CATALYTIC STUDIES ON ZEOLITES

A Thesis Submitted For The Degree Of

Doctor Of Philosophy

By

Muzaffar Khan M.Sc.

At

Department of Chemistry

The City University

London

August 1986

ACKNOWLEDGEMENTS

I would like to acknowledge my gratitude and respect to my supervisor Dr. R.P. Townsend for his guidance and encouragement throughout this work. I would also like to thank my ex-supervisor Dr. R.W. Joyner for his advice and help during my stay at the University of Bradford. I am also grateful to the staff and my colleagues at the department for their endurance and assistance.

My thanks are also due to the Ministry of Education, the Government of Pakistan for the scholarship, the City University for an ORS award and the University of Baluchistan for granting the study leave to complete the present studies.

Finally, I am indebted to express my sincere thanks to every member of my family for their support and [redacted] for looking after my family in my long absence.

INDEX

LIST OF FIGURES

List of Figures cont.

LIST OF TABLES

ABSTRACT

Transition metal exchanged zeolites (prepared by different methods) were characterized using conventional chemical and thermal analyses (TGA, DTA and DSC). Structural stability of the samples was checked by monolayer equivalent surface area (MESA) and X-ray powder diffraction analysis. The catalytic studies of these samples (activated under different atmospheres) were carried out in static or flow systems.

Kinetics of nitrous oxide decomposition reaction were observed on transition metal (cobalt or copper) exchanged 5A zeolites in Pyrex glass static system under vacuum. First order Arrhenius plots for cobalt-5A zeolites were linear over experimental temperature range but deviated from linearity at high temperature for copper-5A zeolites, where it is thought that reaction becomes diffusion limited over 920K.

A copper-glass built flow system (operating at atmospheric pressure) was used for methane oxidation studies on the above cobalt or copper-5A zeolites, and nickel, copper and platinum mordenites (activated under air or nitrogen). Transition metal exchanged -5A zeolites being less reactive for this oxidation reaction, further study was followed on sodium or ammonium forms of nickel and copper mordenites. The catalytic activities of these samples were compared by varying physical parameters like ion exchange, mode of activation, oxygen dilution of the feed (1% methane in air) and/or mode of mixing of the samples. Mixed-catalyst study being a very promising field, can be easily extended by either varying the mixing proportions, oxygen dilution levels, or involving other metal ions or other hydrocarbons as a feed.

CHAPTER 1

GENERAL INTRODUCTION

1.1. INTRODUCTION TO ZEOLITES.

Zeolites are crystalline aluminosilicate compounds composed of three-dimensional framework of AlO_4 and SiO_4 tetrahedra which are linked to each other by the sharing of all the oxygens. Channels and cavities of specific sizes occur in the framework, in which reside mobile exchangeable cations, and water molecules which can be removed from the lattice reversibly. The term 'zeolite' was coined by a Swedish mineralogist Cronstedt[1] in 1756. The Greek roots of the name zeolite mean together 'boiling stone', and refer to the frothy mass which can result when a zeolite is fused in the blowpipe[2], due to rapid water evolution. When heated, this intercrystalline 'zeolitic' water can however be continuously removed over a wide temperature range to give an open empty porous structure which can be filled by other suitable molecules; hence the great importance of zeolites as 'molecular sieve' sorbents. Thus as early as 1925, Weigel and Steinhoff[3] reported that the zeolite chabazite adsorbed water vapour, methyl and ethyl alcohol, but acetone and benzene were largely excluded. McBain[4] discussed the significance of these results and was probably the first to propose the term "molecular sieves" for zeolites which can selectively adsorb different molecules subject to their shape and size. Perhaps the best overall definition of a zeolite, and one which encompasses the complex

physical properties of these materials is due to Smith[5], *viz* "a zeolite is an aluminosilicate with a framework structure enclosing cavities occupied by large ions and water molecules, both of which have considerable freedom of movement, permitting ion exchange and reversible dehydration".

Pauling[6] and Taylor[7] were first to apply X-ray diffraction techniques to study the crystal structure of the zeolites analcite and natrolite, in early 1930's. Around the same time Barrer (who with his co-workers has made a substantial contribution in the development of zeolite chemistry), was the first physical chemist to report during 1938 the results of his studies of the sorption of gases on crystals of the zeolite chabazite and analcite[8]. Two years later, Barrer and Ibbitson[9] found that chabazite, active analcite and gmelinite rapidly occluded the small molecules of methane and ethane, slowly occluded n-paraffins (e.g. propane) but excluded the branched chain iso-paraffins. After these and similar studies[10], Barrer arranged the zeolites into three classes, distinguished by their ability to occlude or exclude certain standard molecules (*viz* H_2, O_2, N_2, Ar, CH_4, C_2H_6, C_3H_8 and iso-C_4H_{10}), which are used to measure the interstitial channel dimensions of the zeolite. Barrer and co-workers [11] also prepared synthetic analogues of the natural zeolites mordenite and analcite using high pressure hydrothermal methods. In 1947, Barrer[12] reported that molecular sieving at low temperature was sufficiently sensitive to separate argon from oxygen. Attracted by the potential application of crystalline zeolites to the separation of gases, Milton and associates at Linde Division of Union Carbide Corporation in 1948 initiated a study of zeolite mineral synthesis and characterization. By 1952, scientists working at Linde research laboratory had prepared many different

synthetic zeolites[13,14]. Some synthetic zeolites are related structurally to naturally occurring minerals, (e.g. mordenite, erionite, faujasite, chabazite and gismondite), whereas others such as A and L have no known natural analogues. Synthetic zeolites have many advantages over natural zeolites in research and industrial applications because of their greater uniformity in composition and purity.

Zeolites are unique as crystalline porous materials, with structure as well as composition controlling properties. Since 1954, this unique class of materials has generated a mass of scientific literature describing their synthesis, properties, structure and application, which probably number well over 15,000 scientific contributions and over 10,000 issued patents[15]. Worthy of mention are the proceedings of the international conferences on molecular sieves[16-22], a comprehensive treatise on zeolite molecular sieves by Breck[23], an excellent monograph on zeolite chemistry and catalysis by Rabo[24], and more recently still a book by Barrer on their sorption properties[25]. There are several review articles on occurrence, origin, sythesis, the nature of chemical reactions involving zeolites, structure, ion exchange, catalysis and industrial applications of zeolites[26-39].

During this period of almost thirty years of research and development, over 150 species of synthetic zeolites have been synthesized and some 7 mineral zeolites have been found in substantial quantities and purity[29]; known natural zeolites are more than 38 so far. Yet commercially only twelve basic types, listed in Table 1-1, are utilized on a large scale[40].

Table 1-1. Zeolite Types in Commercial Applications[40].

Zeolite Minerals	Synthetic Zeolites	Forms
Mordenite	A	Na,K,Ca forms
Chabazite	X	Na,Ca,Ba forms
Erionite	Y	Na,Ca,NH_4 rare earth forms
Clinoptilolite	L	K, NH_4 forms
	Omega	Na, H forms
	'Zeolon',Mordenite	H, Na forms
	ZSM-5	various forms
	F	K forms
	W	K forms

1.1.1. Classification

Attempts to classify zeolites on the basis of their structure have been made by Smith[5], Fischer and Meier[41,42] and Breck[43]. Smith[5] classified zeolites on the basis of common structural units such as parallel six-rings, or "Archimedean polyhedra"[44]. The framework structure of a zeolite is composed of TO4 (where T = Si^{4+}, Al^{3+}) tetrahedra, linked to each other by the sharing of the oxygen ions. The SiO_4 and AlO_4 tetrahedra are then referred to as primary building units PBU). Rings are formed by joining T atoms through the oxygen bridges. For example, the two simplest units are the rings of four tetrahedra (4-ring) and six tetrahedra (6-ring). These subunits have been called secondary building units (SBU) by Meier[42] in his modified classification of zeolites into seven main groups. As shown (Figure 1.1), these units (single 4-ring, single

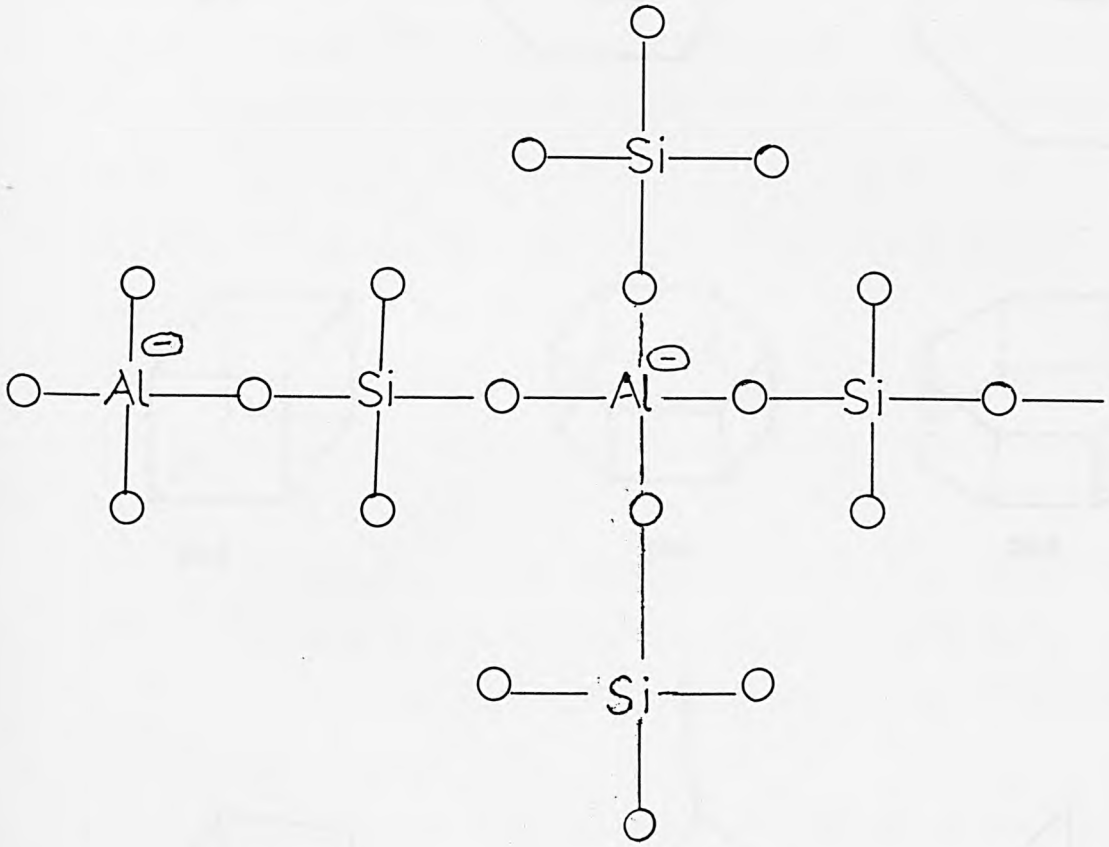

AlO4 and SiO4 tetrahedra , a 2-dimensional representation

Fig.1.1 PRIMARY BUILDING UNITS

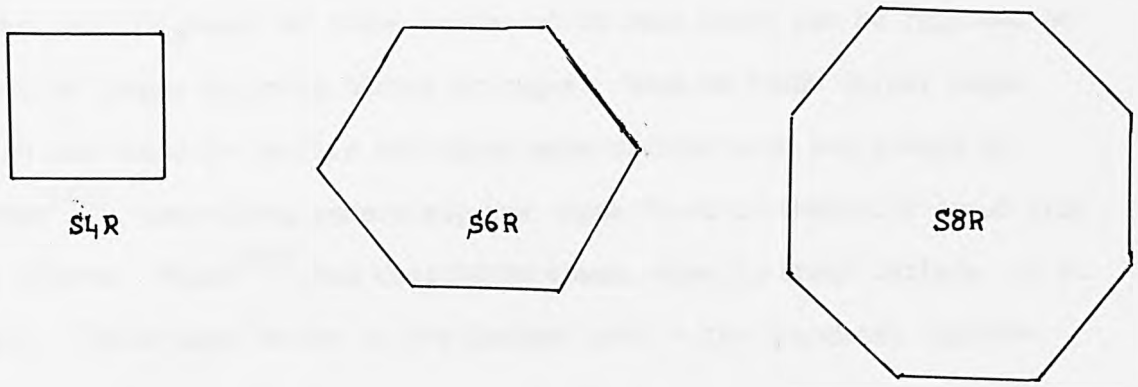

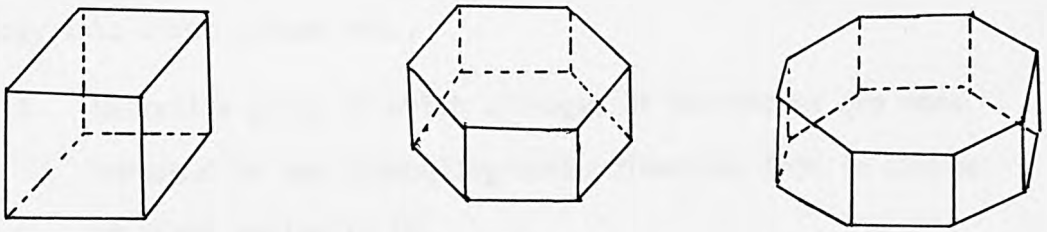

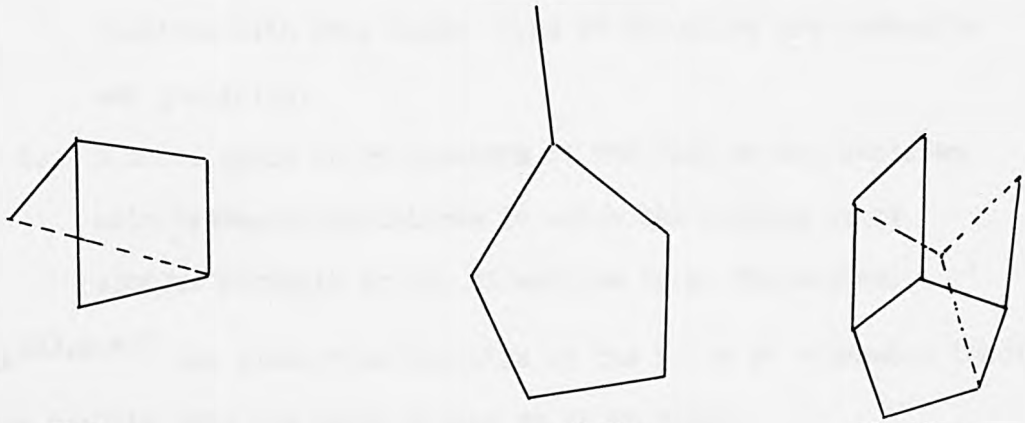

S = SINGLE D = DOUBLE R = RING

Fig.1.2 SECONDARY BUILDING UNITS

6-ring, single 8-ring, cube, hexagonal prism, 4+1 combination, 5+1 combination, 4+4+1 combination) are sufficient to construct zeolite frameworks, but oligomers of these units can be made which can be regarded as a set of larger building blocks or cages. Some of these larger cages which are found in zeolite structure were divided into two groups by Barrer[45], describing separately the cages found in chabazite group from the others. Meier[42] has designated these cages by Greek letters: α, β, γ etc. The α-cage refers to the largest unit - the truncated cuboctahedron.

Deer et al[46] divided zeolites on the basis of their structure and morphology into three groups *viz.*,

1. Natrolite group in which linkages of tetrahedra are more numerous in one crystallographic direction than in planes at right angles to it;
2. Heulandite group have linkages which are more numerous in one plane than in the direction at right angles to it. Zeolites with this layer type of structure are chabazite and gmelinite;
3. A third group which consists of the rest of the zeolites with framework structures in which the binding is of similar strength in all directions (e.g. faujasites).

Breck[23,p.47] has classified zeolites on the basis of framework topology of the zeolite into the seven groups as given below:

Table 1-2

Group	Secondary Building Units (SBU)
1	Single 4-ring, S4R
2	Single 6-ring, S6R
3	Double 4-ring, D4R
4	Double 6-ring, D6R
5	Complex 4-1, T_5O_{10} unit
6	Complex 5-1, T_8O_{16} unit
7	Complex 4-4-1, $T_{10}O_{20}$ unit

Breck[23,p.48] has given tables of zeolite classification in terms of the typical unit cell contents, the polyhedral cage type, the void space of the dehydrated zeolite based on the amount of water contained in the fully hydrated zeolite, the type of channel system, and the free aperture size of the main channels for each zeolite. Synthetic zeolites with (at that time) unknown or uncertain structure are listed in a separate table[23,p.51].

More recently, Barrer[2,p.9] enumerated various ways of generating zeolite framework topologies involving structural units of greater complexity than the secondary building units (SBU) proposed by Meier[42]. Tables classifying some zeolites and tetrasilicates of related topology which list a total of ten groups with their idealized unit cell composition, pore volume and suggested designation of topology are given[2,p.16].

1.1.2. Structure

The structures of zeolites have been described and reviewed by many authors[23,38,47-50].

The fundamental building block of all zeolites is a tatrahedron of four oxygen anions surrounding a smaller silicon or aluminium ion (Fig.1-1). These tetrahedra are arranged so that each of the four oxygen anions is shared in turn with another silica or alumina tatrahedron.

The silica tetrahedra can be regarded in the framework as electrically neutral, because each silicon ion has its +4 charge balanced by the four shared oxygens surrounding it. However each alumina tetrahedron has a residual charge of -1 since the trivalent aluminium ion is also bonded to four shared oxygen anions. This net negative charge in the framework of a zeolite is therefore counter-balanced by cations within the cages (generally Ca^{2+}, Na^{+} or K^{+} in the natural minerals). These ions may be coordinated partly with the lattice and partly with water molecules, or in some cases wholly with water molecules, depending on the zeolite and the degree of hydration. These cations can be replaced readily by ion exchange with other suitable cations with consequent alterations in the zeolite properties.

As described earlier (1.1.1), the silica and alumina tetra (PBU) are combined into more complicated secondary units (SBU), which form the complex building blocks (cages) of the framework zeolite crystal structures. The silica and alumina tetrahedra are geometrically arranged, with (despite some recent assertions to the contrary[51]) Al-O-Al bonds excluded[42]. The structural or unit-cell formula is usually written as

$$\left[M^{n+}_{x/n} \quad (AlO_2)_x \, (SiO_2)_y \right] \; .Z\ H_2O$$

where M^{n+} is a charge compensating cation of valence n and z is the number of water molecules. The ratio of x to y is characteristic of

the zeolite and is generally within the range of 1 to 5. (However, in case of the high silica ZSM-series the Si/Al ratio varies from 10 to 100 or higher[15]. The sum (x+y) gives the total number of tetrahedra in the unit cell while the portion $[\quad]$ represents the framework composition of the zeolite.

Considerations of size and charge show that in principle other atoms should be capable of replacing isomorphously the silicon or aluminium ions in the framework. (e.g. P^{5+}, Ga^{3+}, Ge^{3+}). However, such replacements occur only rarely in natural zeolites[29]. The substitution of Si^{4+} by Ge^{4+} and of Al^{3+} by Ga^{3+} has however been reported in synthetic varieties[52,53].

The physical and chemical properties of zeolites are very dependent upon the arrangement and free dimensions of the intracrystalline channel structure. It is in the cavities and channels of the zeolite framework that the loosely bounded cations and water molecules are found. This molecular water which is presented as an intercrystallyne fluid can be removed by heating in a vacuum and can normally be re-sorbed when the zeolite crystals are exposed to water vapour without disrupting the framework structure (sodium X is an exception because it looses its structure if exposed to steam at 623 K[23,p.492]). Similarly, the poistion and loose bonding of the cations provide a continuous or sometimes partially reversible cation exchange in such a way that the framework structure is normally unaffected. Three types of channel systems are identified[23,p.59]:

(i) A one-dimensional system which does not permit intersection of the channels (e.g. analcime).

(ii) Two dimensional systems, as present in natrolite, mordenite and clinoptilolite.

(iii) In case of three-dimensional intersecting channels, two types arise:

(a) channels which are equidimensional, i.e. regardless of direction, the free diameter of all channels is equal. Examples are faujasite, synthetic zeolites **X**, **Y** and zeolite A.

(b) channels which are not equidimensional, so that the diameter depends upon the crystallographic direction (e.g. gmelinite and offretite). In this case one or two equidimensional channels intersect a smaller second or third channel.

Tables of dimensions, and the nature of the cavities in the zeolites and the dimensions of the appertures, leading into the cavities are given by Breck[23,p.133-180].

1.1.3. Synthesis

The importance of zeolite synthesis is due mainly to two factors[2,p.43]:

i) The need to understand reactions, occurring in lithosphere on or near the surface or in abyssal rock which can be as vast in scale as in the range of variables such as pressure, temperature and time.

ii) The search for cheaper or better replacement for natural minerals and to produce new synthetics of better quality having specific built-in properties.

Zeolites are formed in nature or in the laboratory under conditions in which water is present in considerable amounts and often at elevated temperatures so that the conditions are hydrothermal[2]. The term "hydrothermal" is used in a broad sense and includes the crystallization of zeolites from aqueous systems which contain the necessary chemical

components. The nature of the zeolite obtained is determined by the synthesis conditions, i.e. reactant concentrations, pH, time, temperature, and the nature and concentrations of added promoters. Many of the phases formed are not equilibrium phases but only metastable ones, which in time convert to other more stable phases, which may or may not be zeolitic.

Typical reactants are sodium aluminate, sodium silicate, silicic acid and sodium hydroxide, the latter being used mainly to control the pH. The first step is the formation of a hydrous alumino silicate gel which then crystallizes under carefully controlled conditions to give the desired zeolitic phase. The sequence of events is clear from the following illustration[23, p.250]:

$$NaOH(aq) + NaAl(OH)_4\ (aq) + Na_2SiO_3(aq) \xrightarrow{298K}$$

$$Na_p(AlO_2)_q\ (SiO_2)_r.\ NaOH.H_2O \xrightarrow{298\text{-}448K}$$

Gel phase

$$Na_x\ (AlO_2)_x(SiO_2)_y\ .ZH_2O + \text{solution} \qquad \ldots(1\text{-}1)$$

Zeolite phase

The resultant zeolite must be removed from the mother liquor at the proper time. Finally the zeolite is thoroughly washed to remove sodium silicate from the pore structure.

Typical synthesis conditions for some important zeolites are summarised in Table (1-3).

Table 1-3 Typical zeolite Synthesis Conditions.

Taken from ref.[23].

Zeolite Type	Reactant Composition,[a] (moles/Al_2O_3)			Typical conditions		Composition (moles/Al_2O_3)	
	Na_2O	SiO_2	H_2O	Temp(^oC)	Time(h)	Na_2O	SiO_2
A	2	2	35	100	2-4	1	2
X	3.6	3	144	100	7	1	2.5 (2-3)
Y	8	20	320	100	7		5 (3-6)
Mordenite (large port)	6.3	27	61	100	168	1	(9-12)

[a] NaOH was used to adjust pH.

1.1.4. Properties

1.1.4.1. Dehydration.

The behaviour of "zeolitic water" is a distinctive property of zeolites, and is manifested in their dehydration properties. The amount of crystal water not only depends on zeolite composition and structure but also on the temperature and humidity of the environment. Most zeolites undergo reversible dehydration below about 200^oC without substantial change occurring in the basic framework structure. Many zeolites, however, suffer structural collapse on complete dehydration. Properties of the zeolitic water are commonly interpreted by X-ray crystal structure analysis, thermal analysis, infrared spectra, nuclear magnetic resonance

measurements and dielectric measurements[23].

The zeolites which undergo reversible and continuous dehydration, retain the topology of the framework structure. Exchangeable cations located in the channels and coordinated with water molecules (e.g. in X,Y or chabazite) may migrate to different sites on the channel walls, or other positions or coordination. In zeolites with several possible cation sites (such as zeolite X which has at least five) the effect of dehydration or partial dehydration may be pronounced. Zeolites, like analcime, have water molecules which are tightly coordinated to the framework oxygen, the exchangeable cations and also to other water molecules. In some zeolites complete dehydration causes irreversible changes in the framework topology due to weaker linkages in the framework structure in certain directions. Exchangeable cations initially located in the channels then become trapped.

Zeolites can be classified on the basis of their dehydration behaviour into two groups[23]:-

(i) Zeolites which do not show major structural changes and which exhibit continuous dehydration curves as a function of temperature. Zeolite A, zeolite X and Y, and chabazite belong to this group.

(ii) Zeolites in which dehydration causes structural changes, and the dehydration curves show steps or other discontinuities This type of dehydration is characteristic of natrolite, scolecite and mesolite. In these zeolites, water molecules are present in groups within the structure which have different volatilities.

1.1.4.2. Molecular Sieving.

The molecular sieve action of a zeolite depends upon the degree of

dehydration. The structure must remain intact after dehydration. Large numbers of separations can be carried out through the molecular sieve action which can be either a 'total moelcular sieve action' or 'partial molecular sieve action'[23,p.15]. In the former, advantage is taken of one component of mixture being occluded while the other is not sorbed, and quantiative separations are possible by exposing a gas (or liquid) mixture to a suitable quantity of the appropriate zeolite. Separation of the mixtures C_3H_8/iso-C_4H_4 and nC_4H_{10}/iso-C_4H_{10}, have thus been effected on chabazite crystals, the first named being removed from the second[10], by sorption in the zeolite. When 'partial sieve action' operates, differences in rates of adsorption are exploited either by exposing the mixtures to the zeolite in a static system for an appropriate length of time, or by allowing it to flow through a column of the zeolite at an appropriate rate. For example , the mixtures C_2H_5OH/n-C_7H_{16}, C_2H_6/C_3H_8 and CH_3OH/C_2H_5Br have been separated by removing the first-named molecules first[10].

Sieving and partial sieving effects of zeolites towards various exchange cations are also possible by one or more of the following mechanisms[23]:

1. the size of the cation may hinder entrance to the channels and cavities within the zeolite structure. In some zeolites, the exchangeable cation is "locked in" during synthesis and cannot be replaced (e.g. K^+ in zeolite L).

2. the distribution of charge on the zeolite structure may be unfavourable for the cation, and

3. the size of the hydrated cation in aqueous solution may influence and retard exchange of the cation. If the cavities in the zeolite are too small to contain sufficient entering cations due to their size, ion exchange is restricted.

The separation of molecules is performed by adsorption on zeolites taking advantage of the dimensions of the zeolite channels and the differences in the sizes of the molecules. The most well-known example is zeolite A, which has a channel system with pores of 0.42 nm (8-rings). It is very commonly used for dehydration of gases and of organic solvents [38]. These pores permit diffusion of n-paraffins, but are inaccessible to iso-paraffins.

1.1.4.3. Sorption

Sorption is used to describe uptake of gas and vapours in zeolites and selective adsorption of zeolites is, in part, related to that of their ion or molecular sieving action. The sorption properties of zeolites are influenced by three important factors: the pore volume, the pore size and the presence of cations along the walls of the zeolitic channels[38].

The pore volume per unit mass of zeolite determines the total amount of material which can be sorbed. Zeolite A, with a framework density of 1.27 g ml^{-1} (real density in the hydrated state 1.99 g ml^{-1}) has a void volume of 0.47 ml per ml of zeolite. Zeolite X and Y, with density of 1.93 g ml^{-1} and 1.92 g ml^{-1} respectively, have void volume of ~0.5 ml per ml of zeolite. Thus in X and Y, 50% of the material is void.

However, pore openings limit the size of the zeolitic channels. These dimensions are regulated by the number of silicate tetrahedra in the rings forming the mouths to the zeolite pores. A list of the crystallographic free diameter for rings with different numbers of tetrahedra is given in the following table 1-4 [38].

Table 1-4 Theoretical Dimensions of Pore Opening in Zeolites. Taken from ref. (38).

No. of tetrahedra in the rings	Pore dimensions (nm)
4	0.16
5	0.15
6	0.28
8	0.43
10	0.63
12	0.80
18	1.50

The 4 and 5 rings are very small, so diffusion of molecules through these is not possible. Six membered rings are sufficiently large to allow the passage of small molecules such as ammonia and water. They also permit diffusion of cations, although in some structures these rings are distorted which results in a reduction in the free diameter.

Diffusion problems sometimes limit the usefulness of some zeolites for adsorption, the slow diffusion being a result of the small pore sizes. Zeolites with a tri-dimensional pore system (A, X and Y) are less easily affected by diffusion problems than zeolites with unidimensional pores such as mordenite, where the diffusion process is normally anisotropic. Also, synthetic zeolites are better sorbents than the natural zeolites, which often contain impurities and stacking faults which can seriously affect their sorption properties.

Adsorption selectivity is another important factor in determining the sorbent behaviour of zeolites. The charge compensating cations are present inside the zeolite cages and these produce electrostatic fields which generate a typical affinity in zeolite for polar sorbate molecules when substantial quantities of aluminium are present in the material. Adsorption selectivity is exploited in removing CO_2, water and CO from hydrogen produced by steam reforming[38]. Zeolite Ca-A is used as a selective adsorbent for the nitrogen in air, to produce nitrogen free oxygen[38].

The sorption capacity of a zeolite for a given sorbate is determined by several factors, including the volume available to the sorbate, the nature of the interaction between the sorbate and the zeolite, and physical parameters such as sorption temperature and sorbate pressure. The volume available to the sorbate depends of course on its shape and size, the volume occupied by the cations, and the state of dehydration of the zeolites. The interaction between the sorbate and the zeolite determines the affinity of the sorbate (and thus the quantity sorbed) under a given set of physical conditions.

Sorption in zeolites has been reviewed by Breck[23], Rickert[37], Uytterhoeven[38], Lee[54] and Sanderson[55].

1.1.4.4. Stability

Most zeolites are thermally stable and structural break-down does not occur below around 873K. When heating is continued above this temperature, the crystal structures of zeolites break down and they metamorphose into non-zeolitic solids. Thus zeolite A changes to a β-cristobalite[56]. However, Ca-A zeolite is very stable and retains its structure over 1073K. Similarly, mordenite is another very stable structure. Mordenite dehydration is continuous and there is no evidence of structure change at

high temperature up to 1073K[57].

The stability and structure of zeolites changes when exposed to water vapours at elevated temperature, and pressures (i.e. under hydrothermal conditions). For example, when zeolite A is subjected to a hydrostatic pressure of 137.9×10^6 Pa at 493K, its structure remains stable for one day but after longer periods, finally converts to analcime-like zeolite [58] via zeolite P[23,p.488]. On the other hand, the introduction of calcium ions into zeolite A improves the hydrothermal stability[23,p.490].

In aqueous suspension, hydrolysis involving the removal of some of the intracrystalline Na^+ ions results in the formation of hydroxyl ions, with Na A is in a water slurry. Partial exchange of sodium by calcium reduces the hydrolysis and inhibits the cation migration[59]. Dyer et al[60] observed that different cationic forms exhibit different thermal and hydrothermal stabilities. Zeolites are normally stable to basic conditions and do not generally dissolve or recrystallize below pH 11. The acid stability of zeolites is usually only to about pH 4-5 although some are stable to pH 2[61]. Their acid stability generally depends upon the silicon to aluminium ratio, zeolites becoming progressively more stable with the increase in Si/Al ratio. Zeolites with a Si/Al ratio of 1.5 or less gelatinize upon the acid treatment[23,p.503]. When the Si/Al ratio in a zeolite is greater than 1.5, it decomposes and forms a hydrous silica. Zeolite A for example is readily decomposed by HCl and precipitates as a clear gel. Zeolite X behaves similarly while zeolite Y with Si/Al ratio of greater than 1.5, decomposes and forms silica precipitate with HCl[23,p.503]. Some zeolites, such as mordenite, resist acid treatment, although the cations may be removed by strong acids to produce a hydrogen form of the zeolite. These silica-rich zeolites when treated with dilute mineral acids undergo ion exchange (i.e. $Na^+ \longrightarrow H_3O^+$)

without framework breakdown[62]. A similar pattern of stability is seen when the zeolites are exposed to anhydrous HCl, as shown in table 1-5[63].

Table 1-5. Stability of Zeolites to Anhydrous HCl at 228 torr. (Taken from ref. (63)).

Zeolite	$Si_{/Al}$ ratio	Temperature 473 K	873K
Na Mordenite	4.75	stable	stable
Na Clinoptilolite	4.65	stable	stable
Zeolite L	3.0	stable	stable
Na Y	2.4	stable	stable
Na X	1.33	not stable	-
Na A	1.0	not stable	-

1.1.4.5. Ion-Exchange

Zeolites exhibit the property of ion-exchange. By the term ion-exchange it is normally understood that this refers to one form of isomorphous replacement which takes place between the mobile cations in the zeolite and the cations in the external solution in which the zeolite is immersed.

The deficiency in the positive charge generated by the isomorphous replacement of silicon by aluminium within the framework of zeolites, is compensated by the occluded cations. So both natural and artificial zeolites consist of an immobile anionic framework (the insoluble zeolite structure) and mobile cations in sufficient numbers to result in electroneutrality. The loose bonding of these cations, and their mobility inside the cavities of the framework, makes it possible for zeolites to

exchange other cations easily.

The exchange of a cation A^+ on the zeolite for a cation B^+ in solution can be expressed as

$$Z^-A^+ + B^+(aq.) \rightleftharpoons Z^-B^+ + A^+(aq.)$$

Ion-exchange can take place in aqueous and non-aqueous media. Included in the latter are exchanges involving fused salts. The ion-exchange capacity of the zeolite is a function of the silica to alumina ratio of the zeolite framework. It is therefore highest in zeolite A(~8 $meq.g^{-1}$), for which the silicon to aluminium ratio is about unity. At elevated temperatures large cations may be admitted to previously inaccessible sites, thus increasing the ion-exchange capacity. Breck[23,p.529] has summarised the factors which can influence the cation exchange property of zeolites. These are:-

i. the nature of the cation species (i.e. the cation size both hydrated and anhydrous and the cation charge);
ii. the temperature;
iii. the concentration of the cation in species in solution;
iv. the anion species associated with the cations in solution;
v. the solvent, and
vi. the structural characteristic of the particular zeolite.

Cation exchange in zeolites produced dramatic alterations in stability, adsorption behaviour and selectivity, catalytic activity and other important physical properties[23].

Despite their remarkable selectivities for some ions, zeolites have limited application as ion-exchangers due to three main reasons:

i zeolites generally offer relatively poor resistance to acid attack (1.1.4.4);

ii organic ion exchange resins have greater flexibility for modifying the selectivity pattern;

iii organic resins have superior technological properties in column operation and regeneration[38].

Ion exchange has been reviewed extensively in literature. Apart from several reviews by Barrer and his co-workers[2,25,64], other important reviewing authors include Breck[23], Sherman[33], Maes[65], Sherry[66], Kellerman and Klier[67], Cremers[68], Dyer et al.[69] and Townsend[70].

1.1.4.6. Catalysis

The subject of zeolite catalysis has been reviewed extensively over the last two decades[23-24, 31-32, 34-39 & 71-77].

Zeolites have rugged, robust and thermally stable structures, which make them very useful for surface chamistry applications generally[28]. Heterogeneous catalysis is a surface phenomenon, and in fact has been characterised as 'the chemistry of defect surface states'; this definition can be safely applied to zeolite catalysts[38].

Catalytic activity requires the creation of active sites (1.2.1.) which can occur when an ion-exchanged zeolite is subjected to thermal treatments. Activation procedures can result in the formation of active and stable forms of the zeolites which resist high temperature and even extreme hydrothermal environment. Catalytic activity in the zeolites can be created by the following procedures[38].

(a) Acid zeolite catalyst

Proton acidity is introduced in zeolites by

i) ion exchange with NH_4^+ ions, followed by dehydration and thermal decomposition of the ammonium ions (usually at around 773K) or

ii) ion exchange with polyvalent cations, mostly a mixture of rare earth cations (e.g. La^{3+}), followed by drying and calcination. Acidity increases markedly with an additional NH_4^+ exchange and deammonation.

Mechanisms for the creation and dehydroxylation of acidic hydroxyl in zeolites are shown in figure 1-2. Hydrogen-exchanged zeolites are usua-usually prepared by decomposition of the ammonium-exchanged forms or by dehydration of the hydroxonium-exchanged forms. There is a general tendency for a loss of crystallinity in the hydrogen-exchanged zeolites but to varying extents. For instance, structural breakdown is virtually complete with zeolite X[78], but is only minimal with mordenite[79] and chabazite[80].

Cations and the hydroxy groups attached to the framework in zeolites provide a strong electrostatic field as centres for both Brønsted acid sites and Lewis acid sites. Possible Brønsted and Lewis acid sites in zeolites are given in figure 1-3. Two Brønsted acid sites are lost for every Lewis acid site generated and that acid-base and positive-negative site pairs are generated. Figure 1-4 represents Brønsted and Lewis acid sites in a silica alumina cracking catalyst. Silicon, being tetravalent is surrounded by four tetrahedrally disposed oxygen atoms, and when a silicon atom is replaced by a trivalent aluminium atom the structure shown in figure 1-4(a) arises. Now aluminium is prone to become four coordinate which it can do by passing to the structure shown in figure 1-4(b). The negative charge acquired by the Al atom is delocalised over the four oxygen atoms. Hence the proton which is liberated from

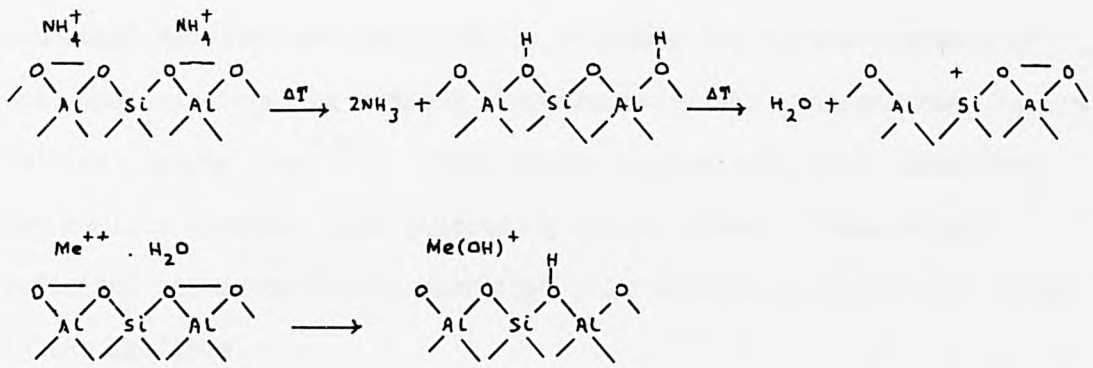

Fig.1.3 (a) PREPARATION OF HYDROGEN-ZEOLITES
(b) FORMATION OF ACID SITES IN ZEOLITES

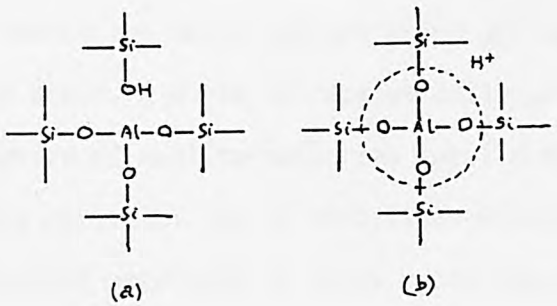

Fig.1.4 (a) LEWIS ACID SITES , and
(b) BRONSTED ACID SITES in SILICA-ALUMINA CATALYST

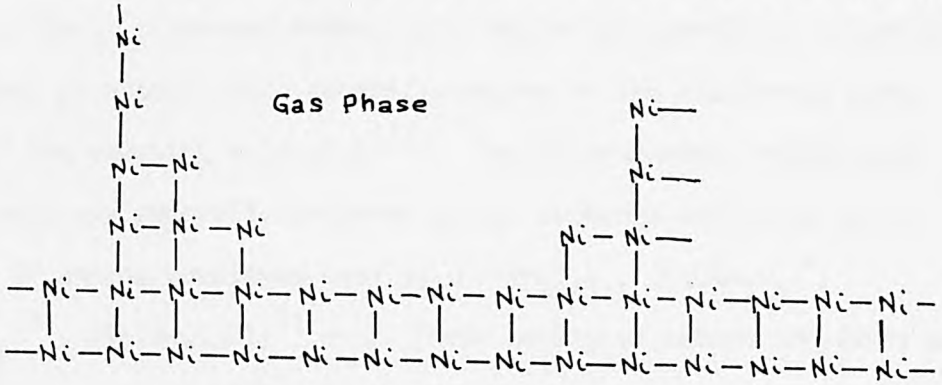

Fig.1.5 REPRESENTATION OF ACTIVE CENTRES

the Si-OH group, is used to create carbonium ions. In case of zeolites, protons attached to framework oxygens apparently act as Brønsted acids in the catalytic properties of zeolites[81]. Rare earth exchanged zeolites are very stable, probably due to the presence of occluded oxide species arising from the trivalent ions and some 'extra lattice' oxygen ions[38]. These extra oxygens originally came from the zeolite crystal, thus generating defect sites. These oxygen deficient sites constitute electrophilic centres or Lewis acid sites in the zeolites.

(b) Metal loaded zeolites

Reactions such as hydrocracking require a combination of acid centres and a supported metal catalyst. When the cations of a zeolite are exchanged with certain transition metal cations which are capable of being reduced *in situ* at the sites, a phase of catalytically active metal is produced. A specific feature of zeolite-supported metal catalysts is certainly that very small particles can be stabilised within the framework, which affords interesting materials to study metal-support interaction and particle size effects[82].

Noble metals have an important role in heterogeneous catalysis and are used in a finely dispersed state, to catalyse hydrogenation, oxidation or in other processes which generally depend on the electronic properties of the reacting molecules[38]. Zeolite-supported noble metal (Pt, Pd etc) are generally propared by ion exchange technique with a solution of ammine complexes such as $(Pt(NH_3)_4)^+$, $(Pd(NH_3)_4)^+$, $(Ru(NH_3)_6)^{3+}$, $(Rh(NH_3)_5Cl)^{2+}$ etc. These amminated cation complexes are generally stable in solutions over a wide pH range and hence are suitable for preparative techniques involving cation exchange[77]. The exchanged zeolite is then thermally treated in various atmospheres, followed by

reduction in hydrogen at elevated temperatures. It was suggested[77] that direct reduction of $(Pt(NH_3)_4)^{2+}$ by H_2 forms a neutral highly mobile platinum hydride such as $H_2Pt(NH_3)_2$, which results in a very rapid particle growth. By contrast[83], in oxidized samples, Pt^{2+} cations are strongly held on the zeolite surface thus hindering the particle growth.

In many cases involving metals supported in zeolites, the nature of the metal-support interaction, and the parameters which determine the nature and extent of this interaction are yet unclear[77].

1.2. INTRODUCTION TO HETEROGENEOUS CATALYSIS

A catalyst is a substance which facilitates the rate of approach towards equilibrium of a thermodynamically feasible chemical reaction. This action of the catalyst is described as catalysis. When the reaction takes place within any one phase, the process is referred to as homogeneous catalysis. In heterogeneous catalysis the reaction occurs at an interface (i.e. at a solid/gas and/or solid/liquid interface). Broadly, the overall catalysis process may be broken down into five steps[84] *viz*:-

i) transport of reactants to the catalyst surface (which is commonly into the catalyst pores),

ii) adsorption of the reactants on the active sites on the external or internal surface of the catalyst,

iii) activation of adsorbed reactants and interaction to form products,

iv) desorption of products from the catalyst surface, and

v) transport of the products away from the catalyst.

Step (i) and (iv), which involve no chemical change can be rate-limiting under certain conditions. The subject of mass transfer through the fluid phase to the catalyst surface has been discussed extensively in several

texts[85-87], and is a physical process.

In contrast, steps (ii) to (iv) involve chemical change and provided one of these is rate limiting, the reaction will obey the Arrhenius equation:

$$K = A \exp(-E/RT) \qquad \ldots.(1.2.a)$$

where K is the velocity constant, A the pre-exponential factor and E is the activation energy.

The most important step in the overall process of catalysis is adsorption of the reactant. Adsorption is basically of two types: physisorption and chemisorption.

(i) Physisorption: in physisorption (or physical adsorption)[88], the molecules are held to the surface by weak Van der Waals forces. Physical adsorption occurs at temperatures close to the boiling point of the gaseous adsorbate. The rates of physical adsorption and desorption are rapid provided the surface is accessible and the processes are readily reversible[89]. Physisorption processes involve relatively small heats of adsorption similar in magnitude to heats of liquefaction. Moreover, because Van der Waals forces are involved, physical adsorption is essentially non-specific with respect to the adsorbent and adsorbate.

(ii) Chemisorption: strong interactions involving valence bonds are termed activated adsorption or chemisorption. During chemisorption[90], considerable changes occur in the distribution of the electrons in the molecules of the adsorbate, and much higher temperatures are required for attainment of equilibrium than those involved in physisorption processes. New chemical bonds[91] are formed between the reactants and the surface atoms of the catalyst. The heat evolved when the extent of previous adsoprtion is low is usually large but falls considerably as

the surface becomes covered with adsorbate. This phenomenon is due to the heterogeneity of the catalyst surface. The rates of desorption from chemisorbed layers are often very low due to the high values of the heats of chemisorption. Thus at low temperatures, the chemisorption of many gases is an irreversible process. However, the rate of chemisorption and the rate of desorption from a chemisorbed layer vary enormously from system to system.

A reaction over a catalyst surface may involve only chemisorption, or a combination of chemisorption and physisorption. For a bimolecular reaction, the former case conforms to Langmuir-Hinshelwood kinetics, whereas the latter case is governed by Rideal-Eley kinetics[92-93]. In any case, the number of active sites and hence the rate of reaction is a function of properties of the catalysts such as the total surface area, active surface area and the porosity. The total surface area and the porosity are easily determined from low temperature nitrogen physical adsorption-desorption isotherms[94].

1.2.1. Active Centres.

It was proposed long ago by Taylor[95] that reactions which are catalyzed by solids actually occur on the surfaces of the solids at points of high chemical activity which are termed as active sites or active centres, but he added "the amount of surface which is catalytically active is determined by the reaction catalysed. There will be all extremes between the cases in which all the atoms in the surface are active and that in which relatively few are so active". Taylor's work gave clear expression to the concept of a geometrically and energentically heterogeneous surface[96], as shown in figure 1-5. There is little difference, except in terminology between his picture and that of small particles having atoms of different

coordination number at their surface. Theoretical concepts given by Balandin's "Multiplet Hypothesis"[97] and Taylor's theory of "Active Centres"[95,98], have helped to understand the nature of the surface atoms constituting a catalytic active site. Balandin's basic idea that each catalytic reaction has a specific requirement for one atom or a specific geometric grouping of two, three, four or whatever number of surface atoms has stood the test of time.

Other authors[99-100] assume that all heterogeneous catalysis is due to the existence of a variety of crystal planes, of atoms of low coordination number at edges and corners, and of atoms of high coordination number at the base of steps on planes. Somorjai[101] has shown that stepped surfaces can be obtained by cutting a single crystal at a slight angle to a low index plane. Such surfaces exhibit higher sticking coefficients for hydrogen and oxygen, and a higher catalytic activity in n-heptane dehydrocycliziation than do the corresponding plane surfaces. However, Kwan[102] has argued strongly against the idea that the edges and corners of crystals are specially active in catalysed reactions although agreeing with Taylor [103] that there is evidence that these isolated spots can affect the heat of physical adsorption.

1.2.2. Transport in Catalyst Pores.

The operating conditions of a catalytic reaction affect the rate of transport of gaseous molecules through the porous structure, and the observed reaction kinetics are influenced by the rate of transport if it is comparable with the rate of chemical reaction. The collisions of molecules with the pore walls and other molecules during transport through the catalyst structure give rise to random molecular motion. So the rate at which molecules diffuse through molecular media is very much less than that associated with the translation velocity of molecules.

When reaction occurs at rates comparable with mass and molecular transfer rates within pore structure, a hyperbolic concentration gradient is established and interior surfaces are exposed to lower reactant concentrations than surfaces near the exterior. The ratio of actual reaction rate to that which would occur if all of the surface throughout the inside of the catalyst particle were exposed to reactant of the same concentration and temperature as that existing at the outside surface of particle is called the effectiveness factor. When a catalyst is operating with low values of effectiveness factor, the reactant concentration drops rapidly with distance of penetration into the interior. Hence the catalytic cations in the interior contribute relatively little to the overall rate of reaction.

Thus even when transport to the catalyst external-surface is not rate-determining, transport along the pores to the active sites within the solids may substantially alter the effectiveness of the catalyst. Transport of a gas in such a catalyst pore may be by one, or a combination of more than one of three types of mass transport in pores.

(i) Bulk diffusion

(ii) Knudsen diffusion, and

(iii) Poiseuille or forced flow.

As a general statement,

(a) if there is no pressure gradient in the pores the mode of transport is just diffusion and

(b) if a pressure gradient is present the mode of the transport is diffusion plus forced flow.

Pure bulk diffusion occurs when the collisions of molecules with the pore wall are relatively few compared to the frequency of molecular collisions

in the free space of the pores, and there is no pressure gradient in the pore. A criterion for this mode of molecular transport is therefore that the pore diameter must be larger than the mean free path of the gas molecules.

By contrast, Knudsen diffusion arises when the mean free path of the gas molecules is greater than the average pore diameter. At atmospheric pressure, in pores $< 10^{-7}$ m diameter, Knudsen diffusion is the mode of molecular flow.

Poiseuille or forced flow is the result of pressure gradient in the pores and is a mass flow process rather than a molecular transport phenomenon. Both Knudsen and bulk diffusive processes are independent of total pressure difference across the pores. If however, the chemical reaction in the pores is such that there is a volume change on passing from reactants to product, a pressure gradient will build along the pore causing a mass flow either in or out of the pore. When the mean free path of the molecule is large compared to the pore diameter so that Knudsen diffusion is occurring, the pore diameter is so small that even at high pressure gradients Poiseuille flow is insignificant. Thus Knudsen flow is indistinguishable from Knudsen diffusion. On the other hand, if a pressure difference occurs in a pore when the mean free path is small compared to the pore diameter, bulk flow will occur which is a combined transport process, consisting of Poiseuille flow superimposed on top of bulk diffusion.

Under ambient conditions diffusion in the micropores is usually of the Knudsen type, while that in the macropores is predominantly in the bulk of transition range (a range of molecular concentrations in which both the collisions of molecules with the pore wall and molecular collisions

in the free space of the pore are important). As a general principle and at atmospheric pressure, in small pores Knudsen diffusion predominates, in intermediate pores (>1000^{o}A) bulk diffusion plus Poiseuille flow give the overall flux, while in very large pores Poiseuille flow is effective. Thus in a typical catalyst (small pores) it is often adequate to just consider Knudsen diffusion even when there is a total pressure gradient in the pores.

1.2.3. Catalytic Activity and Selectivity

The activity of a catalyst for a particular reaction can be defined in terms of the value of the rate constant for that reaction which results under specified conditions of temperature and partial pressures per unit weight of catalyst[104]. The term specific activity is used when the surface area of the catalyst is known, and where the rate or rate constant may be referred to unit surface area. The number of active sites per unit area is also termed as activity[86], and an increase in the number of active sites enhances the rate of reaction. A catalyst speeds the reaction by lowering the activation energy of the rate limiting step. Therefore, although it does not disturb the thermodynamically determined equilibrium composition of the reaction system, it increases the rate at which it is attained. However, it is most important to note that an increase in the activation energy of the reaction may not lead to the expected decrease in the rate constant due to a simultaneous increase in the pore-exponential factor A, which compensates for the change in the exponential term of the Arrhenius equation(1.2.a). This is called the compensation effect. For a series of catalysts and for a given reaction, the relation between A and E is

$$\log A = aE + b \qquad \ldots(1.2.b)$$

where a and b are constants. The occurrence of the compensation effect

is the prime reason for not accepting the magnitude of the value of the activation energy of a reaction as a quantitative measure of the catalytic activity of the catalyst. Catalytic activity is widely correlated to the temperature required to attain an arbitrary degree (or rate) of conversion. Schuit[105] has summarized the advantages of preferring the criterion of temperature at fixed conversion rather than conversion (or rate) at fixed temperature.

The chemical composition of the catalyst, in addition to physical properties like surface area, pore size distribution and particle size, affects the activity. The nature of the carrier, or support, can also effect both the catalytic activity and selectivity because the support can influence the surface structure of the atoms of the dispersed catalytic agent through the ease with which sintering can occur, which, of course, affects the active surface area[106].

1.3. OXIDES AS CATALYSTS

1.3.1. Nitrous Oxide Decomposition

The heterogeneous decomposition of nitrous oxide on various oxides was extensively studied by Schwab and associates[107] during 1930-1940. In general, the reaction was found to be first order with respect to nitrous oxide decomposition. Dell, Stone and Tiley[108] classified various metal oxides on the basis of their activity studies for this reaction. The first group comprised Cu_2O, Ni_2O and CoO which cause decomposition below 673K. The second group consisted of CuO, MgO, CeO_2 and CeO, which brought about decomposition between 673-823K. The correlation indicated that the electronic structure of the catalyst is an important factor in the decomposition of nitrous oxide on metal oxide catalysts. Wagner[109] suggested

that the first step in the reaction involves the production of a nitrogen molecule and an adsorbed oxygen ion as,

$$N_2O + e(\text{from catalyst}) \longrightarrow N_2 + \bar{O}\ (\text{ads}) \quad \ldots I$$

Followed by

$$\bar{O} + \bar{O} \longrightarrow O_2 + 2e(\text{to the catalyst}) \quad \ldots II$$

and

$$\bar{O} + N_2O \longrightarrow O_2 + N_2 + e(\text{to the catalyst}) \quad \ldots III$$

This consideration can be applied to the decomposition of nitrous oxide on metal oxides in general.

More recently, solutions containing active transition metal ions (t.m.i.) dispersed in an inert matrix have been used[110-115] as model catalysts to classify the role of the structural and electronic parameters which affect the catalytic activity. It is now considered that catalytic activity is influenced by four factors:

i) the concentrations of t.m.i.,

ii) the electronic configuration of t.m.i.,

iii) the symmetry of the site occupied by the t.m.i., and

iv) the nature of the matrix in which t.m.i. are dispersed.

Cimino *et al*[116] studied the role of matrix by measuring the catalytic activity of CoO-ZuO-MgO solid solutions for the decomposition of nitrous oxide, and found (perhaps somewhat obviously) that the turnover frequency (molecules decomposed per cobalt ion per second), decreases with increasing zinc content (matrix effect) and also with increasing cobalt concentration. Activity increased strikingly at low zinc contents (dilution effect). This increase in catalytic activity due to the addition of cobalt confirmed that the Co^{2+} ions are the active centres for the decomp-

osition of nitrous oxide. They presented a mechanism for the decomposition of nitrous oxide on the basis of their studies.

Cimino and Indovina[117] investigated activity of Mn^{4+}, Mn^{3+} and Mn^{2+} ions dispersed in MgO for the same reaction and reported that Mn(II) ions are more active than either Mn(IV) ions or Mn(III)ions. Dilute catalysts having a given Mn^{3+}/Mn^{2+} ratio were more active than concentrated catalysts having a similar Mn^{3+}/Mn^{4+} ratio, while the catalysts containing a mixture of Mn^{2+} and Mn^{4+} were very active.

Many surface catalyzed reactions of gases[89] occur by the reactants becoming chemisorbed onto sites on the surface to give 'surface compounds'. There are often fragments of the reactants bonded to the surface by covalent or ionic bonds. When the bonds are not too strong, the fragments can react to give first the chemisorbed product and then the gaseous products. The nature and stability of the surface complexes are very important in the catalytic process and depend on the structural and electronic properties of the adsorbent atoms. The dilute solid solutions of transition metal ions in inert oxide, have the advantage of allowing investigations of the catalytic properties of the ions free from strong interferences between themselves. The study of the decomposition of nitrous oxide over MgO catalysts doped with NiO and NiO + Li_2O[118] showed that the activity for pure MgO is low but increases by addition of Ni^{2+} ions. The apparent activation energy decreases in the presence of Ni^{2+} but increases in the case of Li.

Semiconducting oxides and mixed oxides show a maximum activity when the energy of thermal activation of charge carriers is equal to an energy term of the adsorbed molecule by a probable process of collision between excited charge carriers and adsorbed gas molecules. Scheve and Schulz[119] chose

the decomposition of nitrous oxides on CuO/Cr_2O_3 as a test reaction to investigate this resonance effect on solid surfaces and reported that the activation energy of the gas-phase reaction is lowered by an amount corresponding to the amount of energy transferred by the charge carriers. They concluded that a good catalyst should possess energetically favourable charge carriers.

Rudham and Sanders[120] studied nitrous oxide decomposition on nine transition metal oxides and arranged the activity series of the samples as

$Co_3O_4 > NiO > CuO > Fe_2O_3 > Mn_2O_3 > Cr_2O_3 > TiO_2 > ZnO > V_2O_5$. The results were in good agreement with those reported by other workers[121] for the same reaction.

The effect of collective and localized properties on the catalytic activity of solid solutions of NiO-MgO[122] and on $NiO-Al_2O_3$ and NiO-ZnO catalysts [123] has been investigated. The activity related to a unit Ni^{2+} ion, tended to increase with decreasing NiO concentration in the solid solution which suggested that localized properties of the Ni^{2+} ions and not the collective properties of NiO, are rate determining in these reactions.

The oxides $NiO-TiO_2$ do not form solid solutions, but mixtures of these two compounds have also been investigated[124]. The kinetics of nitrous oxide decomposition on $NiO-TiO_2$ catalysts containing 12.1-100% NiO[124] showed that pure TiO_2 and catalysts containing up to 35% NiO have near-identical activities while a sharp increase in activity was observed for catalysts containing more than 35% NiO. It was concluded that the isolated and weakly interacting Ni^{2+} ions present in the structure of $NiTiO_3$ and the pure TiO_2, have little activity for the reaction while the rapid increase in activity is caused by the presence of free NiO phase.

Cobalt oxide is known[125] to be a very active catalysts for nitrous oxide decomposition. Cimino and Pepe[126] established that cobalt ions are very active also when dispersed in the MgO matrix. Their study for the reaction over pure CoO and CoO-MgO solid solutions indicated that the activity per cobalt ion increases with dilution and the apparent activation energy ranges from 17k cal mol^{-1} on dilute solid solutions to 29k cal mol^{-1} on pure CoO. Lower activity was observed for the CoO-ZnO system[127]. Milton and Reddy[128] studied the catalytic decomposition of nitrous oxide on Co and C O-MgO. Activity of CoO was compared to that of the solid solution (0.60 Co, 0.40 Mg)O to determine the effect of cation dilution. The CoO-MgO catalyst was found to have a lower activity than the pure CoO.

Cu^{2+} ion does not enter easily into solid solutions, not because of its charge, but because of its electronic configuration[110]. Solid solutions of Cu^{2+} in MgO and ZnO can only be formed with difficulty as evidenced by X-ray, magnetic and optical measurements[129]. However, Cu^{2+} can be reduced to Cu^{+} at high temperatures under vacuum. When measuring catalytic activities over CuO-MgO or CuO-ZnO solid solutions it is questionable whether Cu^{2+} ions or Cu^{+} ions are active and whether they stay in solid solutions. It has been shown[130] that whilst in MgO, there is a definite indication of reduction to Cu^{+} but not of a marked segregation, whereas in ZnO segregation can occur.

1.3.2. Methane Oxidation

Oxides of the metals of period IV generally have high activity for many oxidation-reduction reactions with molecular oxygen. A systematic study of the catalytic properties of metal oxides for different reactions involving the participation of oxygen enables an elucidation of some

general principles and also a determination of the properties of other oxides essential for catalysis. Several workers have investigated the activity of oxides for the complete oxidation of methane[131-135]. The first systematic study of the oxides of the fourth period and some other catalysts was conducted by Anderson[134]. Kainz and Horwatitsh[136] while explaining the reaction mechanism of methane oxidation catalyzed with oxides, reported that the catalytic activity decreases in the order: $Pd > Co_3O_4 > MnO_2 > Pt > NiO > CuO >> Cr_2O_3 > Fe_2O_3 > Mn_2O_3 > CeO_2 > ZnO > WO_3 > SiO_2$. So on the basis of the suggested oxidation mechanism the oxides were grouped as:

i) oxides on which oxidation occurs due to oxygen in the lattice (CuO, MnO_2), and

ii) oxides on which oxidation occurs via chemisorbed oxygen molecules (Co_3O_4, NiO, Fe_2O_3 and Mn_2O_3).

Studies of methane oxidation by a continuous flow method[137] on TiO_2, v_2O_5, Cr_2O_3, MnO_2, Fe_2O_3, Co_3O_4, NiO, CuO and ZnO showed markedly different catalytic activities, arranged in the decreasing order as $Co_3O_4 > NiO > MnO_2 > CuO > Cr_2O_3 > Fe_2O_3 > Ti_2O > ZnO$. The reaction orders with respect to methane were 1 for Co_3O_4, 0.8 for ZnO, 0.6 for MnO_2, Cr_2O_3, Fe_2O_3, 0.5 for NiO, CuO and 0 for TiO_2.

Anderson *et al*[134] studied catalytic oxidation of methane on 28 samples in a microcatalytic reactor and observed that the activity of metal or metal oxides per gram of active metal decreases in the order Pt > Pd > Cr > Mn > Ce > Co > Fe > Ni > Ag. They compared the temperature required for complete oxidation of methane, 2-pentene and benzene on four of the most active catalysts (Co_3O_4, Cr_2O_3 on alumina, Pt on alumina and Pd on alumina) and reported that methane was the most difficult hydrocarbon

to oxidize, whilst 2-pentene could be oxidized very easily. Though Co_3O_4 was found to be the most active single-component catalyst in the oxidation of hydrocarbons, its activity decreased on impregnation onto alumina due to the probable formation of $CoAl_2O_4$. Precipitation of $Co(NO_3)_2$ solution with K_2CO_3 prior to addition to the support increased the activity five-fold. Cohn and Haley[138] gave the reactivity order Rh > Pd > Ir > Ru > Pt > Ag, and found that NiO on alumina was inactive under their testing conditions for methane oxidation. Yant and Hawk[133] examined both pure metal oxides and mixtures of oxides, and concluded that Co_3O_4 was the most effective while Vendt *et al*[133] showed that most active of the supported catalyst was Cr_2O_3 for the same reaction.

The chemical composition and the related mobility of lattice oxygen can affect the activity and selectivity of the oxide catalyst in reactions of complete oxidation of olefins and also in their partial oxidation at the C-H bond. The studies[139] conducted on metal oxides (V_2O_5, Cr_2O_3, MnO_2, NiO, CuO) and their composite binary systems (Bi_2O_3-MoO_3, Fe_2O_3-MoO_3, Co_3O_4-MoO_3, Fe_2O_3-Sb_2O_3, Co_3O_4-Sb_2O_4, SnO_2-Sb_2O_4) showed that a functional relation existed between the change in activity and selectivity of the catalysts with composition, and the change of parameters like activation energy or the electrical conductance.

Catalytic properties of oxide catalysts for oxidation reactions are largely determined by the oxygen bond energies in their near-surface layers due to the fact that the strength of oxygen bonding with the catalyst is a contributary component to the activation energies of these reactions. Boreskov *et al*[140] found good correlations between the activation energies of the reactions of homo-molecular exchange, methane and hydrogen oxidation, and the oxygen bond energy on oxide surface of period IV metals.

The sequences of the increase of oxygen bond energy on metal oxide surfaces conincided generally with the sequence for decreasing catalytic activities of the metal oxides, *viz* Co_3O_4 > CuO > NiO > MnO_2 > Cr_2O_3 > Fe_2O_3 > ZnO > V_2O_5 > TiO_5. They suggested that to obtain the intermediate oxidation products, the reactivity of oxygen on the surface must be sufficiently high to guarantee the required oxidation rate of initial product but not too high to oxidize the valuable products of incomplete oxidation.

Electron transfer plays an important role in oxidation-reduction reactions. Redox-reactions in solution involve electron transfer between reagents while in some other oxidation-reduction processes electron transfer results during intermediate interactions of reagents with a catalyst. The latter include complete or partial oxidation of various compounds by molecular oxygen and reactions involving the transfer of oxygen atoms between molecules. Catalytic oxidation by molecular oxygen[141] can follow two mechanisms characterized by separation or combination of intermediatelectron transfers. Further investigations[142] of the atomic catalytic activity (ACA) in some reactions of iron, cobalt, nickel and copper in simple oxides, spinels, salts, solid solutions and zeolites showed that for the same transition metal ion it can vary within the limits of 4-5 orders of magnitude, depending on the nature of catalyst support. The highest values of ACA were found for transition metal ions in simple oxides, while small concentrations of these ions in zeolites gave the lowest values.

Catalytic activity studies[143] of copper-containing zeolites, divalent copper salts and copper oxide with respect to hydrogen oxidation show that at high dilutions, the catalytic activity of one copper ion (ACA) is 10^4 times lower in zeolites than in CuO. The different catalytic activity

is attributed to the different characters of the copper-oxygen bond. The bond has a pronounced ionic character in zeolites and oxyacid salts, whereas in copper oxide the covalent character is most important.

Extensive data on the rates of propene oxidation over various metal oxides have been reported [144] for complete oxidation of hydrocarbon. Margolis [145] has compared the activities of several catalysts for oxidation of hydrocarbons. The formation of oxygen-hydrocarbon complexes capable of isomerization was suggested to be the limiting step of the reactions. The level of hydrocarbon oxidation is correlated to the number of unfilled cation d-levels, and it is reported that oxides of metals with unfilled d^3, d^7 or d^9 shells (Cr, Co, Cu) have a maximum activity while minimum activities correspond to d^0, d^5, d^8 shells (eg. Pb, Fe, Ni). This dependence does not hold for partial oxidation, possibly due to the high importance of bonding between oxygen and the surface which is responsible for the stability of the oxygen hydrogen stability complex. Dowden[146] suggests that oxygen is the complexing ligand and is capable of intrusion between the metal and the hydrocarbon radical to give

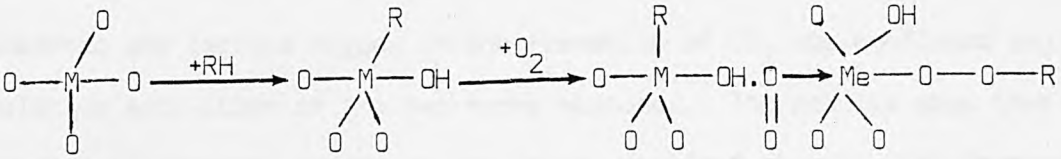

Hydrocarbon-oxygen complexes with the excess of carbon atoms as compared to those of oxygen atoms were observed[147] over selective propene oxidation catalysts, whereas the catalysts for total oxidation induced the formation of complexes with excess oxygen atoms. Decomposition of these complexes at higher temperature yields carbonyl compounds in the first case and carbondioxide and water in the second.

Catalysis activities can be drastically changed by varying the support used and its method of preparations. The latter are on their part strongly dependent on the temperature and the ambient conditions. Yao and Kumar [148] conducted a study of the high temperature treated supported and unsupported metal oxide catalysts for C_2H_4 and CO oxidations. The catalysts used were CuO, Co_3O_4, NiO, $CuCr_2O_4$ and the supports were γ-Al_2O_3, α-Al_2O_3 and ZrO_2. The activity of all supported catalysts per total surface area was reported to be less than the corresponding un-supported metal oxide.

Paetow and Rickert[149] investigated the kinetics of oxidation of propene and carbon monoxide to compare the catalytic activity of copper oxide (CuO), copper aluminium spinel ($CuAl_2O_4$) and copper exchanged zeolites. The highest rate per unit of mass of a catalyst was observed with CuO for both reactions. They also therefore proposed that lattice oxygen is an intermediate in catalytic oxidation on metal oxides.

The role of adsorbed and lattice oxygen in catalytic oxidation was again examined recently by Brown and Patterson[150]. They examined reactivity of tin oxide and antimony-tin oxide catalysts for the oxidation of methane and for the isotropic exchange of oxygen at 673K. The participation of both adsorbed and lattice oxygen in the formation of CO_2 was confirmed and the relative activities of the two forms measured. The results show that utilization of adsorbed oxygen on tin oxide, declined sharply with increasing antimony content in the mixed oxide catalysts. The rate of exchange of oxygen also decreased with increasing antimony content.

1.4. ZEOLITES AS CATALYSTS

Zeolites offer remarkable opportunities for studies on the properties of heterogeneous catalysts because of their unique structural and ion-exchange

properties. Although the subject of zeolite catalysis is only twenty years old, an extensive body of literature already exists and continues to develop rapidly. In addition to original papers, frequent reviews summarize the progress in zeolite catalysis. Reactions such as cracking, hydrocracking, alkylation, isomerization and reforming have attracted special attention due to their importance in industrial applications. However, there is a scarcity of information concerning zeolite activity for processes involving oxidation.

The studies described in this thesis are concerned with nitrous oxide decomposition on transition metal exchanged-5A zeolite and methane oxidation on mordenite in the presence of transition metal ions. In this section such published information as there is on these reactions is presented, followed by the structural and ion exchange properties of synthetic zeolite A and mordenite.

1.4.1. Nitrous Oxide Decomposition.

As discussed earlier (§1.3.1.) decomposition of nitrous oxide has attracted much attention during the past three decades in order to establish the respective rôles of both collective and local properties within an oxide matrix. Redox sites in zeolites which can mediate one-electron-transfer reactions make them also of interest for such studies.

On the basis of extensive investigation of N_2O on oxides (§1.3.1), the mechanism for this reaction may be safely represented as;

$$N_2O_{(gas)} \rightleftharpoons N_2O_{(ads)} \qquad \text{I}$$

$$N_2O_{(ads)} + e \rightleftharpoons N_2O^-_{(ads)} \qquad \text{II}$$

$$N_2O^-_{(ads)} \longrightarrow N_2 + \bar{O}_{(ads)} \qquad III$$

$$\bar{O}_{(ads)} \rightleftharpoons O + e \qquad IV$$

$$2\ O \longrightarrow O_{2\,(g)} \qquad V$$

Step IV can also go by the mechanism

$$\bar{O}_{(ads)} + N_2O_{(gas)} \longrightarrow N_{2(gas)} + O_{2(gas)} + e \ . \qquad VI$$

An electron is transferred to the adsorbed molecule from the solid (step II) and is trapped by acceptor sites in step IV or VI. In case of insulators, positive lattice defects which have affinity to $\bar{e}$ take part in these steps. Active sites in zeolites possibly act like lattice defects. The oxidizing sites (acceptor) in zeolites can form positive radical cations and reducing (donor) sites are capable of forming radical anions [151]. Considering the presence of donor (D) and acceptor (A) sites in zeolites, the step II to IV of the mechanism can be re-written as;

$$N_2\bar{O}_{(gas)} + D \rightleftharpoons \left[N_2\bar{O}_{(ads)}\ D^+\right] \qquad II$$

$$\left[N_2\bar{O}_{(ads)}\ D^+\right] + A \longrightarrow N_{2(gas)} + \left[O_{(ads)}\ A\right]^- + D^+ \qquad III$$

$$\left[O_{(ads)}\ A\right]^- \rightleftharpoons O_{(ads)} + \bar{A} \qquad IV$$

$$\bar{A} + D^+ \rightleftharpoons A + D \qquad VII$$

The formation and continuation of the reaction is carried out by regeneration of a donor site in step VII.

Published literature lacks systematic kinetic studies of this reaction on zeolites. Addison and Barrer[152] were first to investigate the adsorption isotherm for N_2O on chabazite which they found to be reversible up to

623K, decomposition starting only at higher temperatures. Klier studied the reaction on Ni(II)-A zeolites[153] and Co(II)-A zeolite[154] and reported that reversible adsorption occurs at 423K.

The first systematic study of the kinetics of nitrous oxide decomposition involving zeolites was carried out by Rudham and Sanders[120] on both transition metal exchanged-13X zeolites and bulk transition metal oxides. They observed similar sequences for both types of catalysts except in the case of nickel, and decomposition was inferred to follow first order kinetics for all zeolites other than those having Cu^{2+} ions, where kinetic order was 0.5. They proposed that the mechanism for decomposition involves a single cation site and that adsorbed oxygen species are immobile.

Slinkin *et al*[151] conducted investigations of the catalytic activities for N_2O decomposition of H-mordenites of different exchange levels, H-Y zeolite and amorphous alumino-silicate. They deduced that the activity of H-mordenites for this reaction is due to the presence of redox sites. The nature of the active sites required investigation of the different cationic forms of mordenite. When Ni^{2+} ions were exchanged to a level of 50%, the activity of completely inactive Na-mordenite was found to increase sharply. Their further studies[155] on dealuminated H-mordenite and Ni(II)-mordenite showed that the activity of a single Ni^{2+} cation is lower by a factor of 10^3 compared to the activity of the strong oxidation centres responsible for the formation of benzene radical-cations. It was concluded that oxidizing centres are mainly responsible for activity of cations containing zeolite catalysts.

Sidamonidze *et al* carried out kinetic studies of N_2O decomposition reaction on transition metal exchanged erionite[156]. They found that Co/K/Na-erionite was more active than Cu/K/Na-erionite and that the

activity increased with increasing Co^{2+} concentration. Further studies for this reaction[157] emphasised the importance of the ion exchange preparation technique employed. Thus sodium mordenites exchanged with transition metals at pH ≃ 7 were more active than the ones exchanged at pH ≃ 4.

Akbar and Joyner[158] used transition metal (Co^{2+}, Cu^{2+}, Ni^{2+}, Mn^{2+}) exchanged-A zeolites, in their studies, for N_2O decomposition. All the catalysts except those containing Cu^{2+} ions, followed first order kinetics. Catalytic activities of the catalysts, though lower than the metal ions in either oxides or solid solutions, were comparable to transition metal ions (t.m.i) in X zeolites.

Slinkin *et al*[159] observed the activities of polyvalent (alkaline-earth or rare-earth) cation-exchanged mordenites towards nitrous oxide decomposition and arranged them in the following sequences by comparing the reaction rates;

H/NaM(50%) > Be/NaM > Ce/NaM > Mg/NaM > Ca/NaM > Sr/NaM > Ba/NaM > NaM.

They reported that an increase in the catalytic activity of the MeH-zeolite parallels the increase in the number of strong oxidizing centres, except for the Be/HM catalyst. Only Ce^{3+} ions could probably contribute to the catalytic activity.

1.4.2. Methane Oxidation

The properties and specificity of zeolite catalysts in various oxidation reactions in general, and especially for methane oxidation, have been reported in only a limited number of papers in the literature.

Initial studies of the methane oxidation over zeolites using a microcalorimetric technique were carried out by Firth and Holland[160] in order to compare the catalytic activity of different forms of palladium for the reaction. The catalysts were prepared

(i) by thermal decomposition by aqueous ammonium chloropalladite solution;

(ii) by impregnation of NaX zeolite with an aqueous solution of ammonium chloropalladite followed by heating in air at 673K and finally reducing at 573K, and

(iii) by ion-exchanging NaX with tetramminopalladium (II) ions and subsequent activation.

The reaction order was found to be first order in methane for each sample. For oxygen, it was 0,0.3-0.4 and 0.05, respectively. It was also reported that CH_4 and O_2 may be chemisorbed simultaneously on certain Pd species. The apparent activation energies for samples (i) and (ii) were 50 k J mol^{-1} each whereas for catalyst (iii) the value was 88 k J mol^{-1}.

Extending their work, Firth and Holland[161] described the kinetics of complete oxidation of methane over 13X zeolite which had been exchanged to a relatively low extent ($\sim$1%) with ammine complexes of either Rh, Ir, Pd or Pt, and which had been calcined in air. First order kinetics with respect to methane were again observed. The order with respect to oxygen was approximately zero except in the case of platinum where the order was negative. This was interpreted as indicating adsorption of both gases, oxygen the more strongly. The oxygen therefore poisoned the catalyst. It was suggested[161] that the observed identical true activation energies for all catalysts suggested the rate-determining step did not involve bonds to the metal ion, but possibly involved the formation of adsorbed

water molecules from a hydroxyl group and a methyl fragment bonded to the metal ion. The activity sequence at 788K, corrected to the same cation concentration, was

Pd X > Pt X > Ir X > Rh X.

Further studies of the reaction in a stainless steel flow system involving zeolite X were conducted by Rudham and Sanders[162] in which ~ 20% of the sodium ions were replaced by transition metal ions, contrary to very low ~ 1% of the Na^+ exchanged X zeolites used earlier[161]. The observed kinetics for complete methane oxidation were first order in methane and zero order in oxygen giving a methane combustion activity series for X zeolite of Pd >> Cu > Cr > Ni > Fe > Mn > Co. No specific mechanism was proposed and the authors neither supported the Firth-Holland[161] rate-determining step, nor agreed to a proposed mechanism of methane oxidation on palladium catalysts which had been forwarded by Cullis *et al*[135]. Catalysts containing (Pd^{2+}, Cu^{2+}) ions which preferred a square planar or distorted octahedral coordination were most active, followed by those with octahedral coordination (Cr^{3+}, Fe^{3+}, Mn^{2+}), and lastly by those preferring tetrahedral coordination (i.e. Co^{2+}, Zn^{2+}). Catalysts identical to these, were used for a nitrous oxide decomposition reaction study by Rudham and Sanders[135], where the activity series was similar to that obtained on the corresponding bulk oxides. However, obvious differences in both the activation energies and activity series exist for the complete oxidation of methane on the bulk oxides[137] and on the corresponding oxides on high area supports e.g.γ-alumina[163].

Incomplete mechanism for the reaction can be attributed to the very complex

and remarkably sensitive nature of the gas-phase oxidation of the hydrocarbon. Baker and Yorke[164] have reviewed two present theories on the slow, gas-phase oxidation of hydrocarbons.

Mahony, Rudham and Stockwell[165] studied the oxidation of low concentration of H_2, CH_4 (1% in air) and of C_3H_6 (2.33% in air) over a series of Cu-HX catalysts in a flow system operating at atmospheric pressure. First order kinetics were observed for all three reactions. Increasing acidity at constant Cu^{2+} content decreased CH_4 oxidation, increased C_3H_6 oxidation but did not change H_2 oxidation. The activity for all three reactions increased with the extent of ion exchange. The apparent activation energy for CH_4 oxidation remains constant initially but decreases when Cu^{2+} content exceeded 25% exchange. Decrease in CH_4 oxidation activity with increasing acidity was interpreted as indicating probable Cu^{2+} position in α-cage sites being taken by additional protons, hence affecting the catalysis. It was inferred that CH_4 oxidation does not involve carbonium ion intermediates. It was suggested that due to high temperatures required (for activation and reaction itself), the first step in methane oxidation involves reduction of a Cu^{2+} ion in an α-cage site:

$$Cu^{2+} + \bar{O}_z + CH_4 \longrightarrow Cu^{+} - CH_3 + O_zH.$$

Fletcher and co-workers[166] carried out methane oxidation on transition metal exchanged synthetic mordenites, using a copper and glass flow system operating at atmospheric pressure. The catalysts containing (Cu^{2+}, Pd^{2+}, Pt^{2+}) ions were termed as most active while mordenites exchanged with (H^{+}, Mn^{2+}, Ni^{2+}, Ag^{+}, VO_2^{2+}, UO_2^{2+}) ions were found to be the least active catalysts. Activity order deduced from the value of free energies of activation ($\Delta G^{\neq}$) was arranged as,

$$Pd > Pt \sim Cu > Ni > Mn \sim Ag > VO_2 \sim UO_2 > H.$$

The correlation coefficient (-R) of all the twelve mordenite catalysts was reported to be > 0.998, based on the best computer-analyzed fitting reaction order values. The reaction mechanism was supposed to be the same for zeolite X and mordenite.

The kinetic oxidation of propane and carbon monoxide CO was also investigated on Cu^{2+}-exchanged mordenite and Y zeolites by Paetouw and Rickert[149]. They observed that in Cu-MOR approximately 2 molecules of CO per Cu^{2+} ions were chemisorbed whereas in Cu-Y zeolite only 0.25 molecules of CO per Cu^{2+} were chemisorbed indicating the partial accessibility of Cu^{2+} ions in zeolites for CO-chemisorption. The kinetics of both the oxidation reactions were found to be first order. Mordenite was more active than zeolite Y for the reactions.

Weisz[167] showed that Pt-Ca A catalysts have a high selectivity in the oxidation of n-paraffins and n-olefins from a mixture containing isoparaffins and isoolefins.

Rouchaud *et al*[168] have described liquid-phase batch oxidation of hydrocarbons at 423-438K on metal exchanged zeolites. The products of the oxidation of n-hexane without catalysts at 430K and 25 atmospheric oxygen were largely acetic, propionic and butyric acid. The rate of acid formation was approximately doubled when the reaction was carried out on dehydrated Co(II)x, Ni(II)X, or Mn(II)X zeolites. The selectivity to total acids also increased slightly in the latter case.

Agudo, Badcock and Stone[169] observed that the rate of oxidation of hexane at 473-623K was increased in the presence of zeolite X. Activity for the

oxidation of all five hexane isomers tested decreased when Na^+ ions in NaX were exchanged with either Ca^{2+} or Mn^{2+} ions. The reported sequence of activity for different ion exchanged forms of the zeolite X was NaX > MnX > CaX. The higher catalytic activity of NaX was suggested to be due to its greater ability to initiate reactions by H-atom abstraction and to sustain free-radical reactions, whereas CaX and MnX tended to sustain carbonium-ion reactions.

1.4.3. Structure of Zeolite A.

Breck *et al*[13] announced the discovery of zeolite A in 1956. Zeolite A has no natural analogue and hence may be termed as the first truly man-made zeolite. Reed and Breck[170] proposed its structure and gave an ideal unit cell composition as

$$\left[Na_{12} \ (AlO_2)_{12} \ (SiO_2)_{12} \right] .27H_2O.$$

Their basic conclusions on overall structure and composition remain unchallenged to this day. Further investigations into the structure and the properties of zeolite A were carried out by other workers[31,51,171-181]. The composition formula suggests three distinct components, *viz* the aluminosilicate framework $\left[(AlO_2)_{12}(SiO_2)_{12} \right]^{12-}$, the twelve sodium ions and 27 water molecules.

(a) The unit cell framework of zeolite A consists of 24 AlO_4 and SiO_4 tetrahedra, sharing all their corners. Zeolite A is the only known clear example of a zeolite containing double four-membered rings as secondary building units (8-linked tetrahedra or 4-4 rings).

The structure consists of three types of rings and two types of cavities.

Each unit cell (as originally defined) contains three 8-rings, eight 6-rings and twelve 4-rings. The large cavity is termed the α-cage and the small cavity the β- or sodalite cage. The 8-rings connect the α-cages of neighbouring cells and the 6-rings connect the α-and β-cages (fig.1.6). Basically, three-dimensional array of 24 $(Si,Al)O_4$ tetrahedra forms truncated octahedra (fig. 1.6.) which in turn link in a cubic array(fig.1.6.) through their four rings, each four ring linking with a four ring of another truncated octahedra to form a tetragonal prism. The overall result of these linkages is the formation of truncated cuboctahedra (fig.1.6.) and the structure of zeolite A (Fig.1.6.)

The true unit cell of zeolite A is however 8 times greater than the so-called "pseudo unit cell". The lattice constant of a true cell is 24.6^{o}A (23,p.86) but it is convenient for many purposes to consider the pseudo cell only. For zeolite A, the pseudo unit cell constant is 12.32$\overset{o}{A}$. Due to the symmetrical distribution of silicon and aluminium atoms, there is a doubling of the cubic cell constant which lowers the overall symmetry (176).

The large cavity, or α-cage (truncated cubo-octahedron) is located in the centre of the cubic unit cell and is almost spherical, with a free diameter of 11.4$\overset{o}{A}$. Molecules can enter this cavity through six windows, each of these having a virtually planar 8-ring with an opening of 4.2$\overset{o}{A}$. The distorted 6-ring of diameter 2.2$\overset{o}{A}$ gives access to the smaller cavity or β-cage (the sodalite unit), of 6.6$\overset{o}{A}$ mean free diameter. The α-cage is linked to six other α-cages of neighbouring unit cells through the 8-rings and each β-cage is surrounded cubically by eight α-cavities (fig.1.6).

The mean effective pore diameter depends on the nature of the cation.

POLYHEDRA

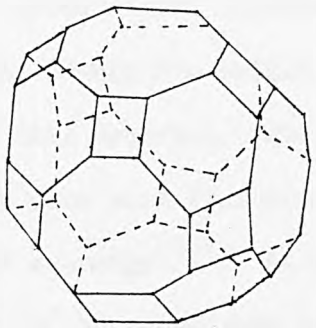

α CAGE

Truncated cuboctahedron

(26- hedron)

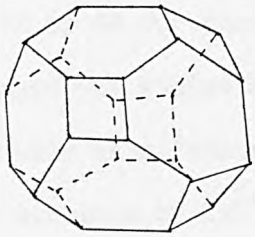

β CAGE

Truncated octahedron

(14- hedron)

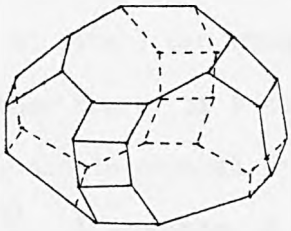

γ CAGE

(18- hedron)

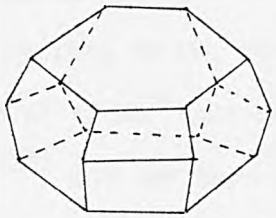

ε CAGE

(11- hedron)

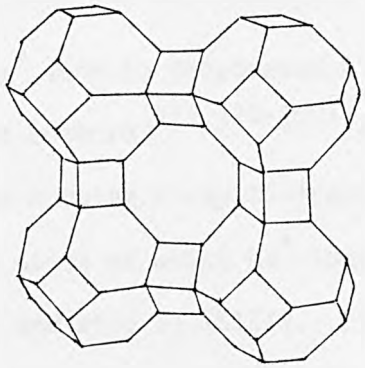

Fig.1.6 ZEOLITE A

Thus, K^+ gives a mean diameter of about 3Å, Na^+ of 4Å and Ca^{2+} of 5Å, for zeolite A. Hence the origin of the terms 3A, 4A or 5A for commercial forms of this material. When calcium is exchanged for sodium in A, the effective pore size increases, but not continuously as a function of the extent of exchange[13]. At a point around 30% exchange of Ca^{2+}, (*viz* 4 of the Na^+ ions replaced out of the 12 per pseudo unit cell), molecules not normally adsorbed are readily occluded. In fact, calcium-exchanged type A has an apparent pore size of 5 to 5.6Å[13]

(b) The net 12-ve charge on the framework due to $24(Si,Al)O_4$ are balanced by 12 Na^+ ions in the unit cell of sodium A zeolite. There are several possible cation site locations in zeolite A. Site I is at the 6-ring, site II is at the 8-ring and site III is near the 4-ring. Cations at site I can occupy the plane of the ring or may be displaced into either the α- or β-cage. The position of 12 Na^+ ions was investigated by single crystal X-ray diffraction[176] and has been reviewed by Seff[179]. In hydrated A zeolite, 8 Na^+ ions are located at site I(SI), near the centre of the 6-rings on the 3-fold axis inside the α-cage. Three of the remaining four Na^+ ions are positioned at site II(SII) in the 8-rings, with water molecules. This site is only one-quarter occupied to avoid unreasonably close interionic contact. Each sodium is coordinated with three water molecules[179]. The twelfth sodium ion is associated only with water molecules near the centre of the α-cavity.

The location of the 12 Na^+ ions in dehydrated A zeolite was presented and reviewed by different authors[175,178-180] on single crystals of dehydrated sodium zeolite A using X-ray diffraction methods. There are three non-equivalent sites at which Na^+ ions are located, namely site I(SI), site II(SII) and site III(SIII). Eight of the 12 Na^+ ions

per unit cell occupying site I (SI) are displaced 0.4Å into the α-cage from the centres of the 6-ring, with three nearest oxygens at 2.3Å and another three oxygens at 3Å. Three sodium ions at site II (SII), are located in the plane of the 8-rings but off-set somewhat from their centres. The coordination of the site II(SII) Na^+ ions is with oxygen atoms at statistical distances of 2.5, 3.0, 3.4, 4.0 and 4.1Å. Subramanian and Seff[180] proposed that, in dehydrated Na-A zeolite, the twelfth Na^+ ion lay in the large cavity opposite a 4-ring which is too small to allow entry of a Na^+ ion. Alternative positions such as double occupancy of the 8-ring and statistical location of three 8-rings by four sodium have also been suggested[181]. It was suggested that Na_{III} had "zero coordination"[180], because its nearest neighbours were about 2.83Å away, *viz* the four oxygens of the nearest 4-ring. Dehydration of zeolite may indeed lead to unusual coordination of cations as water of hydration is lost and the unhydrated cations are forced into rings or even onto surfaces of the aluminosilicate framework. However, Firor and Seff[182] suggested that if the distance between two ions exceeds the sum of their corresponding radii by more than 1.0Å, then these ions may be considered to be not bonded or uncoordinated. "Zero coordinated cations"[183] are supposed to occur only in a zeolite with high Al/Si ratio, and large monovalent cations are required which 'coat' the inner surface of the zeolite, filling all possible coordination sites before all the negative charge of the framework has been balanced. However, studies by Pluth and Smith[181] on dehydrated potassium-exchanged zeolite A proved the absence of supposed zero-coordinated potassium. They noted that all the cations lie adjacent to framework oxygen atoms and that all the K^+ atoms have between 2- and 6-oxygen neighbours within 3.0Å. Nitta *et al*[184] conducted a theoretical study of the site

selectivity of transition metal ions, in dehydrated zeolite A and reported that the cations (Mn^{2+}, Co^{2+}, Fe^{2+}, Ni^{2+}, Zn^{2+}) preferentially occupy the 6-ring site, so it is the last incoming ions which go into the 8-ring sites. Barrer and Meier[171] suggested occlusion of sodium aluminate in A, but extensive studies by Dyer and Enamy[185] on different samples of dehydrated zeolite A showed that no sodium aluminate was occluded in any of the samples studied.

Structural investigation studies of the calcium-exchanged zeolite A by De Roy and Vansant[186] using X-ray powder diffraction techniques lead to coordination 4- and 6- for the fully hydrated structure and coordination 4- after dehydrating the samples at 353K. When the zeolite samples were dehydrated at 423K, it was found that cations were present in the centre of β-cage (sodalite cage) and also in the usual position at the centre of 6-rings. It was concluded that in the transition range between hydrated and dehydrated zeolites, a multiplicity of coordinations is found for Ca^{2+} ions.

c) It is well-known that framework unit cell of hydrated sodium zeolite A contains approximately 27 water molecules. X-ray diffraction studies on a single crystal of hydrated NaA by Gramlich and Meier[176] suggested the presence of water molecules in both α- and β-cages of the structure, as summarised below. (table 1-6).

The water molecule present at site I is ~ 2.3-2.4Å from the cation at the 6-ring, while one water molecule is linked to each cation at site II. The water molecules located near site II form hydrogen bonds with framework oxygen atoms. Seff[179] observed that water molecules positioned in the large α-cage form cubically distorted pentagonal dodecahedral clusters, similar to those found in clathrates. The 20 water molecules

lying at the corners of the cubically-distorted pentagonal dodecahedra in the large cavities are linked to sodium ions or oxygen atoms in the framework. The cluster has a radius of 3.85Å and one water is assigned to its centre. The four water molecules present in β-cage form a distorted tetrahedron, having four edges of 2.9Å and other two of 3.3Å. It was reported[23,p.88] that generally cations in small zeolite cavities like the β-cage are linked with few water molecules. As the size of the cavities increases, water molecules surround the cations, and behave as an isolated liquid phase in large cavities like the α-cage. Water molecules in zeolite clusters have been described as 'crystal water', 'zeolitic water', or 'loosely-bound water' due to their complex nature.

Table 1-6 (taken from 176)

Location	No of H_2O	Designation
In central cavity (α-cage)	1	H_2O_α
Site I (near to 6-ring)	8	H_2O_I
Bridge across 8-ring (near to site II)	6 x 2	H_2O_B
Site II(near to 8-ring)	3	H_2O_{II}
In β-cage	4	H_2O_β

1.4.4. Ion Exchange in Zeolite A.

Breck *et al*[13] were the first to produce ion exchange isotherms for sodium zeolite A, when they replaced (amongst other exchange studies) Na^+ for H^+ in zeolite A. Ammonium exchanged zeolite A was heated at 623K-673K to liberate ammonia. The sample became thermally unstable when more than 35% sodium was exchanged for ammonium. They also reported an order of decreasing selectivity for divalent ion exchange in zeolite A of Zn > Sr > Ba > Ca > Co > Ni > Cd > Hg > Mg whereas the order was Ag > Tl > Na > K > NH_4 > Rb > Li > Cs for monovalent cation exchange. Subsequent studies of ion exchange isotherms and the evaluation of thermodynamic constants have been reported by Barrer *et al*[163-164], Ames[189], Sherry *et al*[190-192], Gal *et al*[193-195], Rees[196] and Weirs *et al*[197]. Less quantitative studies include those of Barrer and Meier[171], Wolf *et al*[198-200], Zhdanov *et al*[201], Dubinin *et al*[202], Seff *et al*[203-209], Schwuger *et al*[210] and Dyer *et al*[60,220] studied exchanges on a mixed Ca^{2+}/Na^+ zeolite A, while Dyer *et al*[69] et.op.cit., Radak *et al*[211], Gauz and Lutze[212,213], and Drummond *et al*[214] carried out isotopic exchange studies on zeolite A. Trivalent cation exchange in zeolite A of Ce^{3+} and Fe^{3+}[13], Ru^{3+}[215], Cr^{3+}[216] and Ti^{3+} has been reported[217], and divalent studies were undertaken by Ames[189] of the Sr/Ca-A system. Similarly, Lomic *et al*[195] studied Cd^{2+} exchange into Zn-A and the converse. Exchanges of Cu^{2+}, Zn^{2+}, Co^{2+}, Ni^{2+}, Cd^{2+}, Pb^{2+} and Mn^{2+} with a mixed Ca^{2+}/Na^+ zeolite A have been reported by Schwuger *et al*[210].

Partial or total collapse of the framework structure after or during the course of the exchange reaction has been observed and reported in the literature. For example, Breck *et al*[13] reported that although exchange of Ba^{2+} for Na^+ proceeded readily, it caused collapse of structure of

zeolite A. Dyer *et al*[60] found that both Ba-A and Ni-A undergo structural decomposition on dehydration at as low a temperature as 343K due to insufficient coordination of ions with the framework after dehydration. Sherry[190] reported that the exchange of Ba^{2+} for Na^{+} in zeolite A does not disrupt the structure provided the exchanged zeolite is not dehydrated. Barrer and Meier[171] noted that instability of NH_4^{+}, Ba^{2+}, Zn^{2+}, Ni^{2+} and Co^{2+} ion exchanged zeolite A increased with increasing degree of removal of the sodium ion. Klier and Ralek[153,218] studied the stability of Ni-A, and found that $Ni_{1.7}A$ lost its structure above 623K; in another study, Gal *et al*[194] reported the preparation of $Ni_{4.9}$-A but the DTA and X-ray patterns showed destruction of the structure above 343K. Other investigations support these conclusions. Thus Egerton and Vickerman[219] found $Ni_{3.73}A$ zeolite to be thermally unstable, and Dyer and Wilson[220] reported that a 81.7% exchanged NiA sample underwent structural collapse during exchange. Coughlan *et al*[221] outgassed a set of Ni exchanged A zeolite samples (8.3 to 80% exchange levels), and described that crystal instbaility occurred only for the samples with exchange levels above 75%. Similar studies have been undertaken on the transition metal exchanged A zeolite. Weirs *et al*[197] found that Cu^{2+} exchange into Ca-A was not reversible, probably due to $Cu(OH)_2(s)$ precipitation upon and within the zeolite. The exchange of Ca-A zeolite with Hg^{2+}, Fe^{3+} and Al^{3+} caused structure degradation while Cr^{3+} exchanged partially and then formed a precipitate.

Zeolite A has a double sieving effect for cations[171]. Small cations can penetrate the single 6-rings into the β-cages. Very large cations like tetramethylammonium cannot even pass through the 8-rings into the α-cages while potassium can penetrate the α-cage[23,p.537, 171] only. Similarly silver but not thallium can enter the β-cage. So in general critical

dimensions for a cation to display ion exchange properties in zeolite A correspond to ~ 4.5Å for the 8-ring and ~ 2.5Å for the 6-ring, though incomplete exchange cannot solely be attributed to an ion-sieve effect. The possibilities could be that incoming ions have the only choice of residing in sites not available to the exchanging ions, or additional exchange results in energetically unfavourable charge distribution.

Heat immersion studies in zeolite A were conducted by Coughlan and Carrol [222] for bivalent exchanged samples. They reported an order of increasing heat of immersion of

$$Cd^{2+} < Zn^{2+} < Cu^{2+} < Ni^{2+} < Co^{2+} < Mg^{2+}$$

whereas heats of hydration of the cations varied in the sequence

$$Cd^{2+} < Mg^{2+} < Zn^{2+} < Co^{2+} < Cu^{2+} < Ni^{2+} .$$

The fact that Cu-A zeolite (31% exchange) had a high heat of immersion was interpreted as evidence of two Cu^{2+} ions per unit cell being exposed to the polar solvent molecules. The still larger heat of immersion value for Ni-A(69% exchanged) was taken as proof of retention crystal stability of the sample on outgassing.

There has been less interest in the exchange of other transition metals in zeolite A. Kellerman *et al* [223] observed the exchange of divalent chromium in zeolite A under oxygen free conditions to prevent oxidation of Cr^{2+} to Cr^{3+}. Yanagida *et al* [203] reported the preparation of two samples of a Mn(II)-exchanged A sample ($Mn_{4.4}A$ and $Mn_{4.5}A$). Akbar [224] prepared $Mn_{3.5}A$ zeolite. An exchange level of up to 64% iron in A has been claimed by Delgas *et al* [225,226]. Cobalt(II) exchanged A zeolite was thoroughly investigated by Klier *et al* [67,227]. They presented a standard method

for preparing Co-A. Heilbron and Vickerman[228] also prepared Co-A. Breck[23,p.540] reported that the cobalt exchange terminated at 89%, while the nickel exchange isotherm extrapolated only to a value of 80%. Akbar[224] also described the preparation of cobalt(II), Ni(II) and Cu(II) exchanged A zeolite samples of different exchange levels, and Gal *et al* [194] found that the selectivity values among the transition metal ions at low loading increase in the following order

$$Ni < Co \lesssim Zn < Cu < Cd \quad .$$

The complete exchange of Cd^{2+} and Zn^{2+} is claimed to be possible, but again a maximum of about 80% was obtained for Ni^{2+} and Co^{2+}[194,195]. Nickel and cobalt ions appear reluctant to penetrate the small cages, and have been shown to exist as fully hydrated octahedral coordinated species in hydrated zeolite A[219]. Upon dehydration these ions pass through an intermediate near-tetrahedral stage and finally return to an octahedral coordination[229].

Rees[196] studied binary and ternary exchange in zeolite A. Binary exchange involved displacing sodium ions in zeolite A by calcium or magnesium ions, for which exchange isotherms at 298K and 338K were constructed. Ternary ion exchange studies on the system Na/Mg/Ca-A were carried out at 298K only. Barri and Rees[230] demonstrated high selectivities of sodium A zeolite for Ca^{2+} ions especially, but low exchange rates for magnesium ions. Polynomial expressions were derived from which the binary isotherms at 298K and 338K could be calculated. A mode of prediction of the ternary isotherms from the binary isothers was also suggested.

Drummond *et al*[214] studied the kinetics of the Na^{+}/Ca^{2+} exchange in

zeolite A at 298K, and hence followed the effect of the presence of Mg^{2+} ions on the exchange. They determined rates for complete replacement of Na^{+} ions by Ca^{2+} ions. The observed degrees of hydrolysis of zeolite A as a function of pH were explained on the basis of a tentative mechanism. Cook *et al*[231] studied the solution degradation of sodium and calcium forms of zeolite A, by measuring the uptake of acid and the solubilization of Si and Al with time over a pH range 3-9. In another recent study, Gaus and Lutze[212] investigated the ion-exchange equilibrium for the system Sr/Ca-A, and found a slight preference for Sr^{2+}, accompanied by an additional uptake of water. In view of these observations, they carried out some kinetic measurements[213] on the Sr/Ca-A and Sr/Ba-A systems. At equilibrium, the latter system did not show any selectivity for either ion. Their equilibrium studies are in accord with Sherry, who also conducted alkalkine earth ion exchange studies in zeolite A much earlier on[232].

The ion exchange of Pb^{2+} and Cd^{2+} for Na^{+} in zeolite A has been studied recently by Hertzenberg *et al*[192]. The system $Pb(NO_3)_2$/Na-A showed extreme selectivity for lead. Selectivity was found to increase with temperature over the range of 323K. They[192] reported that the selectivity of Na-A for Pb^{2+} ion was more from nitrate solution than from acetate solution. However, reversibility was not tested for, or established. It was also reported that Na-A was selective for cadmium but that lead was preferred to a much greater degree. Regarding the effect of co-anions, the preference of Na-A for Cd ions varied[192] in the order

$$NO_3^- > CH_3COO^- \simeq Cl^- \ .$$

1.4.5. Structure of Mordenite

Mordenite is a highly siliceous zeolite (silica to alumina mole ratio > 5:1) occurring in a number of localities as solid or fibrous crystals. It is an interesting member of the zeolite family in that it shows a great thermal stability after dehydration as well as high resistance to acid[32].

The structure of mordenite was determined by Meier[233] as refined subsequently by Gramlich[234].

The orthorhombic unit cell (illustrated in fig.1.7) has the dimensions a=18.13Å, b=20.49Å and c=7.52Å. The unit cell contents of an ideal hydrated sodium mordenite can be expressed by the formula

$$Na_8 Al_8 Si_{40} O_{96} .24H_2O.$$

Describing the structure broadly, one can say that the aluminosilicate consists of characteristic tetrahedral chains which lie parallel to the c-direction. Within these chains, each $(Si,Al)O_4$ tetrahedron is part of one or more 5-membered rings. The prevalence of 5- and 6- membered rings (salient features of the structure) is responsible for the outstanding stability of mordenite as compared to many other zeolites[233].

The main channel is bounded by 12-membered oxygen rings, and forms a one dimensional pore system. The channel diameters are comparable to the dimensions of small molecules such as benzene, pyridine, hexane, etc[235]. The exchangeable cations in mordenite stick out from the channel walls. As would therefore be expected, mordenite ion-exchanged by protons (H-MOR), has a larger pore dimension and can adsorb simple aromatic compounds and paraffins, in contrast to the case of some multi-valent cation-exchanged

mordenites which cannot easily adsorb such compounds[236].

Electron and X-ray diffraction studies by Sherman and Bennett[237] revealed the occurrence of intergrowths and stacking faults in mordenite, but conversion of the "small-pore" to the "large-pore" variety by simple chemical treatment, such as acid leaching, suggests that channel blocking by occluded species is a major difference between the two materials[238]. Certainly cations on channel walls hinder or restrict diffusion; H-mordenite has been shown to have wider channels than Na, Ca or Ba-mordenite[239]. The classification of mordenite samples as "large port" or "small port" is based on whether or not they sorb large molecules[238]. The former can sorb 6.7% of benzene or cyclohexane, while the latter can sorb only a negligible amount of these molecules. Thus a plausible explanation for the difference between "small port" and "large port" mordenite must be that small port mordenite contains extraneous amorphous matter within the structure, affecting its ion-exchange and sorption properties[240]. As would therefore be expected, natural mordenites are usually "small port", while the nature of synthetic varieties depends on the conditions employed in their synthesis[23,p.122].

Yet other mordenite varieties can possibly be prepared by removing aluminium from the structure by strong acid treatment with hydrochloric acid [241]. Mordenite crystallinity survives substantial dealumination[241].

The molecular sieve properties of mordenite can be attributed to a system of large elliptical channels, parallel to [001] (fig.1.7.), having a free diameter of 6.6Å. These channels are interconnected by smaller staggered channels, parallel to [010] (fig.1.7) of 2.8Å free diameter. Some of the cations are thought to be located in these channels[242].

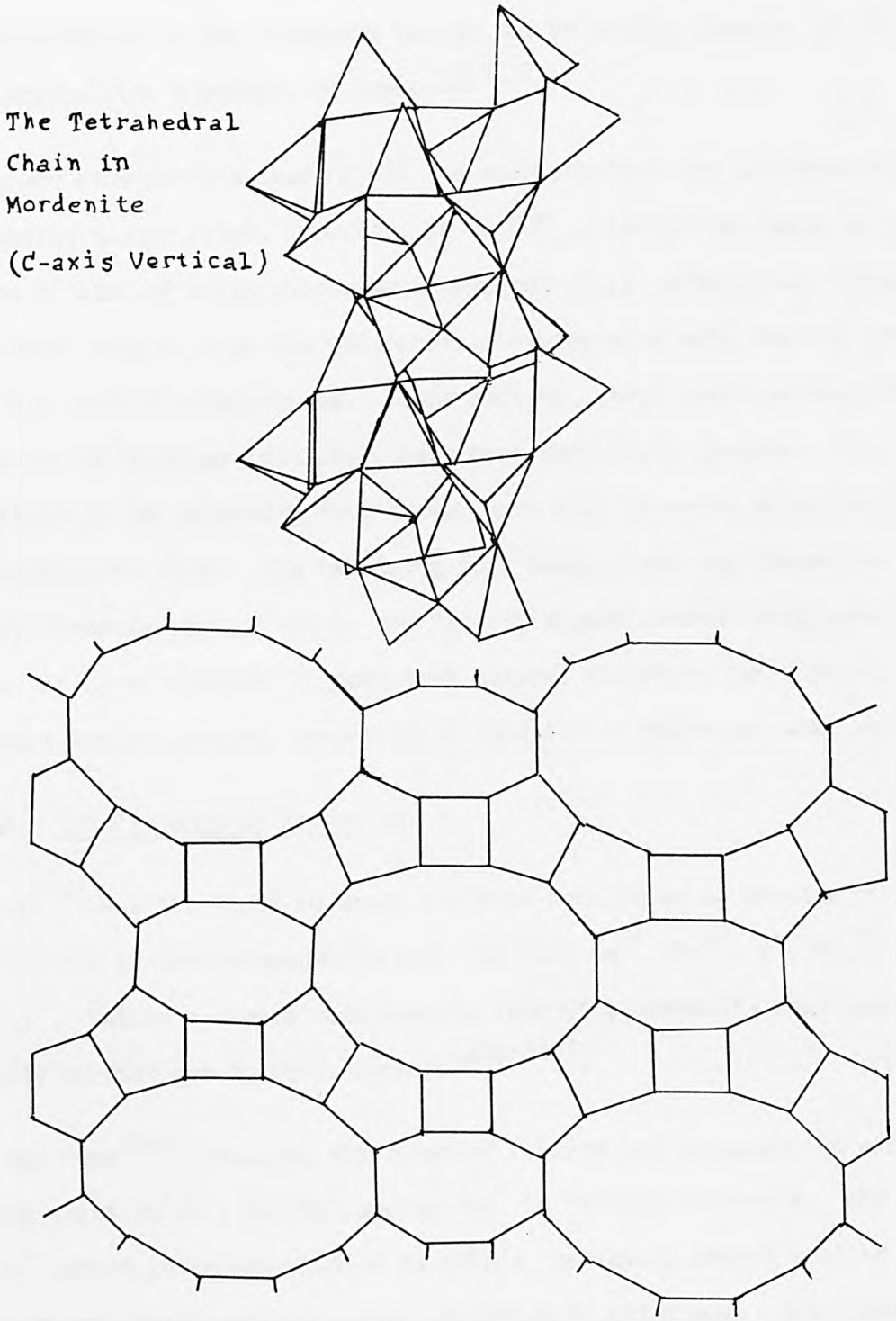

THE MAIN CHANNELS IN MORDENITE, BASED ON THE 5-RING CHAIN

Fig.1.7 THE MORDENITE STRUCTURE

Stacking faults in the framework reduce the effective diameter of the intercrystalline channels to about 4Å[233].

Staggered side-pockets leading off the main channels are connected through 8-membered oxygen rings. However, in Na-MOR, a sodium ion rests at the centre of each of these distorted 8-membered rings, effectively isolating each main channel from its neighbours, leaving each main channel lined with two rows of side-pockets. These sodiums, which comprise four of the eight sodium ions per unit cell, have been definitely located. The positions of the remaining four sodium ions and the water molecules is apparently not fixed. The remaining four sodium ions may therefore occupy randomly some of the 8- and 12-fold oxygen windows which are available. It is of interest to note that natural mordenite has a fairly constant sodium content, amounting to four sodium atoms per unit cell[233].

1.4.6. Ion Exchange in Mordenite.

Barrer[11] was the first to study exchange equilibria on samples of both natural and synthetic mordenite with the ions Ca^{2+}, Ba^{2+}, K^+, NH_4^+, Na^+ and Li^+. Cation exchange measurements involving mordenite were subsequently carried out by other workers[243-249].

Rao and Rees[250] measured the rates of forward and backward ion exchange of the pairs Na^+/K^+, Na^+/Rb^+ and Na^+/Cs^+ in natural mordenite. The Na^+/K^+ system which was studied in detail, employing parent zeolite samples containing various ratios of sodium to potassium. They also determined Na/K, Na/Rb and Na/Cs isotherms and were the first to present detailed isothers in natural mordenite. Wolf *et al*[251] examined the exchange of alkali, alkaline-earth cations, but also transition metal ions (Mn^+, Co^{2+}, Cu^{2+} and Ag^+) in synthetic mordenite. Grivkova *et al*[252]

published exchange isotherms for the ion pairs Na/Cs, K/Cs and Rb/Cs while Wolf *et al*[253] presented similar studies of ion pairs Na/Ca, Na/Mg and Na/Mn, also using synthetic sodium mordenite .

Ion exchange isotherms of NH_4^+, alkali and alkaline-earth metal ions in synthetic mordenite are given by Barrer and Klinowski[254]. The thermodynamic affinity sequence for monovalent cations given by them was Cs > K > Na > Li. The extent of divalent ion exchange obtained were 0.60 for Ca, 0.62 for Sr and 0.84 for Ba. On the whole, the thermodynamic affinity varied as $Cs^+ > K^+ > NH_4^+ > Na^+ > Ba^{2+} > Li^+$. They observed[254] that selectivity for caesium over sodium in synthetic mordenite was greater than that determined for the natural mordenite[250]. In confirmation, a systematic study conducted by Chelishchev and Volodin[255] using natural mordenite gave a similar selectivity sequence. Susuki *et al*[256] have also presented exchange isotherms of alkaline-earth metals, hydrogen and ammonium ions involving synthetic sodium mordenite.

Literature on the transition metal ion exchange in mordenite is more limited. Apart from the work of Wolf *et al*[251] mentioned above, Minachev *et al*[257] reported 70% exchange of zinc in mordenite. However, transition metals in solution can only apparently exchange with ammonium ions in the main channels of mordenite[234,254]. It is suggested[260] that the difference between transition metals and alkali and/or alkaline-earth metals is to be assoicated with the strong hydration of transition metal cations[258,259] and the consequential difficulties in entering the side pockets in mordenite[260].

Barrer and Townsend[260] observed the ion exchange of Mn^{2+}, Co^{2+}, Ni^{2+}, Cu^{2+} and Zn^{2+} in ammonium mordenite and presented a thermodynamic affinity sequence of $Mn^{2+} > Cu^{2+} > Co^{2+} \sim Zn^{2+} > Ni^{2+}$. It was reported

that mordenite can selectively separate Mn^{2+} or Cu^{2+} from a binary solution mixture of one of these ions with Co^{2+}, Ni^{2+} or Zn^{2+}. Their subsequent studies[261] (involving solutions of higher pH) involved ammine complexes of Co^{3+}, Cu^{2+} and Zn^{2+} in mordenite and two other zeolites *viz*, clinoptilolite and phillipsite. Fletcher and Townsend[262, 263] investigated the exchange of hydrated and amminated silver(I) ions in zeolites X, Y and mordenite, all the three zeolites having different silica to alumina ratios. They extended this work by examining the selectivity of the same synthetic sodium zeolites for the tetrammine-platinum(II) and tetramminepalladium(II) ions[264], using the same zeolites. They reported a selectivity sequence for both the $\left[Pt(NH_3)_4\right]^{2+}$ and $\left[Pd(NH_3)_4\right]^{2+}$ ions of

MOR > Y > X.

1.5. Catalytic Activity and Reactor Design

Catalysis is a kinetic process and catalysis research mainly involves investigation of kinetic phenomena (i.e. quantitative studies of reaction rates and the factors effecting it). Kinetic experiments provide a basis for developing a fundamental rate equation that fits the kinetic data, and which is consistent with observations on the reaction mechanism.

Rate studies of catalytic reactions are conducted in a variety of ways employing different kinds of reactors. Kinetic studies for the reactions at the catalyst surface are carried out avoiding as far as possible the complexities of mass and heat transfer, thus using simple theoretical models for the determination of the kinetics of a catalytic reaction. The results of the established kinetics can then be extrapolated to

satisfy the practical situation, enveloping mass and heat transfer effects to a reasonable degree of approximation. Different types of catalytic reactor design, reaction kinetics and related problems are well covered in the available literature[85-87,265-273].

Kinetic information obtained on small laboratory reactors proves to be a useful guide in the design and prediction of the performance of industrial-scale reactors using solid catalysts. Different types of reactors have been described in several texts[267-268,271-273].

Anderson[268,p.6] outlined the following types of small experimental reactors.

A. Flow reactors as integral fixed-bed reactors, differential reactors, stirred flow reactors and microcatalytic reactors of pulse type.

B. Static reactors.

Different types of commercial catalytic reactors described by Satterfield[271,p.313] include,

a. Adiabatic reactors, such as the trickle bed reactor and flooded bed reactor.

b. Multitube reactors with heat exchange.

c. Fluidized-bed reactors.

d. Slurry reactors.

He also described[271,p.355] the following experimental laboratory reactors.

i) A scouting laboratory reactor .

ii) A catalyst-optimization reactor.

iii) The prototype reactor.

iv) Gradientless reactors.

Idealized reactor models detailed by Butt[272,p.205] are,

(a) Plug-flow reactors .

(b) Continuously stirred-tank reactors.

(c) Semi-batch reactors.

(d) Batch reactors.

(e) Laminar flow reactors.

Anderson and Boudart[273,p.48] have recently given descriptions of the following reactor systems:-

(a) The constant-volume batch reactor

(b) The semi-batch reactor

(c) The continuous stirred-tank reactor

(d) The plug-flow, or tubular reactor.

They also describe[273,p.162] fixed bed, slurry bed and fluidized bed reactors.

Out of the different methods available, static methods are often employed by catalyst chemists, while chemical engineers prefer flow methods. The following sections describe different types of flow- and static-reactors, stressing mainly the static (or batch) reactor and tubular (or plug-flow) reactor.

1.5.1. Adiabatic Reactor.

The adiabatic reactor is a packed bed of catalyst, consisting of a pre-heater in which feed is heated to the reaction temperature and, an adiabatic reaction chamber which is designed to produce the extent of conversion needed, in addition to that obtained in the pre-heater. The

diameter is usually sufficiently large to ensure that heat transmitted through the outside walls is small relative to that evolved or absorbed by reaction. The fluid moves through the reactor in near plug flow mode, and the temperature increase (or decrease) for a simple reaction is roughly in proportion to the percent conversion. This type of reactor can be used for either an exothermic or endothermic reaction. Reacting gases are fed to the bed at the ignition temperature, at which the rate becomes economically rapid.

An adiabatic reactor is the cheapest kind to build and usually it is a first choice if it is applicable for large-scale processes. It is generally most practical for large scale, relatively slow reactions which do not involve large heat effects.

When several adiabatic beds are used in series, the individual beds are often varied in depth to obtain an optimum temperature at the exit of each. This optimum is determined either by (i) the temperature at which the reaction rate drops to too low a level, or, (ii) the temperature at which a side reaction becomes significant, or at which the catalyst life may be badly affected.

To make the temperature change through a reactor suffuciently small that an adiabatic reactor can be used,

(i) a portion of the product may be recycled and mixed with fresh feed;

(ii) an excess of one component may be used, or

(iii) an inert gas may be added to the feed.

In a trickle-bed reactor, liquid and gas flow concurrently downward through a packed bed while reaction (essentially adiabatic) takes place. Several

beds in series may be used with interstage cooling or cold-shot cooling with a gas, analogous to that used in the gas-solid adiabatic beds. Alternatively, the two phases (gas-, and liquid phase) may flow concurrently upwards, with the liquid being the continuous phase, a process termed as flooded flow.

1.5.2. Multitube Reactor with Heat Exchange.

Reactions in multitube reactors are very rapid and sometimes highly exothermic. A multitube reactor is preferable to adiabatic reactors if

(i) the adiabatic temperature rise is so great that poor selectivity is encountered, or

(ii) there is a possibility of a runaway reaction or unacceptable catalyst deactivation. Desired temperatures can be achieved by using heat-exchange using (for example) thermally stable organic fluids.

The tubes of the reactor are typically 2.5 to 5 cm^3 in diameter and 4 to 7m long. Small tube diameters help to achieve very close isothermal operation but, on the other hand, for a given capacity the number of tubes increases inversely with the square of internal diameter. Thus the use of tubes much smaller than 2.5 cm^3 would need an unacceptably large number. Isothermicity can be improved by diluting the catalyst with inert material, but additional reactor volume is then required. In practical terms this is not normally justified economically.

1.5.3. Fluidized-bed Reactor.

In the fluidized bed reactor, the solid catalyst is in the form of a powder which is carried by the product stream and in a turbulent fluidized state, forms a relatively dense bed in the reactor. The fine particles of the solid

catalyst are contained in a vertical cylindrical vessel. The fluid stream is passed upwards through the particles at a rate great enough for them to lift, but not so great that they are prevented by carry-over in the gas stream, from falling back into the fluidized phase above its free surface. A bed of particles in this state seems to be 'boiling'; bubbles of the up-flowing fluid (usually a gas) can be seen bursting at the upper surface.

The theoretical treatment of the fluidized bed reactor is difficult because of the lack of a simple model which can account for the reactor performance without the induction of arbitrary variables. However, a particulat advantage of this reactor type is the excellent uniformity of temperature, achieved throughout the bed by the motion of solid particles and by the good heat exchange between solid and gas. The ease of adding or removing solid is an additional advantage. The system is also less expensive to construct than a multitube reactir if the same capacity and heat exchange may be simpler than for an adiabatic multitube reactor. Yet another advantage is that the external surface area presented to the gas is greater than that for a fixed bed and so reactions limited by diffusion in pores will tend to yield higher conversions in a fluidized bed.

1.5.4. The Slurry-Phase Reactor

In a slurry reactor, the reaction of a liquid is often carried out by suspending a solid catalyst in a finally divided form in the liquid. The reacting gas may be introduced through a distributor in the bottom of the vessel, or it may be dispersed into the liquid by a mechanical stirrer, hence keeping the solid suspended. The mode of operation involves the gases first dissolving in the medium, and then diffusing up to the surfaces of the solid particles. Mass transfer is therefore complicated here, and the

process is intrinsically slower than the chemical reaction. The important advantages of this type of reactor include the high heat capacity of the liquid phase, and the ease of achieving very good heat transfer, resulting in constancy of temperature and easy control of temperature to any desired level.

1.5.5. Fixed-Bed Reactor

The fixed-bed reactor consists of a series of narrow tubular reactors thermostatted by a surrounding heat-transfer medium such as a molten salt solution[270,p.384]. The tubes are frequently a few centimetres in diameter and can be up to several metres in length[267,p.4]. The reactor is packed with particles of the solid catalyst. The particles rest on each other and are not removed by the fluid so the bed is considered as a collection of particles.

Fixed bed reactors are used in many important heterogeneous reactions such as ammonia and methanol synthesis.

1.5.6. The Continuous Stirred-tank Reactor.

The continuous stirred-tank reactor (CSTR) is a reactor in which all elements of volume contain fluid indentical in properties and is continuously stirred, or circulated to make it perfectly or completely mixed. The products are continuously removed while the reactants are continuously added in the reactor[273,p.50].

Stirred reactors are often used for liquid-phase reactions employing a fine mesh catalyst. The feed enters one side of the reactor and the exit stream passes out at the other, while the catalyst and the solution are stirred effectively by a mechanical device[268,p.11]. The reactors are normally used in series so that the product of one tank serves as a feed to the

next one *et sequens*.

1.5.7. Integral Fixed-Bed Reactor.

The reactor consists of a cylindrical tube of internal diameter of 1.5 cm^3 or less, with a definite zone of the catalyst, and is surrounded by a constant temperature medium. The feed at measured constant flow passing through a preheater medium is led to the catalyst bed and then passes to a section for recovering or measuring the products. Appropriate compressors, feed pumps, reducing valves and back-pressure regulators are used to maintain constant operating pressure. The kinetics follow the plug flow equation.

Integral reaction rate αiSi (where αi is the fractional feed component and Si is the hourly space velocity of component i), instead of differential reaction rate τ, is obtained from an integral reactor[268,p.8].

Integral fixed-bed reactors are used effectively with catalysts, for which the activity changes continuously with time, as samples are easily obtainable from any part in short time intervals.

1.5.8. Differential Reactor.

A differential reactor is one in which the gas and solid composition, pressure are temperature and essentially uniform throughout the reactor. It also employs a reactor in which the conversion is limited to not more than a few percent. A laboratory fixed-bed reactor can possibly be operated in a differential mode, but it is difficult to do so over a varying range of operating conditions due to possible heat-and-mass-transfer gradients[271,p.359].

The analysis of the data is simplified if operated at small conversions (less than 5%) provided the analytical methods employed for measuring

small changes in conversion of reactants (or small concentration of products), are reasonably accurate. For a differential reaction, the rate of reaction r is defined as,

$$\lim_{\alpha i \to 0} \quad \alpha i \; Si = \frac{d\alpha_i}{d(\frac{1}{Si})} = \tau \qquad \ldots\ldots(1)$$

where αi = fractional feed of component i

Si = hourly space velocity of component i.

Under ideal conditions, the composition of the fluid contacting the catalyst is almost the same as the feed. In principle compositions, corresponding to any conversion can be prepared and then used as feed to the catalyst (268,p.10). For relatively simple reaction mixtures, gas-chromatographic methods involving flame ionization detectors are quite adequate. The requirements implicit, in equation (1) are met well by using a recycle system. In a system studying the catalytic decomposition of a distillable liquid to gaseous products (e.g. decomposition of formic acid to hydrogen and carbon dioxide), recycle is conducted by boiling the liquid at a constant rate. The vapour flows upwards through a bed of catalyst, condensed and returned to the distillation flask. The reactor can be maintained at any desired temperature above the boiling point. The differential reaction rate is then obtained from the flow of the product gas.

The composition of the recycle gas and the differential reaction rate can be changed by varying the feed rate or composition. Removal of reaction products from the recycle stream by cold traps or chemical adsorbent, can be used as an advantage.

1.5.9. Microcatalytic Reactor of Pulse Type.

Pulse type microcatalytic reactors consist of a small reactor attached to a gas-chromatographic column. A carrier gas (either an inert gas or one of the reactants) passes through the system at a constant rate. A small pulse of reactant, (which may consist of a few cm^3 of gas or a few thousandths of a cm^3 of liquid) is injected into the carrier gas before the reactor. The inlet system is carefully designed so that the pulses are reproducible with respect to both amount and concentration profile. The reactor (usually of glass or quartz) contains $5cm^3$ of catalyst and $5cm^3$ of inert solids to serve as a preheater. The catalyst bed broadens the concentration profile of the pulse entering the column. The column should be selected to give a sharp separation of the components of interest.

Microcatalytic experiments are conducted in the same way as in integral flow reactors with temperature, pressure and size of pulse being held constant, and the flow of carrier gas changed to give a plot of conversion versus time.

The pulse-type reactor has the following advantages for studying catalytic reactions[268,p.16].

(i) Microquantity of reactant in the pulse does not effect significantly the temperature of the catalytic bed, even for highly exothermic or endothermic reactions.

(ii) The process of conditioning the catalyst can be followed by means of successive pulses at the same temperature. The amount of reactant remaining on the catalyst in either a chemisorbed or degraded form can be determined from the material balances.

(iii) The adsorbed complex on the conditioned catalyst can be

studied if desired, by treating with pulses of reacting gas like hydrogen or oxygen. More information can be obtained by increasing the temperature of the conditioned catalyst in a stream of inert or reactive carrier gas. The products can be either pursued continuously during the heating period of they can be collected in a cold trap and released to the chromatographic column at the end of the experiment.

1.5.10 Static (or batch) Reactors.

Static reactors are also termed batch reactors because this type of reactor is normally used for small scale or batch-wise expensive products. These reactors, though common, or the norm in chemistry laboratories (for small scale experimental research) but are uncommon on the large scale in industry. This type of reactor also tends to be used for complicated processes or for processes employing long reaction time. Batch reactors (§2.2.3.2.3.) were used in this work for monolayer surface area measurements and for the kinetics of nitrous oxide decomposition on transition metal(II) exchanged zeolites.

In static reaction systems, the reactants are introduced at the start of the experiment and the system is closed. The rate of the reaction is followed by observing changes within the reactor of concentration, pressure, or volume. Reactants are generally introduced at room temperature, and the reactor is heated rapidly to the desired temperature. The heating period generally, contributes no useful kinetic information. The contents of the vessel are removed from the reactor after a fixed time. The mixing of the reactants (if needed) is done within the reactor; however in some reactions no mixing is required.

The composition data are often extrapolated to zero conversion to establish a fictitious zero time. Rate equations may be treated in either a differential or integral mode, as for other reactors. The integration, however, may be made from the fictitious zero time or from the time that the reactor attained a desired temperature[268,p.17].

In the case of liquid and liquid-gas reactions on powdered catalysts, the closed vessel used as a reactor contains a device for stirring efficiently both the catalyst and liquid phase in the constant temperature bath. The volume of reactant is made sufficiently large to ensure that small liquid samples can be removed for analysis at frequent intervals without their removal significantly decreasing the amount of liquid. For gas-liquid reactions, the decrease in pressure can be used as a measure of the extent of reaction, provided that other volatile products are not produced. In gas-liquid reaction reactions, mass transport of the gas to the catalyst is a rate-limiting step, even when the liquid is effectively stirred. Effective stirring helps maintain constant composition throughout the liquid phase.

Reactions of gases, especially involving volume changes, are often studied in static reactors. Investigations of catalytic reactions can be conducted in a large glass bulb containing a small amount of catalyst placed in a constant temperature bath. The rate can be measured by following the change in pressure, the change in volume at constant pressure, or the change in composition. Diffusion control can be avoided by keeping the pressure very low or the reaction quite slow. Most of the complications can be limited by using static glass systems consisting of a small fixed-bed reactor and the gas circulation.

Different static systems have been described by Carberry[274], Weller[275]

Chambers and Boudart[276] and Kemball[277].

Consider a differential volume element (dV) of a reaction mixture, for a given (reactant or product) species A, over a small time increment (dT) as shown in figure 1.8[272,p.5].

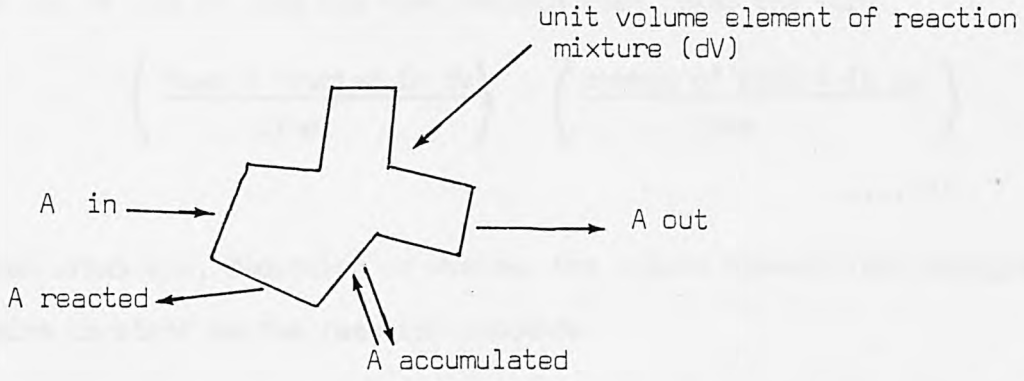

Figure 1.8. (Mass balance with chemical reaction on a volume element of reaction mixture)

The mass balance equation under a steady state (an operation that does not vary with time) can be stated as,

$$\left(\frac{\text{mass A entering dV}}{\text{time}}\right)=\left(\frac{\text{mass A leaving dV}}{\text{time}}+\frac{\text{mass A reacted in dV}}{\text{time}}\right) \quad .....(2)$$

The L.H.S. of equation 2 is the input term and the R.H.S. is the output term. An equivalent molal expression (mol dm^{-3} or mol kg^{-1}) can also be used.

The mass balance equation under non-steady state is,

$$\left(\frac{\text{mass A entering dV}}{\text{time}}\right) - \left(\frac{\text{mass A leaving dV}}{\text{time}} + \frac{\text{mass A reacted in dV}}{\text{time}}\right)$$

$$= \left(\frac{\text{change of mass A in dV}}{\text{time}}\right) \qquad \text{.....(3)}$$

Here input/output terms remain the same, but an accumulated time dependent mass balance term appears on R.H.S.

For a homogeneous batch reaction, there is no flow of reactant or product into or out of the dV, and the mass balance them takes the form

$$\left(\frac{\text{Mass A reacted in dV}}{\text{time}}\right) = \left(\frac{\text{change of mass A in dV}}{\text{time}}\right)$$

.....(4)

Two cases arise now, depending on whether the volume element (dV) changes or remains constant as the reaction proceeds.

(i) For the volume change during course of reaction the left-hand side term can be expressed as $T_A dV$, where r_A is reaction rate w.r.t.A (rate is +ve for change in product & -Ve for change in reactant), and can be integrated to $r_A.V$. The right side term can be written as

$\frac{d(c_A v)}{dt}$ where c_A = concentration of specied A.

So mass balance equation can be written as

$$r_A \cdot V = \frac{d(c_A.V)}{dt} \qquad \text{.....(5)}$$

(ii) For a constant-volume batch reaction, the volume element (dV) does not change during reaction (which for liquid-phase reactions can be invariably taken to be the case), so we finally obtain the following:

$$r_A' = \frac{dc_A}{dt} \qquad \text{.....(6)}$$

Equations 5 and 6 are the appropriate batch reactor equations.

For an enthalpy balance, we can proceed, similarly, now considering a

Heat entering volume element (dV) = (Heat leaving dV +
Heat absorbed by reaction + change of heat within dV) .....(7)

Three different conditions can then be written for batch reactors, *viz.*

(i) The equation is irrelevant for an isothermal batch reactor.

(ii) For a homogeneous adiabatic reactor

$$r_A . \Delta H . V = - \frac{d(\rho . C_s . V . T)}{dt} \qquad .....(8)$$

where ρ = the density, T = Temperature

C_s = Specific heat of reactor contents

ΔH = Heat of reaction (+ve for endothermic and -ve for exothermic reaction)

(iii) For a constant volume batch reactor the equation becomes

$$r_A . \Delta H = \frac{\rho . C_v . dT}{dt} \qquad .....(9)$$

r_A = rate of reaction per unit volume

C_v = specific heat at constant volume.

Equations 8 and 9 are the enthalpy balances for a batch reactor system.

1.5.11. Tubular (or Plug-Flow) Reactor.

A tubular reactor is a continuously operating reactor in which one or all of the reagents show a steady movement in a selected spatial direction, the fluid moving through it like a plug[267,p.4]. In a tubular-flow reactor the feed normally enters one end of a cylindrical tube packed with particles of solid catalyst, and the product stream leaves at the other end. The system operates under steady state conditions, thus

enabling the properties at any point in the reactor to remain constant with respect to time. The packed tubular reactor, also called a plug-flow reactor (PFR), obeys the basic plug flow equation. The ideal plug flow model rules out any axial or radial diffusion effects and assumes that the bed is isothermal. It also assumes the absence of boundary layer diffusion control (film diffusion) between the gas stream and catalyst particles.

The properties of the flowing stream vary from point to point in the absence of complete mixing due to the tube being long and lacking a stirring facility. Variations in the properties can in reality also be present in the axial or radial directions. The plug flow model assumes that there is complete mixing in the radial direction (uniform velocity across the radius) and no mixing in the axial direction, hence allowing variations in composition along the direction of flow but not longitudinal diffusion.

Tubular or plug flow reactors are used most often to determine the catalytic activity of heterogeneous gas/solid catalytic reactions, though treatment of heterogeneous or homogeneous systems do not differ much. Normally conversion of reactants is measured as a function of residence time or space velocity in reactor (space velocity is a convenient unit for expressing the relationship between feed rate and reactor volume in a flow process. It is defined as the volume of feed per unit volume of the reactor, having the dimensions of reciprocal time). Each run is taken at the same temperature and pressure, repeating experiments over the enitre range of reaction conditions. If the conversions are high, the PFR is called an integral reactor since the measured conversions are the itegral result of reaction kinetics over a range of reaction mixture composition. On the other hand if the conversion is very low,

the PFR is termed a differential reactor (see earlier - section 1.5.8). An integral flow reactor was used (§2.3.4.1) in this work for methane oxidation on transition metal (II) exchanged zeolites.

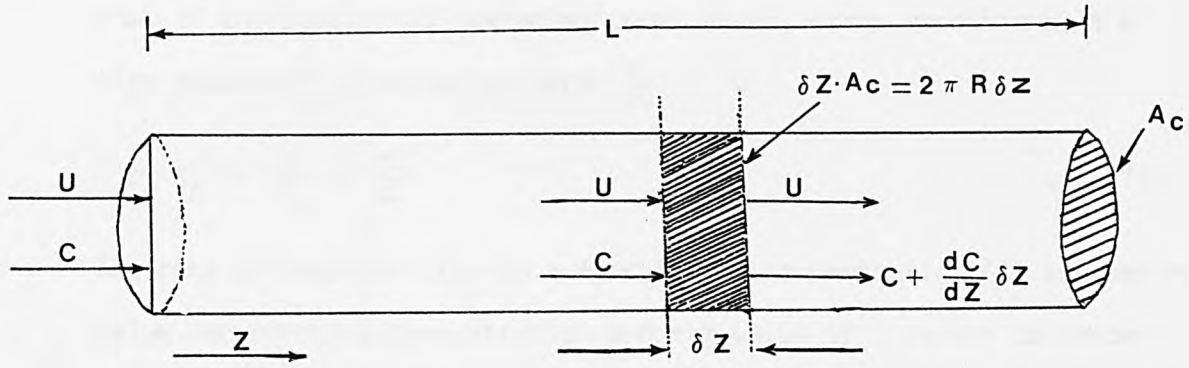

Figure 1.9 (Plug Flow Model)

To derive a plug-flow model (PFR) equation, consider an infinitesimally small volume element length (δZ) of tubular reactor (a cylindrical conduit) of cross section A_c, as shown in figure 1.9 . Assume that the gas is flowing through the uniform particle bed with a constant volumetric velocity U (corresponding to a linear velocity $\bar{U} = \frac{U}{A_c}$).

The mass balance equation under non-steady condition can be as,

(Accumulated mass in elemental volume) =(net mass flowing through elemental volume due to concentration gradient) - (net mass reacting in elemental volume) .....(10)

In mathematical terms this becomes

$$\frac{dC}{dt} \cdot A_c \cdot \delta Z = U\left[(C + \frac{dC}{dZ}\ \delta Z) - C\right] - r_v \cdot A_c\ \delta Z \qquad .....(11)$$

where r_v = rate of reaction per unit volume of reactant, and

C = concentration of reactant or product

Simplifying,

$$\frac{dC}{dt} \cdot A_c = U\frac{dC}{dZ} - r_v A_c \qquad .....(12)$$

Now, if the reactor is operating under steady state conditions, the time dependent accumulation term $\frac{dC}{dt} = 0$

$$r_v A_c = \frac{U}{A_c} \cdot \frac{dC}{dZ} \qquad .....(13)$$

The rate of reaction (r_v) is a function of concentration (C) and has +ve value for reactant concentration and -ve value if C refers to concentration of product, so we can transform equation 13 as

$$\frac{dC}{r_v} = -\frac{dZ}{U} \cdot A_c \qquad .....(14)$$

Here we define a fractional conversion (which is a dimensionless quantity) as $\alpha = \frac{C_2 - C_o}{C_i}$

where C_i = concentration of (reactant or product) species flowing into the reactor, and

C_o = concentration of species (reactant or product) flowing out of reactor.

and

$$d\alpha = \frac{C - (C - dC)}{C} = \frac{dC}{C}$$

or

$$dC = C.\ d\alpha \qquad .....(15)$$

Replacing dC equation 13 becomes

$$T_v = \frac{U}{A_c} \cdot \frac{C.d\alpha}{dZ} \qquad .....(16)$$

Total mass flowing is molal flow rate of reactant = $F(\text{mol } s^{-1}) = C.U$

.....(17)

$$r_v = \frac{F.\ d\alpha}{A_c.dZ} \qquad .....(18)$$

In terms of mass (m) of the catalyst, volume change ($A_c.dZ$) can be replaced by mass change (dm) which (assuming uniform packing in the catalyst bed) can be related as

$$dm = \rho.\ A_c.\ dZ \qquad .....(19)$$

where ρ = density of catalyst particle.

Combining equation 18 and equation 19

$$r_v = Fd\alpha.\ \frac{\rho}{dm} \qquad .....(20)$$

Now $\frac{r_v}{r_m} = \rho$ where r_m = rate of reaction per unit mass of catalyst

therefore $r_v = r_m\ .\ \rho \qquad .....(21)$

Comparing equation 19 and equation 20 we get

$$r_m = F.\ \frac{d\alpha}{dm} \qquad .....(22)$$

For a feed containing more than one reactant (multicomponent), the rate of reaction can be expressed in terms of rate constant and partial pressure, which is

$$r_m = Km\ .\ P_i^x \qquad .....(23)$$

where Km = observed rate constant

P_i = particle pressure of the ith component, and

x = observed order of reaction.

Again P_i = P. mole fraction = $P.\ \frac{n_i}{n_t}$ .....(24)

here n_i = no. of moles of reactant (i) at inlet

n_t = total no. of moles

P = total pressure

At point (Z + δZ) in the reactor, the no. of moles of reactant i after reaction for conversion $\alpha = n_i - n_i\,\alpha = n_i(1 - \alpha)$ .....(25)

Considering the change in no. of moles due to product formation, the total no. of moles at conversion $\alpha = n_t + \delta . n_i . \alpha$ .....(26)

where δ = increase in no. of moles in the system per mole of reactant i converted into products.

Adding up equation 24, 25 and 26, and simplifying

$$P_i = P . \frac{n_i(1 - \alpha)}{n_t + \alpha . \delta n_i} \qquad .....(27)$$

From equation 22,23 and 27, we get the relationship

$$Km \,.\, P^x \,.\, \left[\frac{n_i(1 - \alpha)}{n_t + \delta n_i\, \alpha}\right]^x = \frac{F . d\alpha}{dm} \qquad .....(28)$$

which simply gives

$$Km \,.\, dm = \frac{F}{P^x} \cdot \left[\frac{n_t + \delta n_i \alpha}{n_i\,(1 - \alpha)}\right]^x \,.\, d\alpha \qquad .....(29)$$

Integrating left side of equation 29 w.r.t. m and right side w.r.t.α ,

$$\int_0^m Km \,.\, dm = \frac{F}{P^x} \cdot \int_0^\alpha \left(\frac{n_t + \delta\, n_i \alpha}{n_i\,(1 - \alpha)}\right)^x . d\alpha \qquad .....(30)$$

Consider now a specific system and apply boundary conditions

$\alpha = 0$ at $n = 0$

and $0 < \alpha < 1$ at $m = m$

The simple chemical reaction

$CH_4 + 2O_2 \longrightarrow CO_2 + 2H_2O$ suggests that there is no change in the

no. of moles ($\delta = 0$) therefore $\delta \cdot n_i \cdot = 0$.

Equation 30 under these conditions becomes

$$Km \cdot m = \frac{F}{P^x} \int_0^{\alpha} \left(\frac{n_t}{n_i (1 - \alpha)} \right)^x \cdot d\alpha \qquad .....(31)$$

$$\text{or} \quad Km = \frac{F}{m} \cdot \frac{1}{P^x} \cdot \left(\frac{n_t}{n_i} \right)^x \int_0^{\alpha} \frac{1}{(1 - \alpha)^x} \cdot d\alpha \qquad .....(32)$$

$$\text{From equation 24} \quad P_i = P \cdot \frac{n_i}{n_t} \quad \text{or} \quad \frac{1}{P_i} = \frac{n_t}{P \cdot n_i} \qquad .....(33)$$

Equation 32 and equation 33 when combined, give

$$Km = \frac{F}{m} \cdot \frac{1}{P_i^x} \cdot \int_0^{\alpha} \frac{1}{(1 - \alpha)^x} \cdot d\alpha \qquad .....(34)$$

Equation 34 is the basic, simple plug flow equation in which m, P_i, F and α are the measureable quantities, while two unknowns are (the observed rate constant) and x (the observed order).

The calculation of Km and x become simple by introducing Arrhenius equation

$$Km = B \cdot \exp^{(-E_a/RT)} \qquad .....(35)$$

where B = pre-exponential function

E_a = energy of activation

R = gas constant and

T = absolute temperature

Comparing equation 34 and equation 35 we get

$$\frac{F}{m} \cdot \frac{1}{P_i^x} \cdot \int_0^{\alpha} \frac{1}{(1 - \alpha)^x} \cdot d\alpha = B \cdot \exp^{(-E_a/RT)} \qquad .....(36)$$

Let rate function $\psi_x = \frac{1}{P_i^x} \cdot \int_0^\alpha \frac{1}{(1-\alpha)^n} \cdot d\alpha$ .....(37)

Equation 36 can be written as

$$\frac{F}{m} \cdot \psi_x = B \exp(-E_a/RT) \quad .....(38)$$

or $$\psi_x = \frac{B.m}{F} \cdot \exp(-E_a/RT)$$

and $$\ln \psi_x = \ln(Bm/F) - (E_a/RT) \quad .....(39)$$

Here we have three unknowns, namely B, Ea, and X.

The degree of conversion α is normally measured over a range of temperatures and equation 39 is solved iteratively by a suitable computer program for order of reaction (x), by plotting $\ln\psi_x$ as a function of absolute temperature against $(\frac{1}{T})$ for the most linear plot. The criterion for best value of X which enables the computer to iterate, is the value which can give the best fit straight line for Arrhenius plot. This linearity is assessed by carrying out regression analysis to calculate best fit data for the correlation coefficient (R) which is defined as

$$R = (m\sigma_x/\sigma_y) \quad .....(40)$$

where m = gradient

δ_x = standard deviation in abcissa

and δ_y = standard deviation in ordinate.

As a general rule R has a value of

$0 \rightarrow 1$ for +ve gradient

$0 \geq R \geq -1$ for -ve gradient.

The perfect correlation being R = 1 (+ve gradient). If R = -1 or R = 0 there is no correlation.

From the linear regression analysis of apparent reaction order (x), the intercept gives value of pre-exponential function (B), while the energy of activation (Ea) is usually calculated from the gradient.

CHAPTER 2

EXPERIMENTAL METHODS

2.1. INTRODUCTION

This chapter describes the methods used for the studies carried out at the University of Bradford and the City University, London.

The research work started at Bradford University is described as the 'Static System Studies'; while the work carried out at the City University is referred to as the 'Flow System Studies'

Kinetics of nitrous oxide decomposition reaction by cobalt or copper exchanged synthetic calcium or 5 A zeolites, together with their monolayer surface area measurements by krypton adsorption at 77K, were studied in a Pyrex glass-built Static System under vacuum ($\sim 10^{-6}$ torr) at Bradford. A comparative study of the catalytic activities of the samples for methane oxidation at atmospheric pressure on a copper-Pyrex glass plug-flow system was undertaken at the City University. These oxidation studies were then extended to include more active copper or nickel exchanged synthetic mordenites.

2.2. STATIC SYSTEM STUDIES

2.2.1. Chemicals Used.

The starting material was Union Carbide synthetic Ca-A zeolite (5A) in powder form (Lot No. 99626 B25981), as supplied by Hopkins and Williams Limited. Cobalt chloride ($CoCl_2.6H_2O$), copper nitrate ($Cu(NO_3)_2.3H_2O$), hydrochloric acid and ammonia solution used for ion exchanges were AnalaR grade from B.D.H. Saturated solutions of calcium nitrate or sodium chloride (laboratory analytic reagents from B.D.H.), were used in the

desiccators for equilibrating and storing ion-exchanged zeolites. Analar grade HNO_3, H_2SO_4, HF(40%), EDTA, murexide and erichrome Black T indicators (also supplied by B.D.H.) were used in chemical analyses of the ion-exchanged samples.

2.2.2. Preparation of Transition Metal(II) Exchanged-CaA Zeolites.

The method employed was similar to that used by numerous authors[120,153, 221b,278]. The parent zeolite (synthetic-CaA was placed in a desiccator over saturated ($Ca(NO_3)_2.4H_2O$) for several days to ensure complete hydration.

Difficulties can be encountered when weighing dehydrated zeolites due to their rapid sorption of moisture from the atmosphere. So not only the parent zeolite, but also all their exchanged forms, were stored over saturated salt solutions allowingthe zeolites to be fully hydrated, but avoiding the problem of condensation, as their vapour pressure was lower than the saturated vapour pressure of water (at any given temperature).

It was observed that to standardize the state of hydration, the zeolite samples should be equilibrated over saturated salt solution for at least two weeks.

The concentration of the appropriate transition metal solution, contact time and solution temperature all can govern the ion exchange extent. For a given weight of the hydrated CaA-zeolite, the number of transition metal(II) ions required depend on the number of Ca^{2+} ions to be exchanged. Simple valency rules demand one Ca^{2+} ion exchanged per unit cell for each transition metal(II) ion introduced. So in each case, 5 grams of hydrated CaA-zeolite was accurately weighed. A calculated amount of transition metal(II) salt to give the desired number of M^{2+} ions per unit cell was

dissolved in 200 cm^3 of deionised water. A slurry of the weighed hydrated parent zeolite was made up in ~50 cm^3 water. The pH of the slurry was recorded by a direct reading E.I.L. pH meter, which had been calibrated previously using ammonium chloride/ammonia buffer. The pH of the slurry (~ 10.5) was adjusted to ~pH7 by adding slowly to the constantly stirred slurry, very dilute (0.001M) hydrochloric acid. For this purpose the slurry was placed on a hot plate and was stirred at 353K with a magnetic stirrer. The 200 cm^3 of transition metal(II) salt solution was added very slowly, in small quantities, to the slurry. Stirring was continued over several hours until it was assumed that the required maximum exchange had occurred. The solution was next filtered. The ion-exchange zeolite was next washed three times with hot water (~ 353K). The wet ion-exchanged zeolite was dried partially hydrated and the sample was then placed in a desiccator over saturated ($Ca(NO_3)_2.4H_2O$) solution for a week, and rehydration was indicated by a clear change in the colour of the sample. Cobalt(II) exchanged-CaA zeolite samples were pink and copper(II) exchanged-CaA forms developed a turquoise-blue colour, the intensity differing according to the level of transition metal ion (TMI) content.

2.2.2.1. Preparation of Co(II) exchanged CaA zeolites.

Six cobalt(II) exchanged-CaA zeolite samples with different transition metal ion (TMI) contents were prepared. They were named as Co-5A(X) where X varied from 1 to 6 with increasing metal ion contents. The methods given below are also summarised in Table 2.1.

(a) Co-5A (1) was prepared (§2.2.2)by exchanging 5g hydrated parent sample with a (0.1347g/200 cm^3) solution of $CoCl_2.6H_2O$ for five hours at 353K. The colour of the rehydrated zeolite was whitish-pink.

Table 2.1. Preparation of Cobalt-Exchanged 5A Zeolites

Zeolite	Weight ($g.200cm^{-3}$)		Exchange Time (Hours)	Final Colour
	5A	$CoCl_2.6H_2O$		
Co-5A(1)	5	0.1347	5	Whitish Pink
Co-5A(2)	5	0.2694	5	Very Light Pink
Co-5A(3)	5	0.4041	6	Light Pink
Co-5A(4)	5	0.5389	12	Clear Pink
Co-5A(5)	5	1.1617	48	Bright Pink
Co-5A(6)	5	2.6940	60	Very Bright Pink

Table 2.2. Preparation of Copper-Exchanged 5A Zeolites

Zeolite	Weight ($g.200cm^{-3}$)		Exchange Time (Hours)	Final Colour
	5A	$Cu(NO_3)_2.3H_2O$		
Cu-5A(1)	5	0.1368	8	Pale Blue
Cu-5A(2)	5	0.2736	18	Light Turquoise Blue
Cu-5A(3)	5	0.4104	20	Turquoise Blue
Cu-5A(4)	5	0.5471	20	Bright Turquoise Blue
Cu-5A(6)	5	1.0942	28	Bright Turquoise Blue

(b) Co-5A (2) was prepared (§ 2.2.2) by exchanging 5g hydrated parent zeolite with a (0.2694g/200cm^3) or (0.269g/200cm^3) solution of $CoCl_2,6H_2O$ for five hours at 353K. The colour of the final rehydration sample was very light pink.

(c) Co-5A (3) was prepared (§ 2.2.2) by exchanging 5g hydrated sample with a (0.4041g/200 cm^3) solution of $CoCl_2.6H_2O$ for six hours at 353K. The final rehydration zeolite was light pink in colour.

(d) Co-5A (4) was prepared (§ 2.2.2) by exchanging 5g parent sample with a solution of $CoCl_2.6H_2O$ (0.5389g/200 cm^3) for twelve hours at 353K. The final rehydration ion-exchanged zeolite was a clear pink.

(e) Co-5A (5) was prepared (§ 2.2.2) by exchanging 5g parent zeolite with a solution of $CoCl_2.6H_2O$ (1.16167g/200 cm^3) for two days at 353K. The final rehydration sample was bright pink.

(f) Co-5A (6) was prepared (§ 2.2.2) by exchanging 5g parent sample with a solution of $CoCl_2.6H_2O$ (2.6940g/200 cm^3) for 2½ days at 353K. The final rehydration ion-exchanged sample had a very bright pink colour.

2.2.2.2. Preparation of Cu(II) exchanged-CaA zeolites.

Six ion-exchanged samples were named as Cu-5A(Y), where Y varies from 1 to 6 with increasing metal ion content. The methods summarised in Table 2.2 are given below:

(a) Cu-5A (1) was prepared (§2.2.2) by exchanging 5g of hydrated starting material with a solution of $Cu(NO_3)_2.3H_2O$ (0.1368g/200 cm^3) for eight hours at 353K. The final treated sample was pale blue coloured.

(b) Cu-5A (2) was prepared (§ 2.2.2) by exchanging 5g of hydrated CaA zeolite with a solution of $Cu(NO_3)_2.3H_2O$ (0.2736g/200 cm^3) for 18 hours at 353K. The colour of the rehydrated zeolite was light turquoise blue.

(c) Cu-5A (3) was prepared (§2.2.2) by exchanging 5g of hydrated CaA zeolite with a solution of $Cu(NO_3)_2.3H_2O$ (0.4104g/200 cm^3) for 20 hours at 353K. The final rehydrated sample was turquoise blue in colour.

(d) Cu-5A(4) zeolite was prepared (§ 2.2.2) by exchanging 5g hydrated starting material with a solution of $Cu(NO_3)_1.3H_2O$ (0.5471g/200 cm^3) for 20 hours at 353K. The rehydrated end product was again turquoise blue in colour.

(e) Cu-5A(5) zeolite was prepared (§ 2.2.2) by exchanging 5g hydrated Ca-A zeolite with a solution of $Cu(NO_3)_2.3H_2O$ (0.8207g/200 cm^3) for 30 hours at 353K. The colour of the rehydrated ion-exchanged zeolite was bright turquoise blue.

(f) Cu-5A(6) was prepared (§ 2.2.2) by exchanging 5g hydrated parent sample with a solution of $Cu(NO_3)_2.3H_2O$ (1.0942g/200 cm^3) for 28 hours at 353K. The colour of the final rehydrated Cu(II) exchanged-CaA zeolite was again bright turqouise blue.

2.2.3. Characterization of Zeolites

Zeolite samples Co-5A(X) and Cu-5A(Y) (§ 2.2.2) were chemically analysed by conventional standard methods. The characterization of the catalysts was completed by the volumetric surface area measurements at different temperatures and by X-ray powder studies. The last two techniques were also used as a mode of checking the crystal structure stabilities of the samples.

2.2.3.1. Chemical analyses.

The determination of the catalyst composition required the exact number of transition metal(II) ions per unit cell in the exchanged sample. The quantity of transition metal(II) in the original exchanging salt solutions was found by carrying out volumetric analyses (§ 2.2.3. 1.1-2) but the filtrates of the above could not be analysed due to interference from Co^{2+}, Cu^{2+} and Ca^{2+} ions, in the presence of each other. So determinations of exact composition of the samples was completed by carrying out the direct chemical analyses (§ 2.2.3. 1.3.-9) as follows.

2.2.3.1.1. Analysis of Cobalt(II) ions in original solution.

Out of a 250 cm^3 solution of known concentration, 200 cm^3 were used for ion-exchange (§ 2.2.2.1), and the 50 cm^3 retained in each case was then utilized for determining the amount of cobalt(II) ions in the original solution as given below[279,280].

The 50 cm^3 of the above original solution were diluted to 500 cm^3 in a volumetric flask, from which a 50 cm^3 aliquot was taken for analysis. The pH of the solution was raised to 6 with dil. NH_3 solution. On adding a few drops of freshly prepared murexide indicator, the solution gained an orange-yellow colour which changed to yellow on addition of one

drop of very dilute NH_3 solution. It was next titrated against 0.01M EDTA solution. During titration, whenever the orange-yellow colour recurred (due to an increase in H^+ concentration) another drop of very dilute NH_3 solution was added to regain the yellow colour. The titration was continued until a sharp colour change from yellow to violet took place, indicating the end point.

2.2.3.1.2. Analyses of Copper(II) ions in original solution.

Analyses of copper(II) ions in 50 cm^3 of original exchanging solutions (§ 2.2.2.2) were carried out in the same way as for the cobalt(II) solutions (§2.2.3.1.1), except that the colour changes in murexide indicator in this case were yellow (acidic solution) to orange (weak alkaline solution). During titration, the colour change is from a greenish yellow to a sharp violet end-point[279,280].

2.2.3.1.3. Water

An aliquot of 0.2 → 0.3g of the zeolite was placed in a pre-heated and pre-weighed platinum crucible and ignited at ~ 1273K using two Meker Burners for 1-2 hours. The crucible was weighed after cooling in the desiccator. The procedure was repeated until a constant weight for the crucible was obtained. The difference in the weights of the crucible gave the weight of the water loss and hence the percentages of water in the samples were calculated. The procedure was repeated six times.

2.2.3.1.4. Silica

(a) By fusion mixture method.

In this procedure[260], which was repeated thrice, either the samples from the water determination were used or an aliquot of 0.2 → 0.3 g of the

zeolite was taken into a dried, pre-weighed platinum crucible. To it, 1.5 → 2.5 g of Na_2CO_3/K_2CO_3 fusion mixture was added and mixed with the zeolite using a glass rod. The crucible was heated slowly at first and then to ~ 1273K using Meker Burners for 1-2 hours.

After cooling the crucible to below red heat, it was immersed so that its outside walls *only* were in distilled water in a beaker. The cold crucible was placed sideways together with its lid in a platinum evaporating dish which was half-filled with distilled water. Then 30 cm^3 of conc. HCl were slowly added to the dish, covering it by a clock glass. When effervescence ceased, this dish was placed on a water bath. After one hour, the clock glass was washed and removed, the washings being added to the dish. One cm^3 of conc. sulphuric acid was added to the contents in the dish. The platinum crucible and the lid were removed after washing all residues in them back into the dish. The suspension in the dish was then evaporated to complete dryness.

30 cm^3 of 1:1 HCl were added to this residue followed by 3-4 drops of conc. sulphuric acid. The residue was broken up with a glass rod and evaporated to dryness again. Then 30 cm^3 of 5% HCl were added to the dried contents in the dish and digested on the steam bath for another fifteen minutes. The hot suspension was filtered using a Whatmann No.42 ashless filter paper, washing the precipitate thoroughly with very dilute hot HCL and finally with water. The filtrate was made up to 250 cm^3 for probable use for analysis of Al^{3+}, Ca^{2+} and M^{2+} ions later.

The wet filter paper was folded into a dry, preweighed platinum crucible. The paper was charred off using a *very small* flame. The temperature was slowly raised and finally ignition at ~ 1273K was carried out until a constant weight of the crucible.

The difference in the weights of the crucible gave silicon in the zeolites as silica. The percentage of SiO_2 was then calculated. Finally any Al_2O_3 present was checked by treatment of the SiO_2 precipitates with 40% HF and a correction, if required, was applied accordingly.

(b) Silica by the HF method

This method[5] was used frequently due to improved results, and for a given sample, was normally repeated thrice. The samples from the water analyses were used to determine the silica content each time. 1-2 drops of distilled water and 3-4 drops of conc. sulphuric acid were added to the contents of the crucible and then about three quarters of the crucible capacity was filled with 40% HF solution. The crucible contents were heated to dryness on a hot plate in a fume-cupboard. This was done three times. The final dried residue was ignited to a constant weight, on the Meker burners at ~ 1273K. The reaction $SiO_2 + 4HF \rightarrow SiF_4\uparrow + 2H_2O$, involved evolution of SiF_4 gas, hence removing silicon.

Difference in weights of the crucible gave the silica content, and hence the percentage SiO_2 was calculated.

2.2.3.1.5. Alumina

0.2 → 0.3g of the zeolite were treated with HF in the normal manner as above. The final dried residue in the platinum crucible was digested in 1:1 HCl on a water bath. The resulting solution was diluted to 250 cm^3. This solution was used for the analysis of Al^{3+}, Na^+, Ca^{2+} and the transition metal(II) content.

A 50 cm^3 aliquot of the solution was pipetted into a 600 cm^3 beaker and just neutralised with 1:1 ammonia solution. 4 cm^3 of 1:1 HCl were then added and the solution was diluted to 100 cm^3. The solution was warmed

and 8 cm^3 of 5% oxine solution added to it. It was warmed a little further to ~323K and then 20 cm^3 of 40% ammonium acetate were added slowly with continuous stirring. The suspension was warmed to 343K on a water bath for 20 minutes and then allowed to settle. The suspension was filtered through a preweighed P4 sintered crucible, washed thoroughly with hot water until a clean filtrate (no yellow tinge) was obtained. The crucible with its contents was dried at ~ 413K, for more than two hours in an electric oven. The dried sintered crucible was weighed again. The difference in weights of the crucible gave the weight of Al as $Al(C_9H_6ON)_3$, from which percentage of Al as Al_2O_3 was calculated. The whole procedure was repeated thrice.

2.2.3.1.6. Sodium

A 5 cm^3 aliquot of the HF-treated zeolite solution (§2.2.3.1.5.) was diluted to 50cm^3 (a 10 times dilution). This solution was used for sodium ions determination, with the help of appropriate filter and standards (1.25,2.5,5,10,15,20,25ppm) in a CORNING 400 Flame Photometer.

2.2.3.1.7. Calcium

The analysis of Ca^{2+} and M^{2+} ions (Cu^{2+}, Co^{2+}) in the zeolite samples was a difficult problem. Different methods and techniques were tried to get accurate results. Not only the transition metals, but sodium ions on one hand and silicon or aluminium on the other, interfered in calcium analysis.

Out of the different methods/techniques tried (including the common EDTA titration[279], the tungstate method[280], flame photometry and atomic absorption spectrophotometry), AAS was most satisfactory, using a nitrous oxide-acetylene flame.

A 5 cm^3 aliquot of the HF-treated zeolite solution (§2.2.3.1.5.) was mixed together with 5 cm^3 of 2,000 ppm La^{3+} ions and 5 cm^3 of 10,000ppm K^+ ions. These additions controlled the interference due to slight calcium ionization, and any interference arising from the presence of transition metal ions in the sample solution. The calcium ion standards (0,015, 1 → 10ppm) were prepared with matching aluminium ion concentrations and using a similar background to that for the samples.

These sample and standard solutions were used to determine calcium content employing a Perkin Elmer 370 Atomic Absorption spectrophotometer in a nitrous oxide-acetylene flame under appropriate operating conditions.

2.2.3.1.8. Cobalt

To determine cobalt in the zeolite samples, the Perkin Elmer 370 Atomic Absorption Spectrophotometer was again used, the zeolite sample solutions (§2.2.3.1.5) again being diluted ten times, with samples and standards (of 0.5,1,1.5,2,2.5,3,3.5,4,4.5,5ppm) being analysed using an air-acetylene reducing flame (recommended conditions).

2.2.3.1.9. Copper

Copper analysis of the zeolite samples was also carried out with the help of atomic absorption spectorscopy. The copper contents in the zeolite sample solutions (§2.2.3.1.5.) of ten times dilution and the copper standard solutions (0.5,1,1.5,2,2.5,3,3.5,4,4.5,5ppm) were determined by AAS using an air-acetylene blue oxidizing flame, again following recommended operating parameters of the instrument.

2.2.3.2. Surface Area Determination.

The evaluation of the surface area is of growing importance as an

essential requirement of any study of catalysis, and helps in specifying the efficiency of a catalyst or an absorbent. A solid will posses a large surface area if it exists in the form of fine particles because there is an inverse relationship between the specific surface area (the surface area of 1 gram of solid) and its particle size, given by the relationship

$$S = \frac{6}{Pl} \qquad \text{where}$$

S = the specific surface, l = an edge length and P is the density of the solid.

A large specific surface may arise not only by the aggregation of primary particles, but also by the removal of parts of a parent solid in such a manner as to leave pores. The walls of these pores will comprise the 'Surface Area' of the resultant solid[94,p.2]. Zeolites normally have very large "surface areas". The determination of surface properties is frequently achieved by the use of a nitrogen or krypton adsorption method. A very common adsoprtion method is the static one, which relies on determining the quantity of vapour adsorbed or desorbed from a catalyst at (say) a liquid nitrogen temperature, as a function of the relative pressure of nitrogen above the sample[106,p.88]. Detection can be by observing either (or both) weight and volume changes. This procedure enables a complete adsorption-desorption isotherm to be obtained. The surface area may be determined from these data using the now famous work of Brunauer, Emmett and Teller[281]. The B E T equation is not suitable for Type I, IV, and V isotherms, and zeolites generally give Type I, so with these the 'Point A' or 'Point B' methods are applicable.

2.2.3.2.1. Methods of Measuring Surface Area

There are two main methods for surface area measurements *viz*; the dynamic

and the static methods.

Static methods can be either gravimetric or volumetric and operate on the same principle. The former measures weight changes whilst the latter measures gas volume changes as a function of pressure.

Dynamic methods have been used for measuring the adsorption of vapour for many years. Davies[283] used a dynamic method for measuring the adsorption of benzene from an air stream. Development of gas chromatography has helped to revive the technique, which is more commonly known as the continuous flow gas chromatographic technique. This popular technique was first used by Nelsen and Eggertsen[284]. The relative pressure of nitrogen passing over the catalyst was varied by appropriate dilution with helium. The concentration of the amount of nitrogen adsorbed or desorbed was monitored by thermal conductivity measurements using a microkatharometer detector. This technique was later modified by other workers[285,286] who used commercially available chromatographs and who also simplified the operation procedures and calculations.

All gravimetric methods employ adsorption balances or vacuum balances of two types *viz*: "Beam Balances" and "Coil Spring Balances". The sensitivity of each type is to some extent a matter of choice, though in cases of spring balance it is dependent on the total (mass) capcity of the balance. McBain and Baker[282] were the first to introduce a spring vacuum microbalance (sorption balance) in 1926 and since then, the basic principles of the method have not changed. This balance is the most widely used of all gravimetric techniques for adsoprtion measurements. The essential part of the device is a freely suspended fused silica helical spring with a hook at the lower end to which a light bucket containing the adsorbent is attached. The system is connected to a

vacuum system. The uptake of the adsorbate by the catalyst sample is followed by measuring the extension of the spring using a travelling micrscope.

2.2.3.2.2. Volumetric Method.

Volumetric methods are the commonest ones used for the surface area determination of solids. In this method, successive charges of measured volumes of gas are admitted to the adsorbent until equilibrium is obtained, when the pressure of the gas in the dead-space is read on a manometer. The quantity of gas which has not been adsorbed is calculated by applying the gas laws. In addition, the volume of the dead space is accurately measured. The volume of the gas adsorbed is calculated by subtracting the amount remaining unadsorbed from the total admitted volume. The surface area is then determined from the calculated effective area(5) occupied by each adsorbed species. Gases such as nitrogen, krypton, argon or oxygen at 77K or 90K can be used, but generally nitrogen and kryptonare preferred for the determination of adsorption isotherms. A simple volumetric apparatus consisting of a small glass bulb attached to a vacuum line by means of a standard ground-glass joint, and which also is connected to a mercury manometer, can be used for the solids of specific area of at least 5 m^2g^{-1}. In the volumetric technique, there are two potential sources of error which need much care[94,p.312], first the errors in the measured doses are cumulative, and second, the amount remaining unadsorbed in the dead space becomes relatively more and more important with the increasing pressure. These errors can be avoided by careful calibration of the standard, dosing and the reaction vessel volumes (§2.2.3.2.3.6). Krypton was used as an adsorbent for surface area measurements of the zeolite samples used in this work. Krypton adsorption has special advantages[287] in studying low area solids because

at 77K the saturation vapour pressure of Krypton is only 1.76 torr, so that even at saturation the quantity of gas vapours remaining unadsorbed is small. The measurement of the low pressure, however, becomes a bit more difficult than when the pressure is in the cm of mercury range.

2.2.3.2.3. The High-Vacuum System

The apparatus employed for surface area determination was a standard high vacuum system shown in figure 2.1. It was possible to attain a maximal vacuum of 1×10^{-6} torr (1 torr = 1mm of Hg = 133.3Pa). The system is fully described in the following sub-sections.

2.2.3.2.3.1. Construction

The apparatus was constructed mainly of Pyrex glass and involved greased ground-glass taps and joints. It consisted of four main parts, *viz:* a rotary oil pump (R_p), a mercury diffusion pump (M_d), a McLeod gauge (M_1) which comprised a thin ∿ 25cm long capillary tube of 2mm diameter, and a static reactor (§ 2.2.3.2.3.2.) connected by a common main vacuum line (V_1). Gases used were stored in glass bulbs (B1, B2, B3) while an empty bulb (E_b) was used as a volume expansion section if and when required. Like any other system involving a mercury diffusion pump and a McLeod gauge, mercury remained in this system at 10^{-3} torr (vapour pressure of mercury at room temperature). So to avoid mercury vapours affecting the catalyst surface, the reaction vessel was isolated from the source of mercury by means of liquid nitrogen traps (U, C_1 and C_2) at 77K. The cold fingers (F_1, F_2 and F_3) near the gas bulbs were used to condense gases at 77K and then evacuate any impurities if present, while the side lines (M_1, M_2 and M_3) contained glass-encased magnets for breaking the seals of the glass bulbs. The numbers in the figure represent the taps and (J) is a greased standard ground-glass joint. Mercury in the diffusion pump was heated by an

electric heater (H) attached at the base while cold water (W_1 to W_2) was circulated around the pump to cool the system and condense mercury escaping into the system.

2.2.3.2.3.2. Reaction Vessel.

The reaction vessel (R_v) (§ fig.2.1.) was a batch type static reactor made of quartz. The length of the reaction vessel was 15cm and the diameter was 12mm. A piece of sintered glass (S_g) 3mm wide was inserted in the opening near the detachable end of a greased ground-glass joint (J) which was connected to the vacuum line V_1. This was used to stop the powdered sample being sucked into the 'U' tube of the main vacuum system during outgassing of the sample prior to adsorption or kinetic reaction studies. The sample was placed in the reaction vessel through a second opening which could be closed by a greased stopper (numbered as 1 in figure 2.1.).

2.2.3.2.3.3. Heating Arrangement.

A cylindrical electric furnace was used to dehydrate samples under dynamic vacuum conditions, and during the kinetic experiments. The temperature of the furnace, which was controlled by a Variac, was measured using a chromel-alumel thermocouple, which was in turn calibrated against a reference junction at 273K via a potentiometer bridge.

2.2.3.2.3.4. Materials

The materials investigated were transition metal(II) exchanged-5A zeolite samples (§ 2.2.2.) in the powdered form.

Research grade krypton (99.97% purity) used in the surface area determinations and nitrous oxide (99.998% purity) used in the kinetics study experiments, were supplied by British Oxygen Company Ltd in Pyrex bulbs. After attachment to the gas handling line of the high vacuum system, these

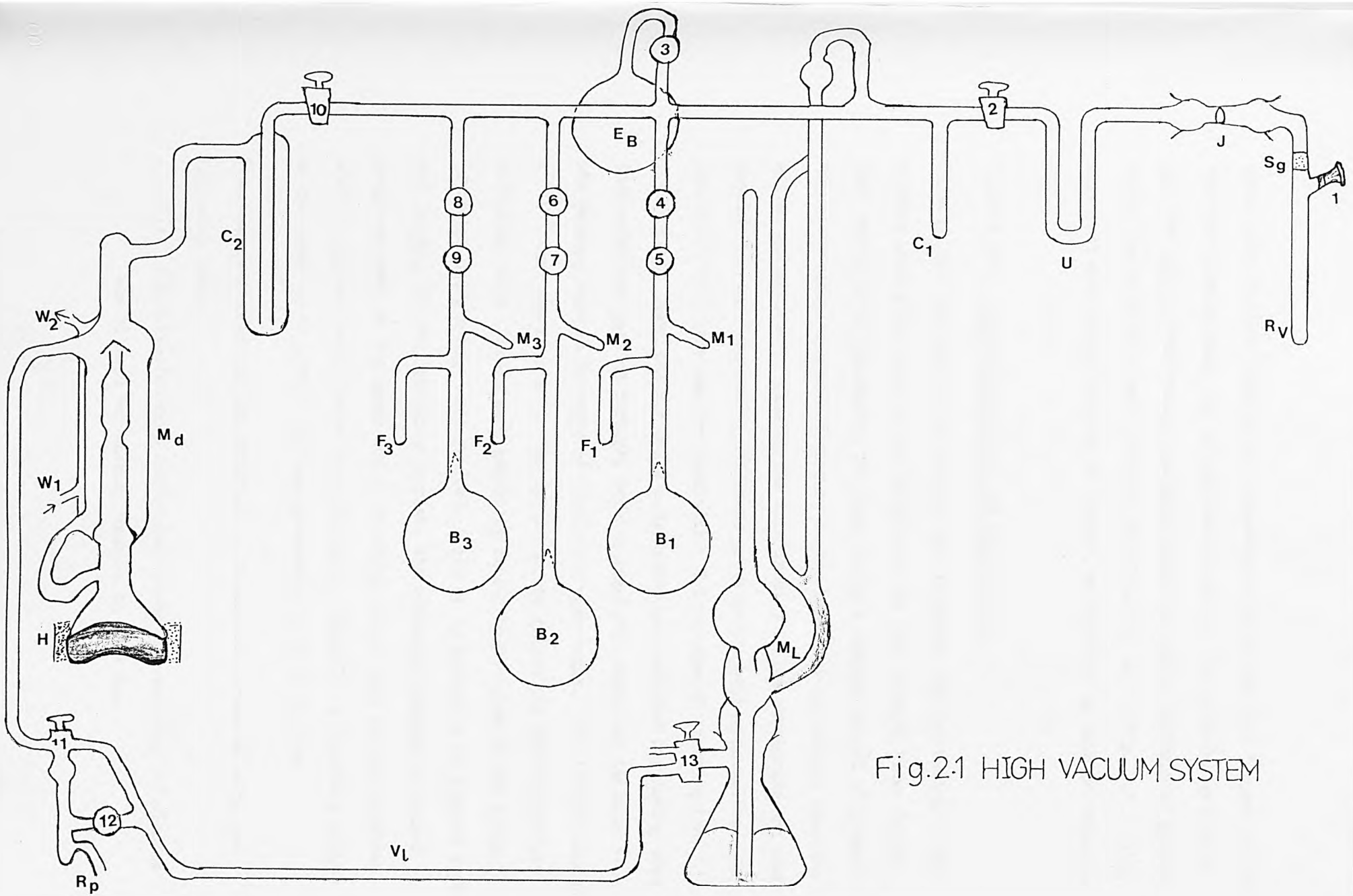

Fig.2-1 HIGH VACUUM SYSTEM

gases were further purified by condensing them in the cold fingers at 77K, and then pumping away any uncondensed impurity. The ground-glass joint and the taps in the vacuum line were sealed by yellow 'Apiezon L' grease while the reaction vessel entrance was closed by tap 1 (fig. 2.1.) using more resistant black 'Apiezon M' grease, as supplied by Apiezon Products Ltd.

2.2.3.2.3.5. Vacuum Generation and Degeneration.

Firstly, all the taps in the system were inspected for "streaking". Any streaks were eliminated either by turning the taps several times (using both hands) or by regreasing the taps (using a minimum amount of grease). Any undesirable movement of mercury in the reservoir on pumping down the system was avoided by closing the taps leading to the atmosphere and then opening the taps connecting different parts in the main vacuum line. A vacuum of $\sim 10^{-2}$ torr was produced within 3-5 minutes of starting the rotary pump. Next the diffusion pump heater was switched on, making sure that water was passing through, and the reaction vessel was isolated from the mercury sources by means of liquid nitrogen traps. An ultimate vacuum $\sim 10^{-6}$ torr was created in the system by the rotary oil and the mercury diffusion pumps. Leaks were generally caused by pinholes in the glass (detected using a high voltage Tesla coil) or by streaking of greased taps and joints. In the leak-proof system, the pressure measured by McLeod gauge was zero on the gauge scale 'sticking vacuum' and did not increase when the system was isolated from the pumps. Usually, a 'sticking vacuum of the order of $\sim 1 \times 10^{-6}$ torr was generated in 15-20 minutes.

The evacuated apparatus was returned to atmospheric pressure using the following steps:

(i) The diffusion pump heater was turned off and about 10 minutes was allowed for mercury vapours to cool down.

(ii) All liquid nitrogen traps were removed and water supply turned off.

(iii) The taps connecting different parts of the system to the main vacuum line were opened.

(iv) Finally, the rotary pump was switched off and air was slowly admitted into the system through T_{13} (see fig.2.1.).

2.2.3.2.3.6. Volume Calibration

The high vacuum system was evacuated to a 'sticking vacuum' (§ 2.2.3.2.3.5). The maximum krypton pressure required for volume calibration was ∿ 0.6mm. ($P/_p$ ∿ 0.3) so it was convenient to reduce the pressure in the storage bulb (B_1) to ∿2mm (vapour pressure of Kr at 77K) by cooling (B_1) with liquid nitrogen. The experimental volume of the system, conveniently divided into three parts, was calibrated by standard methods as;

(i) Standard Volume (V_s): The volume of McLeod gauge bulb down to the point A (which had been pre-determined by filling it with water (∿58.7 cm^3) from a burette) was taken as the standard volume.

(ii) Dosing Volume (V_1): This is made up of the McLeod gauge volume (V_s) plus the volume between taps (2,4,6,8 and 10) (Fig.2.1). Bulb (E_B) is used to increase the dosing volume, which can be reduced by closing tap (T_5). V_1 was determined by introducing a krypton dose from bulb (B_1) to the dosing volume area, isolating a quantity of gas in V_s, evacuating V_1, and then expanding the gas from V_s into V_1, The resulting pressure was measured by the McLeod gauge and then V_1 calculated applying Boyle's Law.

(iii) Reaction Vessel Volume (V_2): This part consists of the experiment volume beyond tap 2, including the volumes of the 'V'

tube and the reaction vessel (R_v). The reaction vessel volume (V_2) was determined by expansion from the dosing volume through V_2, then measuring the equilibrium pressure, and finally applying Boyle's law for calculation.

2.2.3.2.3.7. Mode of Operating

The high vacuum apparatus (§ 2.2.3.2.3.) was used for measuring the monolayer equivalent surface area of the transition metal(II) exchanged- 5A zeolite samples (§ 2.2.2). The reaction vessel was detached from the system after closing tap 2. The 'sticking vacuum' of the order of$\sim 10^{-6}$ torr was produced in the system (§ 2.2.3.2.3.5.) An accurately weighed quantity ($\sim$ 150 mg) of the hydrated sample was placed carefully in the reaction vessel through entrance 1 which was closed by a greased stopper (see fig. 2.1). The reaction vessel was then attached to the main vacuum line of the system through the greased ground-glass joint (J) by opening tap (2) very slowly. The system was evacuated for at least five minutes and the out-gassing was continued overnight at room temperature ($\sim$ 298K) by placing a liquid nitrogen trap under the 'V' tube to isolate the zeolite from the grease, water and mercury vapours. A cylindrical electric furnace coupled with a Variac was placed around the reaction vessel tube and the temperature was increased to $\sim$393K. The sample was heated at this temperature for two hours under vacuum, when the system was checked for maintenance of the sticking vacuum. The furnace was removed and after allowing some time to let the reaction vessel cool down to room temperature, a liquid nitrogen Dewar flask was placed around the sample in the reaction vessel. Then taps 2 and 10 were closed and a dose of Kr gas was admitted to the dosing volume, the pressure measured and expanded into the reaction vessel volume by opening tap 2, slowly when the adsorption of Kr at 77K on the partially dehydrated sample surface commenced.

When equilibrium was reached (after ∿2 hours for first dose at ∿ 2 torr initial pressure), the pressure in the system was measured. Tap 2 was closed and the pressure of the second dose of Kr admitted to the dosing volume was noted. Then the gas was expanded into the reaction vessel by opening tap 2 and the equilibrium pressure was measured after ∿30 minutes. The process was repeated with further doses until the equilibrium relative pressure (P/P_o) at 77K had reached to ∿ 0.35. The volume of Kr adsorbed at N.T.P. (∿ 273K & 760 mm) was calculated from the known values of dosing and the reaction vessel volumes and the initial and equilibrium pressure. The volume (V_c) of krypton adsorbed at 77K was plotted against the relative equilibrium pressure (P/P_o) to obtain an adsorption isotherm, from which the monolayer equivalent surface area or partially dehydrated zeolite sample at ∿393K was determined by the "point B" method.

The sample was then outgassed at 623K for complete dehydration for 2-3 hours. The above procedure of Kr adsorption at 77K was carried out to measure the monolayer equivalent area of the dehydrated zeolite samples at ∿623K.

2.2.3.3. X-ray Powder Diffraction Analysis

2.2.3.3.1. Introduction.

The powder method of X-ray diffraction was devised by Deby and Scherrer in Germany (1916) and by Hull in the United States (1917). This method basically involves the diffraction of monochromatic (the strong K characteristic component) X-rays by a powder specimen. There are three common powder methods in use, differentiated by the relative position of the specimen and film[288],

(1) The Debye-Scherrer Method: The film is placed on the internal surface of a cylinder, and the specimen on the axis of the cylinder.

(2) Focussing Method; The film, specimen and X-ray source are all placed on the surface of a cylinder.

(3) Pinhole Method: The film is flat, perpendicular to the incident X-ray beam, and located at any convenient distance from the specimen.

Powder camera techniques involve various steps including powder preparation (grinding and sieving), specimen preparation and mounting in the camera, loading the camera with X-ray film and selection of the appropriate X-radiation (avoiding radiation at which the specimen would fluoresce), alignment of the camera in X-ray beam, rotation of the specimen after setting of the X-ray tube controls, exposure time, processing of the exposed film and finally film measurement for interpretation of results.

A good X-ray powder photograph of a crystalline solid is suitable for two types of measurements:

(1) the positions of the diffraction lines on the film and the Bragg angle of reflection,

(2) the relative intensities of the diffracted lines.

The Bragg equation can be expressed simly as

$$n\lambda = 2d \sin\theta$$

where n = an integer, the order of reflection

λ = the X-ray wave length,

θ = the Bragg angle

and d = the interplanar spacings.

Approximate d-values are usually read off a powder film directly using special calibrating rulers, with scales of d-values engraved according to X-ray wavelength and diameter of the camera. More accurate work requires

either a travelling microscope, or a specially designed glass vernier ruler accurate to 0.05mm.

The relative intensities of the observed reflections are determined by the number and positions of the atoms in the unit cell and by their scattering powers in the direction of the reflected X-rays. Normally, visual estimation is sufficient for approximate relative assessment of the intensities of the diffraction lines to the nearest 10% taking the intensity of the strongest line as 100%. Alternatively, more accurate graphic intensity data is obtained by using a 'microdensitometer' (a specially designed photometer) for measurement of line intensities.

2.2.3.3.2. Method

The crystallinities of the zeolites 4A, 5A and maximally exchanged transition metal(II) - 5A zeolite Co-5A(4-6) and Cu-5A(4-6) were examined by the powder X-ray diffraction method using a Phillips Debye-Scherrer camera. The operating conditions employed were:

Target	Cu K α
Wavelength	1.542 $\mathring{A}$
Tube voltage	40 K υ
Tube current	14 mA
Exposure time	6 hours

In the case of Co-5A(5) and Co-5A(6), fluorescence on the X-ray films occurred, so the Cu Kα target was replaced by the Co Kα target (λ = 1.790 $\mathring{A}$). The intensities of the exposed or blackened films were measured using a microdensitometer.

2.2.4. Kinetics of Nitrous Oxide Decomposition Reaction

Kinetics of nitrous oxide decomposition reaction were monitored to study the catalytic activity of the zeolites (§2.2.2).

2.2.4.1. Apparatus

The high vacuum system described in section 2.2.3.2.3. and shown in figure 2.1, was used as a static reactor for catalytic studies. Pressure measurement was taken by a McLeod gauge, which was separated from the reaction vessel by a 'U' shaped cold trap immersed in a mixture of acetone and dry ice (solid CO_2) at 195K. Thus the reaction surface was free of any water, mercury or grease contamination. The total volume of the high vacuum apparatus was 340 dm^3, and it could produce an ultimate vacuum of 10^{-6} torr. The dosing volume (260 cm^3) of the system consisited of the volume between taps (2, 4,5,6,8, and 10) plus the McLeod gauge volume. The reaction vessel volume (80 cm^3) was the volume beyond tap 2, including the 'U' tube and the reaction vessel. The nitrous oxide bulbs (of 99.998% purity, supplied by B.O.C), were purified further before use (§2.2.3.2.3.4).

2.2.4.2. Operating Procedure

The procedure employed[158] involved creating a vacuum of 10^{-6} torr, using both the rotary and mercury diffusion pumps (§2.2.3.2.3.5). Before the catalytic studies each hydrated zeolite sample (~150 mg) was outgassed under vacuum overnight. The monolayer equivalent surface area of the partially hydrated sample at 493K and then of the dehydrated sample at 623K were measured using krypton adsorption (§2.2.3.2.3.7.).

The out-gassing of the sample was continued at ~ 635K for two hours in a vacuum to remove any remaining zeolitic water. The high vacuum system was frequently checked for 'sticking vacuum' (§2.2.3.2.3.5.). During subsequent heating of the sample at high temperatures, the greased entrance of the reaction vessel was cooled by compressed air to avoid any leakage through melting of the grease. The activated sample was then heated to the temperature required for the N_2O decomposition reaction (which varied for

different samples used). Heating was by an electric furnace and temperatures (measured by a chromel-alumel thermocouple) were kept constant to ± 2K. When a stable temperature had been obtained, tap 2 was closed and a dose of N_2O at 1-2 torr pressure was introduced into the dosing volume (by entrapping a quantity of gas between taps (6-7), from bulb B_1 and then releasing it from tap 6) and the pressure was measured. The decomposition reaction (which started when tap 2 was opened and N_2O reached the zeolite surface) was monitored by reading the pressure rise as a function of time. The pressure of nitrous oxide during reaction was calculated from the known values of dosing pressure, dosing and reaction vessel volume using the general gas equation. A continuous record of pressure changes against time (in secs) was used to determine the kinetics of the nitrous oxide decomposition reaction.

Normally, a run was performed to ~50% decomposition of nitrous oxide, and in several cases the run was continued to ~95% decomposition. The tap 10 (fig. 2.1) was opened and the system was evacuated at the reaction temperature for 15 minutes and temperature of the furnace was then increased for a subsequent run. After ensuring stable temperature and sticking vacuum had been attained, the above procedure was repeated at the elevated temperature by introducing second dose of nitrous oxide at 1-2 torr pressure. At least five runs were carried out at different temperatures for each zeolite sample studied. After reaction, the krypton monolayer equivalent area was again measured at the highest reaction temperature.

2.3. Flow System Studies

2.3.1. Chemicals Used

Synthetic sodium mordenite (zeolon 100) was supplied by the Norton Company in the powder form. Copper(II), ammonium(I), nickel(II) chloride, nickel(II)

nitrate, hydrochloric, hydrofluoric (40%) sulphuric and nitric acid, ethylenediaminetetra-acetic acid (EDTA), di-sodium tetraborate and 8-hydroxyquinoline (all of AnalaR grade) were supplied by B.D.H. Johnson-Matthey supplied the precious metal complex (K_2PtCl_4) while ampoules of 0.1N sodium thiosulphate were supplied by May and Baker Ltd.

2.3.2. Preparation of Transition Metal(II) Exchanged Sodium Mordenite-Zeolites

Due to its ready availability, its acid-stable nature and its catalytic potential[289-290], mordenite was chosen for these studies. The transition metal ion exchanges were done in two stages. Initially Ni(II), Cu(II) and Pt(II) ion exchanged samples were prepared for the preliminary catalytic activity study, which was extended to mixtures of the catalysts. The later study required further amounts of the catalysts than had been prepared initially. At this stage, it was decided to drop Pt(II) ion exchange for further studies due to difficulties in platinum analysis and to concentrate on copper and nickel mordenites. Thus, only nickel(II) and Cu(II) ion exchanged-mordenite were subsequently prepared for the second stage studies of catalytic activity.

2.3.2.1. Sample Preparation for Preliminary-Catalytic Studies.

The parent sodium mordenite was stored in a desiccator over saturated NaCl solution for a fortnight in order to accomplish complete hydration. Prior to the transition metal ion exchange, sodium mordenite was exchanged for the ammonium form due to the following reasons[260]:

(i) An ammonium zeolite imparts a less alkaline reaction to solution than the corresponding alkali metal form.

(ii) The presence of ammonium chloride in solution suppresses precipitation of certain transition metal hydroxides e.g. those of nickel and cobalt.

(iii) The use of ammonium ion as the other exchanging species avoids the problem of a ternary ion exchange system involving Na^+, NH_4^+ and Cu^{2+} ions when ammonia complexed transition metal specimens are used.

(iv) Since exchange does not proceed to 100%, preparation of the hydrogen zeolite by removing ammonia was thought to possibly lower the mobility of pre-exchanged transition metal ions.

2.3.2.1.1. Preparation of Ammonium Exchanged-Mordenite

A slurry of 100g of hydrated sodium mordenite in 400 cm^3 1M NH_4Cl was stirred for 24 hours using a magnetic stirrer, then centrifuged. The slurry of residue was again exchanged with 400 cm^3 1M NH_4Cl on a magnetic stirrer for another 24 hours. The procedure was repeated five times, with two final exchanges being carried out at 343K. The resulting slurry was centrifuged, washed with distilled water and dried overnight at 343K. The exchanged ammonium mordenite (NH_4-MOR) was equilibrated over a saturated solution of NH_4Cl in a desiccator for a fortnight to complete re-hydration to constant weight.

2.3.2.1.2. Preparation of Nickel(II)-Exchanged-Mordenite.

A weighed portion of hydrated NH_4-MOR was exchanged with a 5-fold excess of equivalent of Ni^{2+} in aqueous solution for several days. The resulting exchanged samples were light green in colour.

Three samples with different levels of nickel(II) exchange were made as follows:

(a) Ni-MOR (1) : This was prepared by ion exchang-ing 10g

NH_4-MOR with 500 cm^3 of 0.1M $Ni(NO_3)_2.6H_2O$ aqueous solution for a few days. The resulting slurry was washed with distilled water, dried at 333K and stored over saturated NaCl solution for two weeks to ensure equilibrium rehydration.

(b) Ni-MOR (2): This was prepared by exchanging 10g of hydrated NH_4-MOR with 500 cm^3 0.1M aqueous $Ni(NO_3)_2.6H_2O$ for two weeks. The suspension was centrifuged and the residue was exchanged with another 500 cm^3 0.1M aqueous $Ni(NO_3)_2.6H_2O$ solution for one week. After, again centrifuging and washing thrice with distilled water, the exchanged sample was dried at 333K and stored in a desiccator over saturated solution of NaCl for fifteen days.

(c) Ni-MOR (3): This was prepared by exchanging 5g of NH_4-MOR with 250 cm^3 0.1M$(NO_3)_2.6H_2O$ aqueous solution for two weeks and repeating the exchange for four times over a period of a month. The final centrifuged sample was washed twice with distilled water and dried over $CaCl_2$ in a vacuum desiccator for one hour. Ni-MOR (3) was also stored over saturated NaCl solution for a fortnight before analysis.

2.3.2.1.3. Preparation of Copper(II) Exchanged-Mordenite.

First of all, a $Cu(NH_3)_4(H_2O)_2 Cl_2$ solution was prepared by adding concentrated ammonia to an aqueous 0.1M solution of $CuCl_2.2H_2O$ until the initially precipitated salt had completely redissolved and adjusting the final solution strength to 1 mol dm^{-3}. The final pH value was maintained at ∿10.5, slightly in excess of that required for solution stability[2.91].

The samples of Cu(II) exchanged-mordenite were prepared by adding a quantity of solution containing around ∿12 m eq g^{-1} metal ion to ∿ 20 m eq NH_4-MOR (§ 2.3.2.1.1.) This assured that all Cu(II) ions would be taken

up by the zeolite. The resulting samples were blue in colour.

Three different samples were again prepared as follows:

(a) Cu-MOR (1): This was prepared by stirring 10g NH_4-MOR in 500 cm^3 of 0.1M copper ammine solution for six days using a magnetic sitrrer. The final slurry was centrifuged and washed twice with dilute NH_3 solution (pH 10.5). The sample was placed under vacuum over anhydrous $CaCl_2$ in a vacuum desiccator for one day. The dried sample was finally stored over saturated NH_4Cl solution in a desiccator for at least two weeks.

(b) Cu-MOR (2): This was prepared by exchanging 10g NH_4-MOR with 500 cm^3 0.1M Cu(II) ion solution, first for 4 days and then after a subsequent centrifugation, the residue was exchanged with another 500 cm^3 of 0.1M Cu(II) ion solution for six days. The final processed samples were stored over sat. NH_4Cl solution.

(c) Cu-MOR (3): This was prepared by exchanging 10g NH_4MOR three times for 6,4 and 5 days respectively. The dried Cu-MOR (3) was finally stored over a saturated NH_4Cl solution.

2.3.2.1.4. Preparation of Platinum(II) Exchanged Mordenite.

Metal complexed salt $Pt(NH_3)_4\ Cl_2$ was prepared first, employing the method described by Cooley and Bush[292].

10g K_2PtCl_4 (Pt=46.57%) were dissolved in 50 cm^3 H_2O in a 150 cm^3 beaker. A small quantity of HCl was added to the solution after heating it slightly. An excess of 50% ammonia solution was added very slowly to the hot solution with concinuous stirring until a colourless solution was obtained. Next the solution was evaporated until only a faint ammonia odour was detected.

After adding 1cm of conc. HCl, the salt was precipitated by the addition of 10 times its volume of 1:1 alcohol/acetone mixture. The suspension was allowed to stand for 1 hour, filtered, then washed with pure acetone and finally dried in air. The prepared complexed salt had a slight yellow colour, which could be due to either unreacted potassium salt or the impurities in the starting salt.

A known weight of NH_4-MOR (§2.3.2.2.1) was then exchanged extensively with a sixfold excess of the above prepared complexed salt solution for several days to prepare the Pt(II) exchanged-mordenites.

A stock solution of 0.1M $Pt(NH_3)_4\ Cl_2$ in water was used for preparing subsequently four platinum zeolite catalysts.

(a) Pt-MOR (1):

5g NH_4-MOR were exchanged with 250 cm^3 of Pt stock solution. The suspension was stirred continuously using a magnetic stirrer for 8 days. The final slurry, after centrifuging and washing thrice with distilled water, was dried at 443K overnight. The exchanged sample (light grey in colour) was stored over saturated NH_4Cl in a desiccator for fifteen days to complete rehydration.

(b) Pt-MOR (2):

5g NH_4-MOR, first exchanged with 200 cm^3 stock solution for 4 days, was re-exchanged with a further 100 cm^3 of stock Pt(II) in solution for two days. The residue was exchanged with a third volume of 100 cm^3 stock solution for another six days. The final exchanged sample, after centrifuging and washing thrice with distilled H_2O, was dried at 443K. The dehydrated sample was equilibrated over saturated NH_4Cl solution in a desiccator for two weeks.

(c) Pt-MOR (3):

5g of NH_4-MOR were exchanged with three volumes of 250 cm^3 stock solution for 9 days the first time, then 3 days and finally 6 days. The sample was further processed as described before.

(d) Pt-MOR (4):

The filtrate from the above preparations was used to exchange 10g of NH_4-MOR for ten days. The sample was then processed as above.

Pt-MOR (2), Pt-MOR (3) and Pt-MOR (4) were all dirty-white in colour.

2.3.2.2. Sample Preparations for Mixed-Catalytic-Studies.

Four zeolite samples *viz.* Ni-NaMOR, Ni-NH_4MOR, Cu-NaMOR and Cu-NH_4MOR were prepared by exchanging ammonium mordenite with respective metal(II) salt solutions. These zeolites were subsequently intimately mixed up in a known ratio to obtain samples for catalytic studies on the flow system.

2.3.2.2.1. Preparation of Ammonium-Exchanged Mordenite.

100g of hydrated parent zeolite were exchanged with 1M solution of NH_4Cl as described in sec. 2.3.2.1.1.

2.3.2.2.2. Preparation of Nickel(II) Exchanged-Sodium Mordenite.-

Nickel(II) exchanged-sodium mordenite (Ni-NaMOR) was prepared by exchanging 20g of hydrated parent zeolite with two 200 cm^3 volumes of aqueous 0.1M $Ni(NO_3)_2.6H_2O$ for 2 and 3 days respectively. The final slurry (after centrifuging and washing thrice with distilled water) was dried at 353K. The dried partially hydrated sample was stored over saturated NaCl for rehydration. The final sample was green in colour.

2.3.2.2.3. Preparation of Nickel(II)-Exchanged-Ammonium Mordenite.

Nickel(II) exchanged-ammonium mordenite (Ni-NH_4MOR) was prepared by stirring 25g of hydrated NH_4MOR (§ 2.3.2.2.2.) with four 250 cm^3 volumes

of aqueous 0.1M $Ni(NO_3)_2.6H_2O$ for 2, 3,2 and 5 days respectively. The final slurry was centrifuged, washed twice with distilled water and dried overnight at 353K in an oven. The dried sample was placed over saturated NaCl in a desiccator for 15 days to equilibrate. The colour of the sample was light green.

2.3.2.2.4. Preparation of Copper(II) Exchanged-Sodium Mordenite.

Copper(II) exchanged-sodium mordenite (Cu-NaMOR) was prepared by introducing Cu(II) ions into 25g of the hydrated parent zeolite from two 250 cm^3 volumes of 0.1M $Cu(NH_3)_4.(H_2O)_2\ Cl_2$ (§2.3.2.1.3). Each time the suspension was stirred for 3 days. The resulting slurry, after washing first with distilled water, and then with three volumes of dilute ammonia solution (pH10.58), was dried at 308K overnight. The partially hydrated sample was stored for at least two weeks in a desiccator over saturated NH_4Cl solution in order to rehydrate it completely. The colour of the rehydrated sample was grey-blue.

2.3.2.2.5. Preparation of Copper(II) Exchanged-Ammonium Mordenite.

(Cu-NH_4MOR) was prepared by introducing Cu(II) ions into 25g of hydrated NH_4MOR (§2.3.2.2.2.) from two 250 cm^3 volumes of 0.1M $Cu(NH_3)_4(H_2O)_2\ Cl_2$ (§2.3.2.1.3), again using a magnetic stirrer, with contact times of 3 and 4 days, respectively. The resulting slurry was centrifuged, washed thrice with dilute NH_3 solution (pH 10.55) and finally dried overnight at 308K. The partially dehydrated sample was stored over saturated NH_4Cl solution for two weeks.

2.3.3. Characterisation of Zeolite Samples.

The zeolites used were characterized by chemical and thermal analysis, followed by powder X-ray diffraction as described in the following sections.

2.3.3.1. Chemical Analyses.

2.3.3.1.1. Volatiles. An aliquot of ∿ 0.25g of the sample in a platinum crucible was heat-treated (§ 2.2.3.1.3). The difference in the initial and final weights of the crucible gave the weight of volatiles *viz*, H_2O, NH_3 and $(NH_4)_2O$ from which total volatile content was calculated for each sample.

2.3.3.1.2. Silica and Alumina. Each sample was then treated with 40%HF for the percentage determinations of silica (§ 2.2.3.1.4) and the alumina content was determined as before (§ 2.2.3.1.5).

2.3.3.1.3. Ammonia and "Ammonium oxide". The $NH_3/(NH_4)_2O$ content in each of the samples was determined in duplicate using the Kjeldahl method, on a Gallenkamp Kjeldahl apparatus which has a facility of running six samples simultaneously.

0.25 g of zeolite sample were placed in each Kjeldahl flask containing 50 cm^3 of 20% NaOH solution and a small quantity of fused silica (to avoid bumping and assist boiling). ∿20 cm^3 of standard 0.1M HCl and a few drops of methyl red indiactor were placed in each conical flask under the condenser such that the end of the condenser was just immersed in the acid surface. The water supply and the heaters were switched on. Heating was continued for 45 minutes, during which time all the evolved NH_3 was trapped in the standard HCl. To avoid any suck-back, all the connical flasks were removed before switching off the heaters. Next the contents of the conical flasks were titrated against standard 0.1M borax solution ($Na_2 B_4 O_7 . 10H_2O$) to estimate $NH_3/(NH_4)_2O$ in zeolite samples.

2.3.3.1.4. Water. The water content in each sample was calculated by subtracting the separately determined $NH_3/(NH_4)_2O$ content (§ 2.3.3.1.3) from the total volatile content (§ 2.3.3.1.1).

2.3.3.1.5. Sodium. Sodium content of the HF-treated zeolite sample solutions (§2.3.3.1.2) was determined using flame photometry as described before (§ 2.2.3.1.6).

2.3.3.1.6. Nickel. Atomic absorption spectrophotometry was used to determine the nickel content in the HF-treated zeolite samples (§ 2.3.3.1.2). Before analysis, the solutions were diluted to a tenth concentration and compared with standard solutions (0.5, 1, 1.5, 2, 2.5, 3, 3.5, 4, 4.5, 5ppm). Experience led to the choice of suitable operating parameters in an oxidizing air-acetylene flame.

2.3.3.1.7. Copper. The method used for copper content determination in zeolite solutions (§ 2.3.3.1.2) using atomic absorption spectrophotometry was as described above (§2.2.3.1.9).

2.3.3.1.8. Platinum. The Perkin Elmer 370 Atomic Absorption Spectrophotometer was also used to determine the platinum content. All the HF-treated sample solution (§2.3.3.1.2) was dried completely, digested in 50 cm^3 of 1:1 HCl for several days on a hot-plate to dissolve it completely (giving a yellow coloured solution) and then diluted to 250 cm^3 solution.

The interferences of the other ions during platinum analysis was controlled by making all solutions (samples and standards) to contain 2,000 p.p.m. La^{3+} and 0.1 mol dm^{-3} HCl. Then a 5 cm^3 aliquot each of the above HF-treated samples solutions together with 5 cm^3 each of 0.1 mol dm^{-3} HCl and 2,000 p.p.m. La was diluted to 50 cm^3. The standard solutions (0, 5, 10, 15, 20, 25, 30, 40, 50, 60, 75 p.p.m.) also contained 5 cm^3 0.1M HCl and 5 cm^3 2,000 La to match the concentration of the sample solutions. These solutions were observed for absorbance readings using an air-acetylene oxidizing (lean, blue) flame.

2.3.3.2. Thermal Analysis

Thermal analysis covers a group of techniques in which a physical property of a substance and/or its reaction product(s) is measured as a function of temperature whilst the substance is subjected to a controlled temperature programme[293]. A number of books, monographs, review articles and special publications deal with the methods of thermal analysis and their applications[294-300]. In each thermoanalytical method, the sample is heated in a controlled manner and a certain physical property is continusously monitored. The property of interest is measured or recorded as a function of time and/or the sample temperature, as a curve which is called a thermogram. Thermograms provide information concerning the microscopic processes occurring in the sample during heating. The techniques, sometimes called as thermally stimulated processes (TSP), are used as standard methods in research. As with other analytical methods, complementary or supplementary information furnished by other themral analysis techniques are required. It is fairly common to complement all DTA or DSC data with thermogravimetry. If a gaseous product(s) is evolved, evolved gas analysis (EGA) may prove useful in solving the problem at hand.

The methods of thermogravimetry (TG), differential thermal analysis (DTA) and differential scanning colorimetry (DSC), described in the following sections, were used to characterize and to determine the thermal stability of the preapred zeolite samples. The thermal analysis results were assessed with complementary data from chemical and X-ray diffraction analyses.

2.3.3.2.1. Thermogravimetric Analysis (TGA).

(a) Introduction.

TGA provides a quantitative measurement of any weight change associated with a transition. For example, it can directly record the loss in weight with

time or temperature, due to dehydration or decomposition. Normally the weight of a sample is recorded as a function of temperature, while its environment is heated or cooled at a controlled rate. The measurement is carried out continuously with a thermobalance. The term thermobalance was used for the first time by a Japanese scientist Honda[301] in 1915 and the technique was developed further during the 1920's by Guichard[302]. The plot of the sample weight versus time or temperature is called a thermogravimetric (TG) curve. If the first derivitive of weight with respect to time or temperature is recorded, the technique is called differential thermogravimetry (DTG) and the resulting curve is called a DTG curve. Three modes of thermogravimetry may be described[300].

(i) Isothermal or static thermogravimetry, in which the sample weight is recorded as a function of time at constant temperature.

(ii) Quasistatic thermogravimetry, in which the sample is heated to constant weight at each of a series of increasing temperatures.

(iii) Dynamic thermogravimetry, in which the sample is heated in an environment whose temperature is changing in a predetermined manner (preferably linear).

TGA curves can give information about the thermodynamic, reaction mechanism, and the initial and final products of a chemical reaction. TG applications in the case of zeolites are concerned mainly in determining the ease and the temperature at which water molecules or other occluded volatiles (eg ammonia) are evolved from the different sites within the zeolite framework structure.

(b) Procedure

Initial TG experiments were performed at the University of Salford on a Du Pont

900 Thermal Analyzer with a DU PONT 950 Thermogravimetric attachment. But due to a lack of suppression and scale enlargement facilities, and the time taken to cool the TG head assembly with compressed air after each run, the need for a more reliable and efficient apparatus was felt. So the TG runs were repeated on a Stanton Redcroft TG 750 thermogravimetric analyzer attached to a Servoscribe 250 chart-recorder. A cold circulating water stream enabled the furnace to cool down within 2-5 minutes after each run, so that measurement on new samples could be carried out at once. Both the instruments had Pt/Pt:Rh 13% thermocouples and employed null-balances. Duplicate runs were carried out using nitrogen and air atmospheres in each case.

The balance consisted of a symmetrical beam with a sample pan on one end and a counter balance weight on the other. The balance arm carried a shutter which moved between a light beam and a photocell. The sample was placed in a shallow platinum dish or crucible. A sensing element (a transducer) detected the deviation of the balance beam and maintained the balance arm in the null-position. Any change in sample weight caused the balance to move and the excess current to flow through the photocell, which was amplified and passed to the moving coil, restoring it to its original position. The current flowing through the motor operated the weight scale on the recorder and was directly proportional to the applied weight. Furnace temperature was continually monitored by the thrmocouple using as a reference temperature melting ice. The operating conditions employed were as given in Table 2.3.

2.3.3.2.2. Differential Thermal Analysis (DTA)

(a) Introduction

DTA is a technique in which the temperature difference between the sample

Table 2.3.

Operation	Du Pont 900/950	Stanton TG 750
Sample weight/mg	5	10
Heating rate K min^{-1}	10	10
Air or nitrogen flow rate/cm^3 min^{-1}	50	100
Sample holder	Pt	Pt
Temperature region	23 - 950K	23 - 2050K
X-axis	50K/inch	300 mm/hr
Y-axis	1mg/inch	2% wt/cm

and a reference material is recorded as a function of temperature when both are heated (or cooled) under similar controlled conditions. The reference material is preferably one with thermal properties (heat capacity and thermal conductivity) which do not change abruptly within the working temperature range, but which are as close as possible to those of the sample. The resulting data, although only qualitative, provides information of the temperatures at which any exothermic or endothermic changes within the sample accur. DTA measurements can be used to determine the heat of reaction Δ H(the enthalpic change) and also for determining the kinetics of reactions.

The sample and the reference material are usually placed in two cells as close to each other as possible, permitting moderately free exchange of heat between them. Thus the temperature difference $\Delta T = T_S - T_T$ is nearly constant avoiding any abrupt enthalpy change where T_S, T_R and ΔT are sample ,reference,differential temperatures. The deviations of ΔT from a horizontal line are caused by processes such as phase transitions, change of crystalline structure, any exothermic or endothermic chemical changes, hence forming peaks in upward and downwards directions.

DTA measurements of the prepared zeolite samples and their mixtures under air and nitrogen atmospheres, were taken.

(b) Procedures

DTA measurements were first carried out at the University of Salford using a Du Pont 900 Thermal Analyzer with a 500 DTA attachment under air atmosphere, but due to undesired distortions of the peak form and base-line shifts, a more sophisticated Stanton Redcroft DTA 674 was used for DTA runs under nitrogen atmospheres.

DTA 500 attachment head consisted of a heating block with three identical and symmetrical chambers which were equidistant from the central temperature control. Two were used for the sample and reference materials while the third was used to monitor the furnace temperature. Both sample and reference material (α-alumina) were placed in quartz tubes of small size to minimize the effects of heat transfer or temperature gradient within the sample. Thermocouples were carefully embedded in quartz tubes in the sample and reference material after placing them in the heating block. When a physical or chemical change in the sample occurred, the voltage output transmitted by the thermocouples was no longer zero and the differential temperature signal (ΔT was plotted against the environmental

temperature (T) measured by the other thermocouple, through a reference ice junction temperature compensator.

Stanton Redcroft DTA 674 mainly comprised the temperature programmer, a head assembly and an amplifier. Temperature sensing was by means of a compact platinum resistance sensor (50 ohm resistance at 273K) mounted in the heater assembly. The head assembly consisted of sample platforms, heater and cooling assembly, outer jacket and flowmeters. The sample platform had two small flat metal bases on which sample and reference dishes rested in good thermal contact. The amplifier had a stable amplification obtained by an input chopper consisting of four insulated transistors in a bridge configuration, an a.c. amplifier, a demodulator and a d.c. amplifier to give a 10 mv output for a potential recorder.

Small amounts of sample were placed in the dish and after selecting and setting the required mode, the apparatus was switched on. Temperature (T) was recorded from the sample thermocouple via the ice cold junction while the differential temperature (Δ T) reached the recorder via the amplifier in the form of repeat signals to give exothermic and endothermic peaks.

The operating conditions used are summarised in Table 2.4.

2.3.3.2.3. Differential Scanning Calorimetry (DSC)

(a) Introduction

Differential scanning calorimetry (DSC) measures the differential energy needed to maintain both sample and reference at the same temperature as a function of temperature when both are heated (or cooled) at a uniform controlled rate, so this technique is closely related to DTA. Two separate electric heaters supply heat to the sample and reference materials

Table 2.4.

Operation	Du Pont 900/500	Stanton Redcroft DTA674
Sample height	5-6 mm	-
Sample weight	-	10-15 mg
Holder	quartz tube	Pt crucible
Thermocouple	Pt:Pt/Rh 13%	Pt:Pt/Rh 13%
Reference Material	α -alumina	α -alumina
Atmosphere	air	nitrogen
Flow rate	50 cm^3 min^{-1}	100 cm^3 min^{-1}
Heating rate	10 K min^{-1}	10K min^{-1}
Sensitivity	-	20 kv
Chart Speed	-	12 cm kv^{-1}
T scale	50 K/in	-
Δ T scale	1K/in	-
Chart Recorder	-	Servoscribe 220

and the heat flow required to sustain a null temperature difference (T_S-T_R = 0) is recorded as a function of temperature (or time). The environment of the sample and heater holders is 'passive' and no energy flow except from the heater, is possible. Out of the two separate circuits one controls the average temperature while the other control circuit corrects any temperature difference between the reference and the sample. For the same material, DSC curve is approximately similar to DTA curve in

position and shape but peaks have opposite directions, an endothermic peak being expressed as a positive DSC peak ($^{dH}/dt$ for endothermic process is positive). The differential scanning calorimeters are more sensitive than DTA instruments and the heat flow is measured directly in DSC, thus DSC can be used to observe reaction in a detailed manner. In DTA, the transition of the sample results in liberation or absorption of energy with an equivalent deviation of its temperature from that of the reference. The resulting record of ΔT versus T gives the information about the nature (endothermic or exothermic) and the temperature of the transition. On the other hand, in DSC, when a sample undergoes a transition, thermal energy is added or subtracted from the sample or the reference holders, to maintian both sample and reference material at the same temperature. Since the input energy is equivalent to the energy absorbed or evolved, in a particular transition, so a recording of this balancing energy yields a direct calorimetric measurement of the transition energy. DSC is also preferable to DTA for obtaining kinetic data since it provides a plot of $^{dH}/dT$, rather than ΔT versus T.

(b) Procedure

A Du Pont 910 Differential Scanning Calorimeter in conjunction with the 990 Thermal Analyzer was used for DSC measurements. Two aluminium pans (in which one was used as a sample holder and the other as a reference) were placed in the cell of the 910 DSC head assembly. The cell was heated linearly at 10K min^{-1} and the difference single ($^{\Delta H}/dt$) was recorded on the recorder of the 990 Thermal Analyzer. The initiation point for a phase change or any chemical reaction on the thermogram is the point at which the curve first deviates from the base line. When the transition is complete, thermal diffusion brings the sample back to equilibrium quickly and the peak (minimum or maximum) temperature is the temperature at which

the reaction is completed. The operating conditions used for DSC runs are given in Table 2.5.

Table 2.5.

Operation	Du Pont DSC 910/990
Weight of sample	20 mg
Atmosphere	air and nitrogen (Duplicate)
Heating rate	10K min^{-1}
Reference	empty aluminium pan
Temperature region	0 - 500 K
T scale	25K cm^{-1}
Δ E scale	20 mv cm^{-1}
Starting temperature	room temperature

2.3.3.3. X-ray Powder Diffraction Analysis

X-ray diffraction measurements (§ 2.2.3.3) were made on the prepared zeolite samples in four different ways, *viz:* in the hydrated forms, after activation under air atmosphere, after activation under nitrogen atmosphere and finally after the oxidation of methane experiments, in order to find out the structure-stability and the crystallinity of these cation exchanged forms, and the effect of activation methods on them.

The apparatus consisted of a Philips X-ray diffractiometer set PW 1051 including an X-ray generator type 1010 coupled to a scintillation counter

and an automatic chart recorder to produce diffractograms of intensity (I) versus angle of diffraction '2θ'. The data obtained was used to calculate interplanar crystal 'd' spacings by applying the Bragg's relation, while the intensities were assessed by visual comparison of each line against the most intense line of mordenites.

The operating conditions used are listed in Table 2.6.

Table 2.6.

Target used	Cu Kα
Wave length (λ)	1.542$\overset{o}{A}$
High voltage (HV)	1650 V.
Tube current (TC)	14 mA
Time constant	4
Chart speed	1600 mm hr^{-1}
Range (2 θ)	$5^o \rightarrow 60^o$
Rate	2^o min^{-1}

2.3.4. Catalytic Activity Studies of the Catalyst Towards Methane Oxidation

2.3.4.1. The Integrated Flow System

When studying porous catalysts in experimental reactors, the effects of mass and heat transfer must be considered. Mass and heat transfer effects

in catalytic beds and the role of diffusion in catalysis have been outlined by Watson[265] and Satterfield[266]. Gas phase mass transfer is essentially of two types, one involving diffusion of molecules (reactants, intermediates, products) to and from the catalyst particle from the bulk gas phase through a boundary layer, while the other involves diffusion into and out of the pores. Either can affect the overall rate of reaction and, in the extreme, be rate determining. Similarly, heat arising from the catalytic reactions can cause either overheating or cooling of the catalyst if its rate of heat transfer is too low. Thus for meaningful results, the experimental reactor must operate under conditions that minimise these effects. In an ideal case, the catalyst bed should be isothermal, with mass and heat transfer processes being rapid compared with the rates of both reaction and heat generation. Anderson[268] has outlined various types of experimental reactors.

The flow system used for the work described here was a copper and glass system based on the integral plug-flow model (§1.5.11), operating at atmospheric pressure and employing tubular flow-reactor (§ 1.5.11). In the tubular-flow reactor used (fig. 2.2), the feed enters one end of a cylindrical tube (through a thin capillary). The catalyst bed itself was 2 to 3cm long, and the product stream leaves the opposite end. Since the catalyst bed is short and compact, the chances of overheating caused by poor heat transfer are minimal. In addition, the reactor was placed in an isothermal plateau within the air-bath which minimised any axial temperature gradient. The flow-rate was self-controlled and the carrier gas used provided an inert atmosphere as diluent, so mass and heat transfer was rapid compared with rates of reaction.

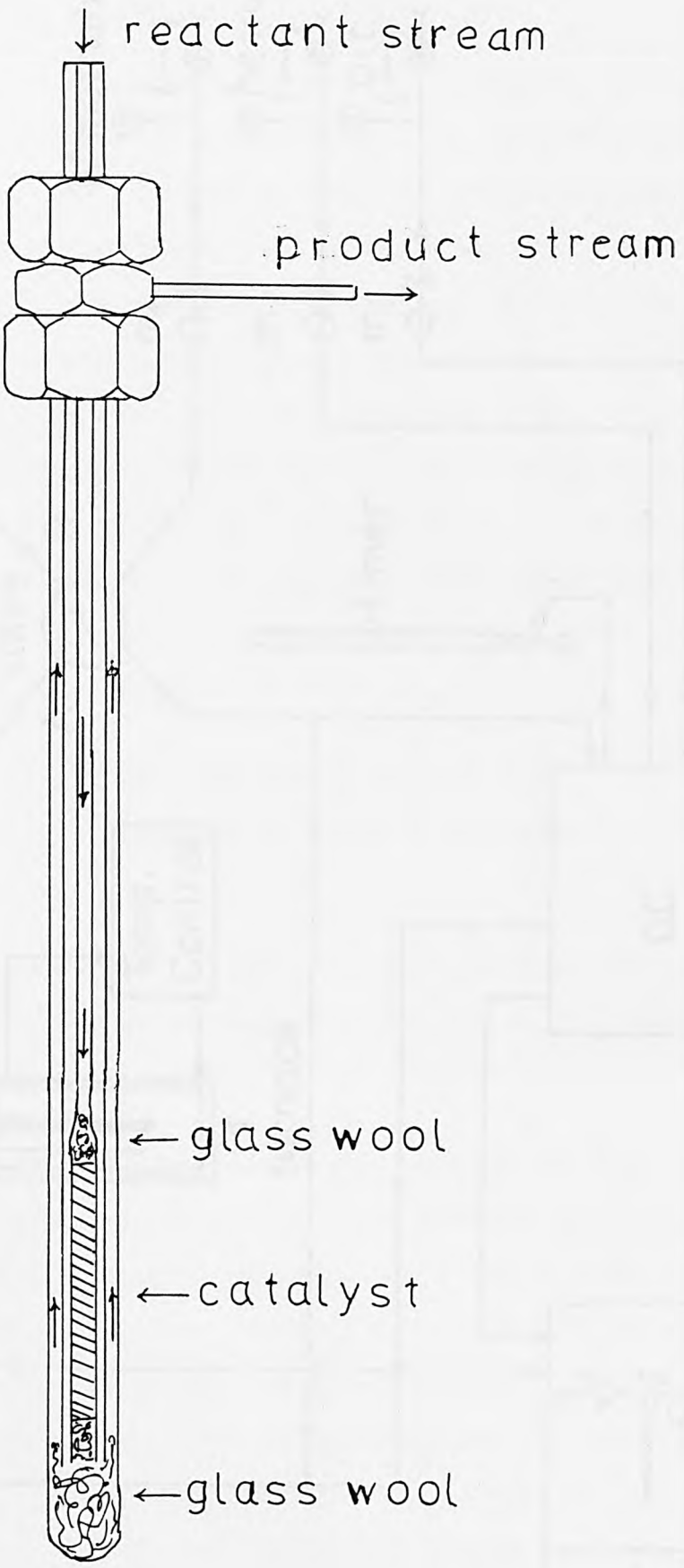

Fig. 2·2 TUBULAR FLOW REACTOR

Fig.2-3 THE CATALYTIC RIG

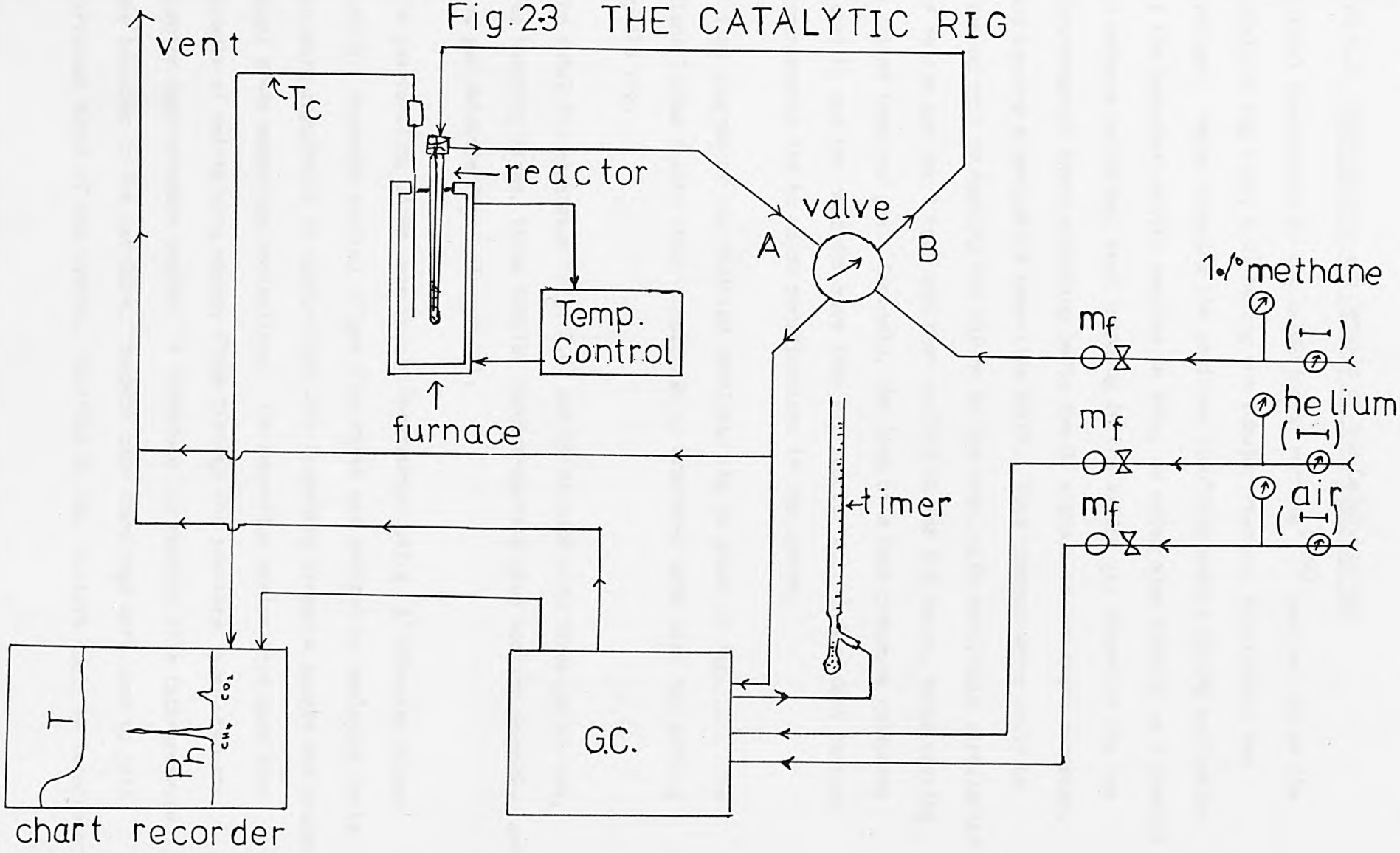

2.3.4.2. Modification and Details of the Catalytic Rig.

Initial experiments on the oxidation of methane[166] carried out on the catalytic rig (fig. 2.3) having one tubular reactor, highlighted two problems. Water escaping the cavities (zeolitic water) during activation of the hydrated zeolite samples *in situ*, or water also forming as a product of methane oxidation, kept trapping in the silica gel column of the gas chromatograph hence affecting badly the GC signals to the chart recorder, and causing a cumulative base-line shift. This trapped water could be removed only by heating the column in the oven, with continuous circulation of helium gas for 1 hour and then cooling it for 4-5 hours, hence wasting a lot of time and gas. Secondly, the lack of a back-pressure measuring facility and the need for more than one reactor with independent heating arrangements led to major modifications in the system.

A flow diagram of the modified catalytic rig is given in fig. 2.4. The items listed (with their suppliers in brackets) were used for setting up the rig.

The catalytic apparatus (fig. 2.4) can be divided into three parts, *viz*, gas handling lines, three tubular reactor-systems plus heating assembly, and the gas detection/analysis network.

The gas-handling lines were mainly constructed using $\frac{1}{8}$" diameter copper tubing. Accurate control of gas flow-rates was ensured by employing Watts pressure regulators in conjunction with Budenberg pressure gauges and Brooks model 8744A mass-flow controllers. The mass-flow controllers were also capable of maintaining steady flows through the reactors, even when the reactor back-pressure varied. A transducer to measure this back-pressure was included in the gas-line. Swagelok pipe couplings were used to join different parts of the system. Gas-flow to the reactors could be terminated,

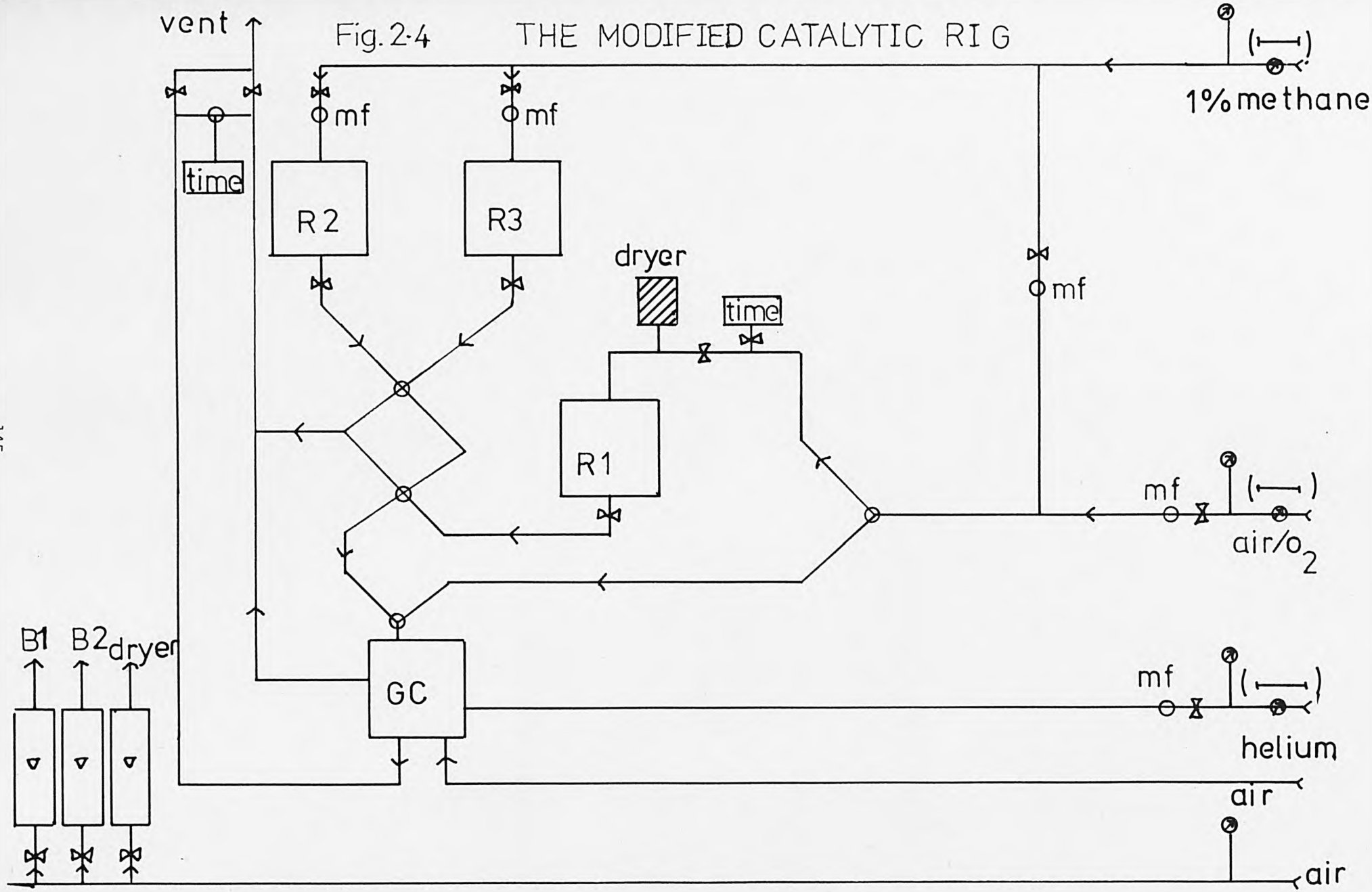
vent
Fig. 2-4 THE MODIFIED CATALYTIC RIG
1% methane
mf
mf
time
R2
R3
dryer
time
mf
R1
mf
air/O_2
B1
B2
dryer
GC
mf
helium
air
air

Table 2.**7.**

Quantity	Item	Suppliers
3	Watts pressure regulators	Watts Regulators Ltd
6	Hoke two-way needle valves (3700 series, panel mounted 1/28" gyrolok)	Hoke International Ltd.
5	Mass-flow controllers model 8744A	Brooks Instruments Ltd.
4	Budenberg Pressure gauges (0-30 psi)	Budenberg Ltd.
3	Hoke 3-way ball valves (brass, 500 psi, $\frac{1}{8}$" gyrolok)	Hoke International Ltd.
5	Toggle 3-way valves	-
2	Rotameter with needle valves (0-50 dm^3 min^{-1})	Rotameter Ltd. England
2	Four way valves	Scientific Instruments Ltd.
5	Chromel-Alumel thermocouples (type K, 4m & 3m leads)	Lab. Facility Ltd.
1	Pressure transducer	Bell & Howell Ltd.
2	Molecular sieve 5A column	B.D.H.
2	Calcined $CaCl_2$ drying columns	B.D.H.
1	Union Cross ($\frac{1}{8}$" brass)	Phase Separation Ltd.
13	Union Tees ($\frac{1}{8}$" brass)	"
10	Swagelok coupling ($\frac{1}{8}$" brass)	"
50	Front & back ferrules	"
2	Reducing Unions ($\frac{1}{8}$"brass)	
3	Pyrex glass reactors	Fissons
2	Soap air bubblers (0-50 dm^3)	"

Table 2.7. (continued)

Quantity	Item	Suppliers
1	Electric furnace attached to a resistance thermometer controller and power regulator.	Assoc. Electrical Ind.
1	Six point electric switch box	-
1	Stanton Redcroft cylindrical furnace coupled to Eurotherm controller	Stanton Redcroft
1	Taylor Servomex GC system with an air circulating oven type A.0221	Taylor Servomex Sybron Corporation
1	Katharometer control unit MK158	Servomex
1	Temperature controller T.C.201	"
1	Sampling automatic solenoid valve	Taylor Servomex
2	Dewar ice flasks	Thermos
1	Dual channel chart recorder CR 600 with an integrator	J.J. Lloyd Instruments Limited.
1	Poropak Q-S GC column (half metre long)	—

if required, at any stage during the experimentwith the help of three toggle valves on the gas-line near the reactors. Gas distribution to the three reactors was controlled by an assembly of a Union Cross, three Hoke 2-way valves and two Scientific Instrument 4-way valves. Three Hoke 2-way valve assemblies provided independently a facility of either letting gas-flow to the reactors (products subsequently coming out of the GC were passed through gas bubbles in order to measure the rate of flow of the products) or of by-passing the gas from the reactors to analyse the feed by GC, and then measuring the rate of flow of the feed. Silicone O-rings

of 3/16" diameter (Alltech Associates) and PTFE sealing tape (Fisons) was used for all glass-to-copper joints, and leaks were tested using soap solution. A drying column containing calcined $CaCl_2$ between glass wool plugs was inserted between the reactors and GC to trap the water molecules which escaped during activation of the zeolite or which were formed in the catalytic reaction, and these had to be replaced by fresh drying material quite frequently. Two molecular sieve 5A columns were attached at the end of the gas lines to absorb any harmful CO formed, before letting the products to vent.

Concerning the three reactor-systems, each one (fig. **2.2**) consisted of a tubular reactor made of ~32mm long Pyrex capillary tubing (internal diameter ~4mm and external diameter <7mm) placed in a ~27mm long Pyrex tube of ~ 12mm diameter. Reactor-system 1 was heated independently in a Stanton Redcroft elecric furnace attached to a Stanton Redcroft Eurotherm controller while reactor systems 2 and 3 were heated in an AEI electric furnace which was coupled to a power regulator and a resistance thermometer controller. Temperature profiles of the individual reactor were followed by three separate chromel-alumel thermocouples in Pyrex glass holders placed in 'plateau' regions, at a height in the catalyst bed close to the reactor positions, and these temperatures were monitored on the dual channel CR 600 chart recorder via a 6-point electric switch-box. This facilitated selective recording of any reactions. Thermocouples were calibrated against a fourth thermocouple which was placed in an ice/water mixture as reference.

Gas samples from the product or reactant streams were taken by means of an automatic solenoid valve and were analysed using a Taylor Servomex gas chromatograph. The automatic solenoid valve was operated by air supplied

from a compressed air cylinder. Gas detection was be means of a Servomex microkatharometer MK 158, bridge network (to control the potential sensitivity across the detector) and a dual channel J.J. Lloyd CR600 chart recorder with analogue integrator. A half metre long separating column (Poropak Q-S) was employed using helium as the carrier gas. Product streams from three reactors could be directed through the GC one at a time by suitably adjusting two Scientific Instruments 4-way valves A and B, to the positions given in Table 2.8, (see also fig.2.4).

Table 2.8.

Direction of reactor			Position of Valve	
R1	R2	R3	A	B
GC	V	V	→	←
V	GC	V	←	←
V	V	GC	←	→
GC	V	V	→	→

GC = Gass Chromatograph, V = vent

Vertical position of valves (⇅) denoted by '→' and

Horizontal position (⇄) denoted by '←'

2.3.4.3. Gases

Cylinders of air, nitrogen and helium supplied by B.O.C., were of the purest grade available. For the oxidation experiments, cylinders of 1% methane in air or 1% methane in nitrogen were of research grade, also supplied by B.O.C. Trace hydrocarbons were not detected when analyzed

chromatographically.

2.3.4.4. Operation of the Catalytic System

The catalyst beds were prepared by accurately weighing out ~ 0.25 g of the catalyst, then lightly pressurising the powder into a 4mm inner diameter Pyrex glass tubular reactor between pads of silica glass wool. The catalyst bed length was maintained between 25-30 mm in all cases. Since methods of activation affect the catalytic properties, the catalysts were either activated under air or under a nitrogen atmosphere. The activation of the catalyst was accomplished by passing a stream of a gas (say 1% CH_4 in air, for activation under air) in dynamic flow conditions over the catalyst bed for 12 - 16 hours at 723K. This procedure not only dehydrated the catalyst, but had the additional effect of removing the ammonium ion as ammonia, yielding either mixed metal/H-mordenite catalysts, or, in the case of ammonium mordenite, the corresponding hydrogen mordenite. Under any given set of reaction conditions, samples of reactant (feed) or product stream for a range of temperatures were taken by automatic solenoid valve for analysis by gas chromatography. Normally, a temperature was selected and the sample analysed by GC and microkatharometer bridge network for reproducible methane and carbon dioxide peaks on the chart recorder at 1 mv sensitivity. Then the reaction temperature was increased gradually in 10-15 K increments. On obtaining a stable temperature (indicated by the temperature profile) a new sample was taken for analysis by GC. This was repeated until 100% conversion of reactant (methane) was obtained, as indicated by the disappearance of the CH_4 peak altogether, or when 823K was obtained, whichever occurred first. At temperatures greater than 823K, the glass wool began to melt out and the reactor softened and deformed. Due to the back-off facility on the chart recorder, CR600, high temperature could also be measured easily on a 10 mv scale. The peak

heights of CH_4 or CO_2 were used as a measure of the extent of reaction. The conversion of methane (α) was found by comparing the methane peak in the product stream with that observed in the feed. In some cases, life tests were also undertaken with the catalyst continuously operating under one set of reaction conditions for at least one week; no significant change in conversion (α) and hence activity, was taken to indicate catalytic stability of the catalysts.

CHAPTER THREE

RESULTS

3.1. INTRODUCTION

The analytical data for the zeolites (§2.2.2 & §2.3.2.) the surface area measurements, thermal and X-ray studies and the corresponding catalysis data, are summarised in table form in appendices (I-III). The relevant computer programs are given in appendix IV.

3.2. ANALYSES OF ZEOLITES

The oxide and unit cell compositions of the zeolite samples are summarised in table (3.1 -3.4), which are based on the results for the complete analyses of the transition metal-exchanged zeolites given in Appendices Ia and Ib. The difference between the aluminium and total metal content indicative of hydrolysis of the zeolites, is represented by a hydrogen ion content in the unit cell fomulae.

For cases involving amminated zeolites, it was assumed that the difference between the aluminium and metal content of the zeolite was equal to the "ammonium oxide"($(NH_4)_2O$) content of the material. Ammonia complexed to the metal in the zeolite was determined by subtracting the $(NH_4)_2O$ content from the total NH_3/NH_4^+ content as determined by the Kjeldahl method.

The results of the analyses were usually within the normal experimental limits, observed for these analytical methods.

3.3. SURFACE AREAS OF ZEOLITE-A SAMPLES

Monolayer equivalent surface areas of zeolite-A samples (§2.2.2.) were

Table 3.1 Oxide Formulae of Zeolite-A Samples

Zeolite	Oxide Formula
Na-A	Na_2O . Al_2O . 2.05 SiO_2 . 4.51 H_2O
Ca-A	0.81 CaO . 0.16 Na_2O . Al_2O_3 . 1.99 SiO_2 . 4.83 H_2O
Cu-5A(1)	0.04 CuO . 0.75 CaO . 0.13 Na_2O . Al_2O_3 . 1.98 SiO_2 . 4.76 H_2O
Cu-5A(2)	0.07 CuO . 0.72 CaO . 0.11 Na_2O . Al_2O_3 . 1.96 SiO_2 . 4.88 H_2O
Cu-5A(3)	0.09 CuO . 0.72 CaO . 0.08 Na_2O . Al_2O_3 . 1.98 SiO_2 . 4.91 H_2O
Cu-5A(4)	0.10 CuO . 0.72 CaO . 0.08 Na_2O . Al_2O_3 . 1.92 SiO_2 . 4.92 H_2O
Cu-5A(5)	0.20 CuO . 0.72 CaO . 0.05 Na_2O . Al_2O_3 . 1.90 SiO_2 . 5.04 H_2O
Cu-5A(6)	0.24 CuO . 0.59 CaO . 0.04 Na_2O . Al_2O_3 . 1.89 SiO_2 . 5.16 H_2O
Co-5A(1)	0.06 CoO . 0.79 CaO . 0.14 Na_2O . Al_2O_3 . 2.03 SiO_2 . 4.82 H_2O
Co-5A(2)	0.08 CoO . 0.11 Na_2O . 0.76 CaO . Al_2O_3 . 1.99 SiO_2 . 4.87 H_2O
Co-5A(3)	0.11 CoO . 0.73 CaO . 0.09 Na_2O . Al_2O_3 . 1.98 SiO_2 . 4.91 H_2O
Co-5A(4)	0.14 CoO . 0.72 CaO . 0.11 Na_2O . Al_2O_3 . 1.98 SiO_2 . 4.93 H_2O
Co-5A(5)	0.36 CoO . 0.56 CaO . 0.05 Na_2O . Al_2O_3 . 1.99 SiO_2 . 5.21 H_2O
Co-5A(6)	0.51 CoO . 0.41 CaO . 0.03 Na_2O . Al_2O_3 . 1.91 SiO_2 . 5.49 H_2O

Table 3.2 Unit Cell Compositions of Zeolite-A Samples

Zeolite		Unit Cell Composition
Na-A	:	$Na_{11.88}[(AlO_2)_{11.88} \cdot (SiO_2)_{12.12}] \cdot 26.7\ H_2O$
Ca-A	:	$Ca_{4.88} \cdot Na_{1.93} \cdot H_{0.34} \cdot [(AlO_2)_{12.03} \cdot (SiO_2)_{11.97}] \cdot 29.04\ H_2O$
Cu-5A(1)	:	$Cu_{0.24} \cdot Ca_{4.54} \cdot Na_{1.6} \cdot H_{0.92} \cdot [(AlO_2)_{12.06} \cdot (SiO_2)_{11.94}] \cdot 28.70\ H_2O$
Cu-5A(2)	:	$Cu_{0.39} \cdot Ca_{4.35} \cdot Na_{1.28} \cdot H_{1.36} \cdot [(AlO_2)_{12.12} \cdot (SiO_2)_{11.88}] \cdot 29.58\ H_2O$
Cu-5A(3)	:	$Cu_{0.54} \cdot Ca_{4.35} \cdot Na_{0.98} \cdot H_{1.32} \cdot [(AlO_2)_{12.06} \cdot (SiO_2)_{11.94}) \cdot 29.62\ H_2O$
Cu-5A(4)	:	$Cu_{0.58} \cdot Ca_{4.45} \cdot Na_{1.06} \cdot H_{1.12} \cdot [(AlO_2)_{12.24} \cdot (SiO_2)_{11.76}] \cdot 30.07\ H_2O$
Cu-5A(5)	:	$Cu_{1.21} \cdot Ca_{4.4} \cdot Na_{0.57} \cdot H_{0.55} \cdot [(AlO_2)_{12.34} \cdot (SiO_2)_{11.69}] \cdot 31\ H_2O$
Cu-5A(6)	:	$Cu_{1.49} \cdot Ca_{3.63} \cdot Na_{0.47} \cdot H_{1.6} \cdot [(AlO_2)_{12.31} \cdot (SiO_2)_{11.69}] \cdot 31.77\ H_2O$
Co-5A(1)	:	$Co_{0.36} \cdot Ca_{4.71} \cdot Na_{1.67} \cdot H_{0.10} \cdot [(AlO_2)_{11.91} \cdot (SiO_2)_{12.09}] \cdot 28.71\ H_2O$
Co-5A(2)	:	$Co_{0.45} \cdot Ca_{4.57} \cdot Na_{1.33} \cdot H_{0.66} \cdot [(AlO_2)_{12.03} \cdot (SiO_2)_{11.97}] \cdot 29.3\ H_2O$
Co-5A(3)	:	$Co_{0.68} \cdot Ca_{4.39} \cdot Na_{1.12} \cdot H_{0.8} \cdot [(AlO_2)_{12.06} \cdot (SiO_2)_{11.94}] \cdot 29.61\ H_2O$
Co-5A(4)	:	$Co_{0.82} \cdot Ca_{4.30} \cdot Na_{1.32} \cdot H_{0.47} \cdot [(AlO_2)_{12.03} \cdot (SiO_2)_{11.97}] \cdot 29.65\ H_2O$
Co-5A(5)	:	$Co_{2.17} \cdot Ca_{3.33} \cdot Na_{0.30} \cdot H_{0.43} \cdot [(AlO_2)_{12.03} \cdot (SiO_2)_{11.97}] \cdot 31.34\ H_2O$
Co-5A(6)	:	$Co_{3.13} \cdot Ca_{2.52} \cdot Na_{0.41} \cdot H_{0.56} \cdot [(AlO_2)_{12.27} \cdot (SiO_2)_{11.73}] \cdot 33.7\ H_2$

Table 3.3 : Oxide Formulae of Mordenite Samples

Zeolite :	Oxide Formula
Na-MOR	0.99 Na_2O . Al_2O_3 . 11.22 SiO_2 . 7.18 H_2O
NH_4-MOR(1)	0.96 $(NH_4)_2O$. 0.01 Na_2O . Al_2O_3 . 11.31 SiO_2 . 5.65 H_2O
NH_4-MOR(2)	0.94 $(NH_4)_2O$. 0.01 Na_2O . Al_2O_3 . 11.30 SiO_2 . 5.86 H_2O
Ni-NaMOR	0.46 NiO . 0.05 $(NH_4)_2O$. 0.49 Na_2O . Al_2O_3 . 11.48 SiO_2 . 8.62 H_2O
Ni-NH_4MOR	0.38 NiO . 0.58 $(NH_4)_2O$. 0.01 Na_2O . Al_2O_3 . 11.07 SiO_2 . 6.94 H_2O
Ni-MOR(1)	0.32 NiO . 0.52 $(NH_4)_2O$. 0.01 Na_2O . Al_2O_3 . 11.57 SiO_2 . 7.51 H_2O
Ni-MOR(2)	0.40 NiO . 0.54 $(NH_4)_2O$. 0.03 Na_2O . Al_2O_3 . 11 SiO_2 . 7.53 H_2O
Ni-MOR(3)	0.43 NiO . 0.52 $(NH_4)_2O$. 0.03 Na_2O . Al_2O_3 . 11 SiO_2 . 7.45 H_2O
Cu-NH_4MOR	0.61 CuO . 0.39 $(NH_4)_2O$. 0.01 Na_2O . Al_2O_3 . 11.31 SiO_2 . 1.47 NH_3 . 5.96 H_2O
Cu-NaMOR	0.54 CuO . 0.42 $(NH_4)_2O$. 0.04 Na_2O . Al_2O_3 . 11.46 SiO_2 . 1.12 NH_3 . 5.91 H_2O
Cu-MOR(1)	0.57 CuO . 0.43 $(NH_4)_2O$. 0.01 Na_2O . Al_2O_3 . 11.45 SiO_2 . 1.49 NH_3 . 5.65 H_2O
Cu-MOR(2)	0.60 CuO . 0.39 $(NH_4)_2O$. 0.01 Na_2O . Al_2O_3 . 11.09 SiO_2 . 1.42 NH_3 . 5.54 H_2O
Cu-MOR(3)	0.69 CuO . 0.30 $(NH_4)_2O$. 0.01 Na_2O . Al_2O_3 . 11.41 SiO_2 . 1.87 NH_3 . 6.07 H_2O
Pt-MOR(1)	0.54 PtO . 0.24 $(NH_4)_2O$. 0.01 Na_2O . Al_2O_3 . 11.16 SiO_2 . 7.56 H_2O
Pt-MOR(2)	0.58 PtO . 0.24 $(NH_4)_2O$. 0.01 Na_2O . Al_2O_3 . 11.45 SiO_2 . 7.74 H_2O
Pt-MOR(3)	0.70 PtO . 0.09 $(NH_4)_2O$. 0.02 Na_2O . Al_2O_3 . 11.36 SiO_2 . 8.28 H_2O
Pt-MOR(4)	0.50 PtO . 0.28 $(NH_4)_2O$. 0.03 Na_2O . Al_2O_3 . 11.68 SiO_2 . 7.54 H_2O

Table 3.4 : Unit Cell Composition of Mordenite Samples

Na-MOR	:	$Na_{7.3}[(AlO_2)_{7.26}(SiO_2)_{40.74}] \cdot 26.07\ H_2O$
NH_4-MOR(1)	:	$(NH_4)_{6.92} \cdot Na_{0.04} \cdot H_{0.25} \cdot [(AlO_2)_{7.21} \cdot (SiO_2)_{40.79}] \cdot 20.47\ H_2O$
NH_4-MOR(2)	:	$(NH_4)_{6.74} \cdot Na_{0.09} \cdot H_{0.4} \cdot [(AlO_2)_{7.23} \cdot (SiO_2)_{40.77}] \cdot 21.14\ H_2O$
Ni-NaMOR	:	$Ni_{1.64} \cdot (NH_4)_{0.36} \cdot Na_{3.49} \cdot [(AlO_2)_{7.12} \cdot (SiO_2)_{40.88}] \cdot 30.69\ H_2O$.
Ni-NH_4MOR	:	$Ni_{1.4} \cdot Na_{0.04} \cdot (NH_4)_{4.26} \cdot H_{0.25}[(AlO_2)_{7.35} \cdot (SiO_2)_{40.66}] \cdot 25.5\ H_2O$.
Ni-MOR(1)	:	$Ni_{1.13} \cdot (NH_4)_{3.68} \cdot Na_{0.06} \cdot H_{1.07} \cdot [(AlO_2)_{7.07} \cdot (SiO_2)_{40.93}] \cdot 26.57\ H_2O$
Ni-MOR(2)	:	$Ni_{1.49} \cdot (NH_4)3.96 \cdot Na_{0.21} \cdot H_{0.23} \cdot [(AlO_2).38 \cdot (SiO_2)_{40.62}] \cdot 27.8\ H_2O$
Ni-MOR(3)	:	$Ni_{1.59} \cdot (NH_4)_{3.84} \cdot Na_{0.22} \cdot H_{0.15} \cdot [(AlO_2)_{7.39} \cdot (SiO_2)_{40.62}] \cdot 27.55\ H_2O$.
Cu-NH_4MOR	:	$Cu_{2.2} \cdot (NH_4)_{2.81} \cdot Na_{0.02} \cdot [(AlO_2)_{7.22} \cdot (SiO_2)_{40.78}] \cdot 5.31\ NH_3 \cdot 21.49\ H_2O$
Cu-NaMOR	:	$Cu_{1.93} \cdot (NH_4)_{3.0} \cdot Na_{0.3} \cdot [(AlO_2)_{7.13} \cdot (SiO_2)_{40.87}] \cdot 4NH_3 \cdot 21.08\ H_2O$
Cu-MOR(1)	:	$Cu_{2.03} \cdot (NH_4)_{3.06} \cdot Na_{0.03} \cdot [(AlO_2)_{7.14} \cdot (SiO_2)_{40.86}] \cdot 5.32\ NH_3 \cdot 20.16\ H_2O$
Cu-MOR(2)	:	$Cu_{2.2} \cdot (NH_4)_{2.85} \cdot Na_{0.08} \cdot [(AlO_2)_{7.33} \cdot (SiO_2)_{40.67}] \cdot 5.21\ NH_3 \cdot 20.32\ H_2O$
Cu-MOR(3)	:	$Cu_{2.47} \cdot (NH_4)_{2.15} \cdot Na_{0.05} \cdot [(AlO_2)_{7.16} \cdot (SiO_2)_{40.84}] \cdot 6.7\ NH_3 \cdot 21.72\ H_2O$
Pt-MOR(1)	:	$Pt_{1.97} \cdot (NH_4)_{1.75} \cdot Na_{0.07} \cdot H_{1.54}[(AlO_2)_{7.3} \cdot (SiO_2)_{40.71}] \cdot 27.6\ H_2O$
Pt-MOR(2)	:	$Pt_{2.07} \cdot (NH_4)_{1.71} \cdot Na_{0.07} \cdot H_{1.22}[(AlO_2)_{7.14} \cdot (SiO_2)_{40.86}] \cdot 27.64\ H_2O$.
Pt-MOR(3)	:	$Pt_{2.52} \cdot (NH_4)_{0.65} \cdot Na_{0.14} \cdot H_{1.36}[(AlO_2)_{7.19} \cdot (SiO_2)_{40.81}] \cdot 29.75\ H_2O$.
Pt-MOR(4)	:	$Pt_{1.76} \cdot (NH_4)_{1.97} \cdot Na_{0.21} \cdot H_{1.32}[(AlO_2)_{7.02} \cdot (SiO_2)_{40.98}] \cdot 26.45\ H_2O$

measured by a volumetric method (§2.2.3.2.2.), using krypton as an adsorbent at 77K, after outgassing samples in vacuum ($\sim 10^{-6}$mmHg) at 393, 623 and ∿950K for 6 hours. At 393K the sample partially dehydrates, while at 623K all the pores become available for adsorption after complete dehydration. The last temperature (∿950K) denotes the maximum temperature to which samples were exposed during the nitrous oxide deocmposition reaction and this therefore varied somewhat for each sample.

The total volume of Kr adsorbed at N.T.P. was then plotted against P/Po (P being equilibrium pressure and Po, the saturation pressure of Kr at 77K = ∿ 2mmHg). The usual 'Point B Method' was used to obtain the value of the monolayer saturation volume (Vm), by extrapolating the linear section of the isotherm to zero pressure. Surface areas of each sample were then calculated from the relationship

$$(S.A) = \frac{Vm}{2214} .N.\delta.10^{-20} \qquad .....(3.1.)$$

where (S.A) is the specific surface area expressed in m^2g^{-1}, Vm is the volume (cm^3 at N.T.P.) of Kr adsorbed per g of the zeolite, N is the Avogadro constant ($6.023x10^{23}$ mol^{-1}) and δ is the effective area of cross section of Kr molecule ($19.5x10^{-20}m^2$).

Figures 3.1 and 3.2 show representative point B isotherms for Cu-5A(3) and Co-5A(3).

The surface area values were calculated also using a computer program based on the 'Point A' and 'Point B' methods. These surface area values usually matched ones which had been estimated earlier from the isotherms. Computed values will be used in further references.

Table 3.5 summarises the results of surface area measurements. Symbols A,B_1 denote computer calculated 'Point A' and 'Point B' methods while

Table 3.5 : Surface Areas ($m^2.g^{-1}$) of Zeolite A Samples

Zeolites	S.A. at 393K/$m^2.g^{-1}$			S.A. at 623K/$m^2.g^{-1}$			Max Temp. /K	S.A./$m^2.g^{-1}$		
	A	B1	B2	A	B1	B2		A	B1	B2
Co-5A(1)	486.79	520.85	438.40	566.22	571.69	572.84	1001	516.43	518.85	566.99
Co-5A(2)	393.68	407.40	401.52	513.79	516.71	522.92	966	427.35	427.82	513.58
Co-5A(3)	391.75	399.82	391.09	483.30	468.94	482.70	956	465.07	468.22	476.15
Co-5A(4)	284.21	284.77	288.88	438.38	439.58	495.70	963	491.61	498.13	466.67
Co-5A(5)	277.17	291.72	295.50	394.62	400.41	412.94	921	343.48	344.76	392.58
Co-5A(6)	302.84	319.24	252.80	353.92	364.89	378.09	933	349.63	349.63	353.93
Cu-5A(1)	502.10	502.85	511.74	535.17	538.02	538.02	979	512.39	559.58	507.57
Cu-5A(2)	497.13	531.16	522.55	516.86	517.81	542.22	983	514.59	518.25	504.26
Cu-5A(3)	485.19	489.57	493.60	497.26	516.31	510.06	993	423.14	479.64	504.58
Cu-5A(4)	421.71	423.73	437.35	489.07	491.04	501.96	947	463.87	465.20	477.10
Cu-5A(5)	442.11	444.25	446.52	488.92	493.15	491.55	977	479.33	481.88	486.59
Cu-5A(6)	435.73	436.25	440.88	482.08	500.89	497.77	968	434.46	441.53	445.62

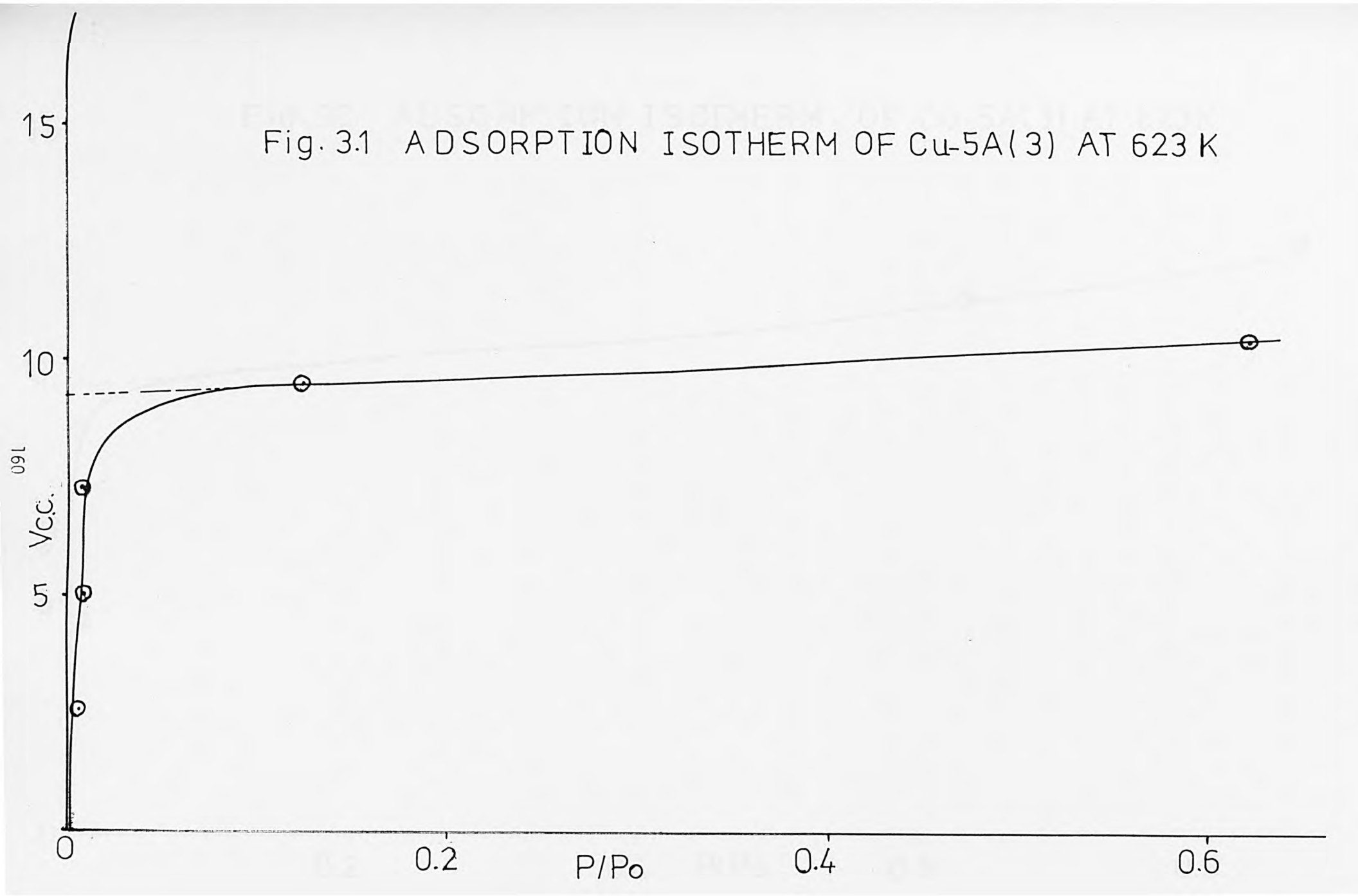
Fig. 3.1 ADSORPTION ISOTHERM OF Cu-5A(3) AT 623 K
15
10
5
0
Vc.c.
160
0.2
P/Po
0.4
0.6

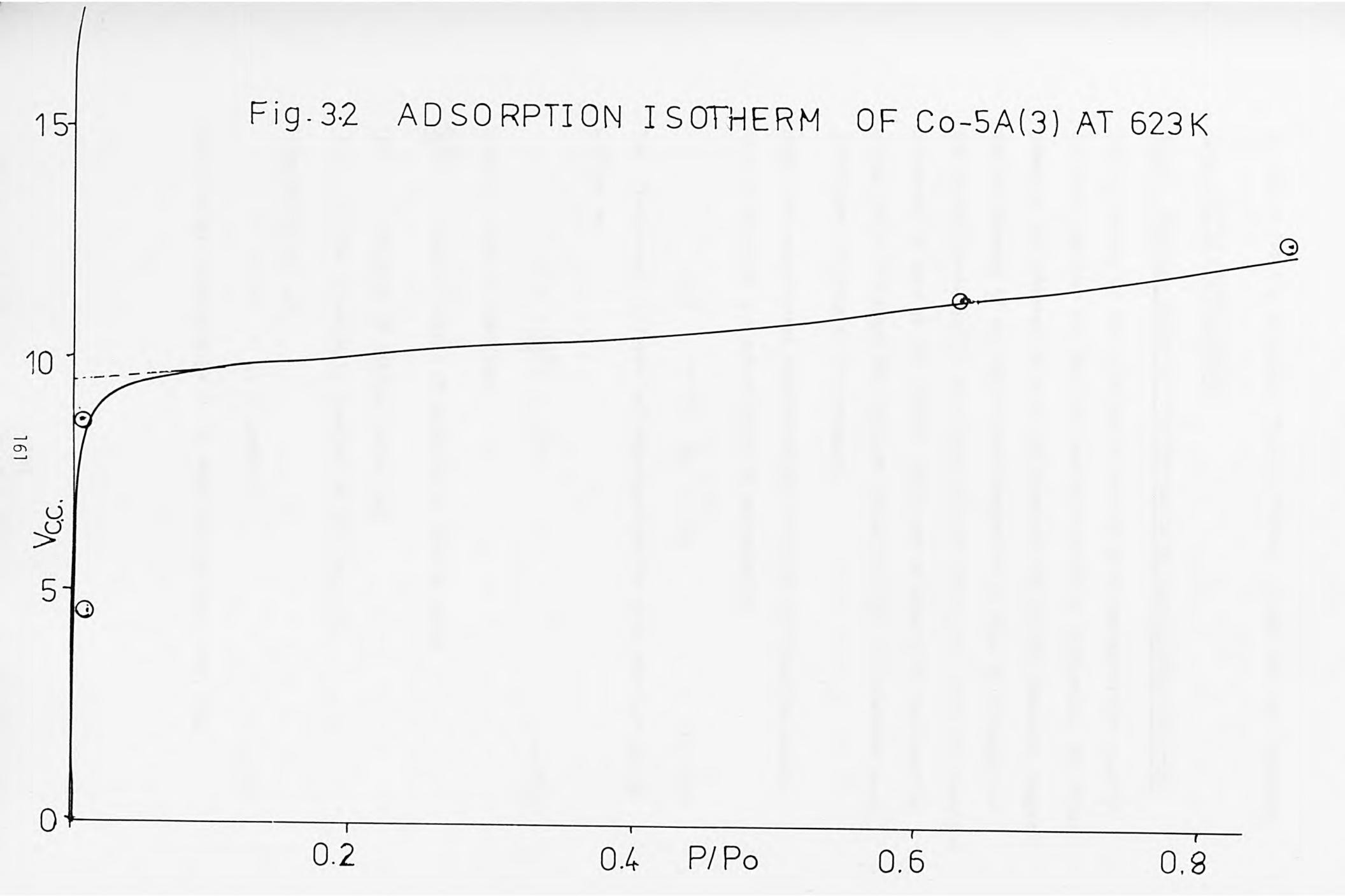
Fig. 3.2 ADSORPTION ISOTHERM OF Co-5A(3) AT 623K
15
10
5
0
Vc.c.
0.2
0.4
P/Po
0.6
0.8

B_2 stands for the estimated 'Point B Method' values from the isotherms.

3.4. STATIC SYSTEM STUDIES

3.4.1. Reaction Rates for the Nitrous Oxide Decomposition Reaction

During studies of the kinetics of nitrous oxide decomposition reaction (§2.2.4) whenever the reaction was carried out to completion, the final pressure was observed to be ∿ 1.5 times of the initial pressure, suggesting the absence of any significant adsorption of N_2O, N_2 or oxygen on the transition-metal(II) exchanged zeolites (§2.2.2.). Also the reaction proceeded as soon as the nitrous oxide was released into the reaction vessel which contained the catalyst (§2.2.3.2.3.2.) as indicated by a consequent increase in the pressure.

Under the experimental conditions the catalysed dissociative adsorption to products can conveniently be expressed as

$$N_2O \longrightarrow N_2 + \tfrac{1}{2} O_2 \qquad .....3.2.$$

The first-order differential rate equation for this reaction can be written as

$$r = -\frac{d(P)}{dt} = k(P) \qquad .....3.3.$$

where r = rate of reaction,

$\frac{d(P)}{dt}$ = rate of change of pressure of nitrous oxide

(P) = pressure of nitrous oxide, and

k = rate or velocity constant of the reaction.

Integrating eq. 3.3,

$$-\ln(P) = kt + \text{constant} \qquad .....3.4.$$

With initial conditions of t = 0, P=Po and for t=t, P=Pt, then

$$\ln \frac{(Po)}{(Pt)} = kt \qquad .....3.5$$

For the reaction $N_2O \rightarrow N_2 + \frac{1}{2} O_2$, the total pressure P is the sum of all the partial pressures:

$$P = P_{(N_2O)} + P_{(N_2)} + P_{(O_2)} \qquad .....3.6.$$

where P is total pressure in the system while $P_{(N_2O)}$, $P_{(N_2)}$ and $P_{(O_2)}$ represent the individual partial pressures of N_2O, N_2 and O_2 respectively.

Let x be decrease in N_2O pressure at any time t.

Then $Pt = P_{(N_2O)} = (Po-x)$ .....3.7.

$$P_{(N_2)} = x \qquad .....3.8.$$

and $P_{(O_2)} = \frac{1}{2}x$ .....3.9.

Inserting these values into eq. 3.6. gives

$$P = (Po - x) + x + \tfrac{1}{2}x \qquad .....3.10.$$

or $x = 2(P-Po)$ .....3.11.

Combining eqns. 3.7. and 3.11

$$Pt = Po - 2(P-Po)$$

or $Pt = 3Po - 2P$ .....3.12.

Similarly, from eqn.3.5 and 3.12 we obtain

$$kt = \ln \frac{Po}{(3Po-2P)} \qquad .....3.13.$$

as a final first order rate equation for the catalytic decomposition of N_2O.

For convenience, the total pressure P is termed as Pt, so

$$kt = \ln \frac{Po}{(3Po-2Pt)} \qquad .....3.14.$$

For simplicity $\ln \frac{Po}{(3Po-2Pt)}$ is termed as the Q_1 factor, where 1 denotes first order reaction.

$$Q_1 = \ln \frac{Po}{(3Po-2Pt)} \qquad .....3.15.$$

For a first order fit, a plot of Q_1 versus t(s) should give a straight line of positive slope, $k(s^{-1})$.

The rate equations for other orders ($\frac{1}{2}$, $\frac{3}{2}$ and 2) can also be derived similarly, as summarised below.

Half Order

For a $\frac{1}{2}$ order, the general integral equation for rate constant is [302],

$$k = \frac{2}{t} \left(\sqrt{a_o} - \sqrt{a_o - x} \right),$$

which for N_2O decomposition reaction yields

$$kt = 2\left(\sqrt{Po} - \sqrt{(3Po - 2Pt)}\right)$$

or

$$Q_{\frac{1}{2}} = 2\left(\sqrt{Po} - \sqrt{(3Po - 2Pt)}\right) \qquad .....3.16.$$

where Pt is the total pressure at time t, and $Q_{\frac{1}{2}}$ is the Q factor for the $\frac{1}{2}$ order reaction.

Thus a plot of $Q_{\frac{1}{2}}$ versus t(s) should be linear for $\frac{1}{2}$ order reaction with a possible slope of k $((mmHg)^{\frac{1}{2}}s^{-1})$.

$\frac{3}{2}$ Order

The integral equation for the $\frac{3}{2}$ order is [302],

$$k = \frac{2}{t} \left(\frac{1}{\sqrt{a_o - x}} - \frac{1}{\sqrt{a_o}} \right)$$

which, following procedures outlined above, finally yields

$$Q_{\frac{3}{2}} = 2\left[\frac{1}{\sqrt{(3Po-2Pt}} - \frac{1}{\sqrt{Po}} \right] \qquad .....3.17.$$

where $Q_{\frac{3}{2}}$ is Q factor for $\frac{3}{2}$ order reaction.

The plot of $Q_{\frac{3}{2}}$ versus time(s) for a $^{2}/_{3}$order reaction would then be linear with a positive slope of k ($(mmHg)^{\frac{1}{2}}s^{-1}$).

Second Order

The integral form for a second order rate constant is

$$k = \frac{1}{t} \cdot \frac{a_o-(a_o-x)}{a_o(a_o-x)}$$

so that

$$kt = \frac{2(Po-2P)}{Po(3Po-2P)}$$

and

$$Q_2 = \frac{2(Po-2Pt)}{Po(3Po-2Pt)} \qquad .....3.18$$

where Q_2 respresents the second order Q factor.

A plot of Q_2 vs. t(s) will then give a straight line of positive slope of k($mmHg\ s^{-1}$).

A computer program (CP1) is given in appendix V, which was written for an input of time t(s), initial N_2O pressure Po(mmHg) and pressure PN_2O at time t. One has a choice of calculating any of the Q factors ($Q_{\frac{1}{2}}$, Q_1, $Q_{\frac{3}{2}}$ or Q_2), followed by a linear regression analysis of the plot of the Q factor versus t, yielding values of the correlation coefficient (R), slope(a) and intercept (b), which enable the relevant rate constant, k and the best fit-data equation.

The data for the twelve static study samples over a range of temperature (at least five different temperatures for each catalyst) were analysed for different orders ($\frac{1}{2}$, 1, $\frac{3}{2}$ and 2), to get a best-fit plot. The criterion for best-fit data was the maximum (closest to 1) value of correlation coefficient, R. The first order plots showed better linearity for most of the samples

(Co-5A samples generally fit better than the Cu-5A zeolites), over the measured range of N_2O decomposition. The un-exchanged 5A zeolite samples were almost totally unreactive in the experimental range studied (1023-1323K).

The results for the first order plots are included in the appendix II. Tables II**c** (1.1 ⟶ 1.6) are for Co-5A zeolites and tables II**d** (1.1 ⟶ 1.6) give results for Cu-5A zeolite samples. In some cases, especially the Cu-5A zeolites, the plots deviated from linearity as the pressure increased. The problem increased at high temperature due to diffusion effects which are then more effective[224]. To retain maximum possible linearity (checked by the value of R), the number of data points taken for analysis (indicated in the tables), are different to the total number of data points. The computer plots of Q versus t(s) are shown in figures (B1-12).

3.4.2. Energies of Activation and Frequency Factors

The rate constant k and the absolute temperature T are related by the Arrhenius equation as

$$k = A.\ \exp^{-E/RT} \qquad \ldots.3.19.$$

where E,R and A are respectively the energy of activation, the gas constant and the pre-expotential or frequency factor. Taking the logarithms,

$$\ln k = -E/RT + \ln A \qquad \ldots..3.20.$$

A linear plot of lnk versus $\frac{1}{T(K)}$ affords a slope $-E/R1$ and enables the evaluation of Ea. Also,

$$\ln A = \ln k + E/R_1T \qquad \ldots..3.21.$$

which provides the value of frequency factor $A(s^{-1})$.

The value of the activation energy E and the frequency factor A were calculated by a computer program CP4 given in appendix V. Linear regression analysis of the plot of ln k versus $\frac{1}{T(K)}$ gave the values of Ea ($J\ mol^{-1}$.), $A(s^{-1})$

and the correlation coefficient R. Due to diffusion effects at high temperature[224], some plots deviated from linearity. Results are tabulated in appendix **II.**

3.4.3. Specific Rates and Free Energy of Activation

Computer program CP**4** was extended to include calculations involving specific rates and free energy values.

Specific rates (R_{sp}) for the decomposition of the nitrous oxide reaction are the number of molecules decomposed per site per second at unit pressure (PN_2O = 1mmHg). Mathematically,

$$R_{sp} = k \cdot \frac{N}{S} \qquad .....3.22$$

where R_{sp} is the specific rate constant, k is the rate constant at a specific temperature and N is the total number of N_2O molecules in the reaction vessel at unit pressure (i.e. PN_2O = 1 mmHg).

Now for the static volume of the system, (342 cm^3)

$$N = \frac{6.02 \times 10^{23} \times 342}{760 \times 22400} = 1.2023 \times 10^{19} \text{ molecules}$$

S is the total number of transition metal ions in the sample, defined as

$$S = \frac{mnL}{w} \qquad .....3.23$$

where m = mass of the activated samples

w = molecular weight of the unit cell of the zeolite

L = Avogadro's number

and n = no. of transition metal ions per unit cell in the zeolite sample.

Then $$R_{sp} = \frac{K.\ N.\ w}{m.\ n.\ L} \qquad .....3.24$$

The units of R_{sp} are molecule (unit cell)$^{-1}$ s^{-1}.

Free energies of activation $\Delta G^{\neq}$ ($J.mol^{-1}$) were calculated from the relationship,

$$\Delta G^{\neq} = R_1 T \ln \frac{kT_1}{h} - \ln k \qquad .....3.25$$

where R_1 = gas constant = 8.314 $J.K^{-1}\ mol^{-1}$,

k = Boltzmann constant = $1.381 \times 10^{-23}\ J.k^{-1}$

h = Planck constant = $6.626 \times 10^{-34}\ J.s^{-1}$

T_1 = 298K = room temperature

T = temperature (K) of the reaction

k = rate constant (s^{-1}) at the temperature T.

Results are presented in appendix II, in tables IIc (1.1-6) for the Co-5A samples and tables IId (1.1-6) for the Cu-5A samples. Each table lists the value of the activation energy Ea ($J.mol^{-1}$), frequency factor A(s^{-1}), correlation coefficient R and the best fit data equation. The temperatures T(K), rate constants k (s^{-1}), free energy of activation $\Delta G^{\neq}$ ($J.mol^{-1}$) and specific rate (R_{sp}) values at temperature T are also included.

The results are summarised in tables (3.6-7) in this section.

3.5. FLOW SYSTEM STUDIES

The conversion factor (α) for methane oxidation (§2.3.4) in a plug-flow reactor (§1.5.11) can be defined either as,

$$\alpha CH_4 = \frac{P_{CH_4(f)} - P_{CH_4(p)}}{P_{CH_4(f)}} \qquad .....3.26$$

or

$$\alpha CO_2 = \frac{P_{CO_2(p)}}{P_{CO_2(100\%)}} \qquad .....3.27$$

TABLE 3.6 Nitrous Oxide Decomposition - 1st Order Fit Data

Zeolite	Temp.of Reaction T/K	Initial Pressure Po/torr	Correlation Coefficient R	Intercept	Rate Constant k/s^{-1}
Co-5A(1)	866	0.6579	0.9961	-7.1654E-3	6.2992E-5
"	919	0.6631	0.9985	-7.8691E-3	1.4164E-4
"	943	0.7496	0.9992	-2.1876E-3	2.7504E-4
"	970	0.9016	0.9957	-9.6713E-3	4.5398E-4
"	1001	0.6475	0.9987	-4.367E-3	8.5085E-4
Co-5A(2)	828	1.0041	0.9990	-6.2705E-2	5.5647E-5
"	858	0.7512	0.9992	-2.3796E-2	1.1632E-4
"	895	0.7291	0.9987	-1.7383E-2	1.8617E-4
"	928	0.9338	0.9981	5.7609E-3	2.5179E-4
"	966	0.7018	0.9989	-6.7941E-3	4.3335E-4
Co-5A(3)	818	0.6845	0.9603	-0.2378	9.8253E-5
"	836	0.7720	0.9901	-3.7518E-2	4.462E-5
"	887	0.7724	0.9972	-6.6662E-2	2.0173E-4
"	922	0.7168	0.9992	-9.1694E-2	3.1148E-4
"	958	0.9010	0.9972	1.2439E-2	3.9076E-4
"	983	0.6223	0.9987	-2.0085E-2	6.2313E-4
Co-5A(4)	817	0.7236	0.9940	-6.6347E-2	6.5182E-5
"	860	1.0799	0.9991	-2.2653E-2	1.8155E-4
"	911	0.4308	0.9879	3.806E-2	2.941E-4
"	925	0.4308	0.9930	-3.6608E-2	3.2921E-4
"	958	0.8826	0.9974	-6.7155E-3	5.6575E-4

TABLE 3.6 continued

Zeolite	Temp.of Reaction T/K	Initial Pressure Po/torr	Correlation Coefficient R	Intercept	Rate Constant k/s^{-1}
Co-5A(5)	792	0.6264	0.9982	-5.440E-2	2.6752E-4
"	806	0.4153	0.9951	3.4623E-2	2.075E-4
"	851	0.5782	0.9974	2.4085E-2	4.567E-4
"	874	0.5397	0.9942	4.0368E-3	4.8814E-4
"	911	0.5980	0.9842	0.1207	5.3447E-4
Co-5A(6)	791	0.5782	0.9988	1.8429E-2	1.8343E-4
"	845	0.6283	0.9876	0.1038	4.6548E-4
"	881	0.5733	0.9937	0.1014	7.1236E-4
"	911	0.6181	0.9968	8.5636E-2	9.2764E-4
"	950	0.4363	0.9918	0.1286	1.2151E-3
Cu-5A(1)	843	0.8005	0.9984	2.9034E-3	2.0438E-4
"	883	0.9010	0.9924	0.1056	3.0854E-4
"	910	0.7167	0.9884	0.2321	4.9354E-4
"	943	0.7834	0.9889	0.1910	7.7387E-4
"	979	0.7442	0.9950	0.2118	8.9766E-4
Cu-5A(2)	829	0.5023	0.9590	6.3644E-3	1.6983E-4
"	885	0.6479	0.9870	0.2255	5.8277E-4
"	910	0.8649	0.9734	0.3669	4.6903E-4
"	939	0.4753	0.9490	0.7139	4.1644E-4
"	982	0.8649	0.9309	0.7113	2.8992E-4

TABLE 3.6 continued

Zeolite	Temp. of Reaction T/K	Initial Pressure po/torr	Correlation Coefficient R	Intercept	Rate Constant k/s^{-1}
Cu-5A(3)	845	0.9629	0.9469	0.3358	2.4501E-4
"	888	1.101	0.9603	0.5141	4.0598E-4
"	915	0.6952	0.9979	0.2384	9.5763E-4
"	951	0.7496	0.9908	0.3241	6.8177E-4
"	977	0.778	0.9793	0.3990	6.9321E-4
Cu-5A(4)	805	0.8894	0.9701	0.1073	2.1752E-4
"	830	1.0085	0.9722	0.3080	3.0238E-4
"	861	0.6631	0.9713	0.4193	5.2093E-4
"	916	0.8006	0.9933	0.3842	6.5893E-4
"	947	1.1078	0.9779	0.3702	4.5959E-4
Cu-5A(5)	800	0.9574	0.9788	1.3187E-2	1.8301E-4
"	829	0.8833	0.9866	0.1442	4.8011E-4
"	887	0.7003	0.9984	0.2976	1.0726E-3
"	912	0.9956	0.9878	0.2688	4.0841E-4
"	951	1.101	0.9806	0.2407	4.7609E-4
"	977	1.1419	0.9792	0.2916	4.2482E-4
Cu-5A(6)	816	1.0214	0.9951	-2.4549E-2	2.5033E-4
"	845	0.6684	0.9717	0.2552	4.4477E-4
"	893	0.8239	0.9866	0.2607	5.5005E-4
"	932	0.6789	0.9719	0.2993	5.2335E-4
"	968	0.6269	0.9750	0.3370	5.03E-4

TABLE 3.7 Static Studies Data

Zeolite	Mass/g	Frequency Factor A/s^{-1}	Correlation Coefficient (R)	Energy of Activation /kJ mol^{-1}	Free Energy of Activation (800K) /kJ mol^{-1}	Specific Rate (Rsp)(800K) molecule $site^{-1}$ s^{-1}
Co-5A(1)	0.1326	170.29	-0.9916	140.67	255.35	7.03E-5
Co-5A(2)	0.1339	51.25	-0.9905	93.71	258.90	5.17E-5
Co-5A(3)	0.0945	799.46	-0.9749	114.38	259.52	3.98E-5
Co-5A(4)	0.1782	53.13	-0.9867	91.64	258.79	2.53E-5
Co-5A(5)	0.0995	0.35	-0.9388	48.07	251.44	6.74E-5
Co-5A(6)	0.2074	9.91	-0.9866	71.42	252.6	2.12E-5
Cu-5A(1)	0.1033	11.36	-0.9799	76.64	249.59	4.76E-4
Cu-5A(2)	0.0967	638.60	-0.9912	110.72	257.53	1.0 E-4
Cu-5A(3)	0.0956	0.98	-0.9995	57.59	247.34	3.04E-4
Cu-5A(4)	0.1055	1.00	-0.9999	55.70	251.4	2.17E-4
Cu-5A(5)	0.1056	0.91	-0.9959	57.83	253.34	8.89E-5
Cu-5A(6)	0.1106	0.98	-0.9991	56.35	251.12	1.13E-4

where $P_{CH_4(f)}$ = peak height of methane in feed,

$P_{CH_4(p)}$ = peak heights of methane in product stream,

$P_{CO_2(p)}$ = peak heights of CO_2 in product stream

and $P_{CO_2(100\%)}$ = peak height of CO_2 at 100% conversion

Methane peak heights only, were used to calculate the conversion factor (α) while $P_{CO_2(p)}$ and $P_{CO_2(100\%)}$ served as a mode of comparison and indication of the completeness of the reaction.

The degree of conversion (α) values were used in a computer program based on the plug-flow equation (§1.5.11),

$$k = \frac{F}{m} \cdot \frac{1}{p^x} \cdot \int_0^{\alpha} \left(\frac{1}{1-\alpha}\right)^x \cdot d\alpha \qquad .....3.28$$

where the quantities F, m, p and α (flow rate, mass of catalyst, pressure and conversion factor) are all measurable quantities while k (the observed rate constant) and x (the observed order) are two unknowns which were calculated with the help of the computer program.

The program iteratively solves the equation by linear regression analysis of the data to enable plots of correlation coefficient (R) versus order (x) and ln k versus $\frac{1}{T}(K^{-1})$.

Eq. 40(1.5.11) defines the correlation coefficient R as

$$R = \frac{a\sigma_x}{\sigma_y} \qquad .....3.29.$$

where a, σ_x, σ_y represent respectively, the gradient of the best fit line, and the standard deviations for $^1/_T$ and ln k respectively.

For N number of points,

$$\sigma_x = \left[\frac{\Sigma X^2 - (\Sigma X)^2}{N - 1} \right]^{\frac{1}{2}} \qquad .....3.30.$$

and

$$\sigma_y = \left[\frac{\Sigma Y^2 - \frac{(\Sigma Y)^2}{N}}{N - 1} \right]^{\frac{1}{2}} \qquad .....3.31.$$

Also,

$$\text{slope} = a = \frac{\Sigma XY - \frac{\Sigma X \Sigma Y}{N}}{\Sigma X^2 - \frac{(\Sigma X)^2}{N}} \qquad .....3.32.$$

and

$$\text{intercept} = b = \frac{\Sigma Y - m\Sigma X}{N} \qquad .....3.33.$$

The plots of R vs order (e.g. see fig.33), usually provide a clear maximum for each zeolite sample studied. The iteration procedure involved changing the order in regular intervals of 0.2 (-2 → +2) to give the best fit. The value of the order was an absolute (maximum) value of R, for a best-fit line. This value of order was used in subsequent calculations.

The plot of ln k versus $1/T$, an almost straight line, enabled the activation energy Ea to be evaluated from the slope, which was further used to evaluate standard free energies of activation, $\Delta G^{\neq}$ from equation (3.25). The $\Delta G^{\neq}$ value can be used to compare the catalyst activity, if it is derived under the same standard conditions. In this study, the temperature chosen for comparing catalytic activities was the same (i.e. 740K for less reactive zeolite 5A samples) and 660K for more reactive mordenites. Two more parameters, $T\alpha 0.5$ (the temperature for 50% conversion) and t factor, used to evaluate the significance of correlation, were also evaluated by the computer program:

Cu/Na-MOR (Air & 4% O_2)

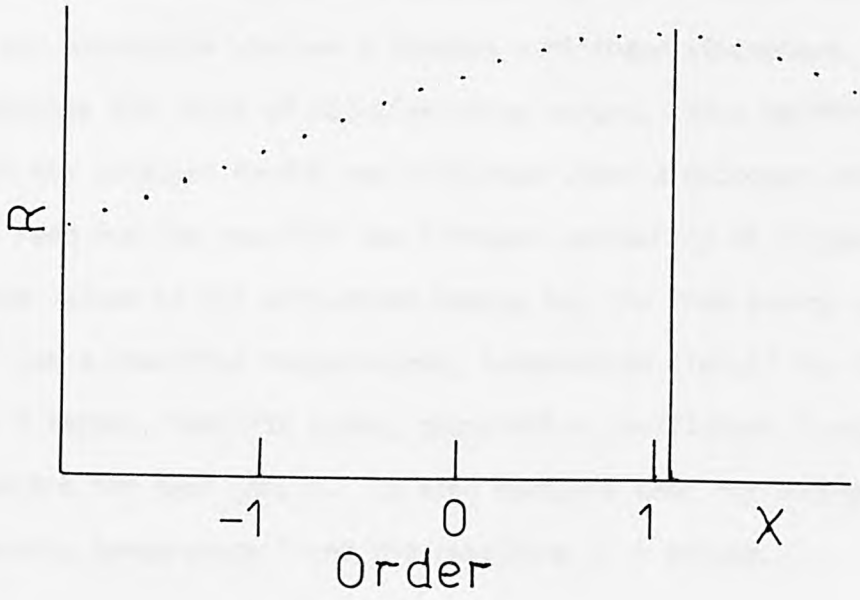

Fig. 3.3 Typical Corr. Coeff. vs. Order Plot

$$t = \frac{R.\sqrt{N-2}}{\sqrt{1-R^2}} \qquad .....3.34$$

where R is the best-fit correlation coefficient and N is the number of data pair values.

Results of the flow-system study are gathered in appendix III. Data sets are given in tables III(a.1→26, b.1→24, c1.1→12, c2.1→12, d1.1→12, d2.1→12 and d3.1→12).

The name of each sample (at top of each table) is followed by the conditions under which the reaction was studied. Symbol A stands for activation under an air atmosphere whereas N denotes a nitrogen atmosphere, while (%) indicates the level of dilution using oxygen. Thus Na-MOR(N+4%) means that the catalyst Na-MOR was activated under a nitrogen atmosphere, and the feed for the reaction was nitrogen containing 4% oxygen. Each table lists values of the activation energy Ea, the free energy of activation $\Delta G^{\neq}$ (at a specified temperature), temperature (Tα0.5) for 50% conversion, the t factor, best-fit order, correlation coefficient R and a best-fit equation for each sample. It also contains data for conversion factor α absolute temperature T and the resulting ln k values.

Four mordenites *viz.*, Cu-NaMOR, Ni-NaMOR, Cu-NH_4MOR and Ni-NH_4MOR (§ table 3.3) were used for subequent mixed-catalytic studies. Six samples were prepared by mixing intimately (with a glass rod), known proportionate (1:3, 1:1, 3:1) weights of, either Na^+- or NH_4^+- exchanged forms of the respective mordenite. For example Cu-Ni-NaM(1) was prepared by mixing one part (by weight) of Cu-NaMOR with three parts (by weight) of Ni-NaMOR; similarly Cu-Ni-NaM(2) contained equal parts (by weight) of Cu-NaMOR and Ni-NaMOR; while the mixture sample Cu- Ni-NaM(3) was obtained from three parts (by weight) of Cu-NaMOR and one part (by weight) of Ni-NaMOR. Six mixed samples prepared are given in table 3.8.

Table 3.8 Mixed Catalytic Studies Samples

S.NO	Samples	Parts by weight			
		Cu-NaMOR	Cu-NH_4MOR	Ni-NaMOR	Ni-NH_4MOR
1.	Cu-Ni-NaM(1)	1	-	3	-
2.	Cu-Ni-HM(1)	-	1	-	3
3.	Cu-Ni-NaM(2)	1	-	1	-
4.	Cu-Ni-HM(2)	-	1	-	1
5.	Cu-Ni-NaM(3)	3	-	1	-
6.	Cu-Ni-HM(3)	-	3	-	1

Plots of ln k versus $^1/_T$ for the tabulated data (IIIa.1-IIId3.12), are presented in figures (P.1-42) and results are summarised in the following tables (3.9-3.12).

TABLE 3.9 Plug-flow Data for Zeolite A Samples

S.No	Zeolite	Mass/g	Activation (mode)	Dilution ($\%O_2$)	Corr.Coeff. (R)	Order	Ea/kJ mol^{-1}	t factor	$T_{o.5}$ /k	$\Delta G^{\neq}$ (660K)	/kJ mol^{-1} (740K)
1	Na-A	0.3687	Air	-	-0.9982	-1.56	105.97	-46.87	881.3	-	321.16
2	Ca-A	0.2984	Air	-	-0.9950	-2	82.14	-24.34	906.8	-	334.07
3	Cu-5A(1)	0.3116	Air	-	-0.9988	1.52	116.02	-61.50	848.1	-	223.19
4	Cu-5A(1)	0.3290	Nitrogen	-	-0.9987	1.52	129.25	-58.86	848.8	-	225.27
5	Cu-5A(2)	0.2330	Air	-	-0.9920	1.30	144.96	-17.53	833.6	-	230.14
6	Cu-5A(2)	0.2491	Nitrogen	-	-0.9859	1.52	181.53	-15.57	833.6	-	223.86
7	Cu-5A(3)	0.2525	Air	-	-0.9966	1.30	136.94	-31.98	805.6	-	227.59
8	Cu-5A(3)	0.3164	Nitrogen	-	-0.9978	0.20	83.33	-52.09	802.7	-	257.14
9	Cu-5A(4)	0.2501	Air	-	-0.9969	1.08	119.80	-40.08	813.6	-	230.75
10	Cu-5A(4)	0.3084	Nitrogen	-	-0.9990	0.64	92.84	-77.27	812.1	-	243.86
11	Cu-5A(5)	0.2130	Air	-	-0.9986	1.08	119.14	-55.96	784.1	-	227.11
12	Cu-5A(5)	0.3152	Nitrogen	-	-0.9995	1.08	115.52	-92.39	779.6	-	228.01
13	Cu-5A(6)	0.2319	Air	-	-0.9986	1.08	131.01	-64.67	802.4	-	230.60
14	Cu-5A(6)	0.3280	Nitrogen	-	-0.9991	1.08	112.04	-68.59	773.8	-	227.61
15	Co-5A(1)	0.2701	Air	-	-0.9965	1.96	126.66	-31.51	951.8	-	218.35
16	Co-5A(1)	0.3021	Nitrogen	-	-0.9931	1.52	89.79	-26.82	925	-	226.58
17	Co-5A(2)	0.2461	Air	-	-0.9986	1.30	82.16	-49.30	886	-	228.36
18	Co-5A(2)	0.3082	Nitrogen	-	-0.9983	1.52	87.42	-51.10	834	-	218.98
19	Co-5A(3)	0.2585	Air	-	-0.9981	0.20	106.91	-42.47	836	-	261.89
20	Co-5A(3)	0.3576	Nitrogen	-	-0.9985	1.30	88.85	-63.85	800.4	-	221.93

Table 3.9 continued

S.No	Zeolite	Mass/g	Activation (mode)	Dilution ($\%O_2$)	Corr. Coeff. (R)	Order	Ea/kJ mol^{-1}	t factor	$T_{o.5}$ /k	$\Delta G^{\neq}$ (660K)	/kJ mol^{-1} (740K)
21	Co-5A(4)	0.2468	Air	-	-0.9960	1.52	84.49	-33.61	784	-	212.20
22	Co-5A(4)	0.3350	Nitrogen	-	-0.9995	1.52	131.42	-86.41	795.5	-	219.19
23	Co-5A(5)	0.2163	Air	-	-0.9993	1.30	93.25	-85.59	751	-	214.84
24	Co-5A(5)	0.2990	Nitrogen	-	-0.9992	1.52	97.62	-88.70	729	-	207.26
25	Co-5A(6)	0.2326	Air	-	-0.9991	0.86	77.15	-68.44	831	-	236.49
26	Co-5A(6)	0.3200	Nitrogen	-	-0.9992	1.52	104.91	-95.43	727	-	207.34

Table: 3.10 Plug-Flow Data For Mordenites

S.No	Zeolite	Mass /g	Activ-ation (mode)	Dilu-tion ($\%O_2$)	Corr. Coeff. (R)	Order	Ea/kJ mol^{-1}	t factor	T 0.5 /k	$\Delta G^{\neq}$ /kJ mol^{-1} (660K)	(740K)
1	Na-MOR	0.3921	Air	-	-0.9946	-2	89.88	-31.88	912	273.97	-
2	NH_4-M(1)	0.3044	Air	-	-0.9976	0.86	100.12	-50.08	798	219.13	-
3	NH_4-M(2)	0.3043	Air	-	-0.9990	0.86	111.52	-74.26	811	204.85	-
4	NH_4-MOR	0.3330	Nitrogen	-	-0.9933	1.08	129.55	-29.87	806	221.75	-
5	Ni-M(1)	0.2447	Air	-	-0.9984	0.64	93.79	-62.73	793	221.74	-
6	Ni-M(1)	0.2011	Nitrogen	-	-0.999	1.52	98.94	-74.7	757	197.14	-
7	Ni-M(2)	0.2282	Air	-	-0.9974	1.08	102.34	-41.43	766	211.42	-
8	Ni-M(2)	0.2548	Nitrogen	-	0.9988	0.86	92.51	-71.97	732	212.41	-
9	Ni-M(3)	0.1905	Air	-	-0.9979	1.08	92.29	-59.73	760	208.03	-
10	Ni-M(3)	0.1425	Nitrogen	-	-0.9970	1.52	102.31	-51.24	775	197.05	-
11	Cu-M(1)	0.2140	Air	-	-0.9991	1.08	101.02	-76.57	638	193.02	-
12	Cu-M(1)	0.2140	Nitrogen	-	-0.9980	0.86	94.57	-52.19	611	194.9	-
13	Cu-M(2)	0.2397	Air	-	-0.9976	0.64	84.40	-40.55	633	204.91	-
14	Cu-M(2)	0.2270	Nitrogen	-	-0.9984	1.08	127.39	-46.43	614	187.31	-
15	Cu-M(3)	0.2532	Air	-	-0.9996	0.86	83.05	-124.40	613	196.76	-

Table 3.10 continued

S.No	Zeolite	Mass /g	Activ-ation (mode)	Dilu-tion ($\%O_2$)	Corr. Coeff. (R)	Order	Ea/kJ mol^{-1}	t factor	T 0.5 /k	$\Delta G^{\neq}$ (660K)	/kJ mol^{-1} (740K)
16	Cu-M(3)	0.2425	Nitrogen	-	-0.9988	0.86	128.20	-60.25	633	198.33	-
17	Pt-M(1)	0.2092	Air	-	-0.9993	0.86	88.56	-73.48	518	207.26	-
18	Pt-M(1)	0.2027	Nitrogen	-	-0.9986	0.86	60.62	-66.97	574	200.51	-
19	Pt-M(2)	0.2818	Air	-	-0.9965	1.08	93.53	-41.41	526	200.85	-
20	Pt-M(2)	0.1997	Nitrogen	-	-0.9986	0.86	55.81	-64.67	582	210.88	-
21	Pt-M(3)	0.2449	Air	-	-0.9983	0.42	71.04	-51.87	521	226.17	-
22	Pt-M(3)	0.2307	Nitrogen	-	-0.9993	1.30	85.91	-77.64	548	190.16	-
23	Pt-M(4)	0.2811	Air	-	-0.9972	1.30	84.06	-47.73	597	201.03	-
24	Pt-M(4)	0.2288	Nitrogen	-	-0.9995	1.08	75.96	-88.93	5554	199.76	-

Table 3.11 Plug-Flow Data for Mordenites

S.No	Zeolite	Mass /g	Activ-ation (mode)	Dilu-tion (% O_2)	Corr.Coeff. (R)	Order	Ea/kJ mol^{-1}	t factor	T 0.5 /k	$\Delta G^{\neq}$ /kJ mol^{-1} (660K)	(740K)
1	Ni-NaM	0.2310	Air	-	-0.9983	1.74	151.28	- 54.30	646	175.75	-
2	Ni-NaM	0.2233	Air	4	-0.9925	1.74	145.63	-28.79	677.5	183.17	-
3	Ni-NaM	0.2252	Air	8	-0.9997	1.96	193.37	-100.07	674	176.55	-
4	Ni-NaM	0.2060	Nitrogen	-	-0.9988	0.86	101.78	-58.76	734	212.31	-
5	Ni-NaM	0.2535	Nitrogen	4	-0.9966	1.74	199.05	-34.28	698	191.92	-
6	Ni-NaM	0.2257	Nitrogen	8	-0.9981	1.30	134.07	-56.12	744	205.87	-
7	Ni-HM	0.2222	Air	-	-0.9965	1.52	120.06	-39.65	747	197.86	-
8	Ni-HM	0.2066	Air	4	-0.9973	1.30	98.53	-45.02	817	208.97	-
9	Ni-HM	0.2181	Air	8	-0.9984	1.30	132.02	-69.52	786	212.47	-
10	Ni-HM	0.2114	Nitrogen	-	-0.9996	1.30	110.25	-120.56	750	204.27	-
11	Ni-HM	0.2166	Nitrogen	4	-0.9995	1.08	101.69	-104.15	804	214.42	-
12	Ni-HM	0.2185	Nitrogen	8	-0.9948	0.42	76.38	-25.79	760	224.80	-
13	Cu-NaM	0.2136	Air	-	-0.9991	1.52	134.70	-69.64	641	180.01	-
14	Cu-NaM	0.2117	Air	4	-0.9991	1.08	111.85	-72.99	650	194.45	-
15	Cu-NaM	0.2248	Air	8	-0.9991	1.30	117.30	-66.73	642	186.96	-
16	Cu-NaM	0.2033	Nitrogen	-	-0.9992	1.52	173.06	-65.31	642	178.53	-

Table 3.11 continued

S.No	Zeolite	Mass /g	Activ-ation (mode)	Dilu-tion ($\%O_2$)	Corr.Coeff. (R)	Order	Ea/kJ mol^{-1}	t factor	T 0.5 /k	$\Delta G^{\neq}$ (660K)	/kJ mol^{-1} (740K)
17	Cu-NaM	0.2176	Nitrogen	4	-0.9989	0.64	103.57	-63.88	625	202.64	-
18	Cu-NaM	0.2153	Nitrogen	8	-0.9989	1.08	154.39	-50.92	645	192.66	-
19	Cu-HM	0.2100	Air	-	-0.9979	1.52	140.13	-43.39	643	180.33	-
20	Cu-HM	0.2560	Air	4	-0.9997	1.08	116.12	-116.02	635	192.79	-
21	Cu-HM	0.2168	Air	8	-0.9977	1.74	146.62	-36.36	635	174.11	-
22	Cu-HM	0.2113	Nitrogen	-	-0.9982	1.52	172.95	-43.95	640	177.34	-
23	Cu-HM	0.2169	Nitrogen	4	-0.9987	0.64	88.78	-51.30	613	230.54	-
24	Cu-HM	0.2153	Nitrogen	8	-0.9997	1.30	155.99	-112.95	617	179.33	-

Table 3.12 Plug-Flow Data for Mordenite Mixtures

S.No	Zeolite	Mass /g	Activ-ation (mode)	Dilu-tion ($\%O_2$)	Corr.Coeff. (R)	Order	Ea/kJ mol^{-1}	t factor	T 0.5 /k	$\Delta G^{\neq}$ /kJ mol^{-1} (660K)	(740K)
1	Cu-Ni-NaM(1)	0.2071	Air	-	-0.997	1.08	119.65	-40.46	692	201.79	-
2	Cu-Ni-NaM(1)	0.1766	Air	4	-0.9988	1.30	119.63	-54.16	694	195.05	-
3	Cu-Ni-NaM(1)	0.2562	Air	8	-0.9963	1.96	186.46	-30.80	673	178.13	-
4	Cu-Ni-NaM(1)	0.1805	Nitrogen	-	-0.9990	1.08	122.90	-71.67	702	203.0	-
5	Cu-Ni-NaM(1)	0.1910	Nitrogen	4	-0.9970	1.52	148.84	-40.83	692	190.44	- -
6	Cu-Ni-NaM(1)	0.2079	Nitrogen	8	-0-9981	0.64	104.04	-55.79	688	212.63	-
7	Cu-Ni-HM(1)	0.1787	Air	-	-0.9989	1.08	109.67	-66.64	689	199.50	-
8	Cu-Ni-HM(1)	0.2247	Air	4	-0.9985	1.30	133.68	-48.13	674	193.62	-
9	Cu-Ni-HM(1)	0.2037	Air	8	-0.9977	1.08	111.60	-43.77	675	198.69	-
10	Cu-Ni-HM(1)	0.2121	Nitrogen	-	-0.9986	1.74	175.43	-56.70	677	194.58	-
11	Cu-Ni-HM(1)	0,1996	Nitrogen	4	-0.9982	1.30	144.02	-50.05	689	196.39	-
12	Cu-Ni-HM(1)	0.2037	Nitrogen	8	-0.9946	1.08	133.01	-28.73	676	199.20	-
13	Cu-Ni-NaM(2)	0.1949	Air	-	-0.9989	1.30	119.81	-63.17	661	190.11	-
14	Cu-Ni-NaM(2)	0.2140	Air	4	-0.9955	1.74	172.41	-31.43	674	181.27	-
15	Cu-Ni-NaM(2)	0.2044	Air	8	-0.9987	0.86	105.73	-63.74	660	202.65	-
16	Cu-Ni-NaM(2)	0.2084	Nitrogen	-	-0.9990	1.52	145.33	-53.98	669	186.0	-
17	Cu-Ni-NaM(2)	0.2023	Nitrogen	4	-0.9995	1.08	121.96	-107.89	675	198.71	-
18	Cu-Ni-NaM(2)	0.2125	Nitrogen	8	-0.9972	0.64	102.55	-44.26	675	210.80	-

Table 3.12 continued

S.No	Zeolite	Mass /g	Activ-ation (mode)	Dilu-tion ($\%O_2$)	Corr.Coeff. (R)	Order	Ea/kJ mol^{-1}	t factor	T 0.5 /k	$\Delta G^{\neq}$ /kJ mol^{-1} (660K)	(740K)
19	Cu-Ni-HM(2)	0.1985	Air	-	-0.9981	1.30	129.32	-48.34	664	109.77	-
20	Cu-Ni-HM(2)	0.1572	Air	4	-0.9976	1.08	110.90	-43.01	665	195.79	-
21	Cu-Ni-HM(2)	0.2059	Air	8	-0.9971	1.08	120.43	-39.56	657	195.73	-
22	Cu-Ni-HM(2)	0.2111	Nitrogen	-	-0.9993	1.30	121.06	-89.54	647	188.54	-
23	Cu-Ni-HM(2)	0.2130	Nitrogen	4	-0.9998	1.30	143.86	-147.58	658	190.04	-
24	Cu-Ni-HM(2)	0.2064	Nitrogen	8	-0.9966	1.30	150.16	-36.49	657	187.15	-
25	Cu-Ni-NaM(3)	0.1681	Air	-	-0.9960	1.74	136.81	-35.10	682	106.0	
26	Cu-Ni-NaM(3)	0.2002	Air	4	-0.9994	1.52	157.45	-89.41	655	183.29	-
27	Cu-Ni-NaM(3)	0.2015	Air	8	-0.9950	1.52	138.21	-31.42	650	182.10	-
28	Cu-Ni-NaM(3)	0.1968	Nitrogen	-	-0.9956	1.52	137.77	-31.93	655	183.32	-
29	Cu-Ni-NaM(3)	0.1912	Nitrogen	4	-0.9979	1.08	123.87	-46.56	660	195.09	-
30	Cu-Ni-NaM(3)	0.2069	Nitrogen	8	-0.9987	1.08	132.70	-58.16	666	194.45	-
31	Cu-Ni-HM(3)	0.1996	Air	-	-0.9991	1.30	119.54	-69.09	664	190.80	-
32	Cu-Ni-HM(3)	0.2233	Air	4	-0.9997	1.52	154.51	-114.52	654	183.29	-
33	Cu-Ni-HM(3)	0.2082	Air	8	-0.9992	1.08	113.35	-78.43	655	195.34	-
34	Cu-Ni-HM(3)	0.2037	Nitrogen	-	-0.9977	1.30	123.62	-41.26	643	111.55	-
35	Cu-Ni-HM(3)	0.1920	Nitrogen	4	-0.9972	1.08	139.91	-40.07	647	192.91	-
36	Cu-Ni-HM(3)	0.2092	Nitrogen	8	-0.9974	1.52	153.49	-45.83	647	180.62	-

3.6. THERMAL STUDIES

Data from the thermogravimetric (TG) traces of the different zeolite samples were fed into a computer program (given in appendix) in order to construct the thermograms which are shown in figures T.1 - T.38. The computer was linked to a sixpen Watanabe data-plotter. Figures (3.4 - 3.6) show some typical DTA traces and in figures (3.7 - 3.14) are found the DSC thermograms of the mordenites. Results are summarised in table 3.13 (TGA) and table 3.14 (DSC and DTA).

3.7. X-RAY STUDIES

Computer X-ray powder diffraction data for Na/Ca-A zeolite samples (i.e. diffraction angle 2θ, **M**iller indices m, interline spacing d, intensity I and unit cell constant a), are summarised in tables IIX.1-8 (presented in an appendix). Intensities of the lines are represented by symbols consisting of letters M, S, V and W (i.e. medium, strong, very strong and weak). Examples of micro-densitometer plots, and taken from the X-ray analysis photographs of these samples are given in figures (3.15-3.17). X-ray diffraction data (angle 2θ and relative intensity I/I_o) for the mordenites in hydrated and activated (dehydrated) forms are compared in tables IIX, IIIX.1-9 (included in an appendix). In addition, distribution plots of the relative intensities for X-ray diffraction of these samples are shown in figures X.1-9. The relevant computer programs for X-ray analyses are also listed in an appendix.

TABLE 3.13 TGA DATA FOR MORDENITES

*Fig. No.	Zeolite	Atmo-sphere	Volatile wieght loss (%w/w) at 373K	473K	573K	673K	773K	873K	973K	1073K
T1	Na-M	Air	2.9	8.7	11.4	11.9	12.6	12.6	12.6	12.6
T2	NH_4-M	"	4.6	9.0	9.4	10.4	12.1	12.8	13.1	13.1
T3	Cu-NaM	"	2.8	6.2	7.3	9.1	9.2	9.2	9.2	9.2
T4	Cu-NH_4M	"	2.5	5.8	7.3	9.6	9.7	9.8	9.8	9.8
T5	Ni-NaM	"	2.6	7.6	9.5	9.9	9.9	9.9	9.9	9.9
T6	Ni-NH_4M	"	2.7	7.4	8.8	9.8	10.6	10.6	10.6	10.6
T7	Cu-NiNaM(1)	"	3.4	9.2	11.4	12.0	12.5	13.2	13.8	13.8
T8	Cu-NiNH_4M(1)	"	2.9	8.8	10.1	11.1	12.6	13.0	13.0	13.0
T9	Cu-NiNaM(2)	"	3.7	8.8	10.6	11.7	12.4	12.5	12.7	12.7
T10	Cu-NiNH_4M(2)	"	3.4	9.0	10.0	11.4	13.2	13.7	13.7	13.7
T11	Cu-NiNaM(3)	"	3.7	8.2	9.5	11.3	11.9	12.0	12.1	12.1
T12	Cu-NiNH_4M(3)	"	3.7	7.9	9.4	10.9	12.4	12.5	12.5	12.5
T13	Cu-M(1)	"	2.7	5.4	7.0	9.0	9.1	9.2	9.2	9.2
T14	Cu-M(2)	"	2.7	5.7	6.8	9.0	9.2	9.2	9.2	9.2
T15	Cu-M(3)	"	2.5	5.7	7.1	9.2	9.3	9.3	9.3	9.3
T16	Ni-M(1)	"	1.0	3.6	5.0	6.2	7.3	7.4	7.6	7.6
T17	Ni-M(2)	"	3.3	7.0	7.6	8.6	9.6	9.8	9.9	9.9
T18	Ni-M(3)	"	3.0	8.1	9.9	11.1	12.2	12.5	12.6	12.7

*Figures (T1 - T18) are given in appendix.

TABLE 3.13 continued TGA DATA FOR MORDENITES

*Fig. No.	Zeolite	Atmo-sphere	Volatile weight loss (%w/w) at 373K	473K	573K	673K	773K	873K	973K	1073K
T19	Na-M	Nitrogen	5.5	11.0	13.6	13.9	13.9	13.9	13.9	13.9
T20	NH_4-M	"	5.1	8.9	9.3	10.1	11.5	12.7	12.7	12.7
T21	Cu-NaM	"	4.3	7.8	8.8	9.7	10.6	11.5	12.1	12.1
T22	Cu-NH_4M	"	3.2	6.4	7.3	8.2	9.1	10.0	10.6	10.6
T23	Ni-NaM	"	3.9	9.1	11.7	12.2	12.4	12.5	12.5	12.5
T24	Ni-NH_4M	"	3.1	8.3	9.7	10.2	11.0	11.9	12.1	12.1
T25	Cu-Ni-NaM(1)	"	4.1	9.2	11.7	12.3	12.8	12.9	12.9	12.9
T26	Cu-NiNH_4M(1)	"	3.2	9.2	10.5	10.7	11.5	12.8	13.3	13.3
T27	Cu-NiNaM(2)	"	4.3	8.7	10.4	11.2	11.8	12.2	12.2	12.2
T28	Cu-NiNH_4M(2)	"	3.4	7.8	8.8	9.6	11.0	11.7	11.7	11.7
T29	Cu-NiNaM(3)	"	3.4	8.2	9.4	10.2	11.0	11.8	12.1	12.1
T30	Cu-NiNH_4M(3)	"	4.3	8.3	9.2	10.1	13.1	14.3	14.8	14.8
T31	Cu-M(1)	"	4.7	8.8	10.1	11.2	12.5	13.9	14.7	14.8
T32	Cu-M(2)	"	5.0	8.9	9.9	11.0	12.1	13.6	14.3	14.3
T33	Cu-M(3)	"	4.5	8.0	9.2	10.3	11.5	13.0	14.1	15.0
T34	Ni-M(1)	"	4.5	9.2	10.3	10.8	11.6	13.1	13.6	13.6
T35	Ni-M(2)	"	4.6	10.1	11.6	12.1	12.8	13.0	13.0	13.0
T36	Ni-M(3)	"	4.3	9.5	10.8	11.6	12.7	13.6	13.8	13.8

*Figures (T19 - T36) are given in appendix

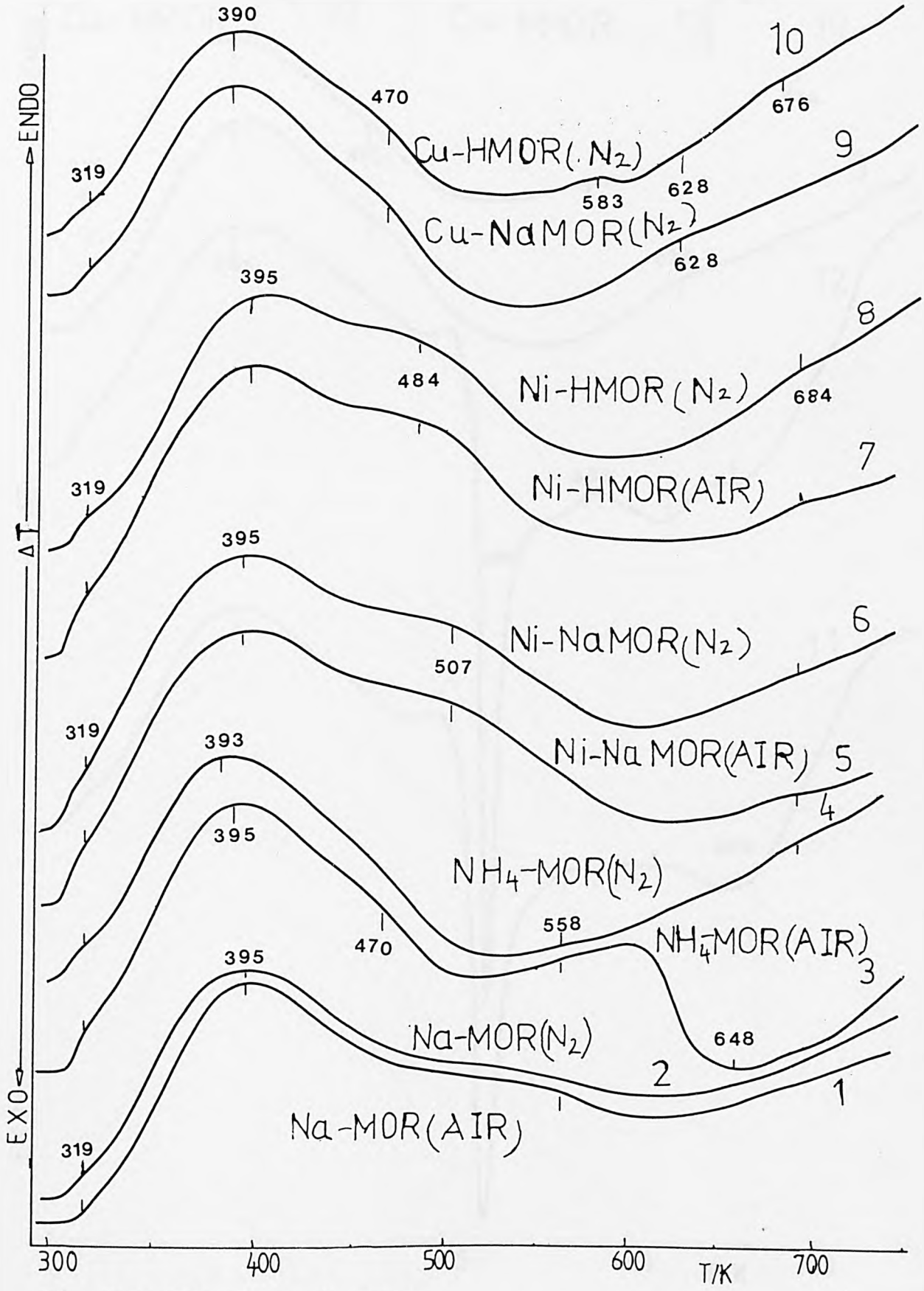

Fig.3.4 DTA of mordenites.

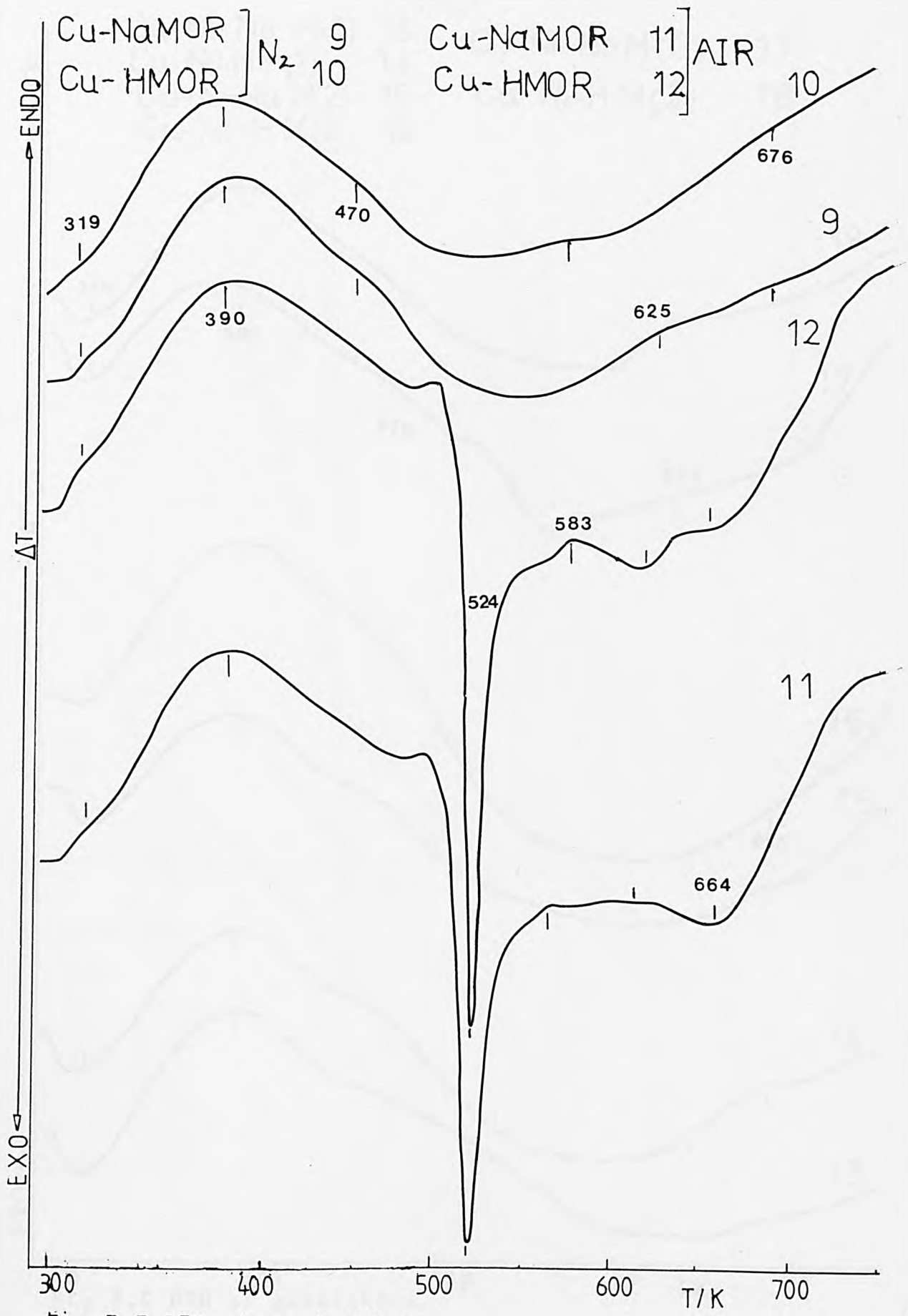

Fig.3.5 DTA of mordenites.

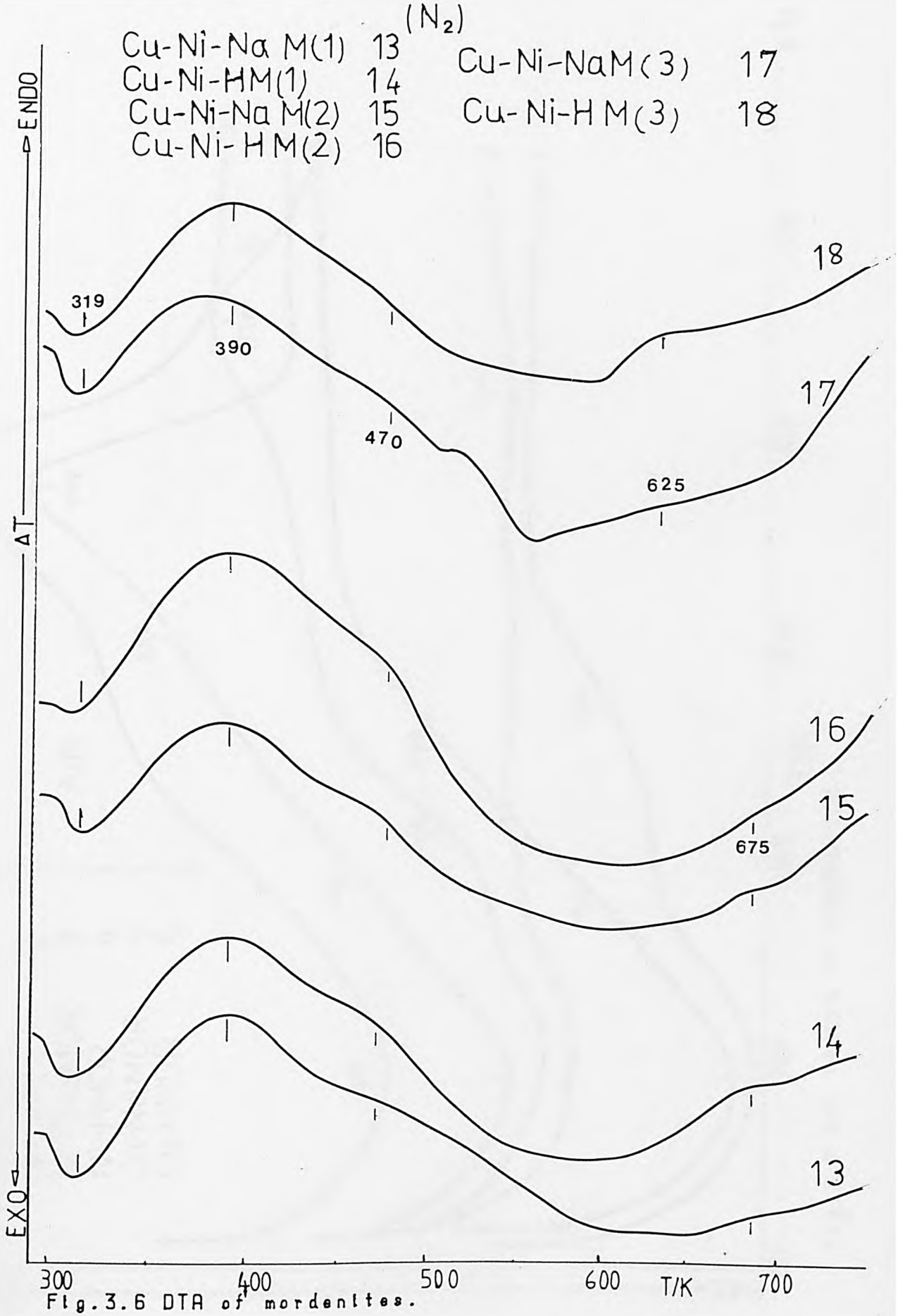

Fig.3.6 DTA of mordenites.

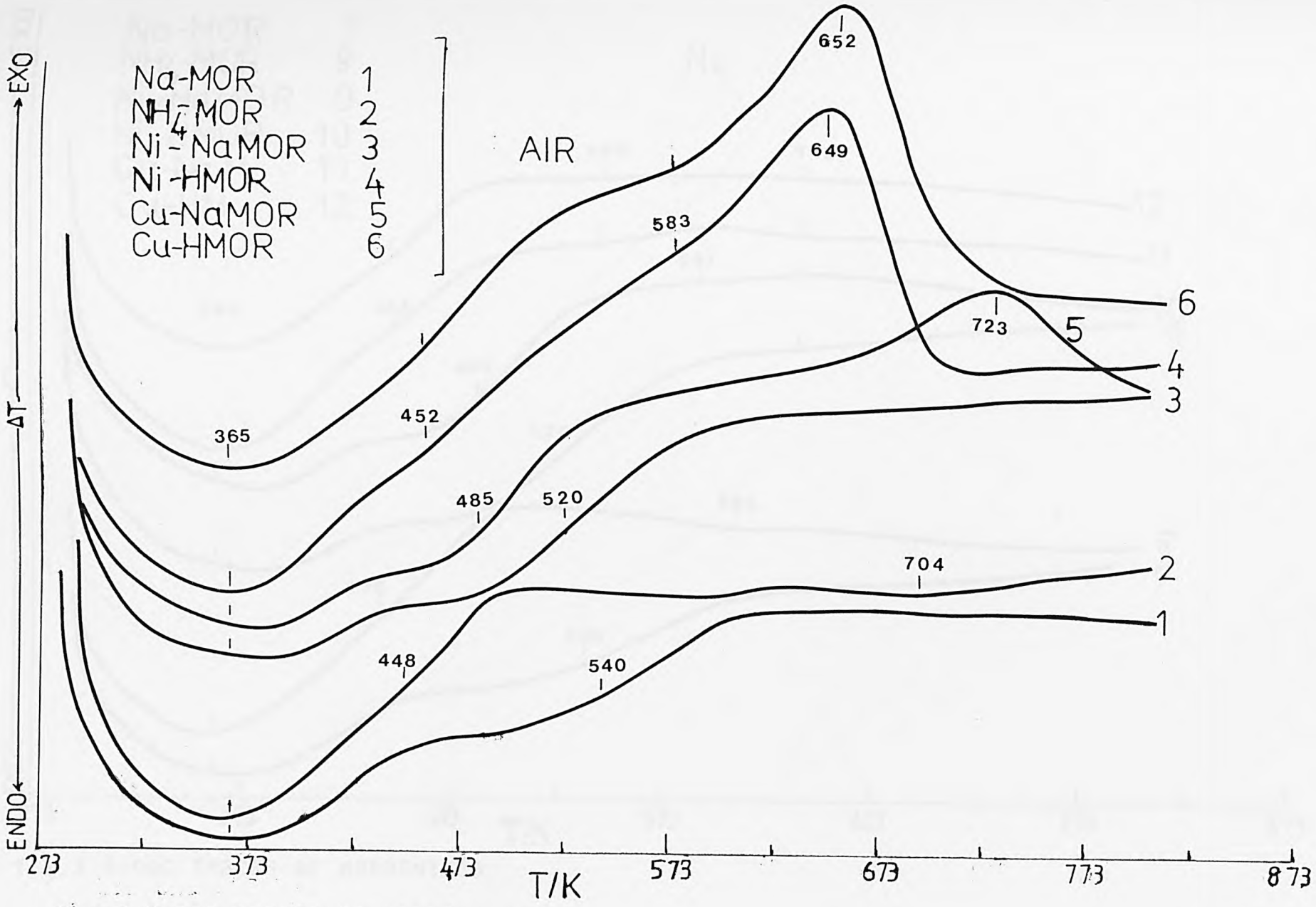

Fig. 3.7 DSC TRACES OF MORDENITES.

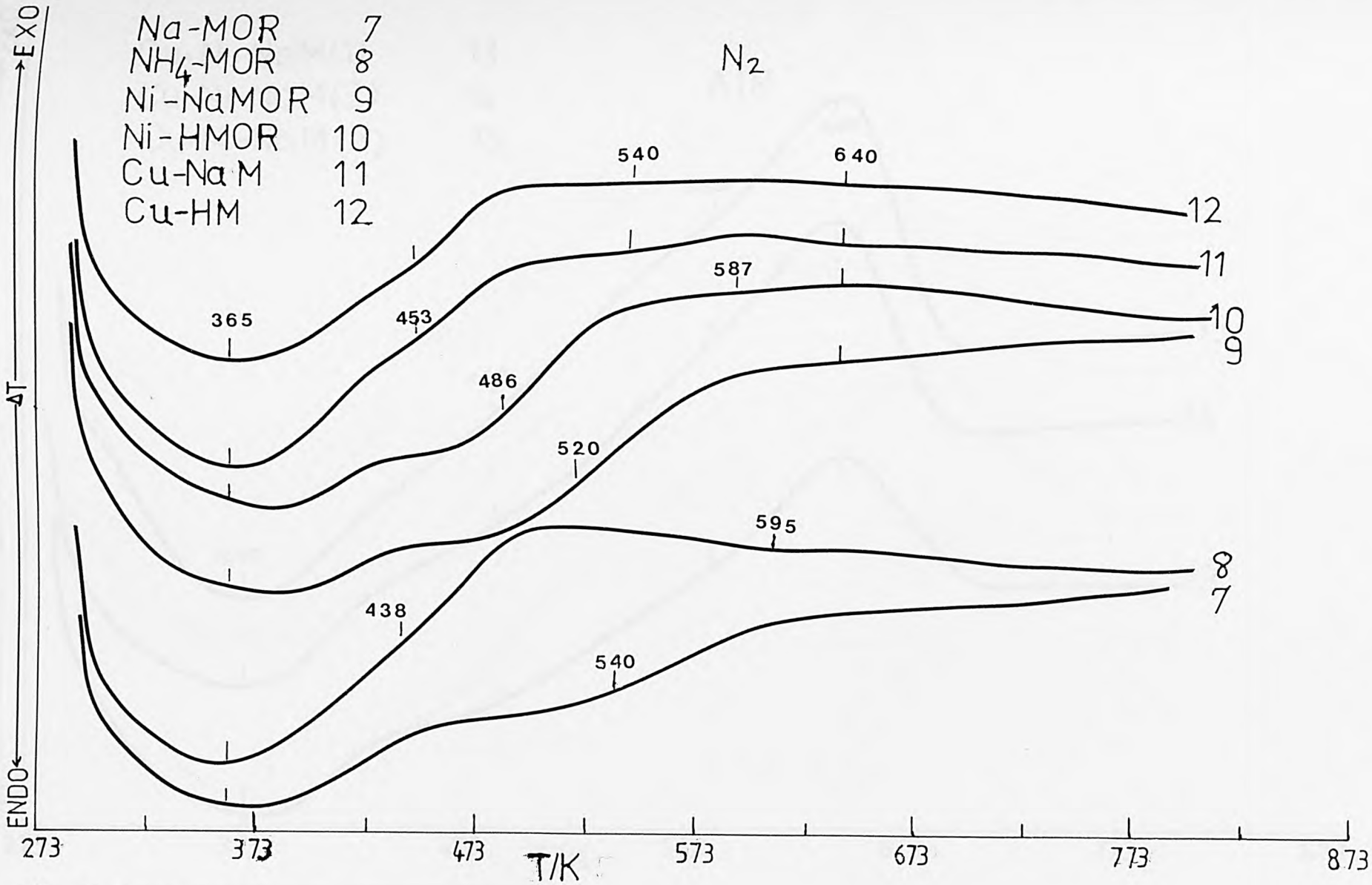

Fig.3.8 DSC TRACES OF MORDENITES.

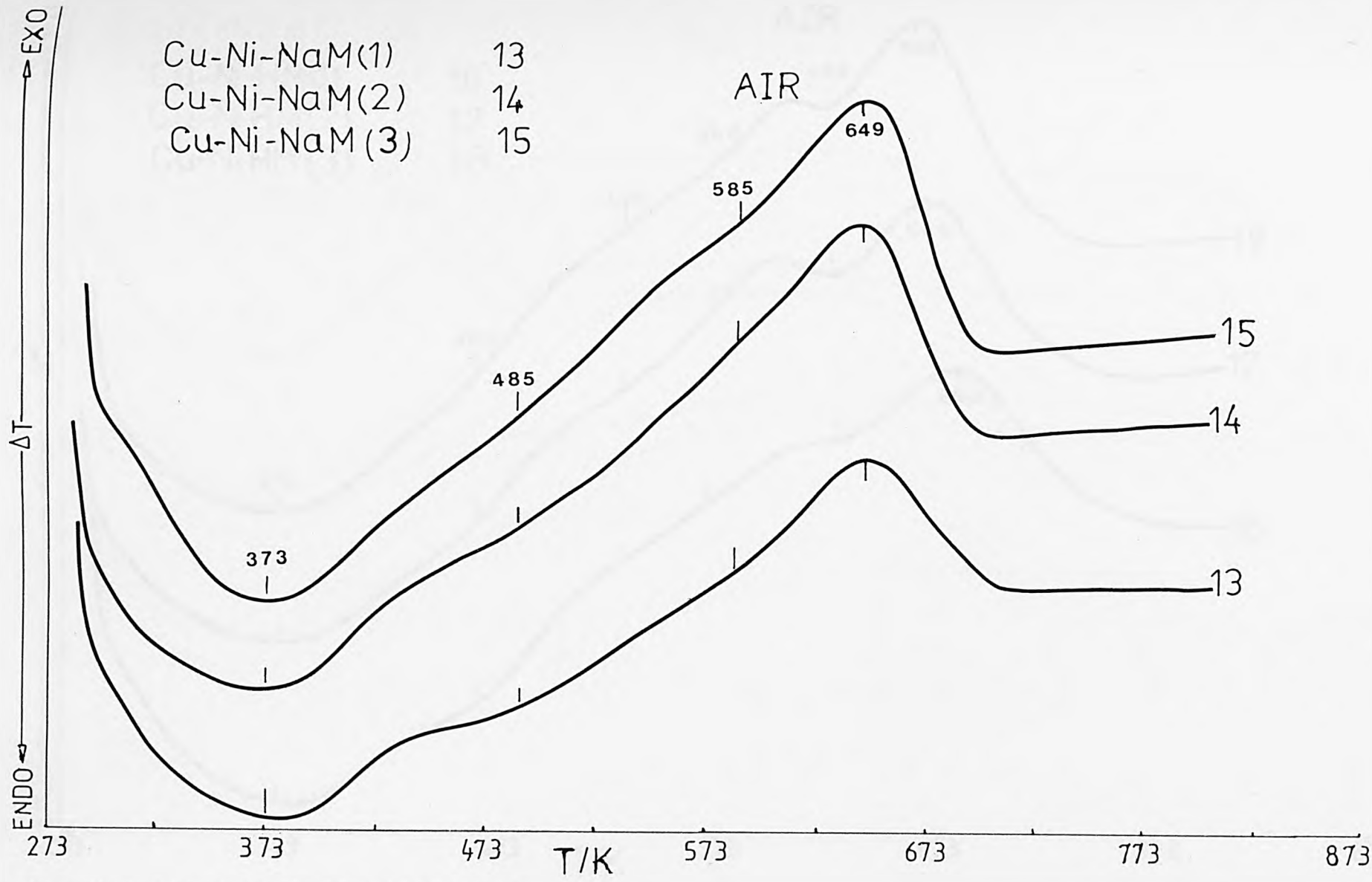

Fig.3.9 DSC TRACES OF MORDENITES.

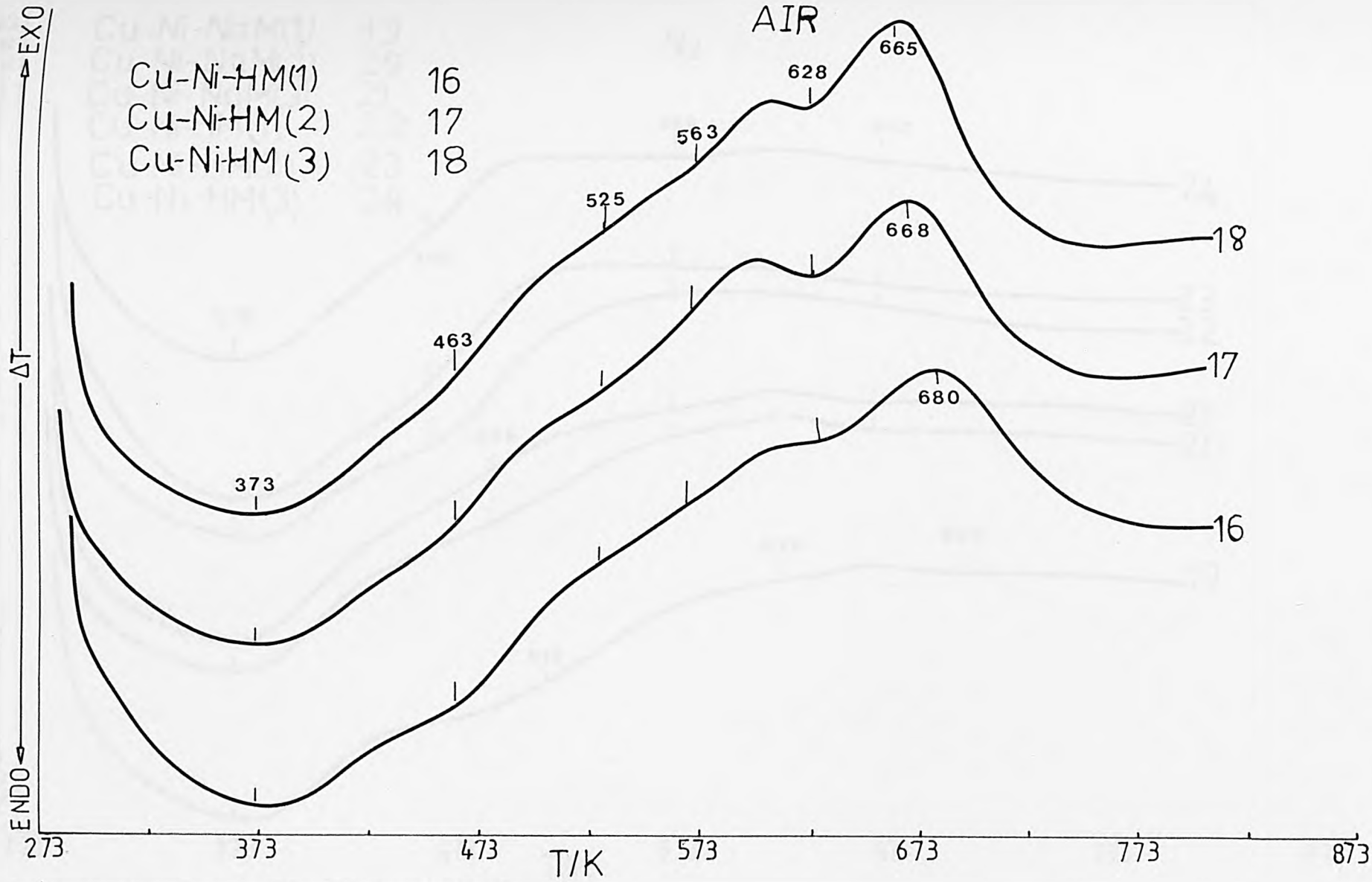

Fig.3.10 DSC TRACES OF MORDENITES.

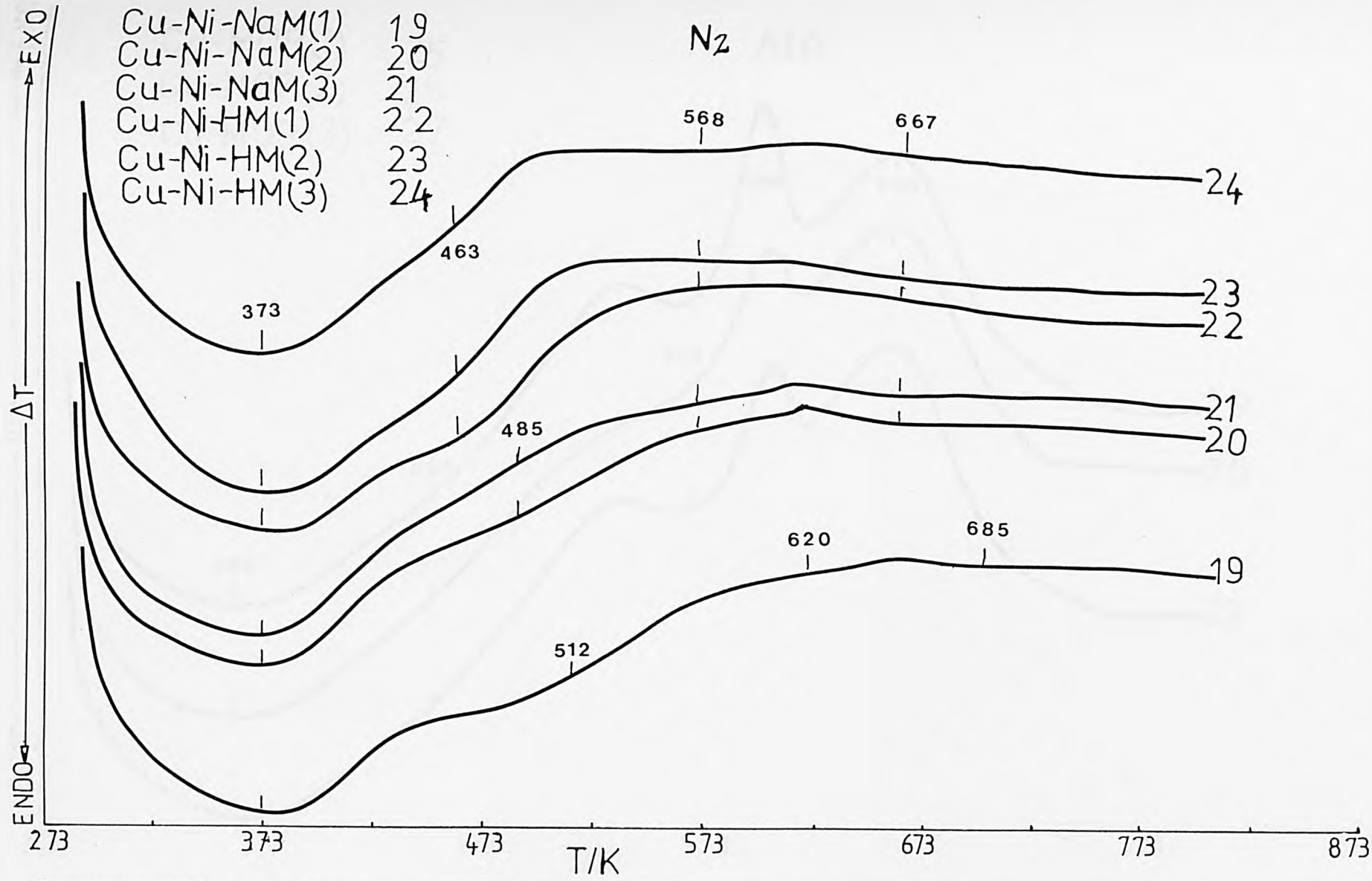

Fig.3.11 DSC TRACES OF MORDENITES.

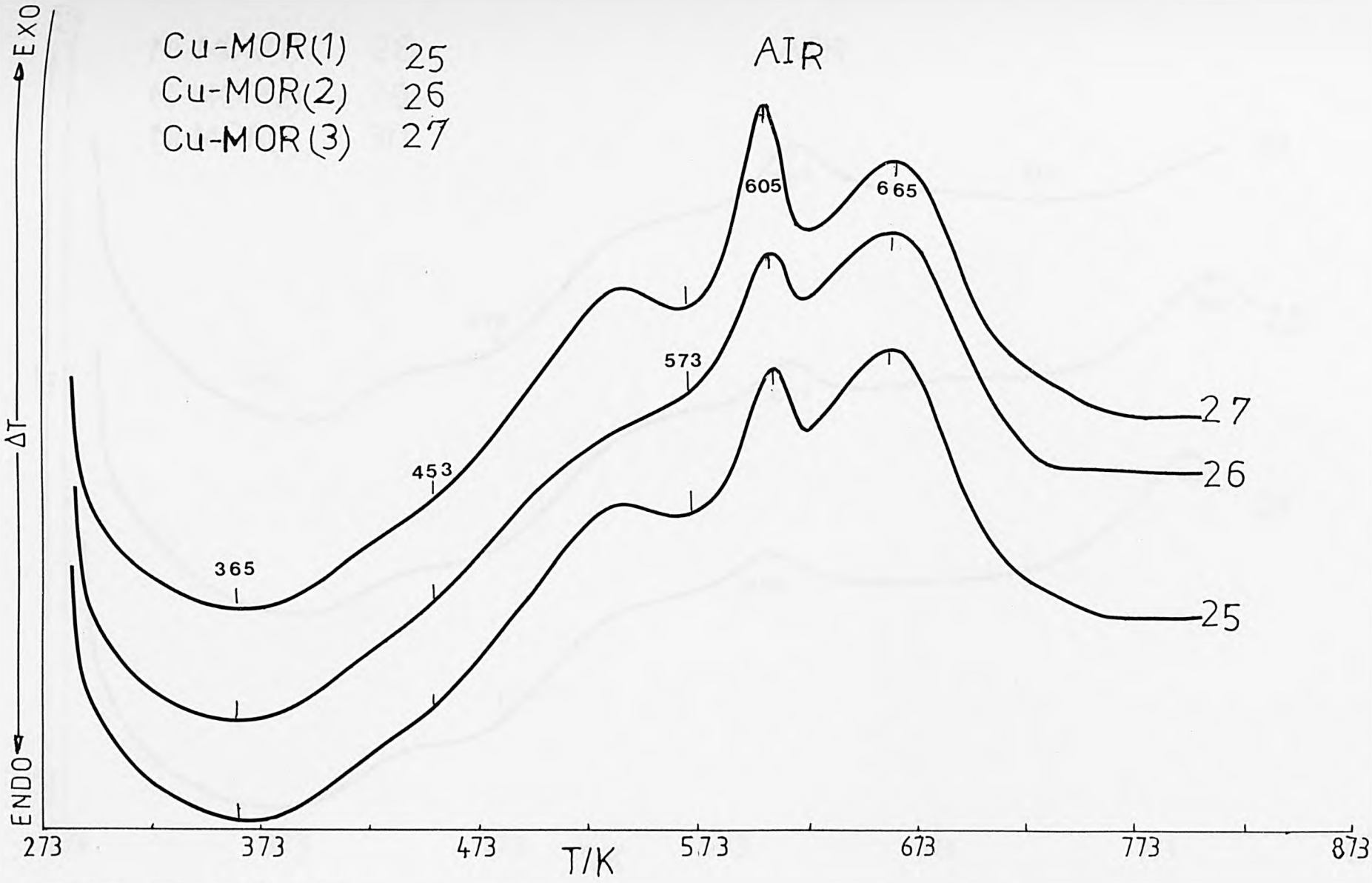

Fig. 3.12 DSC TRACES OF MORDENITES.

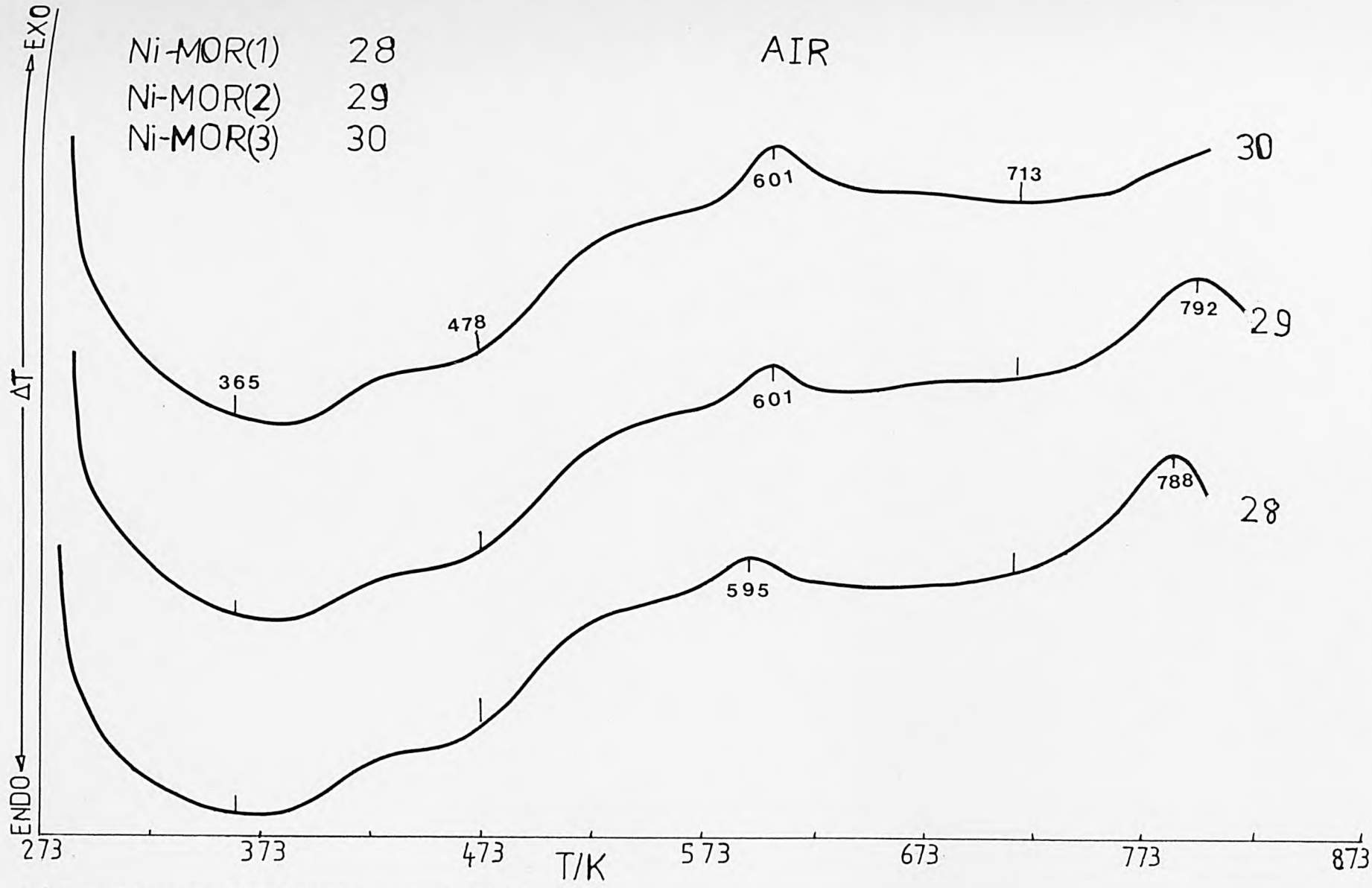

Fig.3.13 DSC TRACES OF MORDENITES.

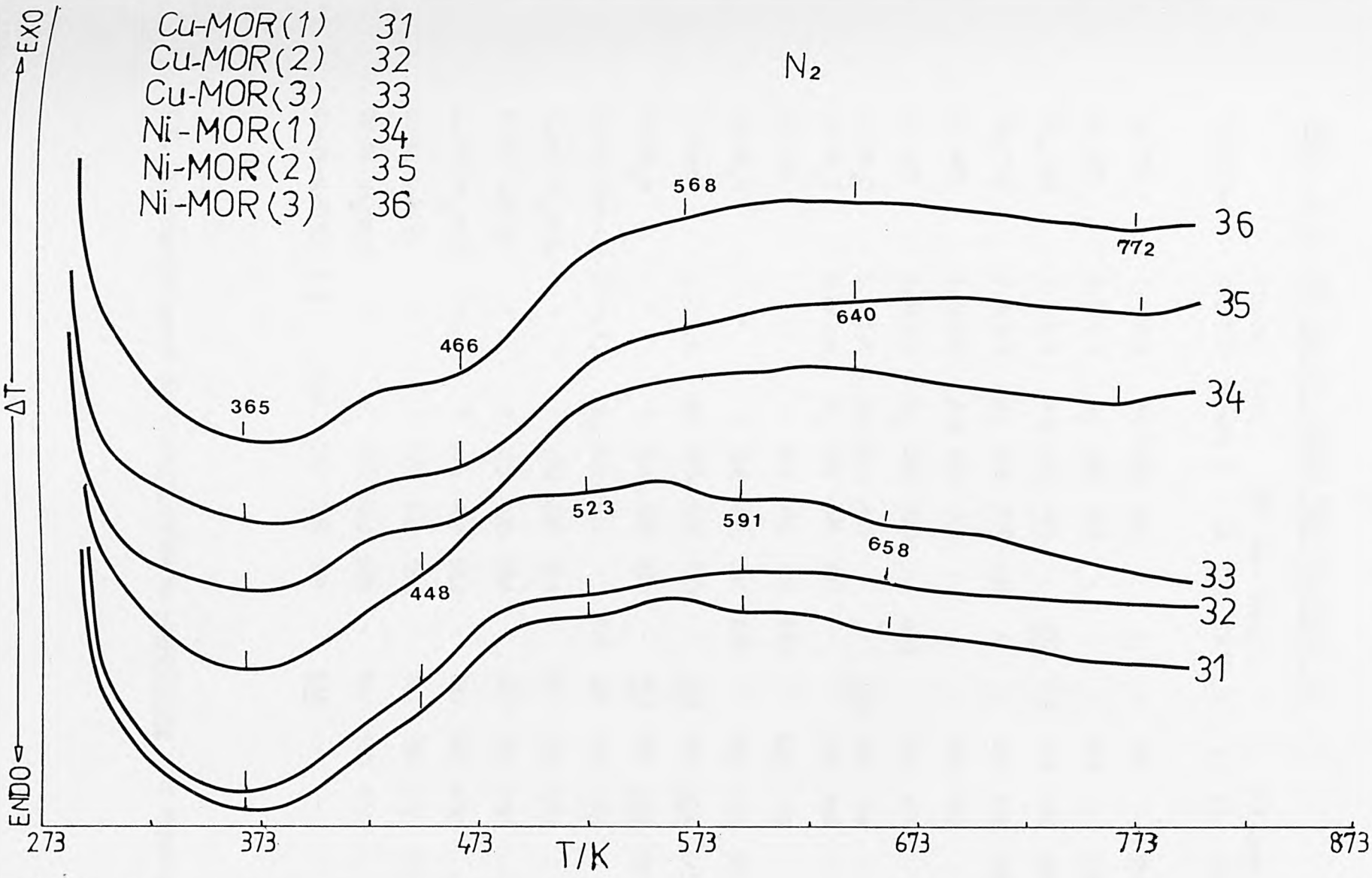

Fig.3.14 DSC TRACES OF MORDENITES

TABLE 3.14 DSC AND DTA CURVES PEAK POSITIONS (K)

Zeolites	figure DSC/DTA	Atmo-sphere	DSC peak temp.(k) I	II	III	IV	V	DTA peak temp.(k) I	II	III	IV	V
Na-MOR	3.7/3.4	Air	365	540	-	-	-	395	-	558	-	-
Na-MOR	3.8/3.4	N_2	365	540	-	-	-	395	-	558	-	-
NH_4-MOR	3.7/3.4	Air	365	448	-	622	704	395	470	558	648	-
NH_4-MOR	3.8/3.4	N_2	365	438	595	-	-	393	470	558	-	683
Ni-NaM	3.7/3.4	Air	365	520	-	-	-	395	507	-	683	
Ni-NaM	3.8/3.4	N_2	365	520	-	640	-	395	507	-	-	684
Ni-NH_4M	3.7/3.4	Air	365	485	-	-	723	395	484	-	-	684
Ni-NH_4M	3.8/3.4	N_2	365	486	587	-	-	395	484	-	-	683
Cu-NaM	"	"	365	453	540	640	-	390	470	-	628	680
Cu-NH_4M	"	"	365	453	540	640	-	390	470	583	628	676
Cu-NaM	3.7/3.5	Air	365	452	583	-	649	390	524	575	625	664
Cu-NH_4M	"	"	365	452	583	-	652	390	524	583	620	664
Cu-Ni-NaM(1)	3.11/3.6	N_2	373	512	-	620	685	390	470	-	-	675
Cu-Ni-NH_4M(1)	"	"	373	463	568	-	667	390	470	-	-	675
Cu-Ni-NaM(2)	"	"	373	485	568	-	667	390	470	-	-	675
Cu-Ni-NH_4M(2)	"	"	373	463	568	-	667	390	470	-	-	675
Cu-Ni-NaM(3)	"	"	373	485	568	-	667	390	470	518	625	-
Cu-Ni-NH_4M(3)	"	"	373	463	568	-	667	390	470	-	625	-
Cu-Ni-NaM(1)	3.9	Air	373	485	585	-	649	-	-	-	-	-

N.B. Exothermic peaks are distinguished by underlining the readings.

continued:

TABLE 3.14 DSC AND DTA CURVES PEAK POSITIONS (K)

Zeolites	figures DSC/DTA	Atmos-phere	DSC peak temp. (k) I	II	III	IV	V	DTA peak temp.(k) I	II	III	IV	V
Cu-Ni-NH_4M(1)	3.10	Air	373	463	563	628	680					
Cu-Ni-NaM(2)	3.9	Air	373	485	585	-	649					
Cu-Ni-NH_4M(2)	3.10	"	373	463	563	628	668					
Cu-Ni-NaM(3)	3.9	"	373	485	585	-	649					
Cu-Ni-NH_4M(3)	3.10	"	373	463	563	628	665					
Cu-MOR(1)	3.12	"	365	453	573	605	665					
Cu-MOR(2)	"	"	365	453	573	605	665					
Cu-MOR(3)	"	"	365	453	573	605	665					
Ni-MOR(1)	3.13	"	365	478	595	713	788					
Ni-MOR(2)	"	"	365	478	601	713	792					
Ni-MOR(3)	"	"	365	478	601	713	798					
Cu-MOR(1)	3.14	N_2	365	448	523	591	658					
Cu-MOR(2)	"	"	365	448	523	591	658					
Cu-MOR(3)	"	"	365	448	523	591	658					
Ni-MOR(1)	"	"	365	466	587	640	765					
Ni-MOR(2)	"	"	365	466	568	640	771					
Ni-MOR(3)	"	"	365	466	568	640	772					

N.B. Exothermic peaks are distinguished by underlining the readings.

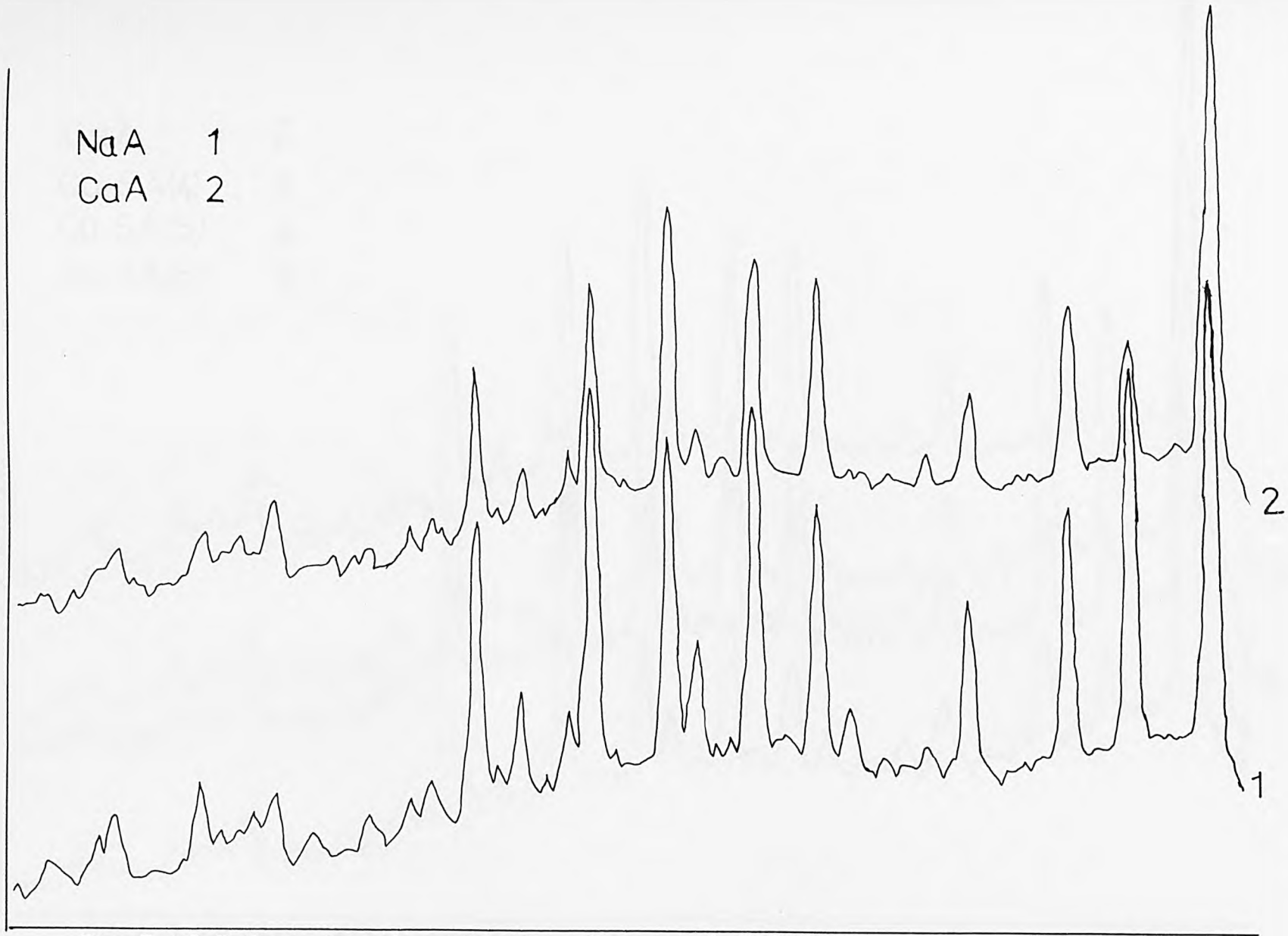

Fig. 3.15 X-Ray microdensitometer traces of NaA, CaA.

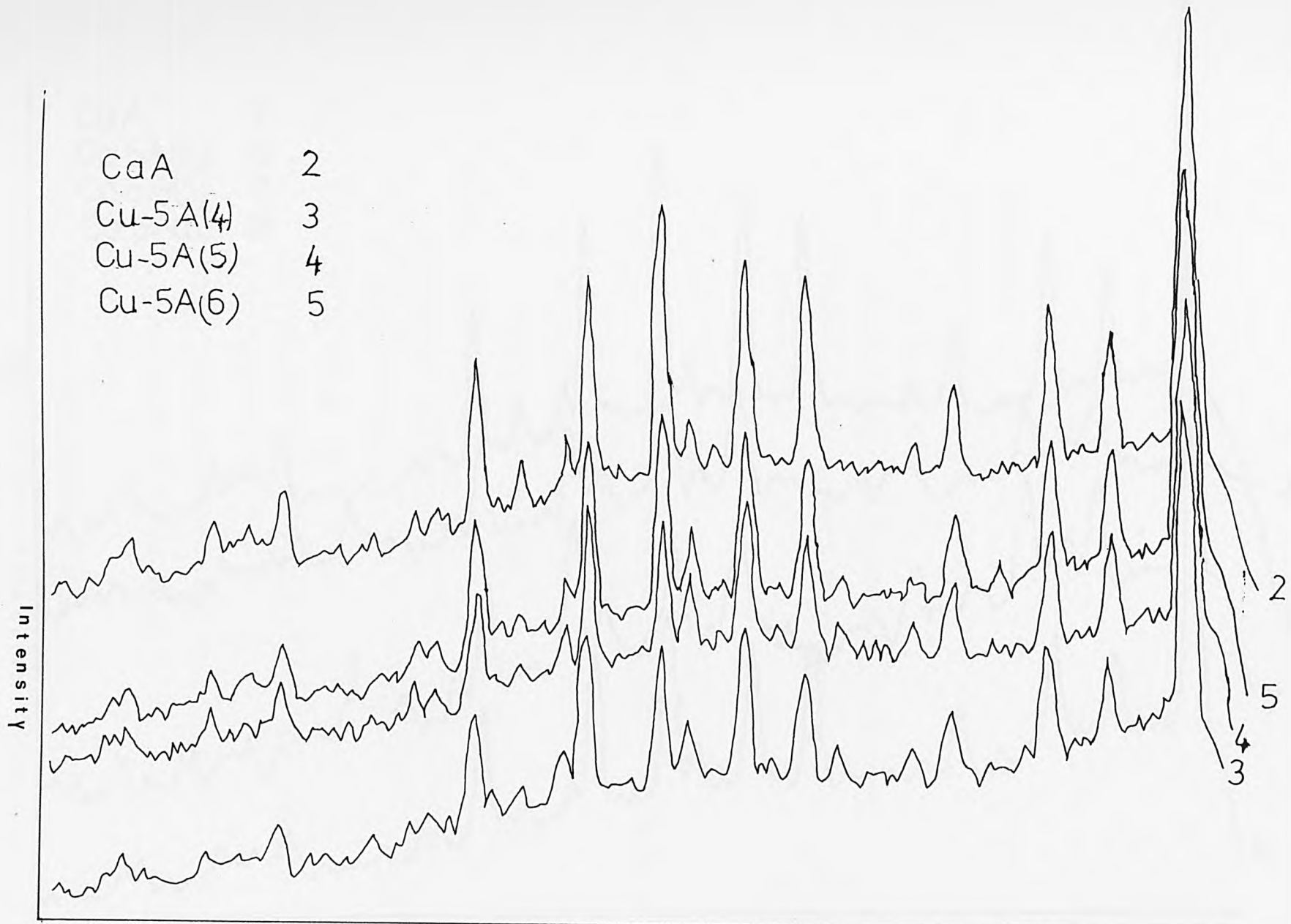

Fig.3.16 X-Ray microdensitometer traces of CaA, Cu-5A(4,5,6). Degrees 2θ

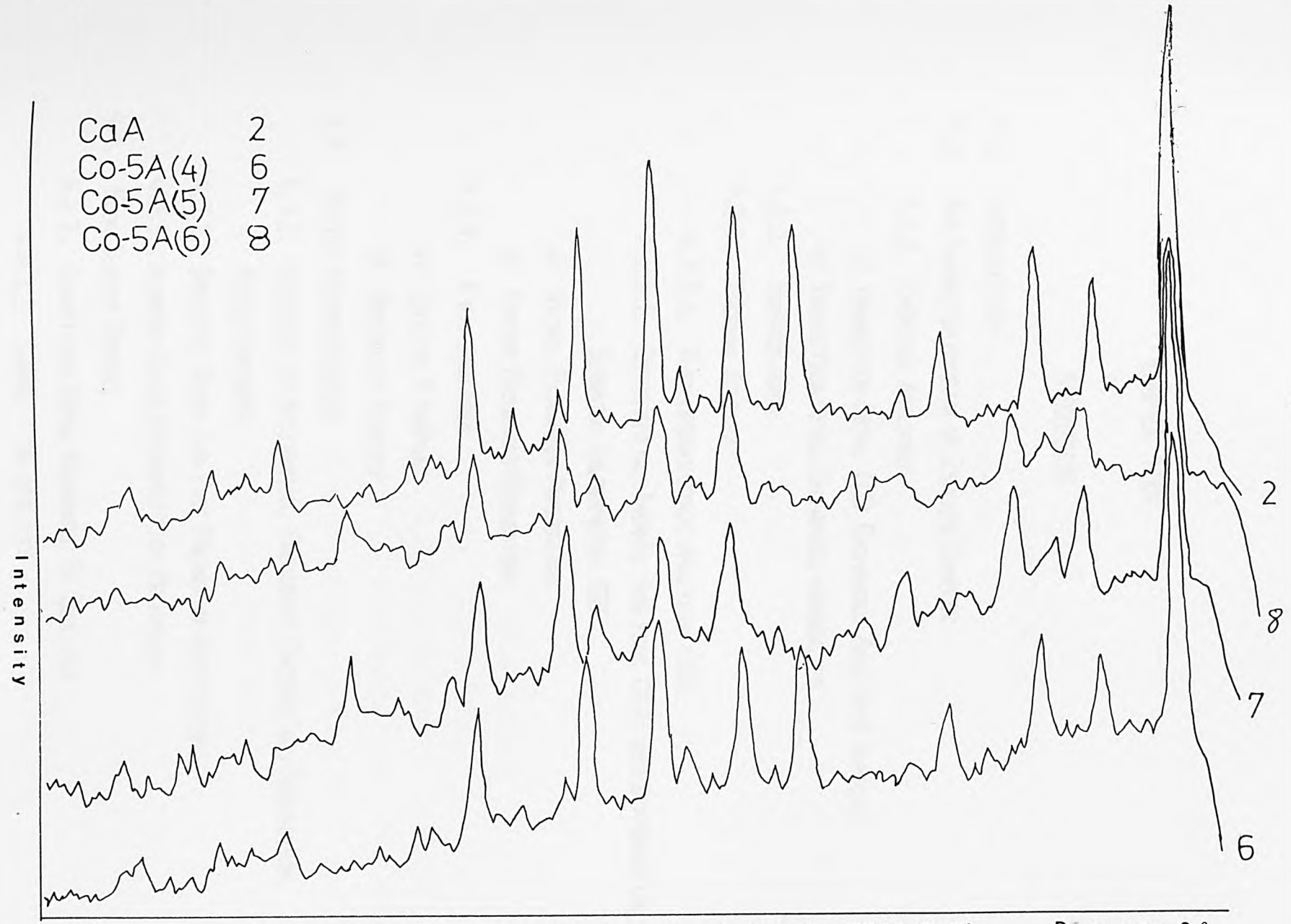

Fig.3.17 X-Ray microdensitometer traces of CaA, Co-5A(4,5,6).

CHAPTER FOUR

DISCUSSION

4.1. INTRODUCTION

This chapter discusses the results obtained when characterising the transition metal exchanged zeolite samples and the results from subsequent experiments on their catalytic activities for both nitrous oxide decomposition and methane oxidation reactions.

4.2. THE CHARACTERIZATION OF ZEOLITE SAMPLES

Characterization of the catalyst samples involved full chemical analyses, surface area measurements, thermal analyses and X-ray diffraction studies of the catalysts prepared.

4.2.1. Chemical Analyses

a) Transition metal (II) exchanged zeolite A samples

Chemical composition data given in appendix Ia (with tables 3.1 and 3.2) show increases in water contents from 4A→5A→M^{2+}-exchanged-5A zeolites. The difference in the water content for 4A and 5A agrees with literature[23] and (obviously) indicates that more void space is available to accommodate intracrystalline water when the monovalent sodium are replaced by divalent calcium ions. The percentage equilibrated water contents for hydrated 4A and 5A-zeolites were 22.23% (26.7 p.u.c.) and 23.69% (29.04p.u.c.) respectively. Breck[23] quotes values for the number of water molecules per unit cell (p.87) of 27 and 30 respectively, close to the values reported here. The slightly lower number of water molecules in 5A reported here was probably due to the fact that the sample was not a fully Ca-exchanged-A zeolite but in fact contained 4.88 Ca^{2+}, 1.93Na^{+} and 0.34H^{+} ions per

unit cell. In the case of hydrated Cu-exchanged 5A-zeolite, the water content increased from 23.51% (28.7p.u.c.) to 25.55% (31.8p.u.c.) for an increase in the copper content per unit cell from 0.24 to 1.49, while in the case of hydrated Co-exchanged 5A-zeolite, the water content increased from 23.38% (28.7p.u.c.) to 26.16% (33.7p.u.c.) when the cobalt content per unit cell increased from 0.36 to 3.13p.u.c. General trends of increase of water content with increase in the number of M^{2+} ions per unit cell of the zeolite were maintained in both the cases *viz*, Cu^{2+} and Co^{2+}. Breck[23] (pp.89 and 428) has discussed the effects that the presence of different cations in the zeolite A has on the pore volume. The Pauling ionic radii [304] (pp.14) for Na^{+} (0.95Å), Ca^{2+} (0.99Å) Cu^{2+} (0.72Å) and Co^{2+} (0.74Å) conform with the data above; when the sodium ions exchange with divalent ions of smaller ionic radii, the change in water content is a maximum. Thus the exchange of sodium by calcium increases the pore volume (and hence the water content) due to the 50% change in the total cation density (no. of cations per unit cell). Then the difference in ionic radii of calcium copper and cobalt explains the increase of water content when calcium in 5A was exchanged by either copper or cobalt metal ions. The somewhat higher water content for Co-5A zeolites as compared to Cu-5A zeolites was probably due to more specific coordination and consequently a greater ordering of water molecules around Co^{2+} ions than round Cu^{2+} ions. Riley and Seff[204] found that for each Co^{2+} ion entering into A zeolite after the first one, three additional water molecules were added into the zeolite cages, High water content in M^{2+} exchanged A zeolite was also due to the fact that Co^{2+} and Cu^{2+} ions have the capability of forming complexes with water molecules, in which the water molecules are strongly coordinated with M^{2+} ions giving rise to a tightly packed environment. Fletcher and Townsend [262] showed that water contents of the silver X and Y zeolites and Ag-

mordenite were higher than the sodium forms, indicating that the tight binding of Ag^+ ions at cationic sites within the zeolite framework provides more space for intra-crystalline water. They[262] also consider Sherry's[191] discussions on this matter, noting that in A (which has the higher charge density than X) the "Ag^+ ions co-ordinate directly to lattice oxygen atoms and thereby free the intracrystalline water." Coughlan and Carrol[222] reported a water content for $Cu_{1.8}$-A zeolite as 29.7 p.u.c., which complements the results presented here.

Silica content determinations employing the Na_2CO_3/K_2CO_3 fusion method (only employed for transition metal free samples §2.2.3) or using an HF treatment, were equally good and the results were generally quite consistent. Alumina contents by the oxine method worked well. The SiO_2/Al_2O_3 ratio as from the typical oxide formula of zeolite A ($Na_2O.Al_2O_3.2SiO_2.4.5H_2O$) is theoretically 2. The overall SiO_2/Al_2O_3 variations observed in the results reported here, are within experimental uncertainty consistent with theory.

Attempts to analyse for calcium using the tungstate method (from HF treated sample solutions) were unsatisfactory because the precipitation of calcium as calcium tungstate ($CaWO_4$) was not only very slow but also proved to be non-quantitative. This was probably due to low concentrations of calcium in the sample solutions; interference from ammonium[280] may have been a factor also.

The flame photometric technique, which was successful for Na^+ in 4A and 5A, was not accurate enough for the determination of calcium either, due to the strong interference from sodium, which was always present in the samples. Conventional volumetric methods for Ca^{2+} ion analysis also failed due to the transition metal and silica interferences.

The determination of calcium content using atomic adsorption spectroscopy (AAS) was the only method which proved to be satisfactory, using a nitrous oxide/acetylene flame. AAS was also employed for the analyses of transition metal contents (Cu^{2+}, Co^{2+}) using in these cases a normal air-acetylene flame; other "wet" methods of analyses produced high errors due to interferences from sodium, calcium and silicon. The application of AAS for the analyses of calcium and transition metals in zeolites was recently reported by Evmerides and Dwyer[305]. Experience in this work agreed well with theirs.

Small discrepancies between the sums of the total metal contents and the aluminium contents per unit cell were assumed to be due to the small amounts of ion exchanged hydronium ions; these levels were however not over significant. The deficiency in the metal cation balance in chemical analysis has been reported[306] before and was attributed to partial hydrolysis of the cation replacement by hydronium ion. Firor and Seff[205a] suggested that protons produced by the transition metal ions during hydrolysis do not harm the crystallinity of the zeolite framework, a conclusion not contradicted by X-ray studies conducted in this work (§4.2.4).

b) Transition metal exchanged mordenites.

Results in appendix Ib (and tables 3.3.-4) indicate that the trend of increasing water contents with the increase in transition metal content per unit cell was also observed for (Ni^{2+}, Cu^{2+}, Pt^{2+})-exchanged mordenites. The water content changes for different samples are as follows:

i) Ni-MOR: an increase from 13.3%(2.66p.u.c.) to 15.05%(30.7p.u.c.) for an increase in nickel ions p.u.c. of 1.13 to 1.64 in nickel ion content per unit cell. However, deviations from the general trend occurred at nickel contents of 1.44 and 1.59 p.u.c. ($Ni\text{-}NH_4MOR$ and Ni-MOR(3)), possibly due to analytical errors, or insufficient saturation of the samples with

water vapour.

ii) Cu-MOR: an increase from 10.11% (20.16p.u.c.) to 10.79%(21.7 p.u.c.), for an increase in copper ions per unit cell of 2.03 to 2.47p.u.c., and

iii) Pt-MOR: an increase from 12.44%(26.45p.u.c.) to 13.51%(29.75p.u.c.) with a corresponding platinum content increase of 1.76 to 2.52p.u.c.

In general, the changes in water content p.u.c. for transition metal exchanged mordenites conformed to the series $Ni^{2+} > Cu^{2+} > Pt^{2*}$, which is in accordance to their ionic radii differences[304]. Reasons for this trend are similar to those suggested above for transition metal exchanged A zeolites (4.2.1a).

Results from ammonium analyses by the Kjeldahl method and the transition metal (Ni, Cu, Pt) analyses by AAS were quite consistent.

4.2.2. Surface Area

Table 3.5 summarises the surface areas of transition metal exchanged A zeolites. These are best referred to as "monolayer equivalent surface areas" (MESA's) as recommended by Barrer[25]. He used this term for the area which would be covered by guest molecules in the intracrystalline pores if all the molecules are removed and placed in a close-packed monolayer upon an ideally smooth surface plane. The amount of gas or liquid adsorbed by a zeolite usually depends upon pressure, temperature, the nature of the adsorbate and of the zeolite itself. During adsorption, the intracrystalline voids and channels of the dehydrated zeolite fill with the adsorbate and when filling is complete, the adsorption stops. This gives rise to pseudo-Langmuir behaviour, and a type I isotherm (figure 3.1 and 3.2) because of strong adsorbate-adosrbent interactions during the filling of the micropores (discussed by Ries[307]).

The external "surface area" of a zeolite is normally very low; typical figures quoted are $\sim 3 m^2 g^{-1}$ (Breck[23], pp.385) or between 2 and 20 $m^2 g^{-1}$ (Cscicery[308]). The high surface area of zeolite is therefore an internal property primarily. MESA values reported (§ table 3.5) for the transitional exchanged-5A zeolites in this work are fairly high ($\sim$277-510 $m^2 g^{-1}$) and hence are due to total void space available.

Two types of void spaces are present in zeoliteA *viz*:

i) the small spherical voids within the β-cages with a diameter of 6.6Å and accessible to only small molecules (eg. water), and

ii) the large voids in the α-cages of diameter 11.4Å.

Surface area measurements for 5A zeolites exchanged with either cobalt or copper involved Krypton adsorption at 77K. This adsorption occurred only in α-cavities because β- cavity openings are too small to permit entry of Krypton atoms.

In dehydrated Na-A zeolite, the six 8-rings are partially blocked by sodium ions and adsorption of Krypton at 77K is even more restricted. Thus the MESA value is low. When sodium is exchanged by calcium to give 4 Ca^{2+} ions and 4 Na^{+} ions per unit cell, then the 8 site I positions are all occupied but the site II positions (in the 8-rings) become freely available for adsorption and a much higher surface area is obtained[23].

As mentioned earlier (§4.2.1), the presence of cations in the zeolite voids affects the available pore volume for adsorption. The exchange of Na^{+} (r = 0.95Å) by Ca^{2+} (r = 0.99Å) obviously increases the pore volume due to a reduction in the total cation density by half. On the other hand, exchange by lithium (r = 0.60Å) reduces the available pore volume per unit cell through a reduction in the unit cell dimensions[23](pp.428). So where

Na to Ca exchange caused an increase in pore volume and hence the surface area (table 3.5) exchanging calcium (r = 0.99) either by cobalt (r = 0.74Å) or by copper (r = 0.72Å) induced some reduction in the unit cell dimensions and consequently in the total pore volume per unit cell. This is why the Cu-exchanged samples show higher MESA values than do the cobalt exchanged ones and also why there is a slight decrease in surface area (at a given temperature) with an increase in the metal (Co^{2+} or Cu^{2+}) content per unit cell. (see table 3.5). The decrease in surface area which has been taken as a probable indication of structure collapse by other workers[171,194,224] need not be so construed, especially bearing in mind the well-resolved peaks in the X-ray diffraction studies (§4.2.4).

Table 3.5 also reveals that surface areas of the samples activated at 623K were higher than those at 395K. The reason for this is simply that at lower activation temperature (395K), some of the remaining water molecules obstructed the flow of Krypton within the crystal lattice, so the empty space for adsorption was limited. Outgassing of the sample in vacuum at high temperature (625K) resulted in complete hydration of the zeolite, thus facilitating the Kr adsorption through unrestricted openings until saturation point. Higher MESA values for the transition metal (Co and Cu^{2+}) exchanged 5A zeolite were also seen at this higher temperature (see table 3.5).

4.2.3. Thermal Studies

Results of the thermogravimetric analyses (TGA), differential thermal analyses (DTA) and differential scanning calorimetry (DSC) measurements are discussed in the following subsections.

4.2.3.1. TGA

Beyer et al[309] observed that thermal decomposition of ammonium forms of

faujasite, clinoptilolite and mordenite was completed in three distinct steps. Most of the water was lost during the pretreatment of the zeolites at 453K in air, followed by the release of NH_3 over the range 623-823K. A final loss at 873-993K was taken to be water expiration loss due to dehydroxylation. In another thermoanalytical study[310] weight loss maxima at 805 and 1037K for NH_4-mordenite were ascribed to deammoniation and dehydroxylation respectively.

Breck[23] (pp.474) reported that continued thermal treatment of NH_4-exchanged zeolites causes in addition to dehydration and deammoniation the removal of a water molecule formed from two neighbouring hydroxyl groups . In case of two-step water loss, the first is normally due to loosley bound water, whereas the second weight loss is either from the zeolitic water in cavities or the result of dehydroxylation (usually at higher temperature).

Lechert[311] recently concluded that although much valued information is in principle obtainable from thermal analyses, nevertheless the reproducibility and standardization of the data is quite difficult because factors like the choice of instrument, sensitivity and experimental conditions all affect badly the measured parameters. Thus while thermal analyses are often helpful for direct comparisons by a worker between different samples on a given machine, results reported by different authors can only be compared meaningfully with difficulty.

This divergency of data by different workers is demonstrable for data on mordenite. Barrer and Peterson[312] obtained a total weight loss on H-mordenite by TG of 15.1%, instead of the 14% calculated by chemical analysis. Breck[23] (pp.450) proposed 16% weight loss for mordenites using TGA. In another study[313], the total weight loss noted for Na-MOR and

H-MOR were 13.6 and 14.8%, respectively. Weight losses reported here (table 3.13) for Na-MOR and H-MOR as found by TG were 13.9 and 13.1%, yet the chemical analyses (appendix 1b) gave corresponding values of 13.4 and 15.9%.

According to Kuhl[314], while ammonia from zeolite-Y escaped completely at 733K, this same reaction did not complete until 893K in mordenite. The range reported by him for mordenite dehydroxylation was 798-1153K, whereas Beyer et al[309] suggest this reaction in mordenite to be drawn somewhere between 923-1033K.

TGA thermograms of the different cationic forms of mordenite (figure T1-36) and the resulting data (table 3.13) exhibited somewhat different dehydration/deammoniation phenomena. For the deammonium exchanged mordenites two or three stages of weight loss were observed while the others showed a somewhat similar pattern of a continuous smooth dehydration curve as a function of temperature with higher rate of dehydration at lower temperature range and vice versa, until no further weight losses occurred. In a similar TG study[242] different cationic forms of mordenite shared a 19-30% zeolitic water loss up to 373K, while on increasing temperature to 753K the Na-MOR, Ni-NaMOR and Mn-Na-MOR samples were completely dehydrated. In contrast, samples of CrNa-MOR, CuNa-MOR and CoNa-MOR were found to lose 98,99 and 93% of their zeolitic water respectively. In this study, all the mordenite samples released physically adsorbed loosely -bound water below 550±60K (the presence of ammonium ions affected the temperature range), followed by a smooth combined water/NH_3 loss (obvious from TG curves). Na-MOR and NiNa-MOR completely dehydrated around 700K but for other samples the weight loss continued (due to NH_3) to temperatures in the range 950±60K. In some

samples (eg. Cu/NH_4-MOR and Cu-MOR (1-3), the observed weight loss beyond 900K could be regarded as being due to dehydroxylation.

Analysis of TGA curves gave variations in the water contents of the mordenites with change in size of the exchanged cations which were similar in trend to the results of chemical analysis (§4.2.1). However, the total weight loss obtained by TGA (table 3.13) did not match the data from chemical analyses (appendix 1b). One possibility that the lower observed values of water/NH_3 content were due to partial crystal breakdown at high temperature, can be easily ruled out on the basis of following reasoning:-

i) X-ray diffraction patters of the samples (§4.2.4) at room temperature and even at high temperatures were well resolved and did not show any evidence of significant structure collapse, and

ii) the fact that mordenite has structure related (§1.4.5) high thermal stability[32,233].

More likely reasons can be either imcomplete equilibration[315] of the samples over saturated sodium chloride solution prior to TGA studies, or instrumental error (most likely with Mettler system), or a cumulative effect of both.

Finally, TG thermograms of the mordenites with same cations were identical in shape while for samples having different cations dissimilarity was quite obvious, which could be due to differences in complex-forming properties of the M^{2+} (Ni or Cu) cations with water and/or ammonia.

4.2.3.2. DTA and DSC

The results of DTA and DSC studies in the temperature region 300-800K are dealt with together because these techniques are in many respects complementary to one another. The peak maxima and minima at particular temperature

(K) in table 3.14 are taken from figures 3.4-3.6 (DTA) and figures 3.7-3.14 (DSC curves), and are given for a constant weight of the samples (15mg each for DTA and 20mg each for DSC).

A general view of the thermograms clearly reveals that endothermic peaks (indicative of desorption processes) were predominant. The height and broadness of the main endothermic peaks (preferably in lower temperature range) usually depict qualitatively the effects that zeolite structure and type of exchanged cations have on the amount of the evolved adsorbent as a function of increase in temperature.

The starting shoulder at 319K in DTA curves (common in all samples) is analogous to an idealised second order transition, showing a discontinuity in the heat content of zeolite samples as compared to the reference (Al_2O_3). The first DTA endotherm for dehydration or dehydration/deammoniation was a maximum on all plots at ∿395K, both in air or nitrogen atmosphere. The corresponding first DSC endotherm showed a peak on all plots at ∿365K. The difference in peak positions of DTA and DSC thermograms must be ascibred to the difference in methodology (see §4.2.3.1 and Lechert[311]).

Thermograms of Na-MOR (fig. 3.4, 3.7-8) revealed two broad overlapping endotherms (with DTA peaks at 395K and 558K and corresponding DSC peak positions at 365K and 540K). Both these peaks may be associated with water loss suggesting at least two water sites in sodium mordenite. For the ammonium form, the initial endotherms were close enough to be treated as single broad curve with a peak at ∿450K. This intimacy of endotherms could probably be due to the simultaneous water/NH_3 loss at 450K. Ammonia evolution under air, was demonstrated by an exothermic peak (at 648K for the

DTA and 622K for the corresponding DSC curve) due to the oxidation of ammonia. This has been observed also by other workers[79,309,316]. Mordenite is thermally stable up to 1073K[23] (pp.457) so the criterion of taking the first exothermic peak position as a measure of stability[317] is not relevant, and was ignored here.

The differences in broadness of the endothermic peaks for different exchange forms containing either monovalent (Na^+,NH_4^+) or divalent (Ni^{2+}, Cu^{2+}) cations in mordenite were quite obvious (e.g. figure 3.4 (DTA) and fig. 3.7 (DSC). The size of the endothermic peak (normally proportional to the H_2O/NH_3 content) varied in the order $Na^+ > Cu^{2+}$ for divalent cations. This trend in peak sizes conformed well with the increase of their kinetic radii (*viz* $Ni^{2+} < Cu^{2+} < Na^+ < NH_4^+$). Toth *et al*[318] observed that for zeoliteA and X, the physically adsorbed water and its heat of bonding, decreased with increase in ionic radii for exchanged ions of same charge, and varied directly with cation charge for ions of approximately the same ionic radius.

The asymmetric nature of the endothermic peaks could be attributed to the presence of more than one type of water/NH_3 complexes of the cations within the mordenite framework. Similarly, the dissimilarity in shapes of the thermograms can be assigned primarily to differences in complex-forming capabilities of the exchanged cations in the samples. Recently[319] the differences in respective peak positions for sodium or ammonium forms of copper exchanged Y-zeolite were related to changes in the degree and strength of coordination complexes of copper with water or ammonia as the concentration of copper ions increased in the zeolite lattice.

Particular aspects of the thermal analyses of the nickel and copper exchanged mordenites are discussed below.

(a) Nickel-exchanged mordenites.

Appendix Ib gives the percentage exchange level of Ni/NH_4-MOR and Ni/Na-MOR as 37.9 and 45.7 respectively. The DTA and DSC thermograms of these samples are given in figures 3.4 and 3.7-8, while table 3.14 lists their respective peak positions.

The loss of most of the water from Ni/Na-MOR and Ni/NH_4-MOR was characterised by endothermic peaks at 395K (DTA, fig.3.4) or 365K (DSC fig. 3.7-8), both in air or nitrogen atmosphere. The second, and partially overlapping endotherms for Ni/Na-MOR, had maximum at 507K(DTA) or 520K(DSC) while for Ni/NH_4-MOR, the corresponding peaks had a maximum at 484K(DTA) or 486K(DSC). The difference in respective peak positions (as said earlier) must be due to differences in the technique employed. The overlap of the first and second peak, also observed in a similar study[319], was termed as a "cleavage tendency of the peaks" and difference in its position was attributed to the changes in the complexes with water or ammonia. The DTA endotherm for Ni/NH_4-MOR at 682 ± 2K was due to the release of NH_3 and appeared as a clear DSC exotherm positioned at 723K under air (fig. 3.7); the absence of these peaks for Ni/Na-MOR under similar conditions can be cited in support of this interpretation.

The other nickel-exchanged mordenites (*viz*, Ni-MOR (1-3) having exchange levels of 31.4, 40.2 and 42.6% (app. Ib)), were prepared at room temperature by repeated exchanges (§2.3.2.1.2). For almost constant sodium levels, an increase in nickel level together with a non-concomitant decrease in the ammonium level of these samples was very significant, probably due to the formation of "excess or non-stoichiometric" nickel, as suggested by other workers[320-21] for nickel and copper exchanged zeolites X and Y.

DSC curves of Ni-MOR (1-3) under air are presented in fig. 3.13. Water loss occurred with two endothermic peaks at 365K and 478K. Exotherms at ∿600K were due to the oxidation of NH_3, as discussed earlier. The additional exotherms at 793 ± 5K were most likely due to the excess Ni^{2+}, as the peaks broadened with the increase in the metal content of the samples (see comment below regarding Schoonheydt's study on Ni-Na-Y).

Though the first endothermic maximum (due to water loss) appeared at the same temperature (365K) whether DTA or DSC was employed, other DSC peak positions changed slightly using nitrogen atmosphere (fig. 3.14). The extra exotherm due to non-stoichiometric nickel seems to appear in the same region..

Using DTA, Schoonheydt *et al*[320] observed endotherms with Ni/Na-Y at 673±10K (only for samples having 'excess' metal) and they coordinated this with a weight loss of hydroxylated precipitate as it dehydrates to nickel oxide. It is suggested that similar inferences can be drawn for excess nickel containing mordenites here.

(b) Copper-exchanged mordenites

Cu/Ni-MOR, and Cu/NH_4-MOR had exchange levels of 53.9 and 61% with respect to copper (appendix Ib). The DTA and DSC curves are well-expressed (fig. 3.5, 3.7-8), and the salient points are listed in table 3.14. On the whole, they are more complicated than the nickel samples, especially under air. Both the Cu/Na-MOR and Cu/NH_4-MOR samples were prepared using ammonium mordenite as the starting material (§2.3.2.2.), so each had in common an ammonium content, although with different levels.

The endotherms at 390K (arising from water loss), were followed by very sharp exotherms with peaks at 524K due to oxidation of ammonia within the

zeolite (this ammonia, in addition to that complexed with the metal ions, can be identified on the basis of unit cell composition (table 3.3) for the copper exchanged mordenites). The subsequent exotherms at 622 ± 3K and 664K, were due to the evolution of ammonia complexed to copper(II) ions. These samples when studied under a nitrogen atmosphere showed similar water loss endotherms at 390K, with shoulders at 470K. Additional endotherms at 625K (Cu/Na-MOR) and 583K (Cu/NH_4-MOR) may be interpreted as the release of ammonia. A small endotherm with a peak at 676K was also observed. In a comparative study[319] on Cu/Na-Y and Cu/NH_4-Y, an endothermic peak at 723K (Cu/Na-Y) was connected to the formation of a(Cu-O-Cu) -type bridge. The absence of this peak for Cu/NH_4-Y was taken as proof in support of the conclusion that the presence of NH_3 in coordination sphere of Cu(II) obstructs the formation of such a bridge[319]. No such implication was possible here because both samples (Cu/Na-MOR and Cu/NH_4-MOR) had substantial ammonia contents. Dyer and Barri[322] have also given DTA profiles of Na/Cu-X.

DSC curves obtained for the Cu/Na-MOR and Cu/NH_4-MOR samples show two endotherms for weight loss due to water removal at 365K and 453K (fig. 3.7) and a distinct oxidation exotherm at 650 ± 2K for samples heated in presence of air. Corresponding DSC curves obtained under a nitrogen atmosphere, recorded two identical endotherms at 365K and 453K for water loss, and two additional endotherms at 540K and 640K for water/ammonia or ammonia loss.

The peak temperature of the first DTA exotherm was used as a criterion of stability in copper(II) exchanged X[317] and Y[319] samples, in order to infer that copper(II) ion destabilised the zeolitic structure more effectively than did other divalent transition metal (e.g. Ni^{2+}). No such conclusion

could be deduced here because mordenite was found to be thermally stable up to 1073K[23](pp.457), well beyond the temperature range (R.T.→873K) used for DTA and DSC in this study.

The samples Cu-MOR (1-3) were, like Ni-MOR (1-3), prepared using several exchanges (§2.3.2.1.3) to give copper contents of 56.7, 60.1 and 68.7%. The chemical composition of the samples showed, in common with the nickel samples, that while the sodium level remained almost constant, the increase in copper content was comparatively more than the decrease in ammonium level, suggesting an accumulation of 'excess' copper as some form of non-stoichiometric precipitate. A similar series of non-stoichiometric CuNa-Y zeolites[320] showed a supplementary endotherm at 613 ± 10K, while some NaCu-X[321] samples prepared by ion-exchange involving alkalinity recorded an extra endotherm around 600K due to decomposition of non-stoichiometric metal precipitate.

A DSC study only of Cu-MOR (1-3) was carried out, to give the curves shown in figures 3.12 and 3.14. Water loss was indicated by two endotherms at 365K and 453K (fig. 3.12) while clear exotherms at 605K were again due to oxidation of ammonia complexed to the metal. The other dominant exotherms at 665K were(again) most likely due to non-stoichiometric copper. DSC curves obtained in nitrogen surroundings (fig. 3.14), depicted a starting endotherm in each case at a similar position (365K) but the second endotherm (water/ammonia) was displaced to appear at 448K. The subsequent endotherm at 591K is taken to be ammonia loss, and the final endotherm at 658K is once more attributed to the weight loss associated with non-stoichiometric copper.

(c) Mixed copper-nickel mordenites

These Cu/Ni/Na-MOR (1-3) and Cu/Ni/NH_4-MOR (1-3) samples were prepared by thorough manual mixing of Cu/Na-MOR with Ni/Na-MOR or Cu/NH_4-MOR with Ni/NH_4-MOR respectively in the ratios described earlier (table 3.8). DTA and DSC profiles of these mixtures have almost similar maxima and minima as for their individual components, under the same conditions.

DTA plots under nitrogen are shown in fig. 3.6. The first two endotherms at 390K and 470K were characteristic of all the samples, probably representing two different positions of water molecules in the zeolite framework. The ammonia/ammonium content of the samples is reflected in the endotherms at 625K and 675K. The major difference in shape of the DTA curves was dependent and consistent with the amount of each constituent in the mixtures.

DSC profiles of Cu/Ni/Na-MOR (1-3) and Cu/Ni/NH_4-MOR (1-3) under air are given in fig. 3.9-10, while fig. 3.11 contains the corresponding thermograms observed using nitrogen atmosphere. The common feature of all the curves was a broad endotherm, characteristic of water loss, at 365K with two different cleavage positions in the ranges 463-485 and 525-585K. The width and resemblance of the curves was quite uniform and reflected the behaviour of their primary substances. The samples treated in air had exotherms at 649K for Cu/Ni/Na-MOR (1-3) and 672 ± 8K for Cu/Ni/NH_4-MOR (1-3), with a slight shift towards a lower temperature with increasing copper content. These exotherms could be attributed confidently to the oxidation of NH_3, keeping in view the temperature ranges of the particular changes.

4.2.4. X-ray Analyses

a) Zeolite A samples

Micro-densitometer profiles of Na/Ca-A and M^{2+}(Cu,Co) exchanged-5A zeolites (fig. 3.15-3-17), and taken from the X-ray analysis photographs were obtained using CuKα radiation for all the samples except Co-5A(5) and Co-5A(6) where due to the occurrence of excessive fluorescence, CoKα radiation was employed.

Differences in the relative intensities for 4A, 5A (fig. 3.15) and for other samples with varying amounts of transition M^{2+} ions(fig. 3.16-17) reflect changes in ion sitings for Na^{+}, Ca^{2+} and M^{2+} (Cu,Co) ions. Distance between the peaks and peak widths remained approximately the same for the different samples, suggesting retention of the crystallinity in all cases. X-ray diffractograms for M^{2+}(Cu,Co) exchanged-5A were identical to those of the original 4A and 5A zeolites, which means that no noticeable break-down of the crystal lattice could be detected for these samples. It has been reported[323] that paramagnetic centres formed by the prolonged X-ray irradiation, influence the movements of cations within zeolite framework, so that irradiation time may affect the reproducibility of the diffraction patterns.

X-ray diffraction data (table IIX.1-8), derived from the readings of the X-ray films of the samples, showed almost all the characteristic lines found by other workers[23,324]. The unit cell constants for these samples are summarised in the table below.

Unit-cell constant (a) values reported earlier[324] are 12.32 Å and 12.16 Å respectively for the $Na_{12}A$ and Ca_6A samples which are close enough to the ones given here (considering experimental error and the fact that our 5A

sample was not completely pure Ca_6A). The variations in the unit-cell constant (a) values for different exchanged levels of M^{2+}(Cu,Co) exchanged-5A zeolites may be attributed to cation movements rather than to framework transformations. Recently[325], decrease in the cell parameter (a) of the highly ammonium-exchanged chabazite was taken as an anisotropic shrikage of the unit-cell. No such relationship could be perceived here.

TABLE 4.1. Cell Parameters of the Samples

No.	Sample	Unit-cell constant $a/\AA$
1	4A	12.302
2	5A	12.328
3	Cu-5A(4)	12.150
4	Cu-5A(5)	12.262
5	Cu-5A(6)	12.381
6	Co-5A(4)	12.272
7	Co-5A(5)	12.250
8	Co-5A(6)	12.175

b) Mordenite Samples

X-ray diffraction data for these samples (in both hydrated and activated forms) are compared in tables IIIX.1-9, and the distribution plots of their relative intensities (fig.X.1-9) show that the X-ray diffraction pattern of the mordenites remained almost unchanged under different

environments except for the intensities which may be ascribed to partial or complete dehydration. However, all the samples were sufficiently equilibrated over saturated salt solution prior to X-ray study for the forms to be fully hydrated. Activation of new samples was carried out under air or N_2 at 723K, and the diffraction patters obtained. It is of interest to note the frequent increase in the intensities of low angle peaks for activated samples (fig. X.2). The effect was more profound under N_2 atmosphere than air (e.g. comparing fig. X.2 and 3). Also note that the difference in the relative intensities ($R.I_1$ - $R.I_2$) of hydrated and activated Ni-exchanged mordenites was higher than the Cu^{2+}- containing samples (e.g. Fig. X.3,5 and X.7,9). These observations suggest generally that the mordenites structure did not suffer damage up to the activation temperature. Benesi[326] found that the X-ray diffraction pattern of mordenite remained unaltered upon removal of water molecules at 1073K However substantial crystal collapse was observed by Weeks *et al*[327] for NH_4-mordenite which had been heated in dry air at 1123K. Increases in the intensity reflections in the range of small and intermediate angles during heat treatment of mordenite samples has also been reported by other workers[313,327-28], but no explanations for these changes were put forward. However, Mishin *et al*[328] tried to correlate the reflections in this range for heat treated zeolites to the changes in aluminium content of the zeolitic framwork, assuming that migration of Al from the lattice caused a decrease in the adsorbed water content. The bases of their assumption were:

i) the concept forward by Kerr[329], that heating of NH_4^+ of H-form of zeolites above 773K usually results in a partial migration of aluminium from the framework to form aluminium compounds outside the framework, and

ii) the earlier finding[330] that the number of aluminium atoms in the zeolitic framework and the number of adsorbed water molecules were inter-related.

4.3. STATIC SYSTEM STUDIES

The catalytic activities of the transition metal exchange-5A zeolites were studied by means of the decomposition of nitrous oxide.

$$2N_2O\ (g) \rightarrow N_2\ (g) + O_2\ (g),$$

as the test reaction in a static system. The results summaraised in tables 3.6-7 (§3.3) are discussed in the following sections. The characterization of the catalysts (§4.2) proved their structural and thermal stabilities under the reaction conditions.

Factors such as the concentration of transition metal ion (t.m.i), the electronic configuration of the t.m.i., symmetry of the site occupied by the t.m.i. and nature of matrix for t.m.i. dispersion, generally affect the catalytic activity of a given reation. In activated transition metal exchanged A zeolites the metal ions are known[153-54,278] to be located in distorted six-rings, being trigonally coordinated to three framework oxygen atoms. This situation compels the transition metal ions to be placed wide apart, hence each contributes individually to the catalytic properties of the sieves.

Table 3.6 shows that the experimental temperature range for activity with Co-5A zeolites (792-1001K) and Cu-5A zeolites (800-982K) are quite comparable. Figures B1-12 show the first order kinetic plots for the

catalysts while the Arrhenius plots are given in figure 4.1-2.

4.3.1. Energies of Activation, Frequency Factors and Transition Metal Contents.

The energies of activation and frequency factors found for each of the samples are listed in table 3.7, and the corresponding metal exchange levels (and also %ages) are given in appendix **1**b.

Higher values of activation energies were observed with t.m.i. contents < 1 atom per unit cell (p.u.c.) for cobalt exchanged-5A and with t.m.i. content < 0.5 atom p.u.c. for copper-exchanged 5A zeolites. Similar results for transition metal exchanged 4A zeolites, were correlated[158] with the low monolayer equivalent surface area (MESA) due to blocking of the 8-rings by sodium ions for $M \leq 1.5$, and to the activated diffusion of reactants. It is interesting to report that our samples (5A) have high monolayer equivalent surface area values (§ table 3.5). However, other possible reasons (*viz.* variations of t.m.i. positions within the unit cell, reaction requirement for two (or more) adjacent t.m.i. sites and variations of electrical properties with t.m.i. contents. all proposed by them[158]) cannot be ruled out.

Table 3.7 shows that no clear relationship between activation energies and the t.m.i. content could be drawn for the two (Co-5A and Cu-5A) series of catalysts. Activity series of cobalt-exchanged-5A zeolites varied as

$$Co(1) < Co(3) < Co(2) < Co(4) < Co(6) < Co(5)$$

and copper-exchanged-5A zeolites have an activity series of

$$Cu(2) < Cu(1) < Cu(3) < Cu(5) < Cu(6) < Cu(4) \quad .$$

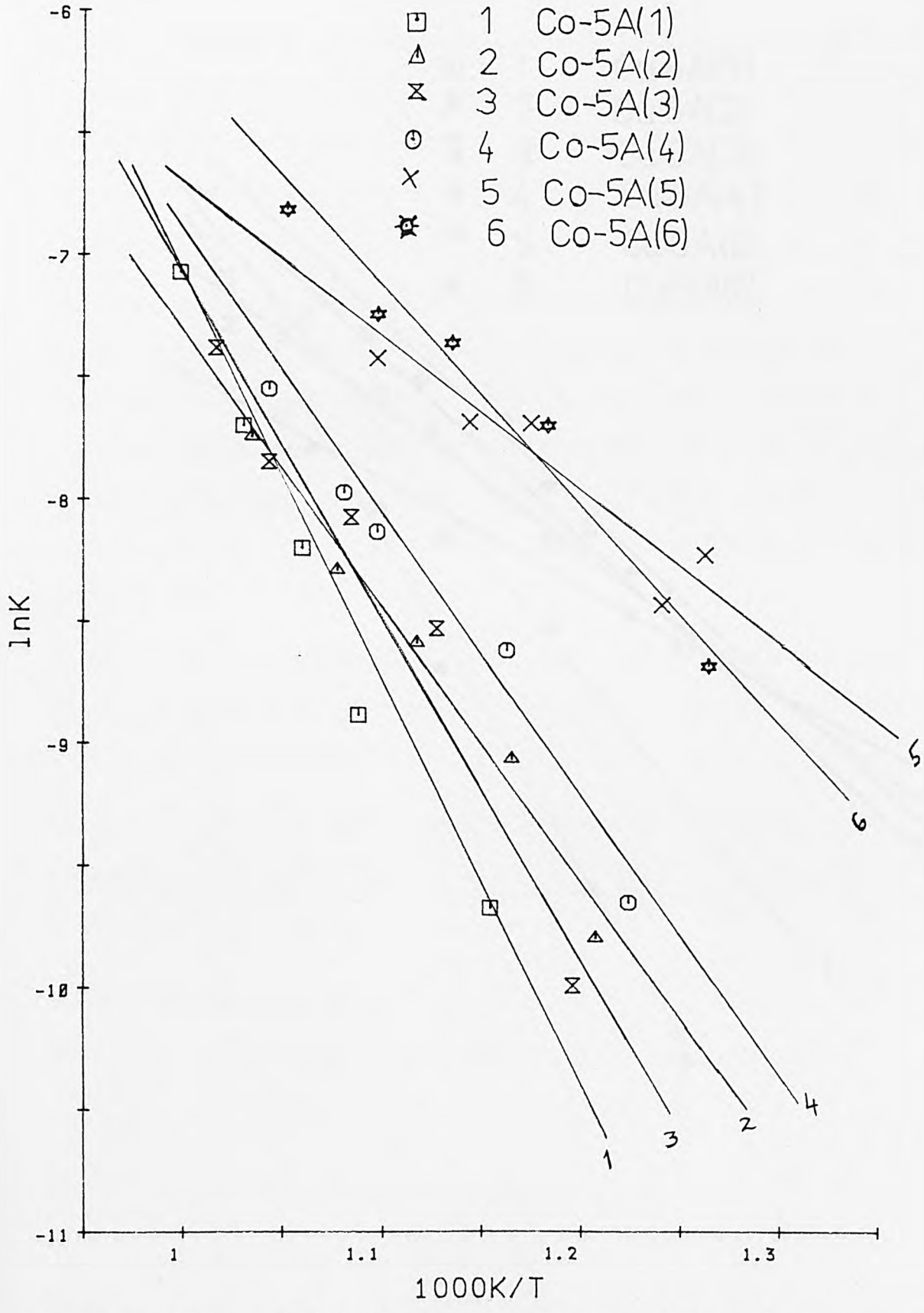

Fig.4.1:Nitrous Oxide Decomp. Arrhenius plots of Co-5A(1-6).

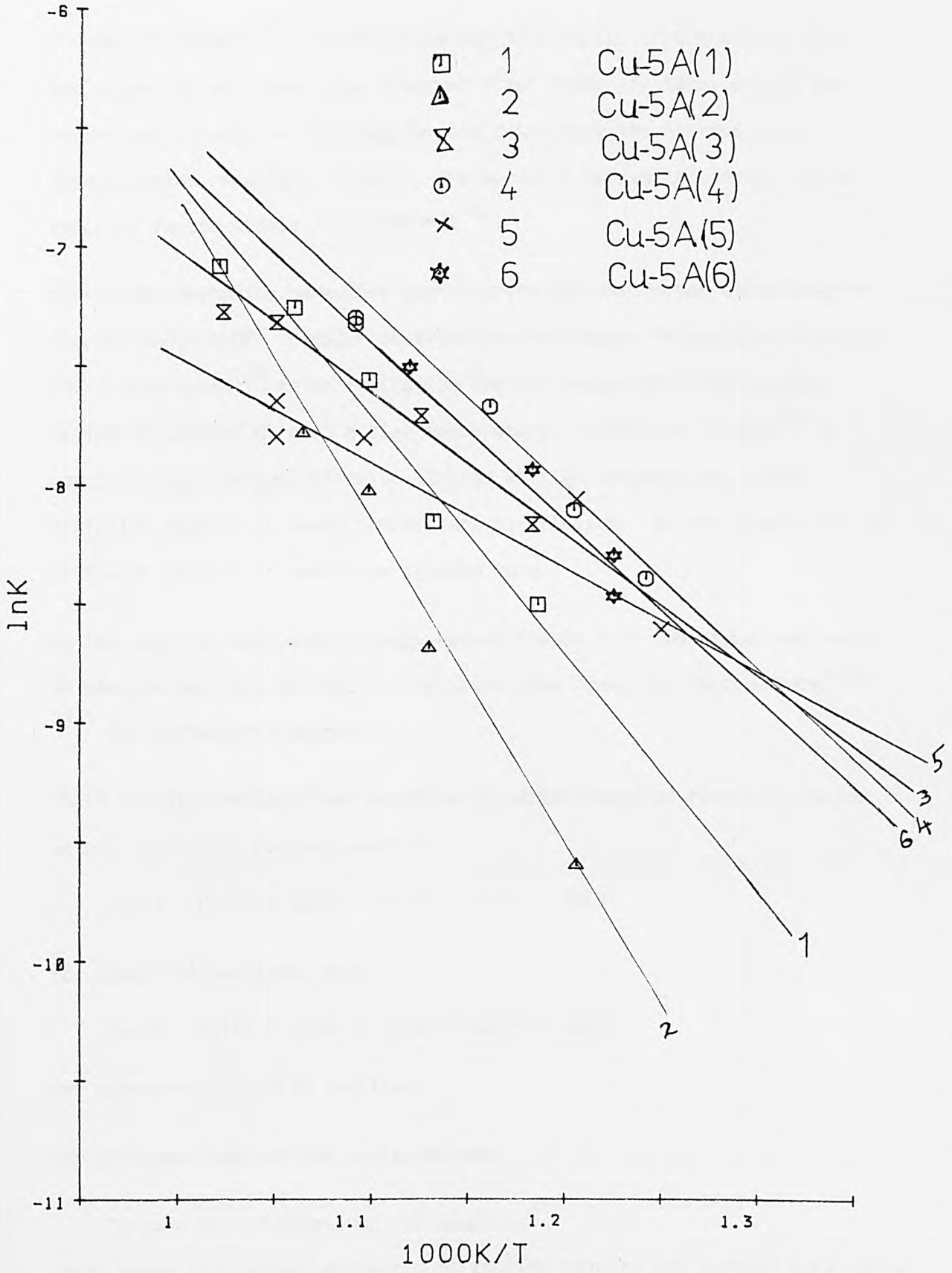

Fig.4.2:Nitrous Oxide Decomp. Arrhenius plots of Cu-5A(1-6).

Rudham and Sanders[120], in their studies of a series of transition metal exchanged 13X zeolites, also observed first order kinetics, except for copper and chromium containing samples catalysing the nitrous oxide decomposition reaction. However, the apparent activation energy values reported varied widely (112-254KJmol^{-1}).

Non-linear Arrhenius behaviour was observed for our copper containing 5A samples above 920K. Similar observations for copper-4A zeolites above 750K, were taken[158] as an indication that on copper activity becomes diffusion limited at such a high temperature. According to Bond[331] a reaction might become diffusion limited at high temperature, where diffusion depends on small temperature coefficient. So the possibility of diffusion limitation cannot be ignored here.

On the basis of activation energy values (table 3.7) the copper-exchanged 5A samples are more active, a conclusion also drawn by other workers[120, 334] for different supports.

Table 3.7 also reveals that an activity series based on frequency factor values and t.m.i. content would be

Co(3) > Co(2) > Co(4) > Co(1) > Co(6) > Co(5)

for cobalt-5A zeolites, and

Cu(2) > Cu(5) > Cu(4) > Cu(6) > Cu(1) > Cu(3)

for copper-exchanged-5A zeolites.

For different cations the series becomes

Co-exch.5A > Copper-exch. 5A samples.

which means that copper-exchanged 5A zeolite samples are overall more active.

4.3.2. Specific Rates and Free Energy of Activation

Zeolite supports for transition metal ions are far less active than their corresponding bulk oxides[120]. Due to the wide variations in the value of activation energies for t.m.i. exchanged zeolites[120,158], the activity series based on E_a values are sometimes misleading. In our work, e.g. a clear trend of activity on the basis of activation energy values and t.m.i. contents for transition metal exchanged-5A zeolites could not be established. Therefore, activity series based on specific rates and/or free energy of activation are normally to be preferred[(120,158,332)].

For cobalt-exchanged-5A series, activity sequence changes with t.m.i. concentration p.u.c. as follows:

Co(1) > Co(5) > Co(2) >Co(3) > Co(4) > Co(6),

while for copper-exchanged-5A samples, the series takes the form

Cu(1) > Cu(3) > Cu(4) > Cu(6) > Cu(2) > Cu(5)

which seem more rational save one or two anomalies.

For different cation exchanged-5A zeolites, the specific rate data from table 3.7, gives the series Cu $\geq$ Co.

This is the same activity series as reported by Rudham and Sanders[120], for their t.m.i. exchanged 13X and as reported by Akbar and Joyner[158] for t.m.i. exchanged 4A zeolites. It is worth noting that differences in pore structure, Si/Al ratios and coordination of metal cations, with framework oxygen atoms, have little effect on the catalytic activity of the catalysts. However, studies by Slinkin *et al*[332] have shown that the rate of the nitrous oxide decomposition reactions on HM (90% exchanged) at 773K was

greater than on zeolite HY under similar conditions. They concluded that apparently mordenite has oxidizing sites of different nature.

Finally, from table 3.7, the activity sequences on the basis of $\Delta G^{\neq}$ values for these two series of catalysts with different t.m.i. contents vary as

Co(3) > Co(2) > Co(4) > Co(1)> Co(6) > Co(5)

and

Cu(2) > Cu(5) > Cu(4) > Cu(6) >Cu(1) > Cu(3).

For different cations, the series still remains Cu > Co, confirming that copper exchanged-5A zeolites are always more active than cobalt-exchanged-5A zeolites.

4.3.3. Nitrous Oxide Decomposition Mechanism

Nitrous oxide, has a small dipole moment, is an oxidising agent and does not readily bond with another oxygen. Therefore, the preferred transformation for nitrous oxide is to produce nitrogen by breaking the nitrogen to oxygen bonding. Nitrous oxide decomposition is an electron-exchange[333] process involving both spin decoupling and charge transfer,as its essential steps. It is now well established[120,151,155,158,334,335] that nitrous oxide decomposition proceeds simply according to the equation $N_2O \rightarrow N_2 + \frac{1}{2}O_2$(i.e. negligible other products are formed), and the ratio of N_2 and O_2 formed is almost 2:1 while the amount of nitrous oxide consumed and nitrogen produced are the same within the experimental error (see §3.3).

A tentative mechanism for nitrous oxide decomposition involving a single cation is forwarded on the basis of studies by numerous workers[335,120,151,158]

as given below,

$$N_2O\ (g) \rightleftharpoons N_2O\ (ads) \qquad \ldots\ldots(1)$$

$$N_2O(ads) + \bar{e} \rightarrow N_2\bar{O}\ (ads) \qquad \ldots\ldots(2)$$

$$N_2\bar{O}\ (ads) \rightarrow N_2\ (g) + \bar{O}\ (ads) \qquad \ldots\ldots(3)$$

$$2\bar{O}\ (ads) \rightarrow O_2\ (g) + 2\bar{e} \qquad \ldots\ldots(4)$$

It seems probable that on t.m.i. exchanged A zeolite, step (2) is rate-determining. The dissociation step (3) is fast and the diffusion step (4) if rate controlling requires second order kinetics with possible oxygen retention.

On the basis of extent of transition metal ion exchange and the kinetic data (§3.3) obtained here for t.m.i. exchanged -5A samples, it is assumed[120] that chemisorption of nitrous oxide on a single cation instantly leads to oxidative-dissociation. It seems likely that immobile adsorbed oxygen becomes mobile in case of copper exchanged-5A above 920K, thus leading to the severe diffusion limitation which is observed.

4.4. FLOW SYSTEM STUDIES

The results of methane oxidation on prepared zeolite samples (§ 2) have been summarised in tables 3.9-12 (§3.5). Contrary to earlier reports[336], products other than water and cardbondioxide could not be detected under the reaction conditions used. Other workers[166,337] have found that computations of the difference in activity based on the amounts of carbon dioxide produced to that based on amount of methane converted are quite significant. All Arrhenius plots drawn in this work were based on the amount of methane converted over a range of temperature . The correlation

coefficient (R) and the 't factor' gave good values generally. The correlation coefficient affords statistical significance of Arrhenius linear relationship between lnk and 1/T and the 't factor' evaluates this significance; and, if both the 't factor' and the correlation coefficient have high values, then and only then can a significant relationship be inferred. The values of both the correlation coefficient and the 't factor' for the catalysts listed in table 3.9-12 (§3.5) are generally high indicating a good correlation.

A similar study[337], on the basis of experiments like catalyst bed design and particle size, concluded that the system obeyed the plug flow model, while considerations of contact time (change of flow rate of reactant gas) hinted[337] that mass transfer was not a limiting factor under the rea ction conditions employed. Using the same batch of exchanged zeolites for the whole range of experiments also improved the reproducibility.

Arrhenius plot positions are exploited to compare the activities of different catalysts. A criterion of activity generally is how high up the graph the plot is found and also how far to the right of the graph that plot is placed. In figure P10, for example, Co-5A(2) is the most active while Co-5A(1) is the least active zeolite sample.

Another common criterion for comparing the activities of the catalysts is the activation energy values but sometimes this proves to be a most misleading oversimplification. This can be illustrated by considering the activation energy values (table 3.9) for NaA, CaA and Cu-5A(1) samples which are 105.97,82.14 and 116.02 $kJmol^{-1}$, respectively. As can be seen clearly sodium and calcium are poisoning the reaction (negative order) yet the activity series based on E_a values alone is CaA > NaA > Cu-5A(1).

This makes CaA the most active while Cu-5A(1) is least active catalyst, which is not true. It is quite evident (§3.5 data) that the activation energy values depend on reaction orders.

The conversion of methane depends on the temperature so a convenient and more realistic mode of comparison can be based on temperature (K). Plots of conversion versus temperature afford $T\alpha.5$ values which is the temperature (K) needed for 50% conversion of methane for a particular catalyst. In the example given above, $T\alpha.5$ values for NaA, CaA and Cu-5A(1) zeolites (table 3.9) are 881.3, 906.8 and 848.1K, respectively.

Hence the activity series becomes

Cu-5A(1) > NaA > CaA which is quite sensible. The comparison of catalytic activities in this work is mostly based on $T\alpha0.5$ (or $T_{\frac{1}{2}}$) values listed for all samples in tables 3.9-12 (§3.5).

However, the most accurate measure of catalytic activity is provided by comparing the free energies of activation ($\Delta G^{\neq}$) values, because the entropy of activation ($\Delta \overset{\neq}{S}$) as well as the energy of activation, are taken into account. However, similar standard states must be employed. In this study the standard reference temperature chosen for comparing the catalytic activities was the same (i.e. 740K for less reactive zeolite 5A samples and 660K for more reactive mordenites). Taking again the above example, zeolites NaA, CaA and Cu-5A(1) have the free energy of activation values of 321.16, 334.07 and 223.19 $kJmol^{-1}$, respectively, Hence once again the activity sequence is

Cu-5A(1) > NaA > CaA which is identical to the $T_{\frac{1}{2}}$ series derived above.

Transition metal exchanged 5A zeolites used for the nitrous oxide decomposition reaction (§4.3) were also tested here for methane oxidation activity and the results obtained will be discussed in the following section.

It was found that transition metal exchanged 5A zeolites were not very active catalysts for this reaction so it was decided to do further work involving synthetic mordenite due to the reasons mentioned earlier (§chapter 2 and 3). The results for these nickel, copper and platinum exchanged mordenites are discussed in later sections. Finally, the results of the nickel and copper exchanged mordenites, both in individual and mixed form, will be dealt with in the last section. Plug flow data (tables 3.9-12) are pictorially represented in figures P1-42.

4.4.1. Transition Metal Exchanged 5A Zeolites

All copper exchanged-5A and cobalt exchanged -5A zeolites were activated under two different atmospheres prior to methane oxidation studies (§chap.2). The mode of activation employed was either air or nitrogen. A comparative study of the catalytic behaviour of these samples towards methan oxidation in these opposing surroundings is presented below.

4.4.1.1. Copper-5A Zeolites

The exchange levels of copper in Cu-5A (1-6) samples given in appendix Ia were 3.85, 6.48, 9.02, 9.4, 19.71 and 24.18% respectively, while their plug flow data summarised in table 3.9 (§3.5) are illustrated in figures P1-6.

a) Air Activation

The data (table 3.9) shows that activation energies of Cu-5A(1-6) vary as

Cu-2 > Cu-3 ≳ Cu-6 > Cu-4 ≳ Cu-5 ≳ Cu 1 . The differences in values for the first three of this series was ±7 $kJmol^{-1}$ whereas for the last three samples the differences were only ±2 $kJmol^{-1}$. However, the Cu-5A(4) and Cu-5A(6) Ea values differed by ∿ 10 $kJmol^{-1}$. It can be seen clearly that activation energy and reaction order are interdependent. The reaction orders for these samples (table 3.9) change from 1.08 to 1.52, consequently adversely affecting the activation energies. A distinct trend on the basis of Ea with changing exchange level cannot be established.

The free energy of activation for these catalysts change as Cu-6 ≃ Cu-4 ≃ Cu-2 > Cu-3 ≃ Cu-5 > Cu-1; it is obvious that the differences in values (table 3.9) is merely ±4$kJmol^{-1}$. Thus no clear relationship between copper ion exchange levels and free energy of activation data could be found here.

However a rational activity trend based on the values of t.m.i. content and the $T\alpha.5$ (or $T_{\frac{1}{2}}$) could be forwarded as Cu-5 > Cu-6 > Cu-3 > Cu-4 > Cu-2 > Cu-1, which though a bit anomalous is justified on the basis of Arrhenius plot positions (fig. P1-3).

b) Nitrogen Activation

In this mode, the activity series in terms of the activation energies of the samples becomes

Cu-3 >Cu-4 > Cu-6 > Cu-5 ≳ Cu-1 > Cu-2, whereas for the free energy of activation data the trend is

Cu-2 ≳ Cu-1 ≳ Cu-6 ≳ Cu-5 > Cu-4 > Cu-3. As is clear, these sequences do not complement each other. It is possible that copper already reduced in nitrogen, is reoxidized by oxygen in the feed (1% CH_4 in air) and variation in degree of oxidation (due to different exposure time during completion of experiment) causes the observed anomalies in the catalytic

behaviour.

The $T_{\frac{1}{2}}$ values of the samples establish a trend as Cu-6 > Cu-5 > Cu-3 ≳ Cu-4 > Cu-2 > Cu-1, which is exactly what would be expected on the basis of exchange level (except Cu-3 and Cu-4 where the metal contents differ by merely 0.4%). The positions of the plots in figures P5-6 also support the conclusion, especially fig. P5 which expects Cu-5A(4) to show higher activity than Cu-5A(3).

4.4.1.2. Cobalt-5A Zeolites:

Exchange levels for Co-5A (1-6) zeolites were respectively 5.6, 9.43, 11.25, 13.69, 35.95 and 50.6%. The plug flow data gathered in table 3.9 is correspondingly represented in figures P7-11, while fig. P12 plots the data for Na-A, Ca-A and Na-MOR. A discussion of the results follows:

a) Air Activation

A trend based on E_A values for the cobalt exchanged 5A samples is

Co-6 > Co-2 ≳ Co-4 > Co-5 > Co-3 > Co-1.

As in the case of copper-5A samples (§4.4.1.1), the orders vary widely within the series, making Ea values difficult to interpret with changing t.m.i. contents. The free energy of activation data for these samples vary within the range (212-262 $kJmol^{-1}$) as Co-3 > Co-6 > Co-2 > Co-1 ≳ Co-5 ≳ Co-4; giving the last three samples an almost equal activity irrespective of cobalt exchange levels.

Once again, $T_{\frac{1}{2}}$ values for these samples afford a better activity trend as

Co-5 >Co-4 > Co-6 ≳ Co-3 > Co-2 > Co-1.

That Co-5A(6) has a lower activity than Co-5A(4) and Co-5A(5), is also reflected in position of the plots in fig. P9, but why this should be is

not clear, as a possible structure collapse seems unlikely on the basis of MESA and X-ray studies (§4.2).

b) Nitrogen Activation:

Cobalt exchanged 5A zeolites activated under nitrogen exhibit activation energy values ranging from 87-132 $kJmol^{-1}$. The Ea related activity sequence can be written as Co-2 $\gtrsim$ Co-3 $\gtrsim$ Co-1 > Co-5 > Co-6 Co-4. The reaction order w.r.t. methane for the above is 1.52 except Co-5A(3) where it is 1.3 (table 3.9). Data values for free energy of activation vary between 207.5-226.6 $kJmol^{-1}$, with a difference of not more than 10 $kJmol^{-1}$ at the most between different samples. The activity sequence thus takes the form Co-6 $\simeq$ Co-5 > Co-2 $\simeq$ Co-4 $\gtrsim$ Co-3 > Co-1.

The plot positions in figure P10-11 justify this series and suggest that Co-5A(2) does have a high activity compared to Co-5A(3) sample (fig. P10) which in turn is more active than Co-5A(1); also Co-5A(5) and Co-5A(6) have a comparable activity (fig. P.11).

The paradox in activity placement of Co-5A(2) is removed by presenting an activity trend based on the values of $T_{\frac{1}{2}}$ (table 3.9) which varies in exact conformity with increasing cobalt exchange levels of the catalysts as

Co-6 $\gtrsim$ Co-5 > Co-4 > Co-3 > Co-2 > Co-1.

In the light of above discussion, it is quite obvious that the mode of activation does have a very significant effect on the catalytic behaviour of the catalysts. As is seen, both copper-5A and Co-5A zeolite samples show a more rational activity trend when activated under nitrogen atmosphere, and also the catalysts treated in this manner are more active overall than the analogous air activated ones. On comparing the activity data (table 3.9), it is seen that copper exchanged 5A samples have higher activities

than the cobalt exchanged 5A zeolites, a conclusion also drawn from the study of nitrous oxide decomposition reaction (§4.3).

4.4.2. Transition Metal Exchanged Mordenites:

As stated earlier, t.m.i. exchanged 5A zeolites are not very active for the methane oxidation reaction (as can be seen, a high temperature 740K was chosen to standardize the $\Delta G^{\neq}$ values) so studies were carried out on the more active mordenites for further studies of the oxidation reaction. All nickel, copper and platinum exchanged mordenites were activated under air or nitrogen atmospheres prior to methane oxidation. The data for these studies are summarised in table 3.10 (§3.5) and the plots are drawn in figures P13-20.

Comparing the data (table 3.10) for activation energy, $T_{\frac{1}{2}}$ and free energy of activation, together with the positions of the Arrhenius plots for Na-MOR and NH_4-MOR, it was soon clear that the former was far less reactive than the latter. Also, the plot positions in fig. P13-14 and the corresponding activity data confirms that H-MOR activated under nitrogen was found to be more active than when activated under air.

4.4.2.1. Nickel Mordenites:

Nickel exchanged mordenites, Ni-MOR (1-3) have ion exchange levels (see appendix Ib) of 31.41, 40.23 and 42.63% respectively. Plug flow data for the zeolites, given in table 3.10 (§3.5) are represented pictorially in figures P15-16.

For air activated Ni-MOR (1-3), the activation energy values indicate that activity of the sample varies as Ni-3> Ni-1 > Ni-2. However, under the same conditions, free energy of activation and $T_{\frac{1}{2}}$ data suggest an activity

series of Ni-1 > Ni-2 > Ni-3, which is also supported by positions of Arrhenius plots in figure P17. In simple terms, the series clearly shows that the activity increases with increasing the cation metal content of the samples. It is also obvious that plots of Ni-MOR(2) and Ni-MOR(3) have comparable activities, which is equivalent to their closeness in the exchange levels (see appendix Ib). The observed increase in the activity with increasing exchange level is probably due to an increasing occupancy by nickel of cation sites in the main channels of mordenite rather than in the side pockets, hence increasing their accessibility for the oxidation reaction.

In case of nitrogen activated Ni-MOR(1-3), both $T_{\frac{1}{2}}$ and activation energy values change in a manner which suggests Ni-MOR(2) is the most active while Ni-MOR(3) is the least active sample. This inferences is neither supported by the free energy of activation ($\Delta G^{\neq}$) values nor the positions of the plots. On the other hand the latter two parameters expect Ni-MOR(2) to be the least active of the three catalyst series i.e. Ni-3 $\geq$ Ni-1 > Ni-2 So it is clear that care should be taken in depending too much on $T_{\frac{1}{2}}$ data values alone. They provide a good measure but are not a definitive tool of assessing catalytic activities.

It is observed above that except for Ni-MOR(3), the catalytic series is reversed, indicating quite different behaviour for the two opposite activation environments. On average, the nitrogen activated samples show a higher activity (compare the $T_{\frac{1}{2}}$ and/or $\Delta G^{\neq}$ values) than their air activated counterparts.

4.4.2.2. Copper Mordenites

The ion exchange levels of copper mordenites, Cu-MOR(1-3) were 56.73,

60.13 and 68.67% respectively (see appendix Ib). The catalytic data for the samples are given in table 3.10 (§3.5) and the plots are given in figures P17-18.

The activation energy and $T_{\frac{1}{2}}$ data for air activated copper mordenites do not provide a clear activity trend. The value of free energy of activation on the other hand do establish a trend in line with the placements of the Arrhenius plots (fig. P17), giving an activity pattern of Cu-1 $\geq$ Cu-3 > Cu-2. Why the first two samples have a matching activity despite having different t.m.i. contents is not clear.

The interpretation of activity behaviour on the basis of Ea and $T_{\frac{1}{2}}$ values for nitrogen activated samples is again difficult. This could be due to differences in reduction/reoxidation levels as explained earlier (§4.4.1.1). However, the free energy of activation data do enable an activity trend of Cu-2 > Cu-1 > Cu-3, matching the plot positions given in figure P18. Here a partial reversal in the expected trend is seen. Also data values (table 3.10) suggest the nitrogen activated copper mordenites are more active as in the case of nickel mordenites (§4.4.2.1.).

4.4.2.3. Platinum Mordenites

Platinum mordenites, Pt-MOR(1-4) have ion exchange levels of 53.63, 57.64, 69.81 and 49.51% respectively (see appendix Ib). The Arrhenius plots of the catalysts are shown in figures P19-20 and the plug flow data are summarised in table 3.10 (§3.5).

No clear trend can be obtained from the data for the platinum mordenite samples which were activated in air. It is possible[161] that with platinum, oxygen inhibits the oxidation process, an inhibition which varies with changes in metal content. Even the activity sequence derived from plot

position (fig. P.19) lacks a clear trend i.e. Pt-2 > Pt-1 > Pt-4 > Pt-3.

On the other hand, a clear trend is noticeable for nitrogen activated platinum mordenites. Both $T_{\frac{1}{2}}$ and free energy of activation values agree to suggest an activity series of Pt-3 > Pt-4 > Pt-1 > Pt-2. An exactly similar trend is seen from the position of Arrhenius plots in figuresP.20. It is quite interesting to observe that this trend is just the opposite to the one for air activated platinum mordenites, so the samples behave in a completely different manner under oxidising and reducing conditions. Like other samples, the platinum mordenites activated under nitrogen are more active than the air activated ones.

To compare the catalytic activities of different t.m.i. exchanged mordenites, it is quite sensible to compare samples of fairly similar metal contents *viz* Ni-MOR(3), Cu-MOR(1) and Pt-MOR(1) with exchange levels (§app. Ib) as 42.63, 53.9 and 53.7% respectively. A comparison of $T_{\frac{1}{2}}$ values for these catalyst under similar conditions clearly gives a logical activity trend of Pt > Cu > Ni. This series is identical to one reported by Fletcher *et al*[166] for mordenites and is quite comparable to that observed by other workers[161,162] for transition and noble metals in zeolite X.

4.4.3. Mixed-Catalysts Study Samples

Four samples (*viz* Ni/Na-MOR, Ni/NH_4-MOR, Cu/Na-MOR and Cu/NH_4-MOR § chap.2) with metal exchange levels (§Ib) varying respectively as 45.74, 37.94, 53.9 and 61.02% were tested at 4, 6 and 20% oxygen levels using a constant flow of the feed (5 cm^3 min^{-1}), after activating the samples under air or nitrogen surroundings. The Arrhenius plots are shown in figures P21-28, and the results are summarised in table 3.11 (§3.5). As is evident from

the data, the reaction orders of these samples vary widely, hence affecting the apparent activation energy values, so that comparison of the catalyst activities on the basis of mere Ea values must be avoided.

As described earlier (§3.5), the feed (1% methane in air) was taken as a 20% oxygen level, whereas 4% and 8% oxygen levels were obtained manually (with the help of mass flow controllers) by diluting a gas sample (1% methane in 99% nitrogen) with proportionate quantities of air. For example a 4% oxygen level was obtained by adjusting a mixture of 4 cm^3min^{-1} of 1% CH_4 in nitrogen and 1 cm^3min^{-1} of air. It is worth mentioning that these oxygen level adjustments affect the amount of methane in the feed e.g. in the case of 4% oxygen level, methane flowing through the catalyst bed is less than that for the gas sample with 8% O_2 level. Variations in the amount of methane flowing through the catalyst bed may partially affect the results because in addition to the probable error in measuring methane heights (used to calculate the conversion factor) for lower oxygen levels, the flow of methane to the active sites of a very active catalyst sometimes can be rate limiting[337].

4.4.3.1. Nickel Mordenites

4.4.3.1.1. Ni/Na-MOR

Arrhenius plots of this catalyst activated under air (fig. P.21) clearly indicate that the activity increases with increase in oxygen level. Both the value of $T_{\frac{1}{2}}$ and standard free energy of activation (table 3.11) decreased with increases in oxygen level, hence supporting the assertion that 20% oxygen level sample gives the highest activity while the 4% O_2 level sample gives the lowest. It can also be observed that activity of 8% oxygen level catalyst approached that seen at 20%.

Nitrogen activated Ni/Na-MOR also show a trend with increasing oxygen level but it is not as obvious as that for the air activated ones. The catalytic activity sequence considering the $T_{\frac{1}{2}}$ data values (table 3.11) with different oxygen levels becomes 4% > 20% > 8%. The position of 4% oxygen level w.r.t. 8% level is clear but the paradox in the position of 8% and 20% oxygen levels can be removed by considering the values of the free energy of activation which increased as the oxygen level increased (table 3.11) to give a catalytic sequence as 4% > 8% > 20%, which was just reverse to that observed for air activated samples. This was also supported from the placement of the Arrhenius plots (fig. P.22) which indicates that a 4% oxygen level behaves as the most active situation while 20% oxygen level was the least active for this oxidation reaction.

4.4.3.1.2. Ni/H-MOR

The trend of increasing activity with increasing oxygen level is maintained for air activated Ni/H-MOR samples. The free energy of activation data (table 3.11) suggest that the catalytic activity tends to change with different oxygen feed as 20% > 4% ≳ 8% but a comparison of $T_{\frac{1}{2}}$ values (table 3.11) with the clear positions of the plots (fig. P.23) adjusts the above catalytic sequence of varying oxygen levels to 20% > 8% > 4%, which is similar to that noted for Ni/Na-MOR under identical reaction conditions.

In the case of nitrogen activated Ni/H-MOR, the $T_{\frac{1}{2}}$ values decrease with the increase in oxygen level of the feed to give the analogous behaviour to air activated sample but both the free energy of activation (table 3.11) and the plot position (fig.P.24) clearly indicate that the 8% O_2 level sample shows a better activity than the sample with 4% O_2 level.

A general comparison of catalytic data (table 3.11) reveals that Ni/H-MOR

samples under different oxygen levels are more active than the equivalent Ni/Na-MOR under similar conditions. This could however be partially due to the higher nickel exchange level (§ app.Ib) for Ni/H-MOR than Ni/Na-MOR.

4.4.3.2. Copper Mordenites

4.4.3.2.1. Cu/Na-MOR

The air activated sample has an explicit catalytic behaviour of increasing activity with increasing oxygen level of the feed, as in the case of Ni/Na-MOR under same conditions.

Data (table 3.11) for free energy of activation and for the $T_{\frac{1}{2}}$ values enable an activity series for three different oxygen levels as 20% > 8% > 4%. The criterion of activity reflected in plots (fig.P.25) is exactly the same.

Unlike Ni/Na-MOR, the Cu/Na-MOR samples retain the above sequence under nitrogen atmosphere. Though $T_{\frac{1}{2}}$ values (table 3.11) for different oxygen dilutions do not give an obvious trend, the free energy of activation data (table 3.11) decrease with increasing oxygen level in the feed. Arrhenius plots in fig. P.26, take such positions that activity sequence for different dilutions remain as proposed above.

4.4.3.2.2. Cu/H-MOR

The sample treated under air lacks any evident trend. The $T_{\frac{1}{2}}$ values (table 3.11) of these samples for 4% and 8% oxygen levels are same (635K) so this cannot be a good basis for comparison here. On the other hand, standard free energy of activation values (table 3.11) are lower for the 8% oxygen level sample than the 4% oxygen level. However, an increase in activity with increased oxygen level could be clearly noticed in the

Arrhenius plot positions (fig. P.28).

For air activated Cu/H-MOR samples, once again the $T_{\frac{1}{2}}$ values (table 3.11) are not quite suitable to provide any obvious catalytic trend. Free energy of activation data (table 3.11), on the other hand, decrease with an increase in oxygen levels (samples at 8% oxygen level and that at 20% oxygen level have almost matching activities) hence supporting the conclusion drawn on the basis of free energy of activation ($\Delta G^{\neq}$) values.

On comparing the above copper mordenites under similar conditions, it is evident that Cu/H-MOR is generally more active than Cu/Na-MOR. A partial explanation for this increased activity is the higher t.m.i. content (see appendix Ib) in the case of former sample. It has been reported[337], that simultaneous changes in oxygen or methane and metal exchange level of the catalyst lead to very complex phenomena so any definitive inferences becomes very idfficult.

4.4.3.3. Mixed Mordenites

A summary of the plug flow data for mixture of mordenites, is presented in table 3.12 (§3.5) while their Arrhenius plots are given in figures P27-42. Mixing ratios of the six samples (Cu/Ni/Na-MOR(1-3) and Cu/Ni/H-MOR(1-3)) can be found in table 3.8 (§3.5). Methane oxidation studies for these six catalysts was carried in both air and nitrogen activated forms with varying oxygen levels (4,8 and 20%).

For all these mixed cetalysts the energy of activation values vary widely as before (probably due to inequalities in the observed reaction orders) so their oxidative activities are generally compared on the basis of Arrhenius plot positions (P29-42), standard free energy of activation values and $T\alpha.5$

(or $T_{\frac{1}{2}}$) data, as detailed in table 3.12 (§3.5).

4.4.3.3.1. Copper/Nickel/Sodium-Mordenites

4.4.3.3.1.1. Cu/Ni/Na-MOR(1)

Arrhenius plot positions (fig. P29) for air activated samples show a higher activity at the 8% oxygen level than at either the 4% or the 20% oxygen levels. This is also reflected in lower free energy of activation values at the 8% oxygen level (178.13kJmol^{-1}) than found either at the 4%(195.05 kJmol^{-1}) or the 20% (201.79kJmol^{-1}) oxygen levels. The $T_{\frac{1}{2}}$ data values also show similar differences for the three oxygen levels. No apparent trend is possible due to anomalous behaviour at 20% oxygen levels, otherwise there is an increase in activity with decrease in oxygen levels.

For the nitrogen activated samples, the above sequences are reversed except for the anomaly in position at 20% oxygen level. Both the data (table 3.12) for the free energy of activation and for the placement of corresponding Arrhenius plots (fig.P30) show a highest activity at 4% oxygen dilution, and a lowest at 8% oxygen level.

The anomalous behaviour at the 20% oxygen levels for mixed zeolites for this oxidation reaction was also observed with the platinum and palladium mordenites[337]. This was explained by assuming that amount of methane in the feed rather than oxygen determine the catalytic activity, and concluding that the catalytic trends cannot be attributed entirely to the effects of oxygen or methane level in the gas feed. Similar assumptions could be taken here to justify the above paradox partially if not in totality.

4.4.3.3.1.2. Cu/Ni/Na-MOR(2)

For this sample, under air activation the 4% oxygen level not only has the

lowest values for the free energy of activation (181.27 $kJmol^{-1}$) but also its plot is above that of 20% and 8% oxygen levels (fig.P33). It appears therefore that for Cu/Ni/Na-M(2) activity decreases with increases in oxygen dilution, except at the 20% level. This sample behaves differently to the above, in a sense that a decrease in activity is observed when going from 4% dilution to 8% dilution, but the 20% oxygen level shows a persistent anomaly to give higher activity than 8% oxygen level in different atmospheres.

In the case of nitrogen activation, the sample shows the same $T_{\frac{1}{2}}$ value (675K) for 4 and 8% oxygen levels, with a lower (669K) value at 20% oxygen. The free energy of activation (table 3.12) and the Arrhenius plot positions (fig. P34) do show a complementary trend of an increase in activity with increase in dilution from the 4% to 8% oxygen level, but once again an anomalous catalytic behaviour is maintained at the 20% oxygen level, which occupies a middle position between the other two oxygen levels.

4.4.3.3.1.3. Cu/Ni/Na-MOR(3)

The activity sequence for this sample, in both air and nitrogen activated forms, is for different (4, 8 and 20%) oxygen levels quite clear.

Under air activation, Cu/Ni/Na-MOR(3) is unique in a sense that a very high activity was obeserved at 20% oxygen level as compared to either 8 or 4% dilutions. The latter are almost of equal activity as suggested by different activity parameters. The values of free energy of oxidation (table 3.12) suggest an activity series of 20% >> 8% > 4%, which is supported in full by the plot positions in fig. P37 (at 8% and 4% oxygen levels) and fig.P41 (at 20% oxygen level).

The above trend (of activity increase with increase in oxygen level of the

feed) persists well for the nitrogen activated samples. Activity at 20% O_2 level is still high but the difference in standard free energy of activation values (table 3.12) also reflected in plot positions (fig.P38), is not as wide as that of air activated one, mentioned earlier. It can be easily observed that activities at the 8% and 4% oxygen levels match. as the difference in $\Delta G^{\neq}$ values is only 0.5 $kJmol^{-1}$ and the plots at these dilutions overlap.

It can be concluded generally that activity increases as the portion of copper mordenite increases in the mixture from Cu/Ni/Na-MOR(1) to Cu/Ni/Na-MOR(3), possibly due to a higher activity associated with copper zeolites. On the other hand, no obvious activity trends with any increase/decrease of oxygen levels in the feed could be established, mainly due to an anomalous behaviour at the 20% oxygen level.

4.4.3.3.2 Copper/Nickel/Hydrogen-Mordenites

4.4.3.3.2.1 Cu/Ni/H-MOR(1)

Air activated Cu/Ni/H-MOR(1) samples show a clear trend of decrease in activity as the percentage of oxygen level in the feed is increased. The observed series on the basis of free energy of activation data (table 3.12) at different oxygen dilutions is 4% > 8% $\gtrsim$ 20%. The difference in $\Delta G^{\neq}$ values between the first two levels amount to $\sim$5 $kJmol^{-1}$, whereas the difference in the last two is merely $\sim$1 $kJmol^{-1}$. The Arrhenius plots for these dilutions (fig. P31) clearly support the said difference. The $T_{\frac{1}{2}}$ data values (table 3.12) also support the trend but the values differ by either 5K or 1K. It can be concluded that though the activity decreases with an increase in oxygen dilution of the feed, there is a distinct limit to this effect.

For the nitrogen activated sample, the situation is rather more complex, as the activity seems to be approximately the same at different oxygen levels, with a free energy of activation varying by only ±2 $kJmol^{-1}$, and giving a sequence of 20% $\gtrsim$ 4% $\gtrsim$ 8%. Similar behaviour is inferred on the basis of either the $T_{\frac{1}{2}}$ values (table 3.12) or the Arrhenius plots (fig.P32), which overlap at certain points. Here the 8% and 20% oxygen level show a nearly matching activity, with the 4% oxygen level becoming a bit less active.

4.4.3.3.2.2. Cu/Ni/H-MOR(2)

The results for air activated Cu/Ni/H-MOR(2) samples do exhibit an apparent trend of an increase in oxidative activity from the lower oxygen levels to the higher ones. Free energy of activation data (table 3.12) suggest the 20% oxygen level to be the most active while at the 8% and 4% oxygen levels, the activity is approximately same (the difference between these two levels is just $\sim$0.7 $kJmol^{-1}$). However $T_{\frac{1}{2}}$ values (table 3.12) at these dilutions are almost equivalent.

For the nitrogen activated forms, the situation is again complicated as the free energy of activation value (table 3.12) at 20% oxygen level are more or less the same as that at 4% oxygen dilution but both these have lower values than at the 8% oxygen level. The values of $T_{\frac{1}{2}}$ also show anomalous behaviour at 20% oxygen level and the Arrhenius plots (fig.P36) nearly overlap each other, portraying activity similarities.

4.4.3.3.2.3. Cu/Ni/H-MOR(3)

Activity pattern of the air activated sample exists only for dilutions at 4% and 8%. Data for the 20% oxygen level lies between the other two plots. The free energy of activation values (table 3.12) give an activity sequence

at different oxygen levels of 4% >20% > 8%. The positions of the Arrhenius plots depicted in fig. P39 agree with this trend.

Nitrogen activated Cu/Ni/H-MOR(3) samples present as interesting a situation as that observed for the air activated Cu/Ni/Na-MOR(3) sample (§4.4.3.3.1.3). Once again the activity at 20% oxygen level is much higher than those at 8% and 4% oxygen levels. The free energy of activation data (table 3.12) for 20% dilution (111.55kJmol^{-1}) is much lower than that at 8% (180.62 kJmol^{-1}) and at 4% (192.91 kJmol^{-1}) oxygen levels. The activity series can be written as 20% > 8% > 4% which sets a trend of increase in activity when the reduced samples are gradually oxidised. The trend is not only verified by the $T_{\frac{1}{2}}$ values (table 3.12) but also by the Arrhenius plots (see figure P40 at 4% and 8% oxygen levels) and figure P42 (at 20% oxygen level). A possible explanation could be that the degree of oxidation of the reduced ions changes with increase in oxygen level of the gas feed.

4.5. CONCLUSION and SUGGESTIONS

In addition to chemical analysis, the techniques like monolayer equivalent surface area (MESA), thermal analysis (TGA, DTA and DSC) and X-ray powder diffraction studies are quite helpful in characterizing the zeolites which is an essential step in catalytic activity determinations. The latter is affected by different modes of activation. Activities of different catalysts tested under nitrogen atmosphere are higher as compared to air activated samples.

Copper containing zeolites are better catalysts than e.g. cobalt or nickel exchanged zeolites, as shown by their activities for different probe reactions *viz* nitrous oxide decomposition and methane oxidation reactions.

Transition metal exchanged mordenites show better activity than corresponding 5A zeolites. Dilutions of the gaseous feed (1% methane in air) with oxygen improved activity, though establishment of clear activity patterns (in some cases) could not be achieved tentatively due to lack of data.

The copper-nickel mordenite mixtures study on methane oxidation offer a very promising field and can be easily extended to involve not only the different proportions but also different metal ions. Similarly levels of oxygen dilution can be varied to enable more data, hence helping establish better activity trends. Change of feed from methane to ethane or ethene is another prospective extension in such studies.

REFERENCES

(1) A.F. Cronstedt, Akad. Handl., Stockholm 17, 120, (1756).

(2) R.M. Barrer, 'Hydrothermal Chemistry of Zeolites' Academic Press, London (1982).

(3) O.Weigel & E.Steinhoff, Z. Krist. 61, 125 (1925).

(4) J.N. McBain, "The Sorption of Gases & Vapours by Solids", Goerge Rutledge & Sons, Ltd., London (1932), Chapter 5.

(5) J.V. Smith, Amer. Mineral. Soc., Spec. Paper 1, 281 (1963).

(6) L. Pauling, Proc. Nat. Acad. Sci., U.S., 16, 453 (1930).

(7) W.H. Taylor, Z. Krist., 74, 1 (1930).

(8) R.M. Barrer, Proc. Roy. Soc. London, A167, 393 (1938).

(9) R.M. Barrer & D.A. Ibbitson, Trans. Faraday Soc., 40, 195 (1944).

(10) R.M. Barrer, J. Soc. Chem. Ind. 64, 130 (1945).

(11) R.M. Barrer, J. Chem. Soc., 2158 (1948).

(12) R.M. Barrer, Nature, 159, 508 (1947).

(13) D.W. Breck, W.G. Eversole & R.M.Milton, J. Am. Chem. Soc., 78, 2338 (1956). (1956).

(14) R.M. Milton, U.S. Patent 2,882,243 & 2,882,244 (1959).

(15) E.M. Flanigen, in 'Proc. Fifth Int. Conf. on Zeolites', (Ed. L.V.C. Rees) Heyden, 1980, p.760.

(16) W.M. Meier, Ed., 'Molecular Sieves', Soc. Chem. Ind., London (1968).

(17) R.F. Gould, Ed., 'Molecular Sieve Zeolites, I and II', Adv. Chem. Ser., 101 & 102, Amer. Chem. Soc. (1971).

(18) W.M. Meier & J.B. Uytterhoeven, Eds., 'Molecular Sieves', Adv. Chem. Ser, 121, Amer. Chem. Soc. (1973).

(19) J.B. Uytterhoeven, Ed., 'Molecular Sieves, Proc. 3rd Int. Conf., Leuven University Press, Belgium (1973).

(20) J.R. Katzer, Ed., 'Molecular Sieves - II', ACS Symp. Ser., 40, Amer. Chem. Soc. (1977).

(21) R.P. Townsend, Ed., 'Proc. of the Conf. on The Properties and Applications of Zeolites', Special Publication No.33, The Chem.Soc., London, (1979).

(22) L.V.C. Rees, Ed., 'Proc. 5th Int. Conf. Zeolites,' Naples, Heyden,(1980).

(23) D.W. Breck, 'Zeolite Molecular Sieves - Structure, Chemistry & Use', Wiley-Interscience, New York (1974).

(24) J.A. Rabo, Ed., 'Zeolite Chemistry & Catalysis', ACS Monograph 171, Amer. Chem. Soc. (1976).

(25) R.M. Barrer, 'Zeolites and Clay Minerals as Sorbents and Molecular Sieves', Academic Press, London (1978).

(26) D.S. Coombs, A.J. Ellis, W.S. Fyfe & W. Taylor, Geochim. Etcosmochim. Acta, 17, 53 (1959).

(27) K.S. Deffelges, J. Sed. Petro., 29,602 (1959).

(28) E.Z. Burzanova, Geol. Ser. 6, 74 (1961).

(29) D.E.W. Vaughan in 'Natural Zeolites, Occurence, Properties & Uses', Eds. L.B. Sand & F.A. Mumpton, Pergamon, London (1978) p.353.

(30) R.M. Barrer, Zeolites, 1(3), 130 (1981).

(31) D.W. Breck, J. Chem. Educ., 41, (12), 678 (1964).

(32) P.B. Venuto & P.S. Landis, Adv. in Catalys., 18, 259 (1968).

(33) J.D. Sherman, 'Adsorption & Ion Exchange separation', AI Ch E Symposium Series, 74, No. 179, 98 (1978).

(34) J. Turkevich in 'Catalysis Reviews, vol.I ed. H. Heienemann, Edward Arnold Pub., London (1968), p.1.

(35) J. Turkevich & Y. Ono., Adv. in Catalys., 20, 135 (1969).

(36) J.A. Rabo, R.D. Bezmann & M.L. Poutsma , Acta Pys. Chem., 24, 39 (1978).

(37) L. Riekert, Adv. in Catalys., 21, 281 (1970).

(38) J.B. Uytterhoeven, Progr, Colloid & Polymer Sci., 65, 233 (1978).

(39) D. Barthomeuf, J. Phys. Chem., 83 (2), 249 (1979).

(40) D.W. Breck, in ref. 21, p.391.

(41) K.F. Fischer & W.M. Meier, Fortschr. Mineral, 42, 50 (1965).

(42) W.M. Meier, in ref. 16, p.10.

(43) D.W. Breck, in ref. 17a, p.1.

(44) P.B. Moore & J.V. Smith, Mineral. Mag., 33, 1008 (1964).

(45) R.M. Barrer, Chem. Ind., London, 1203 (1968).

(46) W.A. Deer, R.A. Howie, J. Zussman, Rock Forming Minerals, p. 351 , vol. 4 , Longmans , London (1963) .

(47) J.R. Anderson, 'Structure of Metallic Catalysts', Academic Press, London (1975), p.74.

(48) J.V. Smith, in ref. 23, p.3.

(49) J.V. Smith, in ref. 21, p. 194.

(50) C.G. Bruce, J.R. Katzer & G.C.A. Schuit, "Chemistry of Catalytic Processes", McGraw-Hill, Inc., N.Y. (1979) p.49.

(51) E.A. Lodge, L.A. Bursil & J.M. Thomas, J.C.S. Chem. Com., 875 (1980); L.A. Bursil, E.A. Lodge & J.M. Thomas, Nature, 286, 111 (1980); J.M. Thomas, L.A. Bursil, E.A. Lodge, A.K. Cheetham & C.A. Fyfe, J.C.S. Chem. Comm., 276 (1981).

(52) R.M. Barrer, J.Chem. Soc., 195 (1959).

(53) J. Selbin & R.B. Mason, J. Inorg. Nucl. Chem., 20, 222 (1961).

(54) H. Lee, in ref. 17, p.311.

(55) R.A. Sanderson, in ref. 19, p.637.

(56) A.S. Berger & L.K. Yakoviev, Zh. PriKl. Khim, 38, 1240 (1965).

(57) M. Koizumi & R. Kiriyama, J. Mineral., 1, 36 (1953).

(58) W.D. Basler & W. Maiwald, J. Phys. Chem. 83, (16), 2148 (1979).

(59) C.R. Allenbach & F.M. O'Connor, U.S. Pat. 3,506,593 (1970).

(60) A. Dyer, W.Z. Celler & M. Shute, in ref. 17a, p.436.

(61) R.M. Barrer & P.J. Cram, in ref. 17b, p.105.

(62) R.M. Barrer & M.B. Makki, Can. J. Chem. 42, 1481 (1964).

(63) R.M. Barrer & A.G. Kannellopoulos, J. Chem. Soc. (A), 765 (1970).

(64) R.M. Barrer, in ref. 22, p.273.

(65) A. Maes & A. Cremers, in ref. 19, p.192.

(66) H.S. Sherry, in ref. 17a, p.350.

(67) R. Kellerman & K. Klier, 'Surface and Defect Prop. of Solids', 4 (1975).

(68) A. Cremers, in ref. 20, p. 179.

(69) A. Dyer, H. Enamy & R.P.Townsend, Sep. Sci. Technol. 16, 173, (1981), **et. op. cit.**

(70) R.P. Townsend, Chemistry and Industry, 246 (1984).

(71) P.B. Venuto, in ref. 17b, p.260.

(72) J.A. Rabo & M.L. Poutsma, in ref. 17b, p.284.

(73) M.L. Poutsma, in ref. 24, p. 437

(74) R. Rudham & A. Stockwell, Catalysis Vol.1, Spec. Periodical Reports, Chem. Soc., London, 87, (1977).

(75) D. Barthomeuf, in ref. 20, p.453.

(76) K.V. Topchieva, 'Application of Zeolites in Catalysis' ed. K. Boreskov & M. Minachev, Akad. Kiado, Budapest, (1979)p.35.

(77) C. Nacccache & Y.B. Taarit, in ref. 21, p.592.

(78) J.A. Rabo, P.E. Pickert, D.N. Stamires & J.E. Boyle, in 'Act. Deux. Cong. Catal', Technip. Paris (1961), p.2055.

(79) R.M. Barrer, Nature, 164, 112, (1949).

(80) A. H. Keough & L.B. Sand, J. Amer. Chem. Soc. 83, 3536, (1961).

(81) W.J. Mortier, J.J. Pluth & J.V. Smith, Mat. Res. Bull., 10, 1319 (1975).

(82) Kh. M. Minachev & Ya. I. Isakov, in ref. 23, p.552.

(83) R.A. Della Betta & M. Boudart, Proc. 5th Inter. Cong. Catalys., North Holland, 2, 1329 (1973).

(84) G.C. Bond, 'Principles of Catalysis', Second Edition (1972), p.p.5.

(85) C.N. Satterfield, 'Mass Trasnfer in Heterogeneous Catalysis', MIT Press, Cambridge (1970).

(86) J.M. Thomas, & W.J. Thomas, 'Introduction to the Principles of Heterogeneous Catalysis', Academic Press Inc., N.Y. (1967).

(87) E.E. Petersen, 'Chemical Reaction Analysis', Prentice Hall Inc., N.Y. (1965).

(88) S. Brunauer, 'The Physical Adsorption of Gases and Vapours', Oxford University Press, London (1943).

(89) P.G. Ashmore, 'Catalysis and Inhibition of Chemical Reactions', Butterworths, London (1963).

(90) B.M.W. Trapnell, 'Chemisorption', Butterworths, London (1955).

(91) I. Langmuir, J.Am. Chem. Soc., 38, 221 (1916).

(92) C.N. Hinshelwood, 'The Kinetics of Chemical Change', Clarendon Press, Oxrord, Chapter 8, (1940).

(93) E.K. Rideal, J. Soc. Chem. Ind., London, 62, 335 (1943); D.D. Eley, 'Adv. Catalys.', 1, 157 (1948).

(94)

(94) S.J. Gregg & K.S.W. Sing, 'Adsorption, Surface Area & Porosity', Academic Press, London (1967).

(95) H.S. Taylor, Proc. Roy. Soc., A108, 105 (1925).

(96) G.C. Bond in 'The Physical Basis for Heterogeneous Catalysis', edited by E. Draughs & R.I. Jaffee, Plenum Press, London (1975).

(97) A.A. Balandin, 'Adv. Catalys.' 10, 96 (1958); E.G. Schlosser, Ber. Bunsen Phys. Chem., 73, 358 (1969).

(98) B.M.W. Trapnell, 'Advan. Catalys.', 3, 1 (1951).

(99) G.C. Bond, 'Fourth Int. Cong. Catalys.', Akademiai Kaido, Budapest (1971), paper 67.

(100) R.V. Hardeveld & F. Hartog, 'Advan. Catalys.', 22, 75 (1972).

(101) G.A. Somorjai, 'Catalysis Reviews', 7, 87 (1973).

(102) T. Kwan, 'Advan. Catalys.', 6, 67 (1954), p.103.

(103) H.S. Taylor, 'Advan. Catalys.', 9, 1 (1957).

(104) G.C. Bond, 'Catalysis By Metals', Academic Press, London (1962), p.125.

(105) G.C.A. Schuit, 'Proc. 2nd Int. Cong. Catal.', EditionsTechnip, Paris (1961), p.916.

(106) E. Noordally, Ph.D. Thesis, The City University, London (1979).

(107) G.M. Schwab & H. Schultes, Zeits.f.Physik.Chemie B 9, 265 (1930);
G.M. Schwab, R. Staeger & von Baumbach, Zeits.f.Physik.Chemie B 21, 65 (1933);
G.M. Schwab & R. Staeger, Zeits.f.Physik. Chemie, B 25, 418 (1934);
G.M. Schwab & H. NaKamura, Ber. d.D.Chem. Ges. 71, 1755, (1938);
G.M. Schwab & G. Driskos, Zeits.f.Physik.Chemie A186, 348 (1940).

(108) K.M. Dell, F.S. Stone & P.F. Tiley, Trans. Faraday Soc. 49, 201 (1953).

(109) C. Wagner, J.Chem. Phys. 18, 69 (1950).

(110) A. Cimino, Chim. Ind. Milan 56, 27 (1974).

(111) F.S. Stone, J. Solid State Chem. 12, 271 (1975).

(112) G.K. Boreskov, Proc. 6th Int. Cong. Catal., London (1976), p.204.

(113) P. Pomonis & J.C. Vickerman, J. Catal. 55, 88 (1978).

(114) A. Cimino, V. Indovina, F. Pepe & M. Schiavello, Zh. Fiz. Khim, 53 2890 (1979).

(115) V. Indovina. A. Cimino, M. Inversi & F. Pepe, J. Catal. 56, 396 (1979).

(116) C. Angeletti, A. Cimino, V. Indovina, F. Pepe & M. Schiavello, J. Chem. Soc., Faraday Trans. I, 77, 641 (1981).

(117) A. Cimino & V. Indovina, J. Catal 17, 54 (1970).

(118) A. Cimino, R. Bosco, V. Indovina & M. Schiavello, J. Catal. 5, 271 (1966).

(119) J. Scheve & I.W. Schulz, Paper 84 Proc. of 4th Int. Congress Catalysis, Moscow (1968), p.483.

(120) R. Rudham & M.K. Sanders in 'Chemisorption & Catalysis' edited by P. Hepple, Institute of Petroleum, London (1971). p.58.

(121) R.M. Dell, F.S. Stone & P.F. Tiley, Trans. Faraday Soc., 49, 201 (1953); Y. Saito, Y. Yoneda & S. Makishima, p.1937, 2nd Int. Congress Catalysis, Paris (1961).

(122) A. Cimino, M. Schiavello & F.S. Stone, Disc. Faraday Soc. 41, 350 (1966); N.P. Keier, I.S. Sazonova & R.V. Bunima, Kinet. Katal. 10, 1037 (1969).

(123) M. Schiavello, M. L. Jacona & A. Cimino, J. Phys. Chem. 75, 1051 (1971); A. Cimino & M. Schiavello, J. Catal. 20, 202 (1971), M.Lo Jacona, M. Schiavello & A. Cimino, J. Phys. Chem. 75, 1045 (1971); M. Schiavello, A. Cimino & J.M. Criado, Cazz.Cimica Ital. 101 ,47 (1971).

(124) T.K. Lavorovskaya, A.A. Slinkin & A.M. Rubinstein, Kinet. Katal 14 , 1202 (1972).

(125) F.S. Stone, R. Rudham & L.R. Gale, Z.Electrochem. 63, 129 (1959); G. Schmid & N. Keller, Naturwissenschaften 37, 43 (1950); C.B. Amphlett, Trans. Faraday Soc. 50, 273 (1954).

(126) A. Cimino & F. Pepe, J. Catal 25, 362 (1972).

(127) F. Pepe, M. Schiavello & G. Ferraris, Z. Phys. Chem. N.F. 96, 297 (1975).

(128) L.V. Milton & J.F. Reddy, J. Catal., 7, 76 (1967).

(129) F.H. Chapple & F.S. Stone, Proc. Brit. Ceram. Soc., 1, 45 (1964).

(130) A. Cimino, F. Pepe & M. Schiavello, Proc. 5th Inter. Cong. on Catalysis, Palm Beach (1972), paper 1; D. Cordischi & M.Lo Jacono, Z. Physik. Chem. N.F. 74, 93 (1971).

(131) I.R. Campbell, Ind. Eng. Chem.,49, 450T, 447T, 432T (1930); T. Wheeler, Rec. Trav. Chim. 50, 874 (1931); I.F. Walker & B.E. Christiensen, Ind. Eng. Chim., 7, 9 (1934); W. Iloughe, Ingenieur Chemiste, 18, 6 (1934).

(132) B.A. Zakharov & L.I. Durynina, Dokl. Akad. Nauk., SSSR, 63, 289 (1948); B.A. Zakharov & T.N. Nikolaeva, Izv. Akad. Nauk SSSR, Otd. Khim. Nauk, 79, (1948); S. Araki, Japan Analyst, 2, 365 (1953).

(133) W.P. Yant & C.O. Hawk, J. Amer. Chem. Soc., 49, 1455 (1927); V.P. Vendt & G.A. Lebedeva, Zavods Kaya Laboratoriya, 24, 819 (1958).

(134) R.W.Anderson, Ind. Eng. Chem., 53, 809 (1961).

(135) C.F. Cullis , D.E. Keene & D.L. Trimm, Trans. Faraday Soc., 67, 864 (1971).

(136) G. Kainz & H. Horwatitsh, Microchim. Acta., N 1-2, 16 (1962).

(137) T.V. Andrishkevich, K.V. Popovskii & G.K. Boreskov, Kinet. Katal 6, 860 (1965).

(138) J.G.E. Cohn & A.J. Haley, C an. Patent 597, 459 (1960).

(139) A.I. Gelbshtein, S.S. Stroeva, Yu.M. Bakshi & Yu.A. Mischenko, paper 22, Proc. of 4th Int. Cong. on Catal., Vol I, Moscow (1968), p.297.

(140) G.K. Boreskov, V.V. Popovskii & V.A. Sazonov, paper 33, Proc. 4th Int. Cong. on Catal. Vol I, Moscow (1968), p.439.

(141) G.K. Boreskov, Kinet. Katal., 11, 374 (1970).

(142) G.K. Boreskov, paper 68, Proc. 5th Int. Cong. Catal. Vol. II, Miami Beach Florida (1972) p.981.

(143) L.P. Davydova, G.K. Boreskov, K.G. Ione & V.V. Popovski, Kinet. Katal., 16, 117 (1975).

(144) L. Ya. Margolis, Adv. In Catal., 14, 429 (1963).

(145) L. Ya. Margolis, Paper 19, Proc. 4th Int. Cong. on Catal. Vol. I, Moscow (1968), p.262.

(146) D.A.Dowden, J. Quim., B-61, 177 (1966).

(147) L.E. Derlyutova, A.V. Krylova, L.Ya.Margolis, Kinet. Katal., 8, 421 (1967).

(148) Y.F.Y. Yao & J.T. Kummer, J. Cat., 46, 388 (1977).

(149) H. Paetow & L. Riekert, Acta Phys. Chem., 24, 245 (1978).

(150) I. Brown & W.R. Patterson, J. Chem. Soc., Faraday Trans. I, 79, 1431 (1983).

(151) A.A. Slinkin, T.K. Lavroviskaya, I.V. Mishin & A.M. Rubinshtein, Kinet. Katal, 19, 922 (1978).

(152) W.E. Addison & R.M. Barrer, J. Chem. Soc., 1, 757 (1955).

(153) K. Klier & M. Ralek, J. Phys. Chem. Solids, 29, 951 (1968).

(154) K. Klier, J. Am. Chem. Soc., 91, 5392 (1969).

(155) A.A. Slinkin, T.K. Lavrovskaya, M.I. Loktev, I.V. Mishin & A.M. Rubinshtein Kinet. Katal., 20, 515 (1979).

(156) Sh. I. Sidamonidze, G.V. Tsitsishvili, T.A. Kheladze, L.M. Scharabidze, Soobshch. Akad. Nauk.Gruz. S.S.R., 88, 605 (1977).

(157) Sh. I. Sidamonidze, G.V. Tsitsishvili, T.A. Kheladze, L.M. Scharabidze, M.D. Rukhadze, Soobshch. Akad. Nauk. Gruz. S.S.R., 96, 597 (1979).

(158) S.Akbar & R.W. Joyner, J.Chem. Soc., Faraday Trans. I, 77, 803 (1981).

(159) A.A. Slinkin, I.V. Mishin, T.K. Lavrovskaya, A.V. Kucherov & A.M. Rubinshtein, Kinet. Katal., 23, 903 (1982).

(160) J.G. Firth & H.B. Holland, Nature, 217, 1252 (1968).

(161) J.G. Firth & H.B. Holland. Trans. Faraday Soc., 65, 1891 (1969).

(162) R. Rudham & M.K. Sanders, J. of Catal., 27, 287 (1972).

(163) R.B. Anderson, K.C. Stein, J.J. Feenan & L.J.E. Hofer, Ind. Eng. Chem., 53, 809 (1961).

(164) R.R. Baker & D.A. Yorke, J. Chem Ed., 49, 351 (1972).

(165) F. Mahoney, R. Rudham & A. Stockwell, in ref. 21, p.329.

(166) P. Fletcher, P.R. Lower & R.P. Townsend, in ref. 21, p.353.

(167) P.B. Weisz, Erdöl Kohle 18, 525 (1965);
N.Y. Chen, P.B. Weisz, Chem. Eng. Progr. Symp. Ser., 63, 81 (1967).

(168) J. Rouchaud, P. Mulkay, J.F. Fripiat, Bull. Soc. Chim. Belges, 77, 505 (1968).

(169) A.L. Agudo, F.R. Badcock & F. S. Stone, paper 59, Proc. of 4th Int. Cong. on Catal., Moscow (1968), p.165.

(170) T.B. Reed and D.W. Breck J. Amer. Chem. Soc., 78(23), 5972 (1956).

(171) R.M. Barrer & W.M. Meier, Trans. Farad. Soc., 54, 1074 (1958).

(172) P.A. Howell, Acta. Cryst.,13, 737 (1960).

(173) L. Broussard & D.P. Shoemaker, J. Am. Chem. Soc., 82, 1041 (1960).

(174) K. Seff & D.P. Shoemaker, Acta. Cryst., 22, 162 (1967).

(175) J.V. Smith & L.G. Dowell, Z. Kristallogr., 126, 135 (1968).

(176) V. Gramlich & W.M. Meier, Z. Kristallogr., 133, 134 (1971).

(177) P.E. Riley, K. Seff & D.P. Shoemaker, J. Phys. Chem. 76, 2593 (1972).

(178) R.Y. Yanagida, A.A. Amaro and K.Seff, J. Phys. Chem. 77, 805 (1973).

(179) K. Seff, Accounts Chem., Res., 9, 121 (1976).

(180) V. Subramanian & K. Seff, J. Phys. Chem., 81, 2249 (1977).

(181) J.J. Pluth & J.V. Smith, J. Phys. Chem., 83, 741 (1979).

(182) R.L. Firor & K. Seff, J. Am. Chem. Soc., 98, 5031 (1976).

(183) P.C. Leung, K.B.Kunz, K.Seff & I.E. Maxwell , J. Phys. Chem, 79, 2157 (1975).

(184) M. Nitta, K.Ogawa and K. Amoura, in ref 22, p.291.

(185) A. Dyer & H. Enamy, in ref.21, p.288.

(186) G. De Roy, W.J. Mortier, J.B. Uytterhoeven & E.F. Vansant, in ref.22, p.214.

(187) R.M. Barrer & W.M. Meier, Trans. Faraday Soc., 55, 130 (1959).

(188) R.M. Barrer, L.V.C. Rees & D. Ward, J. Proc. R. Soc. London, 273A, 180 (1963).

(189) L.L. Ames, J. Am. Mineral, 49, 1099 (1964)

(190) H.S. Sherry, J. Phys. Chem., 70 ,1332 (1966).

(191) H.S. Sherry & H.F. Walton, J. Phys. Chem., 71, 1457 (1967).

(192) E.P. Hertzenberg & H.S. Sherry, ACS Symp. Ser., No. 135, 187 (1980)

(193) P.D. Radovanov, O.M. Gacinovic & I.J. Gal., J. Inorg. Nucl. Chem., 31, 2981 (1969).

(194) I.J. Gal, O. Jankovic, S. Malcic, P.D. Radovanov & M. Todorovic, Tran. Farad. Soc., 67, 999 (1971).

(195) S. Lomic & I.J. Gal, Croat. Chem. Acta. 44, 403 (1972).

(196) L.V.C. Rees, in ref. 21, p.218.

(197) B.H.Weirs, R.J.Grosse & W.A. Gilley, Environ. Sci. Technol. 16, 617 (1982).

(198) F. Wolf & H. Furtig, Kolloid.Z.Z. Polym., 206, 48 (1965).

(199) F. Danes, F. Wolf, Z. Phy. Chem. (leipzig) 251, 339, (1972).

(200) F. Danes & F. Wolf, Z. Phy. Chem. (Leipzig) 251, 339, (1972).

(201) S.P. Zhdanov, M.A.Shubaera & M.M.Piryotko Dokl. Akad. Nauk. SSSR, 203, 874 (1972).

(202) M.M Dubinin & A.A. Isirikyan N.I. Regent, Izv. Akad. Nauk. SSSR, Ser. Khim.,1244 (1974).

(203) R.Y. Yanagida, T.B.Vance & K.Seff Inorg.Chem. 13, 723 (1974).

(204) P.E. Riley & K. Seff, J. Phys. Chem., 79, 1594 (1975).

(205) R.L. Firor & K. Seff, (a) J. Phys. Chem., 82, 1650 (1978);
(b) Inorg. Chem. 17, 2144 (1978);
(c) J. Am. Chem. Soc., 100, 3091 (1978).

(206) W.V. Cruz, P.C.W. Leung & K. Seff, J. Am. Chem. Soc., 100, 6997 (1978).

(207) L.B. McCusker & K. Seff, (a) J. Am. Chem. Soc., 101, 5052 (1978);
(b) J. Phys. Chem., 85, 166 (1981).

(208) V.Subramanian & K.Seff, J. Phys. Chem., 84, 2928 (1980).

(209) H.S. Lee & K. Seff, J. Phys. Chem., 85, 397 (1981).

(210) M.J.Schwuger, H.G.Smolka & C.P.Kurzandorfer, Tenside, 13, 305 (1976).

(211) V.M.Radak, I.J.Gal & I.J.Salai, J. Chem. Soc. Faraday Trans., 72, 1150 (1976).

(212) H. Gaus & W. Lutze, J. Phys. Chem., 80, 2948 (1976).

(213) H. Gaus & W. Lutze, J. Phys. Chem., 85, 79 (1981).

(214) D. Drummond, L.V.C. Rees & A. De Jonge, J. Phys. Chem., 87, 1967(1983).

(215) S.Narayaman and W.M.Carrol, J. Catal., 49, 97 (1977).

(216) Y.S.Khodakov, I.D.Mikheikin, V.S.Nakhshunov, V.A.Shvets, V.B.Kazanskii & Kh.M.Minachev, Izv. Akad. Nauk SSSR, Ser. Khim.523 (1969).

(217) S.M.Kuznicki, K.L.Devries & E.M. Eyring, , J. Phys. Chem., 84, 535 (1980).

(218) K. Klier & M. Ralek , J. Phys. Chem. Solids, 29, 945 (1968).

(219) T.A. Egerton & J.C. Vickerman, J. Chem. Soc. Faraday Trans., 69, 39 (1973).

(220) A. Dyer & M.J. Wilson, Thermochimica Acta, 11, 55 (1975).

(221) B. Coughlan, W.M. Carroll & W.A.McCann, (a) Chem. Ind. 527 (1976); (b) Proc. Roy. Ir. Acad., 76B, 349 (1976).

(222) B. Coughlan, W.M. Carroll, J. Chem. Soc. Faraday Trans., 72, 2016 (1976).

(223) R. Kellerman, P.J.Hutta, & K. Klier, J. Amer. Chem. Soc., 96, 5946 (1974).

(224) S. Akbar, Ph.D. thesis, Bradford University (1980).

(225) W.N.Delgass, R.L.Garten & M.Boudart, (a) J. Chem. Phys., 50, 4603 (1969); (b) J. Phys. Chem., 73, 2970 (1969).

(226) R.L.Garten, W.N.Delgass & M.Boudart; J. Catal., 18, 90 (1970).

(227) K.Klier, R.Kellerman & P.J.Hutta, J. Chem. Phys., 61, 4224 (1974).

(228) M.A. Heilbron & J.C. Vickerman, J. Catal, 33, 434 (1974).

(229) P. Gallezot & B. Imelik, J. Phys. Chem., 77, 652 (1973).

(230) S.A.I.Barri & L.V.C. Rees, J. Chromatogr., 21, 201 (1980).

(231) T.E. Cook, W.A. Cilley & A.C. Savitsky & B.H. Weirs, Environ. Sci. Technol., 16, 344 (1982).

(232) H.S. Sherry, J. Phys. Chem., 77, 4086 (1968).

(233) W.M. Meier. Z. Kristallogr., 115, 439 (1961).

(234) V. Gramlich, Diss. No. 4633 (1971), Eidg. Techn. Hochschule, Zurich, Switzerland.

(235) H.G. Karge, Z. Phys. Chem. (Wiesbaden), 122(1), 103 (1980).

(236) T. Yashima & N. Hara, J. Catal., 27. 329 (1972).

(237) J.D.Sherman & J.M. Bennett, Adv. Chem. Ser., 121, 52 (1973).

(238) L.B. Sand, 'Molecular Sieves', Soc. Chem. Ind., p.71, London (1968).

(239) R.M. Barrer & A.T.T. Oei, J. Catal., 30, 460 (1973).

(240) D.W. Breck, p.124 (Ref. 23); L.B. Sand, p.21 (Ref.31).

(241) M.M. Dubinnin, G.M. Federova, G.M. Plavnik, L.I. Piguzova & E.N. Prokofeva, Isz. Akad. Nauk. SSSR, Ser. Khim, 11, 2429 (1968).

(242) S.A. Aboel-Enein, R. Sh.Mikhail & H.A.E.Wakil, Thermochemica Acta, 165 (1978).

(243) L.L. Ames Jr., Amer. Mineral., 46, 1120 (1961).

(244) H. Takahashi & Y.Nishimura, Seisan-Kenkyu, 20, 466 (1968).

(245) D.B. Hawkins, Materials Res. Bull., 2, 1021 (1967).

(246) G. Lenzi & A. Pozzuoli, Rend. Accad. Sci. Fis. Mat. Naples, 36, 235 (1969).

(247) V.A. Chumakov, V.I. Gorshkov, A.M. Tolmachev & V.A. Fedorov, Vestnik Moscow Univ., 24, 22 (1969).

(248) N.F. Ermolenko, S.A. Levina, L.V. Malashevich & A.A. Prokopovich, Vesti Akad, Navuk Belarus. S.S.R., Ser. Khim Navuk, 5,18 (1968).

(249) L.V.C. Rees & A. Rao, Trans. Faraday Soc., 62, 2103 (1966).

(250) A. Rao & L.V.C. Rees, Trans. Faraday Soc., 62 2505 (1966).

(251) F.Wolf, H.Furtig & H.Knoll, Chem. Tech. (Leipzig), 23, 273 (1971).

(252) A.I. Grivkova & B.A. Zaitsev, Zh.Fiz. Khim, 47, 952 (1973).

(253) C. Golz, K. Pilchowski & F. Wolf, Z. Phys. Chem. (Leipzig), 257, 1137 (1976).

(254) R.M.Barrer & J.Klinowski, J. Chem. Soc., Faraday Trans. I, 70, 2362 (1974).

(255) N.F. Chelishchev & V.F. Volodin, Dokl. Akad. Nauk.USSR (Phys. Chem.), 232, 649 (1977).

(256) N.Susuki, K.Saitoh & S. Hamoda, Radioch. Rad. Letters, 32 (3-4), 121 (1978).

(257) Kh.Minachev,V.Garanin, T.Isakova V.Kharlamov and V.Bogomolov Adv. Chem. Ser., 102, 440 (1971).

(258) O.D. Bonner & C.F. Jumper, Infra-red Phy., 13, 233 (1973).

(259) A. Dyer & R.P. Townsend, J. Inorg. Nucl. Chem., 35, 300 (1973).

(260) R.M. Barrer & R.P. Townsend, J. Chem. Soc., Farad. Trans. I, 72, 661 (1976).

(261) R.M. Barrer & R.P. Townsend, J. Chem. Soc., Faraday Trans. I, 72, 2650 (1976).

(262) P. Fletcher & R.P. Townsend, J. of Chromat., 201, 93 (1980).

(263) P. Fletcher & R.P. Townsend, J. Chem. Soc., Farad. Trans. I, 77, 497 (1981).

(264) P. Fletcher & R.P. Townsend, Zeolites, 3, 129 (1983).

(265) O.A. Hougen & K.M. Watson, 'Chemical Process Principles, Part III', John Wiley, Inc. Chapman & Hall, London (1957).

(266) C.N. Satterfield & T.K.Sherwood, 'The Role of Diffusion in Catalysis', Addison-Wesley, Mass. (1963).

(267) K.G. Denbigh, 'Chemical Reactor Theory', Cambridge (1966).

(268) R.B. Anderson, 'Experimental Methods in Catalytic Research', Academic Press, London (1968).

(269) R. Aris, 'Elementary Chemical Reactor Analysis', Prentice Hall, New Jersey (1969).

(270) B.C. Gates, J.R. Katzer & G.C.A. Schuit, 'Chemistry of Catalytic Processes', McGraw-Hill, New York (1979).

(271) C.N. Satterfield, 'Heterogeneous Catalysis in Practice', McGraw-Hill, London (1980).

(272) J.B. Butt, 'Reaction Kinetics & Reactor Design', Prentice-Hall, New Jersey, (1980).

(273) J.R. Anderson & M. Boudart, 'Catalysis Vol.I', Springer-Verlag, Berlin (1981).

(274) J.J. Carberry, Ind. Eng. Chem. 56, No.11, 39 (1964); D.G. Tajbl, J.B. Simmons & J.J. Carberry, Ind. Eng. Chem., Fundamentals, 5, 171(1966).

(275) S. Weller, J. Am. Chem. Soc., 69, 2432 (1947).

(276) R.P.Chambers and M.Boudart, J. Catalysis, 5, 517 (1966).

(277) C. Kemball, Proc. Roy. Soc., A207, 539 (1951).

(278) K. Klier, in "Molecular Sieve Zeolites, -I", Advances in Chemistry Series, 101, 480 (1971).

(279) G.Schwarzenbach & H.Flaschka, 'Complexometric Titrations', Second English Edition, Methuen & Co. Ltd., London (1969).

(280) A.I. Vogel, 'A Text Book of Quantitative Inorganic Analysis', Third Edition, Longmans (1961).

(281) S. Brunauer, P.H. Emmett & E. Teller, J. Am. Chem. Soc., 60, 309(1938).

(282) J.W.McBain and M.Boudart, J.Am. Chem. Soc., 48, 690 (1926).

(283) R.G. Davies, Chem. & Ind., p.160 (1952).

(284) F.M.Nelson and F.T.Eggertsen, Analyt. Chem., 30, 1387 (1958).

(285) A.J. Haley, J. Appl. Chem., 13, 392 (1963).

(286) J.F. Roth and R.J.Elwood, Analyt. Chem., 31, 1738 (1959).

(287) R.A.Beebe, J.B.Beckwith & J.M. Honig, J. Amer. Chem. Soc., 67, 1554 (1945).

(288) B.D. Cullity in 'Elements of X-ray Diffration' (1959) Addison-Wesley Pub. Co., Inc. U.S.A., p.149.

(289) B.W.Burbridge,M.K. Eyles & I.M. Keen, Adv. Chem. Ser., 102, 401 (1971); V. Bogomolov, V. Garanin, T. Isakova, V. Kharlamov & Kh. Minachev, Adv. Chem. Ser. 102, 440 (1971).

(290) J.A.Gray & J.T.Cobb Jr. Catal., 36, 125 (1975).

(291) R.P. Townsend, DIC Thesis, Imperial College, London (1977), p.99.

(292) W.E.Cooley & D.H. Bush, 'Inorganic Synthesis Vol.5' p.208.

(293) R. Chen & Y. Kirsh, 'Analysis of Thermally Stimulated Processes', Pergammon Press, Paris (1981). p. 82.

(294) C. Durval, 'Thermal Methods in Analytical Chemistry' Elsevier, Amsterdam (1976).

(295) R.C. Mackenzie, ed., 'Differential Thermal Analysis', Vol.1: Fundamental Aspects,' Academic Press, London (1970) & 'Vol.2: Applications', Academic Press, London (1972).

(296) C.J.Keattch & D.Dollimore, 'An Introduction to Thermogravity' 2nd edition, Heyden, London (1975).

(297) M.I.Pope & M.D. Judd, 'DTA: a Guide to the Technique and its Application', Heyden, London (1977).

(298) W. Smykatz-Kloss, 'Differential Thermal Analysis: Applications and Results in Mineralogy', Springer Verlag, Berlin (1974).

(299) D.N. Todor, 'Thermal Analysis of Minerals', Abacus Press, Tunbridge Wells, England (1976).

(300) W.W. Wendlandt, 'Thermal Methods of Analysis', 2nd ed. Wiley, New York (1974).

(301) K. Honda, Sci. Rept. Tohoku Univ., 4, 97 (1915).

(302) M. Guichard, Bull. Soc. Chim., France, 2, 539 (1935).

(303) K.J. Laidler, "Chemical Kinetics", IInd edition, McGraw-Hill, N.Y. (1973) p.7.

(304) F.A. Cotton and G. Wilkinson, "Adv. Inorganic Chemistry" fourth edition, John Wiley N.Y. (1980).

(305) N.P. Evmerides and J. Dwyer, Chim. Chron., New Series, 11, 331 (1982).

(306) P. Fletcher, Ph.D. Thesis, The City University, London (1979); D.W. Breck, ref. 23 p.461.

(307) H.E. Ries, "Cat. vol. I", Reinhold, N.Y. (1954) pp.1.

(308) S.M. Csicsery in 'Zeolite Chemistry & Catalysis, ACS monograph 171, Am. Ch. Soc., D.C.,Ed. J.A. Rabo (1976) pp. 680.

(309) H.K. Beyer, E. Detrekoy, E. Kallo and J. Papp in 'Sym. on Mech. of Hydrocarbon Reactions' Ed. F. Marta and D. Kallo, Elselvier (1975) pp. 369.

(310) H.K. Beyer, A. Kiss, J. Mihalyfe and P.A. Jacob, J.C.S. Faraday I, 76, 332 (1980).

(311) H. Lechart 'Nato ASI, Ser. E, 80, 151 (1984).

(312) R. M. Barrer and D. L. Peterson, Proc. Roy. Soc. London, A280, 466 (1964).

(313) P.K. Bajpai, M.S. Rao and K.V.G.K. Gokhale, 'Proc. of 7th Int. Conf. on Thermal Anal.' ed. B. Miller, Wiley (1982) pp.558.

(314) G.H. Kühl , in ref. 20, p.96.

(315) V. Vucelic, D. Vucelic, D. Karaulic and M. Susic, Thermochimica Acta 7, 77 (1973).

(316) G.V. Tsitsishvili, G.O. Piloyan, L.K. Kvantaliani and D.S. Chipashvili, 'Proc. of 7th Int. Conf. on Thermal Anal.' ed. B. Miller, Wiley (1982) pp. 565.

(317) J. Dwyer, R.V. Parish and N.P. Evmerides, Inorg. Chimica Acta, 75, 229 (1983).

(318) K. Toth and T. Flora, Acta. Chim. (Budapest), 45, 87 (1965).

(319) Van De, M. Tuyen and C. Dimitrov, Dokl. Bolg. Akad. Nauk., 35(8) , 1081 (1982).

(320) R.A. Schoonheydt, L.J. Vandamme, P.A. Jacobs and J.B. Uytterhoeven, J. Catal., 43, 292 (1976).

(321) F.O. Bravo, J. Dwyer and D. Zemboulis, in ref. 21 pp. 369.

(322) A. Dyer and S.A.I. Barri, J. Inorg. Nucl. Chem., 39, 1061 (1977).

(323) M.L. Costenoble, W.J. Mortier and J.B.Uytterhoeven, J. Chem. Soc. Farad. I, 74, 477 (1978).

(324) D.W. Breck, W.G. Eversole, R.M. Milton, T.B. Reed and T.L. Thomas, J. Am. Chem. Soc., 78 (23), 5963 (1956).

(325) H.K. Beyer, I.M. Belenkaja and G. Borbely, J. Chem. Soc., Farad. I, 81, 3049 (1985).

(326) H.A. Benesi, J. Catal., 8, 368 (1967).

(327) T.J. Weeks Jr., H.F. Hillery and A.P. Bolton, J. Chem. Soc. Farad. Trans. I, 71 , 2051 (1975).

(328) I.V. Mishin, G.A. Ashavskaya and I.G. Vorobeva, Izv. Akad. Nauk SSSR, Ser, Khim., No. 8,1720 (1983).

(329) G. Kerr, J. Phys. Chem., 72, 2594 (1968).

(330) I.V. Mishin, G.I. Kapustin, T.V. Alekseeva, A.L. Klyachko, B.K. Nefedov, Z.S. Ameridze and A.M. Rubinshtein, Izv. Akad. Nauk SSSR, Ser. Khim, 2447 (1981).

(331) G.C. Bond, 'Het. Catal. , Principles and Applications', Oxford, 1974, pp. 46-51.

(332) A.A. Slinkin, T.K. Lavrovskaya, I.V. Mishin and A.M. Rubinshtein, Kinet. Katal, 19(4), 922 (1981).

(333) D.D. Eley, A. H. Klepping and P.B. Moore, J. Chem. Soc., F.T.I., 81, 2981 (1985).

(334) M. Iwamoto, S. Yokoo, K. Sakai and S. Kagawa, J. Chem. Soc., F.T.I. 77, 1629 (1981).

(335) J. Legise, J.O. Petunchi and W.K. Hall, J. Catal., 86,392 (1984).

(336) A. Matsui and M. Yasuda, Kogo Kagaku Zasshi, 43, 116B (1940); C. F. Cullis, D.E. Keene and D.L. Trimm, Trans. Farad. Soc., 67, 864 (1971).

(337) S.L. Urwin, Ph.D. Thesis, The City University, London (1983).

APPENDICES

contents

Appendix Ia - CHEMICAL COMPOSITION OF ZEOLITE A SAMPLES

Sample	Na-A	Ca-A	Cu-5A(1)	Cu-5A(2)	Cu-5A(3)
%w/w:					
H_2O	22.23	23.69	23.51	24.20	24.20
Al_2O_3	27.96	27.81	28.04	28.00	27.91
SiO_2	33.69	32.58	32.68	32.31	32.50
Na_2O	17.04	2.704	2.26	1.79	1.36
CaO		12.39	11.59	11.03	11.03
M_xO_y			0.85	1.42	1.96
Total	100.92	99.18	98.92	98.74	98.97
Si:Al Ratio	1.02	1.00	0.99	0.98	0.99
Cation:Al Ratio	1.00	0.97	0.93	0.89	0.89
Exchange Level (%)	11.90	81.20	3.85	6.48	9.02

Appendix Ia - continued

Sample	Cu-5A(4)	Cu-5A(5)	Cu-5A(6)	Co-5A(1)	Co-5A(2)
%w/w:					
H_2O	24.32	24.89	25.55	23.38	23.87
Al_2O_3	28.07	28.00	28.10	27.43	27.89
SiO_2	31.63	31.27	31.14	32.85	32.60
Na_2O	1.47	0.78	0.64	2.30	1.86
CaO	11.21	11.00	9.18	11.91	11.56
M_xO_y	2.06	4.31	5.29	1.13	1.52
Total	98.76	100.25	99.90	99.00	99.30
Si:Al Ratio	0.96	0.95	0.95	1.02	0.99
Cation:Al Ratio	0.91	1.08	0.88	0.98	0.93
Exchange Level (%)	9.40	19.71	24.18	5.60	7.43

Appendix Ia - continued

Sample	Co-5A(3)	Co-5A(4)	Co-5A(5)	Co-5A(6)
%w/w:				
H_2O	24.09	24.09	25.05	26.16
Al_2O_3	27.81	27.71	27.25	27.05
SiO_2	32.37	32.11	31.59	30.42
Na_2O	1.57	1.84	0.83	0.54
CaO	11.12	10.88	8.29	6.01
M_xO_y	2.30	2.28	7.24	10.05
Total	99.27	99.49	100.24	100.22
Si:Al Ratio	0.99	1.00	0.99	0.96
Cation:Al Ratio	0.93	0.96	0.97	0.95
Exchange Level (%)	11.25	13.60	35.95	50.60

Appendix Ib - CHEMICAL COMPOSITION OF MORDENITES

Mordenite	Na-	NH_4-(1)	NH_4-(2)	Ni/Na-	Ni/NH_4-	Ni-(1)
%w/w:						
H_2O	13.37	10.64	10.99	15.05	12.85	13.30
Al_2O_3	10.56	10.61	10.63	9.91	10.49	10.04
SiO_2	69.70	72.94	73.02	69.16	70.56	70.59
Na_2O	6.35	0.03	0.08	2.94	0.03	0.05
$(NH_4)_2O$		5.21	5.06	0.23	3.12	3.18
NH_3						
M_xO_y				3.32	2.91	2.31
Total	99.98	99.43	99.78	100.61	99.96	99.47
Si:Al Ratio	5.61	5.66	5.65	5.74	5.54	5.78
Cation:Al Ratio	0.99	0.97	0.95	0.99	0.97	0.85
Exchange Level (%)	99.40	96.33	93.37	45.74	37.94	31.41

Appendix Ib - continued

Mordenite	Ni(2)-	Ni(3)-	Pt(1)-	Pt(2)-	Pt(3)-	Pt(4)-
%w/w:						
H_2	13.75	13.82	12.86	12.94	13.51	12.44
Al_2O_3	10.35	10.50	9.64	9.49	9.25	9.35
SiO_2	69.22	70.23	65.40	66.03	63.87	66.37
Na_2O	0.18	0.16	0.05	0.07	0.13	0.14
$(NH_4)_2O$	2.83	2.76	1.20	1.14	0.43	1.32
NH_3						
M_xO_y	3.05	3.28	10.70	11.32	12.35	9.58
Total	99.38	100.75	99.85	100.99	99.54	99.20
Si:Al Ratio	5.53	5.53	5.58	5.73	5.68	5.84
Cation:Al Ratio	0.97	0.98	0.79	0.87	0.81	0.81
Exchange Level (%)	40.23	42.63	53.63	57.64	69.81	49.51

Appendix Ib - continued

Mordenite	Cu/Na-	Cu/NH_4-	Cu(1)-	Cu(2)-	Cu(3)-
%w/w:					
H_2	10.67	10.70	10.11	10.24	10.79
Al_2O_3	10.23	10.17	10.14	10.47	10.08
SiO_2	71.28	69.89	70.57	70.57	69.93
Na_2O	0.26	0.02	0.03	0.07	0.04
$(NH_4)_2O$	2.18	2.01	2.23	2.07	1.58
NH_3	1.90	2.49	2.51	2.47	3.14
M_xO_y	4.30	4.84	4.49	4.91	5.40
Total	100.82	100.12	100.08	100.80	100.96
Si:Al Ratio	5.73	5.66	5.73	5.55	5.71
Cation:Al Ratio	1.00	1.00	1.00	1.00	1.00
Exchange Level (%)	53.90	61.02	56.73	60.13	68.67

TABLE IIc.1 Co-5A(1)

Correlation coefficient (R)= -0.9916112705

Energy of activation (Ea)= 140671.2978J/mol.

Frequency factor (A)= 17028.857335sec^-1

Best fit equation : lnK = -16918.9957(1/T) + 9.742664676

	TemperatureT/K	1/T	K(1/sec)	ln K	DELG(J./mol.)
1	866	1.154734411E-3	6.29985E-5	-9.672399644	281743.0482
2	919	1.088139282E-3	1.38975E-4	-8.881216496	292940.5979
3	943	1.060445387E-3	2.7504E-4	-8.198594015	295238.7482
4	970	1.030927835E-3	4.535567E-4	-7.69839027	299657.8995
5	1001	9.990009989E-4	8.5085E-4	-7.069274709	303998.6399

SPECIFIC RATE (Rsp) CALCULATIONS

Molecular weight of catalyst(W)=2193

Number of transition metal ions per unit cell(n)=0.36

Nitrous oxide molecules in apparatus(342CC) at PN2O(1torr)=1.2094E19(molecules)

Mass of catalyst sample=0.1326(g)

Corrected mass of activated catalyst sample=0.10159812(g)

	Temperature(T/K)	Rate ConstantK(1/sec)	Rsp(molecules/site.sec)
1	866	6.29985E-5	7.588468591E-5
2	919	1.38975E-4	1.674019894E-4
3	943	2.7504E-4	3.312987455E-4
4	970	4.535567E-4	5.463305908E-4
5	1001	8.5085E-4	1.024689244E-3

TABLE IIc.2 Co-5A(2)

Correlation coefficient (R)= -0.9905371692

Energy of activation (Ea)= 93712.19592J/mol.

Frequency factor (A)= 51.252717485ec^-1

Best fit equation : lnK = -11271.07139(1/T) + 3.936768642

	TemperatureT/K	1/T	K(1/sec)	ln K	DELG(J./mol.)
1	828	1.207729469E-3	5.564E-5	-9.796608191	270235.2821
2	858	1.165501165E-3	1.1632E-4	-9.059165545	274765.6739
3	895	1.117318436E-3	1.8687E-4	-8.585097369	283086.8138
4	928	1.077586207E-3	2.518E-4	-8.286875438	291223.639
5	966	1.035196688E-3	4.3335E-4	-7.743964843	298788.239

SPECIFIC RATE (Rsp) CALCULATIONS

Molecular weight of catalyst(W)=2196

Number of transition metal ions per unit cell(n)=0.45

Nitrous oxide molecules in apparatus(342CC) at PN2O(1torr)=1.2094E19(molecules)

Mass of catalyst sample=0.1339(g)

Corrected mass of activated catalyst sample=0.10193807(g)

	Temperature(T/K)	Rate ConstantK(1/sec)	Rsp(molecules/site.sec)
1	828	5.564E-5	5.351111612E-5
2	858	1.1632E-4	1.11869393E-4
3	895	1.8687E-4	1.797200264E-4
4	928	2.518E-4	2.421656908E-4
5	966	4.3335E-4	4.167692698E-4

TABLE IIc.3 Co-5A(3)

Correlation coefficient (R)= -0.9748711733

Energy of activation (Ea)= 114378.8562J/mol.

Frequency factor (A)= 799.4574666Sec^-1

Best fit equation : lnK = -13756.71801(1/T) + 6.683933333

	TemperatureT/K	1/T	K(1/sec)	ln K	DELG(J./mol.)
1	836	1.196172249E-3	4.5813E-5	-9.990942664	274197.0403
2	887	1.127395716E-3	1.9811E-4	-8.526688125	280125.6676
3	922	1.084598699E-3	3.1148E-4	-8.074175429	287710.1936
4	958	1.043841336E-3	3.9076E-4	-7.847416997	297137.8198
5	983	1.017293998E-3	6.231299999E-4	-7.380755395	301077.8827

SPECIFIC RATE (Rsp) CALCULATIONS

Molecular weight of catalyst(W)=2203.15

Number of transition metal ions per unit cell(n)=0.6799999999

Nitrous oxide molecules in apparatus(342CC) at PN2O(1torr)=1.2094E19(molecules)

Mass of catalyst sample=9.450000001E-2(g)

Corrected mass of activated catalyst sample=7.173495E-2(g)

	Temperature(T/K)	Rate ConstantK(1/sec)	Rsp(molecules/site.sec)
1	836	4.5813E-5	4.156871113E-5
2	887	1.9811E-4	1.797563434E-4
3	922	3.1148E-4	2.826233197E-4
4	958	3.9076E-4	3.545585217E-4
5	983	6.231299999E-4	5.654008896E-4

TABLE IIc.4 Co-5A(4)

Correlation coefficient (R)= -0.986156849

Energy of activation (Ea)= 92237.54221J/mol.

Frequency factor (A)= 58.07106979Sec^-1

Best fit equation : lnK = -11093.70998(1/T) + 4.061667603

	TemperatureT/K	1/T	K(1/sec)	ln K	DELG(J./mol.)
1	817	1.223990208E-3	6.437350001E-5	-9.650808502	265654.8011
2	860	1.162790698E-3	1.8155E-4	-8.613979463	272222.8981
3	911	1.097694841E-3	2.9353E-4	-8.13353071	284727.2247
4	925	1.081081081E-3	3.4436E-4	-7.973822936	287874.55
5	958	1.043841336E-3	5.268699999E-4	-7.548556719	294757.3365

SPECIFIC RATE (Rsp) CALCULATIONS

Molecular weight of catalyst(W)=2212.82

Number of transition metal ions per unit cell(n)=0.8200000001

Nitrous oxide molecules in apparatus(342CC) at PN2O(1torr)=1.2094E19(molecules)

Mass of catalyst sample=0.1782(g)

Corrected mass of activated catalyst sample=0.13527162(g)

	Temperature(T/K)	Rate ConstantK(1/sec)	Rsp(molecules/site.sec)
1	817	6.437350001E-5	2.579919411E-5
2	860	1.8155E-4	7.276043229E-5
3	911	2.9353E-4	1.176390509E-4
4	925	3.4436E-4	1.380103689E-4
5	958	5.268699999E-4	2.111555437E-4

TABLE IIc.5 Co-5A(5)

Correlation coefficient (R)= -0.9387671789

Energy of activation (Ea)= 48066.995940/mol.

Frequency factor (A)= 0.3508380912Sec^-1

Best fit equation : lnK = -5781.174341(1/T) + -1.047430441

	TemperatureT/K	1/T	K(1/sec)	ln K	DELG(J./mol.)
1	792	1.262626263E-3	2.6752E-4	-8.226316229	248145.5295
2	806	1.240694789E-3	2.1785E-4	-8.431703806	253908.3276
3	851	1.175088132E-3	4.567E-4	-7.691483838	262846.8779
4	874	1.14416476E-3	4.58495E-4	-7.687561171	269922.3424
5	911	1.097694841E-3	5.9545E-4	-7.426193137	279369.5476

SPECIFIC RATE (Rsp) CALCULATIONS

Molecular weight of catalyst(W)=2270.52

Number of transition metal ions per unit cell(n)=2.17

Nitrous oxide molecules in apparatus(342CC) at PN2O(1torr)=1.2094E19(molecules)

Mass of catalyst sample=9.950000001E-2(g)

Corrected mass of activated catalyst sample=7.457525001E-2(g)

	Temperature(T/K)	Rate ConstantK(1/sec)	Rsp(molecules/site.sec)
1	792	2.6752E-4	7.540508065E-5
2	806	2.1785E-4	6.140474289E-5
3	851	4.567E-4	1.287286944E-4
4	874	4.58495E-4	1.292346458E-4
5	911	5.9545E-4	1.678377515E-4

TABLE IIc.6 Co-5A(6)

Correlation coefficient (R)= -0.9829097702

Energy of activation (Ea)= 70392.23248J/mol.

Frequency factor (A)= 8.547941585ec^-1

Best fit equation : lnK = -8466.303341(1/T) + 2.145690504

	TemperatureT/K	1/T	K(1/sec)	ln K	DELG(J./mol.)
1	791	1.264222503E-3	1.69675E-4	-8.681625713	250826.6476
2	845	1.183431953E-3	4.52006E-4	-7.701815104	261066.2526
3	881	1.13507378E-3	6.33075E-4	-7.364921659	269720.8589
4	911	1.097694841E-3	7.13295E-4	-7.245615479	278001.7751
5	950	1.052631579E-3	1.09681E-3	-6.815349312	286504.5199

SPECIFIC RATE (Rsp) CALCULATIONS

Molecular weight of catalyst(W)=2329.57

Number of transition metal ions per unit cell(n)=3.13

Nitrous oxide molecules in apparatus(342CC) at PN2O(1torr)=1.2094E19(molecules)

Mass of catalyst sample=0.2074(g)

Corrected mass of activated catalyst sample=0.1531441601(g)

	Temperature(T/K)	Rate ConstantK(1/sec)	Rsp(molecules/site.sec)
1	791	1.69675E-4	1.656617779E-5
2	845	4.52006E-4	4.413149703E-5
3	881	6.33075E-4	6.181012529E-5
4	911	7.13295E-4	6.964238568E-5
5	950	1.09681E-3	1.070867804E-4

TABLE IId.1 Cu-5A(1)

Correlation coefficient (R)= -0.9799012388

Energy of activation (Ea)= 76640.15048J/mol.

Frequency factor (A)= 11.362776735ec^-1

Best fit equation : lnK = -9217.760811(1/T) + 2.430342814

	TemperatureT/K	1/T	K(1/sec)	ln K	DELG(J./mol.)
1	843	1.18623962E-3	2.0438E-4	-8.495529551	266011.5267
2	883	1.132502831E-3	2.88545E-4	-8.150659505	276101.757
3	910	1.098901099E-3	5.212799999E-4	-7.559223233	280069.4058
4	943	1.060445387E-3	7.068586999E-4	-7.254679771	287837.9994
5	979	1.02145046E-3	8.404E-4	-7.08163259	297417.9418

SPECIFIC RATE (Rsp) CALCULATIONS

Molecular weight of catalyst(W)=2177.86

Number of transition metal ions per unit cell(n)=0.24

Nitrous oxide molecules in apparatus(342CC) at PN2O(1torr)=1.2094E19(molecules)

Mass of catalyst sample=0.1033(g)

Corrected mass of activated catalyst sample=7.901417001E-2(g)

	Temperature(T/K)	Rate ConstantK(1/sec)	Rsp(molecules/site.sec)
1	843	2.0438E-4	4.715476686E-4
2	883	2.88545E-4	6.657340348E-4
3	910	5.212799999E-4	1.202702655E-3
4	943	7.068586999E-4	1.630871768E-3
5	979	8.404E-4	1.938979649E-3

TABLE IId.2 Cu-5A(2)

Correlation coefficient (R)= -0.8687993132

Energy of activation (Ea)= 73678.37259J/mol.

Frequency factor (A)= 3.79547866Sec^-1

Best fit equation : lnK = -8861.538128(1/T) + 1.333810532

	TemperatureT/K	1/T	K(1/sec)	ln K	DELG(J./mol.)
1	829	1.206272618E-3	6.79899E-5	-9.596151393	269179.9755
2	885	1.129943503E-3	1.6983E-4	-8.680712622	280627.3939
3	910	1.098901099E-3	3.2685E-4	-8.026009209	283601.1613
4	939	1.064962726E-3	4.1644E-4	-7.783768164	290747.7688
5	982	1.018329939E-3	2.8992E-4	-8.145905536	307018.8582

SPECIFIC RATE (Rsp) CALCULATIONS

Molecular weight of catalyst(W)=2189.91

Number of transition metal ions per unit cell(n)=0.39

Nitrous oxide molecules in apparatus(342CC) at PN2O(1torr)=1.2094E19(molecules)

Mass of catalyst sample=9.669999999E-2(g)

Corrected mass of activated catalyst sample=7.339530002E-2(g)

	Temperature(T/K)	Rate ConstantK(1/sec)	Rsp(molecules/site.sec)
1	829	6.79899E-5	1.044987956E-4
2	885	1.6983E-4	2.610245118E-4
3	910	3.2685E-4	5.023603701E-4
4	939	4.1644E-4	6.400579855E-4
5	982	2.8992E-4	4.455998732E-4

TABLE IId.3 Cu-5A(3)

Correlation coefficient (R)= -0.9848361516

Energy of activation (Ea)= 46738.20041J/mol.

Frequency factor (A)= 0.2335580103Sec^-1

Best fit equation : lnK = -5621.35577(1/T) + -1.454324795

	TemperatureT/K	1/T	K(1/sec)	ln K	DELG(J./mol.)
1	845	1.183431953E-3	2.84913E-4	-8.163326688	264308.6837
2	888	1.126126126E-3	4.4851E-4	-7.709579581	274408.6075
3	951	1.051524711E-3	6.636549999E-4	-7.317748122	290778.5729
4	977	1.023541453E-3	6.9321E-4	-7.274177575	298374.4238

SPECIFIC RATE (Rsp) CALCULATIONS

Molecular weight of catalyst(W)=2193.28

Number of transition metal ions per unit cell(n)=0.54

Nitrous oxide molecules in apparatus(342CC) at PN2O(1torr)=1.2094E19(molecules)

Mass of catalyst sample=9.56E-2(g)

Corrected mass of activated catalyst sample=7.246479997E-2(g)

	Temperature(T/K)	Rate ConstantK(1/sec)	Rsp(molecules/site.sec)
1	845	2.84913E-4	3.208181715E-4
2	888	4.4851E-4	5.050319153E-4
3	951	6.636549999E-4	7.472898169E-4
4	977	6.9321E-4	7.805693833E-4

TABLE IId.4 Cu-5A(4)

Correlation coefficient (R)= -0.9910246562

Energy of activation (Ea)= 61069.62965J/mol.

Frequency factor (A)= 2.14920461Sec^-1

Best fit equation : lnK = -7345.043499(1/T) + 0.7650978249

	TemperatureT/K	1/T	K(1/sec)	ln K	DELG(J./mol.)
1	805	1.242236025E-3	2.27493E-4	-8.388391089	253303.4085
2	830	1.204819277E-3	3.0238E-4	-8.103826053	259206.202
3	861	1.161440186E-3	4.6611E-4	-7.6710889	265789.559
4	916	1.091703057E-3	6.759E-4	-7.299465422	279937.7019

SPECIFIC RATE (Rsp) CALCULATIONS

Molecular weight of catalyst(W)=2210.84

Number of transition metal ions per unit cell(n)=0.5800000001

Nitrous oxide molecules in apparatus(342CC) at PN2O(1torr)=1.2094E19(molecules)

Mass of catalyst sample=0.1055(g)

Corrected mass of activated catalyst sample=7.984240001E-2(g)

	Temperature(T/K)	Rate ConstantK(1/sec)	Rsp(molecules/site.sec)
1	805	2.27493E-4	2.181912086E-4
2	830	3.0238E-4	2.9001621E-4
3	861	4.6611E-4	4.470515763E-4
4	916	6.759E-4	6.482636295E-4

TABLE IId.5 Cu-5A(5)

Correlation coefficient (R)= -0.9334377551

Energy of activation (Ea)= 34987.397693J/mol.

Frequency factor (A)= 4.141017936E-2Sec^-1

Best fit equation : lnK = -4208.04841(1/T) + -3.184228551

	TemperatureT/K	1/T	K(1/sec)	ln K	DELG(J./mol.)
1	800	1.25E-3	1.8391E-4	-8.601064052	253144.6957
2	829	1.206272618E-3	3.1663E-4	-8.05777666	258576.5032
3	912	1.096491228E-3	4.0841E-4	-7.803238986	282535.2513
4	951	1.051524711E-3	4.7609E-4	-7.649903646	293404.9279

SPECIFIC RATE (Rsp) CALCULATIONS

Molecular weight of catalyst(W)=2254.02

Number of transition metal ions per unit cell(n)=1.21

Nitrous oxide molecules in apparatus(3420C) at PN2O(1torr)=1.2094E19(molecules)

Mass of catalyst sample=0.1056(g)

Corrected mass of activated catalyst sample=7.931616E-2(g)

	Temperature(T/K)	Rate ConstantK(1/sec)	Rsp(molecules/site.sec)
1	800	1.8391E-4	8.677398296E-5
2	829	3.1663E-4	1.493950641E-4
3	912	4.0841E-4	1.926994855E-4
4	951	4.7609E-4	2.246328397E-4

TABLE IId.6 Cu-5A(6)

Correlation coefficient (R)= -0.9322955038

Energy of activation (Ea)= 42232.7724J/mol.

Frequency factor (A)= 0.1382895969Sec^-1

Best fit equation : lnK = -5079.473251(1/T) + -1.978405265

	TemperatureT/K	1/T	K(1/sec)	ln K	DELG(J./mol.)
1	816	1.225490196E-3	2.5033E-4	-8.29273051	256115.6826
2	845	1.183431953E-3	3.5822E-4	-7.934363237	262700.0605
3	893	1.119820829E-3	5.500499999E-4	-7.505501375	274438.4678
4	932	1.072961373E-3	5.233500001E-4	-7.555260101	286809.6041

SPECIFIC RATE (Rsp) CALCULATIONS

Molecular weight of catalyst(W)=3331.85

Number of transition metal ions per unit cell(n)=1.49

Nitrous oxide molecules in apparatus(342CC) at PN2O(1torr)=1.2094E19(molecules)

Mass of catalyst sample=0.1106(g)

Corrected mass of activated catalyst sample=8.234170004E-2(g)

	Temperature(T/K)	Rate ConstantK(1/sec)	Rsp(molecules/site.sec)
1	816	2.5033E-4	1.365732725E-4
2	845	3.5822E-4	1.954351363E-4
3	893	5.500499999E-4	3.000923922E-4
4	932	5.233500001E-4	2.855255949E-4

X-Ray Powder Diffraction Data

Table :IIX.1 : Na-A

No.	Angle	m	d (A)	I	a (A)
1	3.5000	1	12.6277	VVS	12.6277
2	5.0000	2	8.8451	VS	12.5088
3	6.2800	3	7.0474	S	12.2065
4	8.0300	5	5.5186	MS	12.3399
5	10.1500	8	4.3745	W	12.3730
6	10.8500	9	4.0953	MS	12.2860
7	11.9800	11	3.7139	S	12.3177
8	13.0800	13	3.4064	M	12.2818
9	13.5500	14	3.2903	S	12.3112
10	14.9500	17	2.9883	VS	12.3209
11	15.4300	18	2.8975	W	12.2929
12	18.2500	25	2.4617	M	12.3083
13	16.7500	21	2.6749	VVW	12.2580
14	17.0500	22	2.6292	VS	12.3321
15	22.0800	36	2.0508	W	12.3048
16	23.6800	41	1.9194	VW	12.2904
17	26.2800	50	1.7411	M	12.3117
18	29.3000	61	1.5753	W	12.3031
19	34.5800	82	1.3583	VW	12.2997
20	36.4800	90	1.2966	VVW	12.3009
21	77.0800	242	0.7909	W	12.3039
22	77.6800	243	0.7891	VW	12.3004

Unit Cell Constant [taking average of lines 3 - 22]

a = 12.302 (A)

X-Ray Powder Diffraction Data

Table :IIX.2 : Ca-A

No.	Angle	m	d (A)	I	a (A)
1	3.5500	1	12.4500	VVS	12.4500
2	5.0800	2	8.7061	M	12.3124
3	6.2000	3	7.1380	S	12.3634
4	8.0300	5	5.5186	W	12.3399
5	10.6000	9	4.1908	S	12.5723
6	11.9500	11	3.7231	S	12.3482
7	13.0500	13	3.4141	W	12.3096
8	13.5300	14	3.2951	VS	12.3291
9	14.9500	17	2.9883	S	12.3209
10	17.1000	22	2.6217	S	12.2971
11	20.9500	33	2.1560	W	12.3855
12	26.2000	50	1.7461	M	12.3466
13	29.2500	61	1.5777	W	12.3223
14	34.5000	82	1.3610	W	12.3247
15	39.0000	101	1.2250	VW	12.3108
16	76.7000	242	0.7921	VW	12.3229
17	77.3000	243	0.7902	VVW	12.3185

Unit Cell Constant [taking average of lines 6 - 17]

a = 12.328 (A)

X-Ray Powder Diffraction Data

Table :11X.3 : Cu-5A(4)

No.	Angle	m	d (A)	I	a (A)
1	3.6300	1	12.1760	VVS	12.1760
2	5.1500	2	8.5881	S	12.1454
3	6.2500	3	7.0811	S	12.2649
4	8.0800	5	5.4847	M	12.2641
5	10.9000	9	4.0768	S	12.2303
6	12.0300	11	3.6987	S	12.2672
7	13.5800	14	3.2832	S	12.2845
8	15.0300	17	2.9727	S	12.2568
9	16.2300	19	2.7582	VW	12.0227
10	17.1500	21	2.6143	S	11.9804
11	19.0000	26	2.3679	VW	12.0738
12	20.8000	31	2.1709	M	12.0870
13	22.1500	35	2.0447	W	12.0963
14	23.7800	40	1.9118	W	12.0915
15	26.1000	48	1.7523	W	12.1402
16	27.2300	52	1.6848	W	12.1492
17	28.9000	58	1.5951	W	12.1482
18	29.4300	60	1.5689	W	12.1527
19	34.7000	80	1.3542	W	12.1120
20	36.6000	88	1.2930	VW	12.1291
21	39.3000	99	1.2171	VW	12.1102
22	77.6000	236	0.7893	VVW	12.1257

Unit Cell Constant [taking average of lines 1 - 22]

a = 12.150 (A)

X-Ray Powder Diffraction Data

Table : IIX.4 : Cu-5A(5)

No.	Angle	m	d (A)	I	a (A)
1	3.5800	1	12.3458	VS	12.3458
2	5.1300	2	8.6215	S	12.1927
3	6.2000	3	7.1380	S	12.3634
4	8.1000	5	5.4712	S	12.2340
5	8.9000	6	4.9829	W	12.2055
6	10.2300	8	4.3407	W	12.2772
7	10.9000	9	4.0768	S	12.2303
8	12.0300	11	3.6987	S	12.2672
9	13.1300	13	3.3936	W	12.2359
10	13.6300	14	3.2714	S	12.2403
11	14.9800	17	2.9824	S	12.2968
12	15.4300	18	2.8975	W	12.2929
13	16.3800	20	2.7336	VW	12.2251
14	17.1300	22	2.6173	S	12.2762
15	18.3500	25	2.4487	W	12.2435
16	20.8000	32	2.1709	M	12.2804
17	22.1300	36	2.0464	W	12.2784
18	24.0000	42	1.8953	W	12.2831
19	26.3500	50	1.7368	M	12.2813
20	28.2800	57	1.6271	W	12.2845
21	29.4000	61	1.5704	W	12.2650
22	33.5300	77	1.3956	M	12.2465
23	34.6500	82	1.3559	M	12.2780
24	36.6000	90	1.2930	W	12.2662
25	39.2000	101	1.2197	W	12.2581
26	77.6300	242	0.7892	VW	12.2774

Unit Cell Constant [taking average of lines 4 - 26]

a = 12.262 (A)

X-Ray Powder Diffraction Data

Table : IIX.5 : Cu-5A(6)

No.	Angle	m	d (A)	I	a (A)
1	3.5000	1	12.6277	VS	12.6277
2	5.1000	2	8.6721	S	12.2642
3	6.2300	3	7.1038	S	12.3041
4	7.1800	4	6.1678	VW	12.3357
5	8.0500	5	5.5050	S	12.3095
6	8.9300	6	4.9663	VW	12.1648
7	10.8300	9	4.1028	S	12.3084
8	12.0000	11	3.7078	S	12.2975
9	13.5800	14	3.2832	S	12.2845
10	14.9800	17	2.9824	S	12.2968
11	17.1300	23	2.6173	S	12.5521
12	18.3300	26	2.4513	W	12.4991
13	20.7800	33	2.1729	M	12.4823
14	22.2000	37	2.0403	W	12.4105
15	23.7000	42	1.9179	W	12.4295
16	26.3300	51	1.7381	S	12.4122
17	28.3300	59	1.6245	W	12.4779
18	29.4000	63	1.5704	W	12.4644
19	33.4800	79	1.3975	M	12.4208
20	34.7000	84	1.3542	M	12.4112
21	38.1000	99	1.2494	VW	12.4310
22	77.4300	248	0.7898	VW	12.4383

Unit Cell Constant [taking average of lines 2 - 22]

a = 12.381 (A)

X-Ray Powder Diffraction Data

Table : IIX.6 : Co-5A(4)

No.	Angle	m	d (A)	I	a (A)
1	3.6000	1	12.2773	VS	12.2773
2	5.0800	2	8.7061	S	12.3124
3	6.2300	3	7.1038	S	12.3041
4	8.0800	5	5.4847	S	12.2641
5	8.8000	6	5.0390	W	12.3430
6	10.8200	9	4.1066	S	12.3197
7	11.9800	11	3.7139	S	12.3177
8	13.6300	14	3.2714	S	12.2403
9	14.9500	17	2.9883	S	12.3209
10	16.2800	20	2.7500	W	12.2982
11	17.0500	22	2.6292	S	12.3321
12	19.0300	27	2.3643	W	12.2851
13	20.7800	32	2.1729	M	12.2917
14	22.1000	36	2.0490	M	12.2943
15	26.3000	49	1.7399	S	12.1793
16	29.3000	60	1.5753	M	12.2018
17	33.3000	76	1.4041	W	12.2409
18	34.5800	81	1.3583	M	12.2245
19	35.5800	85	1.3249	W	12.2153
20	39.0300	100	1.2242	W	12.2418
21	76.9300	238	0.7914	W	12.2091

Unit Cell Constant [taking average of lines 1 - 21]

a = 12.272 (A)

X-Ray Powder Diffraction Data

Table :IIX.7 : Co-5A(5)

No.	Angle	m	d (A)	I	a (A)
1	4.1800	1	12.2788	VS	12.2788
2	5.9500	2	8.6340	M	12.2103
3	7.2800	3	7.0629	S	12.2333
4	9.3800	5	5.4914	W	12.2792
5	12.7000	9	4.0710	M	12.2131
6	14.0800	11	3.6789	S	12.2017
7	15.2800	13	3.3961	W	12.2449
8	15.8300	14	3.2810	M	12.2763
9	17.5500	17	2.9681	M	12.2379
10	18.0500	18	2.8885	VW	12.2550
11	19.0500	20	2.7421	VW	12.2630
12	20.0500	22	2.6105	W	12.2445
13	24.3000	32	2.1749	VW	12.3031
14	31.0800	50	1.7337	VW	12.2592

Table :IIX.8 : Co-5A(6)

No.	Angle	m	d (A)	I	a (A)
1	4.2300	1	12.1339	S	12.1339
2	5.9500	2	8.6340	W	12.2103
3	7.3300	3	7.0150	W	12.1503
4	9.3500	5	5.5089	VW	12.3182
5	10.4000	6	4.9579	VW	12.1444
6	12.7000	9	4.0710	M	12.2131
7	14.1000	11	3.6738	M	12.1847
8	15.3500	13	3.3810	W	12.1904
9	16.0300	14	3.2411	M	12.1271
10	17.5800	17	2.9632	M	12.2176
11	19.4300	20	2.6905	W	12.0322

Table IIIa - 1 Na-A (A&A)

Best-fit equation: ln k = -12746.27(1/T) - 5.37

Corr. Coefficient = -0.9982 ; t-factor = -46.86

$\Delta G^{\ddagger}$ (740K) = 321.16 kJ/mol ; $T_{(0.5\alpha)}$ = 881.3 K

DATA FOR ORDER -1.56 AND E_A 105972.5 J/MOL

α	T/K	1/T	ln k
1.82E-2	739	1.353E-3	-22.71
3.18E-2	759	1.318E-3	-22.16
4.55E-2	769	1.3E-3	-21.81
7.73E-2	801	1.248E-3	-21.31
0.1091	817	1.224E-3	-20.99
0.1591	833	1.2E-3	-20.65
0.1864	845	1.183E-3	-20.52
0.3	861	1.161E-3	-20.14
0.4955	881	1.135E-3	-19.82
0.6909	893	1.12E-3	-19.69

Table IIIa - 2 Ca-A (A&A)

Best-fit equation: ln k = -9880.05(1/T) -11.54

Corr. Coefficient = -0.9950 ; t-factor = -24.34

$\Delta G^{\ddagger}$ (740K) = 334.07 kJ/mol ; $T_{(0.5\alpha)}$ = 906.8 K

DATA FOR ORDER -2 AND E_A 82142.7 J/MOL

α	T/K	1/T	ln k
8.9E-3	717	1.395E-3	-25.23
1.33E-2	740	1.351E-3	-24.84
1.77E-2	763	1.311E-3	-24.55
2.21E-2	782	1.279E-3	-24.34
3.54E-2	804	1.244E-3	-23.88
5.31E-2	831	1.203E-3	-23.49
8.85E-2	855	1.17E-3	-23.02
0.1328	884	1.131E-3	-22.66

Table IIIa - 3 Cu-5A(1) (A&A)

Best-fit equation: ln k = 13953.88(1/T) + 11.94

Corr. Coefficient = -0.9988 ; t-factor = -61.50

$\Delta G^{\ddagger}$ (740K) = 223.19 kJ/mol ; $T_{(0.5\alpha)}$ = 848.1 K

DATA FOR ORDER 1.52 AND E_A 116012.6 J/MOL

α	T/K	1/T	ln k
4.57E-3	645	1.55E-3	-9.721
9.13E-3	666	1.502E-3	-9.025
1.83E-2	685	1.46E-3	-8.323
2.74E-2	705	1.418E-3	-7.912
4.57E-2	725	1.379E-3	-7.386
0.1005	747	1.339E-3	-6.553
0.1324	772	1.295E-3	-6.25
0.2283	797	1.255E-3	-5.618
0.347	822	1.217E-3	-5.076
0.4658	843	1.186E-3	-4.635
0.6347	868	1.152E-3	-4.056

Table IIIa - 4. Cu-5A(1) (N&A)

Best-fit equation: ln k = -15545.77(1/T) + 13.80

Corr. Coefficient = -0.9987 ; t-factor = -58.86

$\Delta G^{\ddagger}$ (740K) = 225.27 kJ/mol ; $T_{(0.5\alpha)}$ = 848.8 K

DATA FOR ORDER 1.52 AND E_A 129247.5 J/MOL

α	T/K	1/T	ln k
8.9E-3	683	1.464E-3	-9.105
3.13E-2	713	1.403E-3	-7.83
5.36E-2	735	1.361E-3	-7.275
9.82E-2	762	1.312E-3	-6.633
0.1652	785	1.274E-3	-6.055
0.2679	807	1.239E-3	-5.473
0.372	828	1.208E-3	-5.032
0.5134	851	1.175E-3	-4.525
0.6362	871	1.148E-3	-4.105
0.7321	887	1.127E-3	-3.753
0.817	898	1.114E-3	-3.387

Table IIIa - 5 Cu-5A(2) (A&A)

Best-fit equation: ln k = -177436.22(1/T) + 15.66

Corr. Coefficient = -0.9920 ; t-factor = -17.53

$\Delta G^{\ddagger}$ (740K) = 230.14 kJ/mol ; $T_{(0.5\alpha)}$ = 833.56K

DATA FOR ORDER 1.30 AND E_A 144964.7 J/MOL

α	T/K	1/T	ln k
3.21E-2	728	1.374E-3	-8.48
0.1055	756	1.323E-3	-7.239
0.1927	779	1.284E-3	-6.571
0.2982	804	1.244E-3	-6.047
0.4817	830	1.205E-3	-5.382
0.6514	863	1.159E-3	-4.847
0.8807	879	1.138E-3	-3.972

Table IIIa - 6. Cu-5A(2) (N&A)

Best-fit equation: ln k = -21834.42(1/T) + 22.20

Corr. Coefficient = -0.9859 ; t-factor = -15.57

$\Delta G^{\ddagger}$ (740K) = 223.86 kJ/mol ; $T_{(0.5\alpha)}$ = 833.6 K

DATA FOR ORDER 1.52 AND E_A 181531.4 J/MOL

α	T/K	1/T	ln k
4.6E-3	703	1.422E-3	-9.427
3.21E-2	728	1.374E-3	-7.463
0.1055	756	1.323E-3	-6.214
0.1927	779	1.284E-3	-5.534
0.2982	804	1.244E-3	-4.994
0.4817	830	1.205E-3	-4.293
0.6514	863	1.159E-3	-3.71
0.8807	879	1.138E-3	-2.691
0.9771	903	1.107E-3	-1.582

Table IIIa - 7 Cu-5A(3) (A&A)

Best-fit equation: ln k = -16470.62(1/T) + 14.90

Corr. Coefficient = -0.9966 ; t-factor = -31.98

$\Delta G^{\ddagger}$ (740K) = 227.59 kJ/mol ; $T_{(0.5\alpha)}$ = 805.6 K

DATA FOR ORDER 1.30 AND E_A 136936.7 J/MOL

α	T/K	1/T	ln k
3.11E-2	697	1.435E-3	-8.589
5.78E-2	724	1.381E-3	-7.951
0.1022	747	1.339E-3	-7.35
0.2089	769	1.3E-3	-6.554
0.3822	790	1.266E-3	-5.796
0.4978	805	1.242E-3	-5.406
0.5867	828	1.208E-3	-5.127
0.7689	851	1.175E-3	-4.529
0.9422	886	1.129E-3	-3.633

Table IIIa - 8. Cu-5A(3) (N&A)

Best-fit equation: ln k = -10022.53(1/T) + 1.30

Corr. Coefficient = -0.9978 ; t-factor = -52.09

$\Delta G^{\ddagger}$ (740K) = 257.14 kJ/mol ; $T_{(0.5\alpha)}$ = 802.7 K

DATA FOR ORDER 0.20 AND E_A 83327.3 J/MOL

α	T/K	1/T	ln k
8.8E-3	606	1.65E-3	-15.16
1.33E-2	628	1.592E-3	-14.75
2.64E-2	646	1.548E-3	-14.06
3.97E-2	668	1.497E-3	-13.65
5.29E-2	692	1.445E-3	-13.36
9.25E-2	713	1.403E-3	-12.8
0.141	738	1.355E-3	-12.37
0.185	754	1.326E-3	-12.1
0.2599	771	1.297E-3	-11.75
0.4361	795	1.258E-3	-11.21
0.5947	814	1.229E-3	-10.87
0.8018	839	1.192E-3	-10.53
0.9207	859	1.164E-3	-10.35
0.9692	875	1.143E-3	-10.27

Table IIIa - 9 Cu-5A(4) (A&A)

Best-fit equation: ln k = -14409.50(1/T) + 11.34

Corr. Coefficient = -0.9969 ; t-factor = -40.08

$\Delta G^{\ddagger}$ (740K) = 230.75 kJ/mol ; $T_{(0.5\alpha)}$ = 813.6 K

DATA FOR ORDER 1.08 AND E_A 119800.5 J/MOL

α	T/K	1/T	ln k
1.31E-2	667	1.499E-3	-10.47
2.18E-2	681	1.468E-3	-9.956
5.24E-2	698	1.433E-3	-9.062
8.3E-2	716	1.397E-3	-8.585
0.1222	735	1.361E-3	-8.175
0.2184	760	1.316E-3	-7.533
0.3188	786	1.272E-3	-7.084
0.4498	807	1.239E-3	-6.633
0.5721	823	1.215E-3	-6.272
0.738	844	1.185E-3	-5.796
0.8777	865	1.156E-3	-5.314
0.9651	887	1.127E-3	-4.795

Table IIIa - 10 Cu-5A(4) (N&A)

Best-fit equation: ln k = -11166.78(1/T) + 4.98

Corr. Coefficient = -0.9990 ; t-factor = -77.27

$\Delta G^{\ddagger}$ (740K) = 243.86 kJ/mol ; $T_{(0.5\alpha)}$ = 812.1 K

DATA FOR ORDER 0.64 AND E_A 92840.63 J/MOL

α	T/K	1/T	ln k
8.8E-3	619	1.616E-3	-13.11
1.76E-2	642	1.558E-3	-12.41
3.08E-2	661	1.513E-3	-11.85
4.85E-2	677	1.477E-3	-11.39
0.37E-2	707	1.414E-3	-10.83
0.1278	731	1.368E-3	-10.39
0.326	774	1.292E-3	-9.378
0.3524	792	1.263E-3	-9.289
0.5066	813	1.23E-3	-8.85
0.6388	828	1.208E-3	-8.538
0.7709	842	1.188E-3	-8.244
0.8943	860	1.163E-3	-7.946
0.9428	869	1.151E-3	-7.798
0.9692	879	1.138E-3	-7.693

Table IIIa - 11 Cu-5A(5) (A&A)

Best-fit equation: ln k = -14329.80(1/T) + 11.99

Corr. Coefficient = -0.9986 ; t-factor = -55.96

$\Delta G^{\ddagger}$ (740K) = 227.11 kJ/mol ; $T_{(0.5\alpha)}$ = 784.1 K

DATA FOR ORDER 1.08 AND E_A 119137.9 J/MOL

α	T/K	1/T	ln k
1.36E-2	644	1.553E-3	-10.27
3.17E-2	666	1.502E-3	-9.416
6.34E-2	690	1.449E-3	-8.705
0.1131	717	1.395E-3	-8.097
0.1991	739	1.353E-3	-7.478
0.2986	760	1.316E-3	-7.004
0.4525	778	1.285E-3	-6.464
0.6154	**799**	1.252E-3	-5.989
0.7964	816	1.225E-3	-5.453
0.9005	833	1.2E-3	-5.052
0.9774	872	1.147E-3	-4.494

Table IIIa - 12 Cu-5A(5) (N&A)

Best-fit equation: ln k = -13894.99(1/T) + 11.18

Corr. Coefficient = -0.9995 ; t-factor = -92.39

$\Delta G^{\ddagger}$ (740K) = 228.01 kJ/mol ; $T_{(0.5\alpha)}$ = 779.6 K

DATA FOR ORDER 1.08 AND E_A 115523.0 J/MOL

α	T/K	1/T	ln k
2.27E-2	652	1.534E-3	-10.15
5.46E-2	678	1.475E-3	-9.251
0.1046	704	1.42E-3	-8.572
0.2046	730	1.37E-3	-7.839
0.3364	755	1.325E-3	-7.249
0.4955	779	1.284E-3	-6.726
0.6273	795	1.258E-3	-6.347
0.741	811	1.233E-3	-6.018
0.8636	828	1.208E-3	-5.604
0.9455	843	1.186E-3	-5.187
0.9591	854	1.171E-3	-5.081

Table IIIa - 13 Cu-5A(6) (A&A)

Best-fit equation: ln k = -15758.31(1/T) + 13.35

Corr. Coefficient = -0.9986 ; t-factor = -64.67

$\Delta G^{\ddagger}$ (740K) = 230.6 kJ/mol ; $T_{(0.5\alpha)}$ = 802.4 K

DATA FOR ORDER 1.08 AND E_A 131014.6 J/MOL

α	T/K	1/T	ln k
9.13E-3	659	1.517E-3	-10.76
2.74E-2	680	1.471E-3	-9.649
3.2E-2?	685	1.46E-3	-9.491
5.94E-2	707	1.414E-3	-8.857
0.1005	729	1.372E-3	-8.308
0.1644	749	1.335E-3	-7.776
0.3333	778	1.285E-3	-6.953
0.4521	797	1.255E-3	-6.551
0.6301	817	1.224E-3	-6.032
0.79	833	1.2E-3	-5.559
0.8859	847	1.181E-3	-5.204
0.9498	861	1.161E-3	-4.849
0.9726	872	1.147E-3	-4.639
0.9817	883	1.133E-3	-4.516

Table IIIa - 14 Cu-5A(6) (N&A)

Best-fit equation: ln k = -13475.77(1/T) + 10.69

Corr. Coefficient = -0.9991 ; t-factor = -68.59

$\Delta G^{\ddagger}$ (740K) = 227.61 kJ/mol ; $T_{(0.5\alpha)}$ = 773.8 K

DATA FOR ORDER 1.08 AND E_A 112037.5 J/MOL

α	T/K	1/T	ln k
1.82E-2	643	1.555E-3	-10.41
4.55E-2	663	1.508E-3	-9.478
7.27E-2	685	1.46E-3	-8.994
0.15	710	1.408E-3	-8.224
0.2546	736	1.359E-3	-7.626
0.4	761	1.314E-3	-7.065
0.5955	786	1.272E-3	-6.477
0.7364	806	1.241E-3	-6.072
0.8727	826	1.211E-3	-5.607
0.9409	841	1.189E-3	-5.258
0.9636	857	1.167E-3	-5.08

Table IIIa - 15 Co-5A(1) (A&A)

Best-fit equation: ln k = -15234.01(1/T) + 13.93

Corr. Coefficient = -0.9965 ; t-factor = -31.51

$\Delta G^{\ddagger}$ (740K) = 218.35 kJ/mol ; $T_{(0.5\alpha)}$ = 951.8 K

DATA FOR ORDER 1.96 AND E_A 126655.6 J/MOL

α	T/K	1/T	ln k
1.33E-2	744	1.344E-3	-6.473
1.78E-2	758	1.319E-3	-6.178
2.67E-2	774	1.292E-3	-5.763
3.56E-2	785	1.274E-3	-5.467
4.44E-2	804	1.244E-3	-5.237
8.89E-2	823	1.215E-3	-4.496
0.1333	843	1.186E-3	-4.042
0.1911	867	1.153E-3	-3.614
0.2444	886	1.129E-3	-3.301

Table IIIa - 16 Co-5A(1) (N&A)

Best-fit equation: ln k = -10799.81(1/T) + 7.21

Corr. Coefficient = -0.9931 ; t-factor = -26.82

$\Delta G^{\ddagger}$ (740K) = 226.58 kJ/mol ; $T_{(0.5\alpha)}$ = 925 K

DATA FOR ORDER 1.52 AND E_A 89789.6 J/MOL

α	T/K	1/T	ln k
2.25E-2	713	1.403E-3	-8.082
4.51E-2	740	1.351E-3	-7.369
7.21E-2	761	1.314E-3	-6.878
0.1036	781	1.28E-3	-6.489
0.1396	797	1.255E-3	-6.16
0.1487	816	1.225E-3	-6.089
0.1757	829	1.206E-3	-5.898
0.2117	853	1.172E-3	-5.678
0.2748	863	1.159E-3	-5.356
0.3243	876	1.142E-3	-5.138
0.4054	890	1.124E-3	-4.821
0.466	905	1.105E-3	-4.674

Table IIIa - 17 Co-5A(2) (A&A)

Best-fit equation: ln k = -9882.40(1/T) + 5.75

Corr. Coefficient = -0.9986 ; t-factor = -49.30

$\Delta G^{\ddagger}$ (740K) = 228.36 kJ/mol ; $T_{(0.5\alpha)}$ = 886 K

DATA FOR ORDER 1.30 AND E_A 82162.3 J/MOL

α	T/K	1/T	ln k
1.79E-2	668	1.497E-3	-9.124
3.13E-2	687	1.456E-3	-8.556
4.91E-2	709	1.41E-3	-8.094
7.14E-2	737	1.357E-3	-7.704
0.1071	765	1.307E-3	-7.274
0.1652	787	1.271E-3	-6.797
0.2589	820	1.22E-3	-6.273
0.3884	862	1.16E-3	-5.748
0.5089	888	1.126E-3	-5.345

Table IIIa - 18 Co-5A(2) (N&A)

Best-fit equation: ln k = -10515.04(1/T) + 8.10

Corr. Coefficient = -0.9983 ; t-factor = -51.10

$\Delta G^{\ddagger}$ (740K) = 218.98 kJ/mol ; $T_{(0.5\alpha)}$ = 834 K

DATA FOR ORDER 1.52 AND E_A 87422.0 J/MOL

α	T/K	1/T	ln k
1.39E-2	626	1.597E-3	-8.59
2.32E-2	648	1.543E-3	-8.071
3.24E-2	669	1.495E-3	-7.729
6.02E-2	700	1.429E-3	-7.088
0.1157	725	1.379E-3	-6.389
0.1898	758	1.319E-3	-5.828
0.2685	773	1.294E-3	-5.405
0.3565	795	1.258E-3	-5.027
0.4213	815	1.227E-3	-4.783
0.5	834	1.199E-3	-4.506
0.5741	854	1.171E-3	-4.253

Table IIIa - 19 Co-5A(3) (A&A)

Best-fit equation: ln k = -12858.96(1/T) + 4.28
Corr. Coefficient = -0.9981 ; t-factor = -42.47

$\Delta G^{\ddagger}$ (740K) = 261.89 kJ/mol ; $T_{(0.5\alpha)}$ = 836 K

DATA FOR ORDER 0.20 AND E_A 106909.3 J/MOL

α	T/K	1/T	ln k
1.39E-2	673	1.486E-3	-14.7
2.32E-2	704	1.42E-3	-14.19
4.17E-2	720	1.389E-3	-13.6
7.87E-2	746	1.34E-3	-12.96
0.1482	771	1.297E-3	-12.32
0.2361	799	1.252E-3	-11.84
0.375	822	1.217E-3	-11.36
0.6065	848	1.179E-3	-10.85
0.7685	868	1.152E-3	-10.57

Table IIIa - 20 Co-5A(3) (N&A)

Best-fit equation: ln k = -10686.42(1/T) + 759

Corr. Coefficient = -0.9985 ; t-factor = -63.85

$\Delta G^{\ddagger}$ (740K) = 221.93 kJ/mol ; $T_{(0.5\alpha)}$ = 800.4 K

DATA FOR ORDER 1.30 AND E_A 88846.8 J/MOL

α	T/K	1/T	ln k
4.6E-3	578	1.73E-3	-10.87
1.39E-2	608	1.645E-3	-9.753
2.32E-2	638	1.567E-3	-9.235
3.7E-2	659	1.517E-3	-8.759
6.94E-2	691	1.447E-3	-8.108
0.1343	718	1.393E-3	-7.401
0.2407	745	1.342E-3	-6.735
0.3519	767	1.304E-3	-6.256
0.4398	786	1.272E-3	-5.944
0.5278	807	1.239E-3	-5.659
0.6435	828	1.208E-3	-5.297
0.7361	848	1.179E-3	-4.993
0.8194	868	1.152E-3	-4.682
0.8611	886	1.129E-3	-4.496

Table IIIa - 21 Co-5A(4) (A&A)

Best-fit equation: ln k = -10162.80(1/T) + 8.64

Corr. Coefficient = -0.9960 ; t-factor = -33.61

$\Delta G^{\ddagger}$ (740K) = 212.20 kJ/mol ; $T_{(0.5\alpha)}$ = 784 K

DATA FOR ORDER 1.52 AND E_A 84493.5 J/MOL

α	T/K	1/T	ln k
9.25E-2	680	1.471E-3	-6.41
0.141	694	1.441E-3	-5.947
0.2026	713	1.403E-3	-5.529
0.2863	733	1.364E-3	-5.101
0.3965	779	1.284E-3	-4.652
0.5022	784	1.276E-3	-4.276
0.5991	804	1.244E-3	-3.946
0.6388	819	1.221E-3	-3.808
0.7357	840	1.19E-3	-3.451
0.8018	862	1.16E-3	-3.171
0.8767	885	1.13E-3	-2.771

Table IIIa - 22 Co-5A(4) (N&A)

Best-fit equation: ln k = -15806.87(1/T) + 15.25

Corr. Coefficient = -0.9995 ; t-factor = -86.41

$\Delta G^{\ddagger}$ (740K) = 219.19 kJ/mol ; $T_{(0.5\alpha)}$ = 795.5 K

DATA FOR ORDER 1.52 AND E_A 131418.4 J/MOL

α	T/K	1/T	ln k
4.65E-3	629	1.59E-3	-9.766
9.3E-3	653	1.531E-3	-9.079
2.79E-2	681	1.468E-3	-7.966
8.37E-2	715	1.399E-3	-6.823
0.1628	743	1.346E-3	-6.089
0.2884	767	1.304E-3	-5.397
0.5116	797	1.255E-3	-4.549
0.6372	812	1.232E-3	-4.119
0.7302	830	1.205E-3	-3.778
0.7814	843	1.186E-3	-3.568

Table IIIa - 23 Co-5A(5) (A&A)

Best-fit equation: ln k = -11215.39(1/T) + 9.78

Corr. Coefficient = -0.9993 ; t-factor = -85.59

$\Delta G^{\ddagger}$ (740K) = 214.84 kJ/mol ; $T_{(0.5\alpha)}$ = 751 K

DATA FOR ORDER 1.30 AND E_A 93244.72 J/MOL

α	T/K	1/T	ln k
1.75E-2	599	1.669E-3	-9.018
2.63E-2	609	1.642E-3	-8.605
4.39E-2	624	1.603E-3	-8.081
7.46E-2	646	1.548E-3	-7.529
0.1184	665	1.504E-3	-7.036
0.1754	685	1.46E-3	-6.601
0.2851	711	1.406E-3	-6.025
0.3947	733	1.364E-3	-5.597
0.5351	757	1.321E-3	-5.133
0.6798	779	1.284E-3	-4.678
0.8202	805	1.242E-3	-4.176
0.9167	830	1.205E-3	-3.678
0.9737	862	1.16E-3	-3.098

Table IIIa - 24 Co-5A(5) (N&A)

Best-fit equation: ln k = -11741.35(1/T) + 11.73

Corr. Coefficient = -0.9992 ; t-factor = -88.70

$\Delta G^{\ddagger}$ (740K) = 207.26 kJ/mol ; $T_{(0.5\alpha)}$ = 729 K

DATA FOR ORDER 1.52 AND E_A 97617.5 J/MOL

α	T/K	1/T	ln k
9.3E-3	567	1.764E-3	-8.965
1.86E-2	586	1.706E-3	-8.265
3.72E-2	603	1.658E-3	-7.557
5.12E-2	620	1.613E-3	-7.227
7.91E-2	637	1.57E-3	-6.769
0.1256	654	1.529E-3	-6.268
0.1907	673	1.486E-3	-5.792
0.2971	691	1.447E-3	-5.244
0.3814	711	1.406E-3	-4.9
0.5209	732	1.366E-3	-4.404
0.6605	754	1.326E-3	-3.923
0.7814	774	1.292E-3	-3.454
0.8884	797	1.255E-3	-2.886
0.9302	821	1.218E-3	-2.545

Table IIIa - 25 Co-5A(6) (A&A)

Best-fit equation: ln k = -9279.75?(1/T) + 3.66

Corr. Coefficient = -0.9991 ; t-factor = -68.44

$\Delta G^{\ddagger}$ (740K) = 236.49 kJ/mol ; $T_{(0.5\alpha)}$ = 831 K

DATA FOR ORDER 0.86 AND E_A 77151.81 J/MOL

α	T/K	1/T	ln k
2.61E-2	644	1.553E-3	-10.72
3.91E-2	662	1.511E-3	-10.31
5.65E-2	681	1.468E-3	-9.931
8.7E-2	709	1.41E-3	-9.486
0.1217	731	1.368E-3	-9.134
0.187	758	1.319E-3	-8.672
0.2826	779	1.284E-3	-8.208
0.3927	805	1.242E-3	-7.804
0.4957	830	1.205E-3	-7.509
0.6609	861	1.161E-3	-7.079
0.7609	886	1.129E-3	-6.823

Table IIIa - 26 Co-5A(6) (N&A)

Best-fit equation: ln k = -12618.81(1/T) + 12.89

Corr. Coefficient = -0.9992 ; t-factor = -95.43

$\Delta G^{\ddagger}$ (740K) = 207.34 kJ/mol ; $T_{(0.5\alpha)}$ = 727 K

DATA FOR ORDER 1.52 AND E_A 104912.8 J/MOL

α	T/K	1/T	ln k
2.33E-2	597	1.675E-3	-8.104
4.19E-2	622	1.608E-3	-7.502
0.1023	649	1.541E-3	-6.561
0.1814	667	1.499E-3	-5.919
0.2837	694	1.441E-3	-5.372
0.4	712	1.404E-3	-4.898
0.4977	727	1.376E-3	-4.551
0.7023	757	1.321E-3	-3.839
0.7628	768	1.302E-3	-3.601
0.8326	778	1.285E-3	-3.281
0.8558	788	1.269E-3	-3.156
0.893	797	1.255E-3	-2.921
0.9163	807	1.239E-3	-2.741
0.9395	817	1.224E-3	-2.515
0.9535	826	1.211E-3	-2.34
0.9674	837	1.195E-3	-2.113

Table IIIb - 1 Na-MOR (A&A)

Best-fit equation: ln k = -10810.03(1/T) + 10.28

Corr. Coefficient = -0.9946 ; t-factor = -31.88

$\Delta G^{\ddagger}$ (660K) = 273.97 kJ/mol ; $T_{(0.5\alpha)}$ = 912 K

DATA FOR ORDER -2 AND E_A 89874.66 J/MOL

α	T/K	1/T	ln k
3.07E-2	762	1.312E-3	-24.29
3.51E-2	779	1.284E-3	-24.16
4.83E-2	803	1.245E-3	-23.85
6.58E-2	819	1.221E-3	-23.56
9.21E-2	840	1.19E-3	-23.25
0.1404	859	1.164E-3	-22.88
0.2061	880	1.136E-3	-22.57
0.2456	889	1.125E-3	-22.44
0.3289	900	1.111E-3	-22.23
0.4474	909	1.1E-3	-22.06
0.6447	920	1.087E-3	-21.92
0.8158	931	1.074E-3	-21.88
0.9518	941	1.063E-3	-21.87

Table IIIb - 2 NH4-MOR(1) (A&A)

Best-fit equation: ln k = -12042.05(1/T) + 7.39

Corr. Coefficient = -0.9976 ; t-factor = -50.08

$\Delta G^{\ddagger}$ (660K) = 219.13 kJ/mol ; $T_{(0.5\alpha)}$ = 798 K

DATA FOR ORDER 0.86 AND E_A 100117.6 J/MOL

α	T/K	1/T	ln k
3.95E-2	666	1.502E-3	-10.57
6.14E-2	685	1.46E-3	-10.12
9.21E-2	709	1.41E-3	-9.696
0.136	726	1.377E-3	-9.285
0.2105	750	1.333E-3	-8.811
0.2807	763	1.311E-3	-8.485
0.364	766	1.305E-3	-8.176
0.4825	796	1.256E-3	-7.815
0.5965	807	1.239E-3	-7.512
0.6886	819	1.221E-3	-7.278
0.7895	833	1.2E-3	-7.015
0.8553	845	1.183E-3	-6.825
0.9079	854	1.171E-3	-6.645
0.9211	863	1.159E-3	-6.592

Table IIIb - 3 NH4-MOR(2) (A&A)

Best-fit equation: ln k = -13413.68(1/T) + 8.84

Corr. Coefficient = -0.9990 ; t-factor = -74.26

$\Delta G^{\ddagger}$ (660K) = 204.85 kJ/mol ; $T_{(0.5\alpha)}$ = 810.6 K

DATA FOR ORDER 0.86 AND E_A 111521.3 J/MOL

α	T/K	1/T	ln k
1.74E-2	666	1.502E-3	-11.4
3.91E-2	687	1.456E-3	-10.58
6.52E-2	706	1.416E-3	-10.05
0.1	728	1.374E-3	-9.609
0.1652	747	1.339E-3	-9.076
0.2565	773	1.294E-3	-8.588
0.3739	794	1.259E-3	-8.143
0.487	809	1.236E-3	-7.802
0.6174	825	1.212E-3	-7.458
0.7391	840	1.19E-3	-7.149
0.8696	855	1.17E-3	-6.779
0.9174	866	1.155E-3	-6.607
0.9783	885	1.13E-3	-6.265

Table IIIbc - 4 NH4-MOR (N&A)

Best-fit equation: ln k = -15581.94(1/T) + 12.59

Corr. Coefficient = -0.9933 ; t-factor = -29.87

$\Delta G^{\ddagger}$ (660K) = 221.75 kJ/mol ; $T_{(0.5\alpha)}$ = 806 K

DATA FOR ORDER 1.08 AND E_A 129548.3 J/MOL

α	T/K	1/T	ln k
4.4E-3	649	1.541E-3	-11.85
2.22E-2	669	1.495E-3	-10.22
4E-2	693	1.443E-3	-9.625
6.22E-2	718	1.393E-3	-9.171
0.1156	744	1.344E-3	-8.52
0.2	769	1.3E-3	-7.92
0.2844	775	1.29E-3	-7.51
0.3556	785	1.274E-3	-7.233
0.4044	794	1.259E-3	-7.065
0.4933	805	1.242E-3	-6.787
0.6089	819	1.221E-3	-6.454
0.7333	834	1.199E-3	-6.096
0.84	849	1.178E-3	-5.749
0.9289	863	1.159E-3	-5.349

Table IIIb - 5 Ni-MOR(1) (A&A)

Best-fit equation: ln k = 11281.10(1/T) + 5.49

Corr. Coefficient = -0.9984 ; t-factor = -62.73

$\Delta G^{\ddagger}$ (660K) = 221.74 kJ/mol ; $T_{(0.5\alpha)}$ = 792.5 K

DATA FOR ORDER 0.64 AND E_A 93791.0 J/MOL

α	T/K	1/T	ln k
3.69E-2	666	1.502E-3	-11.43
4.64E-2	675	1.481E-3	-11.2
6.09E-2	683	1.464E-3	-10.93
7.83E-2	697	1.435E-3	-10.67
0.113	716	1.397E-3	-10.29
0.1739	744	1.344E-3	-9.836
0.2283	757	1.321E-3	-9.543
0.337	779	1.284E-3	-9.109
0.4717	788	1.269E-3	-8.709
0.6674	819	1.221E-3	-8.242
0.742	828	1.208E-3	-8.077
0.8319	842	1.188E-3	-7.782
0.903	853	1.172E-3	-7.69
0.942	864	1.157E-3	-7.569
0.983	878	1.139E-3	-7.387

Table IIIb - 6. Ni-MOR(1)(N&A)

Best-fit equation: ln k = -11900.32(1/T) + 11.58

Corr. Coefficient = -0.9990 ; t-factor = -74.70

$\Delta G^{\ddagger}$ (660K) = 197.14 kJ/mol ; $T_{(0.5\alpha)}$ = 757 K

DATA FOR ORDER 1.52 AND E_A 98939.2 J/MOL

α	T/K	1/T	ln k
4.5E-3	570	1.754E-3	-9.298
9.1E-3	593	1.686E-3	-8.59
2.26E-2	612	1.634E-3	-7.67
3.62E-2	635	1.575E-3	-7.189
5.88E-2	653	1.531E-3	-6.686
0.1086	674	1.484E-3	-6.031
0.1765	701	1.427E-3	-5.486
0.2896	730	1.37E-3	-4.881
0.457	751	1.332E-3	-4.228
0.5385	763	1.311E-3	-3.947
0.6652	789	1.267E-3	-3.51
0.7466	809	1.236E-3	-3.203
0.8552	828	1.208E-3	-2.695

Table IIIb - 7 Ni-MOR(2)(A&A)

Best-fit equation: ln k = -12308.74(1/T) + 9.72

Corr. Coefficient = -0.9974 ; t-factor = -41.43

$\Delta G^{\ddagger}$ (660K) = 211.42 kJ/mol ; $T_{(0.5\alpha)}$ = 765.5 K

DATA FOR ORDER 1.08 AND E_A 102334.8 J/MOL

α	T/K	1/T	ln k
3.6E-2	643	1.555E-3	-9.355
4.05E-2	656	1.524E-3	-9.235
7.66E-2	672	1.488E-3	-8.577
0.1239	686	1.458E-3	-8.068
0.1689	703	1.422E-3	-7.731
0.2162	719	1.391E-3	-7.453
0.2928	735	1.361E-3	-7.097
0.3941	751	1.332E-3	-6.722
0.4955	765	1.307E-3	-6.403
0.6476	783	1.277E-3	-5.967
0.7599	800	1.25E-3	-5.638

Table IIIb - 8 Ni-MOR(3) (N&A)

Best-fit equation: ln k = -11127.23(1/T) + 7.63

Corr. Coefficient = -0.9988 ; t-factor = -71.97

$\Delta G^{\ddagger}$ (660K) = 212.41 kJ/mol ; $T_{(0.5\alpha)}$ = 732 K

DATA FOR ORDER 0.86 AND E_A 92511.7 J/MOL

α	T/K	1/T	ln k
1.38E-2	581	1.721E-3	-11.45
2.29E-2	606	1.65E-3	-10.94
7.34E-2	634	1.577E-3	-9.753
9.63E-2	652	1.534E-3	-9.471
0.1743	675	1.481E-3	-8.84
0.2523	692	1.445E-3	-8.43
0.3257	707	1.414E-3	-8.133
0.4083	720	1.389E-3	-7.855
0.5275	736	1.359E-3	-7.514
0.6376	751	1.332E-3	-7.229
0.7661	765	1.307E-3	-6.9
0.867	781	1.28E-3	-6.61
0.9404	796	1.256E-3	-6.328
0.9702	808	1.238E-3	-6.153

Table IIIb - 9 Ni-MOR(3)(A&A)

Best-fit equation: ln k = -11100.61(1/T) + 8.42

Corr. Coefficient = -0.9979 ; t-factor = -59.73

$\Delta G^{\ddagger}$ (660K) = 208.03 kJ/mol ; $T_{(0.5\alpha)}$ = 760 K

DATA FOR ORDER 1.08 AND E_A 92290.4 J/MOL

α	T/K	1/T	ln k
3.15E-2	622	1.608E-3	-9.311
4.05E-2	640	1.563E-3	-9.054
6.17E-2	654	1.529E-3	-8.621
9.25E-2	669	1.495E-3	-8.199
0.1542	683	1.464E-3	-7.65
0.2071	700	1.429E-3	-7.322
0.2731	719	1.391E-3	-7
0.3216	735	1.361E-3	-6.801
0.301	727	1.376E-3	-6.883
0.3216	733	1.364E-3	-6.801
0.337	735	1.361E-3	-6.743
0.4427	751	1.332E-3	-6.383
0.533	765	1.307E-3	-6.112
0.6432	783	1.277E-3	-5.798
0.7665	800	1.25E-3	-5.437
0.8678	820	1.22E-3	-5.083
0.9383	839	1.192E-3	-4.732

Table IIIb - 10 Ni-MOR(3)(N&A)

Best-fit equation: ln k = -12305.47(1/T) + 12.24

Corr. Coefficient = -0.9970 ; t-factor = -51.24

$\Delta G^{\ddagger}$ (660K) = 197.05 kJ/mol ; $T_{(0.5\alpha)}$ = 775 K

DATA FOR ORDER 1.52 AND E_A 102307.6 J/MOL

α	T/K	1/T	ln k
2.72E-2	638	1.567E-3	-7.137
4.53E-2	654	1.529E-3	-6.613
0.113	690	1.449E-3	-5.643
0.1765	703	1.422E-3	-5.141
0.2398	715	1.399E-3	-4.775
0.2896	727	1.376E-3	-4.536
0.3258	736	1.359E-3	-4.38
0.371	745	1.342E-3	-4.199
0.4072	761	1.314E-3	-4.063
0.4661	770	1.299E-3	-3.852
0.5249	779	1.284E-3	-3.649
0.5973	793	1.261E-3	-3.402
0.6833	809	1.236E-3	-3.1
0.7376	816	1.225E-3	-2.894
0.7873	825	1.212E-3	-2.687
0.8326	835	1.198E-3	-2.472
0.8552	841	1.189E-3	-2.351
0.914	856	1.168E-3	-1.951

Table IIIb - 11 Cu-MOR(1)(A&A)

Best-fit equation: ln k = -12150.66(1/T) + 12.76

Corr. Coefficient = -0.9991 ; t-factor = -76.57

$\Delta G^{\ddagger}$ (660K) = 193.02 kJ/mol ; $T_{(0.5\alpha)}$ = 637.6 K

DATA FOR ORDER 1.08 AND E_A 101020.6 J/MOL

α	T/K	1/T	ln k
2.69E-2	543	1.842E-3	-9.587
5.83E-2	565	1.77E-3	-8.796
0.1345	588	1.701E-3	-7.915
0.2197	603	1.658E-3	-7.37
0.4036	629	1.59E-3	-6.626
0.538	641	1.56E-3	-6.214
0.6928	652	1.534E-3	-5.773
0.6727	657	1.522E-3	-5.831
0.7623	664	1.506E-3	-5.566
0.8565	672	1.488E-3	-5.244
0.8699	674	1.484E-3	-5.191
0.9147	689	1.451E-3	-4.985
0.9619	697	1.435E-3	-4.669

Table IIIb - 12 Cu-MOR(1)(N&A)

Best-fit equation: ln k = -11374.34(1/T) + 11.15

Corr. Coefficient = -0.9980 ; t-factor = -52.19

$\Delta G^{\ddagger}$ (660K) = 194.9 kJ/mol ; $T_{(0.5\alpha)}$ = 611 K

DATA FOR ORDER 0.86 AND E_A 94566.2 J/MOL

α	T/K	1/T	ln k
4.7E-3	486	2.058E-3	-12.36
9.4E-3	495	2.02E-3	-11.66
1.87E-2	508	1.969E-3	-10.97
2.34E-2	519	1.927E-3	-10.74
3.27E-2	532	1.88E-3	-10.41
6.07E-2	547	1.828E-3	-9.775
0.1215	566	1.767E-3	-9.052
0.1869	580	1.724E-3	-8.589
0.3365	598	1.672E-3	-7.919
0.5421	614	1.629E-3	-7.301
0.729	629	1.59E-3	-6.823
0.9112	650	1.538E-3	-6.28
0.9579	660	1.515E-3	-6.06

Table IIIb - 13 Cu-MOR(2)(A&A)

Best-fit equation: ln k = -10151.15(1/T) + 7.48

Corr. Coefficient = -0.9976 ; t-factor = -40.55

$\Delta G^{\ddagger}$ (660K) = 204.91 kJ/mol ; $T_{(0.5\alpha)}$ = 633 K

DATA FOR ORDER 0.64 AND E_A 84396.6 J/MOL

α	T/K	1/T	ln k
5.65E-2	551	1.815E-3	-10.98
0.1174	571	1.751E-3	-10.23
0.1884	589	1.698E-3	-9.73
0.4096	621	1.61E-3	-8.86
0.4399	628	1.592E-3	-8.774
0.5296	639	1.565E-3	-8.541
0.5171	634	1.577E-3	-8.572
0.8304	657	1.522E-3	-7.855
0.9522	677	1.477E-3	-7.512
0.6522	643	1.555E-3	-8.256

Table IIIb - 14 Cu-MOR(2)(N&A)

Best-fit equation: ln k = -15321.99(1/T) + 18.58

Corr. Coefficient = -0.9984 ; t-factor = -46.43

$\Delta G^{\ddagger}$ (660K) = 187.31 kJ/mol ; $T_{(0.5\alpha)}$ = 614 K

DATA FOR ORDER 1.08 AND E_A 127387.1 J/MOL

α	T/K	1/T	ln k
1.4E-2	529	1.89E-3	-10.31
3.74E-2	547	1.828E-3	-9.311
7.01E-2	567	1.764E-3	-8.664
0.1916	588	1.701E-3	-7.585
0.4159	609	1.642E-3	-6.644
0.6682	623	1.605E-3	-5.903
0.8411	638	1.567E-3	-5.361
0.9252	649	1.541E-3	-4.987
0.9673	660	1.515E-3	-4.676

Table IIIb - 15 Cu-MOR(3)(A&A)

Best-fit equation: ln k = -9988.85(1/T) + 8.70

Corr. Coefficient = -0.9996 ; t-factor = -124.40

$\Delta G^{\ddagger}$ (660K) = 196.76 kJ/mol ; $T_{(0.5\alpha)}$ = 613 K

DATA FOR ORDER 0.86 AND E_A 83047.3 J/MOL

α	T/K	1/T	ln k
4.87E-2	528	1.894E-3	-10.17
6.42E-2	539	1.855E-3	-9.885
0.1012	551	1.815E-3	-9.413
0.1416	562	1.779E-3	-9.058
0.1789	570	1.754E-3	-8.805
0.3233	595	1.681E-3	-8.135
0.4053	605	1.653E-3	-7.858
0.4859	612	1.634E-3	-7.621
0.5815	621	1.61E-3	-7.366
0.6916	633	1.58E-3	-7.086
0.7357	638	1.567E-3	-6.974
0.8282	649	1.541E-3	-6.722
0.8879	655	1.527E-3	-6.534
0.9484	664	1.506E-3	-6.281

Table IIIb - 16 Cu-MOR(3)(N&A)

Best-fit equation: ln k = -15419.52(1/T) + 16.57

Corr. Coefficient = -0.9988 ; t-factor = -60.25

$\Delta G^{\ddagger}$ (660K) = 198.33 kJ/mol ; $T_{(0.5\alpha)}$ = 633 K

DATA FOR ORDER 0.86 AND E_A 128197.8 J/MOL

α	T/K	1/T	ln k
1.31E-2	543	1.842E-3	-11.66
2.18E-2	558	1.792E-3	-11.15
4.59E-2	573	1.745E-3	-10.39
8.73E-2	589	1.698E-3	-9.728
0.179	606	1.65E-3	-8.966
0.3275	621	1.61E-3	-8.281
0.5546	637	1.57E-3	-7.597
0.7555	649	1.541E-3	-7.083
0.8908	660	1.515E-3	-6.685
0.952	671	1.49E-3	-6.423
0.9825	680	1.471E-3	-6.201

Table IIIb - 17 Pt-MOR(1)(A&A)

Best-fit equation: ln k = -10651.32(1/T) + 13.17

Corr. Coefficient = -0.9993 ; t-factor = -73.48

$\Delta G^{\ddagger}$ (660K) = 207.26 kJ/mol ; $T_{(0.5\alpha)}$ = 518 K

DATA FOR ORDER 0.86 AND E_A 88555.04 J/MOL

α	T/K	1/T	ln k
8.41E-2	470	2.128E-3	-9.415
0.1301	483	2.07E-3	-8.957
0.2543	498	2.008E-3	-8.223
0.3405	506	1.976E-3	-7.882
0.457	516	1.938E-3	-7.512
0.5894	523	1.912E-3	-7.155
0.66	529	1.89E-3	-6.976
0.7528	535	1.869E-3	-6.738
0.8985	546	1.832E-3	-6.305
0.9485	553	1.808E-3	-6.09

Table IIIb - 18 Pt-MOR(1)(N&A)

Best-fit equation: ln k = -7291.72(1/T) + 5.35

Corr. Coefficient = -0.9986 ; t-factor = -66.97

$\Delta G^{\ddagger}$ (660K) = 200.51 kJ/mol ; $T_{(0.5\alpha)}$ = 574 K

DATA FOR ORDER 0.86 AND E_A 60623.4 J/MOL

α	T/K	1/T	ln k
1.88E-2	450	2.222E-3	-10.91
3.29E-2	464	2.155E-3	-10.35
6.1E-2	477	2.096E-3	-9.715
7.04E-2	492	2.033E-3	-9.568
0.1033	507	1.972E-3	-9.169
0.1315	512	1.953E-3	-8.914
0.1738	522	1.916E-3	-8.614
0.2488	536	1.866E-3	-8.217
0.338	552	1.812E-3	-7.86
0.4413	566	1.767E-3	-7.527
0.5399	579	1.727E-3	-7.252
0.6667	593	1.686E-3	-6.927
0.8122	610	1.639E-3	-6.546
0.9108	628	1.592E-3	-6.227
0.9484	643	1.555E-3	-6.059

Table IIIb 19 Pt-MOR(2)(A&A)

Best-fit equation: ln k = -11249.79(1/T) + 14.70

Corr. Coefficient = -0.9965 ; t-factor = -41.41

$\Delta G^{\ddagger}$ (660K) = 200.85 kJ/mol ; $T_{(0.5\alpha)}$ = 526 K

DATA FOR ORDER 1.08 AND E_A 93530.7 J/MOL

α	T/K	1/T	ln k
1.92E-2	448	2.232E-3	-10.2
3.33E-2	462	2.165E-3	-9.646
5.82E-2	473	2.114E-3	-9.073
0.1021	490	2.041E-3	-8.486
0.1947	506	1.976E-3	-7.783
0.3309	519	1.927E-3	-7.157
0.4862	525	1.905E-3	-6.641
0.5915	533	1.876E-3	-6.336
0.6787	538	1.859E-3	-6.089
0.7362	547	1.828E-3	-5.921
0.8681	554	1.805E-3	-5.474
0.9645	567	1.764E-3	-4.92
0.9745	579	1.727E-3	-4.811
0.9754	579	1.727E-3	-4.811

Table IIIb - 20 Pt-MOR(2)(N&A)

Best-fit equation: ln k = -6712.95(1/T) + 4.19

Corr. Coefficient = -0.9986 ; t-factor = -64.67

$\Delta G^{\ddagger}$ (660K) = 210.88 kJ/mol ; $T_{(0.5\alpha)}$ = 582 K

DATA FOR ORDER 0.86 AND E_A 55811.5 J/MOL

α	T/K	1/T	ln k
1.4E-2	440	2.273E-3	-11.19
2.34E-2	450	2.222E-3	-10.68
3.74E-2	465	2.151E-3	-10.2
6.54E-2	479	2.088E-3	-9.629
8.41E-2	493	2.028E-3	-9.369
0.1542	523	1.912E-3	-8.729
0.2103	537	1.862E-3	-8.39
0.2897	553	1.808E-3	-8.027
0.3785	567	1.764E-3	-7.707
0.4860	580	1.724E-3	-7.384
0.5654	593	1.686E-3	-7.17
0.7336	611	1.637E-3	-6.742
0.8458	629	1.59E-3	-6.433
0.9252	645	1.55E-3	-6.154

Table IIIb - 21 Pt-MOR(3)(A&A)

Best-fit equation: ln k = -8544.59(1/T) + 6.66

Corr. Coefficient = -0.9983 ; t-factor = -51.87

$\Delta G^{\ddagger}$ (660K) = 226.17 kJ/mol ; $T_{(0.5\alpha)}$ = 520.5 K

DATA FOR ORDER 0.42 AND E_A 71039.7 J/MOL

α	T/K	1/T	ln k
5.75E-2	457	2.188E-3	-12
9.51E-2	471	2.123E-3	-11.49
0.1435	483	2.07E-3	-11.07
0.2414	498	2.008E-3	-10.53
0.3168	506	1.976E-3	-10.23
0.4216	516	1.938E-3	-9.918
0.5453	523	1.912E-3	-9.619
0.638	529	1.89E-3	-9.425
0.7439	536	1.866E-3	-9.221
0.7351	542	1.845E-3	-9.237
0.8455	544	1.838E-3	-9.029

Table IIIb - 22 Pt-MOR(3)(N&A)

Best-fit equation: ln k = -10333.49(1/T) + 13.58

Corr. Coefficient = -0.9993 ; t-factor = -77.64

$\Delta G^{\ddagger}$ (660K) = 190.16 kJ/mol ; $T_{(0.5\alpha)}$ = 548 K

DATA FOR ORDER 1.30 AND E_A 85912.7 J/MOL

α	T/K	1/T	ln k
1.36E-2	450	2.222E-3	-9.337
3.62E-2	469	2.132E-3	-8.343
7.69E-2	492	2.033E-3	-7.562
0.1946	514	1.946E-3	-6.546
0.3891	538	1.859E-3	-5.681
0.5837	556	1.799E-3	-5.046
0.7511	572	1.748E-3	-4.503
0.8462	585	1.709E-3	-4.127
0.9321	599	1.669E-3	-3.628
0.9774	616	1.623E-3	-3.094

Table IIIbc - 23 Pt-MOR(4)(A&A)

Best-fit equation: ln k = -10110.57(1/T) + 11.52

Corr. Coefficient = -0.9972 ; t-factor = -47.73

$\Delta G^{\ddagger}$ (660K) = 201.03 kJ/mol ; $T_{(0.5\alpha)}$ = 597 K

DATA FOR ORDER 1.30 AND E_A 84059.2 J/MOL

α	T/K	1/T	ln k
1.85E-2	486	2.058E-3	-9.224
3.7E-2	512	1.953E-3	-8.518
7.87E-2	521	1.919E-3	-7.735
0.125	534	1.835E-3	-6.952
0.2037	545	1.835E-3	-6.952
0.2037	555	1.802E-3	-6.691
0.3056	570	1.754E-3	-6.199
0.3983	583	1.715E-3	-5.846
0.4907	596	1.678E-3	-5.537
0.5833	607	1.647E-3	-5.245
0.6667	617	1.621E-3	-4.982
0.7639	627	1.595E-3	-4.655
0.8519	639	1.565E-3	-4.299
0.9028	646	1.548E-3	-4.03
0.9445	657	1.522E-3	-3.719

Table IIIb - 24 Pt-MOR(4)(N&A)

Best-fit equation: ln k = -9136.88(1/T) + 10.04

Corr. Coefficient = -0.9995 ; t-factor = -88.93

$\Delta G^{\ddagger}$ (660K) = 199.76 kJ/mol ; $T_{(0.5\alpha)}$ = 554 K

DATA FOR ORDER 1.08 AND E_A 75963.9 J/MOL

α	T/K	1/T	ln k
1.36E-2	449	2.227E-3	-10.34
3.62E-2	469	2.132E-3	-9.352
7.24E-2	491	2.037E-3	-8.638
0.1674	515	1.942E-3	-7.743
0.3394	536	1.866E-3	-6.917
0.5068	555	1.802E-3	-6.372
0.6335	571	1.751E-3	-6.009
0.7602	584	1.712E-3	-5.639
0.8688	598	1.672E-3	-5.262
0.9593	616	1.623E-3	-4.759

TABLE IIIc - 1.1 Ni-NaMOR (A&A)

Best-fit equation: ln k = -18195.30(1/T) + 25.15

Corr. Coefficient = -0.9983 ; t-factor = -54.30

$\Delta G^{\ddagger}$ (660K) = 175.75 kJ/mol ; $T_{(0.5\alpha)}$ = 645.6 K

DATA FOR ORDER 1.74 AND E_A 151275.7 J/mol

α	T/K	1/T	ln k
2.32E-2	570	1.754E-3	-6.82
5.56E-2	587	1.704E-3	-5.916
0.125	600	1.667E-3	-5.04
0.213	613	1.631E-3	-4.415
0.139	602	1.661E-3	-4.92
0.2361	621	1.61E-3	-4.287
0.4074	638	1.567E-3	-3.524
0.5787	652	1.534E-3	-2.885
0.75	668	1.497E-3	-2.193
0.8565	680	1.471E-3	-1.61
0.9213	692	1.445E-3	-1.059
0.963	709	1.41E-3	-0.4268

TABLE IIIc - 1.2 Ni-NaMOR (A&4%)

Best-fit equation: ln k = -17516.57(1/T) + 22.65

Corr. Coefficient = -0.9925 ; t-factor = -28.79

$\Delta G^{\ddagger}$ (660K) = 183.17 kJ/mol ; $T_{(0.5\alpha)}$ = 677.5 K

DATA FOR ORDER 1.74 AND E_A 145632.7 J/mol

α	T/K	1/T	ln k
5E-3	564	1.773E-3	-8.332
2E-2	579	1.727E-3	-6.932
2.5E-2	595	1.681E-3	-6.705
3.5E-2	610	1.639E-3	-6.359
5E-2	626	1.597E-3	-5.989
0.115	642	1.558E-3	-5.095
0.255	656	1.524E-3	-4.15
0.39	668	1.497E-3	-3.554
0.53	680	1.471E-3	-3.027
0.66	691	1.447E-3	-2.537
0.8	707	1.414E-3	_1.908
0.865	719	1.391E-3	-1.513
0.91	732	1.366E-3	-1.139
0.93	743	1.346E-3	-0.9196
0.945	753	1.328E-3	-0.7149

TABLE IIIc - 1.3 Ni-NaMOR (A&8)

Best-fit equation: ln k = -23258.46(1/T) + 32.55

Corr. Coefficient = -0.9997 ; t-factor = -100.0

$\Delta G^{\ddagger}$ (660K) = 176.55 kJ/mol ; $T_{(0.5\alpha)}$ = 674 K

DATA FOR ORDER 1.96 AND E_A 193370.8 J/mol

α	T/K	1/T	ln k
0.1419	640	1.563E-3	-3.788
0.2162	648	1.543E-3	-3.278
0.2973	657	1.522E-3	-2.852
0.3784	665	1.504E-3	-2.491
0.5405	677	1.477E-3	-1.84
0.6689	687	1.456E-3	-1.308
0.7905	699	1.431E-3	-0.6958
0.8514	708	1.412E-3	-0.2886
0.9054	719	1.391E-3	0.21

TABLE IIIc - 1.4 Ni-NaMOR (N&A)

Best-fit equation: ln k = -12242.42(1/T) + ?9.37

Corr. Coefficient = -0.9988 ; t-factor = -58.76

$\Delta G^{\ddagger}$ (660K) = 212.31 kJ/mol ; $T_{(0.5\alpha)}$ = 733.5 K

DATA FOR ORDER 0.86 AND E_A 101783.5 J/mol

α	T/K	1/T	ln k
3.21E-2	616	1.623E-3	-10.39
5.96E-2	643	1.555E-3	-9.755
0.1284	669	1.495E-3	-8.956
0.2248	692	1.445E-3	-8.347
0.3624	715	1.399E-3	-7.791
0.4908	733	1.364E-3	-7.401
0.6321	741.5	1.349E-3	-7.031
0.7703	763	1.311E-3	-6.677
0.8514	772	1.295E-3	-6.447
0.9234	786	1.272E-3	-6.192

TABLE IIIc - 1.5 Ni-NaMOR (N&4)

Best-fit equation: ln k = -23941.03(1/T) + 31.09

Corr. Coefficient = -0.9966 ; t-factor = -34.28

$\Delta G^{\ddagger}$ (660K) = 191.92 kJ/mol ; $T_{(0.5\alpha)}$ = 698.1 K

DATA FOR ORDER 1.74 AND E_A 199045.7 J/mol

α	T/K	1/T	ln k
4.78E-3	604	1.656E-3	-8.455
2.39E-2	626	1.597E-3	-6.829
3.828E-2	646	1.548E-3	-6.345
0.1292	668	1.497E-3	-5.043
0.3158	685	1.46E -3	-3.942
0.512	699	1.431E-3	-3.171
0.7464	714	1.401E-3	-2.25
0.8373	726	1.377E-3	-1.774
0.9067	739	1.353E-3	-1.25
0.9282	747	1.339E-3	-1.019

TABLE IIIc - 1.6 Ni-NaMOR (N&8%)

Best-fit equation: ln k = -16125.26(1/T) + 16.43

Corr. Coefficient = -0.9981 ; t-factor = -56.12

$\Delta G^{\ddagger}$ (660K) = 205.87 kJ/mol ; $T_{(0.5\alpha)}$ = 743.7 K

DATA FOR ORDER 1.30 AND E_A 134065.4 J/mol

α	T/K	1/T	ln k
3.38E-2	649	1.541E-3	-8.391
6.08E-2	669	1.495E-3	-7.786
0.1284	690	1.449E-3	-6.99
0.2229	702	1.425E-3	-6.366
0.2365	711	1.406E-3	-6.296
0.3378	720	1.389E-3	-5.85
0.4054	732	1.366E-3	-5.602
0.4865	742	1.348E-3	-5.331
0.5811	754	1.326E-3	-5.032
0.6757	763	1.311E-3	-4.734
0.7027	771	1.297E-3	-4.646
0.8311	782	1.279E-3	-4.172
0.8851	792	1.263E-3	-3.913
0.9392	804	1.244E-3	-3.548

TABLE IIIc - 1.7 Ni- HMOR (A&4%)

Best-fit equation: ln k = -14440.68(1/T) + 15.19

Corr. Coefficient = -0.9965 ; t-factor = -39.65

$\Delta G^{\ddagger}$ (660K) = 197.86 kJ/mol ; $T_{(0.5\alpha)}$ = 746.6 K

DATA FOR ORDER 1.52 AND E_A 120059.8 J/mol

α	T/K	1/T	ln k
1.38E-2	622	1.608E-3	-8.215
3.2E-2	640	1.563E-3	-7.36
5.5E-2	653	1.531E-3	-6.8
8.26E-2	668	1.497E-3	-6.371
0.1193	681	1.468E-3	-5.973
0.1606	693	1.443E-3	-5.64
0.2431	711	1.406E-3	-5.148
0.4037	728	1.374E-3	-4.465
0.5184	750	1.333E-3	-4.061
0.5875	766	1.305E-3	-3.825
0.6927	786	1.272E-3	-3.455
0.7706	791	1.264E-3	-3.149
0.922	815	1.227E-3	-2.271

TABLE IIIc - 1.8 Ni- HMOR (A&4%)

Best-fit equation: ln k = -11851.45(1/T) + 9.34

Corr. Coefficient = -0.9973 ; t-factor = -45.02

$\Delta G^{\ddagger}$ (660K) = 208.97 kJ/mol ; $T_{(0.5\alpha)}$ = 817.2 K

DATA FOR ORDER 1.30 AND E_A 98532.96 J/mol

α	T/K	1/T	ln k
2.32E-2	658	1. 52E-3	-8.686
4.17E-2	677	1.477E-3	-8.088
8.33E-2	709	1. 41E-3	-7.367
0.1435	739	1.353E-3	-6.78
0.2269	764	1.309E-3	-6.257
0.3657	786	1.272E-3	-5.656
0.4213	805	1.242E-3	-5.458
0.5833	830	1.205E-3	-4.937
0.7361	843	1.186E-3	-4.445
0.7407	859	1.164E-3	-4.429
0.7235	871	1.148E-3	-4.488
0.8387	883	1.133E-3	-4.051
0.8248	880	1.136E-3	-4.11

TABLE IIIc - 1.9 Ni- HMOR (A&8%)

Best-fit equation: ln k = -15878.72(1/T) + 15.01

Corr. Coefficient = -0.9984 ; t-factor = -69.52

$\Delta G^{\ddagger}$ (660K) = 212.47 kJ/mol ; $T_{(0.5\alpha)}$ = 785.5 K

DATA FOR ORDER 1.30 AND E_A 132015.7 J/mol

α	T/K	1/T	ln k
3.45E-2	679	1.473E-3	-8.336
4.14E-2	690	1.449E-3	-8.149
6.89E-2	700	1.429E-3	-7.621
9.66E-2	711	1.406E-33	-7.264
0.131	721	1.387E-3	-6.934
0.1724	731	1.368E-3	-6.628
0.2207	742	1.348E-3	-6.343
0.2709	751	1.332E-3	-6.097
0.3226	760	1.316E-3	-5.876
0.3586	769	1.3E-3	-5.737
0.4552	779	1.284E-3	-5.398
0.531	790	1.266E-3	-5.155
0.6138	801	1.248E-3	-4.896
0.6689	809	1.236E-3	-4.722
0.7793	820	1.22E-3	-4.344
0.8276	831	1.203E-3	-4.153
0.8897	840	1.19E-3	-3.853
0.9586	857	1.167E-3	-3.318

TABLE IIIc - 1.10 Ni- HMOR (N&A)

Best-fit equation: ln k = -13260.97(1/T) + 12.40

Corr. Coefficient = -0.9996 ; t-factor = -120.56

$\Delta G^{\ddagger}$ (660K) = 204.27 kJ/mol ; $T_{(0.5\alpha)}$ = 749.7 K

DATA FOR ORDER 1.30 AND E_A 110251.7 J/mol

α	T/K	1/T	ln k
1.35E-2	609	1.642E-3	-9.335
3.15E-2	635	1.575E-3	-8.476
6.08E-2	659	1.517E-3	-7.798
9.46E-2	674	1.484E-3	-7.333
0.1802	695.5	1.438E-3	-6.625
0.2838	715	1.399E-3	-6.086
0.3761	731	1.368E-3	-5.718
0.473	746	1.34E-3	-5.387
0.5856	761.5	1.313E-3	-5.031
0.6757	775.5	1.289E-3	-4.746
0.7703	791	1.264E-3	-4.424
0.8491	805	1.242E-3	-4.105
0.9144	822.5	1.216E-3	-3.748
0.9595	836	1.196E-3	-3.354

TABLE IIIc - 1.11 Ni-HMOR (N&4%)

Best-fit equation: ln k = -12231.33(1/T) + 8.92

Corr. Coefficient = -0.9995 ; t-factor = -104.15

$\Delta G^{\ddagger}$ (660K) = 214.42 kJ/mol ; $T_{(0.5\alpha)}$ = 804.4 K

DATA FOR ORDER 1.08 AND E_A 101691.3 J/mol

α	T/K	1/T	ln k
1.97E-2	650.5	1.537E-3	-9.915
3.944E-2	673	1.486E-3	-9.21
6.4E-2	693	1.443E-3	-8.712
9.36E-2	711	1.406E-3	-8.314
0.1281	723	1.383E-3	-7.98
0.1823	740	1.351E-3	-7.594
0.2414	754	1.326E-3	-7.274
0.33	772	1.295E-3	-6.897
0.4138	788.5	1.268E-3	-6.604
0.4975	804	1.244E-3	-6.345
0.5813	817	1.224E-3	-6.102
0.6798	833	1.2E-3	-5.823
0.8177	856	1.168E-3	-5.398
0.9261	875	1.143E-3	-4.935

TABLE IIIc - 1.12 Ni-HMOR (N&8%)

Best-fit equation: ln k = -9187.43 (1/T) + 2.41

Corr. Coefficient = -0.9948 ; t-factor = -25.79

$\Delta G^{\ddagger}$ (660K) = 224.8 kJ/mol ; $T_{(0.5\alpha)}$ = 760.4 K

DATA FOR ORDER 0.42 AND E_A 76384.27 J/mol

α	T/K	1/T	ln k
3.55E-2	621	1.61E-3	-12.38
7.09E-2	649	1.541E-3	-11.68
0.1135	679	1.473E-3	-11.2
0.2057	711	1.406E-3	-10.58
0.3262	742	1.348E-3	-10.09
0.5532	766	1.305E-3	-9.487
0.7801	789	1.267E-3	-9.039
0.8865	807	1.239E-3	-8.835
0.922	839	1.192E-3	-8.76

TABLE IIIc - 2.1 Cu-NaMOR (A&A)

Best-fit equation: ln k = -16201.80(1/T) + 21.27

Corr. Coefficient = -0.9991 ; t-factor = -69.64

$\Delta G^{\ddagger}$ (660K) = 180.01 kJ/mol ; $T_{(0.5\alpha)}$ = 640.5 K

DATA FOR ORDER 1.52 AND E_A 134701.8 J/mol

α	T/K	1/T	ln k
1.277E-2	548.5	1.823E-3	-8.309
2.55E-2	563.5	1.775E-3	-7.608
5.96E-2	575.5	1.738E-3	-6.732
0.1362	594.5	1.682E-3	-5.841
0.2255	611	1.637E-3	-5.255
0.3745	627.5	1.594E-3	-4.59
0.5532	646	1.548E-3	-3.958
0.7532	662.5	1.509E-3	-3.237
0.8979	681	1.468E-3	-2.482
0.9745	708	1.412E-3	-1.557
0.885	680	1.471E-3	-2.572

TABLE IIIc - 2.2 Cu-NaMOR (A&4%)

Best-fit equation: ln k = -13453.75(1/T) + 14.4

Corr. Coefficient = -0.9991 ; t-factor = -72.99

$\Delta G^{\ddagger}$ (660K) = 194.45 kJ/mol ; $T_{(0.5\alpha)}$ = 650.2 K

DATA FOR ORDER 1.08 AND E_A 111854.5 J/mol

α	T/K	1/T	ln k
2.45E-2	556	1.799E-3	-9.671
5.39E-2	581	1.721E-3	-8.866
0.1078	599	1.669E-3	-8.142
0.2108	615	1.626E-3	-7.407
0.3039	631	1.585E-3	-6.976
0.4069	642	1.558E-3	-6.604
0.5098	651	1.536E-3	-6.285
0.6422	662	1.511E-3	-5.907
0.7549	673	1.486E-3	-5.578
0.8431	685	1.46E-3	-5.284
0.9118	693	1.443E-3	-4.99
0.9559	702	1.425E-3	-4.71

TABLE IIIc - 2.3 Cu-NaMOR (A&8%)

Best-fit equation: ln k = -14108.14(1/T) + 16.73

Corr. Coefficient = -0.9991 ; t-factor = -66.73

$\Delta G^{\ddagger}$ (660K) = 186.96 kJ/mol ; $T_{(0.5\alpha)}$ = 641.8 K

DATA FOR ORDER 1.30 AND E_A 117295.1 J/mol

α	T/K	1/T	ln k
6.9E-3	527	1.898E-3	-9.981
2.098E-2	549	1.821E-3	-8.873
4.895E-2	570	1.754E-3	-8.007
9.091E-2	591	1.692E-3	-7.359
0.2168	610	1.639E-3	-6.395
0.3706	630	1.587E-3	-5.722
0.6014	651	1.536E-3	-4.965
0.7552	664	1.506E-3	-4.462
0.8671	680	1.471E-3	-4.002
0.9371	692	1.445E-3	-3.562

TABLE IIIc - 2.4 Cu-NaMOR (N&A)

Best-fit equation: ln k = -20815.20(1/T) + 28.40

Corr. Coefficient = -0.9992 ; t-factor = -65.31

$\Delta G^{\ddagger}$ (660K) = 178.53 kJ/mol ; $T_{(0.5\alpha)}$ = 641.8 K

DATA FOR ORDER 1.52 AND E_A 173057.5 J/mol

α	T/K	1/T	ln k
4.27E-3	551	1.815E-3	-9.362
8.55E-3	559	1.789E-3	-8.664
3.85E-2	589	1.698E-3	-7.136
0.137	610	1.639E-3	-5.785
0.333	631	1.585E-3	-4.706
0.658	652	1.534E-3	-3.546
0.8675	668	1.497E-3	-2.634
0.9188	678	1.475E-3	-2.265
0.9615	690	1.449E-3	-1.764

TABLE IIIc - 2.5 Cu-NaMOR (N&4%)

Best-fit equation: ln k = -12456.73(1/T) + 11.42

Corr. Coefficient = -0.9989 ; t-factor = -63.88

$\Delta G^{\ddagger}$ (660K) = 202.64 kJ/mol ; $T_{(0.5\alpha)}$ = 625 K

DATA FOR ORDER 0.64 AND E_A 103565.3 J/mol

α	T/K	1/T	ln k
4E-2	551	1.815E-3	-11.24
7.683E-2	565	1.77E-3	-10.57
0.1005	574	1.742E-3	-10.29
0.2039	592	1.689E-3	-9.549
0.3216	612.5	1.633E-3	-9.045
0.5578	629	1.59E-3	-8.376
0.7789	644.5	1.552E-3	-7.877
0.9045	654	1.529E-3	-7.569
0.9548	664	1.506E-3	-7.405
0.2613	602	1.661E-3	-9.278
0.6719	637	1.57E-3	-8.115

TABLE IIIc - 2.6 Cu-NaMOR (N&8%)

Best-fit equation: ln k = -18569.39(1/T) + 22.47

Corr. Coefficient = -0.9989 ; t-factor = -50.92

$\Delta G^{\ddagger}$ (660K) = 192.66 kJ/mol ; $T_{(0.5\alpha)}$ = 644.6 K

DATA FOR ORDER 1.08 AND E_A 154385.8 J/mol

α	T/K	1/T	ln k
1.37E-2	567	1.764E-3	-10.28
4.79E-2	588	1.701E-3	-9.005
0.1096	609	1.642E-3	-8.141
0.2534	628	1.592E-3	-7.211
0.5206	646	1.548E-3	-6.27
0.6986	655	1.527E-3	-5.762
0.8288	666	1.502E-3	-5.353
0.9384	681	1.468E-3	-4.854

TABLE IIIc - 2.7 Cu-H MOR (A&A)

Best-fit equation: ln k = -16854.30(1/T) + 22.24

Corr. Coefficient = -0.9979 ; t-factor = -43.39

$\Delta G^{\ddagger}$ (660K) = 180.33 kJ/mol ; $T_{(0.5\alpha)}$ = 642.7 K

DATA FOR ORDER 1.52 AND E_A 140126.6 J/mol

α	T/K	1/T	ln k
8E-3	546.5	1.83 E-3	-8.763
2.11E-2	562	1.779E-3	-7.784
5.9E-2	575.5	1.738E-3	-6.725
0.1013	593	1.686E-3	-6.15
0.2025	609	1.642E-3	-5.368
0.3376	627	1.595E-3	-4.719
0.5189	644.5	1.552E-3	-4.057
0.7173	661	1.513E-3	-3.361
0.886	680	1.471E-3	-2.549
0.9578	695.5	1.438E-3	-1.856

TABLE IIIc - 2.8 Cu-HMOR (A&4%)

Best-fit equation: ln k = -13966.31(1/T) + 15.51

Corr. Coefficient = -0.9997 ; t-factor = -116.02

$\Delta G^{\ddagger}$ (660K) = 192.79 kJ/mol ; $T_{(0.5\alpha)}$ = 635.3 K

DATA FOR ORDER 1.08 AND E_A 116115.9 J/mol

α	T/K	1/T	ln k
5.096E-2	565.5	1.768E-3	-9.114
0.1083	587	1.704E-3	-8.327
0.1974	603.5	1.657E-3	-7.671
0.2866	613.5	1. 63E-3	-7.237
0.4076	627	1.595E-3	-6.791
0.535	638.5	1.566E-3	-6.402
0.6529	647	1.546E-3	-6.067
0.7707	658	1. 52E-3	-5.719
0.8917	671	1. 49E-3	-5.276
0.9427	680	1.471E-3	-4.999
0.9682	688	1.453E-3	-4.787

TABLE IIIc - 2.9 Cu-HMOR (A&8%)

Best-fit equation: ln k = -17635.30(1/T) + 24.65

Corr. Coefficient = -0.9970 ; t-factor = -36.36

$\Delta G^{\ddagger}$ (660K) = 174.11 kJ/mol ; $T_{(0.5\alpha)}$ = 635.3 K

DATA FOR ORDER 1.74 AND E_A 146619.9 J/mol

α	T/K	1/T	ln k
6.94E-3	537	1.862E-3	-7.924
1.39E-2	558	1.792E-3	-7.224
4.86E-2	578	1. 73E-3	-5.941
0.1458	599	1.669E-3	-4.749
0.2917	618	1.618E-3	-3.894
0.4514	628	1.592E-3	-3.24
0.5972	650	1.538E-3	-2.7
0.75	664	1.506E-3	-2.077
0.8681	675	1.481E-3	-1.413
0.9236	684	1.462E-3	-0.9172

TABLE IIIc - 2.10 Cu-HMOR (N&A)

Best-fit equation: ln k = -20801.99(1/T) + 28.56

Corr. Coefficient = -0.9982 ; t-factor = -43.95

$\Delta G^{\ddagger}$ (660K) = 177.34 kJ/mol ; $T_{(0.5\alpha)}$ = 640K

DATA FOR ORDER 1.52 AND E_A 172947.7 J/mol

α	T/K	1/T	ln k
4.23E-3	550	1.818E-3	-9.41
1.28E-2	560	1.786E-3	-8.296
5.56E-2	588	1.701E-3	-6.794
0.1496	609	1.642E-3	-5.725
0.355	630	1.587E-3	-4.656
0.6624	651	1.536E-3	-3.569
0.889	666	1.502E-3	-2.534
0.944	677	1.477E-3	-2.047
0.947	690	1.449E-3	-1.558

TABLE IIIc - 2.11 Cu-HMOR (N&4%)

Best-fit equation: ln k
-10678.79(1/T) + 8.91

Corr. Coefficient = -0.9987 ; t-factor = -51.30

$\Delta G^{\ddagger}$ (660K) = 230.54 kJ/mol ; $T_{(0.5\alpha)}$ = 612.5 K

DATA FOR ORDER 0.64 AND E_A 88783.42 J/mol

α	T/K	1/T	ln k
3.54E-2	524	1.908E-3	-11.36
8.08E-2	553	1.808E-3	-10.52
0.1818	577.5	1.732E-3	-9.668
0.3838	603	1.658E-3	-8.837
0.5858	619.5	1.614E-3	-8.307
0.6967	628	1.592E-3	-8.057
0.7978	636	1.572E-3	-7.831
0.8889	646	1.548E-3	-7.608
0.9419	654	1.529E-3	-7.449

TABLE IIIc - 2.12 Cu-HMOR (N&8%)

Best-fit equation: ln k = -18763.121/T) + 25.16

Corr. Coefficient = -0.9997 ; t-factor = -112.95

$\Delta G^{\ddagger}$ (660K) = 179.33 kJ/mol ; $T_{(0.5\alpha)}$ = 617.2 K

DATA FOR ORDER 1.30 AND E_A 155996.6 J/mol

α	T/K	1/T	ln k
6.25E-3	534	1.873E-3	-10.05
3.75E-2	561	1.783E-3	-8.238
0.1125	580	1.724E-3	-7.087
0.2813	601	1.664E-3	-6.037
0.5375	620	1.613E-3	-5.121
0.7125	632	1.582E-3	-4.566
0.8125	640	1.563E-3	-4.202
0.8813	646	1.548E-3	-3.886
0.9313	654	1.529E-3	-3.566
0.975	663	1.508E-3	-3.07

Table IIId - 1.1 Cu-Ni-NaM(1) (A+A)

Best-fit equation: ln k = -14391.36(1/T) + 14.49

Corr. Coefficient = -0.9970 ; t-factor = -40.46

$\Delta G^{\ddagger}$ (660K) = 201.79 kJ/mol ; $T_{(0.5\alpha)}$ = 692K

DATA FOR ORDER 1.08 AND E_A 119649.7 J/MOL

α	T/K	1/T	ln k
2.165E-2	591	1.692E-3	-9.775
4.762E-2	608	1.645E-3	-8.972
6.061E-2	630	1.587E-3	-8.723
0.1602	649	1.541E-3	-7.692
0.303	670	1.493E-3	-6.958
0.4589	688	1.453E-3	-6.416
0.5931	701.5	1.426E-3	-6.024
0.6861	711	1.406E-3	-5.759
0.79	723	1.383E-3	-5.445
0.8636	730	1. 37E-3	-5.183
0.9156	739	1.353E-3	-4.948
0.9545	748	1.337E-3	-4.699

Table IIId - 1.2 Cu-Ni-NaM(1) (A+4%)

Best-fit equation: ln k = -14388.42 (1/T) + 15.77

Corr. Coefficient = -0.9988 ; t-factor = -54.16

$\Delta G^{\ddagger}$ (660K) = 195.05 kJ/mol ; $T_{(0.5\alpha)}$ = 694K

DATA FOR ORDER 1.30 AND E_A 119625.3 J/MOL

α	T/K	1/T	ln k
4.78E-2	607	1.647E-3	-7.790
0.1019	634	1.577E-3	-6.995
0.1911	654	1.529E-3	-6.3
0.3376	675	1.481E-3	-5.606
0.4905	693	1.443E-3	-5.072
0.6943	713	1.403E-3	-4.428
0.809	725	1.379E-3	-4.018
0.9045	742	1.348E-3	-3.554
0.9618	763	1.311E-3	-3.069

Table IIId - 1.3 Cu-Ni-NaM(1) (A+8%)

Best-fit equation: ln k = -22427.06(1/T) + 31.09

Corr. Coefficient = -0.9963 ; t-factor = -30.80

$\Delta G^{\ddagger}$ (660K) = 178.13 kJ/mol ; $T_{(0.5\alpha)}$ = 673.4 K

DATA FOR ORDER 1.96 AND E_A 186458.6 J/MOL

α	T/K	1/T	ln k
1.27E-2	600	1.667E-3	-6.467
4.46E-2	618	1.618E-3	-5.179
0.121	633	1. 58E-3	-4.099
0.2166	648	1.543E-3	-3.404
0.3694	666	1.502E-3	-2.658
0.4968	673	1.486E-3	-2.142
0.7006	698	1.433E-3	-1.292
0.7898	707	1.414E-3	0.8289
0.9299	725	1.379E-3	0.3974

Table IIId - 1.4 Cu-Ni-NaM(1) (N+A)

Best-fit equation: ln k = -14781.86(1/T) + 14.92

Corr. Coefficient = -0.9990 ; t-factor = -71.67

$\Delta G^{\ddagger}$ (660K) = 203 kJ/mol ; $T_{(0.5\alpha)}$ = 702K

DATA FOR ORDER 1/08 AND E_A 122896.4 J/MOL

α	T/K	1/T	ln k
1.73E-2	593	1.686E-3	-9.864
3.03E-2	613.5	1. 63E-3	-9.296
7.9E-2	634.5	1.576E-3	-8.31
0.1255	655	1.527E-3	-7.82
0.2814	678	1.475E-3	-6.91
0.489	701	1.427E-3	-6.188
0.675	718	1.393E-3	-5.654
0.775	730	1. 37E-3	-5.356
0.8615	739	1.353E-3	-5.054
0.9048	746	1. 34E-3	-4.865
0.9351	752	1. 33E-3	-4.699
0.961	761.5	1.313E-3	-4.507

Table IIId - 1.5 Cu-Ni-NaM(1) (N+4%)

Best-fit equation: ln k = -17902.44(1/T) + 21.92

Corr. Coefficient = -0.9970 ; t-factor = -40.83

$\Delta G^{\ddagger}$ (660K) = 190.44 kJ/mol ; $T_{(0.5\alpha)}$ = 692K

DATA FOR ORDER 1.52 AND E_A 148840.8 J/MOL

α	T/K	1/T	ln k
1.01E-2	588	1.701E-3	-8.434
1.52E-3	605	1.653E-3	-8.021
7.1E-2	628	1.592E-3	-6.436
6.06E-2	621	1. 61E-3	-6.602
0.1212	646	1.548E-3	-5.859
0.227	662.5	1.509E-3	-5.136
0.3939	682.5	1.465E-3	-4.405
0.5758	699	1.431E-3	-3.769
0.702	711	1.406E-3	-3.324
0.8131	724	1.382E-3	-2.862
0.899	735.5	1.36E-3	-2.362
0.9242	739	1.353E-3	-2.154

Table IIId - 1.6 Cu-.Ni-NaM(1) (N+8%)

Best-fit equation: ln k = -12513.66(1/T) + 9.60

Corr. Coefficient = -0.9981 ; t-factor = -55.79

$\Delta G^{\ddagger}$ (660K) = 212.63 kJ/mol ; $T_{(0.5\alpha)}$ = 688.3 K

DATA FOR ORDER 0.64 AND E_A 104038.6 J/MOL

α	T/K	1/T	ln k
7.92E-3	559	1.789E-3	-12.82
1.42E-2	568	1.761E-3	-12.23
2.12E-2	585	1.709E-3	-11.83
4.26E-2	602	1.661E-3	-11.13
5.67E-2	618	1.618E-3	-10.84
9.22E-2	634	1.577E-3	-10.34
0.156	647	1.546E-3	-9.788
0.2553	661	1.513E-3	-9.258
0.3901	678	1.475E-3	-8.776
0.539	692	1.445E-3	-8.376
0.6312	702	1.425E-3	-8.16
0.7447	713	1.403E-3	-7.908
0.8298	723	1.383E-3	-7.714
0.9078	735	1.361E-3	-7.514

Table IIId - 1.7 Cu-Ni-HM(1)

Best-fit equation: ln k = -13191.14(1/T) + 13.10

Corr. Coefficient = -0.9989 ; t-factor = -66.64

$\Delta G^{\ddagger}$ (660K) = 199.50 kJ/mol ; $T_{(0.5\alpha)}$ = 688.5 K

DATA FOR ORDER 1.08 AND E_A 109671.1 J/MOL

α	T/K	1/T	ln k
1.27E-2	561.5	1.781E-3	-10.17
2.331E-2	586	1.706E-3	-9.552
5.085E-2	606.5	1.649E-3	-8.757
0.1144	630	1.587E-3	-7.909
0.2627	656	1.524E-3	-6.982
0.3877	672	1.488E-3	-6.499
0.5233	688	1.453E-3	-6.076
0.6674	702.5	1.423E-3	5.666
0.7966	718	1.393E-3	-5.276
0.875	728	1.374E-3	-4.99
0.928	739	1.353E-3	-4.732
0.9619	748.5	1.336E-3	-4.489

Table IIId - 1.8 Cu-Ni-HM(1) (A+4%)

Best-fit equation: ln k = -16078.36(1/T) + 18.64

Corr. Coefficient = -0.9985 ; t-factor = -48.13

$\Delta G^{\ddagger}$ (660K) = 193.62 kJ/mol ; $T_{(0.5\alpha)}$ = 674.2 K

DATA FOR ORDER 1.30 AND E_A 133675.5 J/MOL

α	T/K	1/T	ln k
2.87E-2	591	1.692E-3	-8.554
7.18E-2	613	1.631E-3	-7.608
0.1675	633	1.58E-3	-6.691
0.3014	652	1.534E-3	-5.993
0.4785	672	1.488E-3	-5.352
0.627	687	1.456E-3	-4.884
0.77	701	1.427E-3	-4.408
0.9238	714.5	1.4E-3	-3.666
0.9667	734.5	1.361E-3	-3.245

Table IIId - 1.9 Cu-Ni-HM(1) (A+8%)

Best-fit equation: ln k = -13370.33(1/T) + 13.55

Corr. Coefficient = -0.9977 ; t-factor = -43.77

$\Delta G^{\ddagger}$ (660K) = 198.69 kJ/mol ; $T_{(0.5\alpha)}$ = 675 K

DATA FOR ORDER 1.08 AND E_A 111160.9 J/MOL

α	T/K	1/T	ln k
0.1181	615	1.626E-3	-8.006
0.1458	630	1.587E-3	-7.778
0.2361	645	1.55E-3	-7.238
0.3264	657	1.522E-3	-6.85
0.4097	667	1.499E-3	-6.556
0.5208	677	1.477E-3	-6.214
0.6319	687	1.456E-3	-5.897
0.7431	699	1.431E-3	-5.575
0.8333	709	1.41E-3	-5.281
0.9028	720	1.389E-3	-4.996
0.9514	731	1.368E-3	-4.707

Table IIId - 1.10 Cu-Ni-HM(1) (N+A)

Best-fit equation: ln k = -21100.02(1/T) + 26.08

Corr. Coefficient = -0.9986 ; t-factor = -56.70

$\Delta G^{\ddagger}$ (660K) = 194.58 kJ/mol ; $T_{(0.5\alpha)}$ = 676.5 K

DATA FOR ORDER 1.74 AND E_A 175425.5 J/MOL

α	T/K	1/T	ln k
4.3E-3	575	1.739E-3	-10.69
1.3E-2	592	1.689E-3	-9.572
5.58E-2	613.5	1.63E-3	-8.077
0.133	635	1.575E-3	-7.134
0.3004	655	1.527E-3	-6.135
0.4936	676	1.479E-3	-5.363
0.412	666	1.502E-3	-5.671
0.7124	691.5	1.446E-3	-4.524
0.837	706	1.416E-3	-3.9
0.9142	717	1.395E-3	-3.3
0.9571	727.5	1.375E-3	-2.712

Table IIId - 1.11 Cu-Ni-HM(1) (N+4%)

Best-fit equation: ln k = -17322.75(1/T) + 20.04

Corr. Coefficient = -0.9982 ; t-factor = -50.05

$\Delta G^{\ddagger}$ (660K) = 196.39 kJ/mol ; $T_{(0.5\alpha)}$ = 689.3 K

DATA FOR ORDER 1.30 AND E_A 144021.38J/MOL

α	T/K	1/T	ln k
1.493E-2	591	1.692E-3	-9.098
3.98E-2	618	1.618E-3	-8.101
0.1094	640	1.563E-3	-7.041
0.214	661	1.513E-3	-6.291
0.4129	682	1.466E-3	-5.453
0.617	699	1.431E-3	-4.797
0.771	710	1.408E-3	-4.286
0.893	725	1.379E-3	-3.745
0.9403	734	1.362E-3	-3.415
0.965	743	1.346E-3	-3.149
0.975	758	1.319E-3	-2.994

Table IIId - 1.12 Cu-Ni-HM(1) (N+8%)

Best-fit equation: ln k = -15998.88(1/T) + 17.35

Corr. Coefficient = -0.9946 ; t-factor = -28.73

$\Delta G^{\ddagger}$ (660K) = 199.20 kJ/mol ; $T_{(0.5\alpha)}$ = 675.7 K

DATA FOR ORDER 1.08 AND E_A 133014.6 J/MOL

α	T/K	1/T	ln k
6.54E-3	558	1.792E-3	-10.96
1.96E-2	600	1.667E-3	-9.859
6.54E-2	616	1.623E-3	-8.628
0.1177	633	1.58E-3	-8.01
0.2157	647	1.546E-3	-7.342
0.3726	664	1.506E-3	-6.682
0.5033	676	1.479E-3	-6.266
0.6928	692	1.445E-3	-5.724
0.8039	703	1.422E-3	-5.383
0.8954	713	1.403E-3	-5.031
0.9477	725	1.379E-3	-4.735

TABLE IIId - 2.1 Cu-Ni-NaM(2) (A&A)

Best-fit equation: ln k = -14410.87(1/T) + 16.73

Corr. Coefficient = -0.9989 ; t-factor = -63.17

$\Delta G^{\ddagger}$ (660K) = 190.11 kJ/mol ; $T_{(0.5\alpha)}$ = 661 K

DATA FOR ORDER 1.30 AND E_A 119811.9 J/mol

α	T/K	1/T	ln k
1.087E-2	554	1.805E-3	-9.394
3.261E-2	572	1.748E-3	-8.281
4.89E-2	587	1.704E-3	-7.865
0.1033	603	1.658E-3	-7.079
0.1576	618	1.618E-3	-6.617
0.2826	638	1.567E-3	-5.932
0.4783	659	1.517E-3	-5.21
0.6196	672	1.488E-3	-4.765
0.788	690	1.449E-3	-4.199
0.8587	698	1.433E-3	-3.901
0.9294	709	1.41E-3	-3.481

TABLE IIId - 2.2 Cu-Ni-NaM(2) (A&4%)

Best-fit equation: ln k = -20737.45(1/T) + 27.83

Corr. Coefficient = -0.9955 ; t-factor = -31.43

$\Delta G^{\ddagger}$ (660K) = 181.27 kJ/mol ; $T_{(0.5\alpha)}$ = 673.5 K

DATA FOR ORDER 1.74 AND E_A 172411.1

α	T/K	1/T	ln k
9.524E-3	590	1.695E-3	-7.593
4.762E-2	610	1.639E-3	-5.949
0.1191	630	1.587E-3	-4.965
0.2857	647	1.546E-3	-3.909
0.3905	662	1.511E-3	-3.461
0.5524	679	1.473E-3	-2.853
0.6952	693	1.443E-3	-2.303
0.7714	702	1.425E-3	-1.962
0.8714	713	1.403E-3	-1.375
0.9333	723	1.383E-3	0.7871
0.9714	735	1.361E-3	-9.043E-2

TABLE IIId - 2.3 Cu-Ni-NaM(2) (2.3)

Best-fit equation: ln k = -12718.15(1/T) + 11.83

Corr. Coefficient = -0.9987 ; t-factor = -63.74

$\Delta G^{\ddagger}$ (660K) = 202.65 kJ/mol ; $T_{(0.5\alpha)}$ = 660.4 K

DATA FOR ORDER 0.86 AND E_A 105738.7 J/mol

α	T/K	1/T	ln k
6.85E-3	537	1.862E-3	-11.93
2.06E-2	555	1.802E-3	-10.83
2.74E-2	570	1.754E-3	-10.54
4.79E-2	585	1.709E-3	-9.971
7.53E-2	599	1.669E-3	-9.506
0.137	617	1.621E-3	-8.879
0.2534	635	1.575E-3	-8.204
0.363	647	1.546E-3	-7.781
0.4863	659	1.517E-3	-7.406
0.6027	671	1.49E-3	-7.098
0.7192	683	1.464E-3	-6.802
0.8082	692	1.445E-3	-6.565
0.8904	701	1.427E-3	-6.311

TABLE IIId - 2.4 Cu-Ni-NaM(2) (N&A)

Best-fit equation: ln k = -17481.09(1/T) + 22.01

Corr. Coefficient = -0.9990 ; t-factor = -53.98

$\Delta G^{\ddagger}$ (660K) = 186 kJ/mol ; $T_{(0.5\alpha)}$ = 669 K

DATA FOR ORDER 1.52 AND E_A 145337.8 J/mol

α	T/K	1/T	ln k
2.53E-2	589	1.698E-3	-7.591
5.46E-2	610	1.639E-3	-6.799
0.1366	627	1.595E-3	-5.813
0.2568	645	1.55E-3	-5.07
0.4208	661	1.513E-3	-4.393
0.6066	680	1.471E-3	-3.751
0.765	696	1.437E-3	-3.163
0.8907	711	1.406E-3	-2.509

TABLE IIId - 2.5 Cu-Ni-NaM(2) (N&4%)

Best-fit equation: ln k = -14669.73(1/T) + 15.44

Corr. Coefficient = -0.9995 ; t-factor = -107.89

$\Delta G^{\ddagger}$ (660K) = 198.71 kJ/mol ; $T_{(0.5\alpha)}$ = 674.8 K

DATA FOR ORDER 1.08 AND E_A 121964.1 J/mol

α	T/K	1/T	ln k
1.98E-2	578	1.73E-3	-9.841
4.456E-2	602	1.661E-3	-9.017
8.42E-2	617	1.621E-3	-8.358
0.1485	635	1.575E-3	-7.751
0.2426	647	1.546E-3	-7.2
0.3713	662	1.511E-3	-6.679
0.4604	671	1.49E-3	-6.388
0.5842	683	1.464E-3	-6.025
0.6832	692	1.445E-3	-5.754
0.7871	703	1.422E-3	-5.431
0.8614	712	1.404E-3	-5.169
0.9257	723	1.383E-3	-4.869
0.9703	734	1.362E-3	-4.529

TABLE IIId - 2.6 Cu-Ni-NaM(2) (N&8%)

Best-fit equation: ln k = -12335.0(1/T) + 9.72

Corr. Coefficient = -0.9972 ; t-factor = -44.26

$\Delta G^{\ddagger}$ (660K) = 210.80 kJ/mol ; $T_{(0.5\alpha)}$ = 674.5 K

DATA FOR ORDER 0.64 AND E_A 102553.2 J/mol

α	T/K	1/T	ln k
2E-2	568	1.761E-3	-11.91
4.67E-2	589	1.698E-3	-11.05
6E-2	607	1.647E-3	-10.8
0.1	621	1.61E-3	-10.27
0.1533	636	1.572E-3	-9.829
0.2467	647	1.546E-3	-9.317
0.34	660	1.515E-3	-8.958
0.44	668	1.497E-3	-8.653
0.56	681	1.468E-3	-8.347
0.6733	690	1.449E-3	-8.088
0.78	700	1.429E-3	-7.851
0.8667	711	1.406E-3	-7.646
0.94	721	1.387E-3	-7.435

TABLE IIId - 2.7 Cu-Ni-HM(2) (A&A)

Best-fit equation: ln k = -15554.02(1/T) + 18.40

Corr. Coefficient = -0.9981 ; t-factor = -48.34

$\Delta G^{\ddagger}$ (660K) = 190.77 kJ/mol ; $T_{(0.5\alpha)}$ = 663.5 K

DATA FOR ORDER 1.30 AND E_A 129316.1 J/mol

α	T/K	1/T	ln k
2.12E-2	575	1.739E-3	-8.738
6.355E-2	595	1.681E-3	-7.611
0.1356	615	1.626E-3	-6.802
0.25	635	1.575E-3	-6.1
0.3771	649	1.541E-3	-5.574
0.5042	664	1.506E-3	-5.145
0.6017	673	1.486E-3	-4.84
0.6822	681	1.468E-3	-4.585
0.822	691	1.447E-3	-4.082
0.8941	701	1.427E-3	-3.734
0.9576	714	1.401E-3	-3.236

TABLE IIId - 2.8 Cu-Ni-HM(2) (A&4%)

Best-fit equation: ln k = -13338.35(1/T) + 14.01

Corr. Coefficient = -0.9976 ; t-factor = -43.01

$\Delta G^{\ddagger}$ (660K) = 195.79 kJ/mol ; $T_{(0.5\alpha)}$ = 665 K

DATA FOR ORDER 1.08 AND E_A 110895.0 J/mol

α	T/K	1/T	ln k
1.5E-2	553	1.808E-3	-9.869
2.5E-2	578	1.73E-3	-9.353
5.5E-2	591	1.692E-3	-8.548
0.115	613	1.631E-3	-7.775
0.21	632	1.582E-3	-7.114
0.29	644	1.553E-3	-6.736
0.43	658	1.52E-3	-6.231
0.57	672	1.488E-3	-5.814
0.675	683	1.464E-3	-5.516
0.81	697	1.435E-3	-5.103
0.911	712	1.404E-3	-4.696

TABLE IIId - 2.9 Cu-Ni-HM(2) (A&8%)

Best-fit equation: ln k = -14485.19(1/T) + 15.75

Corr. Coefficient = -0.9971 ; t-factor = -39.56

$\Delta G^{\ddagger}$ (660K) = 195.73 kJ/mol ; $T_{(0.5\alpha)}$ = 657 K

DATA FOR ORDER 1.08 AND E_A 120429.8 J/mol

α	T/K	1/T	ln k
2.66E-2	567	1.764E-3	-9.56
3.54E-2	585	1.709E-3	-9.269
7.08E-2	599	1.669E-3	-8.556
0.1504	615	1.626E-3	-7.755
0.2301	627	1.595E-3	-7.279
0.3628	645	1.55E-3	-6.727
0.5133	658	1.52E-3	-6.247
0.6903	673	1.486E-3	-5.742
0.7788	685	1.46E-3	-5.476
0.885	696	1.437E-3	-5.089
0.9469	704	1.42E-3	-4.751

TABLE IIId - 2.10 Cu-Ni-HM(2) (N&A)

Best-fit equation: ln k = -14560.38(1/T) + 17.32

Corr. Coefficient = -0.9993 ; t-factor = -89.54

$\Delta G^{\ddagger}$ (660K) = 188.54 kJ/mol ; $T_{(0.5\alpha)}$ = 647 K

DATA FOR ORDER 1.30 AND E_A 121055.0 J/mol

α	T/K	1/T	ln k
2.2E-2	559	1.789E-3	-8.762
4.43E-2	575	1.739E-3	-8.047
8.85E-2	588	1.701E-3	-7.324
0.1239	599	1.669E-3	-6.963
0.2035	612	1.634E-3	-6.406
0.2876	626	1.597E-3	-5.99
0.4159	639	1.565E-3	-5.498
0.562	653	1.531E-3	-5.025
0.6858	667	1.499E-3	-4.634
0.8407	683	1.464E-3	-4.063
0.9115	693	1.443E-3	-3.688
0.9602	706	1.416E-3	-3.267
0.9867	721	1.387E-3	-2.779

TABLE IIId - 2.11 Cu-Ni-HM(2) (N&4%)

Best-fit equation: ln k = -17303.17(1/T) + 21.07

Corr. Coefficient = -0.9998 ; t-factor = -147.58

$\Delta G^{\ddagger}$ (660K) = 190.04 kJ/mol ; $T_{(0.5\alpha)}$ = 658 K

DATA FOR ORDER 1.30 AND E_A 143858.5 J/mol

α	T/K	1/T	ln k
1.99E-2	578	1.73E-3	-8.873
5.97E-2	599	1.669E-3	-7.747
0.1393	620	1.613E-3	-6.843
0.2438	635	1.575E-3	-6.201
0.3881	650	1.538E-3	-5.605
0.5124	659	1.517E-3	-5.19
0.6468	669	1.495E-3	-4.768
0.7562	680	1.471E-3	-4.405
0.8607	691	1.447E-3	-3.98
0.9204	700	1.429E-3	-3.637
0.9652	711	1.406E-3	-3.212

TABLE IIId - 2.12 Cu-Ni-HM(2) (N&8%)

Best-fit equation: ln k = -18060.53(1/T) + 22.30

Corr. Coefficient = -0.9966 ; t-factor = -36.49

$\Delta G^{\ddagger}$ (660K) = 187.15 kJ/mol ; $T_{(0.5\alpha)}$ = 657.3 K

DATA FOR ORDER 1.30 AND E_A 150155.2 J/mol

α	T/K	1/T	ln k
6.41E-3	558	1.792E-3	-9.983
1.28E-2	578	1.73E-3	-9.287
5.77E-2	594	1.684E-3	-7.751
8.97E-2	609	1.642E-3	-7.288
0.1667	627	1.595E-3	-6.611
0.3013	641	1.56E-3	-5.909
0.4039	652	1.534E-3	-5.517
0.5321	659	1.517E-3	-5.096
0.6667	671	1.49E-3	-4.674
0.8333	684	1.462E-3	-4.073
0.9359	698	1.433E-3	-3.486

TABLE IIId - 3.1 Cu-Ni-NaM(3) (A&A)

Best-fit equation: ln k = -16455.72(1/T) + 35.40

Corr. Coefficient = -0.9960 ; t-factor = -35.10

$\Delta G^{\ddagger}$ (660K) = 106 kJ/mol ; $T_{(0.5\alpha)}$ = 682.3 K

DATA FOR ORDER 1.74 AND E_A 136812.8 J/mol

α	T/K	1/T	ln k
4.367E-3	558	1.792E-3	5.68
1.747E-2	579	1.727E-3	7.078
4.803E-2	599	1.669E-3	8.117
0.1026	621	1.61E-3	8.927
0.2009	641	1.56E-3	9.699
0.3297	648	1.543E-3	10.35
0.4542	676	1.479E-3	10.84
0.5699	692	1.445E-3	11.27
0.7205	703	1.422E-3	11.86
0.8079	713	1.403E-3	12.28
0.869	722	1.385E-3	12.66
0.9214	730	1.37E-3	13.13

TABLE IIId - 3.2 Cu-Ni-NaM(3) (A&4%)

Best-fit equation: ln k = -18937.86(1/T) + 24.87

Corr. Coefficient = -0.9994 ; t-factor = -89.41

$\Delta G^{\ddagger}$ (660K) = 183.29 kJ/mol ; $T_{(0.5\alpha)}$ = 655.2 K

DATA FOR ORDER 1.52 AND E_A 157449.3 J/mol

α	T/K	1/T	ln k
1.111E-2	570	1.754E-3	-8.385
2.78E-2	588	1.701E-3	-7.455
5.28E-2	596	1.678E-3	-6.794
0.1111	612	1.634E-3	-6.002
0.2028	626	1.597E-3	-5.318
0.3694	643	1.555E-3	-4.545
0.5194	657	1.522E-3	-4.008
0.6389	667	1.499E-3	-3.598
0.7556	677	1.477E-3	-3.162
0.85	688	1.453E-3	-2.72
0.9194	698	1.433E-3	-2.245
0.9639	710	1.408E-3	-1.708

TABLE IIId - 3.3 Cu-Ni-NaM(3) (A&B%)

Best-fit equation: ln k = -16624.10(1/T) + 21.53

Corr. Coefficient = -0.9950 ; t-factor = -31.42

$\Delta G^{\ddagger}$ (660K) = 182.10 kJ/mol ; $T_{(0.5\alpha)}$ = 650 K

DATA FOR ORDER 1.52 AND E_A 138212.7 J/mol

α	T/K	1/T	ln k
1.33E-2	554	1.805E-3	-8.21
1.99E-2	574	1.742E-3	-7.802
6.62E-2	592	1.689E-3	-6.563
0.1325	609	1.642E-3	-5.814
0.1987	620	1.613E-3	-5.349
0.2782	620	1.613E-3	-5.349
0.3775	642	1.558E-3	-4.521
0.4901	649	1.541E-3	-4.115
0.6159	661	1.513E-3	-3.685
0.7152	670	1.493E-3	-3.328
0.8278	681	1.468E-3	-2.843
0.894	690	1.449E-3	-2.452

TABLE IIId - 3.4 Cu-Ni-NaM(3) (N&A)

Best-fit equation: ln k = -16570.52(1/T) + 21.44

Corr. Coefficient = -0.9956 ; t-factor = -31.93

$\Delta G^{\ddagger}$ (660K) = 182.32 kJ/mol ; $T_{(0.5\alpha)}$ = 654.6 K

DATA FOR ORDER 1.52 AND E_A 137767.3 J/mol

α	T/K	1/T	ln k
1.322E-2	562	1.779E-3	-8.192
3.084E-2	578	1.73E-3	-7.331
8.811E-2	593	1.686E-3	-6.236
0.1762	611	1.637E-3	-5.466
0.2952	626	1.597E-3	-4.834
0.3656	642	1.558E-3	-4.543
0.5154	656	1.524E-3	-4.004
0.6696	671	1.49E-3	-3.473
0.8194	685	1.46E-3	-2.861
0.9075	697	1.435E-3	-2.327
0.9714	713	1.403E-3	-1.546

TABLE IIId - 3.5 Cu-Ni-NaM(3) (N&4%)

Best-fit equation: ln k = -14899.47(1/T) + 16.31

Corr. Coefficient = -0.9979 ; t-factor = -46.56

$\Delta G^{\ddagger}$ (660K) = 195.09 kJ/mol ; $T_{(0.5\alpha)}$ = 659.6 K

DATA FOR ORDER 1.08 AND E_A 123874.2 J/mol

α	T/K	1/T	ln k
1.282E-2	557	1.795E-3	-10.22
2.564E-2	581	1.721E-3	-9.523
6.41E-2	601	1.664E-3	-8.585
0.1436	622	1.608E-3	-7.732
0.2923	643	1.555E-3	-6.922
0.4462	657	1.522E-3	-6.376
0.6103	665	1.504E-3	-5.895
0.7333	680	1.471E-3	-5.542
0.841	693	1.443E-3	-5.19
0.9077	703	1.422E-3	-4.909
0.9487	712	1.404E-3	-4.664

TABLE IIId - 3.6 Cu-Ni-NaM(3) (N&8%)

Best-fit equation: ln k = -15961.50(1/T) + 18.15

Corr. Coefficient = -0.9987 ; t-factor = -58.16

$\Delta G^{\ddagger}$ (660K) = 194.45 kJ/mol ; $T_{(0.5\alpha)}$ = 566.2 K

DATA FOR ORDER 1.08 AND E_A 132703.9 J/mol

α	T/K	1/T	ln k
2.26E-2	570	1.754E-3	-9.73
3.76E-2	582	1.718E-3	-9.213
6.77E-2	598	1.672E-3	-8.608
9.77E-2	609	1.642E-3	-8.223
0.203	626	1.597E-3	-7.427
0.3233	639	1.565E-3	-6.877
0.4812	650	1.538E-3	-6.347
0.609	660	1.515E-3	-5.978
0.7519	671	1.49E-3	-5.564
0.8346	680	1.471E-3	-5.292
0.9173	692	1.445E-3	-4.938

TABLE IIId - 3.7 Cu-Ni-HM(3) (A&A)

Best-fit equation: ln k = -14378.02(1/T) + 16.55

Corr. Coefficient = -0.9991 ; t-factor = -69.06

$\Delta G^{\ddagger}$ (660K) = 190.80 kJ/mol ; $T_{(0.5\alpha)}$ = 664.2 K

DATA FOR ORDER 1.30 AND E_A 119538.8 J/mol

α	T/K	1/T	ln k
7.556E-2	602	1.661E-3	-7.436
5.78E-2	592	1.689E-3	-7.716
0.12	611	1.637E-3	-6.941
0.1733	621	1.61E-3	-6.534
0.2578	635	1.575E-3	-6.069
0.32	644	1.553E-3	-5.798
0.3933	652	1.534E-3	-5.521
0.4978	664	1.506E-3	-5.171
0.62	673	1.486E-3	-4.788
0.7422	688	1.453E-3	-4.389
0.8356	697	1.435E-3	-4.03

TABLE IIId - 3.8 Cu-Ni-HM(3) (A&4%)

Best-fit equation: ln k = -18584.19(1/T) + 24.29

Corr. Coefficient = -0.9997 ; t-factor = -114.52

$\Delta G^{\ddagger}$ (660K) = 183.29 kJ/mol ; $T_{(0.5\alpha)}$ = 653.5 K

DATA FOR ORDER 1.52 AND E_A 154508.9 J/mol

α	T/K	1/T	ln k
1.5436E-2	572	1.748E-3	-8.16
3.093E-2	587	1.704E-3	-7.455
9.794E-2	608	1.645E-3	-6.248
0.2474	629	1.59E-3	-5.186
0.3995	646	1.548E-3	-4.54
0.5751	659	1.517E-3	-3.927
0.6933	669	1.495E-3	-3.513
0.7887	678	1.475E-3	-3.13
0.8763	690	1.449E-3	-2.673
0.9381	701	1.427E-3	-2.17

TABLE IIId - 3.9 Cu-Ni-HM(3) (A&8%)

Best-fit equation: ln k = -13634.11(1/T) + 14.52

Corr. Coefficient = -0.9992 ; t-factor = -78.43

$\Delta G^{\ddagger}$ (660K) = 195.34 kJ/mol ; $T_{(0.5\alpha)}$ = 654.5 K

DATA FOR ORDER 1.08 AND E_A 113353.9 J/mol

α	T/K	1/T	ln k
6.99E-3	539	1.855E-3	-10.92
2.1E-2	557	1.795E-3	-9.811
3.5E-2	570	1.754E-3	-9.292
5.59E-2	585	1.709E-3	-8.812
9.79E-2	602	1.661E-3	-8.227
0.1678	616	1.623E-3	-7.646
0.2727	631	1.585E-3	-7.091
0.4336	648	1.543E-3	-6.501
0.5664	661	1.513E-3	-6.105
0.7343	677	1.477E-3	-5.624
0.8392	689	1.451E-3	-5.282
0.9161	700	1.429E-3	-4.951

TABLE IIId - 3.10 Cu-Ni-HM(3) (N&A)

Best-fit equation: ln k = -14868.35(1/T) + 31.83

Corr. Coefficient = -0.9977 ; t-factor = -41.26

$\Delta G^{\ddagger}$ (660K) = 111.55 kJ/mol ; $T_{(0.5\alpha)}$ = 642.8 K

DATA FOR ORDER 1.30 AND E_A 123615.5 J/mol

α	T/K	1/T	ln k
6.55E-2	580	1.724E-3	6.21
0.1354	596	1.678E-3	6.986
0.2096	613	1.631E-3	7.48
0.3843	627	1.595E-3	8.242
0.4411	637	1.57E-3	8.438
0.5939	652	1.534E-3	8.926
0.7467	668	1.497E-3	9.422
0.8777	682	1.466E-3	9.966
0.9476	694	1.441E-3	10.45
0.9869	711	1.406E-3	11.08

TABLE IIId - 3.11 Cu-Ni-HM(3) (N&4%)

Best-fit equation: ln k = -16779.60(1/T) + 19.71

Corr. Coefficient = -0.9972 ; t-factor = -40.07

$\Delta G^{\ddagger}$ (660K) = 192.91 kJ/mol ; $T_{(0.5\alpha)}$ = 646.8 K

DATA FOR ORDER 1.08 AND E_A 139505.6 J/mol

α	T/K	1/T	ln k
5.155E-3	546	1.832E-3	-11.14
3.093E-2	570	1.754E-3	-9.337
4.896E-2	592	1.689E-3	-8.868
0.1392	612	1.634E-3	-7.77
0.2551	626	1.597E-3	-7.088
0.3949	640	1.563E-3	-6.546
0.518	648	1.543E-3	-6.163
0.6598	659	1.517E-3	-5.759
0.7887	668	1.497E-3	-5.374
0.8892	678	1.475E-3	-5
0.9536	689	1.451E-3	-4.631

TABLE IIId - 3.12 Cu-Ni-HM(3) (N&8%)

Best-fit equation: ln k = -18461.85(1/T) + 24.54

Corr. Coefficient = -0.9974 ; t-factor = -45.83

$\Delta G^{\ddagger}$ (660K) = 180.62 kJ/mol ; $T_{(0.5\alpha)}$ = 646.8 K

DATA FOR ORDER 1.52 AND E_A 153491.8J/mol

α	T/K	1/T	ln k
6.5E-3	555	1.802E-3	-8.968
3.29E-2	573	1.745E-3	-7.326
7.24E-2	593	1.686E-3	-6.506
0.1447	609	1.642E-3	-5.752
0.2105	619	1.616E-3	-5.318
0.3092	632	1.582E-3	-4.834
0.4145	641	1.56E-3	-4.42
0.8026	672	1.488E-3	-3.002
0.6711	657	1.522E-3	-3.528
0.7697	667	1.499E-3	-3.147
0.8224	673	1.486E-3	-2.908
0.8947	681	1.468E-3	-2.484
0.9408	691	1.447E-3	-2.075

Comparison of X-ray diffraction data

Table IIIX.1 : Na/NH4-MOR : Nil

	Amminated		Hydrated	
No.	Angle	I/Io	Angle	I/Io
1	6.38	25	6.38	34
2	8.50	25	8.50	26
3	9.60	61	9.60	68
4	13.35	29	13.35	47
5	13.70	29	13.70	34
6	14.50	11	14.50	17
7	15.15	17	15.15	23
8	17.20	5	17.20	7
9	19.50	41	19.50	38
10	22.15	72	22.15	74
11	23.10	15	23.10	17
12	23.50	15	23.50	16
13	25.50	100	25.50	100
14	26.12	50	26.12	74
15	27.72	56	27.72	68
16	30.80	22	30.80	27
17	33.18	4	33.18	5
18	34.95	5	34.95	6
19	35.50	10	35.50	16
20	36.40	4	36.40	5
21	36.80	3	36.80	5
22	39.00	1	39.00	1
23	40.40	1	40.40	1
24	44.25	8	44.25	8
25	44.90	4	44.90	7
26	46.50	7	46.50	9
27	47.30	2	47.30	5
28	48.40	7	48.40	11
29	50.80	4	50.80	7
30	53.10	2	53.10	2
31	53.90	3	53.90	4
32	55.20	2	55.20	4
33	56.70	1	56.70	4
34	57.70	2	57.70	3
35	59.70	3	59.70	5

Comparison of X-ray diffraction data

Table IIIX.2 : NiNa-MOR : Air

	Activated		Hydrated	
No.	Angle	I/Io	Angle	I/Io
1	6.35	20	6.35	14
2	8.50	18	8.50	12
3	9.60	53	9.60	44
4	13.32	42	13.32	35
5	13.72	42	13.72	22
6	14.50	16	14.50	11
7	15.10	28	15.10	23
8	17.50	7	17.50	5
9	19.50	44	19.50	43
10	21.30	9	21.30	7
11	22.15	75	22.15	78
12	23.10	15	23.10	12
13	23.55	16	23.55	12
14	25.50	100	25.50	100
15	26.20	60	26.20	55
16	27.00	13	27.00	12
17	27.70	55	27.70	53
18	30.35	8	30.35	7
19	30.80	25	30.80	24
20	33.07	5	33.07	4
21	34.10	4	34.10	0
22	35.10	7	35.10	7
23	35.50	14	35.50	13
24	36.50	6	36.50	5
25	36.80	6	36.80	5
26	39.60	3	39.60	1
27	40.35	3	40.35	2
28	44.35	9	44.35	9
29	46.50	8	46.50	7
30	47.40	5	47.40	3
31	48.35	8	48.35	8
32	50.25	4	50.25	4
33	50.80	5	50.80	5
34	53.20	2	53.20	1
35	53.95	3	53.95	2
36	55.30	1	55.30	1
37	56.75	1	56.75	2
38	57.70	2	57.70	2
39	59.70	3	59.70	3
40	60.70	5	60.70	4

Comparison of X-ray diffraction data

Table IIIX.3 : NiNa-MOR : Nitrogen

	Activated		Hydrated	
No.	Angle	I/Io	Angle	I/Io
1	6.35	25	6.35	77
2	8.50	26	8.50	12
3	9.60	85	9.60	44
4	13.32	50	13.32	35
5	13.72	26	13.72	22
6	14.50	14	14.50	11
7	15.10	32	15.10	23
8	17.50	6	17.50	5
9	19.50	50	19.50	43
10	21.30	5	21.30	7
11	22.22	84	22.22	78
12	23.10	15	23.15	12
13	23.55	16	23.55	12
14	25.50	100	25.50	100
15	26.20	52	26.20	55
16	27.00	10	27.00	12
17	27.70	48	27.70	53
18	30.35	4	30.35	7
19	30.80	22	30.80	24
20	33.07	2	33.07	4
21	34.50	2	34.10	1
22	35.10	2	35.10	7
23	35.50	9	35.50	13
24	36.50	4	36.50	5
25	36.80	4	36.80	5
26	39.60	1	39.60	1
27	40.35	1	40.35	2
28	44.35	18	44.35	9
29	46.50	7	46.50	7
30	47.40	1	47.40	3
31	48.35	6	48.35	8
32	50.25	3	50.25	4
33	50.85	4	50.85	5
34	53.20	1	53.20	1
35	53.95	3	53.95	2
36	55.30	1	55.30	1
37	56.80	2	56.80	2
38	57.70	2	57.70	2

Comparison of X-ray diffraction data

Table IIIX.4 : NiNH4-MOR : Air

	Activated		Hydrated	
No.	Angle	I/Io	Angle	I/Io
1	6.35	10	6.35	18
2	8.50	16	8.50	24
3	9.50	51	9.50	79
4	13.30	36	13.30	47
5	13.70	15	13.70	20
6	14.50	11	14.50	16
7	15.10	29	15.10	41
8	17.35	8	17.35	6
9	19.50	44	19.50	66
10	21.35	6	21.35	5
11	22.20	78	22.20	98
12	23.10	14	23.10	17
13	23.50	13	23.50	17
14	25.50	100	25.50	100
15	26.18	47	26.18	65
16	27.65	47	27.65	58
17	28.80	7	28.80	9
18	30.30	6	30.30	8
19	30.80	23	30.80	30
20	33.10	5	33.10	5
21	35.10	5	35.00	8
22	35.55	12	35.55	14
23	36.50	5	36.50	7
24	36.90	3	36.90	7
25	39.60	2	39.60	3
26	40.50	2	40.50	3
27	41.60	1	41.60	3
28	44.40	9	44.40	15
29	46.40	6	46.40	11
30	48.38	8	48.40	10
31	50.20	4	50.20	5
32	50.80	5	50.80	9
33	53.20	0	53.20	3
34	53.90	3	53.90	5
35	55.20	2	55.20	4
36	56.80	3	56.80	3
37	57.70	3	57.70	4
38	59.70	4	59.70	6

Comparison of X-ray diffraction data

Table IIIX.5 : NiNH4-MOR : Nitrogen

	Activated		Hydrated	
No.	Angle	I/Io	Angle	I/Io
1	6.35	69	6.35	18
2	8.50	27	8.50	24
3	9.50	92	9.50	79
4	13.30	44	13.30	47
5	13.70	34	13.70	20
6	14.50	10	14.50	16
7	15.10	15	15.10	41
8	17.35	2	17.35	6
9	19.50	36	19.50	66
10	21.35	4	21.35	5
11	22.20	73	22.20	98
12	23.10	13	23.10	17
13	23.50	15	23.50	17
14	25.50	100	25.50	100
15	26.18	57	26.18	65
16	27.65	53	27.65	58
17	28.80	5	28.80	9
18	30.30	5	30.30	8
19	30.80	26	30.80	30
20	33.10	2	33.10	5
21	35.00	4	35.00	8
22	35.60	12	35.55	14
23	36.50	5	36.50	7
24	36.90	6	36.90	7
25	39.60	0	39.60	3
26	40.45	2	40.50	3
27	41.60	0	41.60	3
28	44.40	9	44.40	15
29	46.40	8	46.41	11
30	28.40	7	48.38	10
31	50.22	4	50.20	5
32	50.80	6	50.80	9
33	53.22	3	53.20	3
34	53.95	4	53.90	5

Comparison of X-ray diffraction data

Table IIIX.6 : CuNa-MOR : Air

	Activated		Hydrated	
No.	Angle	I/Io	Angle	I/Io
1	6.35	16	6.35	22
2	8.50	18	8.50	27
3	9.50	48	9.50	73
4	13.35	32	13.35	47
5	15.10	23	15.10	35
6	17.50	6	17.50	6
7	19.50	41	19.50	59
8	21.22	5	21.22	6
9	22.10	76	22.10	98
10	23.10	13	23.10	21
11	23.50	12	23.50	14
12	25.50	100	25.53	100
13	26.10	53	26.15	60
14	27.65	54	27.70	54
15	28.70	9	28.70	11
16	30.30	7	30.30	7
17	30.70	25	30.70	29
18	33.10	4	33.10	4
19	34.10	2	34.10	4
20	34.95	5	34.95	8
21	35.50	13	35.50	13
22	36.30	5	36.35	6
23	36.70	5	36.90	5
24	39.30	2	39.30	3
25	40.40	1	40.40	2
26	41.40	3	41.35	2
27	44.30	10	44.30	10
28	44.80	5	44.82	6
29	46.40	8	46.40	9
30	47.30	3	47.30	4
31	48.40	8	48.40	8
32	50.00	4	50.15	4
33	50.80	5	50.80	6
34	53.20	2	53.20	3
35	53.80	4	54.00	4
36	56.70	2	56.80	1
37	57.60	2	57.70	4
38	59.70	4	59.70	3
39	60.70	4	60.70	5
40	62.60	4	62.60	2

Comparison of X-ray diffraction data

Table IIIX.7 : CuNa-MOR : Nitrogen

	Activated		Hydrated	
No.	Angle	I/Io	Angle	I/Io
1	6.35	38	6.35	22
2	8.50	35	8.50	27
3	9.50	81	9.50	73
4	13.35	44	13.35	47
5	15.10	24	15.10	35
6	17.50	7	17.50	6
7	19.50	49	19.50	59
8	21.25	4	21.22	6
9	22.10	85	22.10	98
10	23.25	19	23.10	21
11	23.70	14	23.50	14
12	25.55	100	25.53	100
13	26.15	55	26.15	60
14	27.60	50	27.70	54
15	28.70	8	28.70	8
16	30.30	6	30.30	7
17	30.70	19	30.70	29
18	33.10	3	33.10	4
19	34.20	2	34.10	4
20	35.35	4	34.95	8
21	35.50	9	35.50	13
22	36.30	3	36.30	6
23	36.90	4	36.90	5
24	39.30	2	39.30	3
25	40.40	1	40.40	2
26	41.40	1	41.35	2
27	44.30	9	44.30	10
28	44.90	5	44.80	6
29	46.40	6	46.40	9
30	47.30	1	47.30	4
31	48.40	6	48.40	8
32	50.00	2	50.00	4
33	50.80	4	50.80	6
34	53.20	1	53.20	3
35	53.90	1	54.00	4
36	56.70	0	56.80	1
37	57.60	1	57.70	4
38	59.70	2	59.70	3
39	60.70	2	60.70	5

Comparison of X-ray diffraction data

Table IIIX.8 : CuNH4-MOR : Air

	Activated		Hydrated	
No.	Angle	I/Io	Angle	I/Io
1	6.35	15	6.35	17
2	8.50	21	8.50	20
3	9.55	56	9.56	71
4	13.35	38	13.35	42
5	14.50	14	14.50	13
6	15.15	29	15.15	34
7	17.50	7	17.50	6
8	19.50	47	19.50	61
9	21.30	7	21.30	5
10	22.15	83	22.15	94
11	23.10	15	23.10	17
12	23.60	14	23.60	16
13	24.70	7	24.60	7
14	25.50	100	25.50	100
15	26.15	54	26.10	60
16	27.65	52	27.70	51
17	28.10	15	28.10	15
18	28.75	9	28.75	6
19	30.80	23	30.80	24
20	33.10	4	33.10	3
21	33.95	3	33.90	4
22	35.02	6	35.00	6
23	35.55	11	35.55	11
24	36.55	4	36.90	5
25	36.90	5	36.90	5
26	39.50	2	39.50	3
27	40.40	2	40.40	2
28	44.10	1	41.10	2
29	44.35	10	44.35	9
30	45.00	5	45.10	5
31	46.45	9	46.40	8
32	47.50	3	47.40	3
33	48.40	7	48.50	7
34	50.10	4	50.10	5
35	50.85	6	50.82	6
36	53.15	3	53.00	3
37	54.00	3	53.90	4
38	55.30	3	55.20	3
39	56.90	2	56.75	3
40	57.70	3	57.70	3
41	59.70	3	59.70	3
42	60.80	4	60.80	5

Comparison of X-ray diffraction data

Table IIIX.9 : CuNH4-MOR : Nitrogen

	Activated		Hydrated	
No.	Angle	I/Io	Angle	I/Io
1	6.35	31	6.35	17
2	8.50	32	8.50	20
3	9.55	85	9.55	71
4	13.35	42	13.35	42
5	14.50	13	14.50	13
6	15.20	26	15.15	34
7	17.45	6	17.50	6
8	19.50	48	19.50	61
9	21.30	3	21.30	5
10	22.30	86	22.15	94
11	23.21	15	23.10	17
12	23.60	15	23.55	16
13	24.70	6	24.60	7
14	25.50	100	25.50	100
15	26.30	53	26.10	60
16	27.70	46	27.70	51
17	28.15	15	28.10	51
18	28.80	6	28.75	6
19	30.80	21	30.80	24
20	33.10	2	33.10	3
21	33.90	0	33.90	4
22	35.30	3	35.00	6
23	35.70	9	35.55	11
24	36.60	4	36.55	4
25	37.00	3	36.90	5
26	39.58	2	39.50	3
27	40.70	1	40.40	2
28	41.70	1	41.10	2
29	44.50	10	44.30	9
30	45.20	5	45.00	5
31	46.60	4	46.40	8
32	47.60	2	47.40	3
33	48.50	5	48.50	7
34	50.10	2	50.10	5
35	50.85	4	50.82	6
36	53.30	0	53.00	3
37	54.10	2	53.90	4
38	55.10	1	55.20	3
39	57.00	1	56.75	3
40	57.80	1	57.70	3
41	59.80	3	59.70	3
42	61.10	3	60.70	5

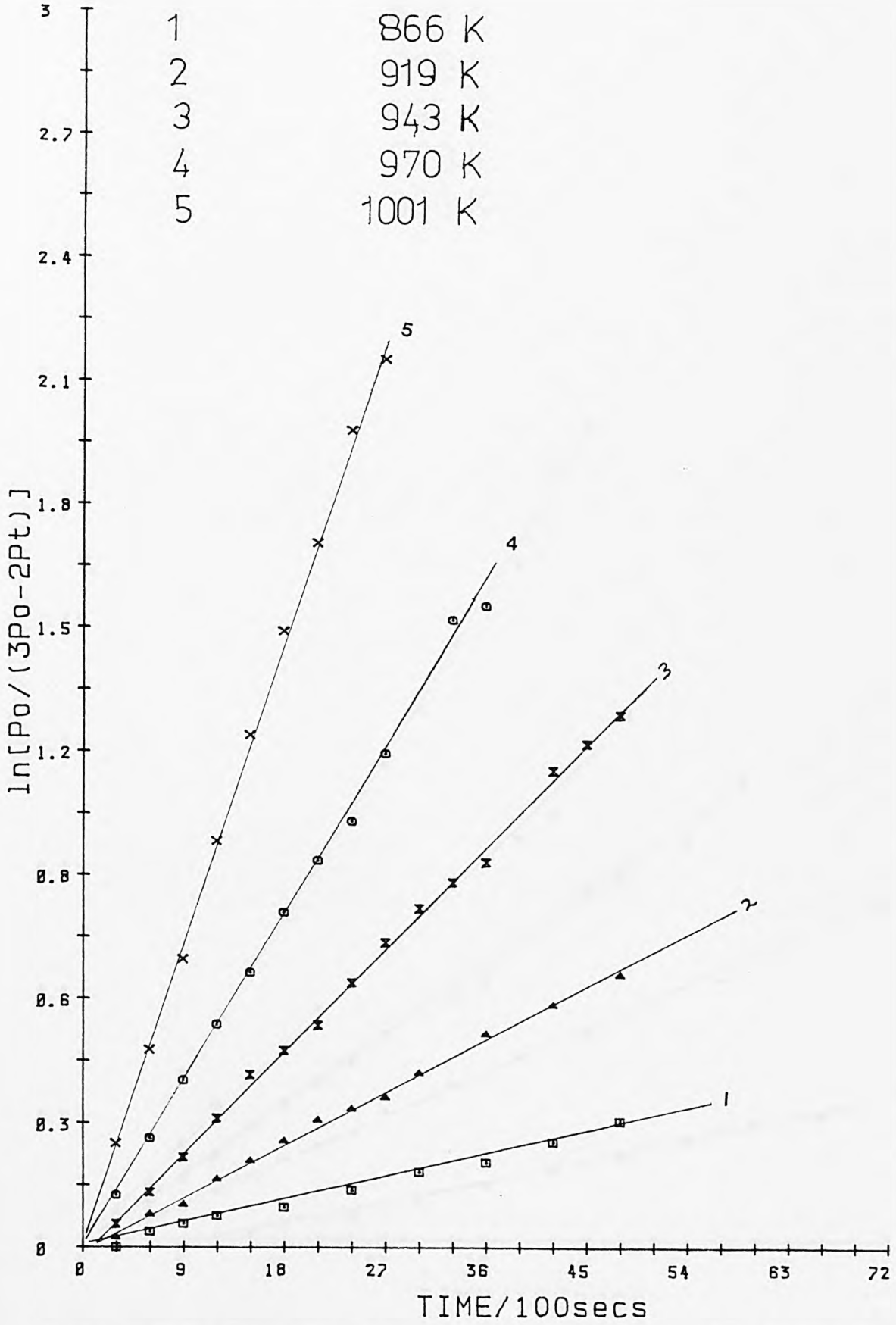

Fig.B1: Ist Order Nitrous Oxide Decomp. plots of Co-5A(1).

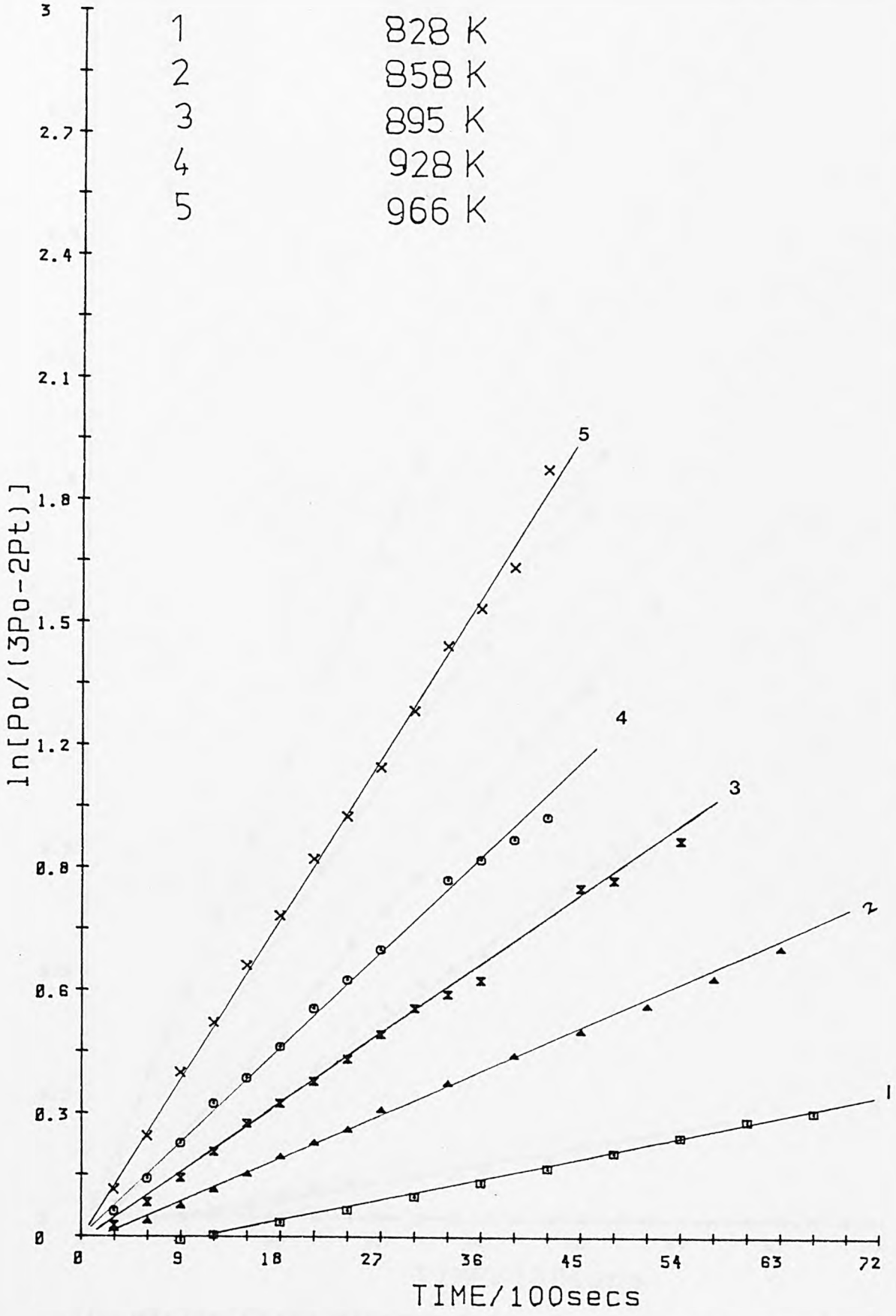

Fig.B2: Ist Order Nitrous Oxide Decomp. plots of Co-5A(2).

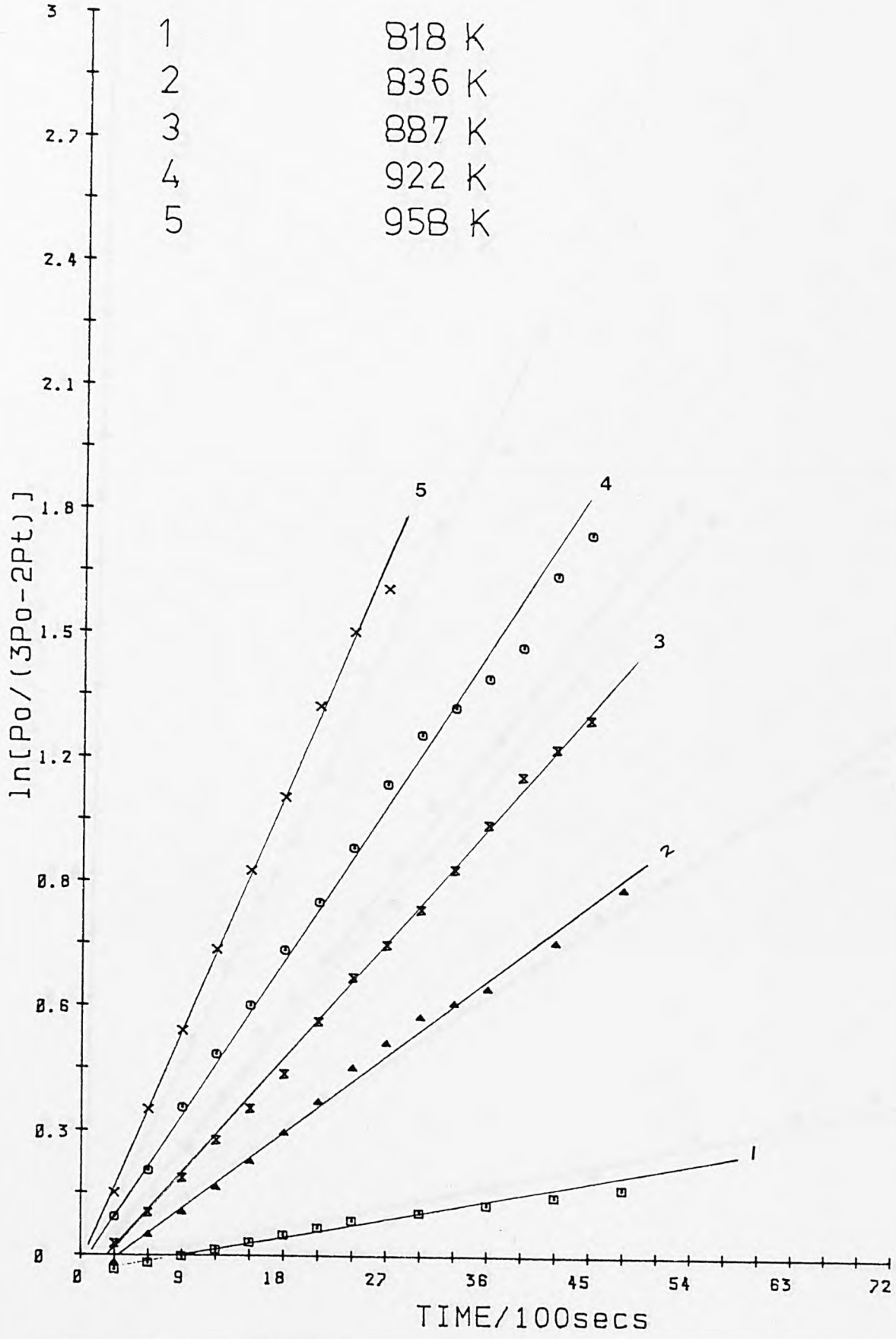

Fig.B3: Ist Order Nitrous Oxide Decomp. plots of Co-5A(3).

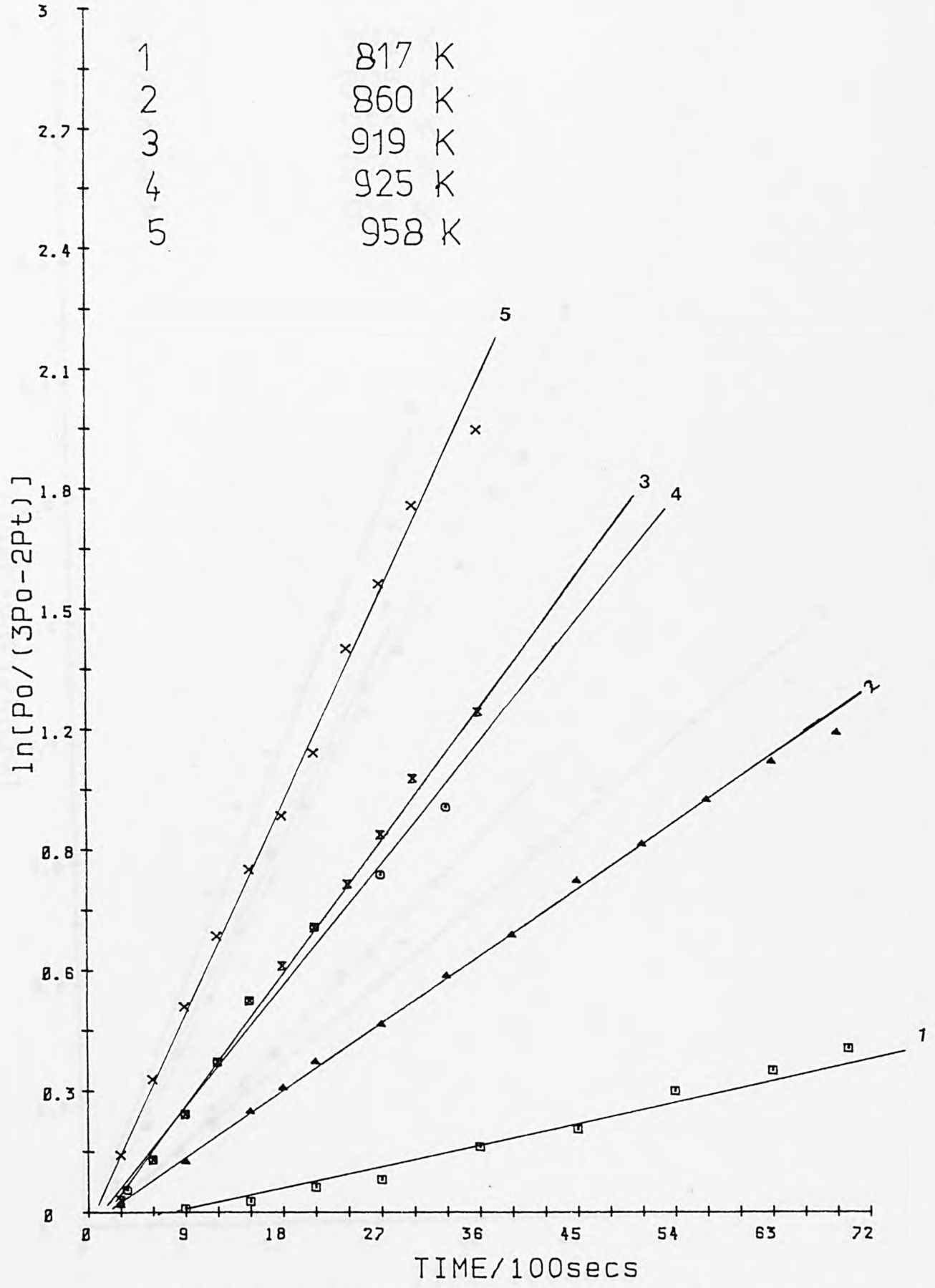

Fig.B4: Ist Order Nitrous Oxide Decomp. plots of Co-5A(4).

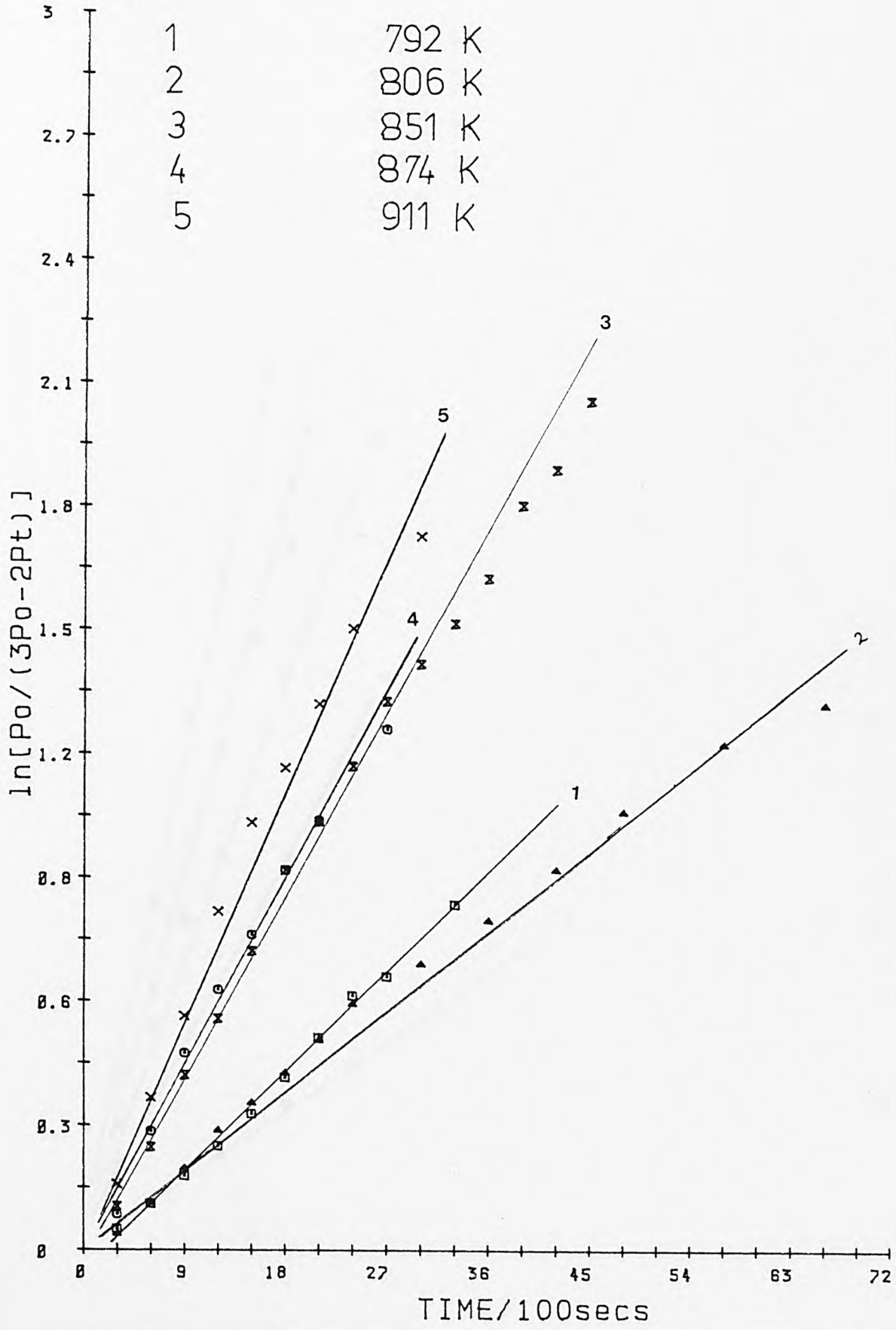

Fig.B5: Ist Order Nitrous Oxide Decomp. plots of Co-5A(5).

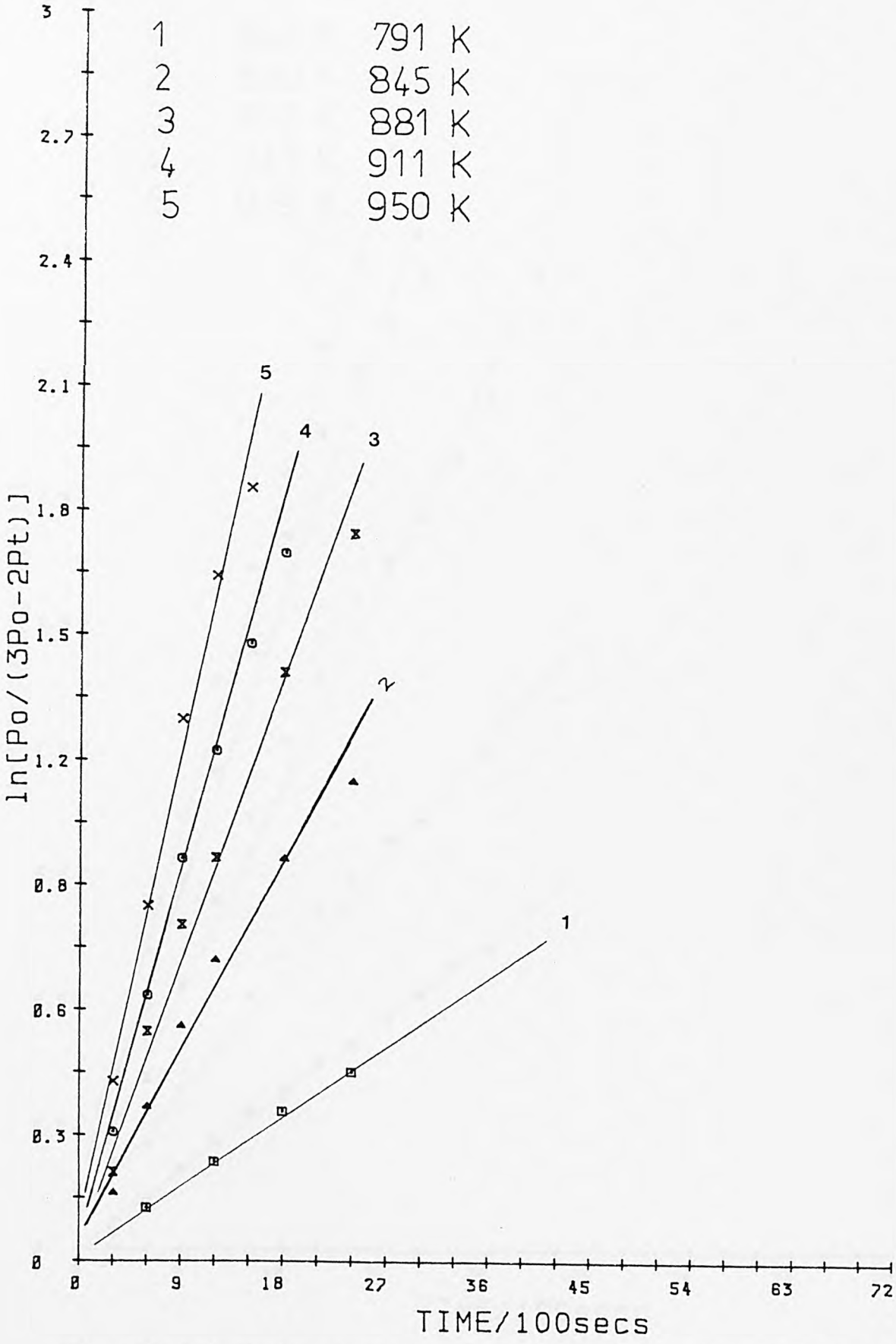

Fig.B6: Ist Order Nitrous Oxide Decomp. plots of Co-5A(6).

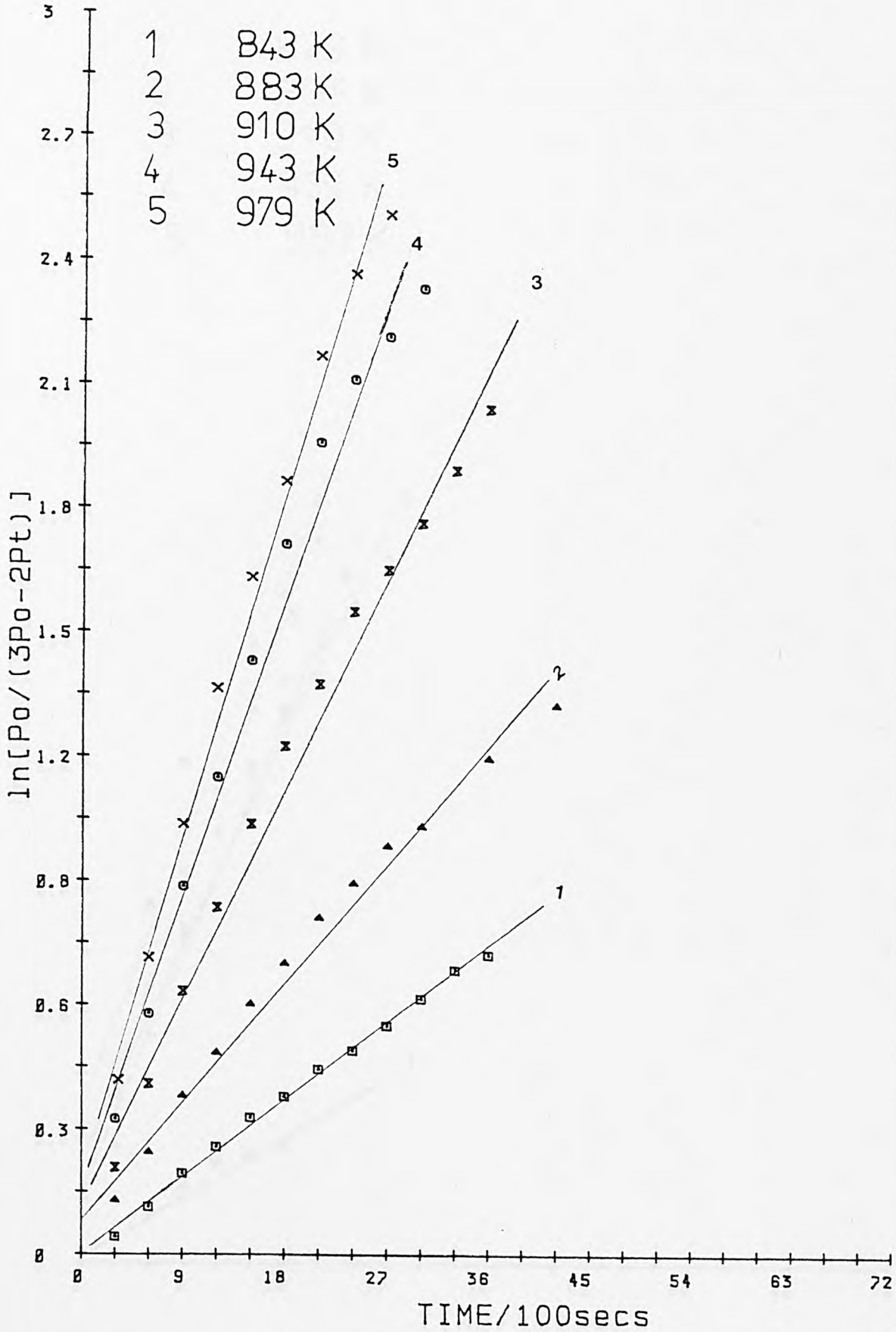

Fig.B7: Ist Order Nitrous Oxide Decomp. plots of Cu-5A(1).

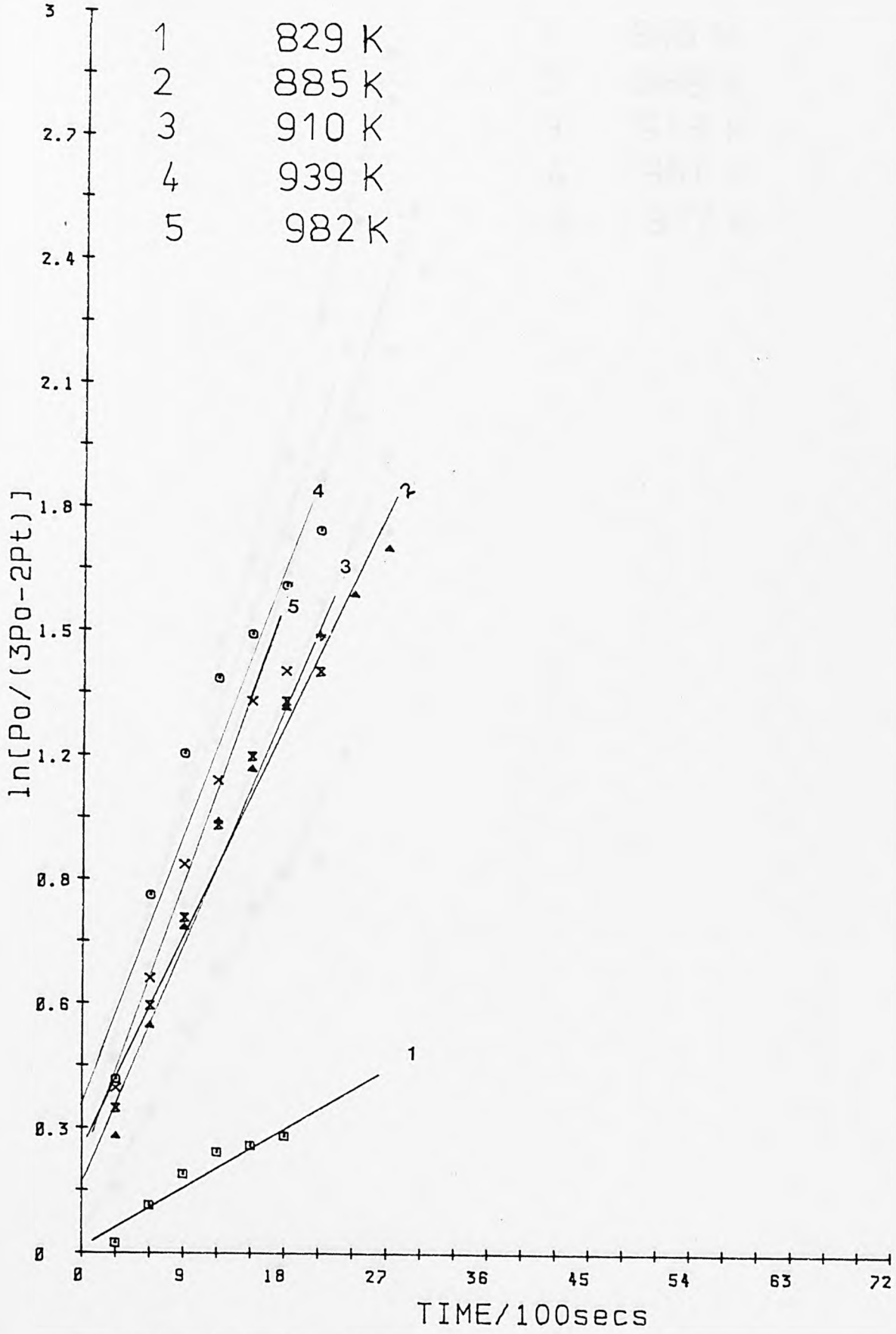

Fig.B8: Ist Order Nitrous Oxide Decomp. plots of Cu-5A(2).

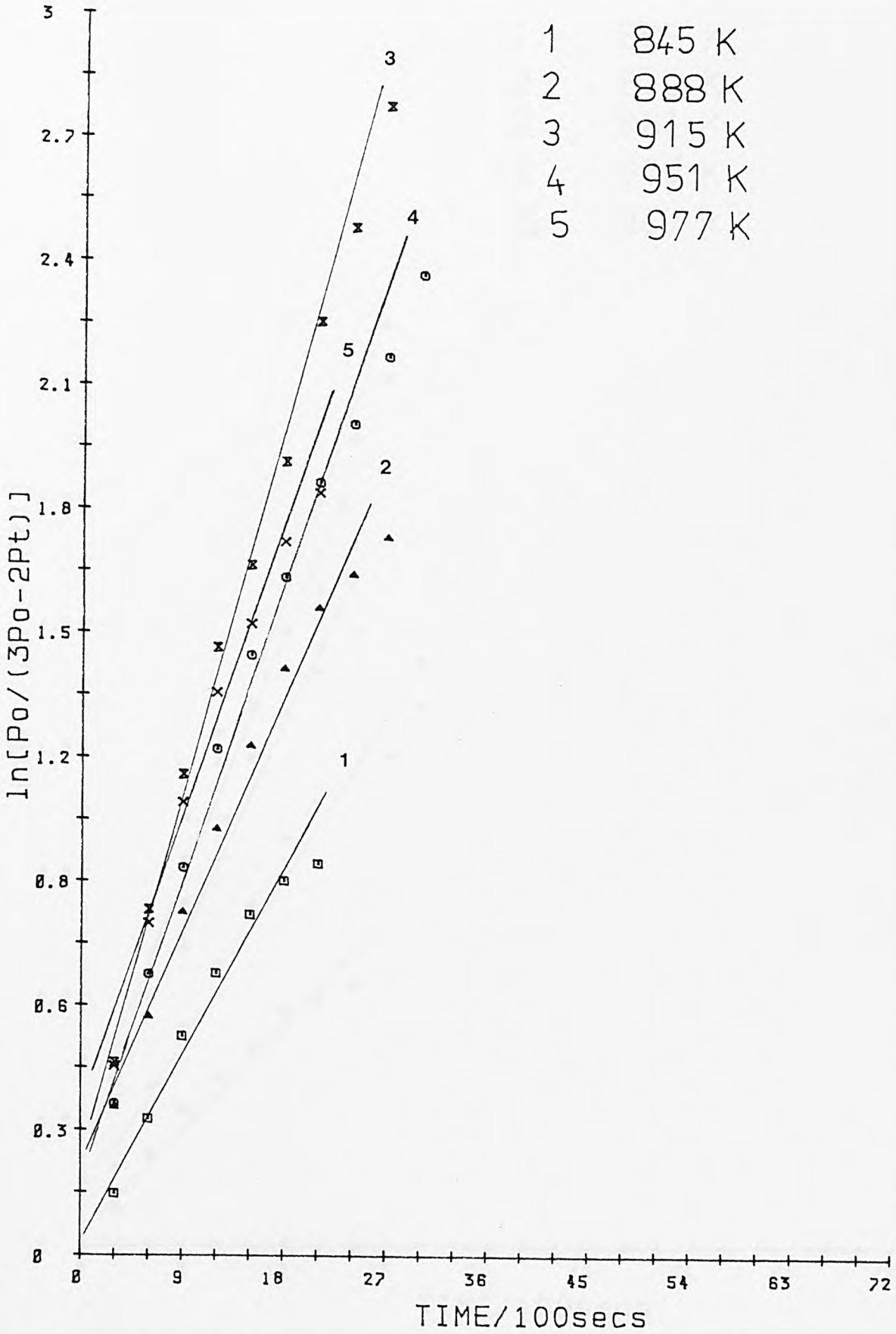

Fig.B9: Ist Order Nitrous Oxide Decomp. plots of Cu-5A(3).

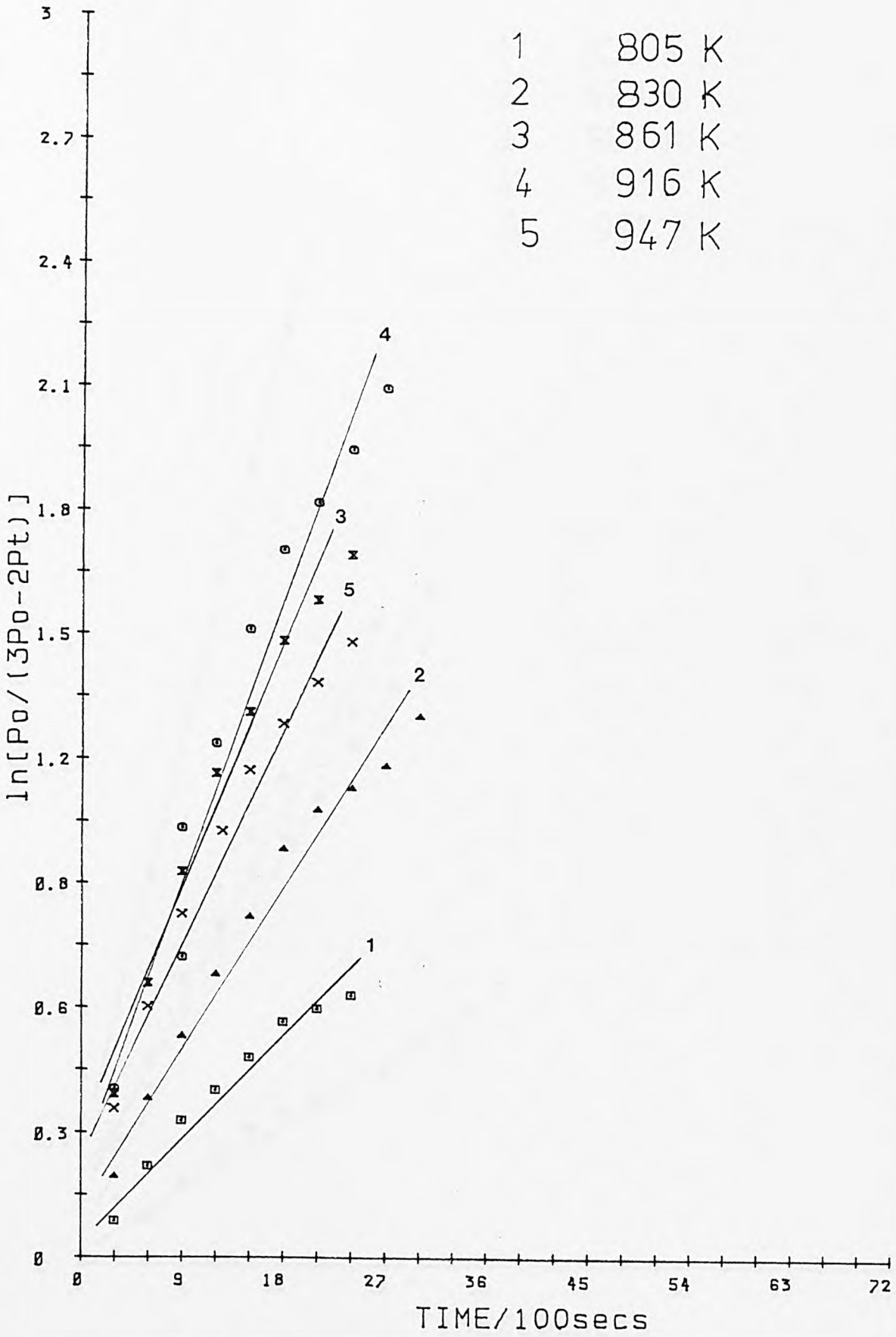

Fig.B10: Ist Order Nitrous Oxide Decomp. plots of Cu-5A(4).

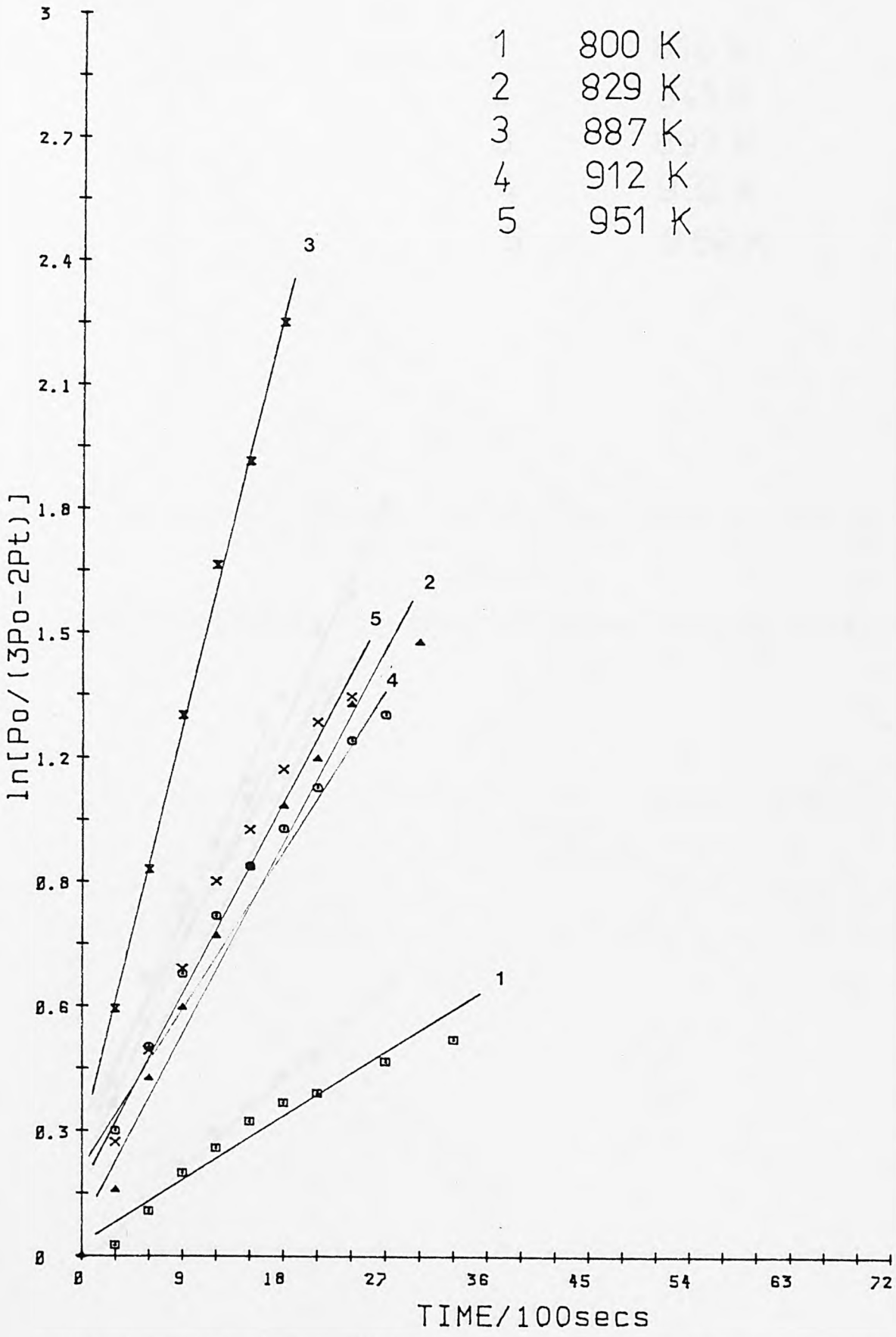

Fig.B11:Ist Order Nitrous Oxide Decomp. plots of Cu-5A(5).

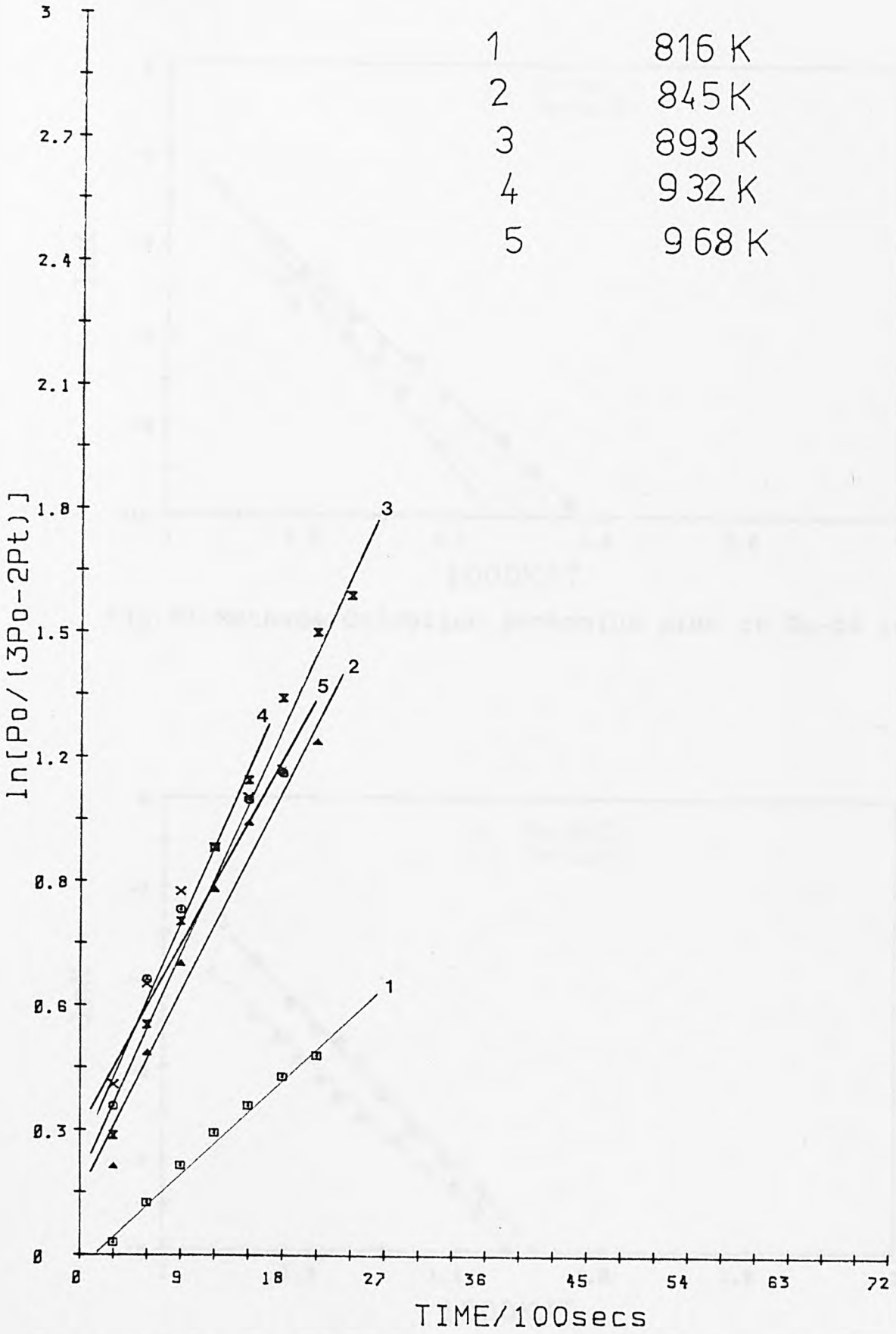

Fig.B12: Ist Order Nitrous Oxide Decomp. plots of Cu-5A(6).

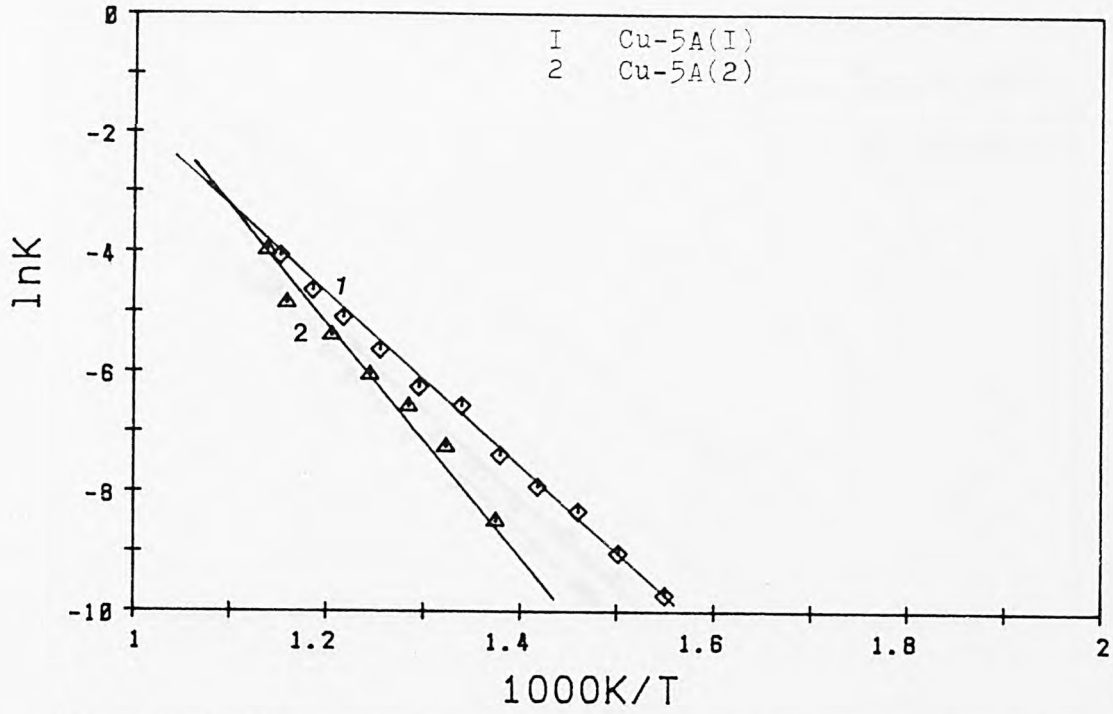

Fig.P1:Methane Oxidation Arrhenius plot of Cu-5A in air.

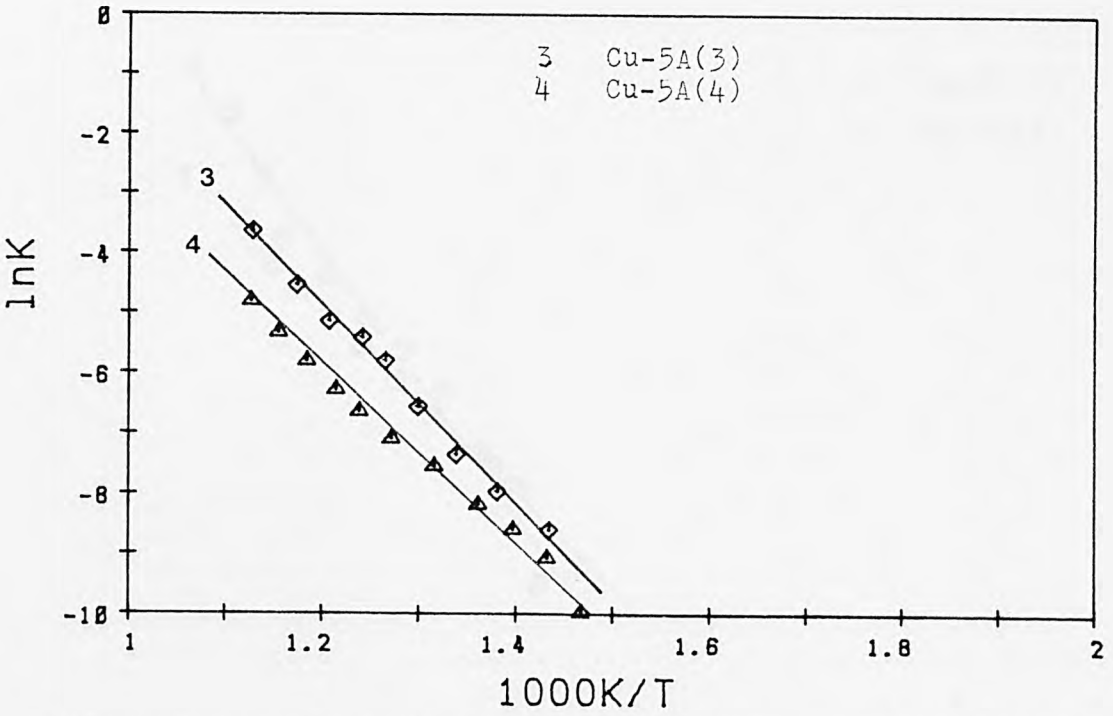

Fig.P2:Methane Oxidation Arrhenius plot of Cu-5A in air.

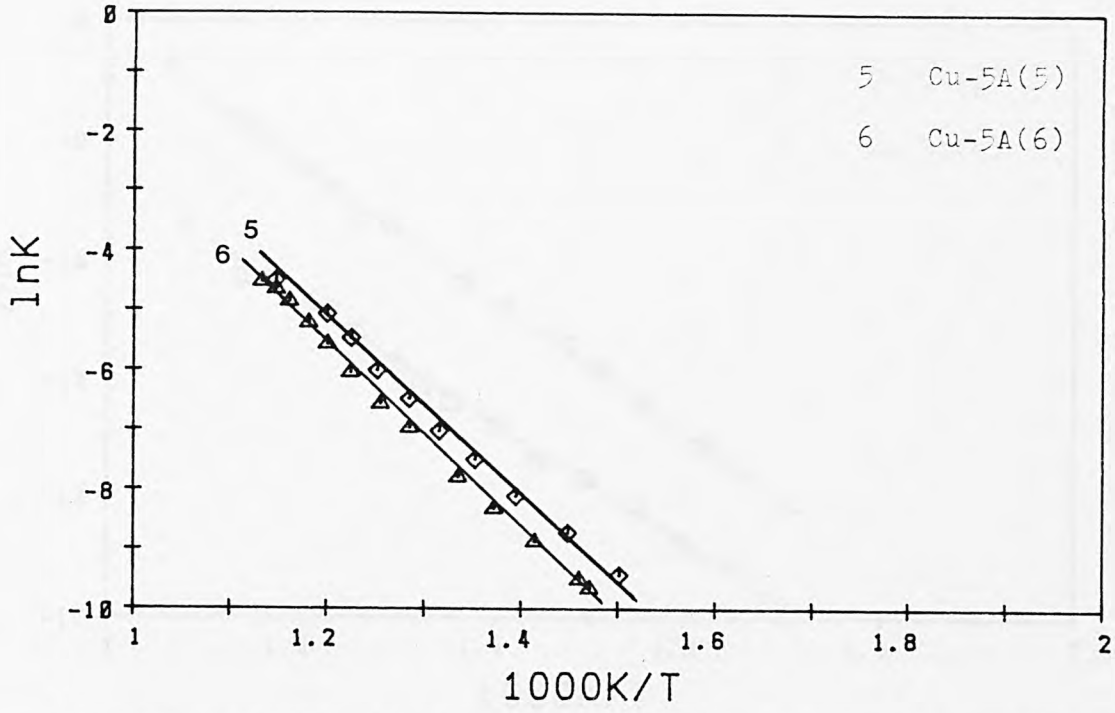

Fig.P3:Methane Oxidation Arrhenius plot of Cu-5A in air.

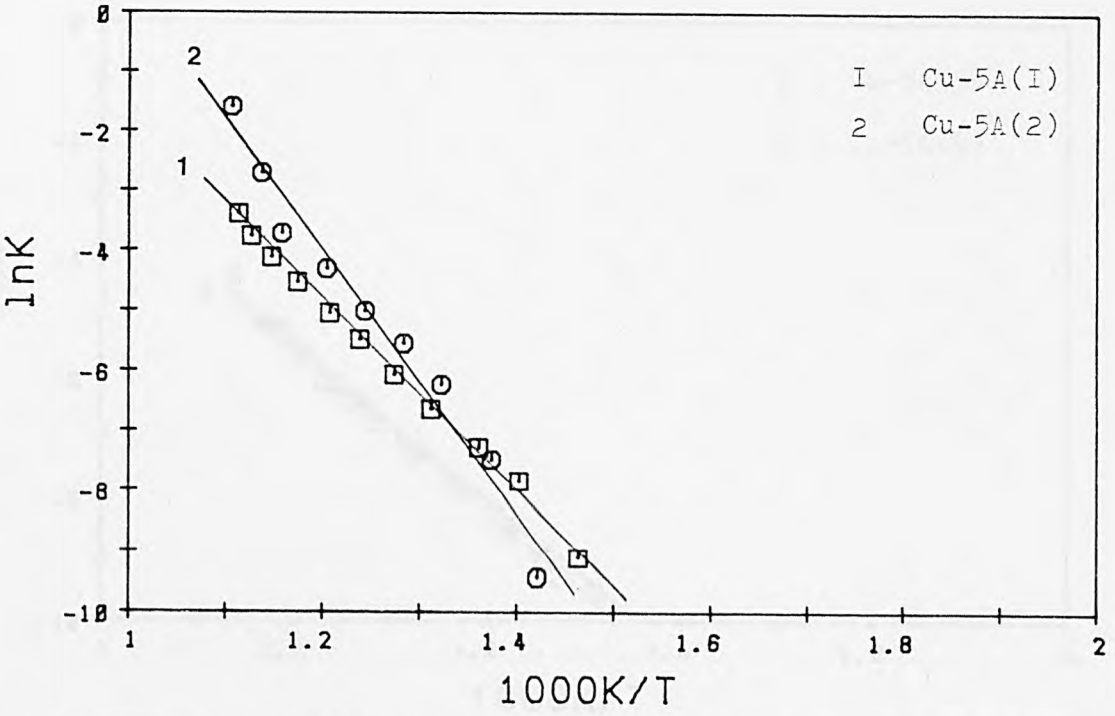

Fig.P4:Methane Oxidation Arrhenius plot of Cu-5A in N_2.

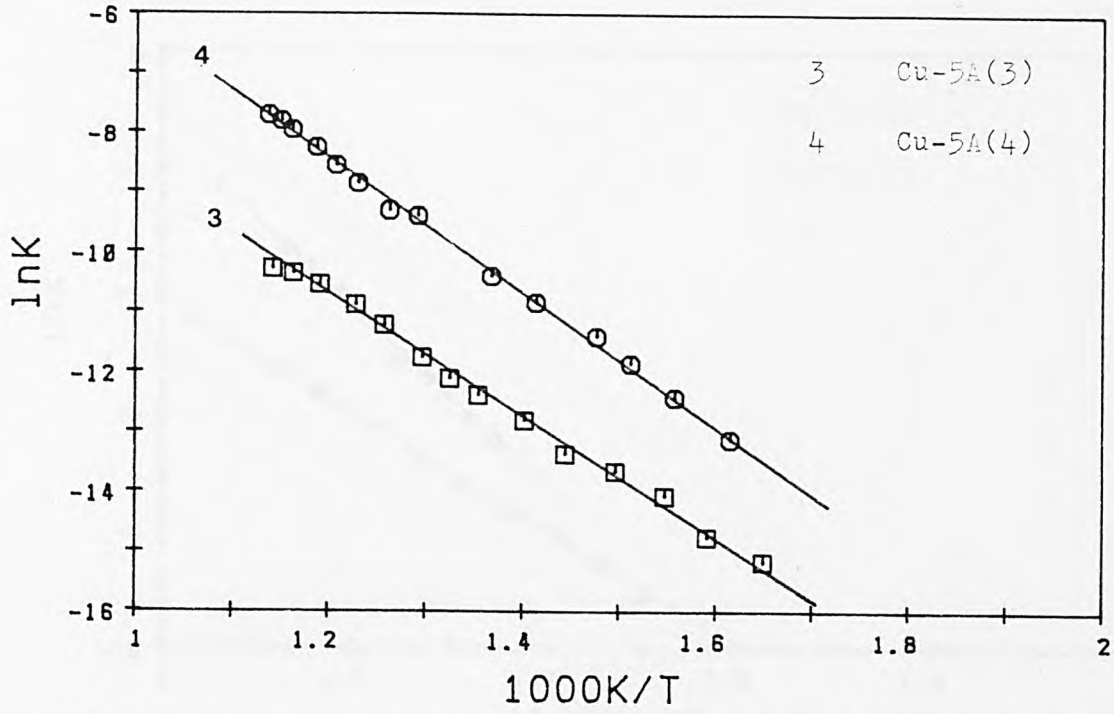

Fig.P5:Methane Oxidation Arrhenius plot of Cu-5A in N2.

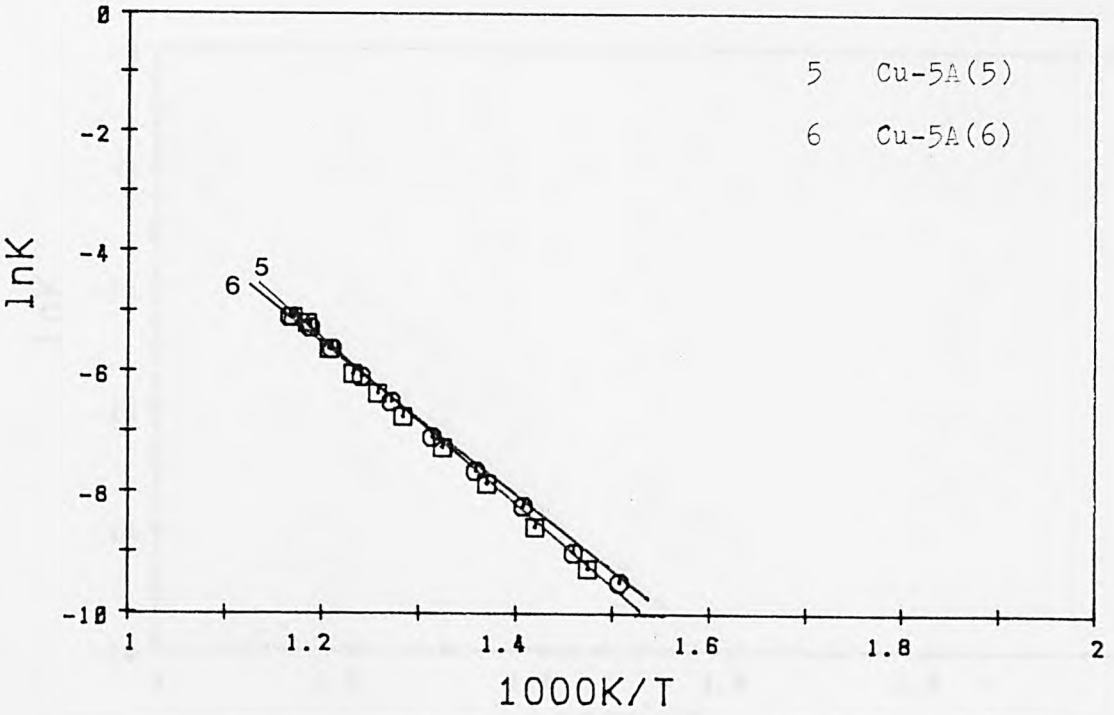

Fig.P6:Methane Oxidation Arrhenius plot of Cu-5A in N2.

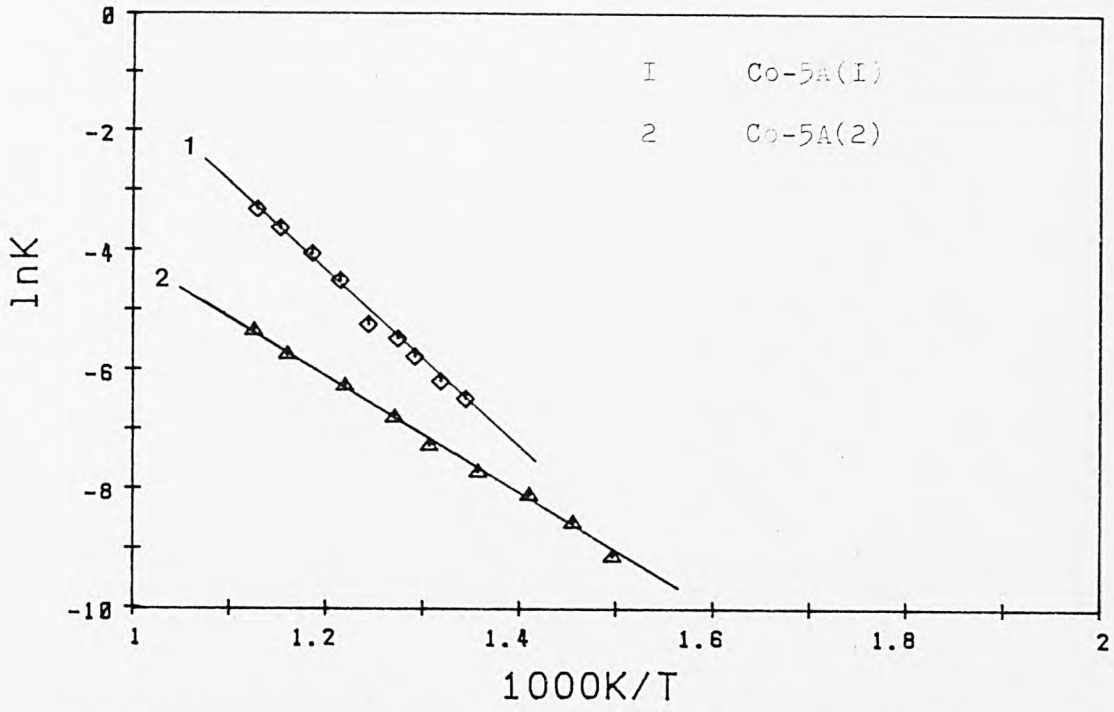

Fig.P7:Methane Oxidation Arrhenius plot of Co-5A in air.

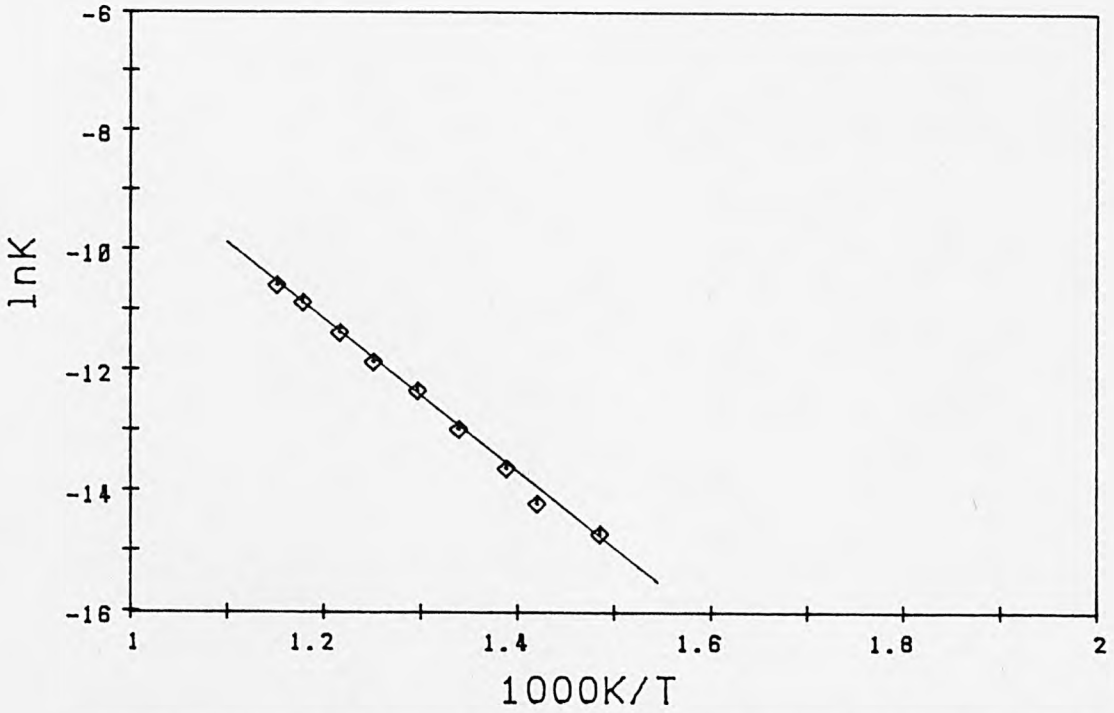

Fig.P8:Methane Oxidation Arrhenius plot of Co-5A(3) in air

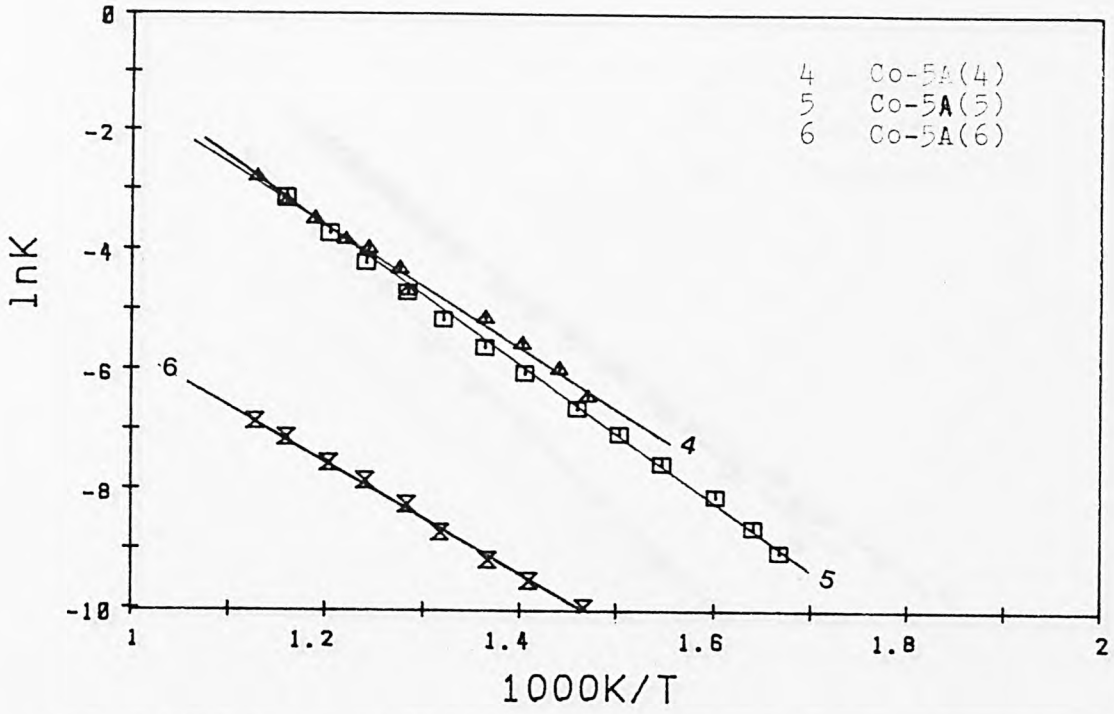

Fig.P9:Methane Oxidation Arrhenius plot of Co-5A in air.

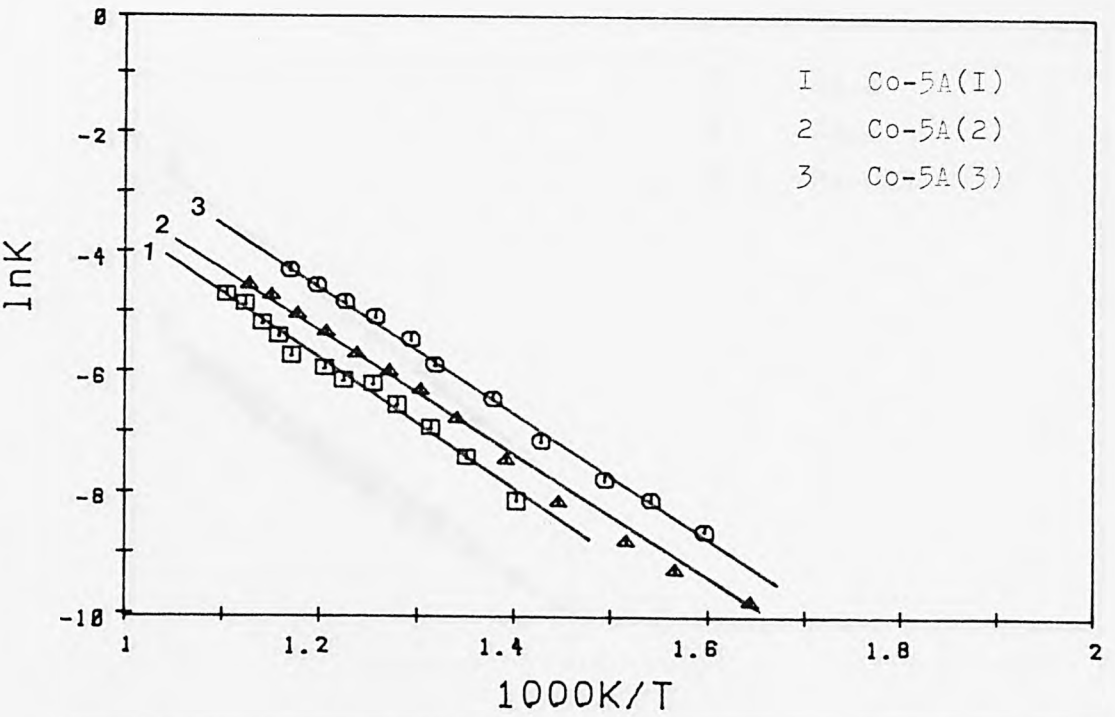

Fig.P10:Methane Oxidation Arrhenius plot of Co-5A in N2.

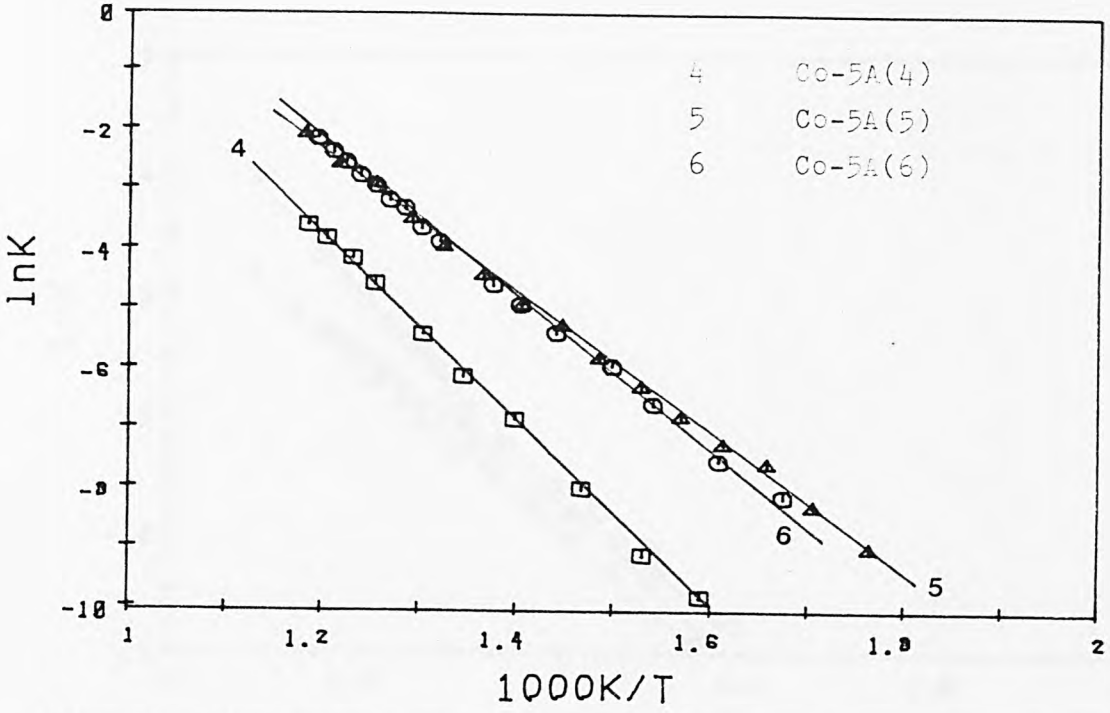

Fig.P11:Methane Oxidation Arrhenius plot of Co-5A in N2.

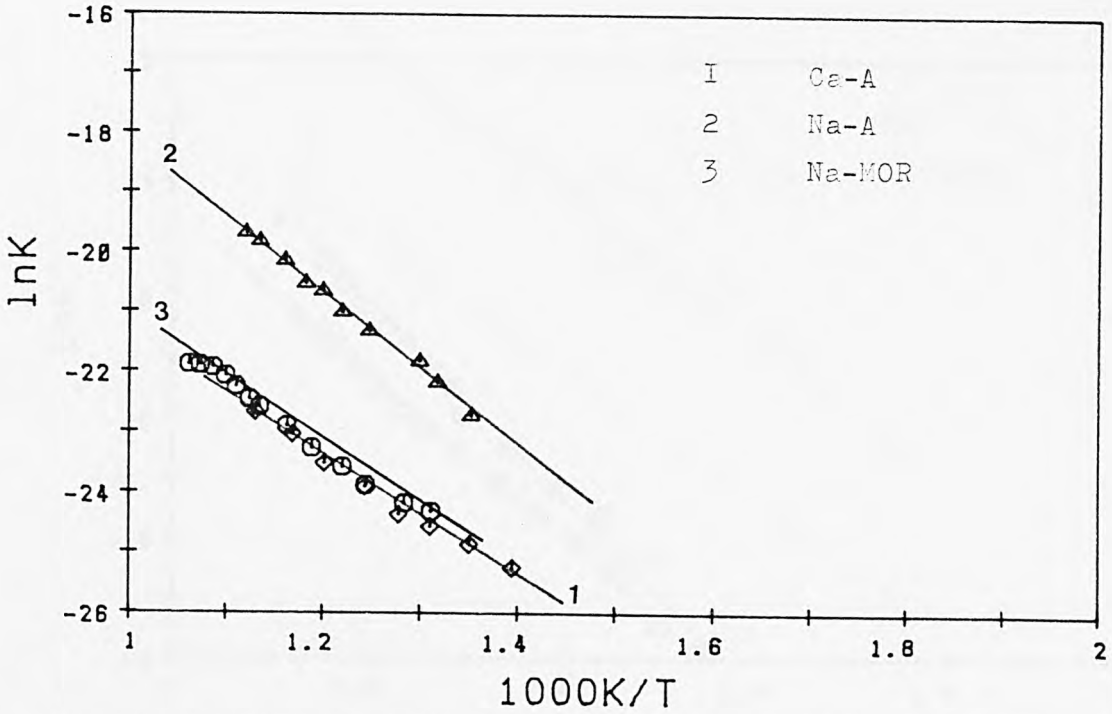

Fig.P12:Methane Oxidation Arrhenius plot of CaA/NaA/NaM in air.

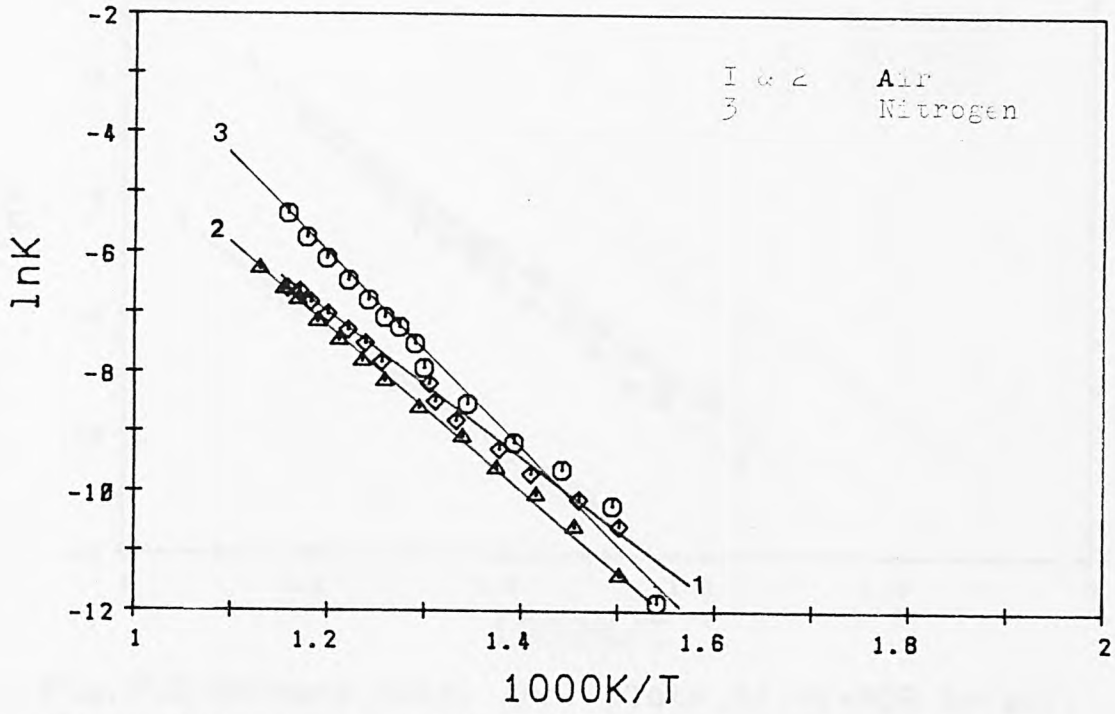

Fig.P13:Methane Oxidation Arrhenius plot of NH4-MOR(1).

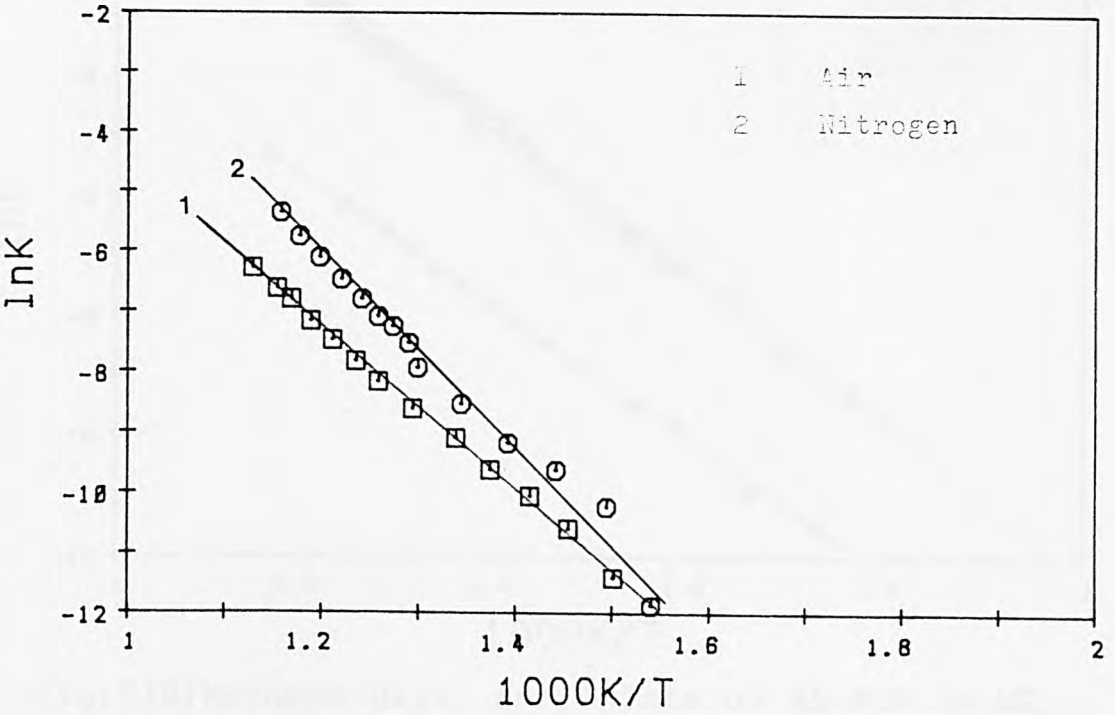

Fig.P14:Methane Oxidation Arrhenius plot of NH4-MOR(2).

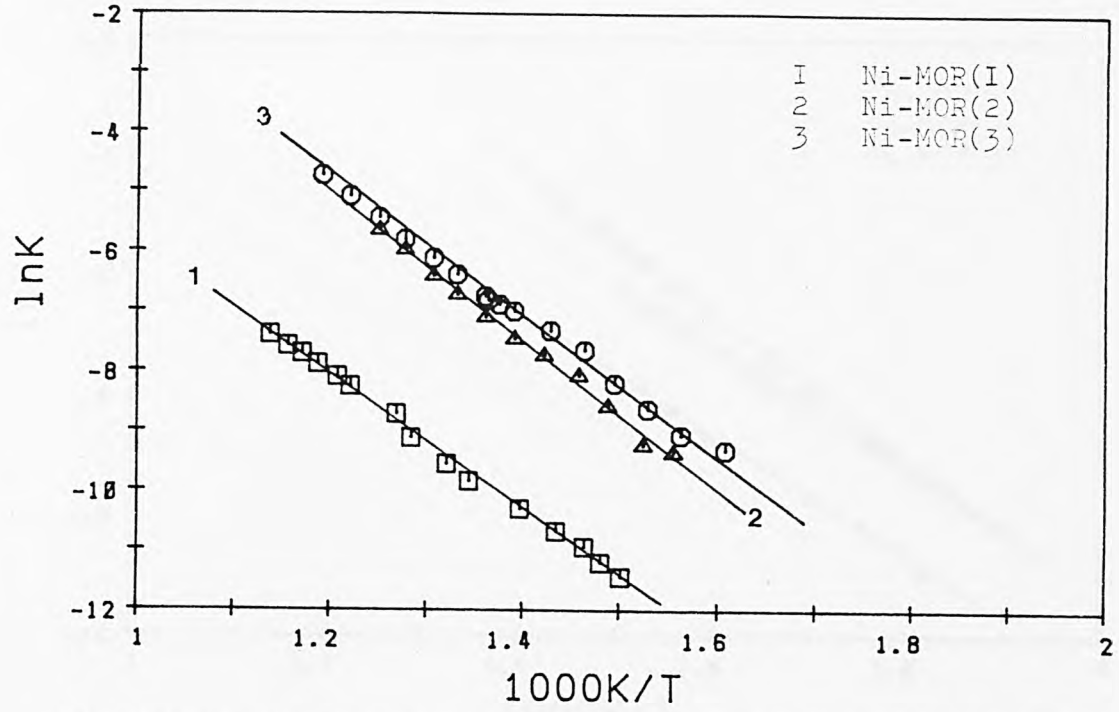

Fig.P15:Methane Oxid. Arr. plots of Ni-MOR in air.

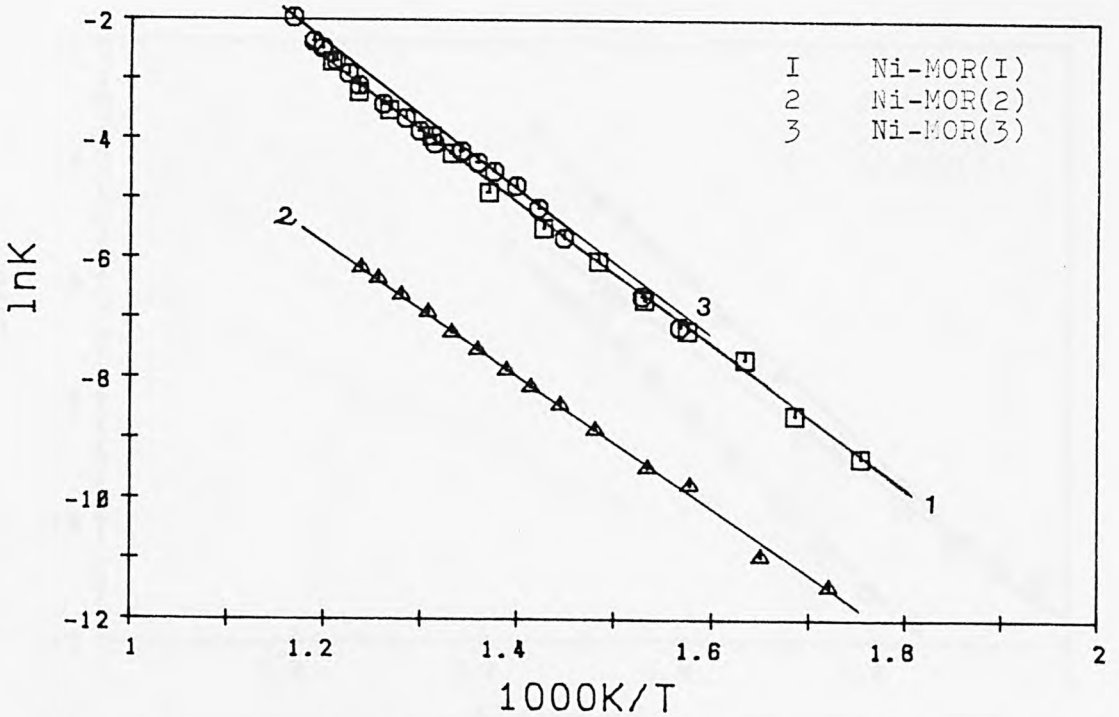

Fig.P16:Methane Oxid. Arr. plots of Ni-MOR in N2.

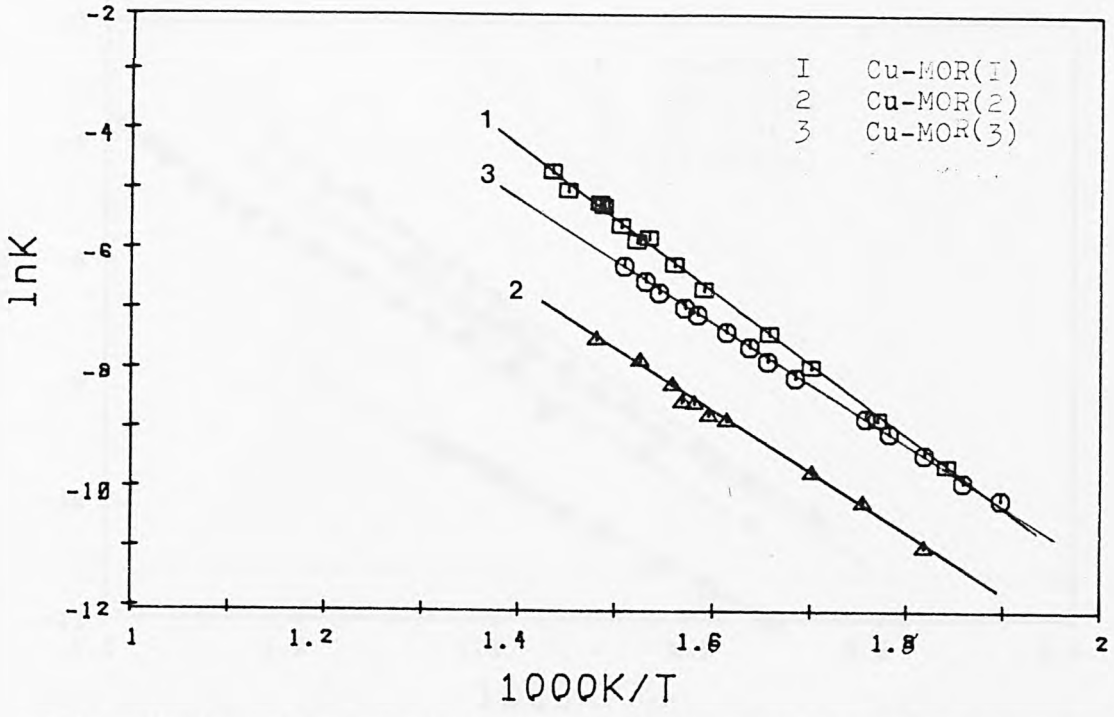

Fig.P17:Methane Oxid. Arr. plots of Cu-MOR in air.

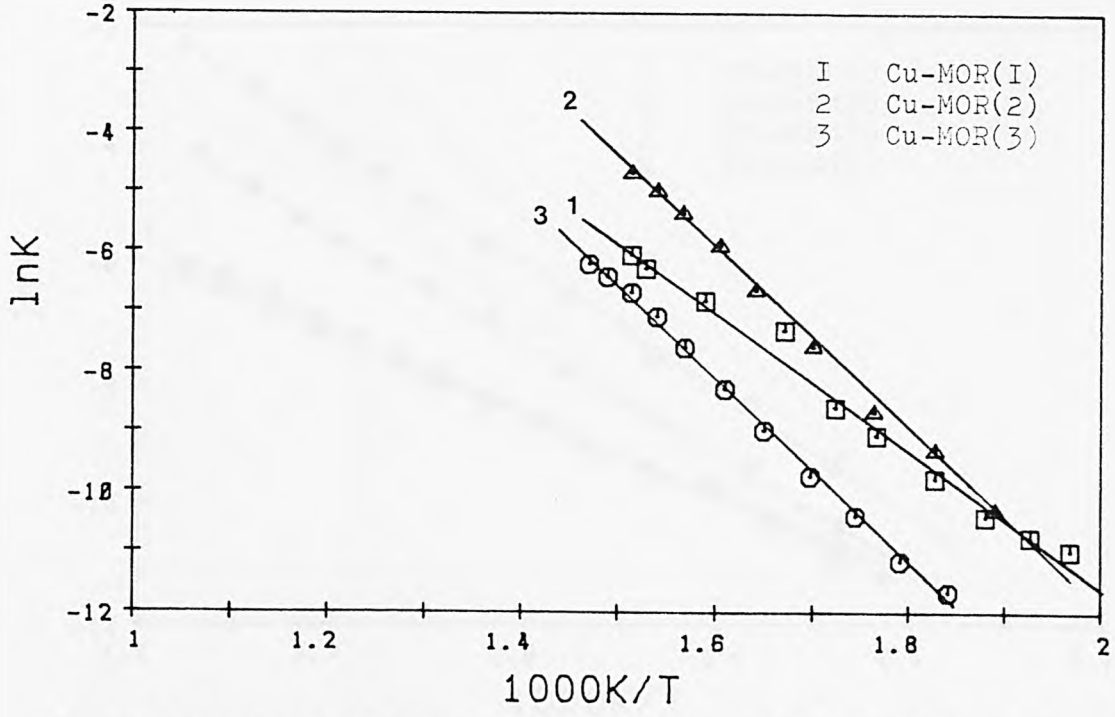

Fig.P18:Methane Oxid. Arr. plots of Cu-MOR in N2.

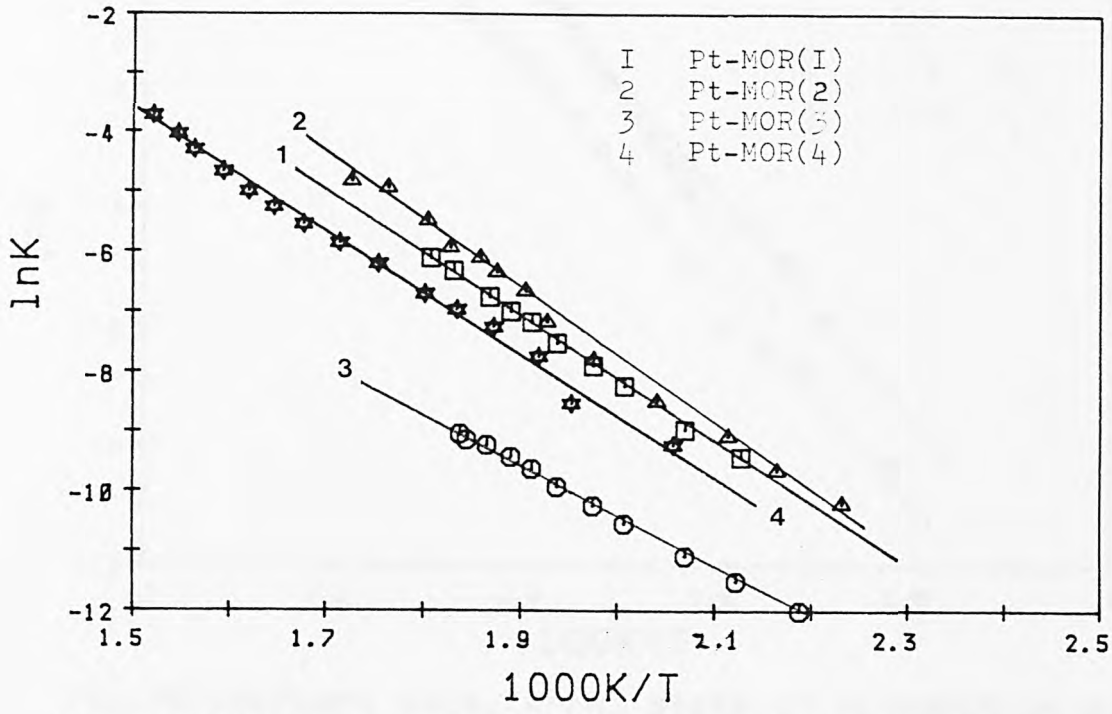

Fig.P19:Methane Oxid. Arr. plots of Pt-MOR in (air).

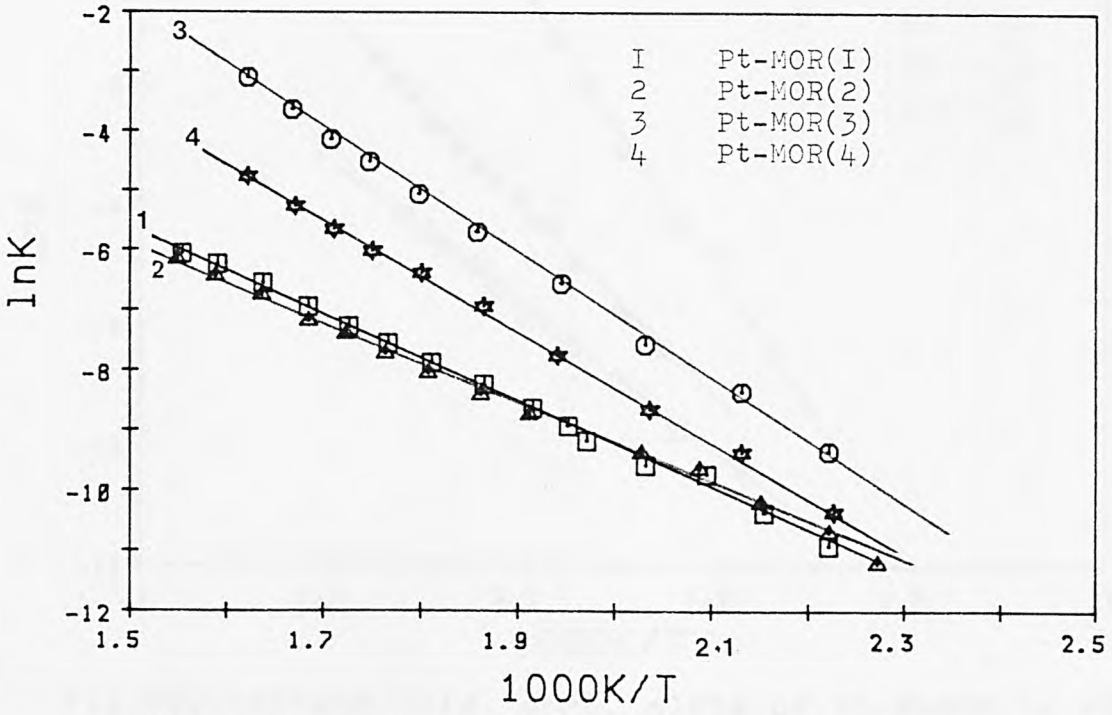

Fig.P20:Methane Oxid. Arr. plots of Pt-MOR in (N2).

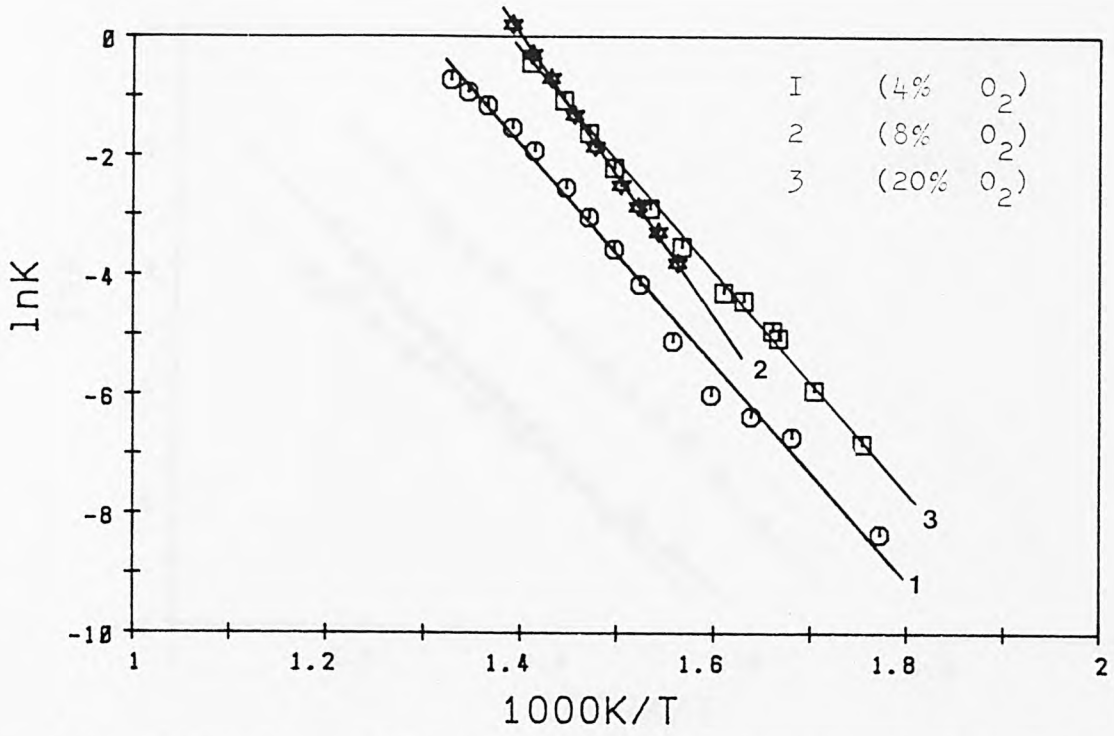

Fig.P21: Methane Oxid. Arrh. plots of Ni-NaMOR in air.

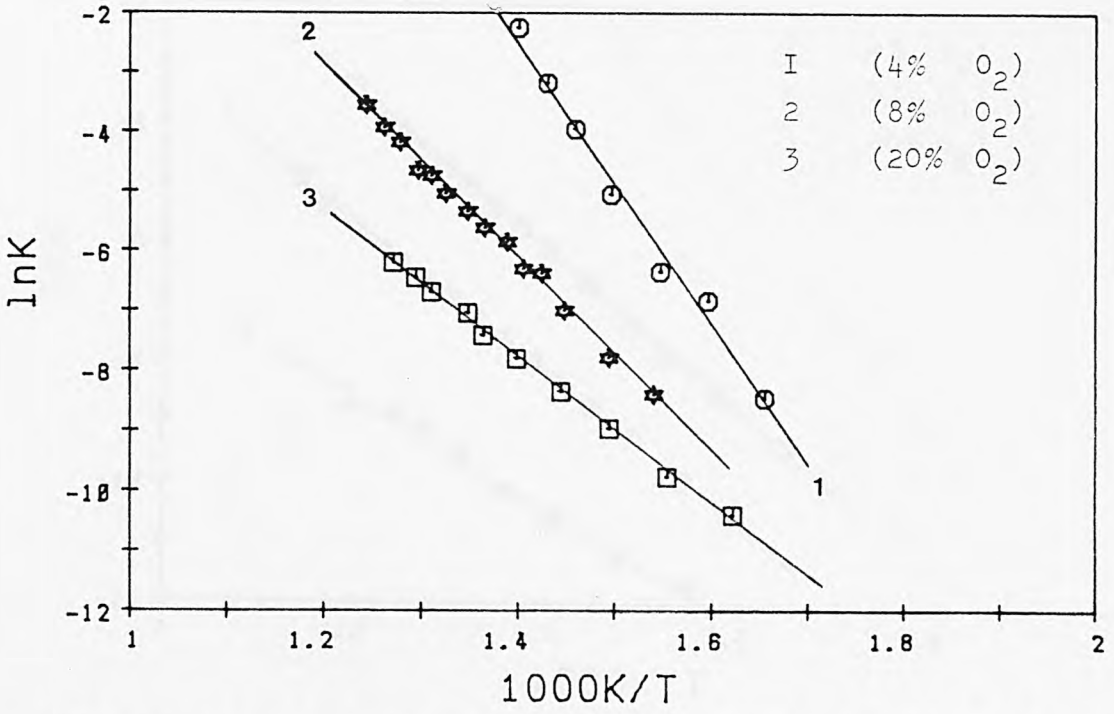

Fig.P22: Methane Oxid. Arrh. plots of Ni-NaMOR in N2.

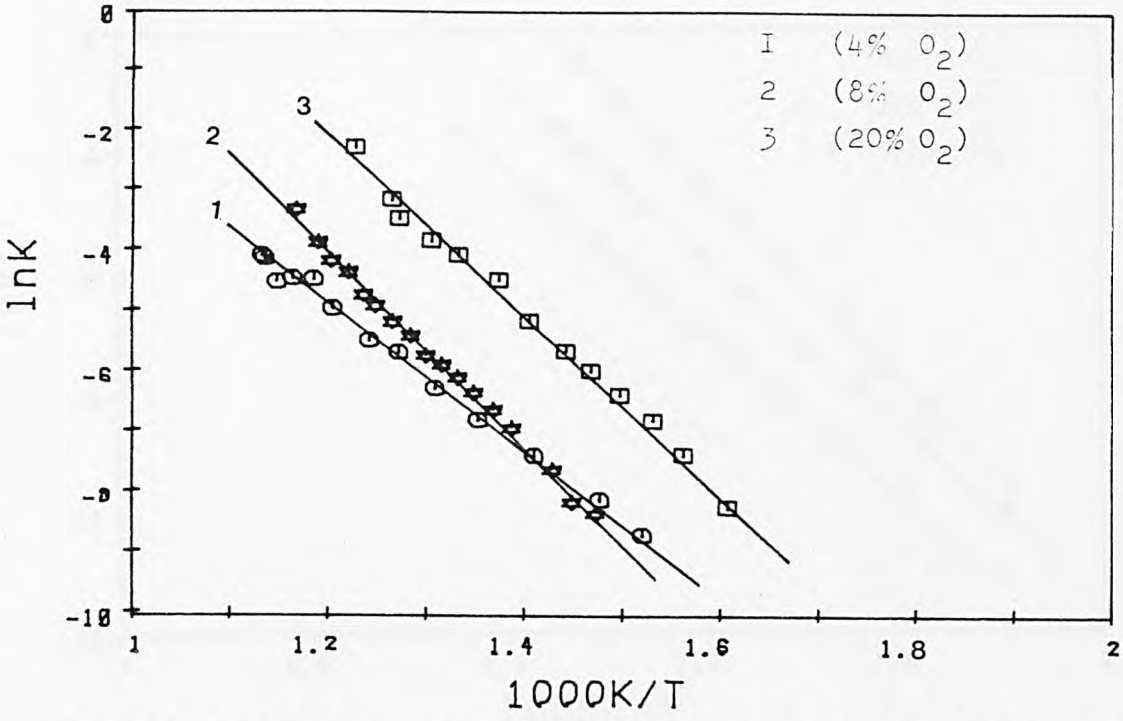

Fig.P23:Methane Oxid. Arrh. plots of Ni-NH4MOR in air.

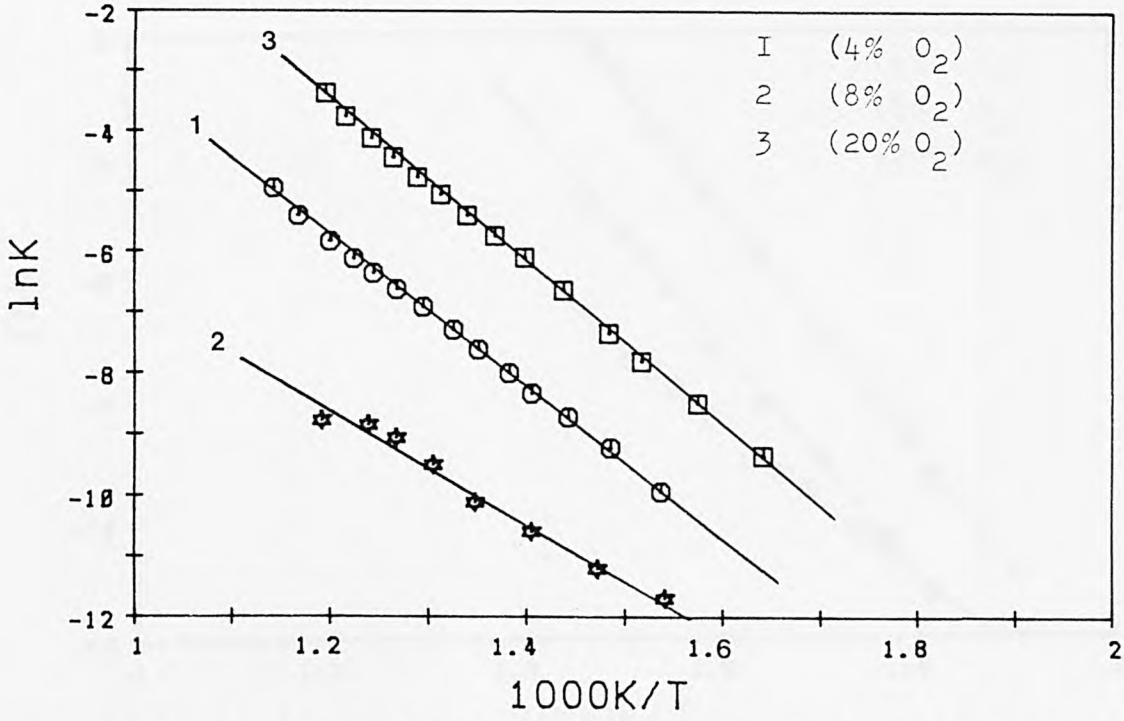

Fig.P24:Methane Oxid. Arr. plots of Ni-NH4MOR in N2.

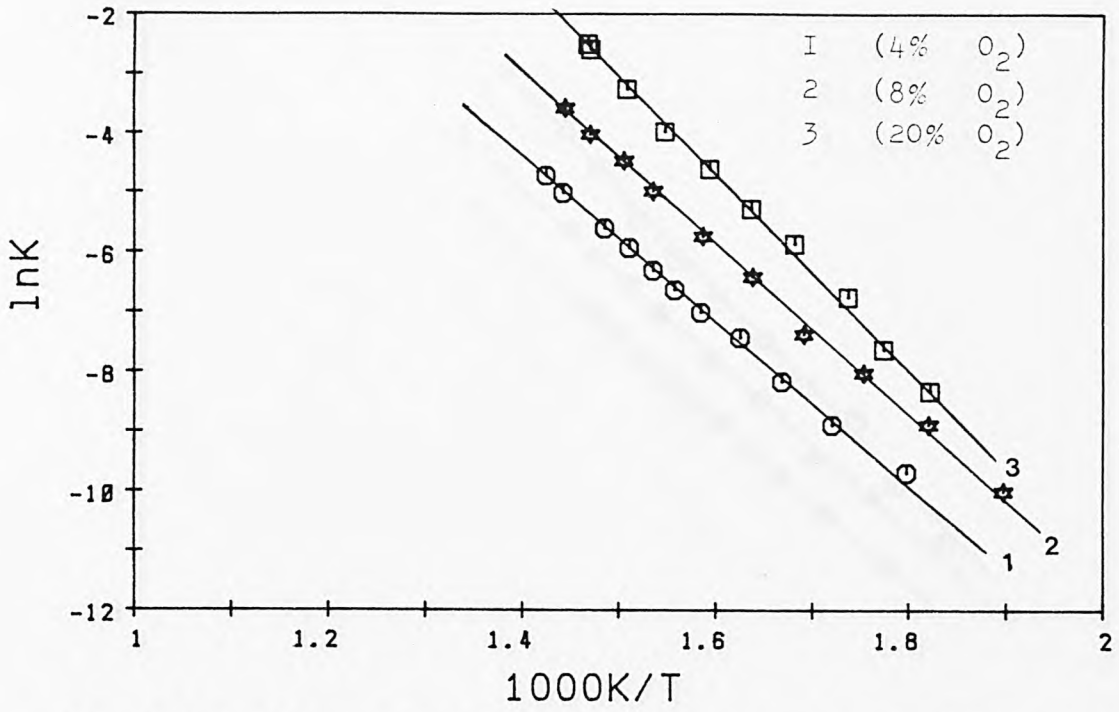

Fig.P25: Methane Oxid. Arr. plots of Cu-NaMOR in air.

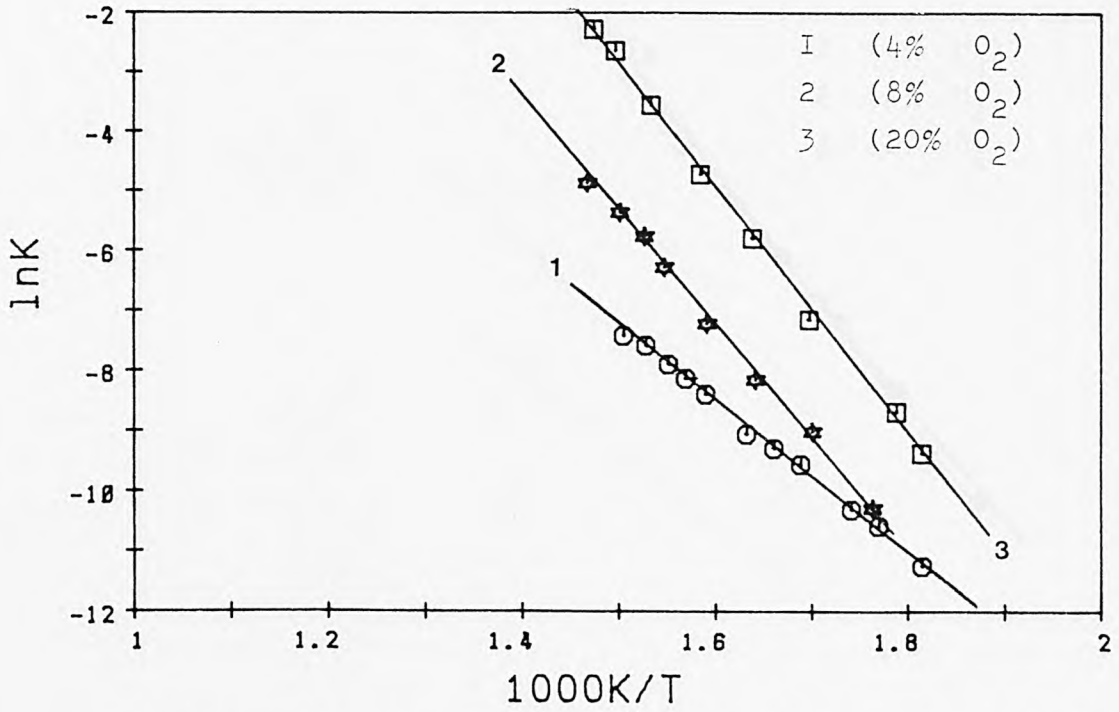

Fig.P26: Methane Oxid. Arrh. plots of Cu-NaMOR in N2.

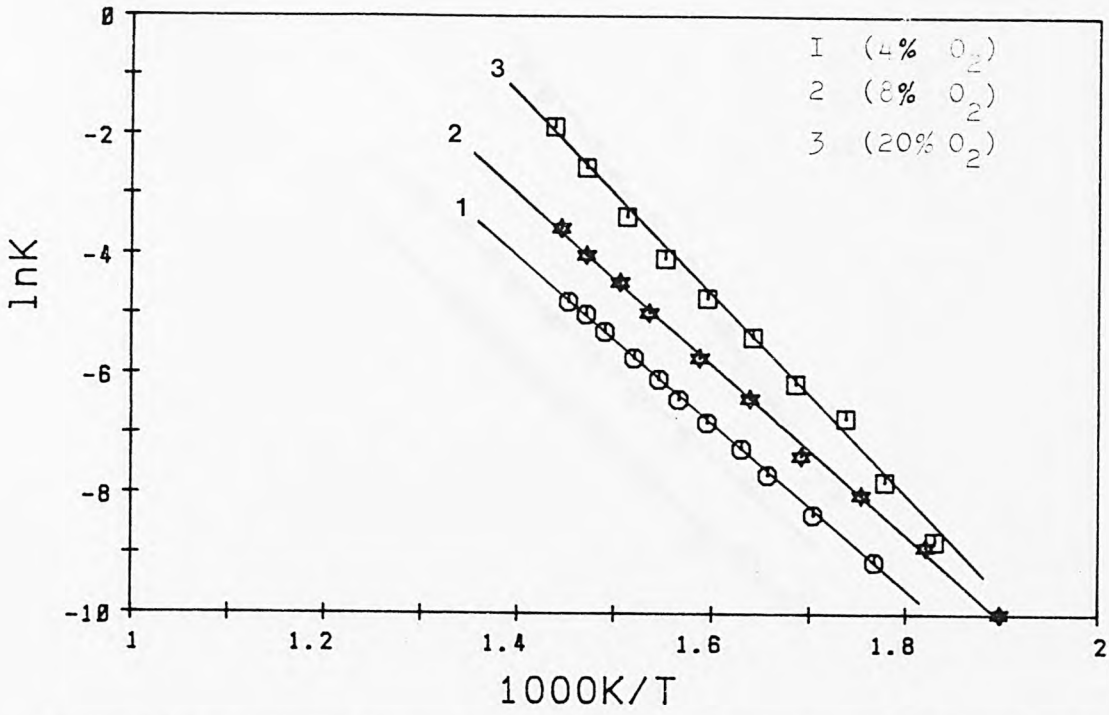

Fig.P27:Methane Oxid. Arrh. plots of Cu-NH4MOR in air.

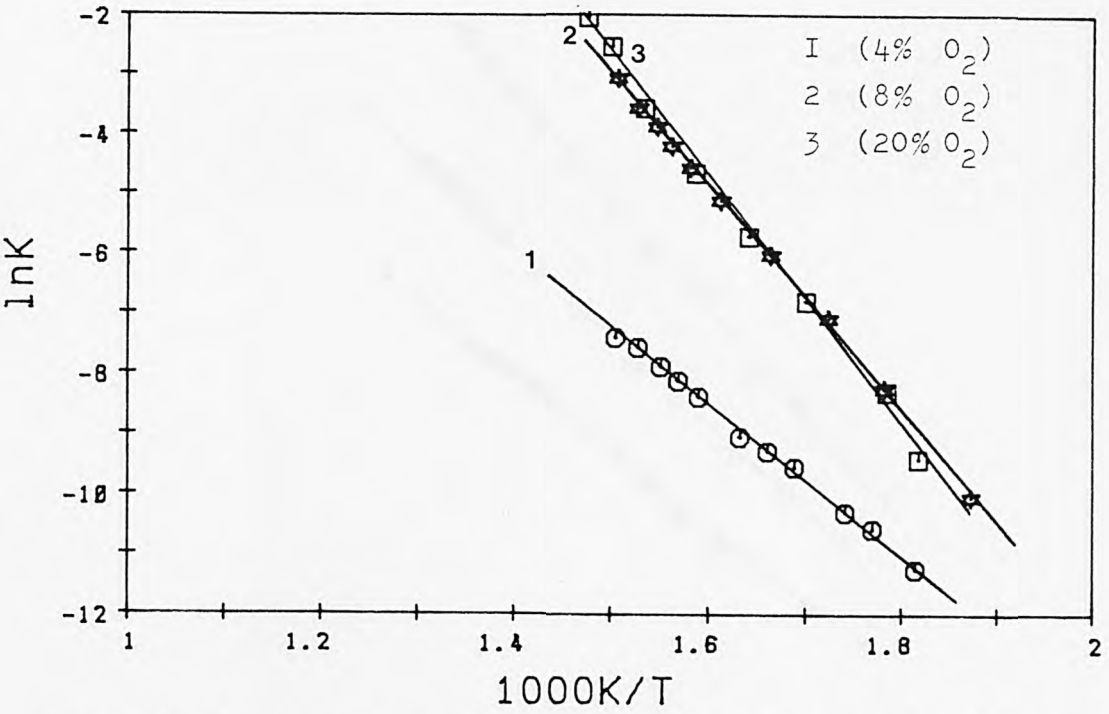

Fig.P28:Methane Oxid. Arrh. plots of Cu-NH4MOR in N2.

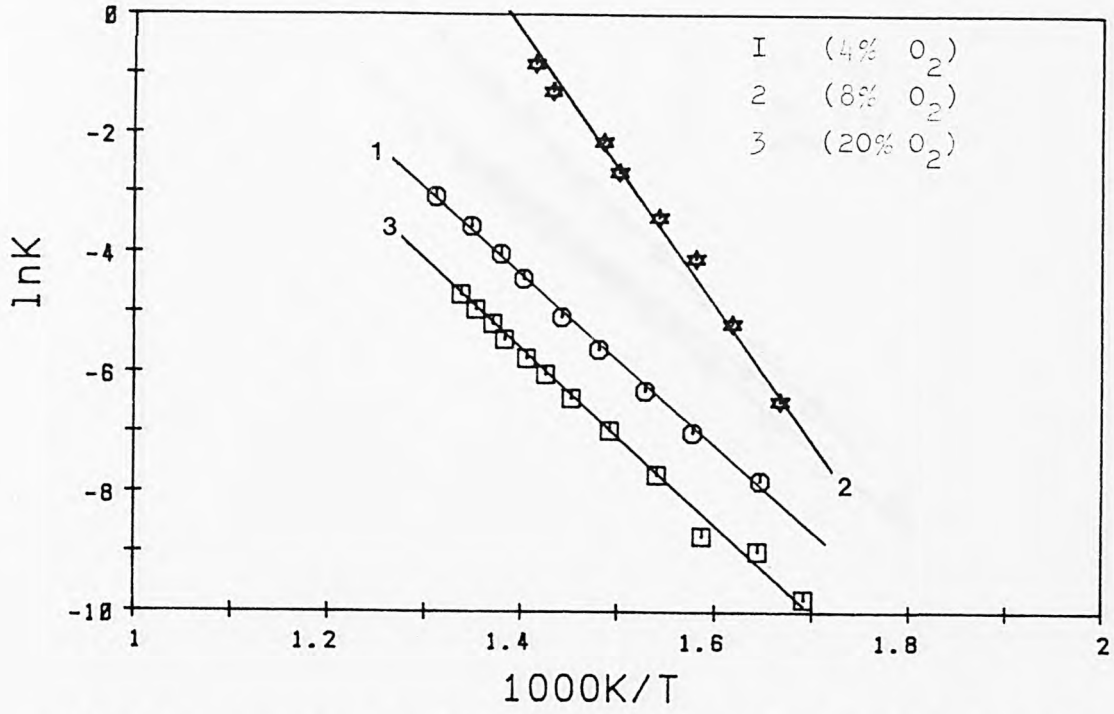

Fig.P29: Methane Oxid. Arrh. plots of Cu-Ni-NaM(1) in air.

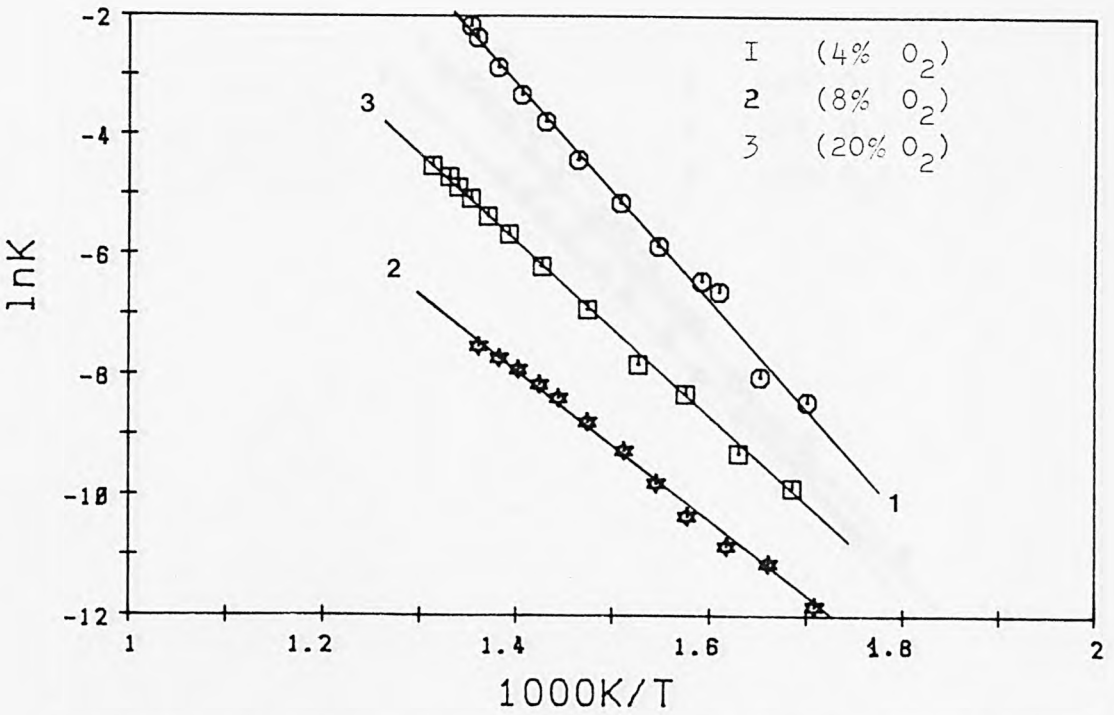

Fig.P30: Methane Oxid. Arrh. plots of Cu-Ni-NaM(1) in N2.

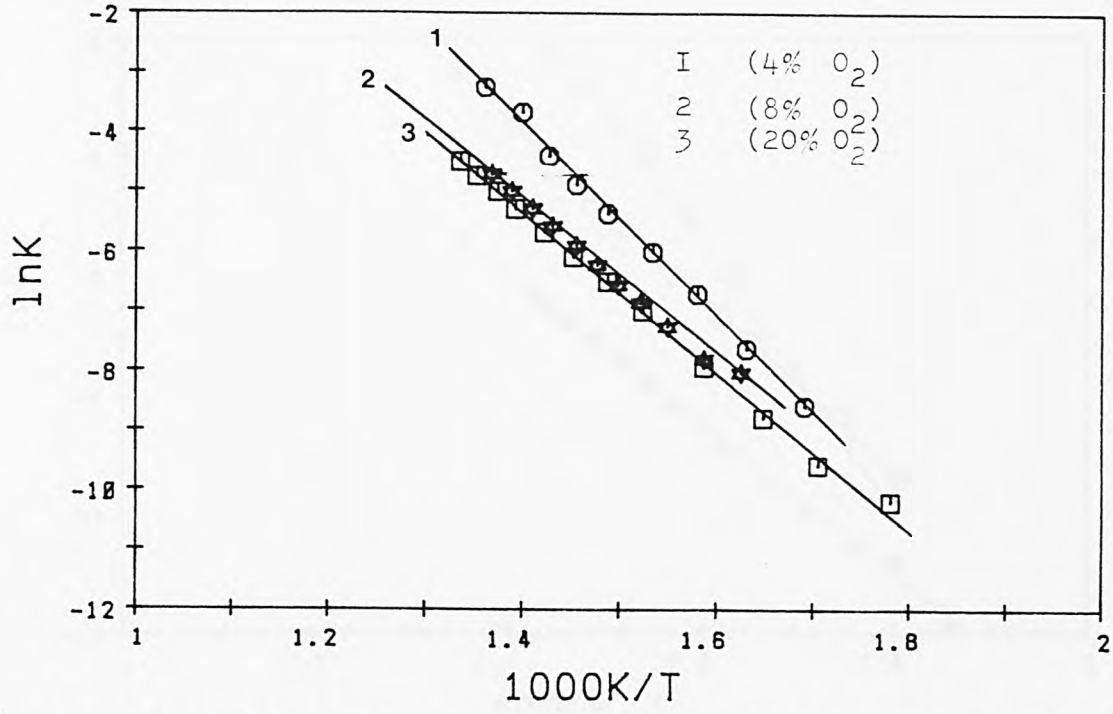

Fig.P31:Methane Oxid. Arrh. plots of Cu-Ni-NH4M(1) in air

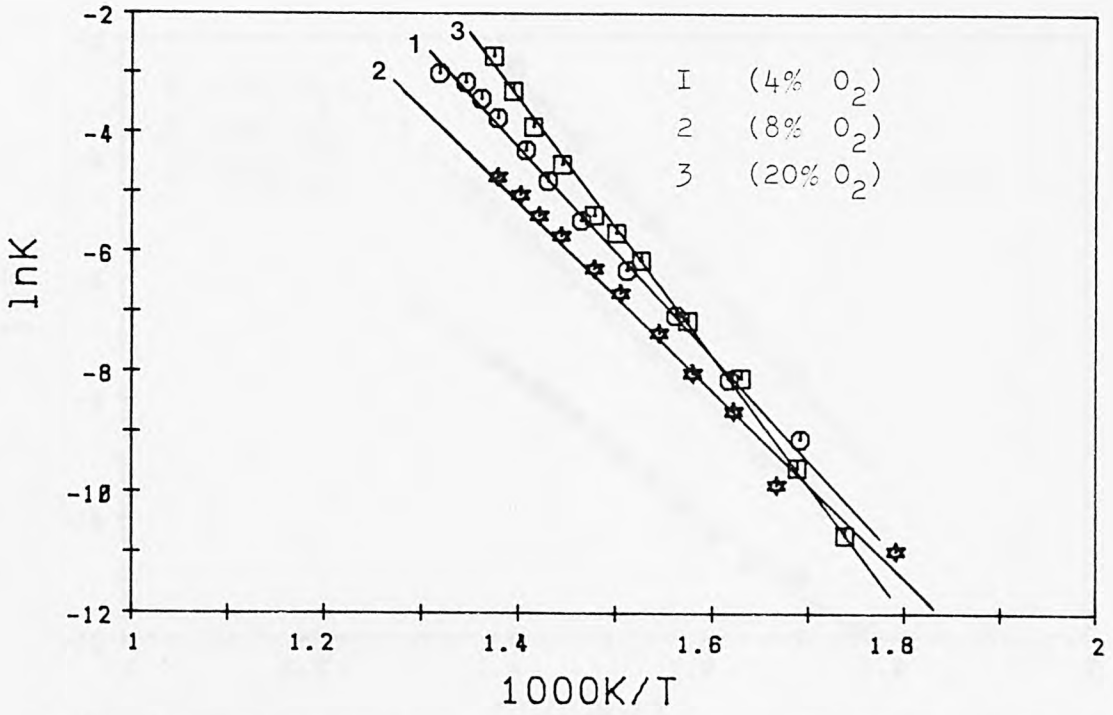

Fig.P32:Methane Oxid. Arrh. plots of Cu-Ni-NH4M(1) in N2.

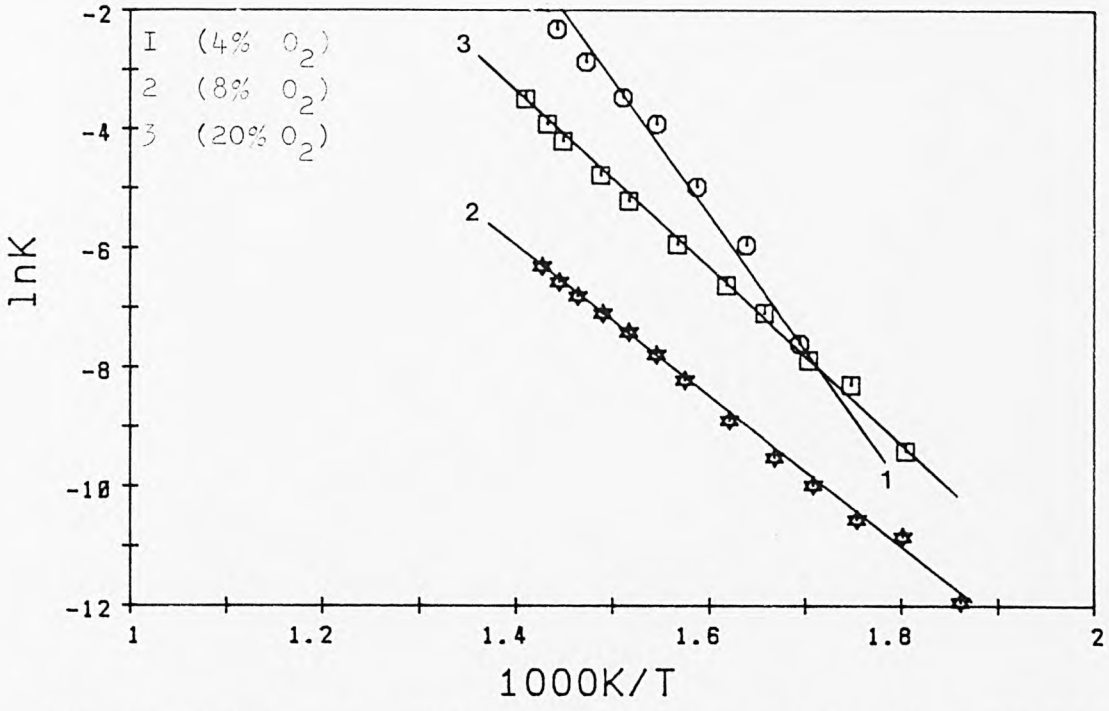

Fig.P33:Methane Oxid. Arrh. plots of Cu-Ni-NaMOR(2) in air.

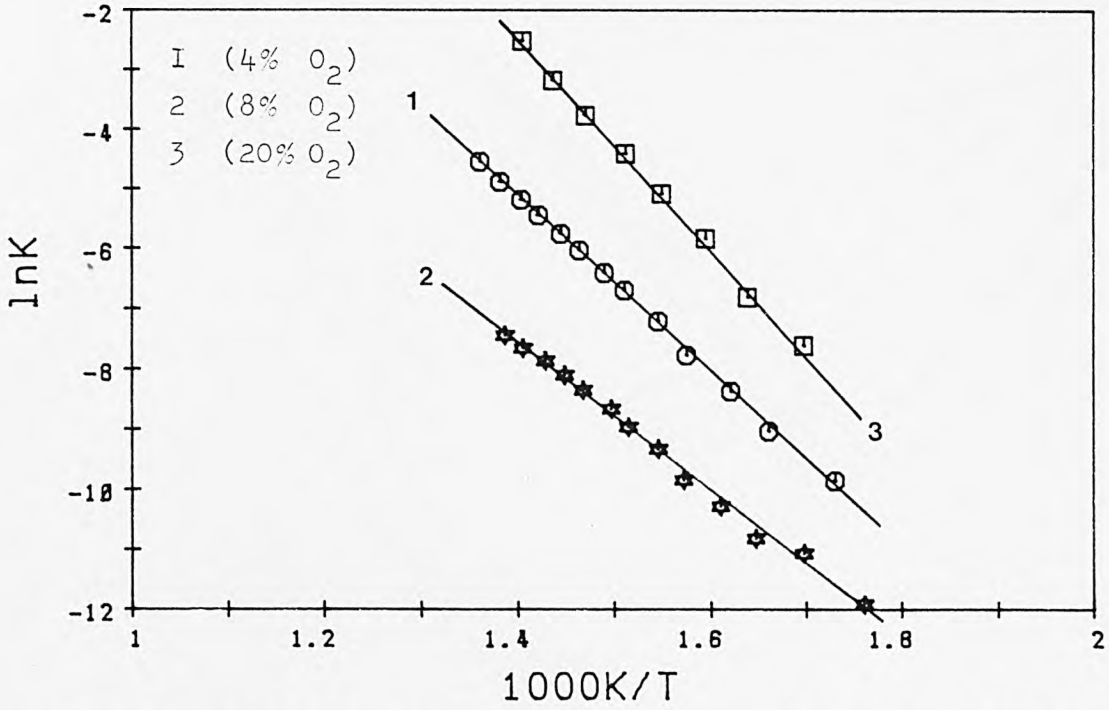

Fig.P34:Methane Oxid. Arrh. plots of Cu-Ni-NaM(2) in N2.

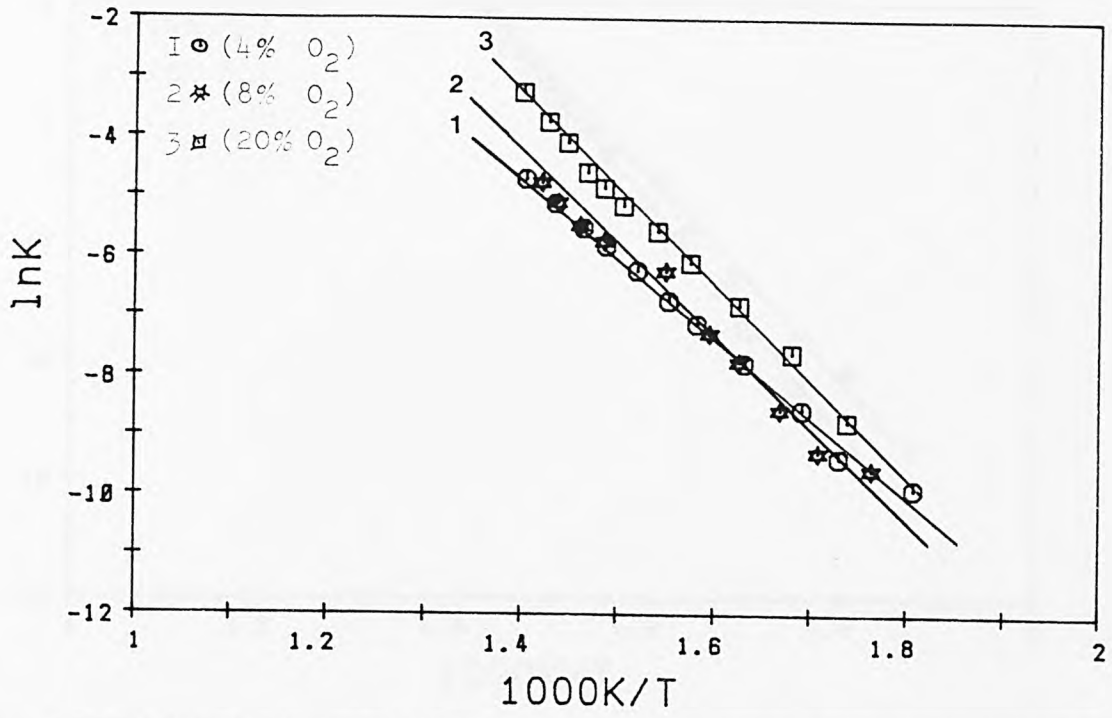

Fig.P35: Methane Oxid. Arrh. plots of Cu-Ni-NH4M(2) in air.

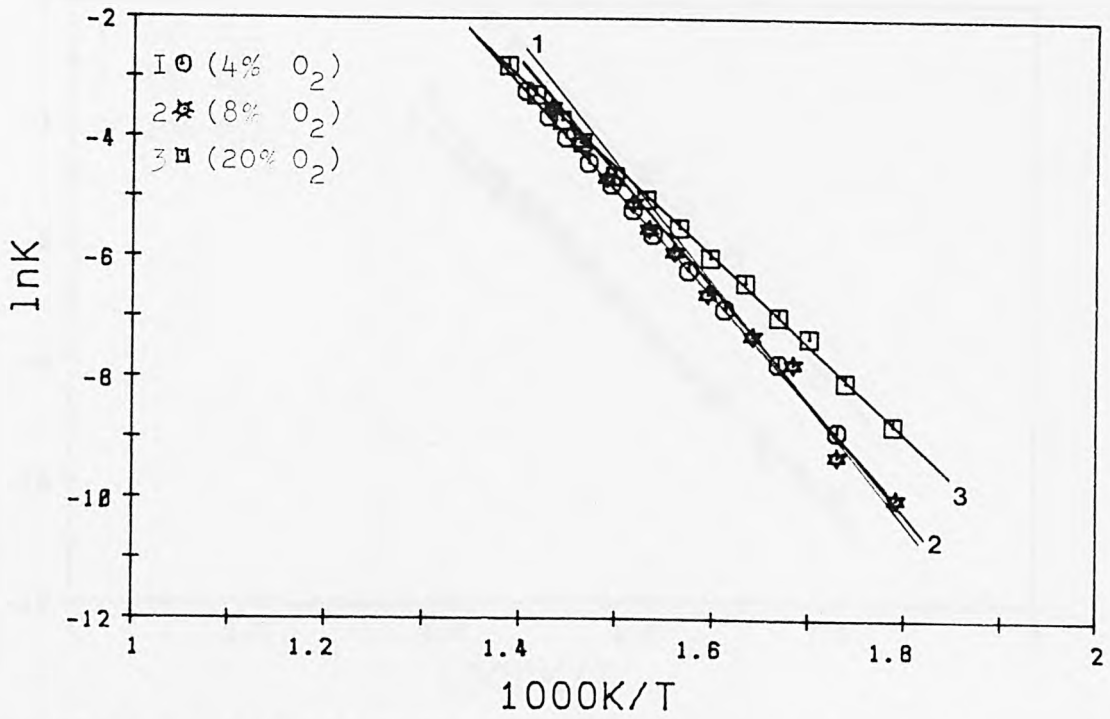

Fig.P36: Methane Oxid. Arrh. plots of Cu-Ni-NH4M(2) in N2.

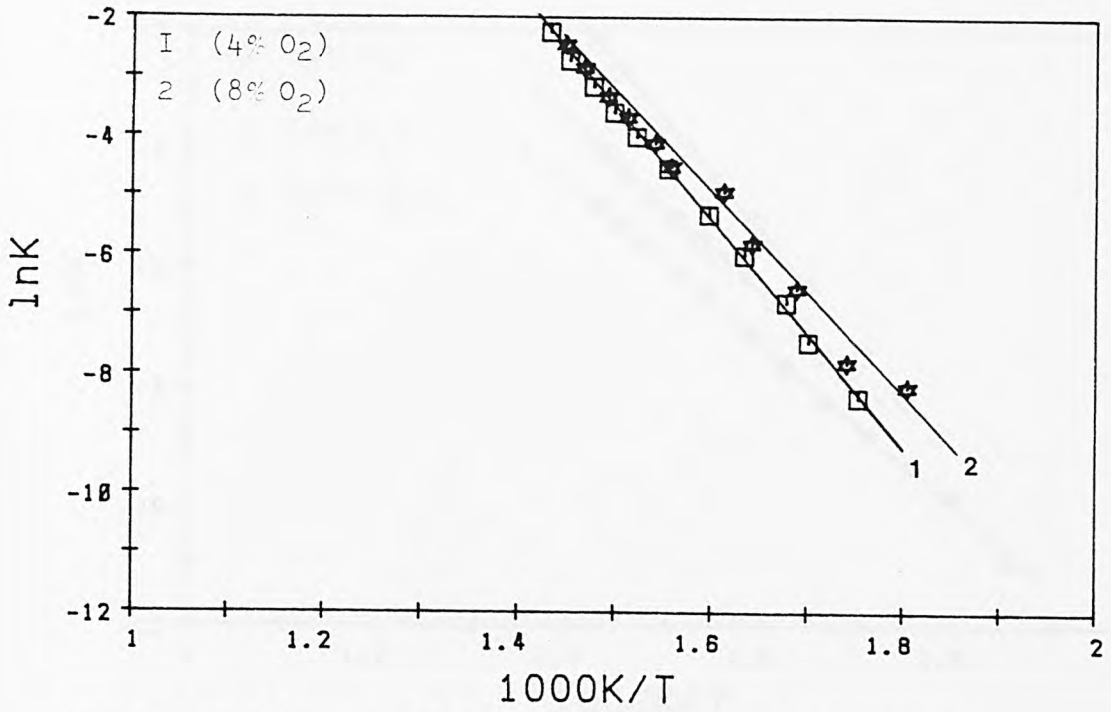

Fig.P37:Methane Oxid. Arrh. plots of Cu-Ni-NaM(3) in air.

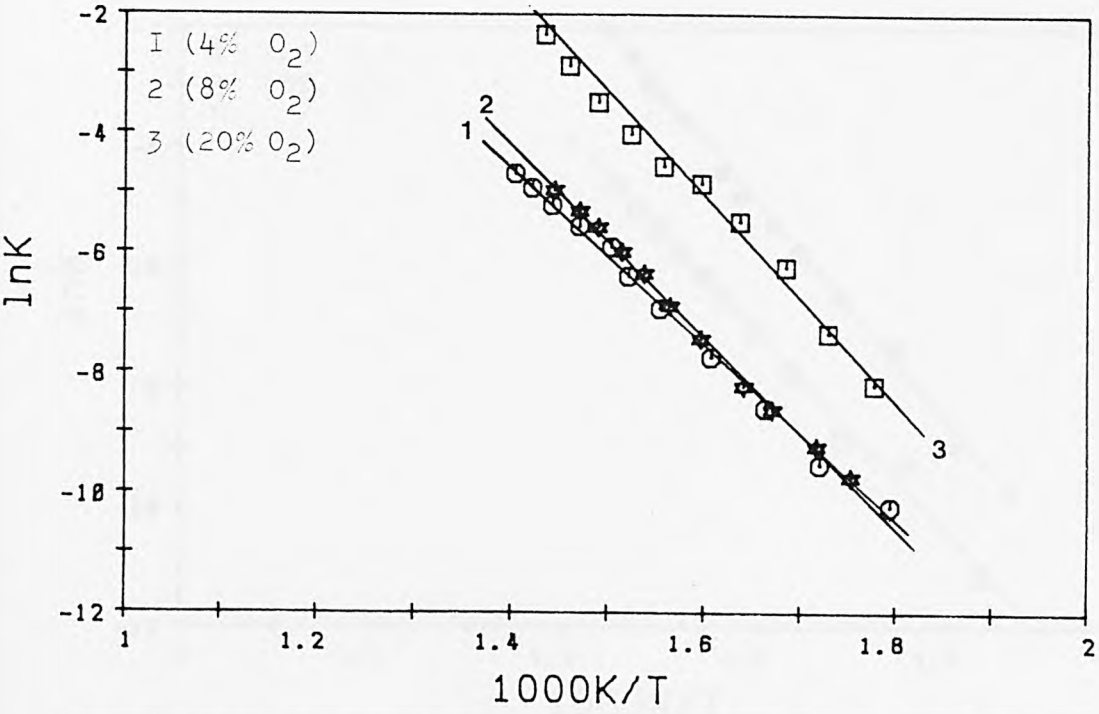

Fig.P38:Methane Oxid. Arrh. plots of Cu-Ni-NaM(3) in N2.

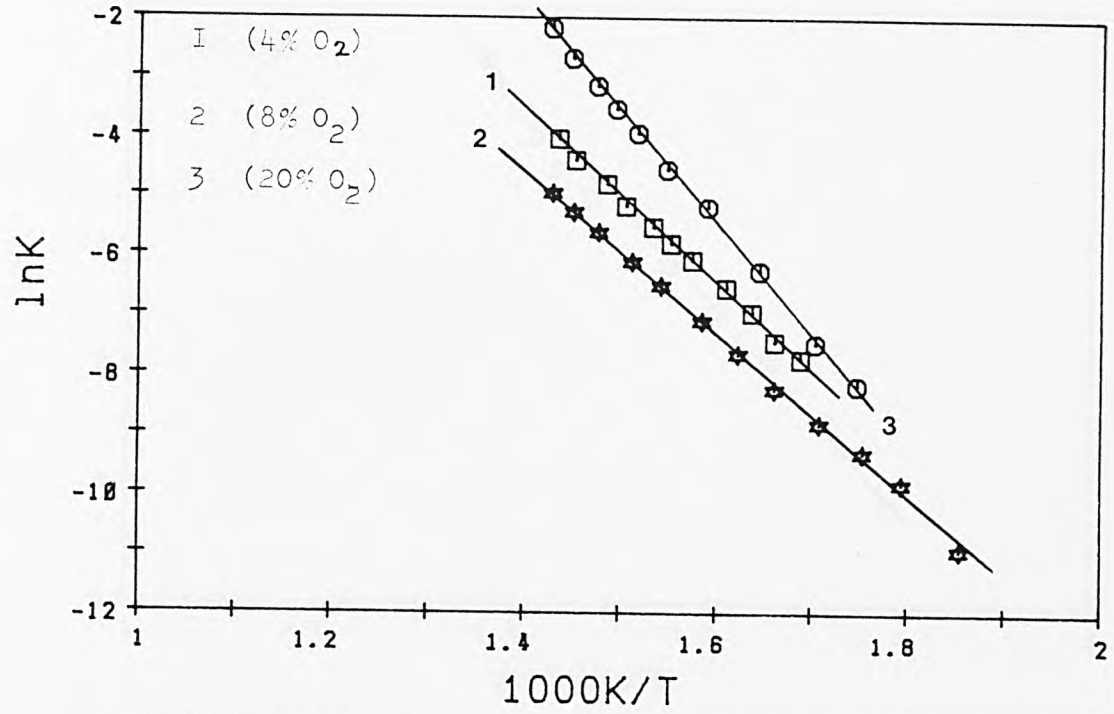

Fig.P39:Methane Oxid. Arrh. plots of Cu-Ni-NH4M(3) in air.

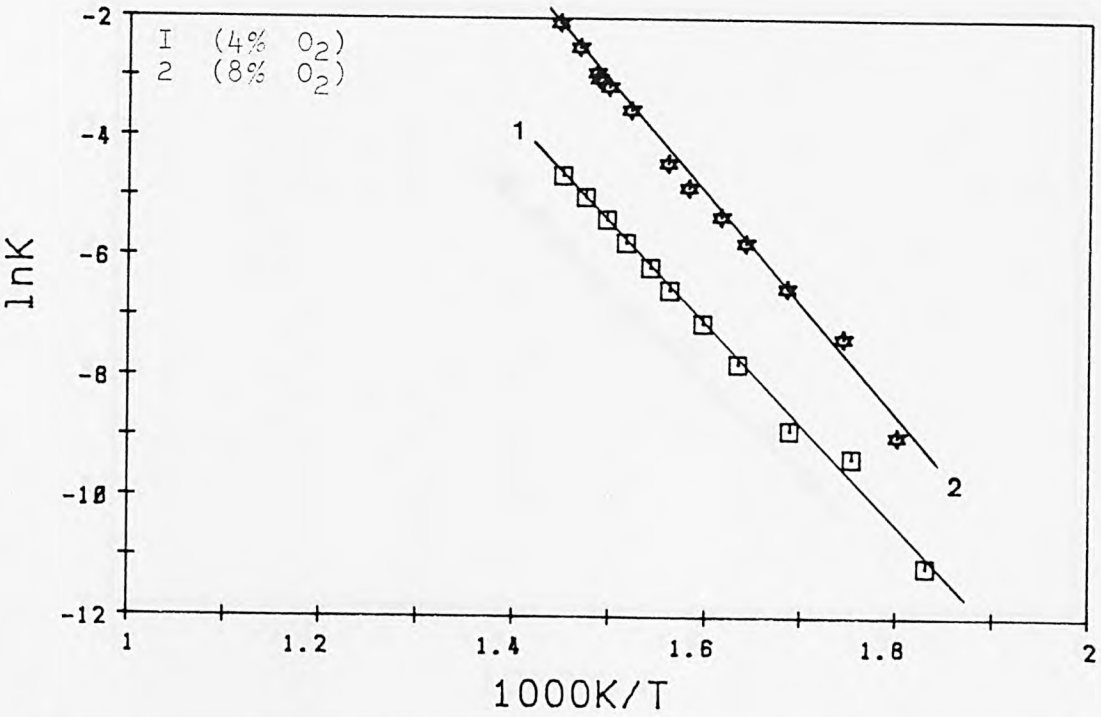

Fig.P40:Methane Oxid. Arrh. plots of Cu-Ni-NH4M(3) in N2.

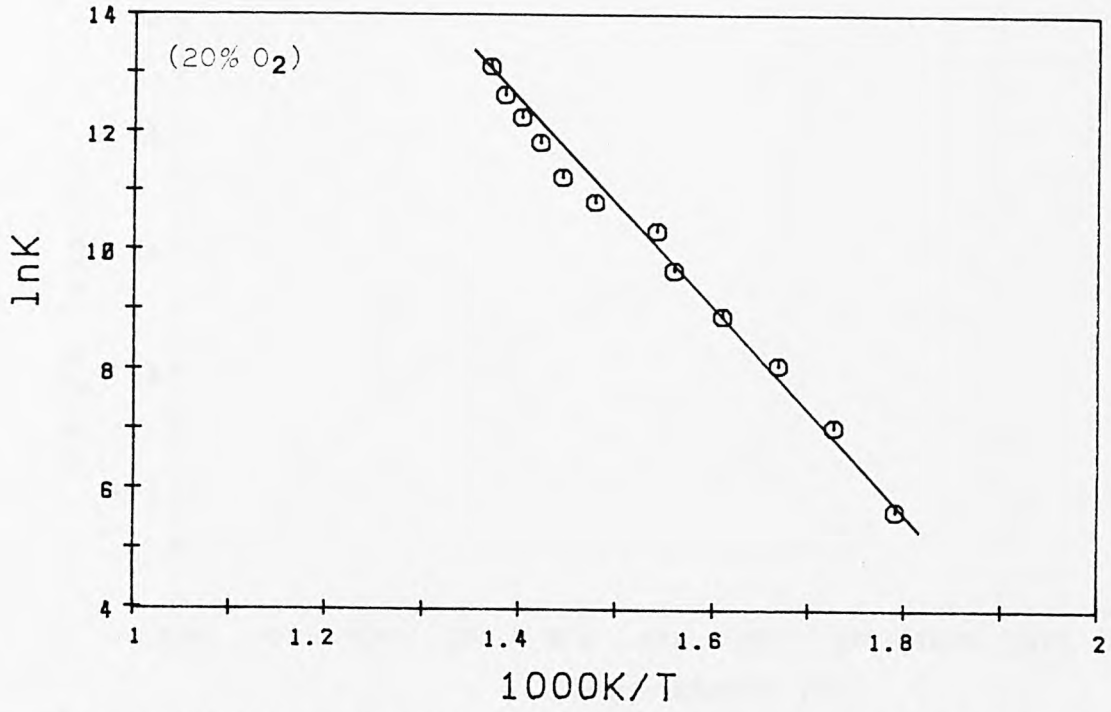

Fig.P41:Methane Oxid. Arrh. plots of Cu-Ni-NaM(3) in air.

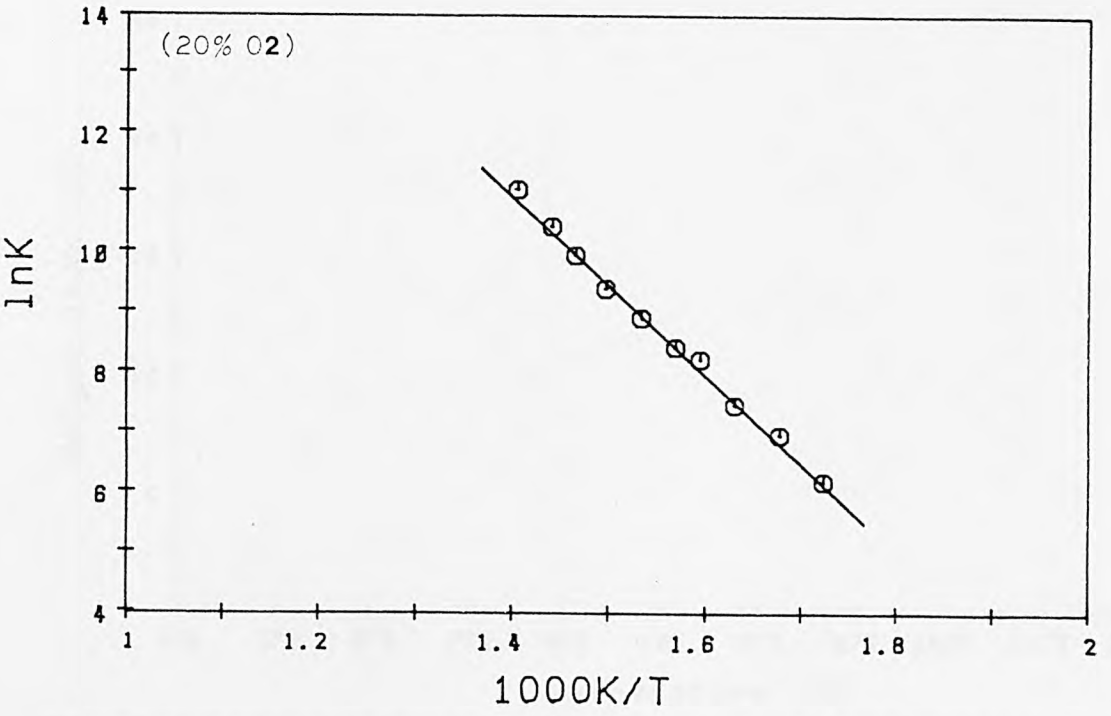

Fig.P42:Methane Oxid. Arrh. plots of Cu-Ni-NH4M(3) in N2.

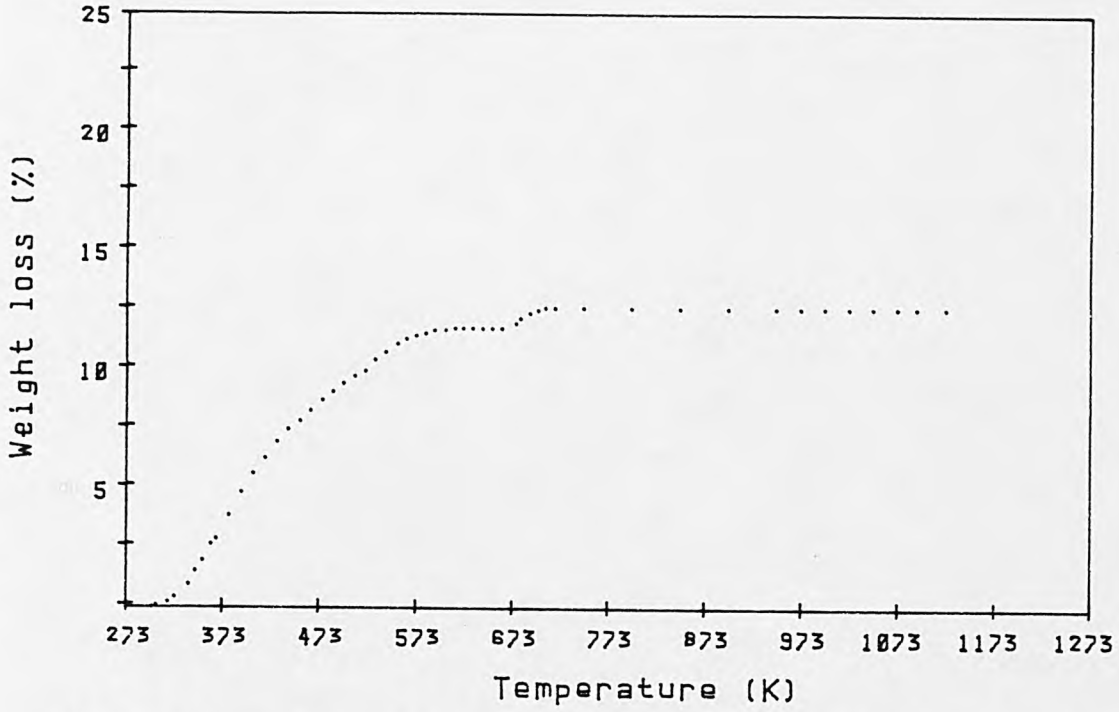

Figure T1 . Thermogram (TG plot) of Na-MOR under air.

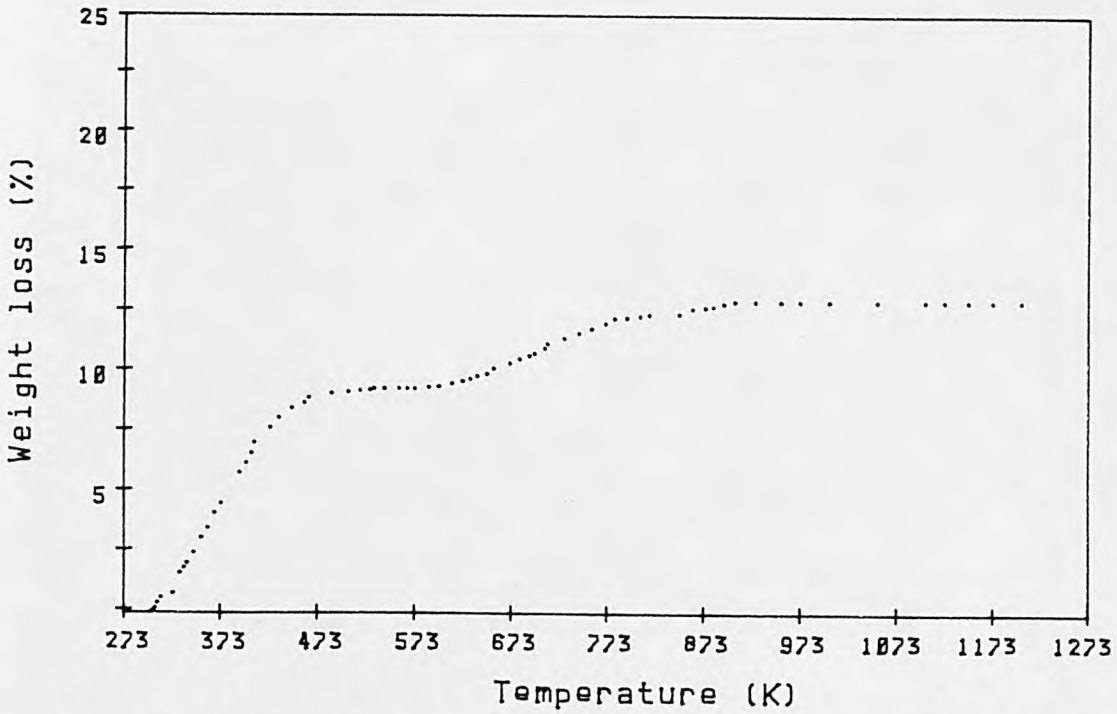

Figure T2 . Thermogram (TG plot) of NH4-MOR under air.

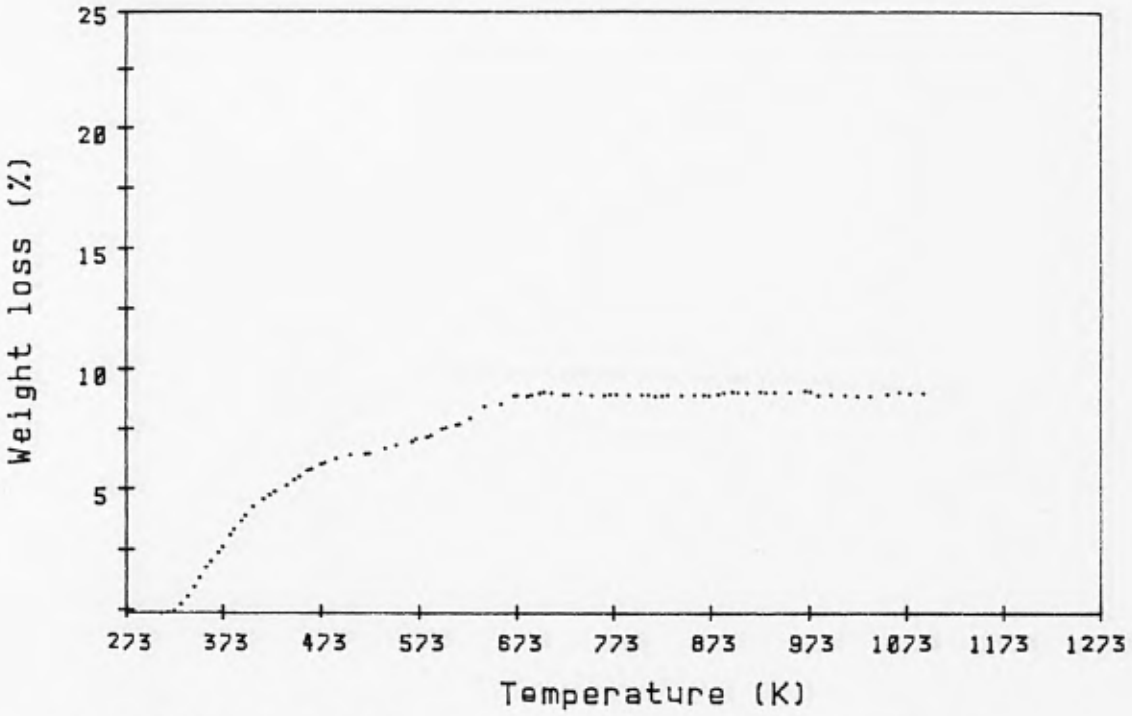

Fig.T3: Thermogram (TG plot) of Cu-NaMOR in air.

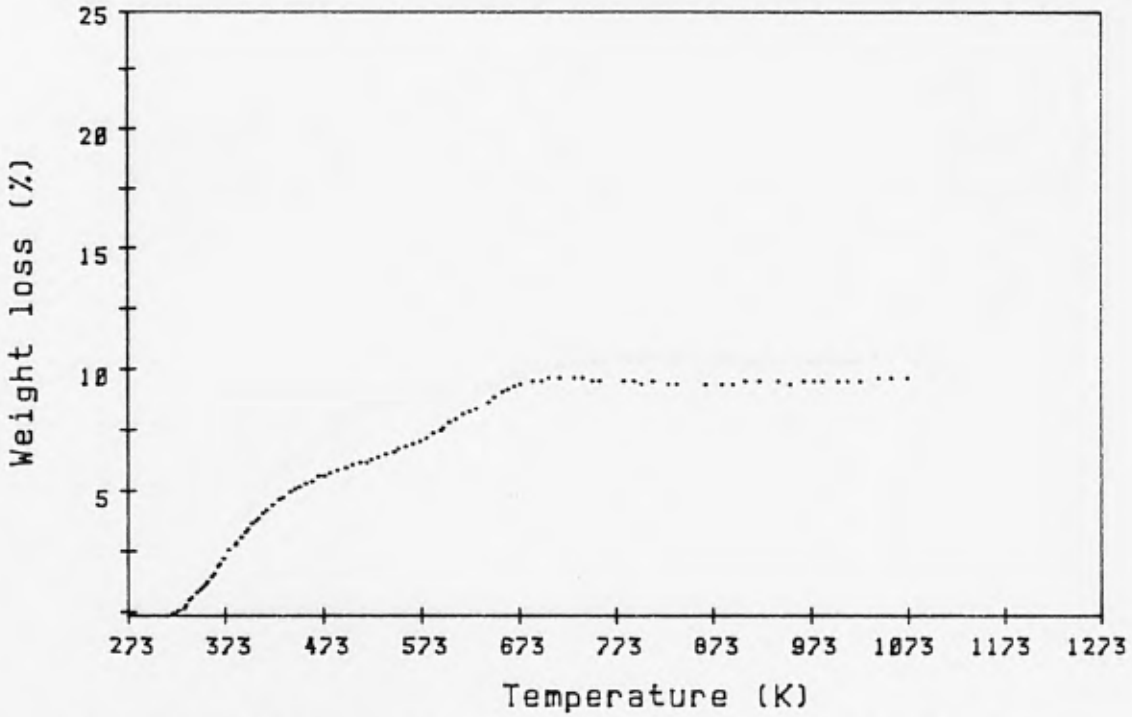

Fig.T4: Thermogram (TG plot) of Cu-NH4MOR in air.

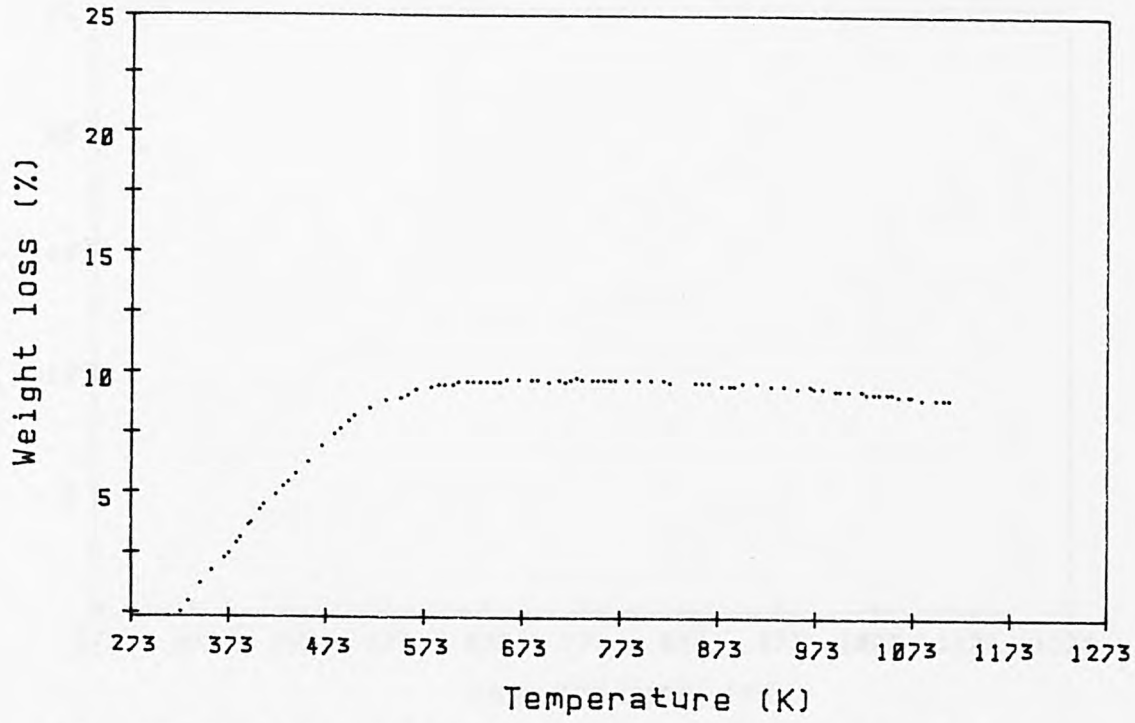

Fig.T5: Thermogram (TG plot) of Ni-NaMOR in air.

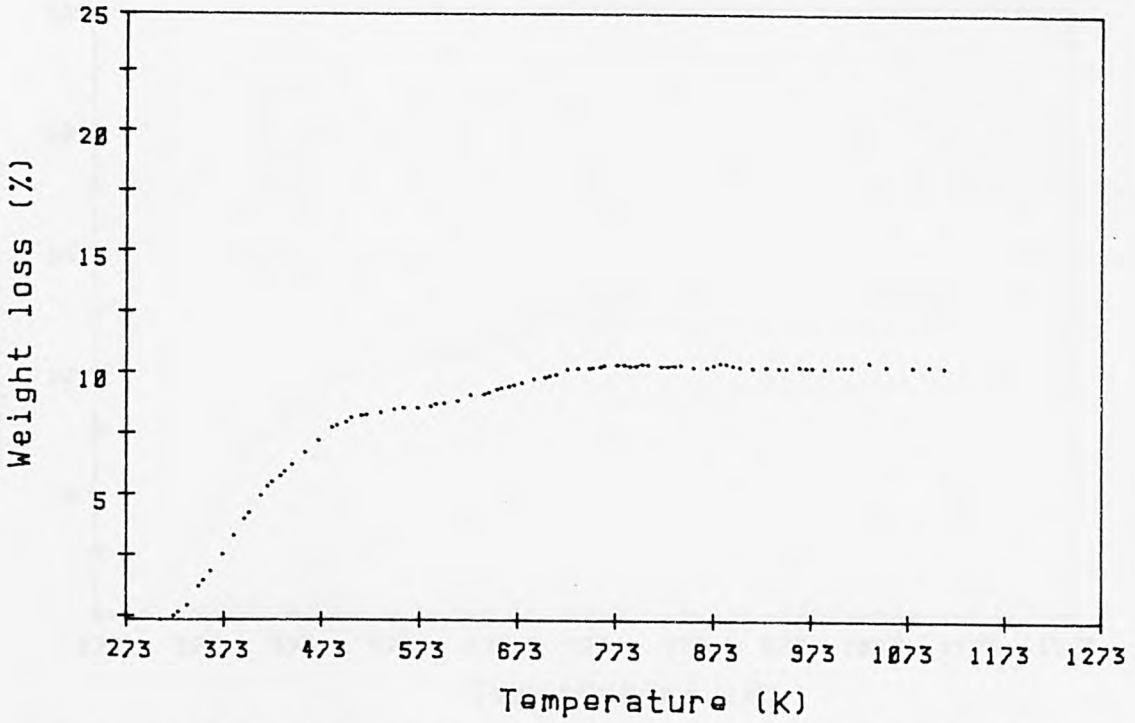

Fig.T6: Thermogram (TG plot) of Ni-NH4MOR in air.

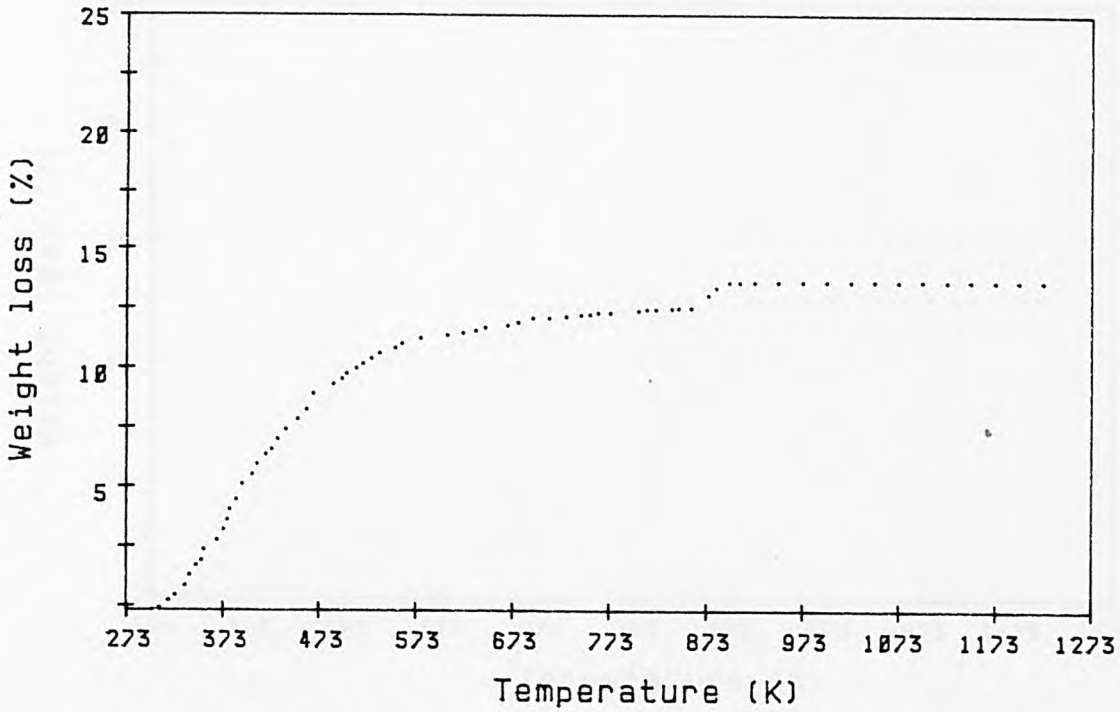

Fig.T7: Thermogram (TG plot) of Cu-Ni-NaM(1) in air.

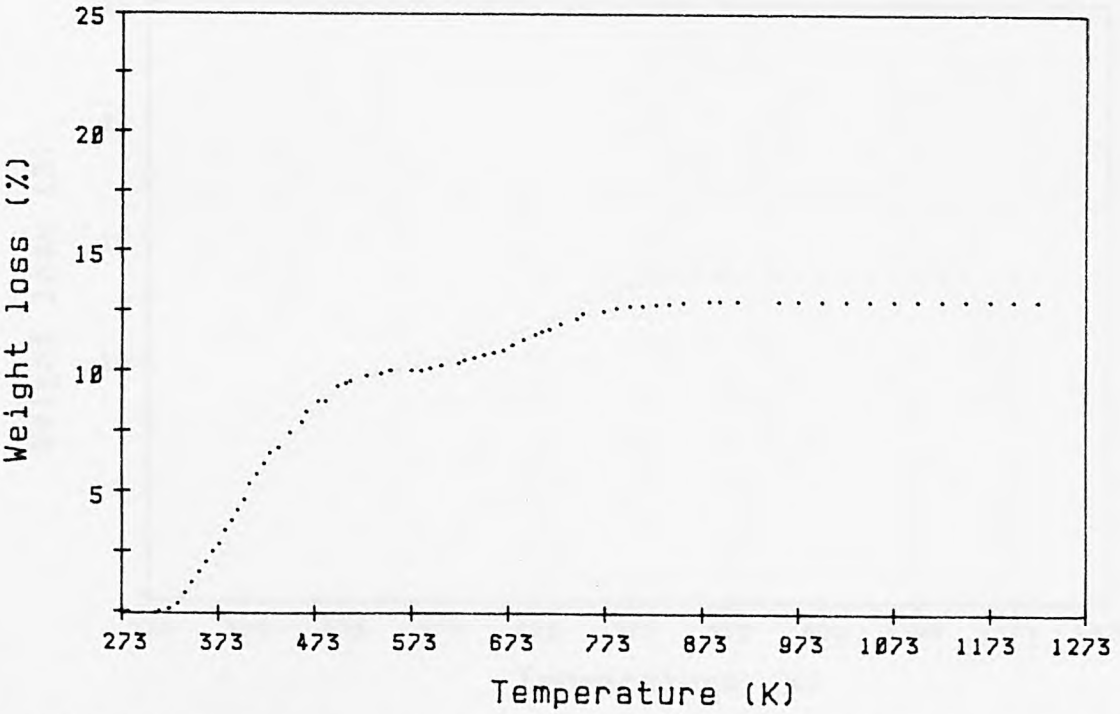

Fig.T8: Thermogram (TG plot) of Cu-Ni-NH4M(1) in air.

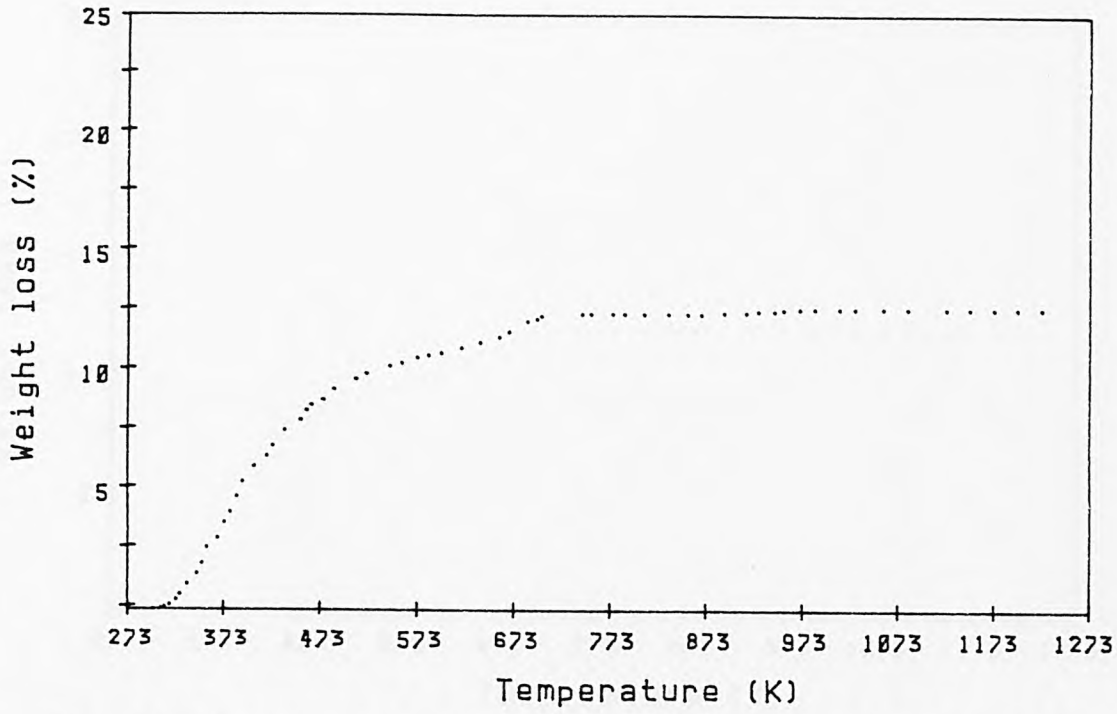

Fig.T9:Thermogram (TG plot) of Cu-Ni-NaM(2) in air.

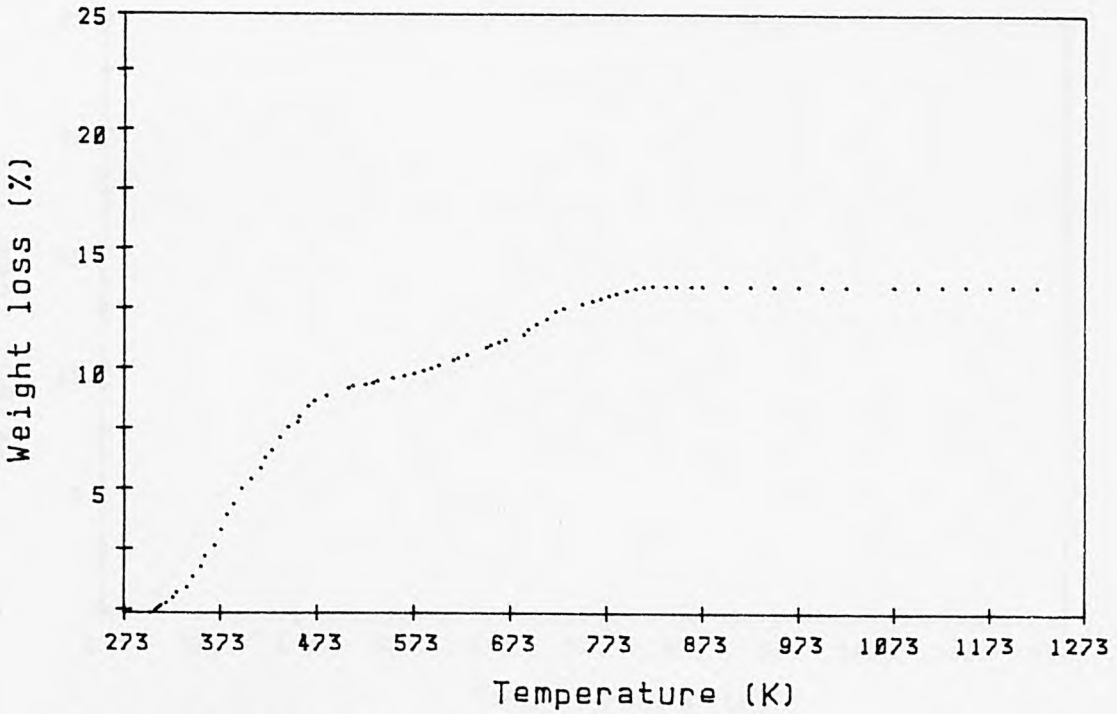

Fig.T10:Thermogram (TG plot) of Cu-Ni-NH4M(2) in air.

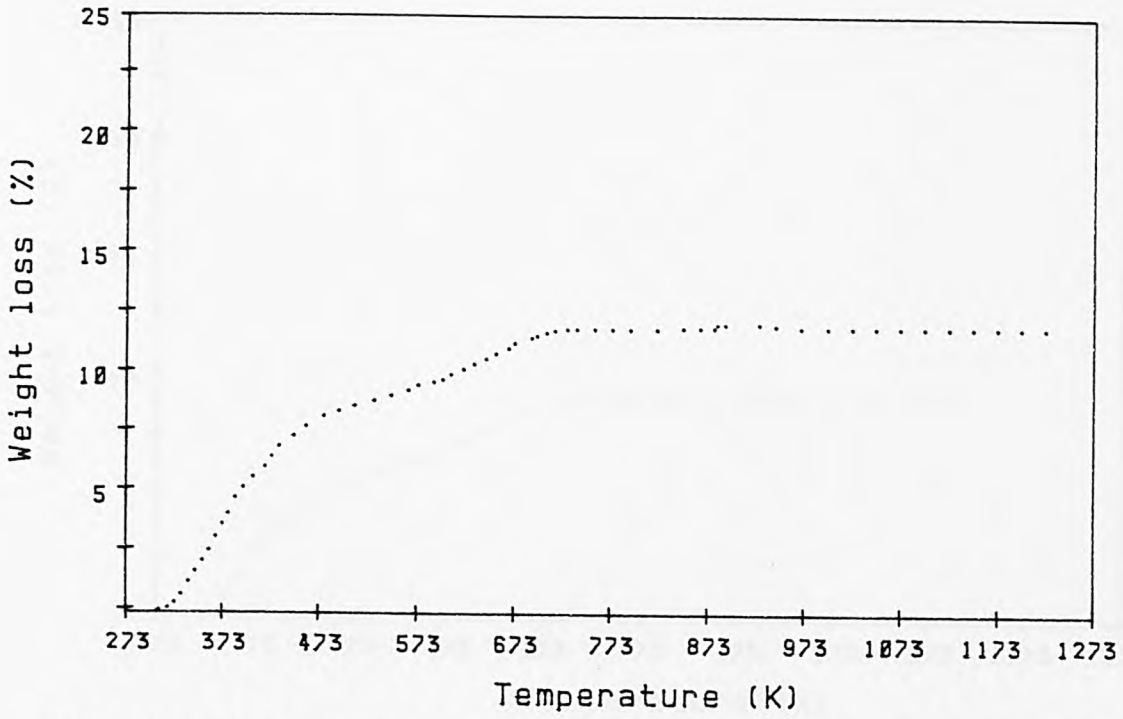

Fig.T11:Thermogram (TG plot) of Cu-Ni-NaM(3) in air.

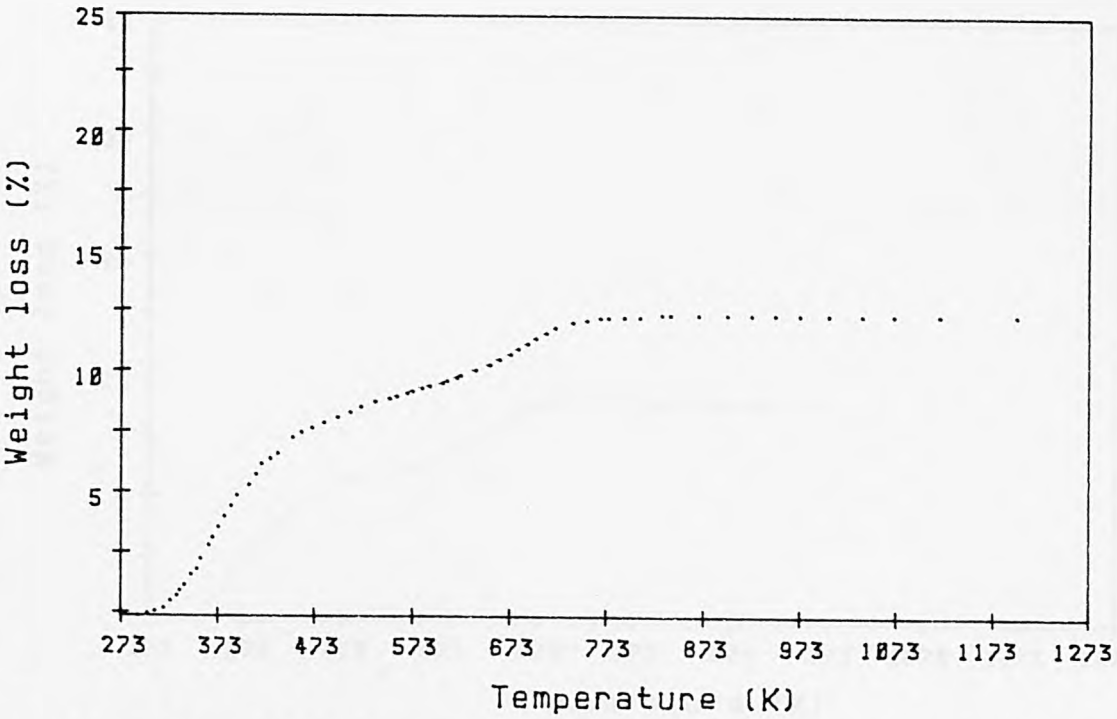

Fig.T12:Thermogram (TG plot) of Cu-Ni-NH4M(3) in air.

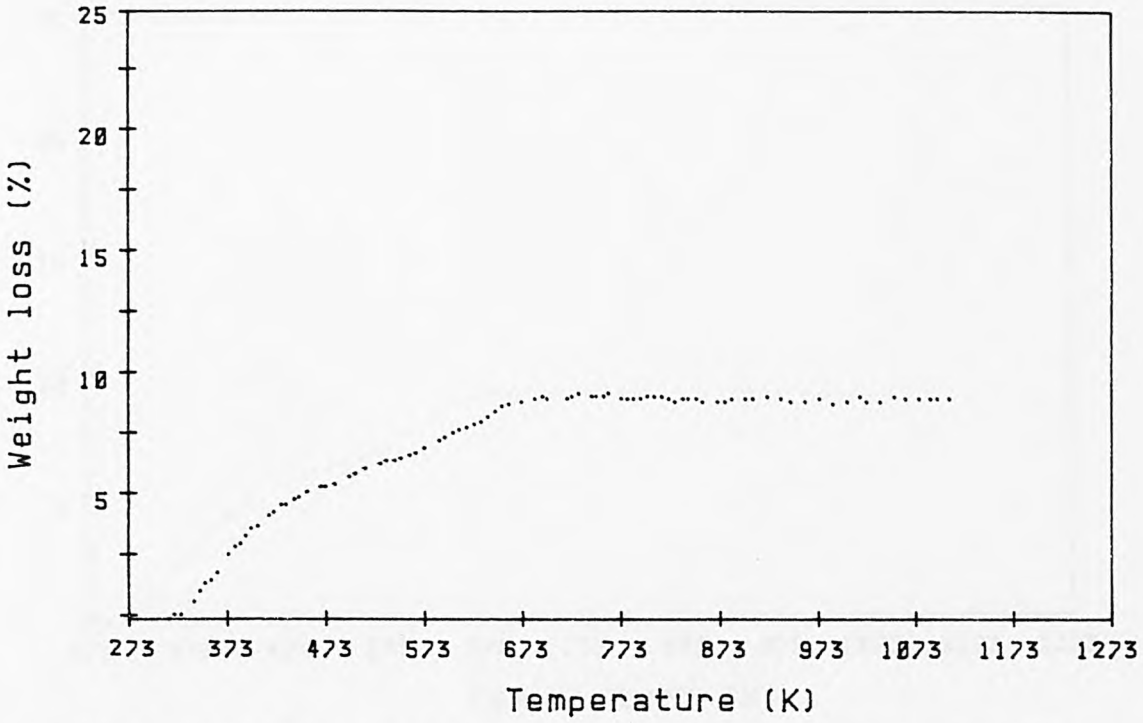

Fig.T13: Thermogram (TG plot) of Cu-MOR(1) in air.

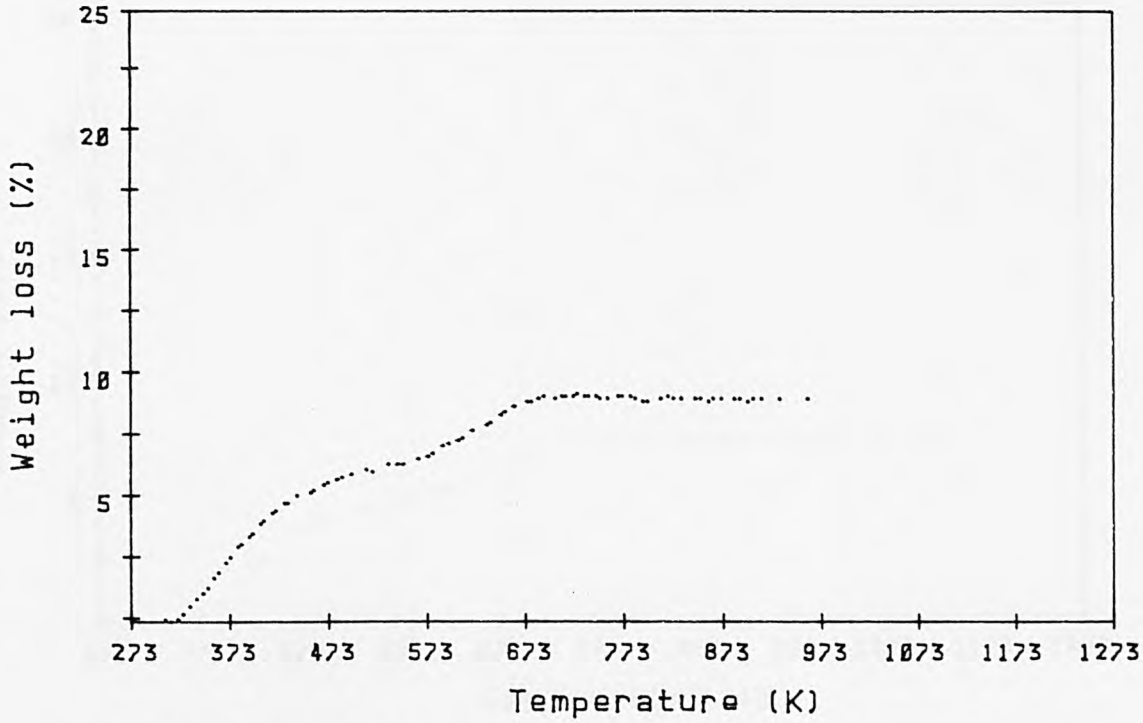

Fig.T14: Thermogram (TG plot) of Cu-MOR(2) in air.

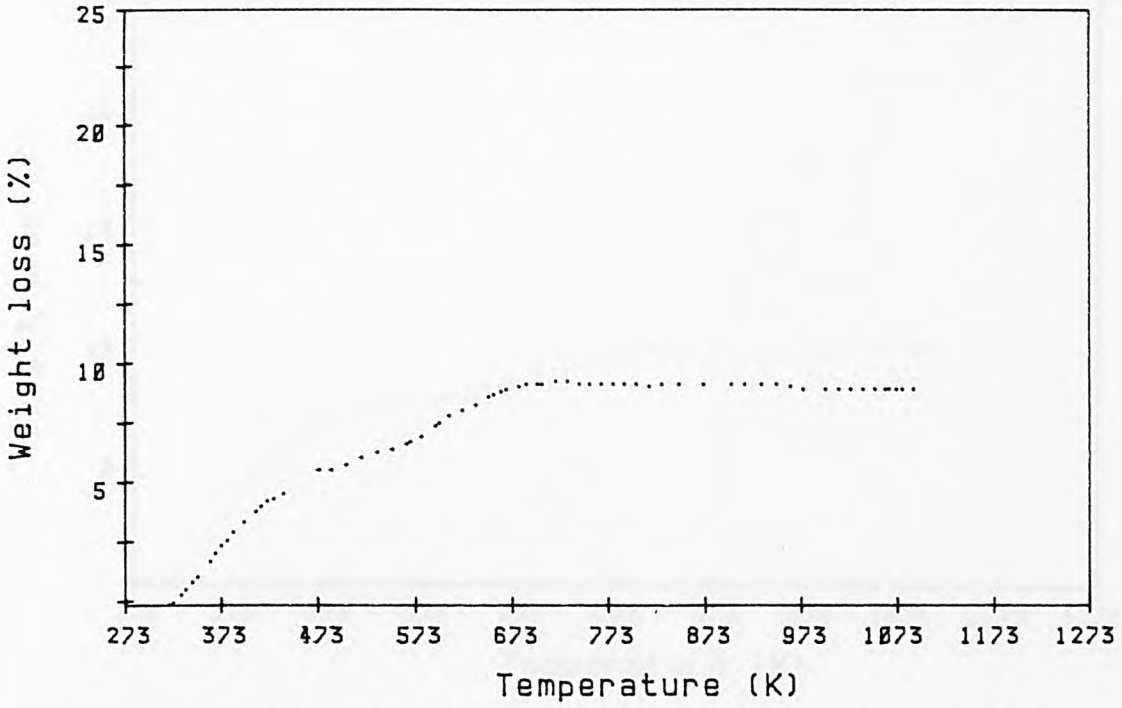

Fig.T15:Thermogram (TG plot) of Cu-MOR(3) in air.

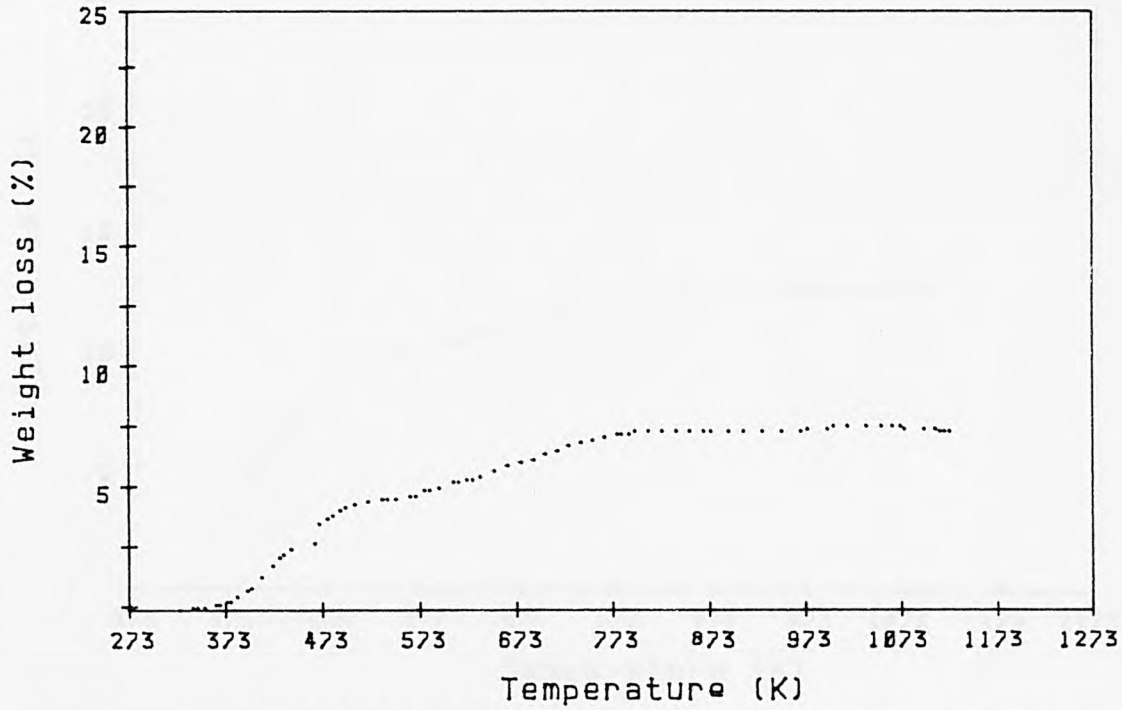

Fig.T16:Thermogram (TG plot) of Ni-MOR(1) in air.

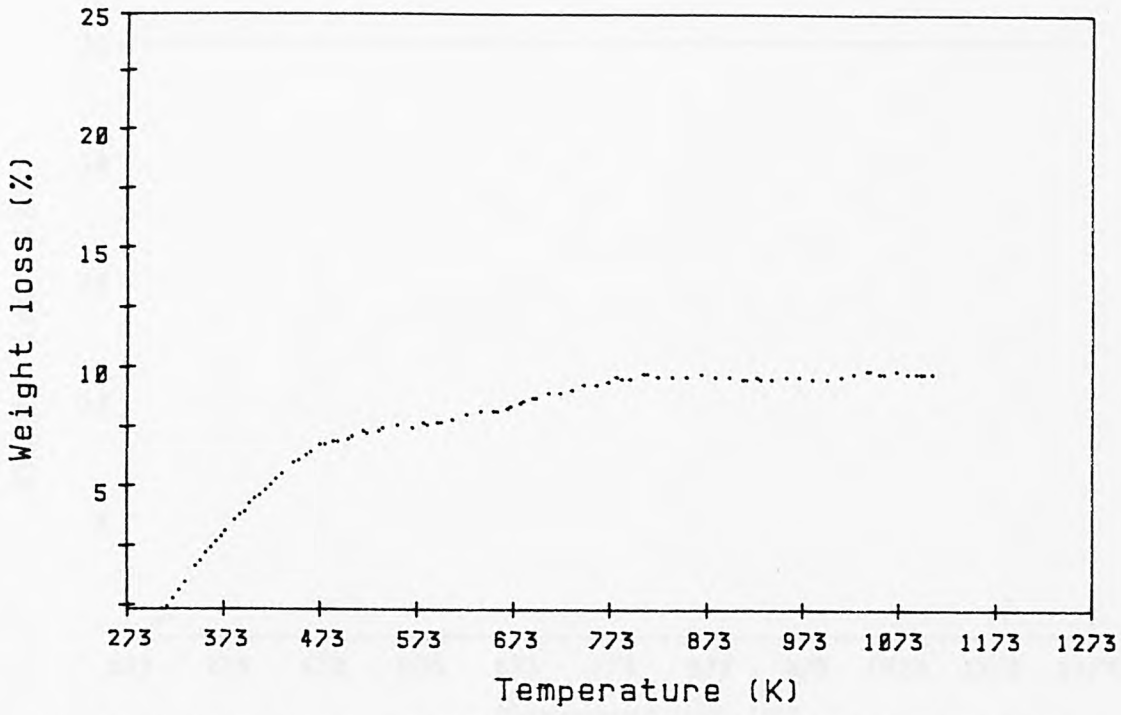

Fig.T17: Thermogram (TG plot) of Ni-MOR(2) in air.

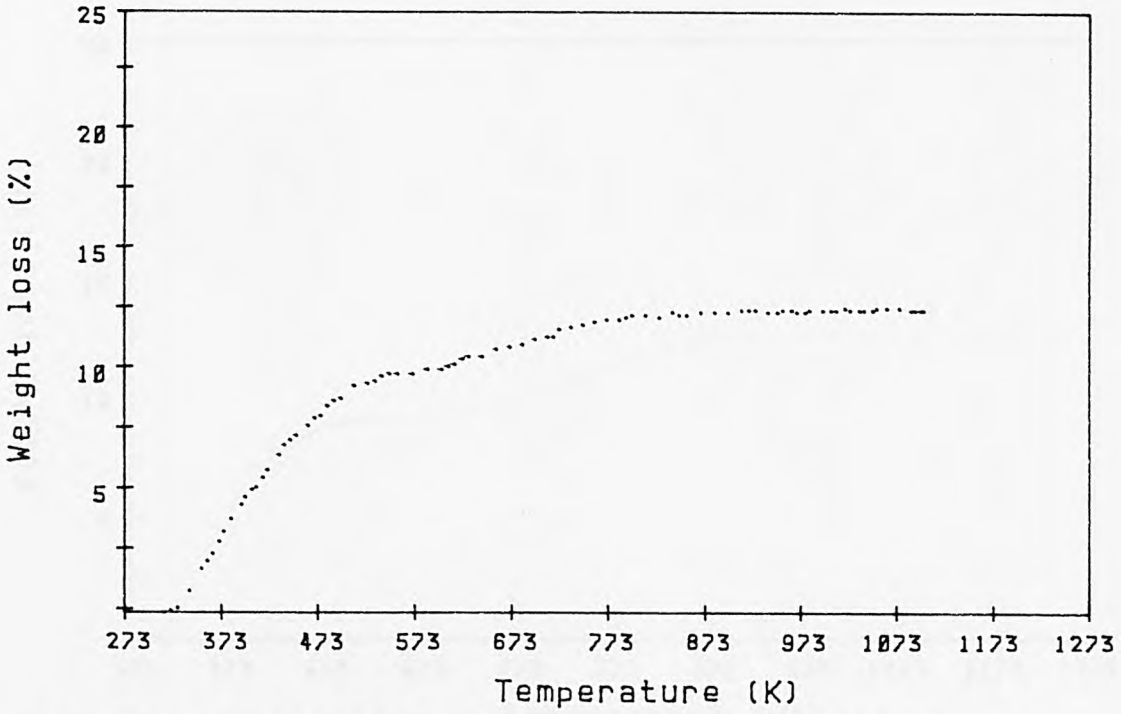

Fig.T18: Thermogram (TG plot) of Ni-MOR(3) in air.

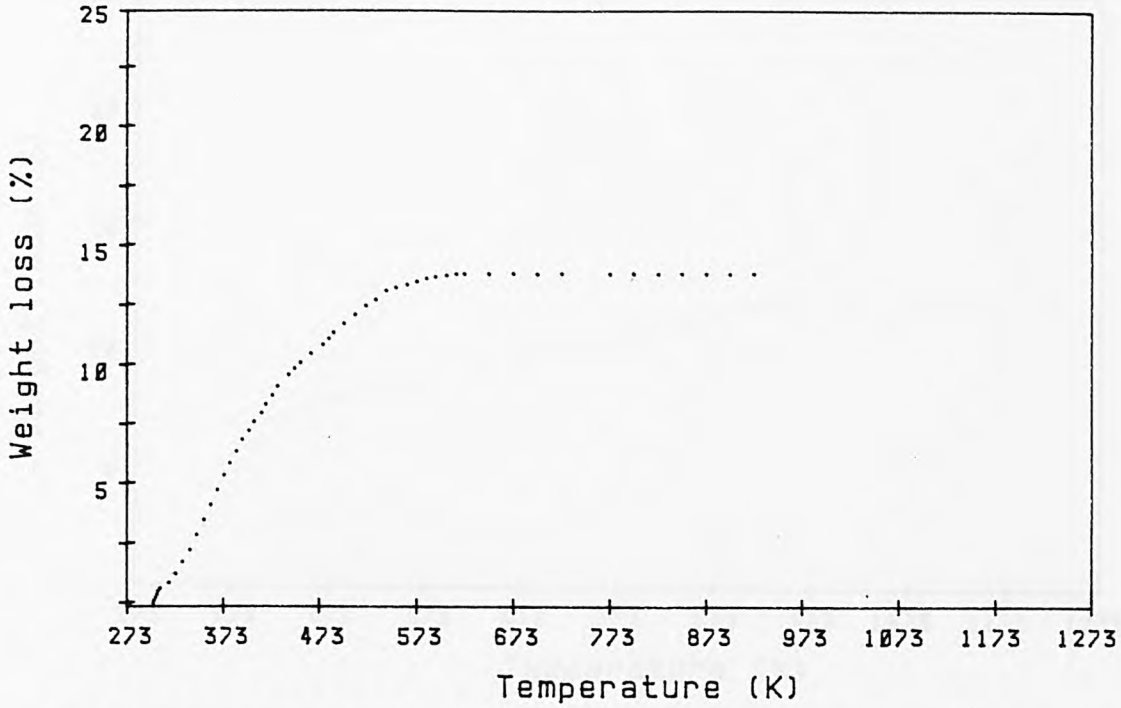

Fig.T19: Thermogram (TG plot) of Na-MOR in nitrogen.

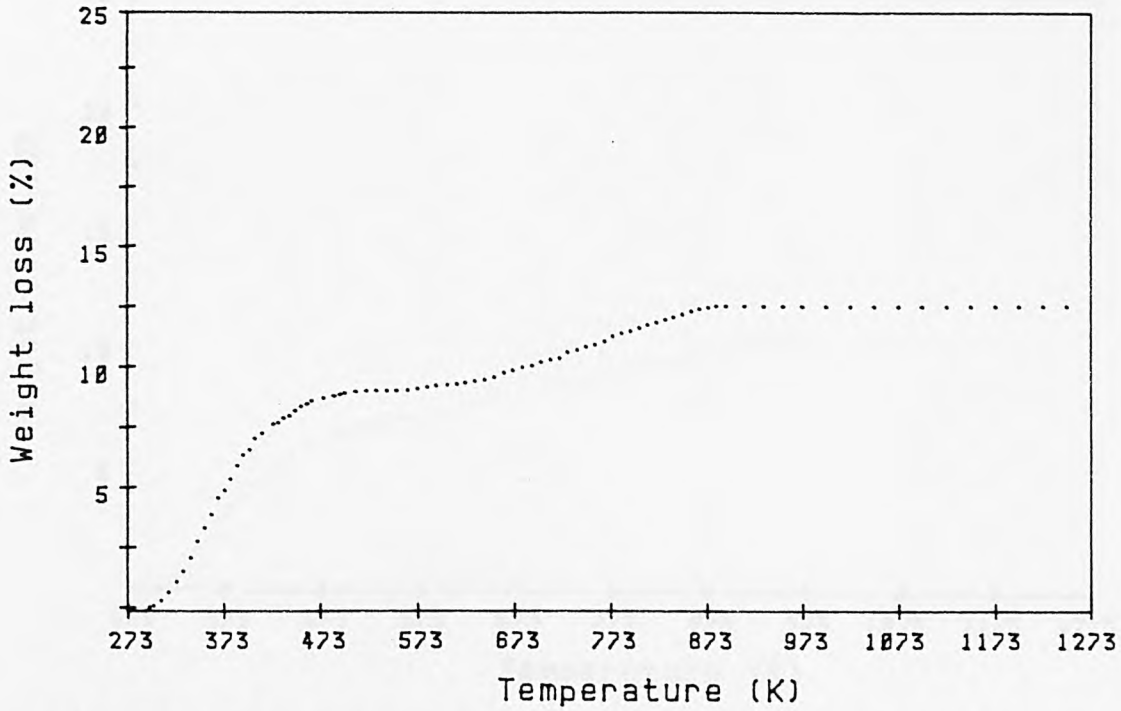

Fig.T20: Thermogram (TG plot) of NH4-MOR in nitrogen.

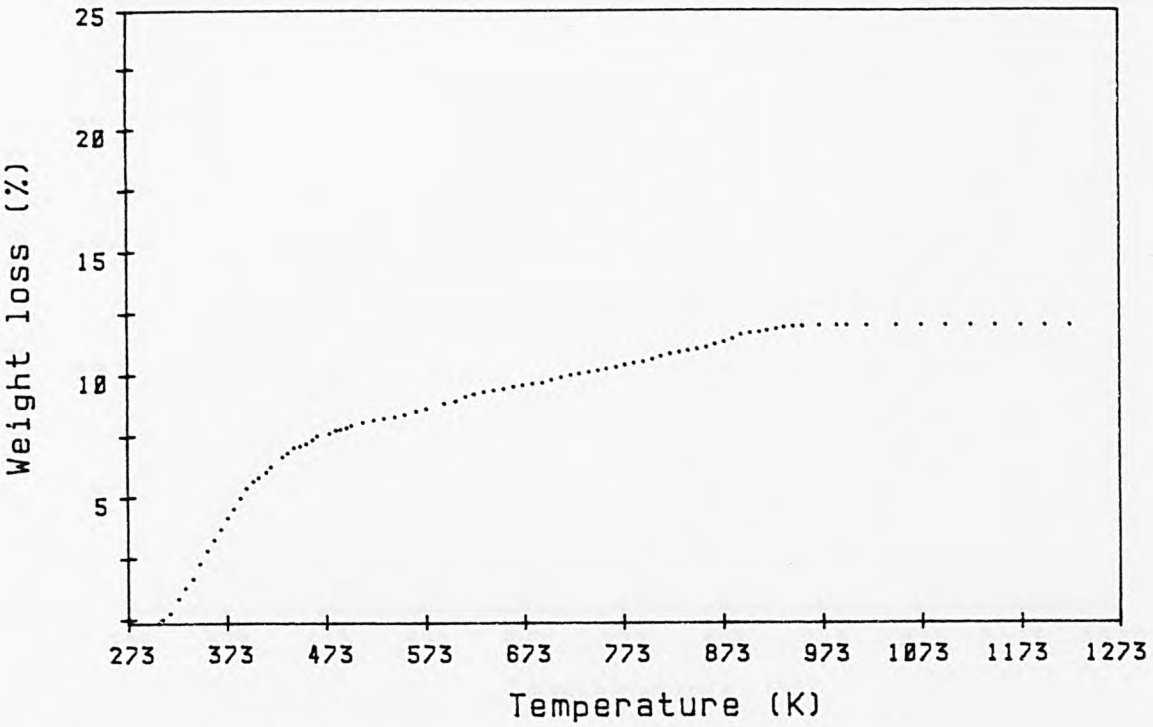

Fig.T21:Thermogram (TG plot) of Cu-NaMOR in nitrogen.

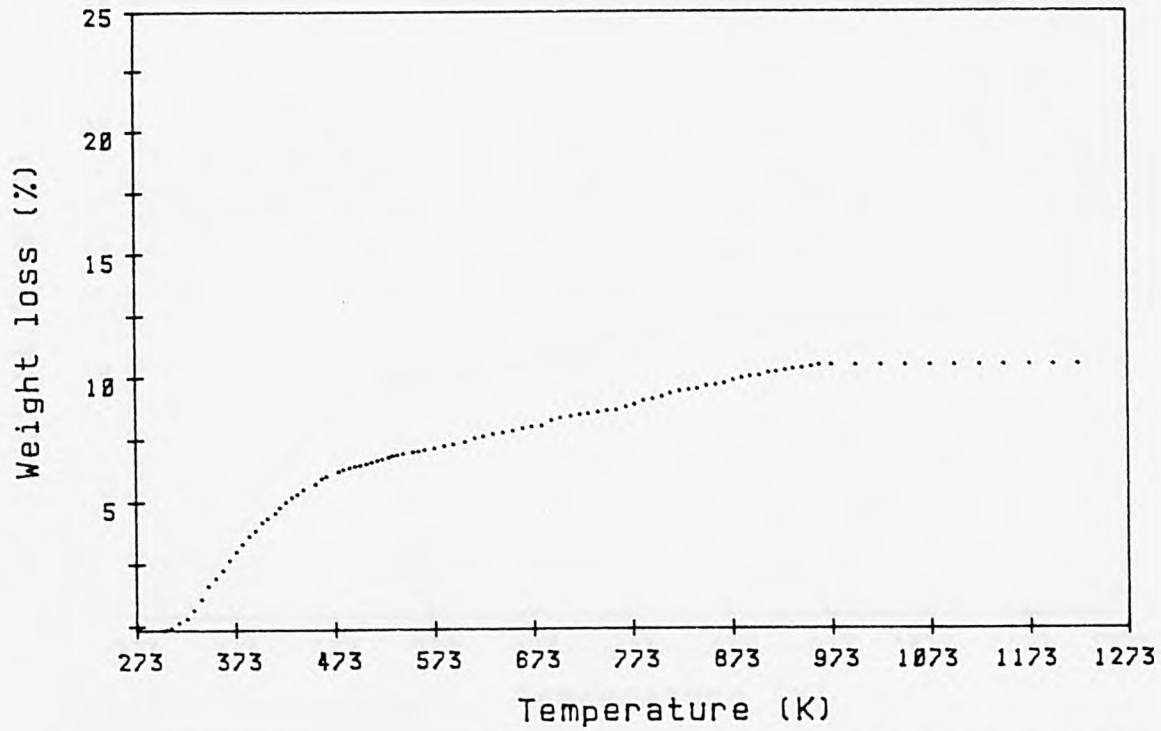

Fig.T22:Thermogram (TG plot) of Cu-NH4MOR in nitrogen.

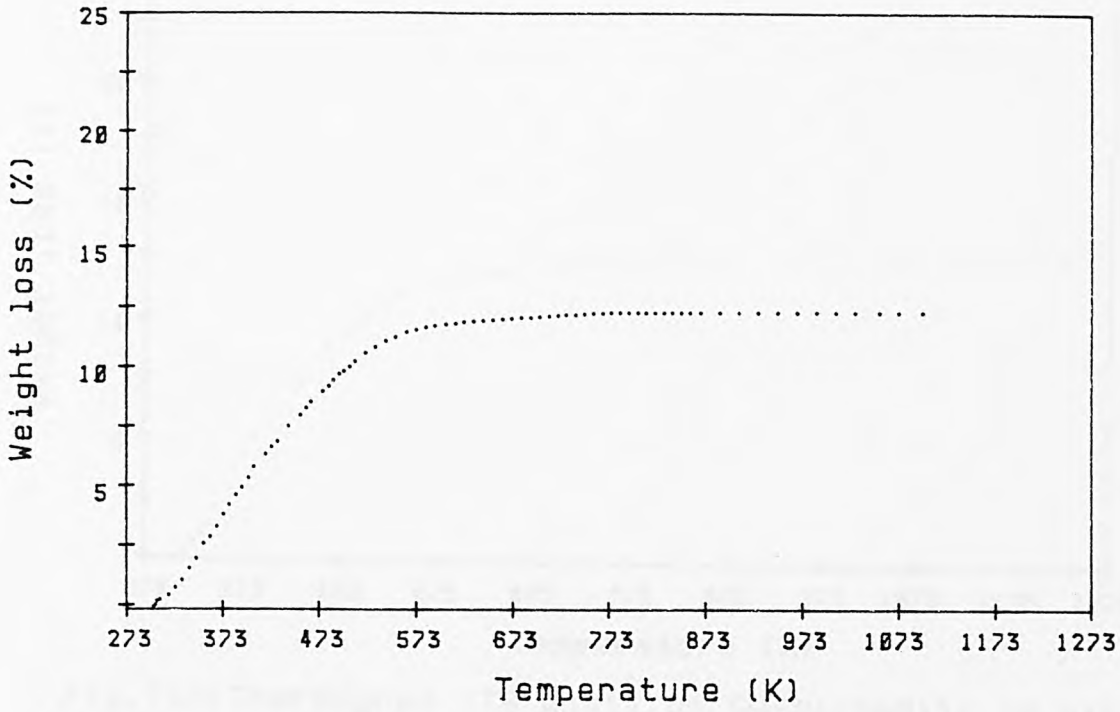

Fig.T23:Thermogram (TG plot) of Ni-NaMOR in nitrogen.

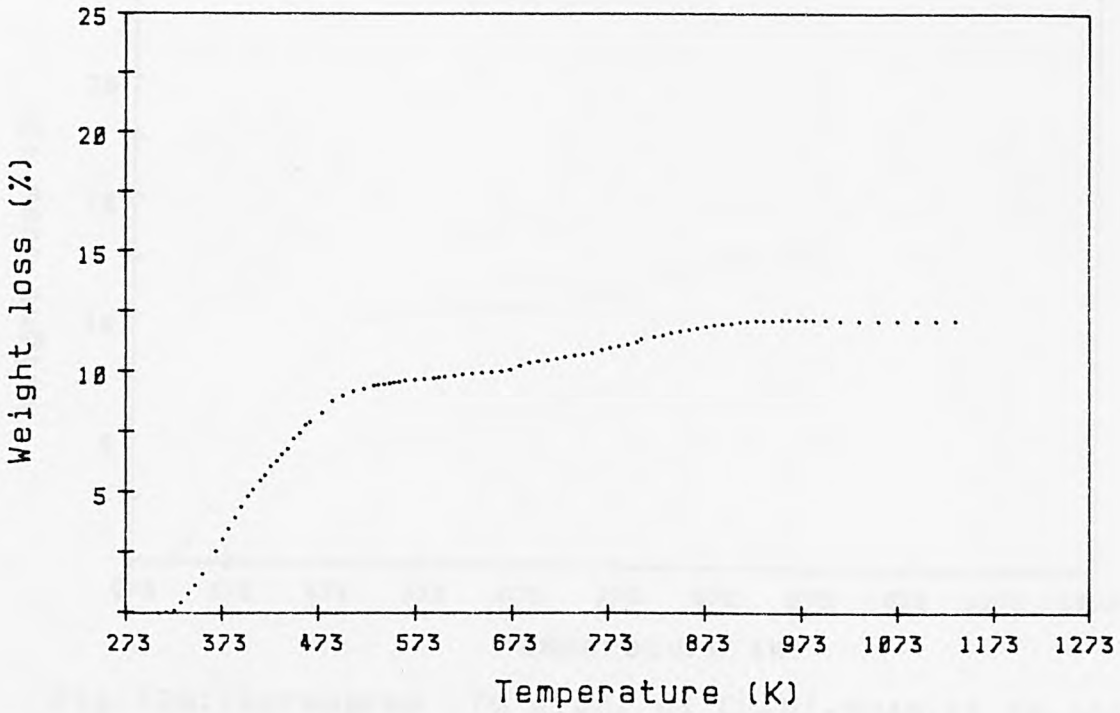

Fig.T24:Thermogram (TG plot) of Ni-NH4MOR in nitrogen.

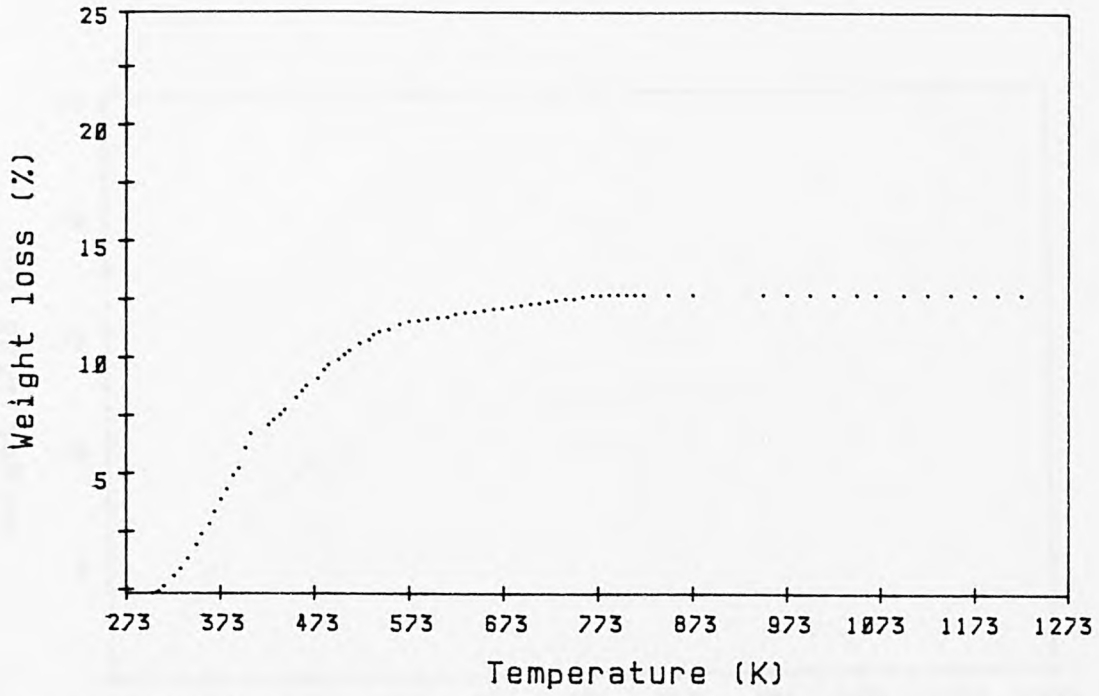

Fig.T25:Thermogram (TG plot) of Cu-Ni-NaM(1) in nitrogen.

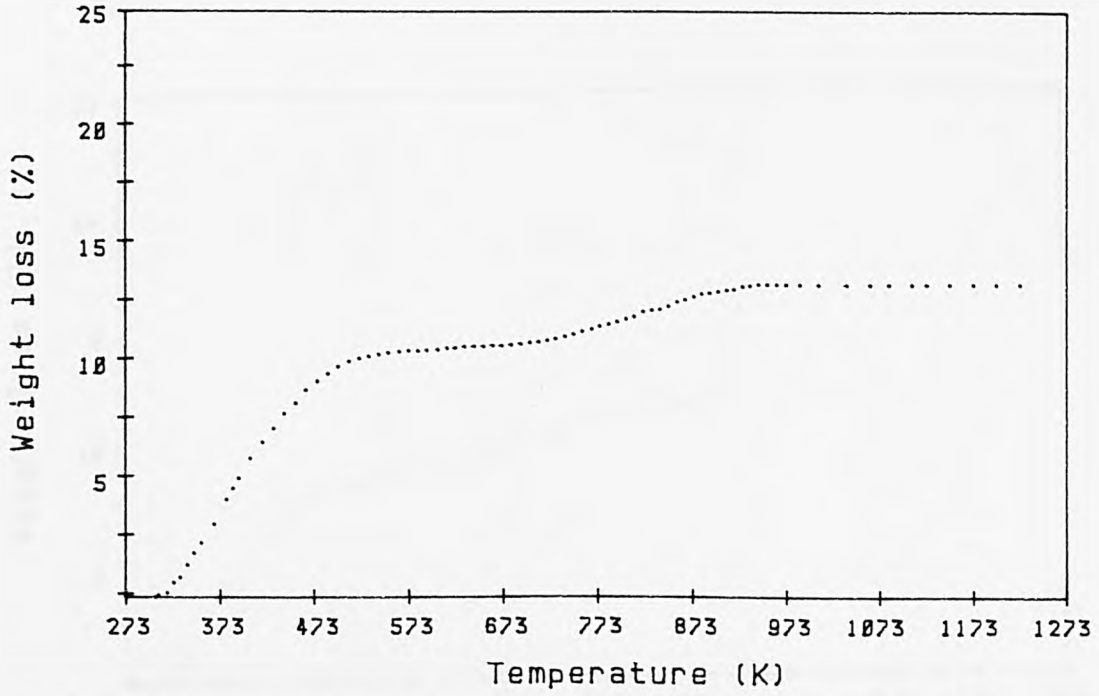

Fig.T26:Thermogram (TG plot) of Cu-Ni-NH4M(1) in nitrogen.

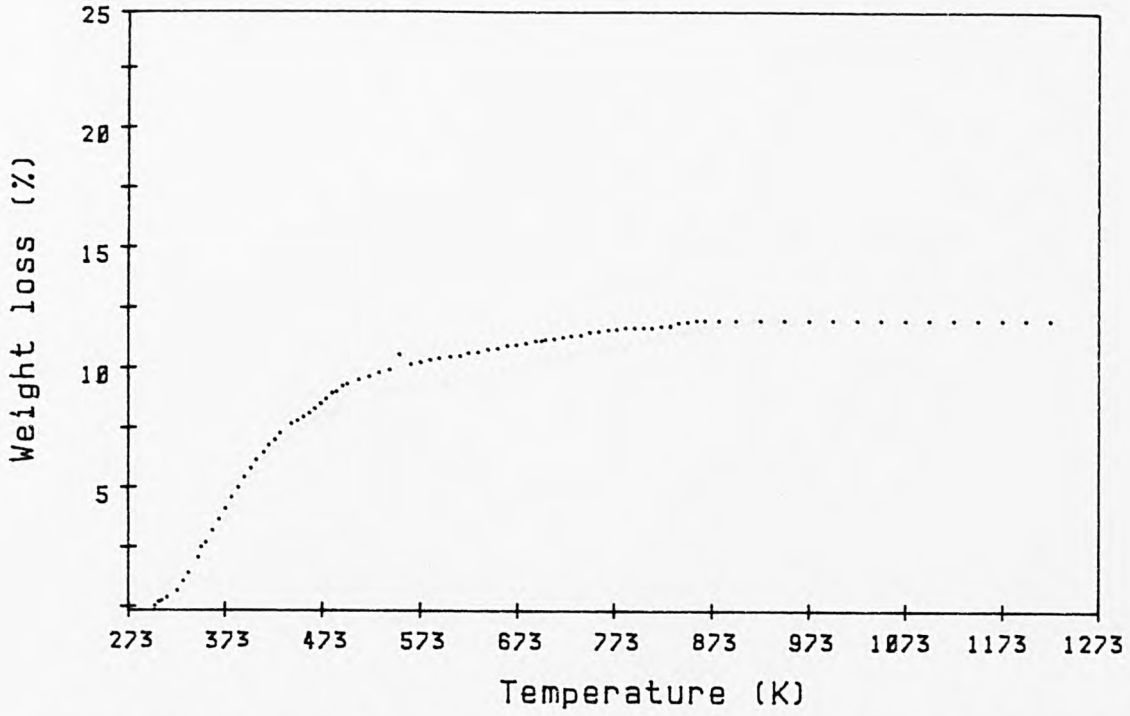

Fig.T27:Thermogram (TG plot) of Cu-Ni-NaM(2) in nitrogen.

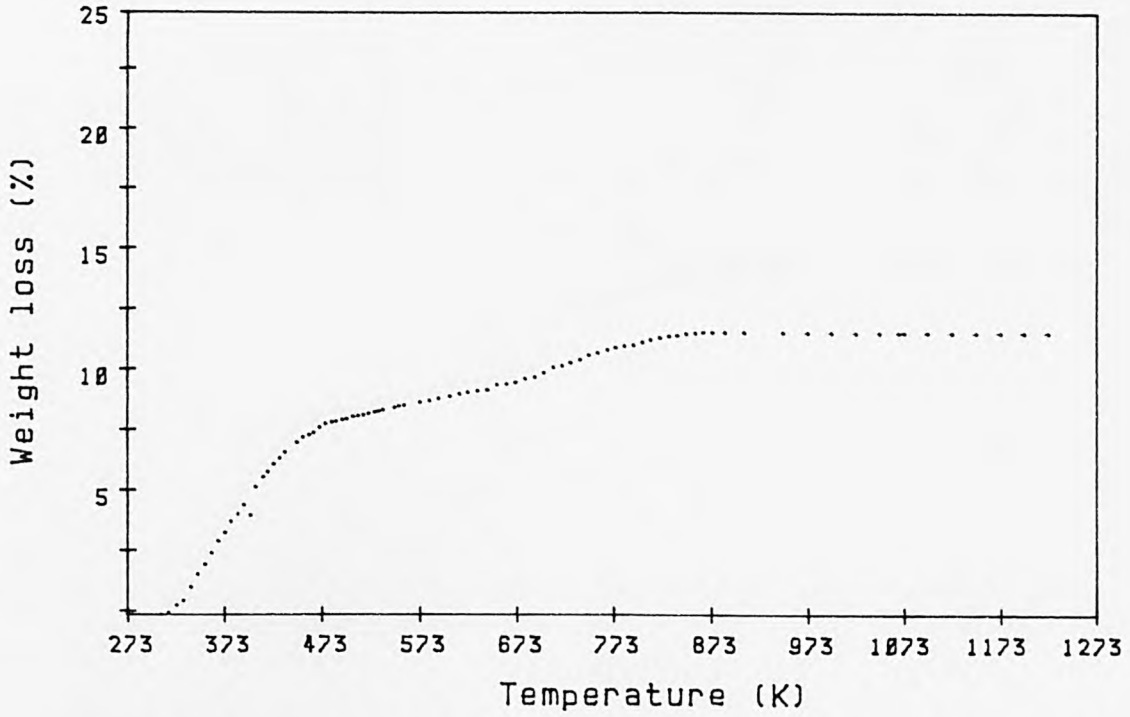

Fig.T28:Thermogram (TG plot) of Cu-Ni-NH4M(2) in nitroge

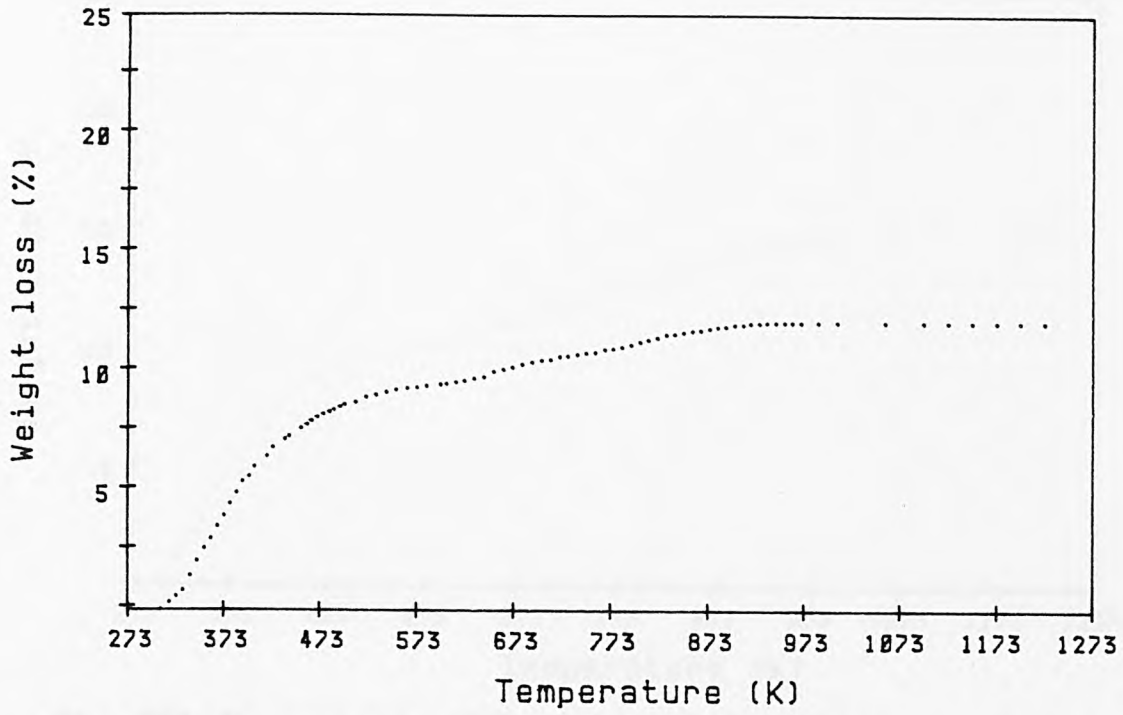

Fig.T29:Thermogram (TG plot) of Cu-Ni-NaM(3) in nitrogen.

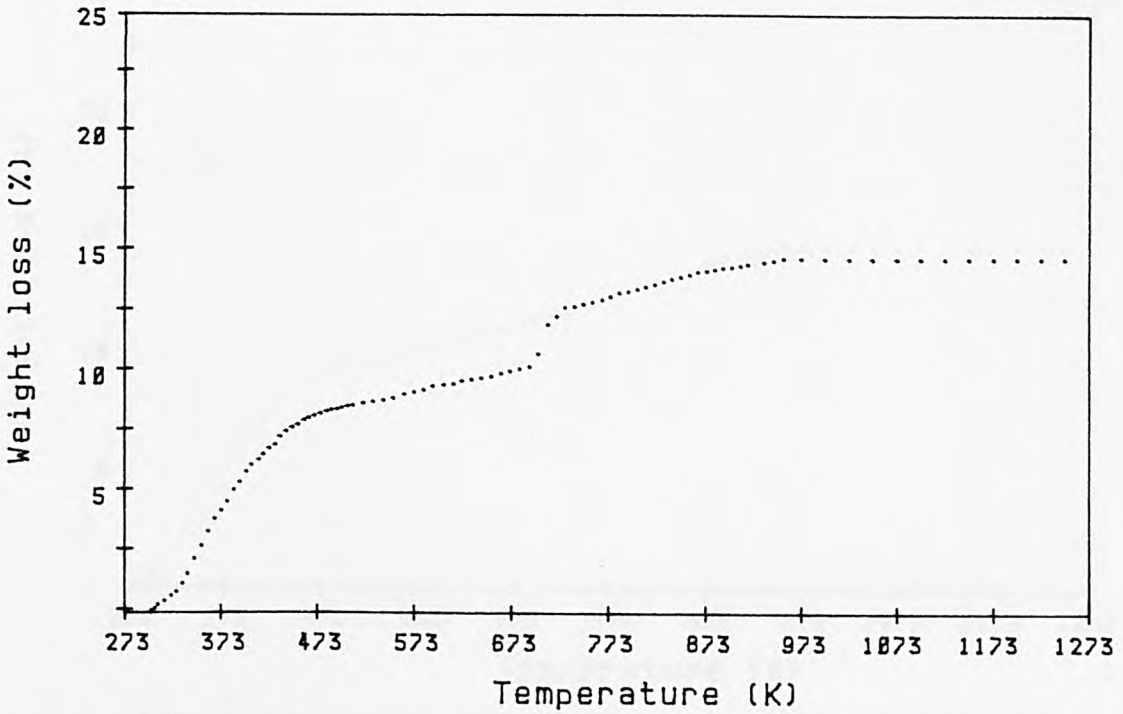

Fig.T30:Thermogram (TG plot) of Cu-Ni-NH4M(3) in nitrogen.

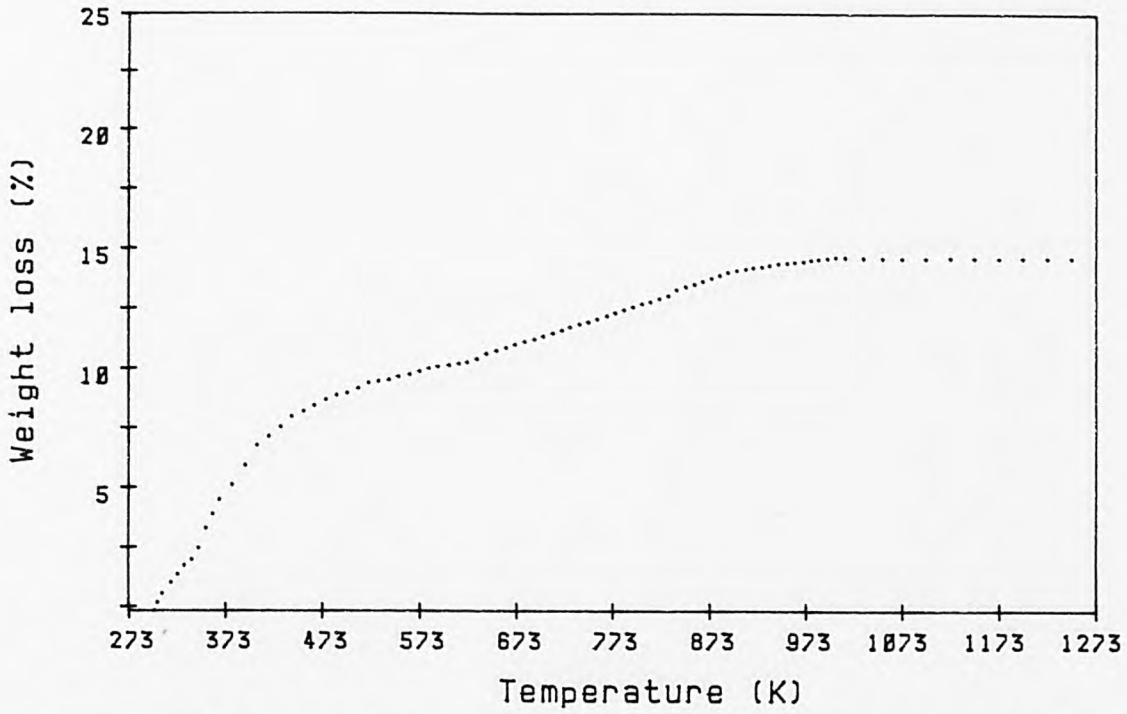

Fig.T31: Thermogram (TG plot) of Cu-MOR(1) in nitrogen.

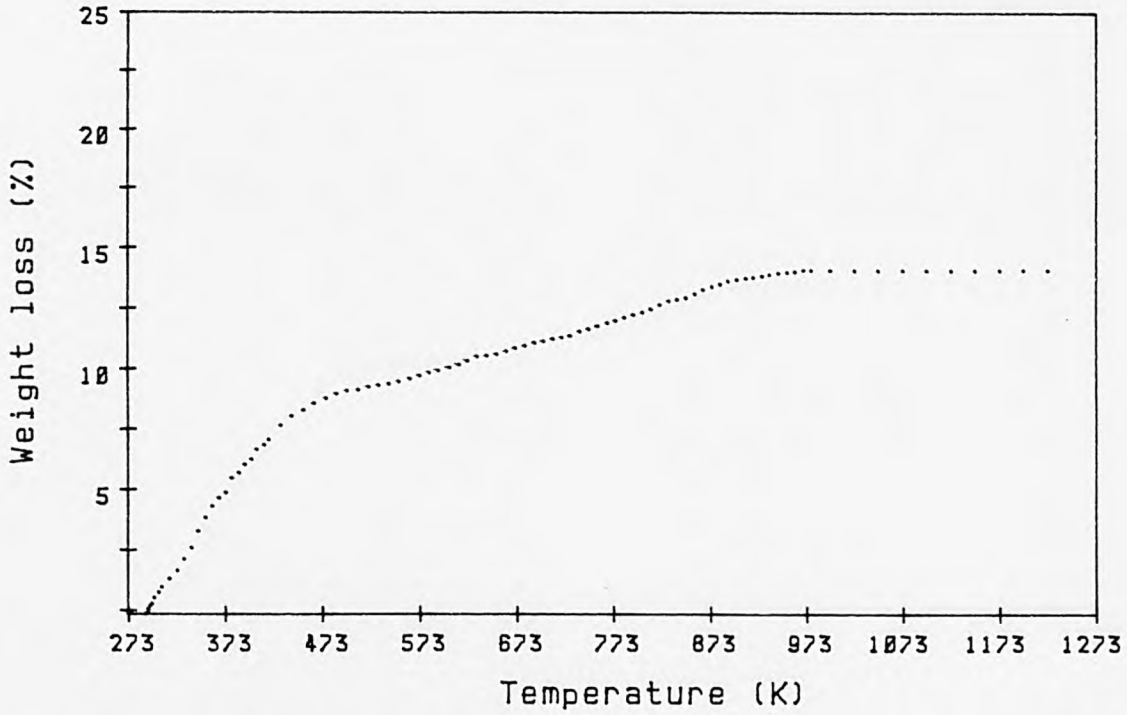

Fig.T32: Thermogram (TG plot) of Cu-MOR(2) in nitrogen.

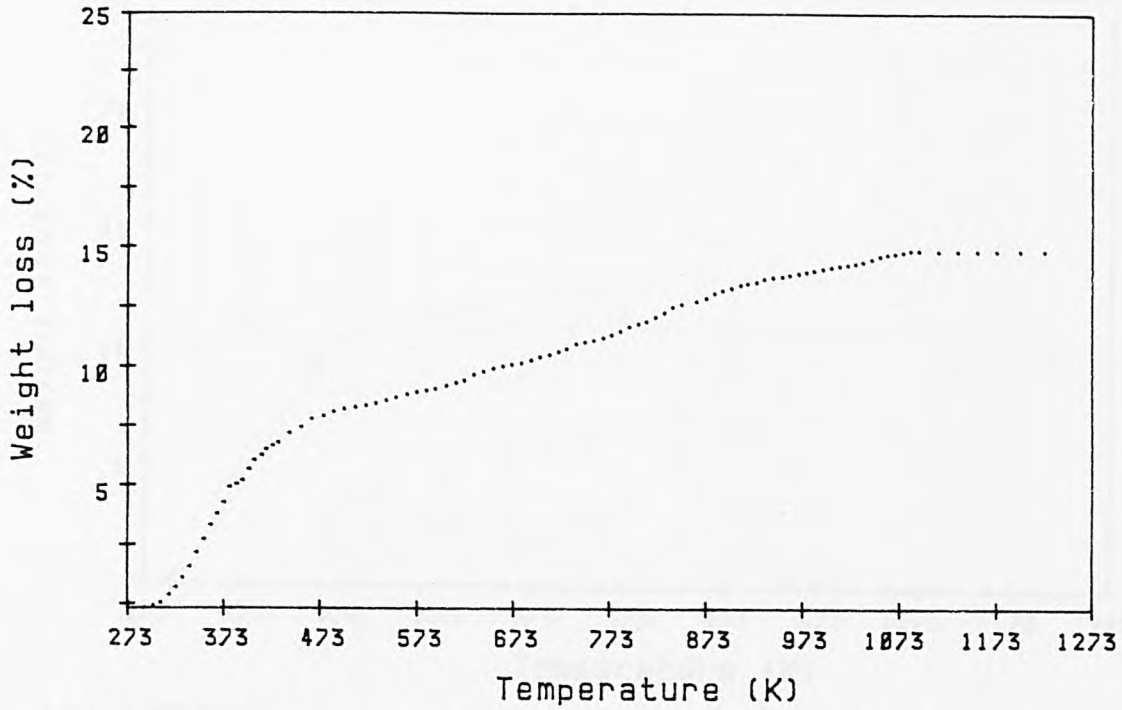

Fig.T33:Thermogram (TG plot) of Cu-MOR(3) in nitrogen.

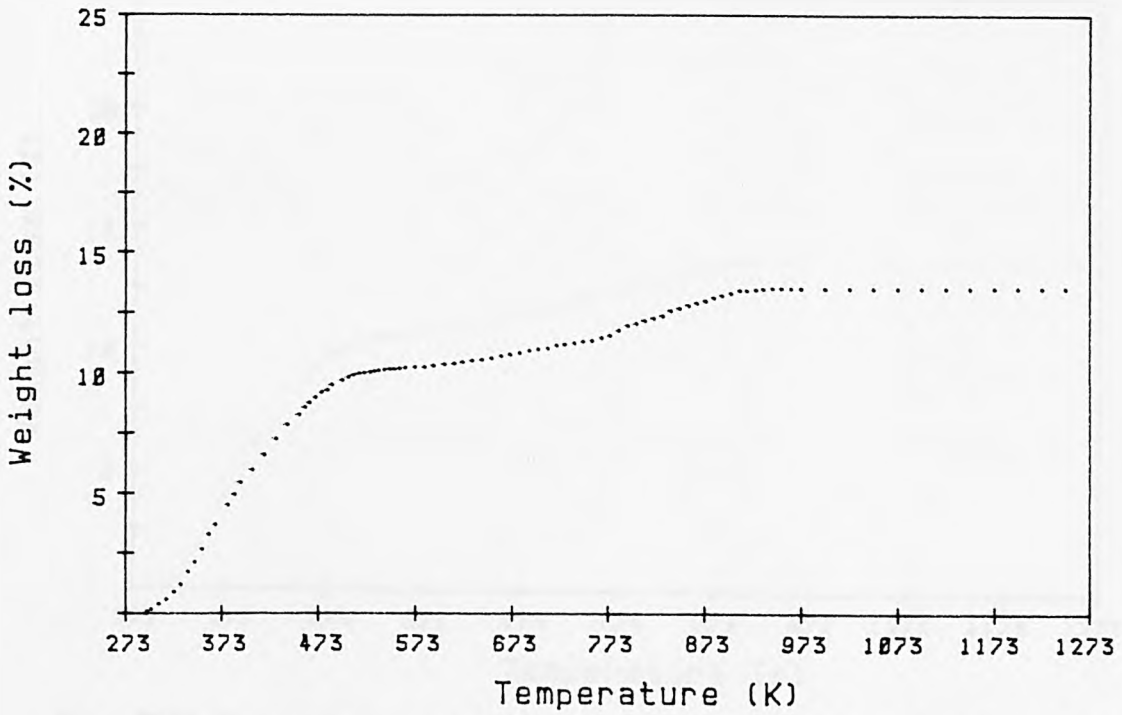

Fig.T34:Thermogram (TG plot) of Ni-MOR(1) in nitrogen.

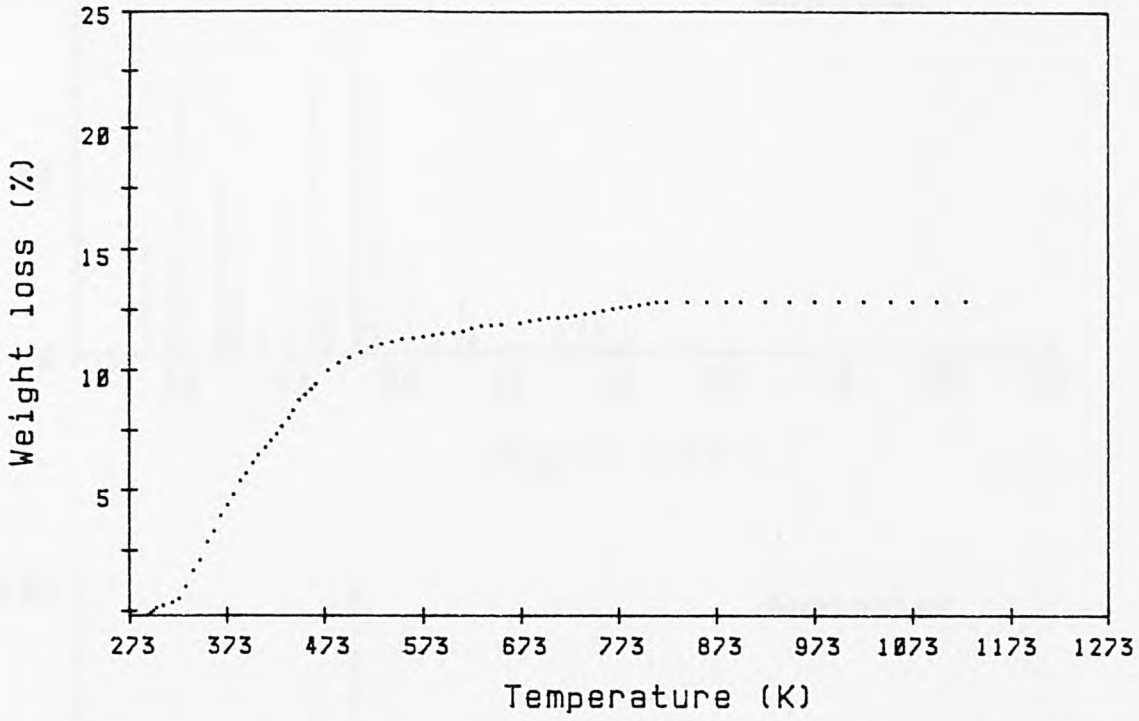

Fig.T35:Thermogram (TG plot) of Ni-MOR(2) in nitrogen.

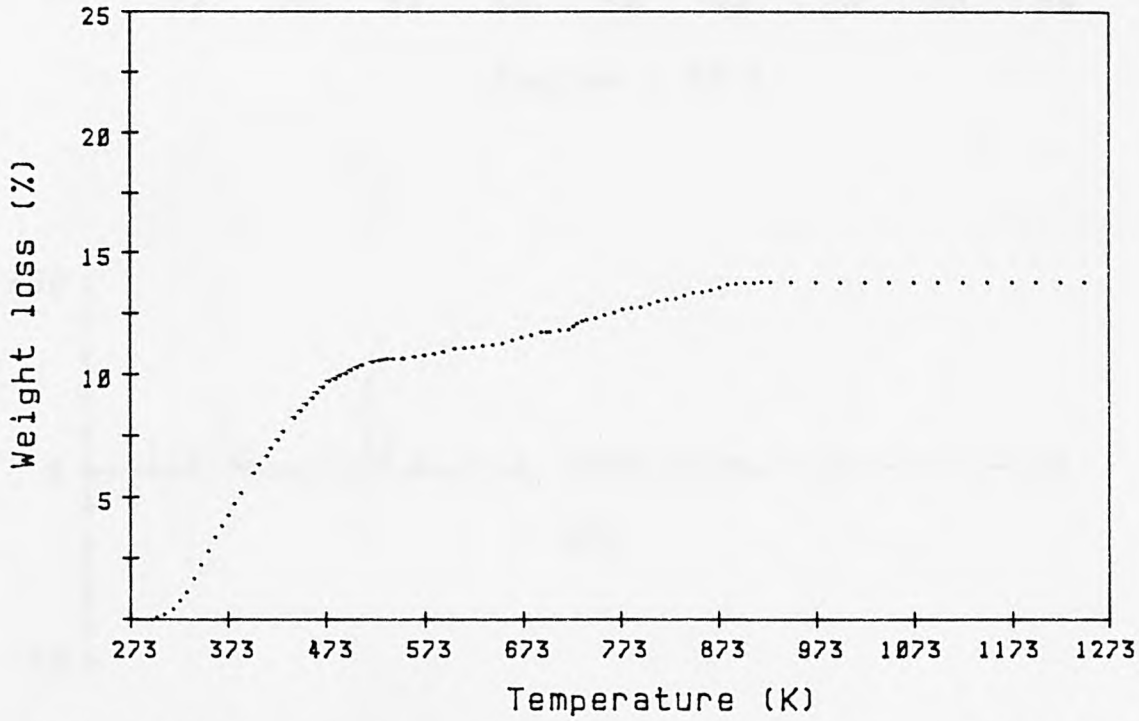

Fig.T36:Thermogram (TG plot) of Ni-MOR(3) in nitrogen.

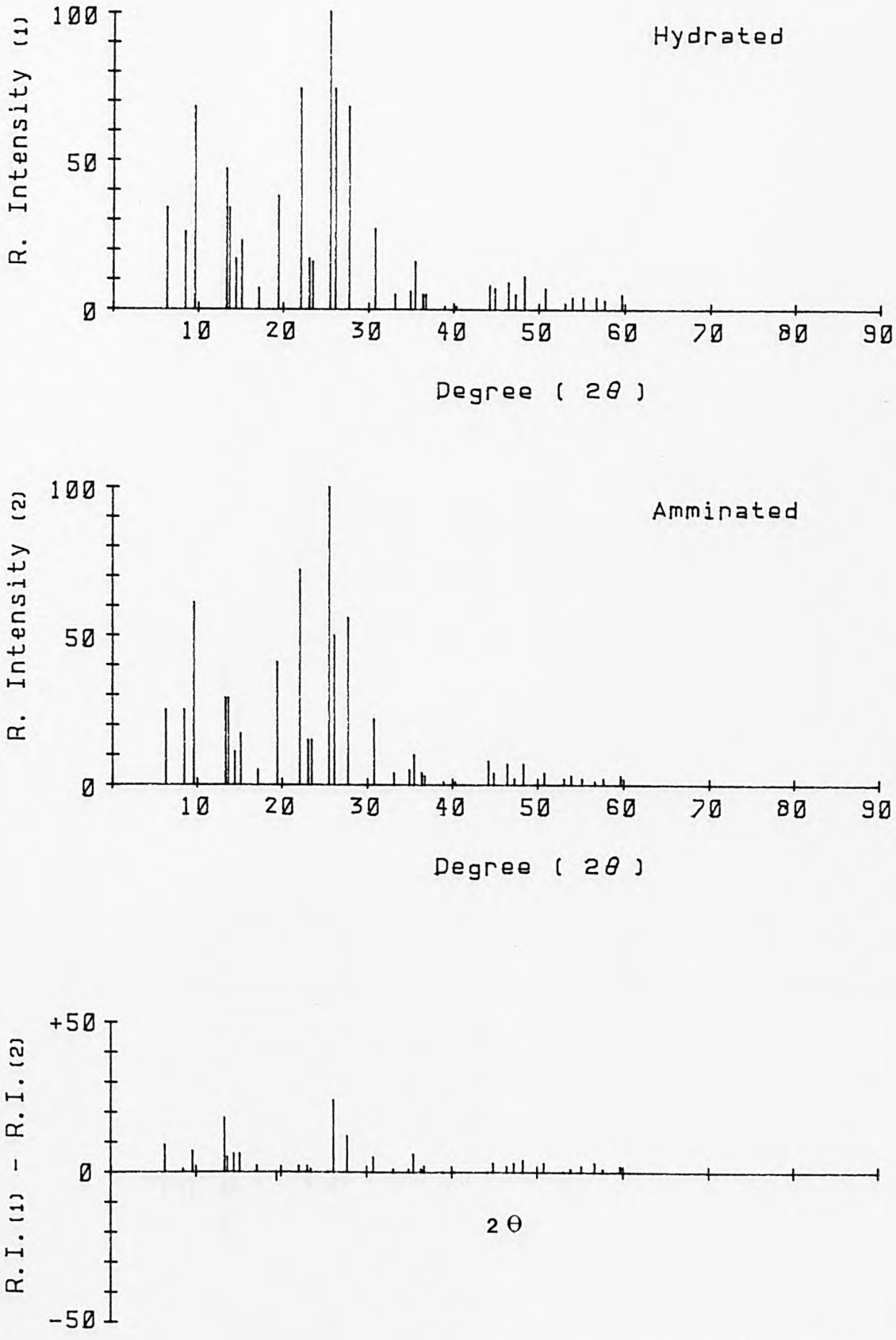

Fig. X.1: Distribution of relative intensity for X-ray diffraction of zeolite Na/NH4-MOR.

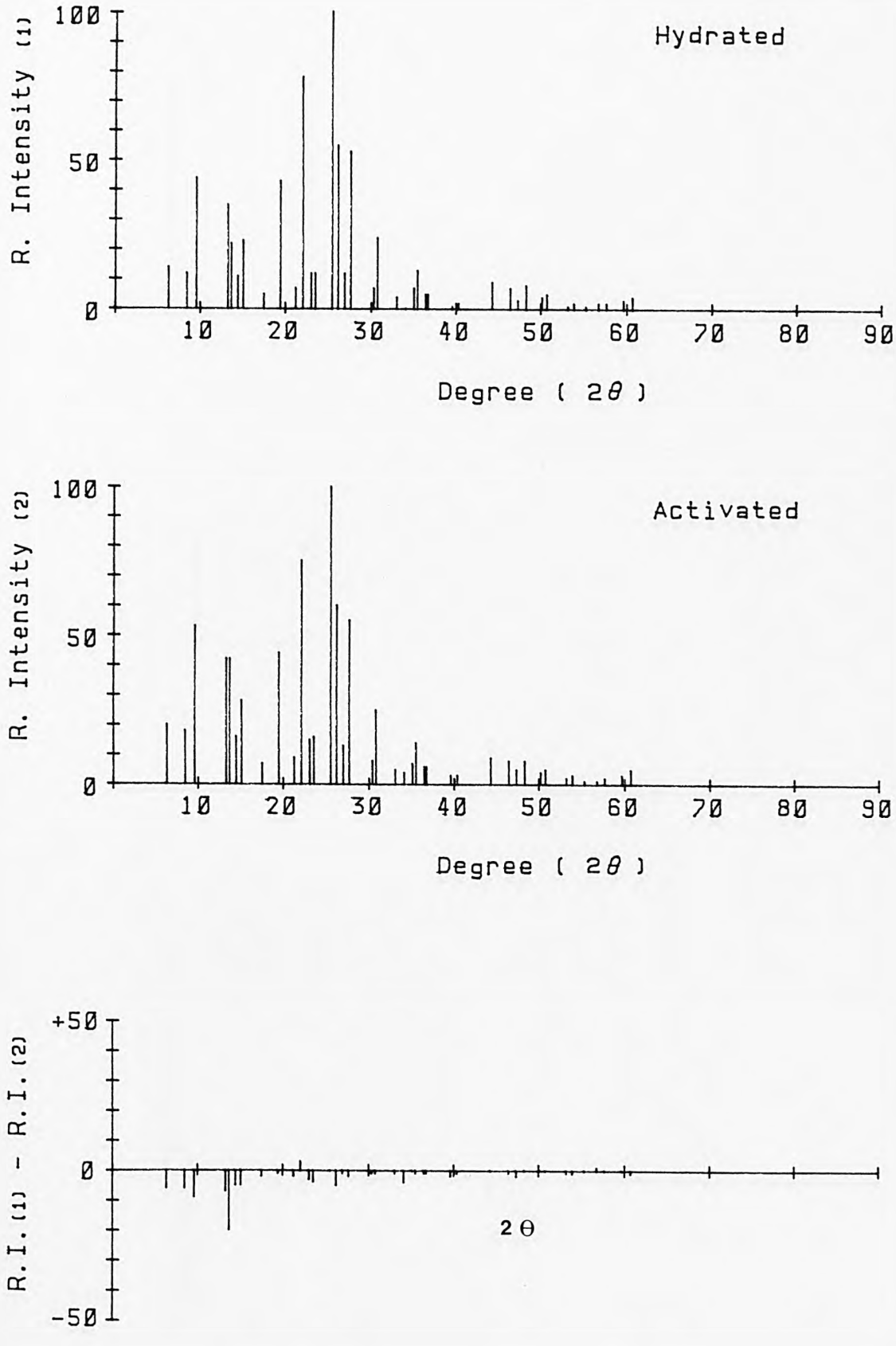

Fig. X.2: Distribution of relative intensity for X-ray diffraction of zeolite NiNa-MOR .

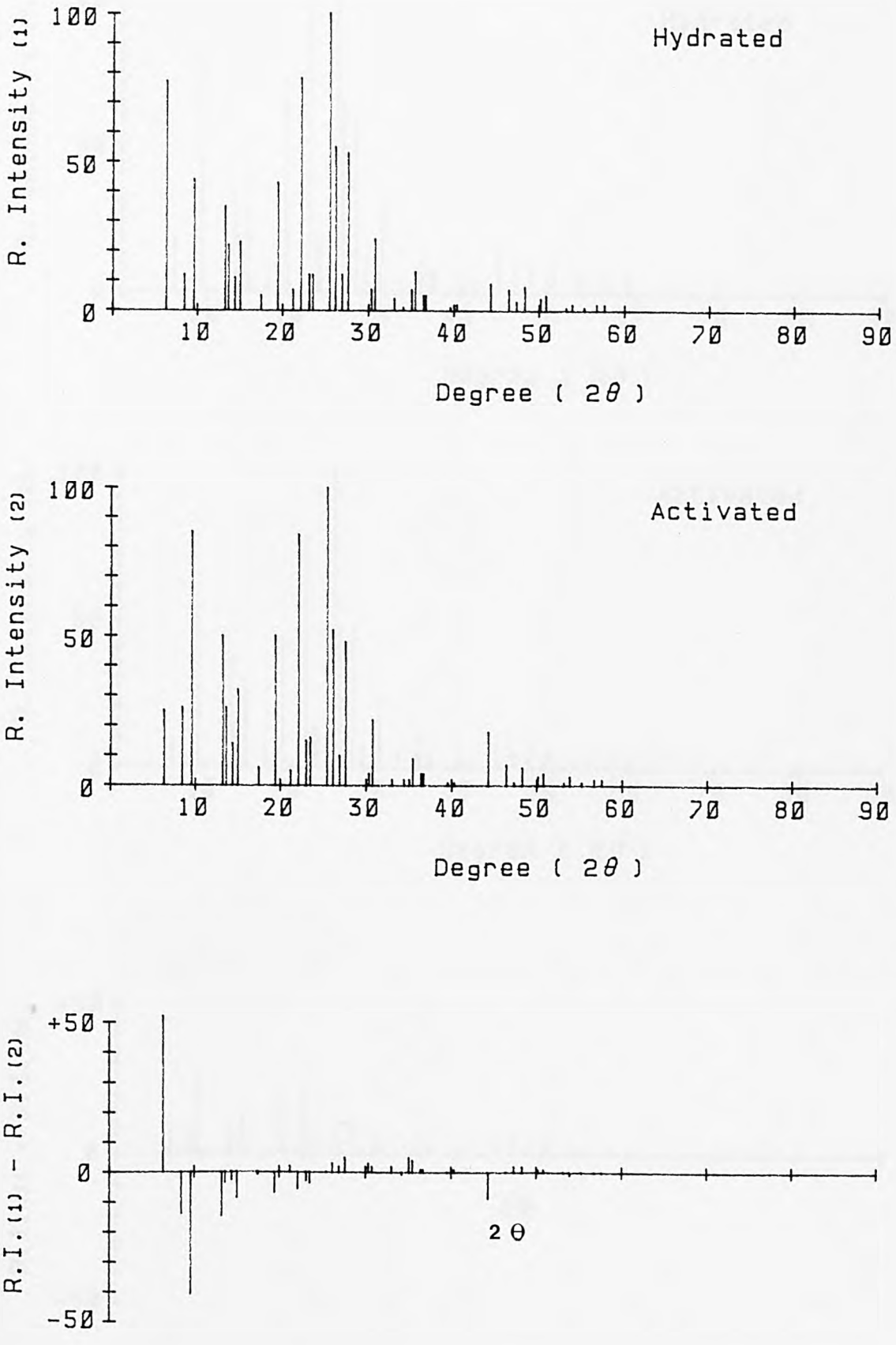

Fig. X.3: Distribution of relative intensity for X-ray diffraction of zeolite NiNa-MOR(N_2).

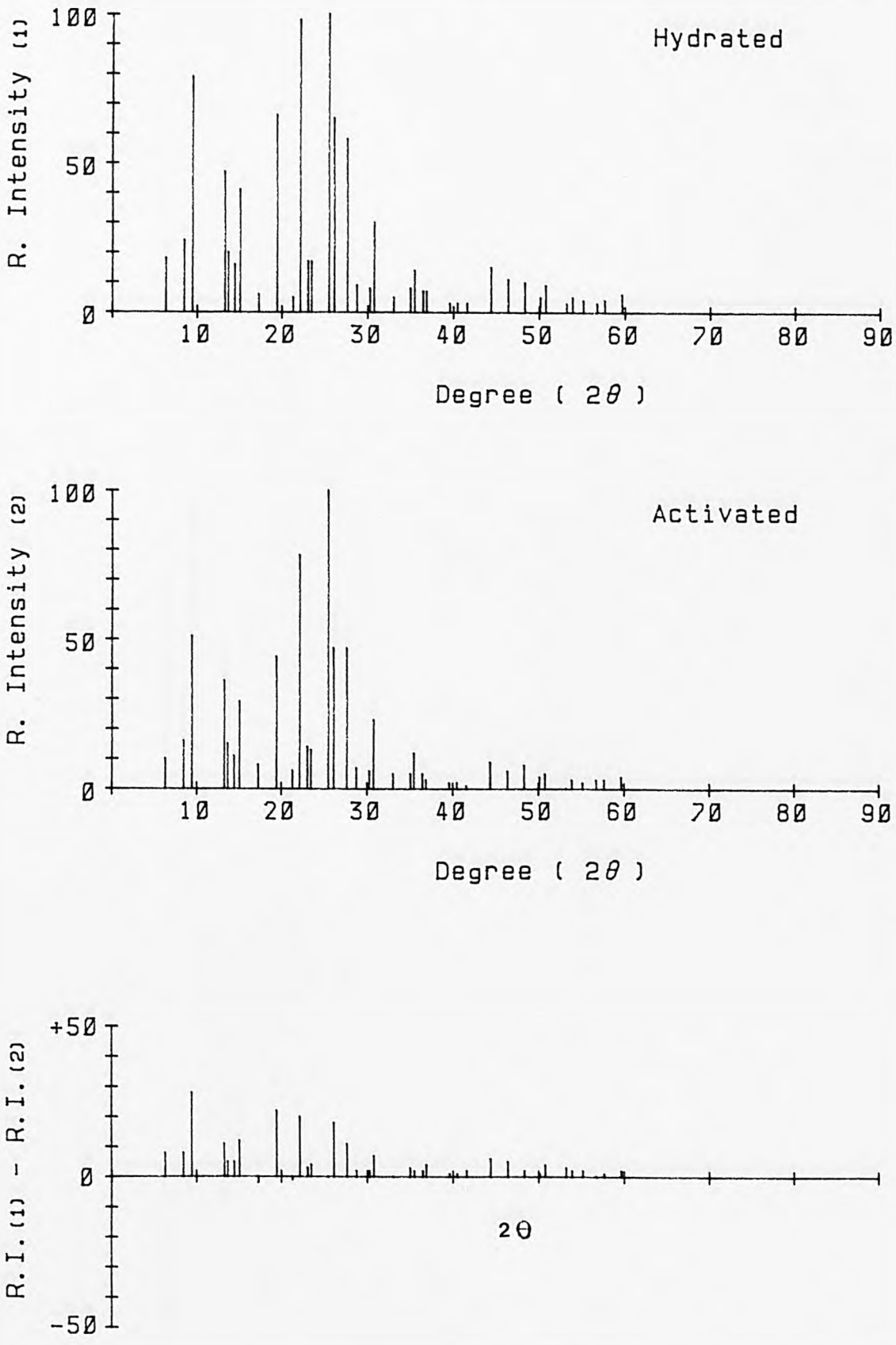

Fig. X.4: Distribution of relative intensity for X-ray diffraction of zeolite NiNH4-MOR .

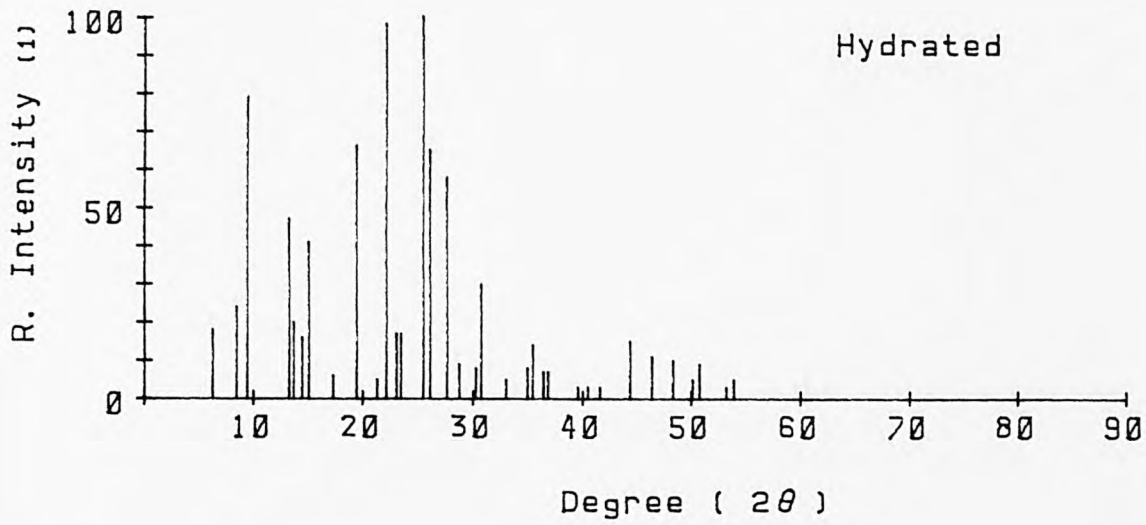

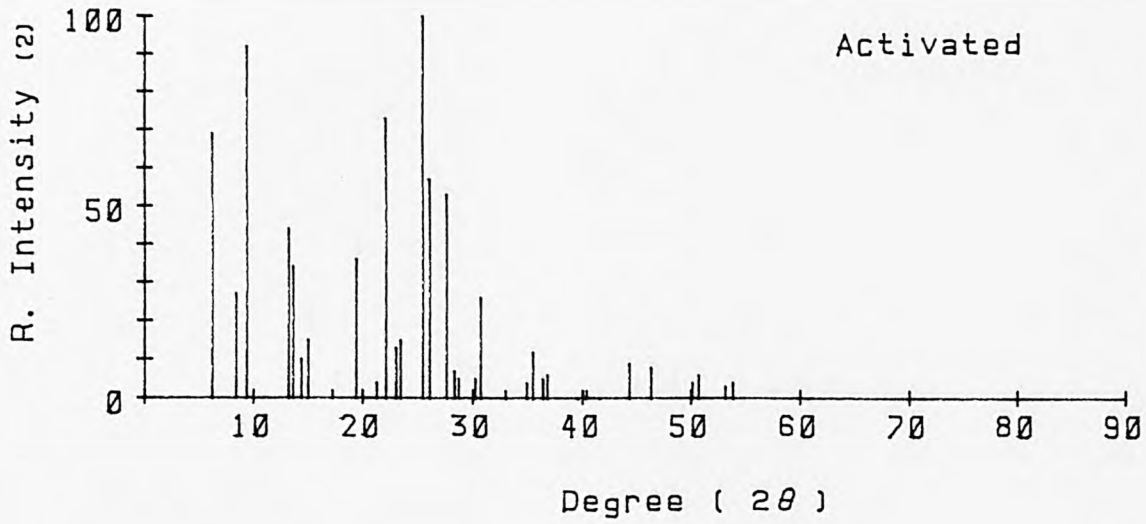

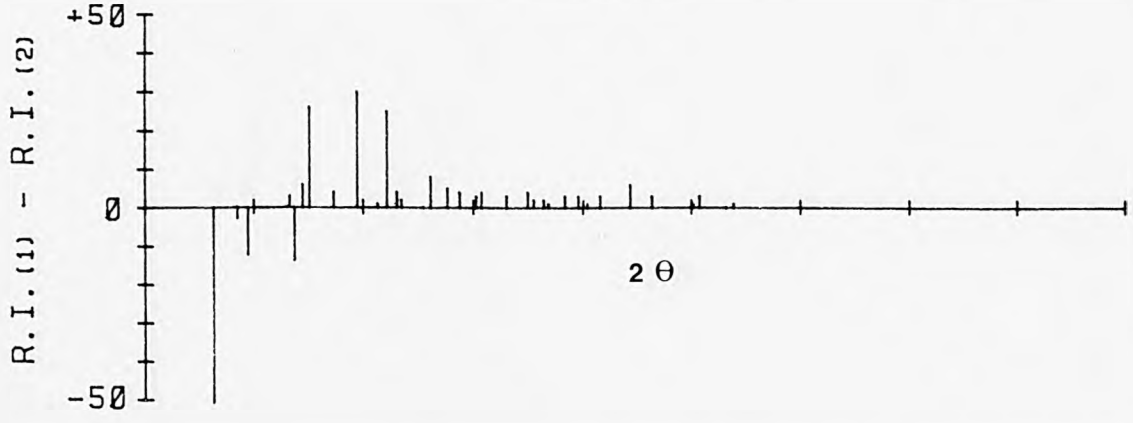

Fig. X.5: Distribution of relative intensity for X-ray diffraction of zeolite NiNH4-MOR (N_2).

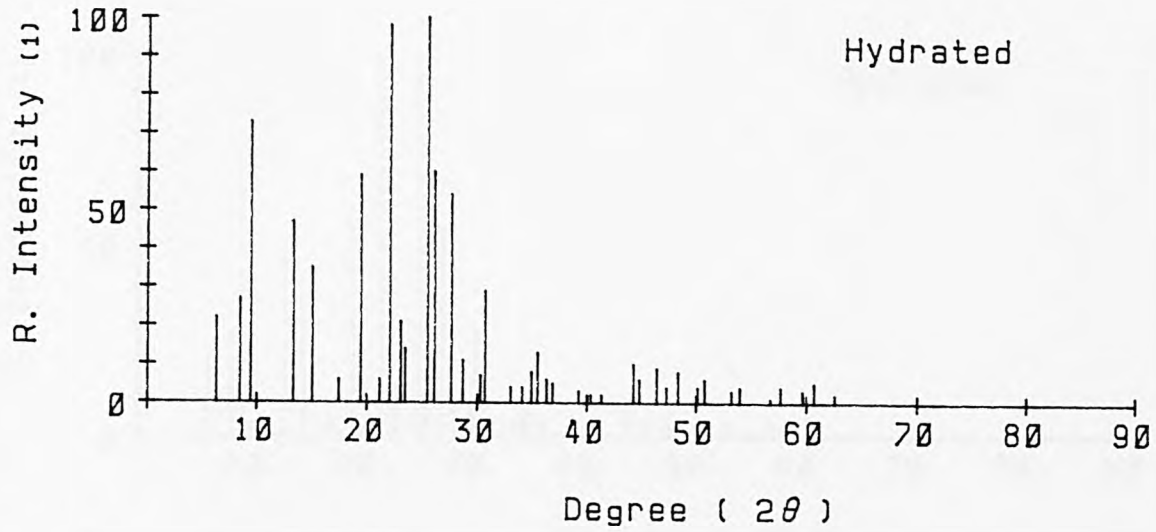

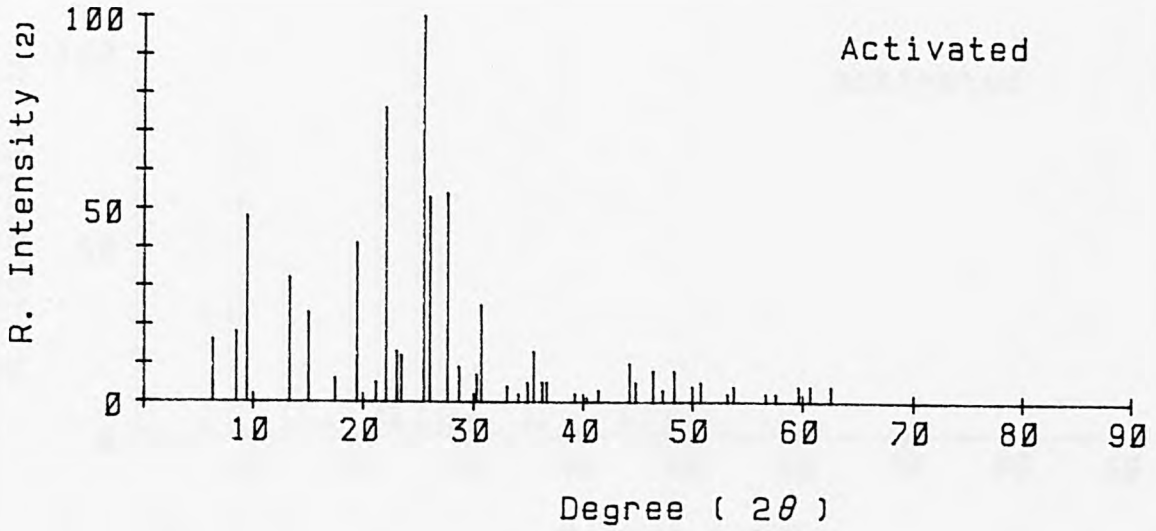

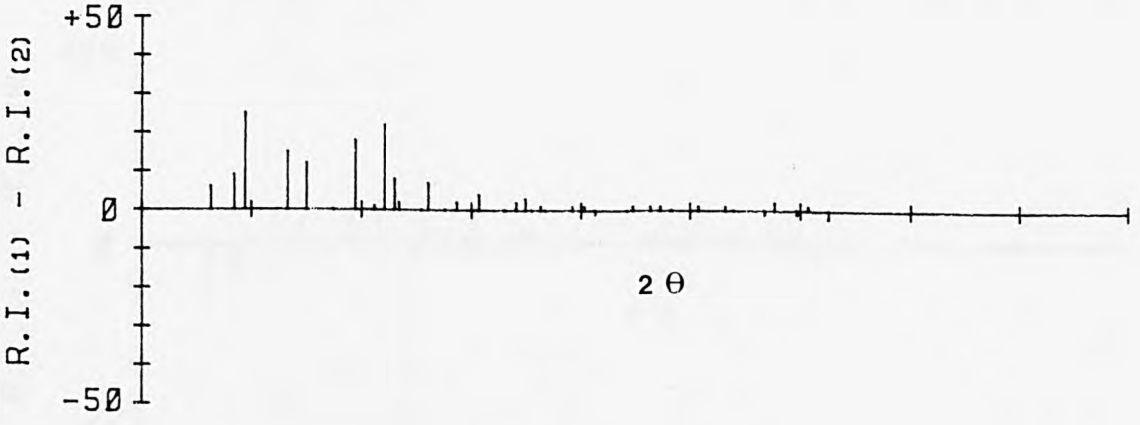

Fig. X.6: Distribution of relative intensity for X-ray diffraction of zeolite CuNa-MOR(Air).

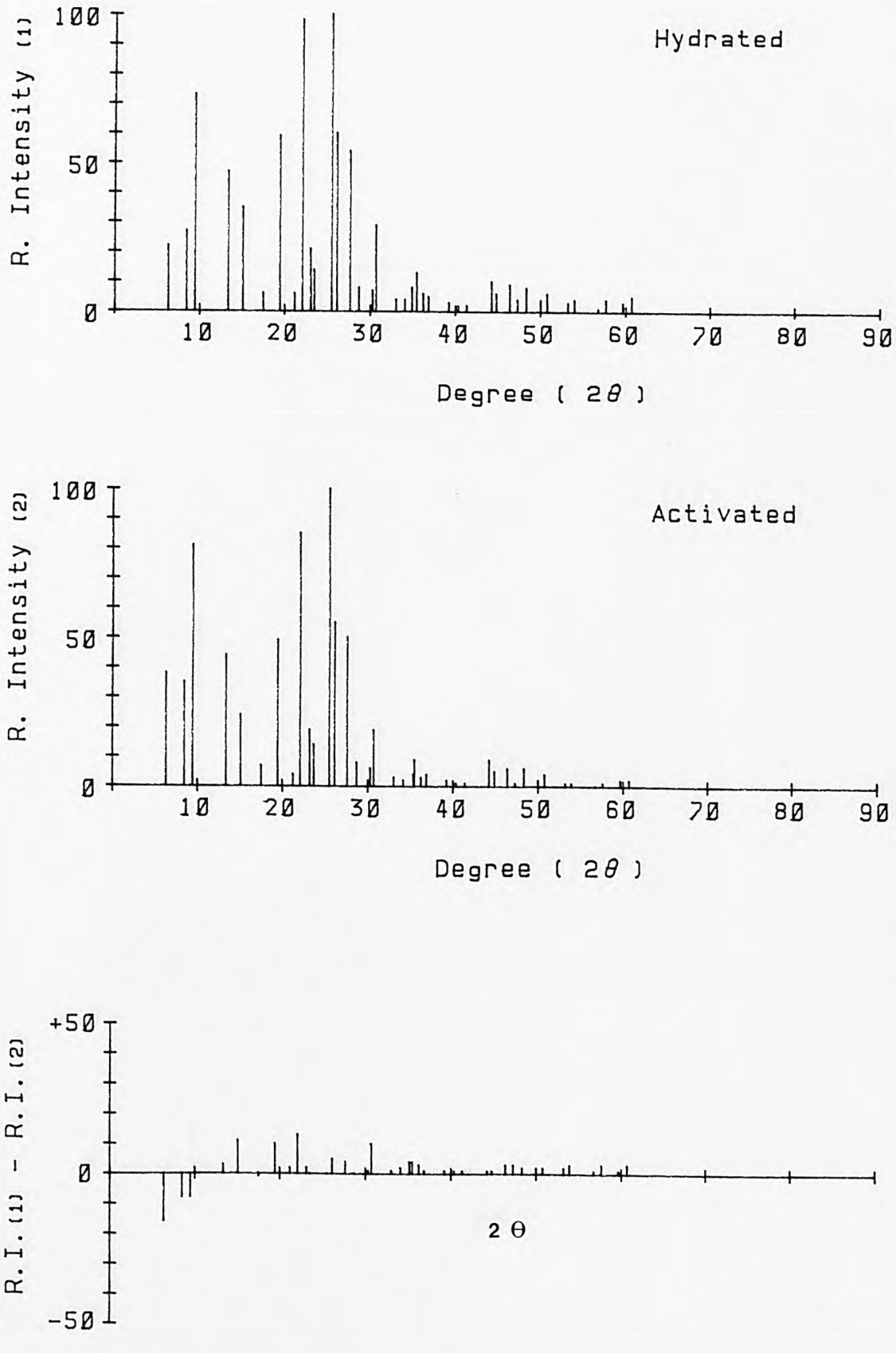

Fig. X.7: Distribution of relative intensity for X-ray diffraction of zeolite CuNa-MOR(N_2).

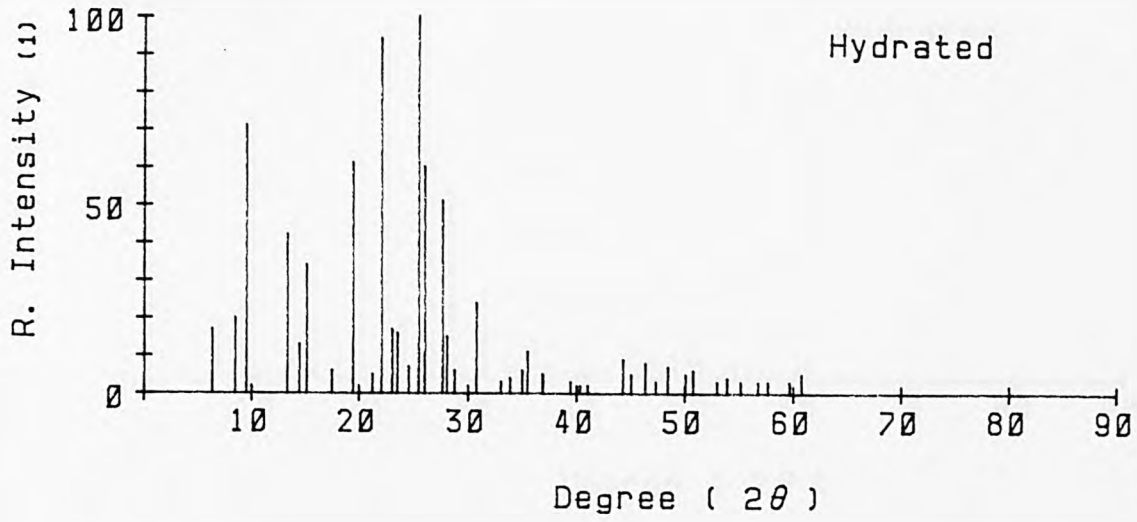

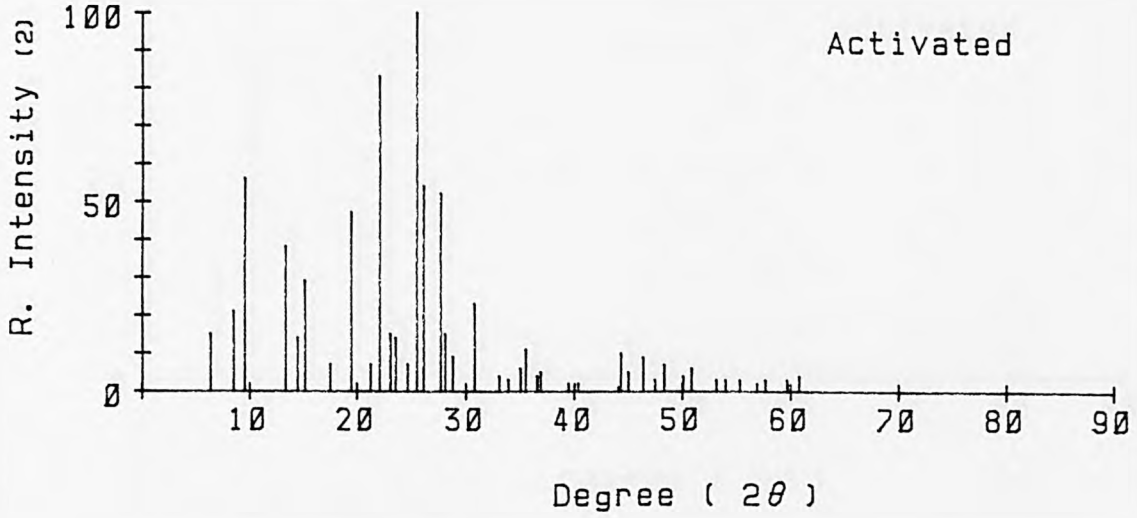

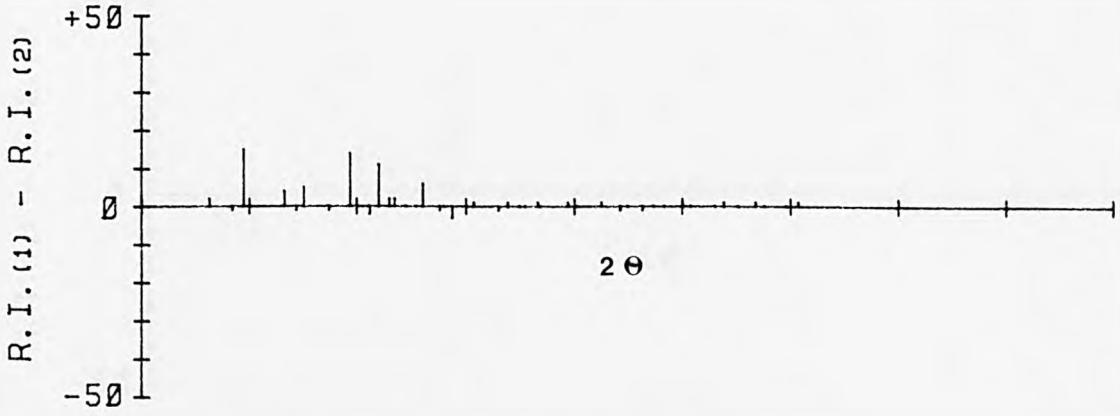

Fig. X.8: Distribution of relative intensity for X-ray diffraction of zeolite CuNH4-MOR(Air).

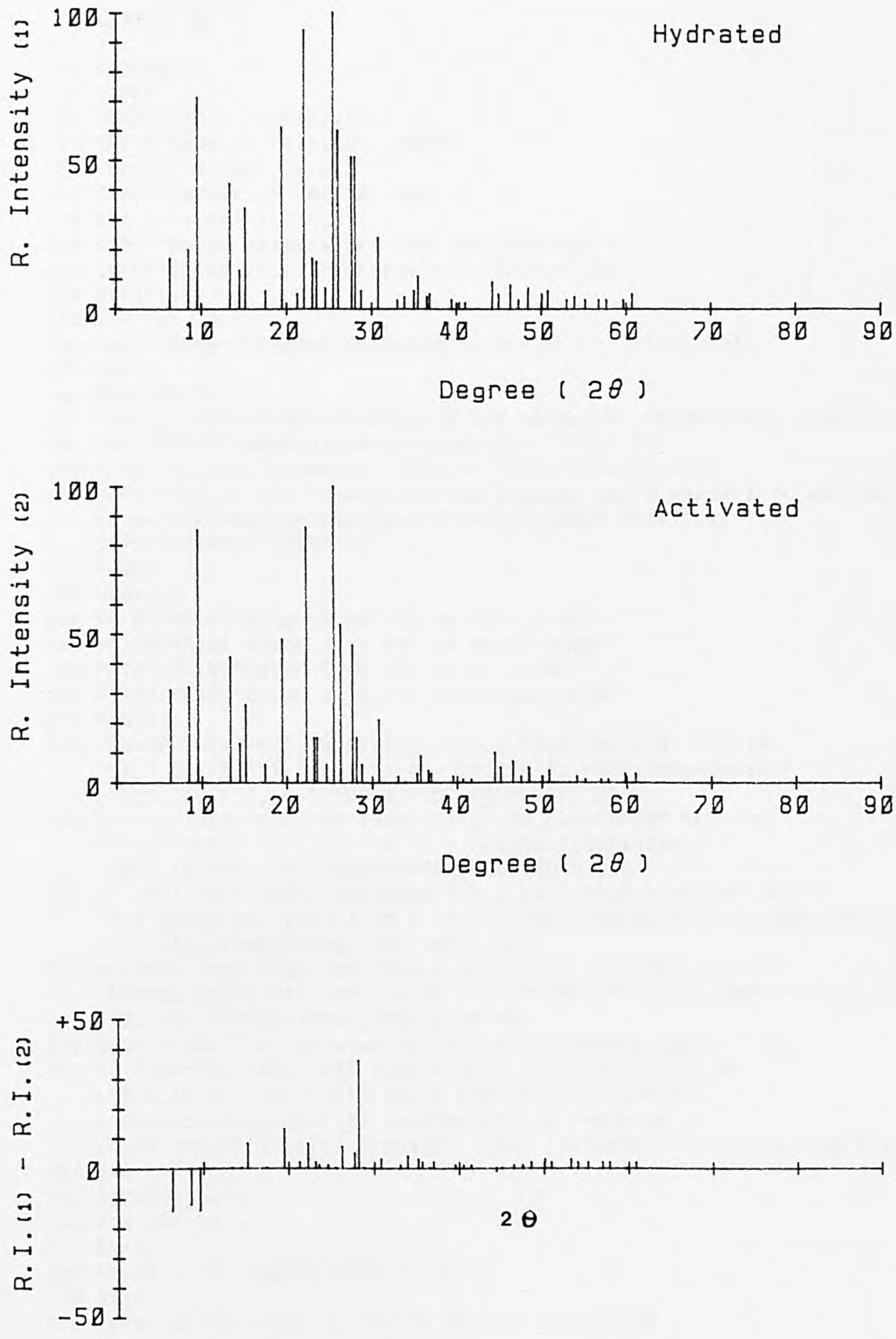

Fig. X.9: Distribution of relative intensity for X-ray diffraction of zeolite CuNH4-MOR(N_2).

Computer programs
(CP-1 to CP-8, pp. 420-448)
have been removed
for copyright reasons